MODEL SYSTEMS TO STUDY THE MECHANISMS OF NEURAL DEVELOPMENT AND DISEASE

EDITED BY: Parthiv Haldipur, Paula Alexandre and Sumru Bayin

PUBLISHED IN: Frontiers in Molecular Neuroscience

frontiers Research Topics

frontiers

ISSN 1664-8714
ISBN 978-2-88976-707-6
DOI 10.3389/978-2-88976-707-6

About Frontiers

Frontiers is more than just an open-access publisher of scholarly articles: it is a pioneering approach to the world of academia, radically improving the way scholarly research is managed. The grand vision of Frontiers is a world where all people have an equal opportunity to seek, share and generate knowledge. Frontiers provides immediate and permanent online open access to all its publications, but this alone is not enough to realize our grand goals.

Frontiers Journal Series

The Frontiers Journal Series is a multi-tier and interdisciplinary set of open-access, online journals, promising a paradigm shift from the current review, selection and dissemination processes in academic publishing. All Frontiers journals are driven by researchers for researchers; therefore, they constitute a service to the scholarly community. At the same time, the Frontiers Journal Series operates on a revolutionary invention, the tiered publishing system, initially addressing specific communities of scholars, and gradually climbing up to broader public understanding, thus serving the interests of the lay society, too.

Dedication to Quality

Each Frontiers article is a landmark of the highest quality, thanks to genuinely collaborative interactions between authors and review editors, who include some of the world's best academicians. Research must be certified by peers before entering a stream of knowledge that may eventually reach the public - and shape society; therefore, Frontiers only applies the most rigorous and unbiased reviews.
Frontiers revolutionizes research publishing by freely delivering the most outstanding research, evaluated with no bias from both the academic and social point of view. By applying the most advanced information technologies, Frontiers is catapulting scholarly publishing into a new generation.

What are Frontiers Research Topics?

Frontiers Research Topics are very popular trademarks of the Frontiers Journals Series: they are collections of at least ten articles, all centered on a particular subject. With their unique mix of varied contributions from Original Research to Review Articles, Frontiers Research Topics unify the most influential researchers, the latest key findings and historical advances in a hot research area! Find out more on how to host your own Frontiers Research Topic or contribute to one as an author by contacting the Frontiers Editorial Office: frontiersin.org/about/contact

MODEL SYSTEMS TO STUDY THE MECHANISMS OF NEURAL DEVELOPMENT AND DISEASE

Topic Editors:
Parthiv Haldipur, Seattle Children's Research Institute, United States
Paula Alexandre, University College London, United Kingdom
Sumru Bayin, Memorial Sloan Kettering Cancer Center, United States

Citation: Haldipur, P., Alexandre, P., Bayin, S., eds. (2022). Model Systems to Study the Mechanisms of Neural Development and Disease.
Lausanne: Frontiers Media SA. doi: 10.3389/978-2-88976-707-6

Table of Contents

frontiers | Frontiers in Molecular Neuroscience

TYPE Editorial
PUBLISHED 31 August 2022
DOI 10.3389/fnmol.2022.1006888

OPEN ACCESS

EDITED AND REVIEWED BY
Gregg E. Homanics,
University of Pittsburgh, United States

*CORRESPONDENCE
N. Sumru Bayin
sumru.bayin@gurdon.cam.ac.uk
Paula Alexandre
p.alexandre@ucl.ac.uk
Parthiv Haldipur
parthiv.haldipur@seattlechildrens.org

SPECIALTY SECTION
This article was submitted to Methods and Model Organisms, a section of the journal Frontiers in Molecular Neuroscience

RECEIVED 29 July 2022
ACCEPTED 03 August 2022
PUBLISHED 31 August 2022

CITATION
Sumru Bayin N, Alexandre P and Haldipur P (2022) Editorial: Model systems to study the mechanisms of neural development and disease. *Front. Mol. Neurosci.* 15:1006888. doi: 10.3389/fnmol.2022.1006888

Editorial: Model systems to study the mechanisms of neural development and disease

N. Sumru Bayin[1]*, Paula Alexandre[2]* and Parthiv Haldipur[3]*

[1]Wellcome Trust/Cancer Research UK Gurdon Institute, Cambridge University, Cambridge, United Kingdom, [2]University College London Great Ormond Street Institute of Child Health, London, United Kingdom, [3]Center for Integrative Brain Research, Seattle Children's Research Institute, Seattle, WA, United States

KEYWORDS

brain, disease, animal models, development, cellular models

Editorial on the Research Topic
Model systems to study the mechanisms of neural development and disease

Experimental models ranging from vertebrate and invertebrate models to *in vitro* cellular systems have been used to study the mechanisms underlying brain development and disease. Each of these models has specific strengths and caveats in recapitulating human biology. Some make use of elaborate genetic manipulations and are suitable for longitudinal studies while others may be more advantageous for large scale experiments. The need of the hour is to compare the differences and commonalties of findings obtained from different model systems and identify the benefits and drawbacks of each model system.

Human developmental studies of the brain have relied heavily on "macro scale" imaging, and pathology which provide discontinuous snapshots of the developing brain that omit evidence for what the brain may have looked like before or what it would eventually develop into. These approaches do not inform on the molecular and cellular mechanisms operational during brain development.

In vitro cellular systems and animal models have an advantage in this regard since they provide the luxury of performing sophisticated and reproducible experimentation which can help us decipher cellular and molecular mechanisms more easily and follow the development and emergence of phenotypes over time. The use of experimental models is also based on the principle that at least some features of human brain development are conserved across vertebrate and invertebrate species and can be recapitulated *in vitro*. In addition, genetically modified animal models what have been used to perform structure-function analyses, *in vivo* imaging and longitudinal studies to follow phenotypes over time, can help elucidate gene function, and vastly improve our understanding of basic neurobiological processes such as neuronal specification, neuronal circuit formation and function. These models also aid in the development of targeted therapies against neurodevelopmental disorders. However, the jury is still out on the extent to which animal and cellular

models truly and fully recapitulate human brain development and associated pathologies.

Recent studies on the human brain that have utilized imaging, histology and other high throughput approaches such as single cell genomics that are aimed at unraveling the molecular complexity of the human brain, have highlighted that many animal models, including rodents do not fully recapitulate human brain development, particularly cerebral and cerebellar development. This is likely due to the large evolutionary expansion of the human brain both in size and complexity to fulfill higher-order functions. For example, the human brain has expanded progenitor zones and cell types that are either absent or reduced significantly in rodents, and even non-human primates. Such findings highlight the necessity of humanized animal and cellular models as well as comparative analyses. Identification of human-specific developmental mechanisms has resulted in a renewed focus on human tissue-based studies which have helped characterize these foundational differences. However, human tissue is rare and not readily available to most labs. A paucity of standardized protocols for sophisticated experimentation, live imaging and human slice cultures are some of the present challenges for human studies. *In vitro* cellular models like brain organoids have also been useful in understanding human diseases, particularly of the cerebral cortex since cerebral organoids have been shown to mimic many early aspects of human cerebral development. However, these models fail to fully recapitulate the later stages of neural development and consume a lot of resources. Additionally, human tissue, particularly from malformed brains is scarce and not readily available to most. Finally, challenges of performing elaborate genetics and whole organ/live imaging approaches present complications for human studies and humanized models. Collectively all these highlight the value and benefit of utilizing multiple models and different expertise when investigating neural development and disease, both for practical and evo-devo angles.

In this Research Topic, our goal is to introduce the functionality of various *in vitro* and *in vivo* models and showcase their effectiveness in improving our understanding of brain development and disease, in order to facilitate a cross model system discussion on neural development and disease mechanisms. Here, we present valuable review articles that discuss brain tumors (Antonica et al.), aging (Chaudhar et al.) and genetic disorders affecting brain development (Biel et al.) from the perspective of the disease models; modeling neural polarity mechanisms and their role in developmental disease (Solecki), and the power of imaging approaches and emerging non-mammalian models in neuroscience (Haynes et al.). In addition to these resources, we have research articles that describe the use of models to identify the molecular mechanisms of various aspects of neurodevelopmental aging from central and peripheral nervous system development (Delalande et al.; Jose et al.; Natarajan et al.), and associated pathophysiology (Roy et al.; Kelani et al.).

Author contributions

All authors listed have made a substantial, direct, and intellectual contribution to the work and approved it for publication.

Funding

This work was supported by Brain and Behavior Research Foundation Young Investigator Award and NIH-R21 NS117848 to PH, NIH/NINDS (K99/R00 NS112605-01) and core support from Wellcome Trust (#092096) to NS, and Wellcome Human Developmental Biology Initiative (#182625) to PA.

Acknowledgments

We would like to thank all the authors for their contributions.

Conflict of interest

The authors declare that the research was conducted in the absence of any commercial or financial relationships that could be construed as a potential conflict of interest.

Publisher's note

frontiers in Molecular Neuroscience

ORIGINAL RESEARCH
published: 21 October 2021
doi: 10.3389/fnmol.2021.746211

Membrane Cholesterol Is a Critical Determinant for Hippocampal Neuronal Polarity

Mini Jose, Aiswarya Sivanand and Chaitra Channakeshava*

Centre for Neuroscience, Indian institute of Science, Bangalore, India

Maintaining a normal cholesterol balance is crucial for the functioning of a healthy brain. Dysregulation in cholesterol metabolism and homeostasis in the brain have been correlated to various neurological disorders. The majority of previous studies in primary cultures focus on the role of cholesterol balance in neuronal development after polarity has been established. Here we have investigated how transient alteration of membrane lipids, specifically cholesterol, affects neuronal development and polarity in developing hippocampal neurons prior to polarity establishment, soon after initiation of neurite outgrowth. We observed that temporary cholesterol perturbation affects axonal and dendritic development differentially in an opposing manner. Transient membrane cholesterol deficiency increased neuronal population with a single neurite, simultaneously generating a second population of neurons with supernumerary axons. Brief replenishment of cholesterol immediately after cholesterol sequestering rescued neuronal development defects and restored polarity. The results showed a small window of cholesterol concentration to be complementing neurite outgrowth, polarity reestablishment, and in determining the normal neuronal morphology, emphasizing the critical role of precise membrane lipid balance in defining the neuronal architecture. Membrane cholesterol enhancement modified neurite outgrowth but did not significantly alter polarity. Cholesterol sequestering at later stages of development has shown to enhance neurite outgrowth, whereas distinct effects for neurite development and polarity were observed at early developmental stages, signifying the relevance of precise membrane cholesterol balance in altering neuronal physiology. Our results confirm cholesterol to be a key determinant for axo-dendritic specification and neuronal architecture and emphasize the possibility to reverse neuronal developmental defects caused by cholesterol deficiency by modulating membrane cholesterol during the early developmental stages.

Keywords: hippocampal neuronal development, membrane cholesterol, axo-dendritic specification, lipid homeostasis, neurite outgrowth, neuronal polarity, cholesterol labeling

OPEN ACCESS

Edited by:
Parthiv Haldipur,
Seattle Children's Research Institute,
United States

Reviewed by:
Raman M. Das,
The University of Manchester,
United Kingdom
Li-Jin Chew,
Brown University, United States

****Correspondence:***
Mini Jose
mini@iisc.ac.in;
minijose2000@gmail.com

Specialty section:
This article was submitted to Methods and Model Organisms, a section of the journal Frontiers in Molecular Neuroscience

Received: *23 July 2021*
Accepted: *04 October 2021*
Published: *21 October 2021*

Citation:
Jose M, Sivanand A and Channakeshava C (2021) Membrane Cholesterol Is a Critical Determinant for Hippocampal Neuronal Polarity. Front. Mol. Neurosci. 14:746211. doi: 10.3389/fnmol.2021.746211

INTRODUCTION

The axo-dendritic specification is a defining feature for the unique architecture of neurons. A well-coordinated orchestra of positive and negative feedback signals is thought to regulate the breaking of symmetry and establishment of neuronal polarity with a singular axon and multiple dendrites in neurons (Arimura and Kaibuchi, 2007; Barnes and Polleux, 2009;

Schelski and Bradke, 2017; Takano et al., 2019). The functional distinction of the different neuronal compartments including the axons and the dendrites is brought about by the selective filtering of molecules giving a distinct molecular composition, allowing a unidirectional flow of signals during synaptic transmission (Song et al., 2009). Different functional and molecular determinants for this specification have been characterized over the years (Leterrier et al., 2015; Gumy et al., 2017; Leterrier, 2018). Membrane lipids including sphingolipids and cholesterol have been shown to have a prominent role in the selective localization of molecules particularly in the axolemma by lipid-protein interactions (Ledesma et al., 1998). Several evidences emphasize the relevance of lipid homeostasis, particularly that of lipid rafts and cholesterol, in various physiological and pathological processes (Vance, 2012; Sviridov et al., 2020; Vona et al., 2021). Cholesterol metabolism and homeostasis are thought to have critical roles in maintaining a healthy brain (Zhang and Liu, 2015). Dysregulation in the lipid balance has been correlated to diverse neurodegenerative conditions including Alzheimer's disease, Parkinson's disease, Huntington's disease, Niemann Pick type C disease, and recently to cancer (Vance, 2012; Wang and Song, 2012; Leoni and Caccia, 2015; Hussain et al., 2019; Vona et al., 2021). Proteins such as amyloid precursor protein (APP) vital in the pathological outcome of neurological disorders such as AD have been recently shown to be critically involved in the cholesterol turnover for neuronal activity, supporting the importance of cholesterol homeostasis in a wider context (Pierrot et al., 2013; Grimm et al., 2017; Cho et al., 2020).

Autonomous cholesterol synthesis has been shown to occur in neuronal soma but not in axons (Vance et al., 1994). The majority of cholesterol synthesis in the brain occurs in glial cells, particularly during active myelination covering the axons, and significantly reduces in the mature brain once the myelination is complete (Quan et al., 2003; Dietschy and Turley, 2004; Funfschilling et al., 2012). Therefore, cholesterol is thought to have a prominent role in regulating neuronal development and neurite outgrowth. Cholesterol mediated neurite outgrowth has been reported to be dependent on the brain regions, being different between the cortical and hippocampal regions (Ko et al., 2005). Cholesterol modulation is also thought to regulate dendritic outgrowth, with little effect on the axonal extension (Fan et al., 2002). Most of these studies have been conducted on later developmental stages of neurons (stages 3–5), when the neuronal polarity establishment and axon determination have already been initiated (Dotti et al., 1988). Though the lipid balance and compositionality of the membrane are thought to be critical in neurite outgrowth, the fine regulation of membrane cholesterol on the axonal and dendritic development particularly at very early stages, from the initiation of protrusions to breaking of symmetry and polarity establishment (stages 1–3), has never been explored in detail. In this study, we have addressed the role of membrane lipid regulation, particularly cholesterol, in regulating neurite outgrowth and development and in determining the axo-dendritic specification at very early stages of neurite growth.

We transiently sequestered cholesterol to different levels in rat hippocampal neurons at DIV1 (days *in vitro*) for varying durations. The alterations in membrane cholesterol levels after transient sequestering were verified using an unesterified cholesterol assay. The neurons were allowed to grow to DIV3 and imaged using axonal and dendritic markers. Interestingly, we observed opposing effects for cholesterol sequestering on the axonal and dendritic growth and a marked shift in neuronal polarity. Along with an increase in the neuronal population with a single neurite, cholesterol sequestering also generated a second population of neurons with supernumerary axons. The neuromorphological and polarity defects were rescued upon briefly replenishing the neurons with exogenous cholesterol, confirming this effect to be cholesterol dependent. The short concentration window of optimal cholesterol replenishment revealed the critical nature of membrane lipid balance on maintaining normal neuronal morphology. Conversely, transient cholesterol enhancement complemented neurite extension but did not alter polarity. Increased duration of cholesterol sequestering elevated the population of cells entering apoptosis. Our results elucidate that membrane cholesterol is a critical determinant for axonal and dendritic outgrowth, and for regulating axo-dendritic specification and neuronal architecture in rat hippocampal neurons.

MATERIALS AND METHODS

Cell Culture

Primary cultures were prepared from P0/P1 rat pups (Sprague-Dawley) as described earlier (Goslin and Banker, 1989). The hippocampus was dissected out from the rodent brain in Hibernate Media (Thermofisher Scientific). The dissected hippocampi were trypsinized (0.25% Trypsin), washed 3×, and dissociated into single cells by syringing using needles of 2 pore sizes sequentially to remove all neurites (21 G and 25 G, BD Precision Glide Needle). The cells were plated on 18 mm diameter thickness corrected coverslips (Marienfeld Superior) coated with Poly-L-Lysine (1 mg/ml, Sigma Aldrich) after resuspending in Neurobasal media (Thermofisher Scientific) complemented with B27, Glutamate, and Normocin (Invivogen; referred to as Complete Neurobasal media) at a density of 50 cells/mm^2.

Drug Treatment and Immunocytochemistry

The cells were fixed at DIV1, DIV2, and DIV3 with 4% PFA+sucrose and labeled with antibodies against Map2 (Merck Millipore #AB5622, rabbit) and Tau (Merck Millipore #05–348, mouse). Alexa 488 and Alexa 647 secondary antibodies (Thermofisher Scientific) marked Map2 and Tau, respectively for dual color labeling.

For cholesterol sequestration, the cells were treated transiently with differing concentrations (2.5 mM, 5 mM, 7.5 mM, and 10 mM) of Methyl β cyclodextrin (MβCD, Sigma Aldrich C4555) for 10 min or 20 min at 37 deg at DIV1. The MβCD stock (100 mM) was reconstituted in water and the working concentrations were prepared in Complete Neurobasal media for treatment. After treatment, the cells were washed thrice in prewarmed Complete Neurobasal media and allowed to grow to DIV3 before fixing them. For cholesterol replenishment, the cells

treated with 5 mM MβCD for 10 min were washed and further treated for 10 min with differing concentrations of exogenous cholesterol (Sigma Aldrich C4951, Cl:MβCD, 0.5 mM, 1.0 mM, 1.5 mM, and 2.0 mM) at 37 deg. The Cholesterol stock (100 mM) was reconstituted in water and the working concentrations were prepared in Complete Neurobasal media for treatment. The cells were again washed thrice in prewarmed Complete Neurobasal media and allowed to grow to DIV3 before fixing them. The treated cells were labeled with antibodies against Map2 and Tau marked by Alexa 488 and Alexa 647, respectively. The coverslips were mounted using Prolong antifade agent (Thermofisher Scientific).

Cholesterol Labeling and Viability Assay

For measuring unesterified cholesterol, the control and cells treated with varying concentrations of MβCD (2.5 mM, 5 mM, 7.5 mM, and 10 mM) for 10 min and 20 min were labeled at DIV3 using a membrane marker for lipid rafts tagged with Alexa 555 (Thermofisher Scientific V34404). Membrane labeling was done in Complete Neurobasal media for 10 min at 4 deg. The cells were then washed, fixed with 4% PFA+sucrose and labeled with Filipin III (Sigma Aldrich F4767) at a concentration of 50 μg/ml in PBS for 2 h at RT and overnight at 4 deg, after which they were washed and imaged in PBS.

The membrane damage to the cells induced on cholesterol sequestering for varying durations was assessed using a Live/Dead Cell imaging kit (Thermofisher Scientific R37601) which uses Calcein AM cell permeable dye and Bobo-3 Iodide as live and dead cell indicators, respectively. The live control and treated cells (10 mM MβCD, 10 min, 20 min, and 30 min) were labeled at DIV3 for 15 min at RT and imaged in an extracellular imaging buffer. For quantifying the viability of cells undergoing cholesterol sequestering, the control and cells treated for varying durations (10 mM MβCD, 10 min, 20 min, and 30 min) were fixed at DIV3 and labeled with an antibody (Cleaved Caspase 3, rabbit, #9661, Cell Signaling Technology) which recognize endogenous levels of activated Caspase 3 marked by Alexa 555. The coverslips were mounted using Prolong antifade agent containing DAPI (Thermofisher Scientific).

Microscope Image Acquisition and Quantitative Analysis

Images were acquired an inverted microscope Zeiss Axio Observer Z1 equipped with a 40× objective, halogen lamp and an ScMOS camera (pco.edge). Specific filters for Alexa 488 and Alexa 647 were used for acquisition. 3D stacks of total volume thickness of 3 μm with a plane thickness of 200 nm were acquired. The images were exported, and all processing and image analyses were performed using Metamorph 7.0. Maximum intensity projections of the images were generated. For analysis of neuronal development profile, length of the longest neurite, length of dendrites, number of neurites per cell and the neuronal polarity ratio were quantified. For specific sets of experiments, additional analysis included calculation of the percentage of cells with single neurite, percentage of neurons with multiple axons, and polarity ratio of neurons displaying multiple axons, as explained. Due to the minimal variability between neuronal cultures, Mean ± SEM is presented for all data. The statistical difference between the means was calculated by One-way Anova (Graph Pad Prism 9). $^{****}p < 0.0001$, $^{***}p < 0.001$, $^{**}p < 0.01$, $^{*}p < 0.05$ and ns non-significant.

Imaging of cells labeled with Filipin III was performed similarly using a 40× objective. Due to the high photobleaching of Filipin III, cells were focused using the lipid raft membrane marker tagged with Alexa 555 and 3D stacks of total volume thickness of 3 μm with a plane thickness of 200 nm were acquired for both channels. DsRed filter was used for Alexa 555 acquisition, whereas Filipin fluorescence was acquired using a filter combination 420–480 nm excitation and 500–550 nm emission. Quantification of Filipin fluorescence was done from maximum intensity projections of 3D stacks. The images were thresholded for automatic detection of light objects to form a mask. The regions mapping the cells were transferred to the original images to quantify the corresponding average intensity of the cells.

For quantifying the viability of cells undergoing cholesterol sequestering, images of control and treated cells were acquired using a 20× objective. For the live cell assay, images were acquired for green and orange channels using GFP and DsRed filters, respectively. The images were thresholded and assessed by the Count nuclei App in Metamorph software. The ratio of orange (dead) to green (live) cells in each field was quantified and normalized using the mean value of control cells. For the caspase 3 assay, images were acquired using DAPI and DsRed filters. The percentage of DAPI marked cells colabeled with Caspase 3 (positive, dead cells) vs. DAPI only cells (negative, live cells) was quantified for each field by a Cell Scoring App in Metamorph software. The ratio of the percentage of dead vs. live cells was assessed and normalized using the mean value of control cells.

The statistical difference between the means of each condition (fluorescence intensity/ratio) was calculated by One-way Anova (Graph Pad Prism 9). $^{****}p < 0.0001$, $^{***}p < 0.001$, $^{**}p < 0.01$, $^{*}p < 0.05$ and ns non-significant.

RESULTS

Assessing Rat Hippocampal Neuronal Development Profile

To understand the role of cholesterol on neuronal development, it was critical to assess a homogeneous neuronal population at different stages of development. Cell culture protocols were optimized to prepare homogenous primary hippocampal neuronal cultures from postnatal day 0 or 1 (P0/P1) rat pups. The morphology of pyramidal neurons in these cultures was assessed at DIV1, DIV2, and DIV3 (**Figure 1**). The homogeneity of cultures was verified using Tau (axonal marker) and Map2 (somato-dendritic marker) antibodies, which showed >90% of the plated neurons to be undifferentiated at DIV1 vs. >90% differentiated at DIV3. A gallery of low magnification images of cells at each developmental stage is presented in **Supplementary Figure 1**. 3D image stacks of total volume thickness of 3 μm of Tau and Map2 labeled neurons at different stages were acquired at higher magnification (**Figure 1**). All quantifications

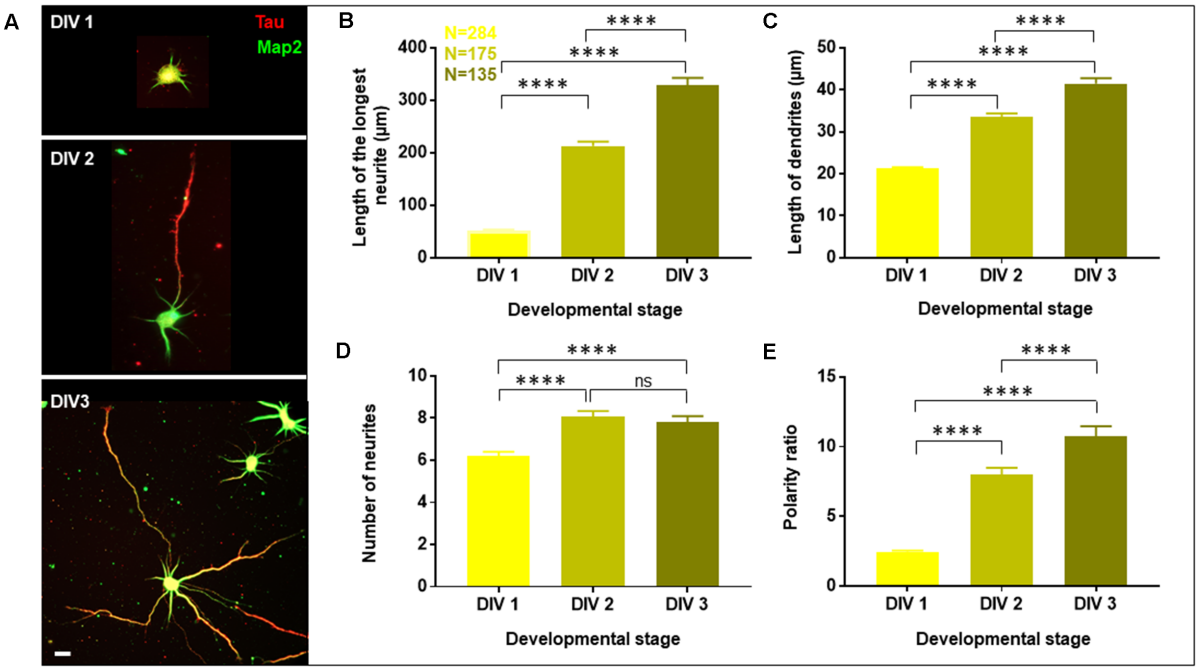

FIGURE 1 | Developmental profile of optimized primary cultures of rat hippocampal neurons. Neurons were grown to three developmental stages namely DIV 1, 2, and 3, fixed and labeled with Tau (red) and Map2 (green) as axonal and dendritic markers, respectively. **(A)** A gallery of cells at DIV 1, 2, and 3 is presented. **(B–E)** Neuronal development was assessed by quantifying the length of the longest neurite **(B)**, length of dendrites **(C)**, number of neurites in each cell **(D)**, and the polarity ratio **(E)**, which was calculated from the ratio of the longest neurite to the average length of dendrites of each cell. N denotes the number of cells from four independent cultures. One-way Anova was performed to test the significance of the difference between the means. ****$p < 0.0001$, ns denotes non-significant. Scale bar indicates 20 µm.

were performed on the maximum intensity projections of the stacks with an overlay of both channels. The experimental and analytical procedures are outlined in **Supplementary Figure 2**.

Neuronal development and growth profile were analyzed by quantifying the length of the longest neurite (axon), length of the dendrites (all neurites except the longest) and the number of neurites per cell. This classification of neurites into axon and dendrites was entirely based on their length and not their specific labeling. Neuronal polarity was assessed based on the ratio of the length of the longest neurite (axon) to the average length of the dendrites, which is referred to as the neuronal polarity ratio. The higher values of the neuronal polarity ratio indicated the asymmetric pattern of the neurons with a single long axon and short dendrites, while small values of polarity ratio showed a symmetric growth pattern, where the neurites were similar in length. The conventional semi-automated software for neuro-morphology assessment including Simple Neurite Tracer (SNT), Neural Circuit Tracer (NCT), AutoNeuriteJ, etc. are limited by various factors such as lack of sensitivity to detect fine neuronal processes for precise characterization, exclusion of overlapping cells, the requirement of additional labeling and lack of distinction of axo-dendritic processes (Chothani et al., 2011; Longair et al., 2011; Boulan et al., 2020). Therefore, manual tracing of neurites was performed from the periphery of the soma to the distal end of the neurites. All projections and bifurcations including the secondary and tertiary processes were considered and added to the length of the primary process. Thresholding of neurite length was performed where a cut-off length of 10 µm was introduced to exclude filopodia. The quantification of all parameters including the length of the longest neurite, length of dendrites, number of neurites per cell, and polarity ratio was done using the filtered values (**Supplementary Figure 2B**).

A gallery of rat hippocampal neurons of different stages namely, DIV1, DIV2, and DIV3 is presented (**Figure 1A**). A steep increase in the length of the longest neurite (referred to as the axon) was observed from DIV1 (51.73 ± 1.86 µm) to DIV3 (328.2 ± 14.53 µm), with DIV2 (212.7 ± 8.38 µm) being intermediate (**Figure 1B**, **Table 1**). The dendrites (rest of the neurites except the longest) also displayed a gradual increase in their length along development, though not as fast as the axon (**Figure 1C**, **Table 1**). The length of the dendrites increased from 21.27 ± 0.3 µm at DIV1 to 41.42 ± 1.35 µm at DIV3. The number of neurites per cell showed a slight increase with the maturity of neurons from 6 ± 0.2 at DIV1 to 8 ± 0.3 at DIV 2 and DIV3 (**Figure 1D**, **Table 1**). Neuronal development involves both growth of the neuronal processes as well as an axo-dendritic specification or neuronal polarity establishment. Different technical challenges including lack of reliable markers at the early developmental stages made it hard to determine whether the specification between the two neuronal processes

TABLE 1 | Developmental profile of primary cultures of rat hippocampal neurons.

Developmental stage	DIV1	DIV2	DIV3
Length of the longest neurite (μm)	51.73 ± 1.86	212.7 ± 8.38	328.2 ± 14.53
Length of dendrites (μm)	21.27 ± 0.3	33.49 ± 0.85	41.42 ± 1.35
Number of neurites per cell	6 ± 0.2	8 ± 0.3	8 ± 0.3
Polarity ratio	2.47 ± 0.09	7.99 ± 0.49	10.72 ± 0.75

*The table shows the morphological properties of primary cultures of rat hippocampal neurons at three developmental stages namely, DIV1, 2, and 3. Mean ± SEM is presented for N number of cells as shown in **Figure 1** from four independent cultures.*

has been established. Therefore, the neuronal polarity ratio or the ratio of the length of the longest neurite (axon) to the average length of the dendrites was assessed, which showed the polarity status of the neuron. The polarity ratio displayed a drastic increase from 2.47 ± 0.09 at DIV1 to 10.72 ± 0.75 at DIV3 (**Figure 1E**, **Table 1**), confirming this to be a reliable parameter to assess the switch of a neuron from a symmetric to asymmetric growth pattern. Along with the qualitative assessment of polarity establishment using Tau and Map2 as axonal and dendritic markers, quantifying the polarity ratio allowed us to make a reliable and additional assessment on the multiple morphological phenotypes observed by membrane lipid perturbations.

To account for the variability between cultures, all quantifications were done across the same cultures at different stages. The minimal error observed for the different parameters across the cultures showed the robustness of the data and purity of the cultures suggesting its homogenous nature, enabling us to quantify the reported parameters in a reliable manner. A significant increase in the length and number of neurites as well as in the percentage of polarized cells was observed during rat hippocampal neuronal development from DIV1 to DIV3.

Cholesterol Sequestering Has Opposing Effects on Axon vs. Dendrites

Having a homogenous neuronal population, which could be developmentally assessed, allowed us to investigate the role of membrane cholesterol in two important aspects of neuronal development, in neurite outgrowth and polarity establishment. In contrast to the majority of studies which employed polarity established cells, the experiments described here were conducted at very early stages of development before the axodendritic specification was established (stages 1–3). Also, instead of chronic deprivation of cholesterol from the membrane surface, we adopted a minimally invasive approach where cholesterol was transiently sequestered for a few minutes. The treated cells were then washed and allowed to grow for 2 more days, after which they were fixed and immunolabeled with Tau and Map2 (**Supplementary Figure 2Ai**). This experimental paradigm allowed us to directly address the effects of a transient membrane lipid alteration on neuronal morphology and development.

Neurons at DIV1 were transiently treated with the cholesterol sequestering drug, Methyl β cyclodextrin (MβCD), at various concentrations (2.5 mM, 5 mM, 7.5 mM, and 10 mM) for 10 min and analyzed at DIV3 (**Figure 2**). Control cells were treated similarly with the highest amount of carrier alone (water). A gallery of cells including the control and those treated with varying concentrations of MβCD is presented (**Figure 2A**). We observed that transient cholesterol perturbation exerted effects on both neurite outgrowth and neuronal polarity establishment. This also revealed two distinct populations of neurons with different phenotypes on neuronal morphology.

The length of the longest neurite (referred to as the axon) was significantly attenuated with the increasing concentration of MβCD. The length of the axon decreased from 307.2 ± 13.12 μm in control neurons to 158.7 ± 5.49 μm when MβCD concentration was increased to 10 mM (**Figure 2B**, **Table 2**). Interestingly, cholesterol perturbation by MβCD increased the length of the dendrites (**Figure 2C**, **Table 2**). In contrast to the control neurons where the average length of dendrites was 37.04 ± 1.13 μm, the dendritic length increased to 62.38 ± 4.39 μm upon augmenting the MβCD concentration to 10 mM. A stark effect on neuronal arborization was observed on transient cholesterol sequestration by MβCD. The neurite number per cell reduced from 6 ± 0.3 to 2 ± 0.1 with increasing MβCD concentration (**Figure 2D**, **Table 2**). The strong effect of cholesterol sequestering on neuronal arborization resulted in a second phenotype, i.e., the population of cells with a single neurite (**Figure 3A**). The percentage of cells with a single neurite increased drastically with cholesterol perturbation (**Figure 3B**). In control cultures, the percentage of neurons with a single neurite was negligible (2 ± 2%). In striking contrast, the MβCD treated cultures exhibited a significant increase in neurons with a single neurite from 26 ± 7% in 2.5 mM MβCD to 55 ± 10% in 10 mM MβCD (**Figure 3B**, **Table 2**).

Quantification of all growth parameters was done from the same cultures to minimize variability between cultures. The minimal error in data obtained from these cultures confirmed the robustness of the data. These results showed distinct effects of transient cholesterol perturbation on the growth of axon vs. dendrites, significantly affecting both neurite outgrowth and neuronal arborization.

Cholesterol Sequestering Affects Neuronal Polarity

We next asked whether the membrane cholesterol perturbation affected neurite outgrowth alone or whether neuronal polarity establishment was also affected. The neuronal polarity ratio displayed a significant change from 11.79 ± 0.73 in control down to 5.97 ± 0.68 with cholesterol sequestering by MβCD (**Figure 2E**, **Table 2**), confirming that neuronal polarity was affected as well. As an independent assessment to dissect out the effect of cholesterol sequestration on neuronal polarity, we performed a qualitative comparison of cells immunolabeled for the axonal marker Tau and classified cells based on three criteria:

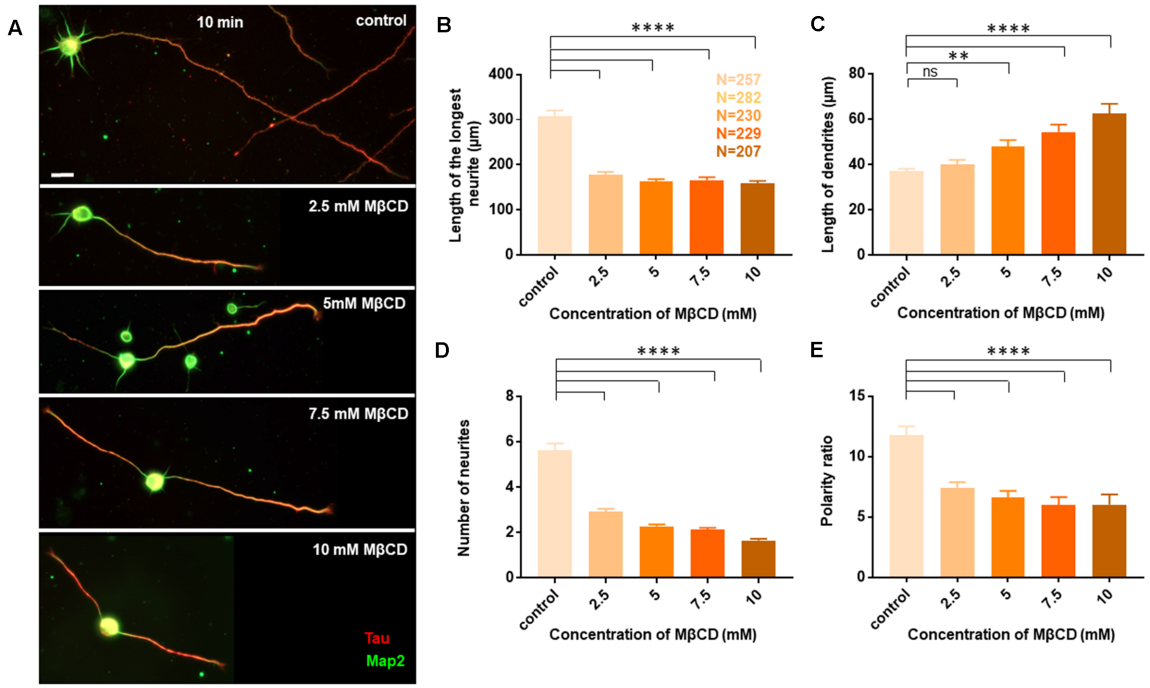

FIGURE 2 | Neurons exhibit opposing effects for axonal and dendritic growth upon transient perturbation of membrane cholesterol. Neurons at DIV1 were transiently treated with varying concentrations of MβCD for 10 min to sequester cholesterol. The cells were labeled with Tau (red) and Map2 (green) and imaged at DIV3. **(A)** A gallery of control and cells treated with varying concentrations of MβCD for 10 min is presented. **(B–E)** Represents the length of the longest neurite **(B)**, length of dendrites **(C)**, number of neurites in each cell **(D)**, and the neuronal polarity ratio **(E)**. Cholesterol sequestered neurons displayed a significant defect in axonal growth but complemented dendritic growth. N denotes the number of cells from five independent cultures. One-way Anova was performed to test the significance of the difference between the means. ****$p < 0.0001$, **$p < 0.01$ and ns denotes non-significant. Scale bar indicates 20 μm.

TABLE 2 | Developmental alterations of rat hippocampal neurons upon transient sequestering of cholesterol for 10 min.

Sample	Control	2.5 mM MβCD	5 mM MβCD	7.5 mM MβCD	10 mM MβCD
Length of the longest neurite (μm)	307.2 ± 13.12	178.0 ± 6.12	162.4 ± 5.66	165.9 ± 6.67	158.7 ± 5.49
Length of dendrites (μm)	37.04 ± 1.13	39.94 ± 2.08	47.82 ± 2.95	54.40 ± 3.26	62.38 ± 4.39
Number of neurites per cell	6 ± 0.3	3 ± 0.1	2 ± 0.1	2 ± 0.1	2 ± 0.1
Polarity ratio	11.79 ± 0.73	7.43 ± 0.46	6.62 ± 0.53	5.97 ± 0.68	6.02 ± 0.85
Percentage of cells with single neurite (%)	2 ± 2	26 ± 7	31 ± 4	43 ± 6	55 ± 10
Percentage of cells with multiple axon (%)	26 ± 5	39 ± 2	46 ± 2	53 ± 3	60 ± 3
Polarity ratio of cells with multiple axon	4.51 ± 0.44	3.45 ± 0.29	2.30 ± 0.29	2.43 ± 0.22	2.24 ± 0.29

*The table shows the neuro-morphological modifications upon transient cholesterol sequestering for 10 min using varying concentrations of MβCD. Mean ± SEM is presented for N number of cells as shown in **Figures 2** and **3** from five and three independent cultures.*

(1) showing no polarity (undifferentiated), (2) polarized (with a single axon), and (3) polarized (with multiple or supernumerary axons).

Using Tau to label axons can be challenging at early developmental stages since Tau labels all neurites initially and then gets restricted to axons in mature neurons (**Supplementary Figure 1**). Since the developmental stage of interest in this study was very early when polarity is just getting established, we assessed the percentage of control neurons displaying multiple neurites with Tau labeling or with supernumerary axons (**Table 2**, **Figures 3C,E**). We observed that the percentage of cells displaying supernumerary axons significantly rose from 26 ± 5% to 60 ± 3% with increasing MβCD concentration (**Table 2**, **Figure 3C**). The multiple axons observed in cholesterol perturbed cells exhibited very strong and comparable levels of Tau labeling among them, whereas the majority of control cells displayed only a single neurite that was strongly labeled for Tau. For a better understanding of the effect of cholesterol sequestering on neuronal polarity, we compared the neuronal polarity ratio of the control cells and the MβCD treated cells displaying supernumerary axons. We observed that the polarity ratio of the MβCD treated cells with multiple axons significantly decreased (2.24 ± 0.29) compared to control cells displaying the same (4.51 ± 0.44, **Table 2**). Low values of the polarity ratio showed that the neurons exhibited a symmetric morphology following cholesterol sequestration compared to an asymmetric growth in control cells, which had a much longer axon compared to the dendrites. Therefore, in addition

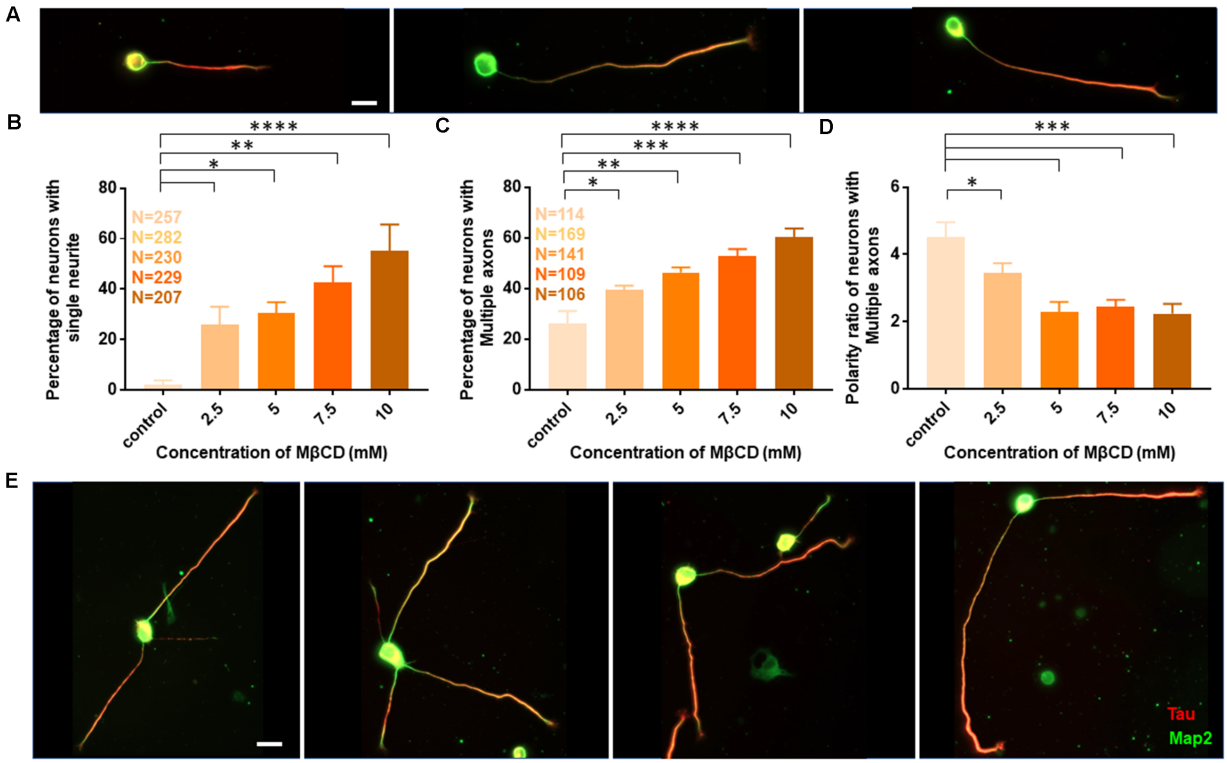

FIGURE 3 | Transient cholesterol sequestering affects neuronal arborization and polarity. **(A)** A gallery of neurons treated with MβCD for 10 min, exhibiting single neurites, is presented. **(B)** Percentage of cells with single neurites upon application of varying concentrations of MβCD. **(C)** Percentage of cells with supernumerary axons upon application of varying concentrations of MβCD for 10 min. **(D)** Polarity ratio of neurons exhibiting supernumerary axons as calculated from **(C)**. **(E)** A gallery of treated neurons displaying supernumerary axons is presented. Cholesterol sequestered neurons treated with MβCD displayed single neurites and multiple axons, exhibiting a severe shift in neuronal polarity. The polarity ratio was significantly reduced in neurons exhibiting multiple axons, showing symmetric growth for the affected cells. N denotes the number of cells from five independent cultures for **(B)** and from three independent cultures for **(C,D)**. One-way Anova was performed to test the significance of the difference between the means. ****$p < 0.0001$, ***$p < 0.001$, **$p < 0.01$, *$p < 0.05$. Scale bar indicates 20 μm.

to a reduction in the length of the axon with increasing membrane cholesterol perturbation, there was also an increase in the percentage of neurons reversing to symmetric growth and displaying supernumerary axons. This unique population of cells with multiple axons would also explain the distinct effects observed previously, where there was an increase in the length of all the neurites except the axon upon cholesterol sequestration (**Figure 2C**). Therefore, the shift in polarity and an elevated population of neurons displaying supernumerary axons would largely account for the increase in length of dendrites observed with higher cholesterol sequestering.

Neuronal Developmental Defects and Opposing Effects on Axon and Dendrites Is Independent of Duration of Cholesterol Perturbation

Since distinct effects of cholesterol perturbation were observed on neuronal growth and polarity, we next addressed whether these effects were dependent on the duration of perturbation. For this, rat hippocampal neurons at DIV1 were treated with varying concentrations of MβCD, but the duration of cholesterol sequestering was doubled to 20 min (**Figure 4**). The cells were washed and allowed to grow to DIV3 when they were immunolabeled with Tau and Map2. All quantifications were done as described previously for the 10 min perturbation. A gallery of cells treated with differing concentrations of MβCD from 2.5 mM, 5 mM, 7.5 mM to 10 mM for 20 min is presented along with control neurons treated with the carrier alone (**Figure 4A**). Similar to that reported for the 10 min treatment, the growth of the axon was strongly attenuated for the 20 min treatment as well, with increasing MβCD concentrations (**Figure 4B**). The length of the axon significantly reduced in MβCD treated neurons (193.7 ± 8.63 μm) when compared to the control cells (344 ± 17.74 μm; **Figure 4B**, **Table 3**). Membrane cholesterol perturbation for 20 min caused an increase in the dendritic length, as observed in 10 mM MβCD treated cells (75.18 ± 8.36 μm), compared to that in the control condition (32.08 ± 1.21 μm; **Figure 4C**, **Table 3**). Neuronal arborization was also severely affected with a longer duration of cholesterol perturbation, wherein the number of neurites per cell reduced from 7 ± 0.4 to 2 ± 0.1 at higher MβCD concentrations (**Figure 4D**, **Table 3**). Similar to that observed with 10 min treatment, cholesterol perturbation for 20 min also resulted in an increase in the population of neurons

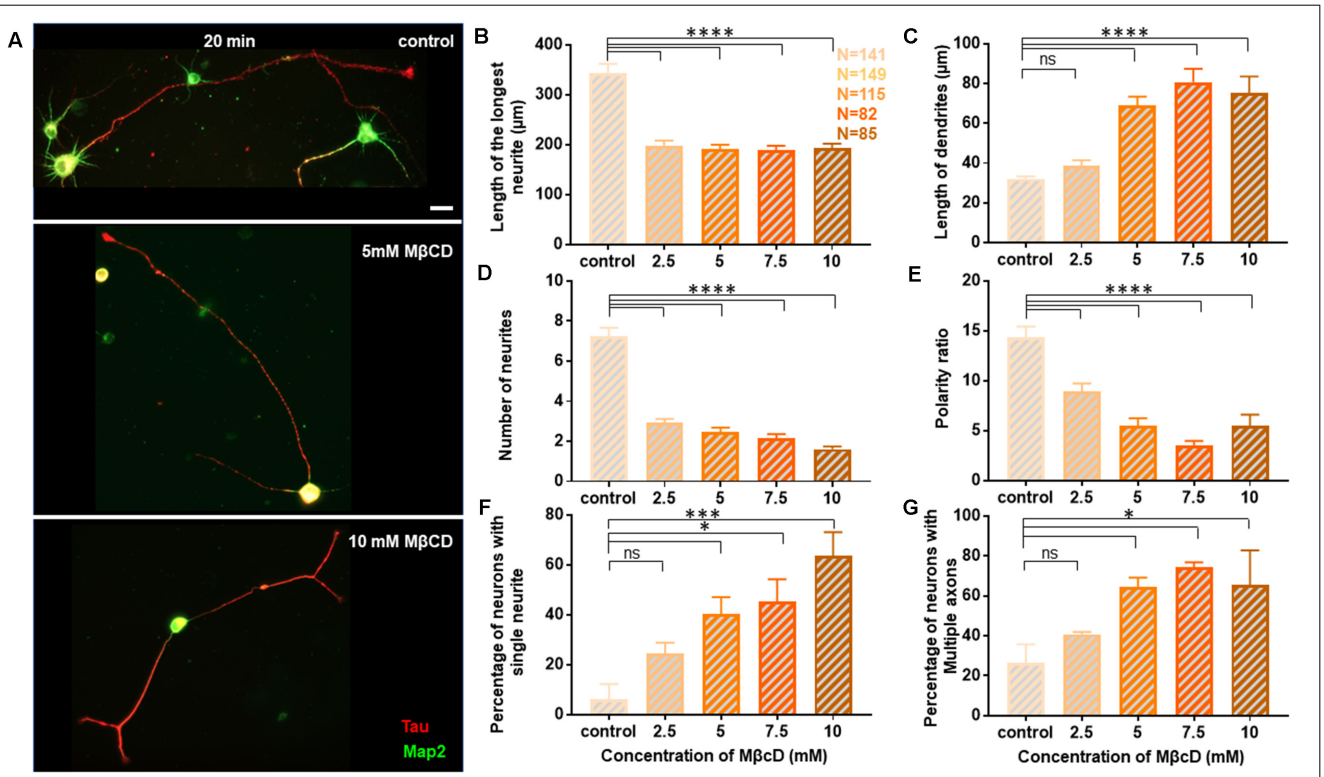

FIGURE 4 | Neuronal developmental defects in growth and polarity are retained independent of the duration of transient cholesterol perturbation. Neurons at DIV1 were transiently treated with varying concentrations of MβCD for 20 min to sequester cholesterol. The cells were labeled with Tau (red) and Map2 (green) and imaged at DIV3. **(A)** A gallery of control and cells treated with varying concentrations of MβCD for 20 min is presented. **(B–E)** Represents the length of the longest neurite **(B)**, length of dendrites **(C)**, number of neurites in each cell **(D)**, and the polarity ratio **(E)** at varying concentrations of MβCD. **(F,G)** Represents the percentage of treated neurons displaying single neurites **(F)** and supernumerary axons **(G)**, respectively. Cholesterol sequestration for a longer duration resulted in neurons displaying significant defects in axonal growth but complementing dendritic growth, similar to shorter perturbation. Consistent with acute transient perturbation, longer cholesterol sequestration also resulted in neurons displaying single neurites and multiple axons, exhibiting a severe shift in neuronal polarity. N denotes the number of cells from three independent cultures. One-way Anova was performed to test the significance of the difference between the means. $^{****}p < 0.0001$, $^{***}p < 0.001$, $^{*}p < 0.05$ and ns non-significant. Scale bar indicates 20 μm.

with a single neurite (6 ± 6% in control to 64 ± 9% in treated cells; **Figure 4F**, **Table 3**). Neurons also displayed a significant decrease in their polarity ratio on longer cholesterol sequestering (14.32 ± 1.13 in control cells; 5.49 ± 1.12 in treated cells; **Figure 4E**, **Table 3**). Cholesterol sequestering for 20 min also resulted in an increase in the number of cells displaying supernumerary axons (26 ± 9% in control; 66 ± 17% in treated cells; **Figure 4G**, **Table 3**). Together these observations suggest that the neuronal developmental defects observed upon cholesterol perturbation were not affected by the duration of perturbation. The effects observed after 10 min and 20 min treatment were similar and followed the same pattern. However, in contrast to membrane cholesterol perturbation for 10 min duration, which resulted in a gradual transition of morphological changes between the different concentrations, the effects observed with 20 min perturbation were abrupt and stronger.

Since we observed acute neuro-morphological and polarity defects in response to varying levels of cholesterol sequestering, we quantified membrane cholesterol in parallel by an unesterified cholesterol assay by labeling with Filipin III after treatment with different MβCD concentrations (**Figure 5**). Filipin III is known to be highly photo-unstable; therefore, a lipid raft membrane marker which labels overlapping regions was used as a reference for focusing the cells. We observed that Filipin fluorescence decreased 2.5 to 3 times from the control condition in response to increased sequestering of membrane cholesterol (**Figures 5A,B**, **Table 4**). The results were consistent with the dose response curve of **Figure 2**. We also extended the study to Filipin labeling of cells which had undergone a longer duration of cholesterol sequestering such as 20 min. We observed a similar pattern for alteration in Filipin fluorescence, but a stronger response with a longer duration of perturbation, consistent with the dose response curve of **Figure 3** (**Figure 5C**, **Table 4**). We also observed a higher membrane damage for the cells undergoing longer cholesterol perturbation (20 min) compared to the short duration (10 min), accounting for the higher variability in Filipin fluorescence in these cells (**Table 4**).

Therefore, we assessed whether the viability was compromised for cells undergoing cholesterol sequestering for longer durations. Cholesterol perturbation was performed at a high concentration (10 mM MβCD) for varying durations

TABLE 3 | Developmental alterations of rat hippocampal neurons upon transient sequestering of cholesterol for 20 min.

Sample	Control	2.5 mM MβCD	5 mM MβCD	7.5 mM MβCD	10 mM MβCD
Length of the longest neurite (μm)	344 ± 17.74	198.1 ± 10.26	190.7 ± 9.08	189.1 ± 8.53	193.7 ± 8.63
Length of dendrites (μm)	32.08 ± 1.21	38.52 ± 2.92	68.98 ± 4.51	80.74 ± 6.61	75.18 ± 8.36
Number of neurites per cell	7 ± 0.4	3 ± 0.2	2 ± 0.2	2 ± 0.2	2 ± 0.1
Polarity ratio	14.32 ± 1.13	8.94 ± 0.81	5.48 ± 0.77	3.52 ± 0.45	5.49 ± 1.12
Percentage of cells with single neurite (%)	6 ± 6	24 ± 4	40 ± 6	45 ± 8	64 ± 9
Percentage of cells with multiple axon (%)	26 ± 9	41 ± 1	64 ± 5	74 ± 2	66 ± 17

The table illustrates the alterations in morphological properties of rat hippocampal neurons upon transient cholesterol sequestering for 20 min using varying concentrations of the cholesterol sequestering drug MβCD. Mean ± SEM is presented for N number of cells as shown in ***Figure 4*** *from three independent cultures.*

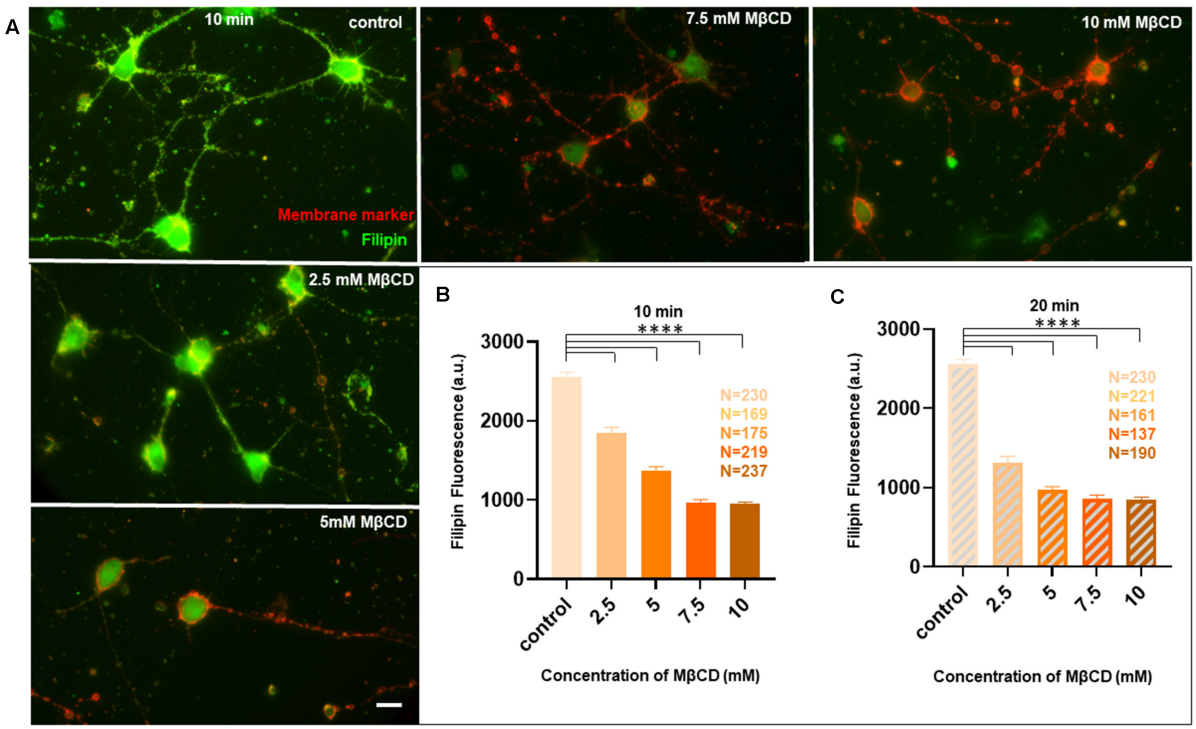

FIGURE 5 | Membrane cholesterol labeling by Filipin III shows altered fluorescence, dependent upon dosage and duration of cholesterol sequestering, consistent with neuro-morphological defects. Neurons at DIV1 were transiently treated with varying concentrations of MβCD for 10 min and 20 min to sequester cholesterol. The cells were labeled with a lipid raft membrane marker (red) and Filipin III (green) and imaged at DIV3. **(A)** A gallery of control and cells treated with varying concentrations of MβCD for 10 min is presented. Both channels in all panels are thresholded with the same values for comparison. **(B)** Represents the absolute fluorescence of Filipin III for cells treated with varying concentrations of MβCD for 10 min. **(C)** Represents the absolute fluorescence of Filipin III for cells treated with varying concentrations of MβCD for 20 min. Fluorescence of Filipin III marks unesterified cholesterol on the membrane. Cholesterol sequestering decreased Filipin III fluorescence, but the effect was severe for 20 min compared to 10 min of cholesterol perturbation, consistent with the corresponding neuro-morphological defects observed. N denotes the number of cells from three independent cultures. One-way Anova was performed to test the significance of the difference between the means. $^{****}p < 0.0001$. Scale bar indicates 20 μm.

TABLE 4 | Alteration in fluorescence of Filipin III, labeling unesterified membrane cholesterol, upon transient sequestering of cholesterol for varying durations.

Sample	Control	2.5 mM MβCD	5 mM MβCD	7.5 mM MβCD	10 mM MβCD
Filipin fluorescence (10 min)	2556 ± 60.27	1855 ± 65.48	1371 ± 52.07	972 ± 33.04	953.8 ± 19.2
Filipin fluorescence (20 min)	2556 ± 60.27	1311 ± 82.02	969.9 ± 44.85	855.6 ± 51.22	842.7 ± 39.26

The table illustrates absolute levels of Filipin III fluorescence in rat hippocampal neurons upon transient cholesterol sequestering for 10 min and 20 min using varying concentrations of the cholesterol sequestering drug MβCD. Since all experiments were performed on the same cultures, a single control is used for both durations of perturbation. Mean ± SEM is presented for N number of cells as shown in ***Figure 5*** *from three independent cultures.*

namely, 10 min, 20 min, and 30 min (**Supplementary Figure 3**). The viability assay was performed by two methods. In the first, the membrane damage to the cells induced upon transient cholesterol sequestering at DIV1 for varying durations was assessed at DIV3 in live cells. The control and cholesterol sequestered cells were labeled using a Live/Dead cell imaging kit

which marked Calcein AM (green) and Bobo-3 Iodide (orange) as live and dead cell indicators, respectively (**Supplementary Figure 3A**). The normalized ratio of dead to live cells showed significantly higher levels for 20 min and 30 min compared to 10 min, whose levels were similar to control values (**Supplementary Figure 3B**, **Supplementary Table 1**). The assay verified a higher population of cells with membrane integrity compromised with a longer duration of cholesterol perturbation. In the second method, the control and treated cells at DIV3 were fixed and labeled with an antibody recognizing endogenous levels of activated Caspase 3 (orange), and counter labeled with DAPI (Blue, **Supplementary Figure 3C**). Similar to the live cell assay, the normalized ratio of the percentage of dead vs. live cells showed similar levels between control and 10 min perturbation, in contrast to a significantly higher population of cells entering apoptosis after 20 min and 30 min cholesterol sequestering (**Supplementary Figure 3D**, **Supplementary Table 1**). Since our results showed minimal membrane damage and viability issues with short cholesterol sequestering similar to control values, subsequent rescue experiments were performed with the short cholesterol perturbation of 10 min.

Transient Application of Exogenous Cholesterol Rescues Neurite Outgrowth and Polarity Defects After Cholesterol Perturbation

Cholesterol sequestering affected axonal and dendritic neurite outgrowth as well as neuronal polarity in a distinct manner. Therefore, we asked whether these developmental defects can be reversed by transient supplementation of membrane cholesterol. This would also address whether the effects we observed upon cholesterol sequestering were specific and direct rather than secondary, since MβCD is also known to affect the cytoskeleton. For this purpose, we treated the hippocampal neuronal cultures at DIV1 with 5 mM MβCD for 10 min, which showed a significant yet moderate effect on neuronal development (**Figure 2**). The treated cells were washed and immediately supplemented with exogenous cholesterol (Cl) at varying concentrations (0.5 mM, 1.0 mM, 1.5 mM, and 2.0 mM) for 10 min. The cells were washed and grown till DIV3, when they were fixed, immunolabeled with Tau and Map2 and imaged (**Supplementary Figure 2Aii**). We found that brief cholesterol supplementation of the MβCD treated cells significantly rescued many of the severe developmental defects generated by cholesterol sequestering (**Figures 6** and **7**).

A gallery of cells including control, MβCD treated (5 mM), and cholesterol supplemented cells is presented (**Figures 6A** and **7A**). On transient cholesterol application, the length of the longest neurite increased from 149.9 ± 7.74 μm to 275.2 ± 14.78 μm, depending on the concentration of the exogenous cholesterol supplemented (**Figure 6B**, **Table 5**). Higher cholesterol concentration resulted in retarded axonal length, emphasizing the critical window of the membrane cholesterol content in supporting growth. Cholesterol replenishment, in general, reduced the average length of dendrites of cholesterol sequestered cells to control values (**Figure 6C**, **Table 5**). The number of neurites per cell also significantly increased from 2 ± 0.1 in MβCD treated cells to 7 ± 0.2 in cholesterol supplemented cells (**Figure 6D**, **Table 5**). The extent of rescue was critically dependent on the amount of replenished cholesterol. Consistently, we observed that the percentage of cells with a single neurite disappeared completely (0 ± 0) or to negligible values from a significant population of 27 ± 4% in MβCD treated cells upon brief cholesterol replenishment (**Figure 7B**, **Table 5**). On the contrary, the neuronal polarity ratio displayed a partial rescue upon replenishment (8.25 ± 0.61) when compared to cholesterol sequestered cells (6.22 ± 0.65; **Figure 6E**, **Table 5**). Similar to neurite outgrowth, the rescue of polarity was also critically dependent on the replenished cholesterol and behaved similar to cholesterol sequestered cells at high cholesterol concentrations (**Figure 6E**, **Table 5**). This strongly supports the critical nature of membrane cholesterol concentration on neuronal polarity. Consistently, we observed that the percentage of cells with supernumerary axons reduced drastically for a small window of replenished cholesterol concentration, emphasizing the critical role of fine membrane cholesterol balance in axo-dendritic specification and neuronal polarity establishment (**Figure 7C**, **Table 5**). The neuronal polarity ratio of the cholesterol replenished cells with multiple axons (4.51 ± 1.27) was higher than that of cholesterol sequestered cells (2.29 ± 0.29) and similar to that of control cells (4.52 ± 0.44), thereby verifying that the asymmetric nature of neurite growth had returned on retaining the membrane cholesterol balance (**Figure 7D**, **Table 5**). The results confirmed the critical nature of membrane cholesterol content in neurite outgrowth and neuronal polarity establishment.

Increasing Cholesterol Content on the Cell Membrane Alters Growth but Not Polarity

Neuronal developmental defects induced by cholesterol sequestering were rescued by the transient application of exogenous cholesterol. Therefore, we wanted to address the effect of increasing the membrane cholesterol concentration on neuronal development. The rat hippocampal neurons at DIV1 were transiently treated with varying concentrations of exogenous cholesterol (0.5 mM, 1.0 mM, 1.5 mM, and 2.0 mM) for 10 min (**Supplementary Figure 2Aiii**). The cells were washed and grown till DIV3, when they were fixed, immunolabeled with axonal and dendritic markers, and imaged. A gallery of cells treated transiently with varying concentrations of cholesterol is presented in **Figure 8A**. We observed that the normal neuronal morphology was retained for a short concentration window of supplemented cholesterol and was lost at high cholesterol concentrations, emphasizing the relevance of the correct membrane lipid balance for the normal neuronal architecture. Cholesterol imbalance altered the shape of the soma and resulted in axons growing and curling back towards the soma instead of leading away from it, increasing the probability of generating ectopic synapses (**Figure 8A**). While supplementing extrinsic cholesterol rescued neurite outgrowth of cholesterol perturbed cells, cholesterol addition to the normal neurons resulted in attenuated growth. This attenuation

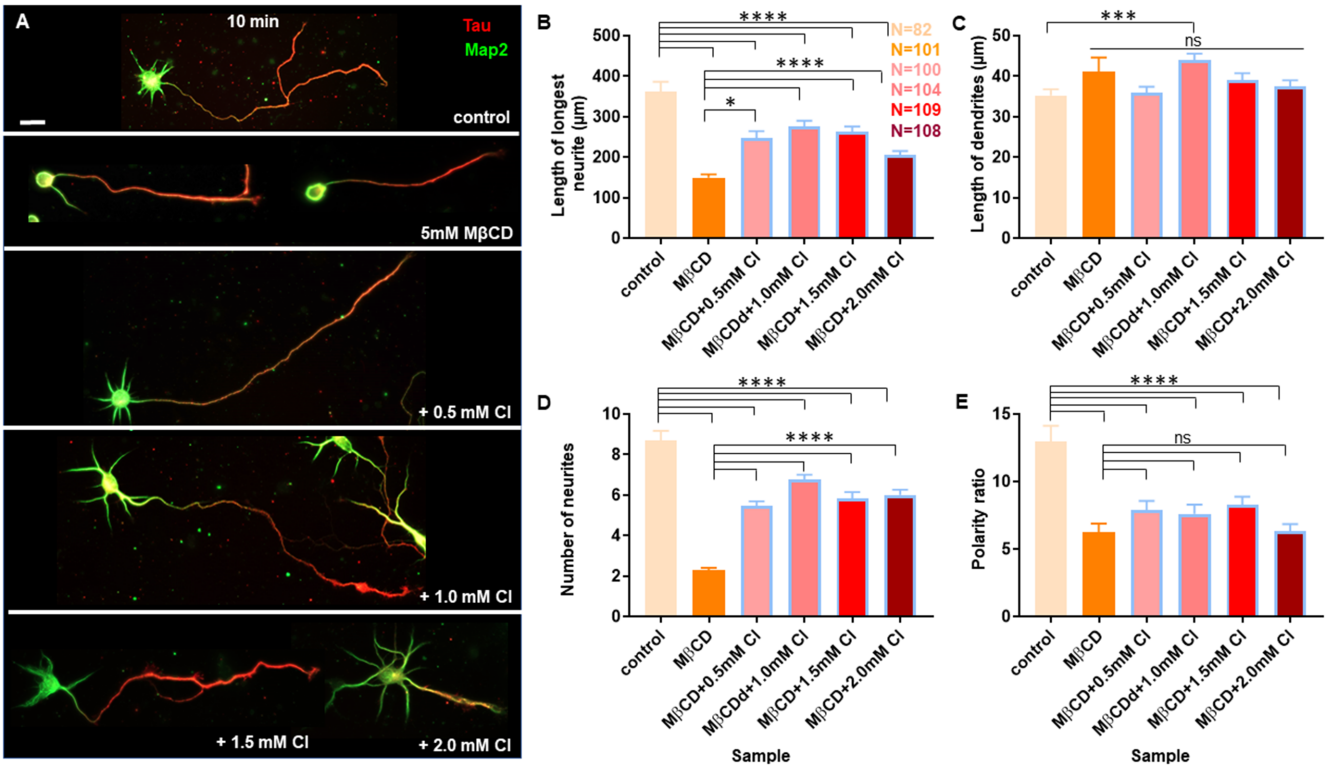

FIGURE 6 | Transient cholesterol replenishment rescues neuronal developmental defects from cholesterol sequestering. Neurons at DIV1 were transiently treated with 5 mM MβCD (referred to as MβCD in the figure) for 10 min to sequester cholesterol. The treated neurons were immediately supplemented with varying concentrations of exogenous cholesterol (Cl) for 10 min. The cells were grown to DIV3 and labeled with Tau (red) and Map2 (green). **(A)** A gallery of control and cells treated with 5 mM MβCD followed by varying concentrations of cholesterol is presented. **(B–E)** Represents the length of the longest neurite **(B)**, length of dendrites **(C)**, number of neurites in each cell **(D)**, and the neuronal polarity ratio **(E)** of the treated cells. The developmental defects observed for cholesterol sequestered neurons were significantly rescued upon supplementing exogenous cholesterol. N denotes the number of cells from three independent cultures. One-way Anova was performed to test the significance of the difference between the means. Significance was tested for each sample against the control as well as against MβCD alone. $^{****}p < 0.0001$, $^{***}p < 0.001$, $^{*}p < 0.05$, and ns non-significant. Scale bar indicates 20 μm.

was significant and augmented with increasing cholesterol concentration. The length of the longest neurite reduced from 361.9 ± 24.58 μm in control cells to 177.1 ± 9.06 μm in cells treated with higher amounts of cholesterol (**Figure 8B**, **Table 6**). In contrast to cholesterol sequestering which affected axon and dendrites in an opposing manner, cholesterol enhancement did not significantly alter the growth of dendrites (**Figure 8C**, **Table 6**). However, cholesterol enhancement negatively affected neurite outgrowth and neuronal arborization and reduced the average number of neurites per cell from 9 ± 0.5 in control cells to 6 ± 0.3 in treated cells (**Figure 8D**, **Table 6**). Contrary to cholesterol sequestering, cholesterol enhancement did not generate a significant population of neurons with a single neurite (**Figure 8F**, **Table 6**). The most significant effect of cholesterol enhancement was observed for the neuronal polarity ratio which sharply decreased from 12.94 ± 1.18 to 6.18 ± 0.5 upon increasing the membrane cholesterol concentration (**Figure 8E**, **Table 6**). The decrease in polarity ratio indicated the reversal of neurons to symmetric growth following cholesterol enhancement. Interestingly, contrary to cholesterol sequestering, cholesterol enhancement did not significantly shift polarity, though it altered neurite outgrowth and extension. Consistently, the percentage of cells displaying supernumerary axons was not significantly altered upon cholesterol enhancement, when compared to control neurons (**Figure 8G**, **Table 6**). These results showed that membrane cholesterol enhancement altered neurite outgrowth but not polarity. Together these observations support the critical nature of membrane cholesterol balance in regulating neurite outgrowth and polarity, and in maintaining the normal neuronal morphology and architecture.

DISCUSSION

Molecular mechanisms underlying neuronal polarity have been investigated for decades. However, our understanding of the complex interplay among various signaling pathways in regulating neurite outgrowth and polarity establishment remains poorly understood. The complexity of the fundamental mechanisms that regulate axonal and dendritic specification makes it challenging, yet interesting. This study addresses the role of one of the key players of this network, namely

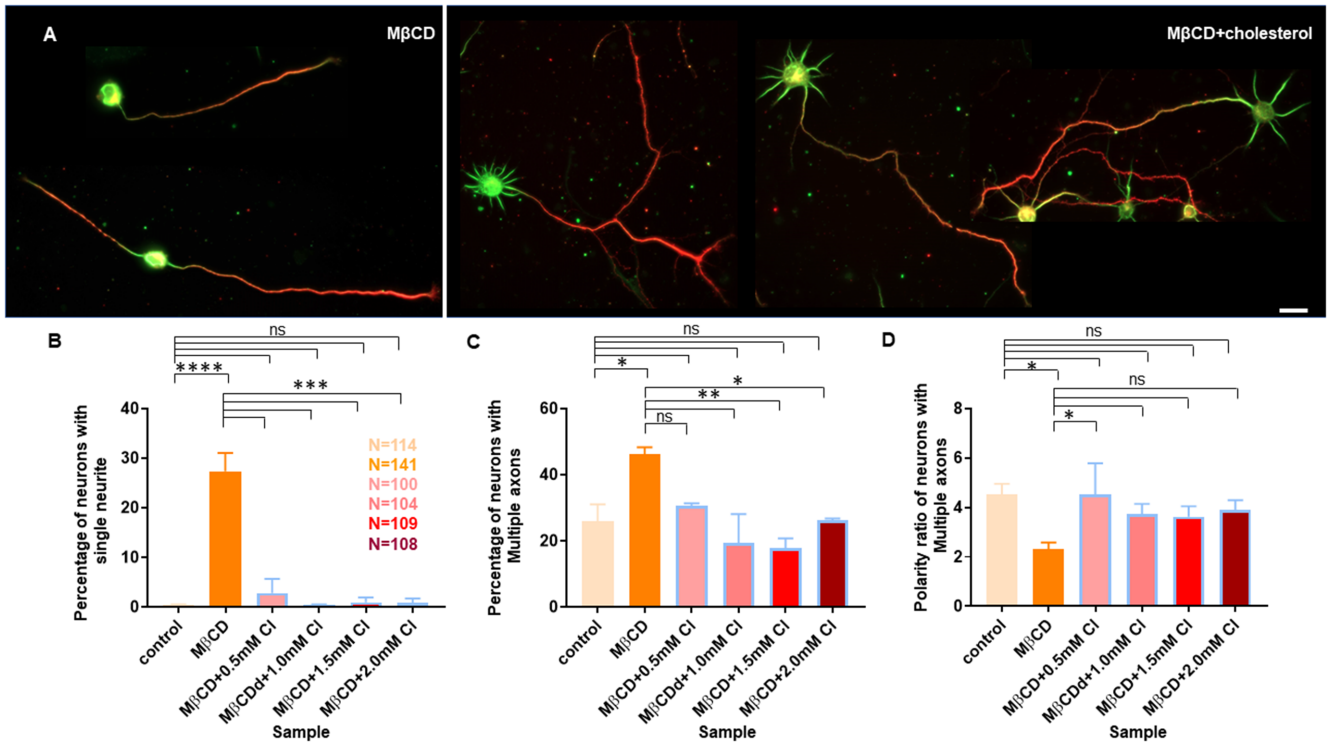

FIGURE 7 | Transient cholesterol replenishment rescues neurite arborization and polarity defects caused by cholesterol sequestering. **(A)** Depicts the morphological transition of neurons upon cholesterol sequestering and transient replenishment with exogenous cholesterol. **(B)** Percentage of cells with single neurites upon transient application of 5 mM MβCD followed by varying amounts of exogenous cholesterol for 10 min. **(C)** Percentage of cells displaying supernumerary axons upon transient application of 5 mM MβCD followed by varying amounts of exogenous cholesterol for 10 min. **(D)** Polarity ratio of neurons exhibiting supernumerary axons as calculated from **(C)**. Neuronal arborization and polarity defects in cholesterol sequestered neurons were significantly rescued upon transient cholesterol replenishment. In the population of neurons displaying supernumerary axons, the polarity ratio was increased to control values in cholesterol supplemented cells, showing their reversal to an asymmetric growth pattern. N denotes the number of cells from three independent cultures. One-way Anova was performed to test the significance of the difference between the means. $^{****}p < 0.0001$, $^{***}p < 0.001$, $^{**}p < 0.01$, $^{*}p < 0.05$. Scale bar indicates 20 μm. ns, non-significant.

membrane cholesterol which has been shown to be a crucial player in orchestrating multiple processes and pathways. Alterations in membrane cholesterol homeostasis have been correlated with different pathophysiological conditions including Alzheimer's disease, Parkinson's disease, Huntington's disease, and Niemann Pick type C disease (Vance, 2012; Wang and Song, 2012; Leoni and Caccia, 2015; Hussain et al., 2019). Recent evidence has linked key proteins involved in these disease conditions to the regulation of lipid and cholesterol homeostasis, further underscoring the consequences of mis-regulation of these pathways and disease pathology (Pierrot et al., 2013; Grimm et al., 2017; Cho et al., 2020). Cholesterol has also been linked to modification and maturation of signaling molecules such as hedgehog proteins, critically involved in embryogenesis (Porter et al., 1996; Blassberg and Jacob, 2017). In addition to neurodegenerative conditions, disorder in cholesterol synthesis has been reported to cause multiple human malformation syndromes including Smith-Lemli-Opitz syndrome (SLOS; Porter and Herman, 2011). Reports show altered signaling of multiple GTPases impairing normal axonal and dendritic growth, potentially in a cholesterol dependent manner, contributing to the neurocognitive deficits found in SLOS (Jiang et al., 2010). All this evidence emphasizes the requisite for a better understanding of the critical regulation of membrane cholesterol during different phases of development, particularly during neurite outgrowth and polarity establishment, the mis-regulation of which can lead to multiple pathophysiological conditions.

Primary cultures of rodent hippocampal neurons are a widely used and amenable system to address molecular mechanisms underlying neuronal growth and polarity. The development of hippocampal neurons in culture has been classified into different stages (Stage 1–5): development of protrusions or lamellipodia (stage 1), neurite outgrowth (stage 2), symmetry breaking and axonal extension (stage 3), dendritic growth (stage 4), and formation and maturation of synapses (stage 5; Dotti et al., 1988). Most of the studies on the effects of cholesterol alterations on neurite outgrowth have been primarily addressed in stages 3–5, when neuronal polarity has already been established (Fan et al., 2002; Ko et al., 2005). In this study, we undertook a detailed biophysical characterization of the neuro-morphological effects after altering the membrane cholesterol in a controlled and minimally invasive manner transiently, so as not to disturb its natural growing environment.

TABLE 5 | Rescue of developmental defects of cholesterol sequestered neurons by transient application of exogenous cholesterol.

Sample	Control	MβCD	MβCD + 0.5 mM Cl	MβCD + 1.0 mM Cl	MβCD + 1.5 mM Cl	MβCD + 2.0 mM Cl
Length of the longest neurite (μm)	361.9 ± 24.58	149.9 ± 7.74	246.5 ± 17.83	275.2 ± 14.78	262.9 ± 12.59	205.1 ± 10.29
Length of dendrites (μm)	35.23 ± 1.54	41.07 ± 3.53	35.93 ± 1.46	44.03 ± 1.55	38.98 ± 1.76	37.54 ± 1.46
Number of neurites per cell	9 ± 0.5	2 ± 0.1	6 ± 0.2	7 ± 0.2	6 ± 0.3	6 ± 0.3
Polarity ratio	12.94 ± 1.18	6.22 ± 0.65	7.87 ± 0.69	7.60 ± 0.69	8.25 ± 0.61	6.33 ± 0.51
Percentage of cells with single neurite (%)	0 ± 0*	27 ± 4	3 ± 2	0 ± 0*	1 ± 1	1 ± 1
Percentage of cells with multiple axon (%)	26 ± 5	46 ± 2	31 ± 0.8	19 ± 9	18 ± 3	26 ± 0.6
Polarity ratio of cells with multiple axon	4.52 ± 0.44	2.29 ± 0.29	4.51 ± 1.27	3.73 ± 0.41	3.63 ± 0.42	3.89 ± 0.41

*The neuro-morphological perturbations induced by transient cholesterol sequestering were rescued upon transient application of exogenous cholesterol. The table compares the alterations in the morphological properties of control, cholesterol sequestered, and cholesterol supplemented neurons. MβCD refers to 5 mM MβCD. *0 values have been replaced with negligible values in* ***Figure 7B*** *for the sake of display. Mean ± SEM is presented for N number of cells as shown in* ***Figures 6*** *and* ***7*** *from three independent cultures.*

Due to the challenging nature of this early developmental stage to determine polarity establishment, in addition to qualitative polarity analysis using conventional axo-dendritic markers, different quantitative parameters were also considered including the neuronal polarity ratio, which is the ratio of the longest neurite to the average length of the dendrites. This gives a reliable readout of the polarity status of a neuron, consistent with the morphological and molecular signatures during neuronal development. The protocols were optimized to generate a homogenous neuronal population, and the different quantitative parameters for assessing neuronal development and polarity were thoroughly assessed for their variability between culturing conditions. Experiments were performed in the same sets of neuronal cultures to minimize the variability between cultures. The robust approach of this study allowed us to decipher multiple components of neuronal development including neurite outgrowth and polarity establishment in a reliable manner.

We observed that transient cholesterol sequestering, irrespective of the duration of perturbation, affected axons and dendrites in a distinct manner, attenuating axonal growth and promoting dendritic growth. This manipulation generated two subsets of neuronal populations, those with a single neurite or with multiple axons. Though both cholesterol sequestering as well as cholesterol enhancement affected neurite outgrowth, only the former shifted neuronal polarity. Transient cholesterol replenishment of sequestered neurons rescued developmental and polarity defects to a significant extent. However, the rescue was critically dependent on the amount of replenished cholesterol, emphasizing the importance of precise membrane lipid balance for optimal neurite outgrowth and neuronal architecture.

Previous studies have reported that cholesterol modulation alters neurite outgrowth in a region-dependent manner in the brain. In one study, cholesterol perturbation promoted neurite outgrowth in the hippocampus, but retarded growth in the neocortex (Ko et al., 2005). Since these reported experiments were performed at later stages (3–5), the effects of the perturbations might be dependent on the developmental stage. On the contrary, the increase in the population of neurons displaying multiple axons following cholesterol sequestering, as we have observed, might also explain the differences in the observations. Membrane cholesterol deficiency has been reported to affect Tau phosphorylation and microtubule depolymerization in axons. It also causes selective inhibition of dendritic outgrowth by affecting MAP2 phosphorylation and microtubule destabilization, consistent with our observation of an increase in the population of neurons with a single neurite on cholesterol sequestering (Fan et al., 2001, 2002). Neuronal cholesterol metabolism has been shown to modulate dendritic arborization and synaptic content, emphasizing its importance in mature neurons as well (Moutinho et al., 2016). Cholesterol is a critical player in defining membrane fluidity, underscoring its key role in regulating the lateral diffusion of molecules involved in different signaling pathways, including polarity establishment, synaptic transmission, and pathophysiological

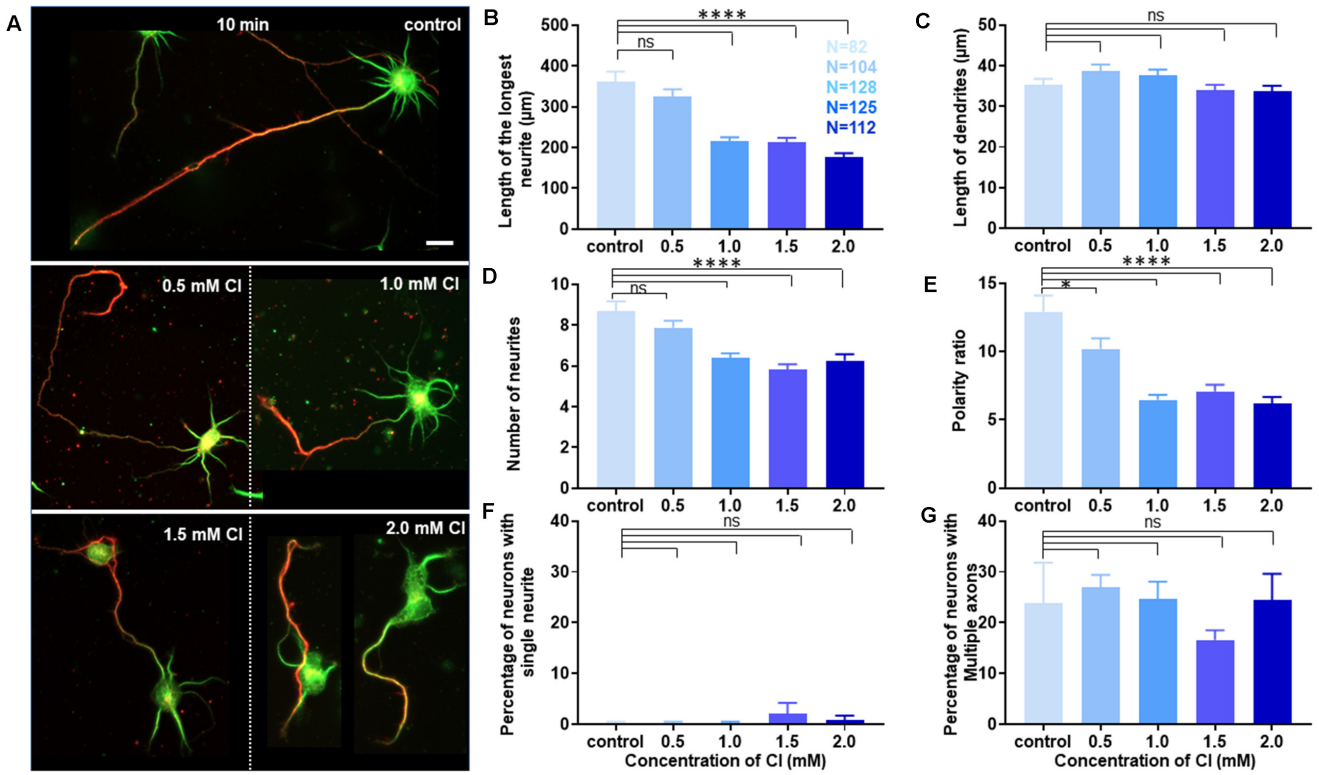

FIGURE 8 | Membrane cholesterol enhancement alters growth but does not shift polarity. **(A)** A gallery of control and cells transiently treated with varying concentrations of cholesterol (Cl) is presented. Higher cholesterol concentrations altered neuronal architecture and morphology, but also generated cells with axons growing and curling back over the soma. **(B–E)** Represents the length of the longest neurite **(B)**, length of dendrites **(C)**, number of neurites in each cell **(D)**, and the neuronal polarity ratio **(E)** of the treated cells. **(F,G)** Represents the percentage of treated neurons displaying single neurites **(F)** and supernumerary axons **(G)**, respectively. Transient membrane cholesterol enhancement significantly perturbed axonal growth and neurite arborization but did not hamper dendritic growth. The neuronal polarity ratio shifted to lower values upon cholesterol enhancement, denoting symmetric growth. Interestingly, there was no significant population of treated neurons with single neurites or displaying multiple axons, confirming that cholesterol enhancement complemented dendritic extension, but not polarity shift to develop supernumerary axons. N denotes the number of cells from three independent cultures. One-way Anova was performed to test the significance of the difference between the means. ****$p < 0.0001$, *$p < 0.05$, and ns non-significant. Scale bar indicates 20 µm.

TABLE 6 | Developmental alterations of rat hippocampal neurons upon transient application of exogenous cholesterol for 10 min.

Sample	Control	0.5 mM Cl	1.0 mM Cl	1.5 mM Cl	2.0 mM Cl
Length of the longest neurite (µm)	361.9 ± 24.58	324.3 ± 18.19	215.4 ± 9.63	212.3 ± 11.57	177.1 ± 9.06
Length of dendrites (µm)	35.23 ± 1.5	38.72 ± 1.6	37.66 ± 1.41	33.99 ± 1.34	33.63 ± 1.44
Number of neurites per cell	9 ± 0.5	8 ± 0.3	6 ± 0.2	6 ± 0.3	6 ± 0.3
Polarity ratio	12.94 ± 1.18	10.19 ± 0.79	6.46 ± 0.37	7.08 ± 0.49	6.18 ± 0.5
Percentage of cells with single neurite (%)	0 ± 0*	0 ± 0*	0 ± 0*	2 ± 2	1 ± 1
Percentage of cells with multiple axon (%)	24 ± 8	27 ± 2	25 ± 3	17 ± 2	25 ± 5

*The table illustrates morphological alterations of neurons transiently treated with varying concentrations of exogenous cholesterol. *0 values have been replaced with negligible values in **Figure 8F** for the sake of display. Mean ± SEM is presented for N number of cells as shown in **Figure 8** from three independent cultures.*

conditions. Previous studies have shown that the lateral diffusion and membrane nano-organization of many of these key molecules is defined by several factors including intracellular ionic levels, genetic alterations or the membrane potential of the cell (Nair et al., 2013, 2020; Kedia et al., 2020a,b; Tanwar et al., 2021). These factors could provide potential feedback to the membrane lipid compartments for defining the protein-lipid compartmentalization to regulate these pathways.

The cholesterol sequestering drug, Methyl β cyclodextrin, has been shown to act as an actin depolymerizing agent as well (Mundhara et al., 2019). The cytoskeletal modifications on cholesterol perturbation by MβCD were similar to that of Latrunculin B, another actin depolymerizing drug (Mundhara et al., 2019). Actin depolymerization at low concentrations has been shown to promote neurite outgrowth and extension in hippocampal neurons, whereas it was inhibited at high concentrations (Chia et al., 2016). Since developmental

defects observed by cholesterol sequestration by MβCD might involve effects from both lipid and cytoskeletal modifications, it was important to dissect out the influence of cholesterol alteration vs. cytoskeletal rearrangement on the developmental outcome. Using an unesterified cholesterol assay, we confirmed that the membrane cholesterol content was effectively reduced by transient cholesterol sequestering, and that the reduction was dependent upon the dosage of MβCD. Also, we observed a stronger reduction in membrane cholesterol levels on increasing the duration of perturbation, consistent with our observations of severe neuro-morphological defects associated with longer cholesterol sequestering. Our transient cholesterol replenishment studies significantly rescued the neuronal developmental defects observed on sequestering, clearly emphasizing a critical role for membrane cholesterol in determining the normal neuronal architecture and polarity.

Interestingly, a significant population of supernumerary axons was observed on cholesterol depletion, which augmented with increasing concentrations of MβCD. Actin depolymerization in developing neurons (stage 2) has been shown to promote multiple axons (Bradke and Dotti, 1999). However, since this population was significantly reduced to normal levels on cholesterol supplementation, a critical role for cholesterol in determining neuronal polarity was concluded, though the overlap of cytoskeletal modifications cannot be overruled. Cholesterol depletion has been shown to alter ion channels (Amsalem et al., 2018) and surface receptor signaling (Fukui et al., 2015; Antonini et al., 2018), as well as lipid raft integrity (Rosello-Busquets et al., 2019). Recent studies emphasize the critical role of the Rap GTPase regulator Sema3A and its receptor Plexin-A1 in suppressing supernumerary axons in hippocampal neurons (Wang et al., 2018). Hippocampal neurons from Sema3A knockout mice displayed multiple axons (Wang et al., 2018). Earlier studies have also shown the involvement of Sema3C in inducing lipid raft dependent endocytosis (Salikhova et al., 2008). It remains to be seen whether cholesterol sequestering alters the membrane binding of Sema3A, which is thought to act as an autocrine signal for the establishment of neuronal polarity. The binding and activation by Sema3A might also be lipid raft dependent processes, which would be compromised by cholesterol depletion. This could in turn leave the Plexin-A type containing receptors in their autoinhibited state, rendering the generation of multiple axons by increased Rap1B activity (Wang et al., 2018).

Cellular toxicity for Methyl β Cyclodextrin has been reported previously (Peake and Vance, 2012; Rosello-Busquets et al., 2019). Our studies also show acute membrane damage and compromised viability with a longer duration of incubation, particularly at higher concentrations. Cholesterol depleting enzymes such as ChOx and statins (Nystatin, Lovastatin) alone or in combination with small molecules to inhibit cholesterol biosynthesis might be alternate choices for studying the influence of membrane cholesterol at early developmental stages (Simons et al., 1998; Rosello-Busquets et al., 2019). However, the effect of dosage and duration of these drugs would need to be optimized as well as toxicity assessed according to the developmental stage of the cells since the outcome might vary.

Emerging evidence suggests cholesterol and lipid rafts to be potential therapeutic targets to address different neurological disorders (Vance, 2012; Vona et al., 2021). Different approaches for regulating cholesterol homeostasis have yielded promising results in addressing neurological disorders such as NPC disease (Peake and Vance, 2012). Although neurons have an autonomous cholesterol synthesis machinery, the majority of their cholesterol need is provided by glial cells—microglia in young neurons and, astrocytes and oligodendrocytes through the myelin sheath in the adult brain (Funfschilling et al., 2012). The metabolic support from the glial cells might be critical either as an extrinsic supply for maintaining the neuronal membrane lipid balance or for triggering the signaling pathways regulating the neuronal intrinsic cholesterol supply. Thus, the neuron-glia exchange of cholesterol might have a strong implication on the polarity establishment and maintenance of the neuronal architecture. Our results emphasize the implications of a transient lipid imbalance on neuronal architecture as well as on neural circuitry. Our findings also show that it is possible to reverse the neuronal developmental defects caused by cholesterol deficiency by modulating membrane cholesterol during the early developmental stages. Together, regulating cholesterol levels is a potential therapeutic platform for addressing many of the neurodegenerative and developmental disorders that depend on cholesterol homeostasis. Though previous studies using small molecules such as cyclodextrin to regulate membrane cholesterol have been promising, their applications have been limited by the toxicity they induce (Peake and Vance, 2012). Therefore, genetic modulation of glial cholesterol exporters to modify the neuronal membrane lipid integrity and cholesterol homeostasis might be key to address many of the disorders depending on cholesterol homeostasis in the brain (Karasinska et al., 2009; Courtney and Landreth, 2016). Multiple studies show altering the overall glial content in the brain as a therapeutic strategy to ameliorate neurotoxicity and neuropathology, indicating the importance of global cholesterol homeostasis in the progression of neurodegenerative conditions such as AD (Asai et al., 2015; Spangenberg et al., 2019). However, the relevance of the glial metabolic support on neuronal development in these diseases still needs to be addressed. Transgenic animals labeling different neuronal subtypes and single gene editing techniques including Crispr-Cas9 provide feasible choices for sparse labeling of neurons and quantification of novel parameters such as the neuronal polarity ratio to study the polarity defects *in vivo* (Young et al., 2008; Ran et al., 2013).

In conclusion, mis-regulation of cholesterol metabolism and membrane lipid homeostasis has been correlated with several neurological disorders. This study addresses the fundamental biophysical aspects of cholesterol regulation on membrane physiology and development using rat hippocampal neurons as a model system. Because of the technical challenges in studying polarity establishment during early neuronal development, most of the previous research in this area has been conducted in later stages of development when neuronal polarity has already been established. This is one of the very few studies

which has addressed the role of cholesterol homeostasis in neuronal development and differentiation at the very early stages of neurite growth. Our study signifies the stark effect of a transient alteration in membrane cholesterol balance on neurite outgrowth and polarity establishment. It also emphasizes the significance of addressing this condition at an early developmental phase, where the developmental defects can be rescued to a significant extent by modulating the lipid membrane balance in a precise manner. We observed distinct effects for transient cholesterol sequestering on the development of axons and dendrites and on neuronal polarity establishment. Differential effects were also observed for cholesterol enhancement and sequestering on neurite outgrowth and polarity. Thus, this study identifies membrane cholesterol as a critical factor for axo-dendritic specification and a key molecule for determining neuronal architecture. It also provides insights into regulating membrane cholesterol levels as a potential therapeutic target to address neurodegenerative and developmental disorders that depend on cholesterol homeostasis.

DATA AVAILABILITY STATEMENT

The original contributions presented in the study are included in the article/**Supplementary Material**, further inquiries can be directed to the corresponding author.

ETHICS STATEMENT

All animal procedures to prepare primary cultures were performed with approval and clearance from Animal Ethics Committee, Indian Institute of Science.

AUTHOR CONTRIBUTIONS

The project was conceptualized and executed by MJ. All experiments including cell culturing, drug treatments and labeling were done by MJ. Microscopy imaging was done by MJ and CC. Data analyses were done by MJ, AS, and CC. The manuscript was written by MJ. All authors contributed to the article and approved the submitted version.

FUNDING

The work was funded by DBT Ramanlingaswami Fellowship, DBT Har Gobind Khorana Innovative Young Biotechnologist Award, and DST-SERB Early Career Research Award to MJ. AS was funded by DST-SERB ECRA and CC by DBT-IYBA. The authors acknowledge DBT-IISc Partnership Program for funding the microscopy imaging system used for this work.

ACKNOWLEDGMENTS

We thank the Central Animal Facility, IISc for providing the animals for preparing the primary cultures used for the experiments, Emma Sabu Kattuman for the initial work done and Dr. Narendrakumar Ramanan and Dr. Deepak Nair, CNS, IISc for critical reading of the manuscript.

SUPPLEMENTARY MATERIALS

The Supplementary Material for this article can be found online at: https://www.frontiersin.org/articles/10.3389/fnmol.2021.746211/full#supplementary-material.

REFERENCES

Amsalem, M., Poilbout, C., Ferracci, G., Delmas, P., and Padilla, F. (2018). Membrane cholesterol depletion as a trigger of Nav1.9 channel-mediated inflammatory pain. *EMBO J.* 37:e97349. doi: 10.15252/embj.201797349

Antonini, A., Caioli, S., Saba, L., Vindigni, G., Biocca, S., Canu, N., et al. (2018). Membrane cholesterol depletion in cortical neurons highlights altered NMDA receptor functionality in a mouse model of amyotrophic lateral sclerosis. *Biochim. Biophys. Acta Mol. Basis Dis.* 1864, 509–519. doi: 10.1016/j.bbadis.2017.11.008

Arimura, N., and Kaibuchi, K. (2007). Neuronal polarity: from extracellular signals to intracellular mechanisms. *Nat. Rev. Neurosci.* 8, 194–205. doi: 10.1038/nrn2056

Asai, H., Ikezu, S., Tsunoda, S., Medalla, M., Luebke, J., Haydar, T., et al. (2015). Depletion of microglia and inhibition of exosome synthesis halt tau propagation. *Nat. Neurosci.* 18, 1584–1593. doi: 10.1038/nn.4132

Barnes, A. P., and Polleux, F. (2009). Establishment of axon-dendrite polarity in developing neurons. *Annu. Rev. Neurosci.* 32, 347–381. doi: 10.1146/annurev.neuro.31.060407.125536

Blassberg, R., and Jacob, J. (2017). Lipid metabolism fattens up hedgehog signaling. *BMC Biol.* 15:95. doi: 10.1186/s12915-017-0442-y

Boulan, B., Beghin, A., Ravanello, C., Deloulme, J. C., Gory-Faure, S., Andrieux, A., et al. (2020). AutoneuriteJ: an imageJ plugin for measurement and classification of neuritic extensions. *PLoS One* 15:e0234529. doi: 10.1371/journal.pone.0234529

Bradke, F., and Dotti, C. G. (1999). The role of local actin instability in axon formation. *Science* 283, 1931–1934. doi: 10.1126/science.283.5409.1931

Chia, J. X., Efimova, N., and Svitkina, T. M. (2016). Neurite outgrowth is driven by actin polymerization even in the presence of actin polymerization inhibitors. *Mol. Biol. Cell* 27, 3695–3704. doi: 10.1091/mbc.E16-04-0253

Cho, Y. Y., Kwon, O. H., and Chung, S. (2020). Preferred endocytosis of amyloid precursor protein from cholesterol-enriched lipid raft microdomains. *Molecules* 25:5490. doi: 10.3390/molecules25235490

Chothani, P., Mehta, V., and Stepanyants, A. (2011). Automated tracing of neurites from light microscopy stacks of images. *Neuroinformatics* 9, 263–278. doi: 10.1007/s12021-011-9121-2

Courtney, R., and Landreth, G. E. (2016). LXR regulation of brain cholesterol: from development to disease. *Trends Endocrinol. Metab.* 27, 404–414. doi: 10.1016/j.tem.2016.03.018

Dietschy, J. M., and Turley, S. D. (2004). Thematic review series: brain lipids. Cholesterol metabolism in the central nervous system during early development and in the mature animal. *J. Lipid Res.* 45, 1375–1397. doi: 10.1194/jlr.R400004-JLR200

Dotti, C. G., Sullivan, C. A., and Banker, G. A. (1988). The establishment of polarity by hippocampal neurons in culture. *J. Neurosci.* 8, 1454–1468. doi: 10.1523/JNEUROSCI.08-04-01454.1988

Fan, Q. W., Yu, W., Gong, J. S., Zou, K., Sawamura, N., Senda, T., et al. (2002). Cholesterol-dependent modulation of dendrite outgrowth and microtubule stability in cultured neurons. *J. Neurochem.* 80, 178–190. doi: 10.1046/j.0022-3042.2001.00686.x

Fan, Q. W., Yu, W., Senda, T., Yanagisawa, K., and Michikawa, M. (2001). Cholesterol-dependent modulation of tau phosphorylation in cultured neurons. *J. Neurochem.* 76, 391–400. doi: 10.1046/j.1471-4159.2001.00063.x

Fukui, K., Ferris, H. A., and Kahn, C. R. (2015). Effect of cholesterol reduction on receptor signaling in neurons. *J. Biol. Chem.* 290, 26383–26392. doi: 10.1074/jbc.M115.664367

Funfschilling, U., Jockusch, W. J., Sivakumar, N., Mobius, W., Corthals, K., Li, S., et al. (2012). Critical time window of neuronal cholesterol synthesis during neurite outgrowth. *J. Neurosci.* 32, 7632–7645. doi: 10.1523/JNEUROSCI.1352-11.2012

Goslin, K., and Banker, G. (1989). Experimental observations on the development of polarity by hippocampal neurons in culture. *J. Cell Biol.* 108, 1507–1516. doi: 10.1083/jcb.108.4.1507

Grimm, M. O., Mett, J., Grimm, H. S., and Hartmann, T. (2017). APP function and lipids: a bidirectional link. *Front. Mol. Neurosci.* 10:63. doi: 10.3389/fnmol.2017.00063

Gumy, L. F., Katrukha, E. A., Grigoriev, I., Jaarsma, D., Kapitein, L. C., Akhmanova, A., et al. (2017). MAP2 defines a pre-axonal filtering zone to regulate KIF1- versus KIF5-dependent cargo transport in sensory neurons. *Neuron* 94, 347–362.e7. doi: 10.1016/j.neuron.2017.03.046

Hussain, G., Wang, J., Rasul, A., Anwar, H., Imran, A., Qasim, M., et al. (2019). Role of cholesterol and sphingolipids in brain development and neurological diseases. *Lipids Health Dis.* 18:26. doi: 10.1186/s12944-019-0965-z

Jiang, X. S., Wassif, C. A., Backlund, P. S., Song, L., Holtzclaw, L. A., Li, Z., et al. (2010). Activation of Rho GTPases in smith-lemli-opitz syndrome: pathophysiological and clinical implications. *Hum. Mol. Genet.* 19, 1347–1357. doi: 10.1093/hmg/ddq011

Karasinska, J. M., Rinninger, F., Lutjohann, D., Ruddle, P., Franciosi, S., Kruit, J. K., et al. (2009). Specific loss of brain ABCA1 increases brain cholesterol uptake and influences neuronal structure and function. *J. Neurosci.* 29, 3579–3589. doi: 10.1523/JNEUROSCI.4741-08.2009

Kedia, S., Ramakrishna, P., Netrakanti, P. R., Jose, M., Sibarita, J. B., Nadkarni, S., et al. (2020a). Real-time nanoscale organization of amyloid precursor protein. *Nanoscale* 12, 8200–8215. doi: 10.1039/d0nr00052c

Kedia, S., Ramakrishna, P., Netrakanti, P. R., Singh, N., Sisodia, S. S., Jose, M., et al. (2020b). Alteration in synaptic nanoscale organization dictates amyloidogenic processing in Alzheimer's disease. *iScience* 24:101924. doi: 10.1016/j.isci.2020.101924

Ko, M., Zou, K., Minagawa, H., Yu, W., Gong, J. S., Yanagisawa, K., et al. (2005). Cholesterol-mediated neurite outgrowth is differently regulated between cortical and hippocampal neurons. *J. Biol. Chem.* 280, 42759–42765. doi: 10.1074/jbc.M509164200

Ledesma, M. D., Simons, K., and Dotti, C. G. (1998). Neuronal polarity: essential role of protein-lipid complexes in axonal sorting. *Proc. Natl. Acad. Sci. U S A* 95, 3966–3971. doi: 10.1073/pnas.95.7.3966

Leoni, V., and Caccia, C. (2015). The impairment of cholesterol metabolism in Huntington disease. *Biochim. Biophys. Acta* 1851, 1095–1105. doi: 10.1016/j.bbalip.2014.12.018

Leterrier, C. (2018). The axon initial segment: an updated viewpoint. *J. Neurosci.* 38, 2135–2145. doi: 10.1523/JNEUROSCI.1922-17.2018

Leterrier, C., Potier, J., Caillol, G., Debarnot, C., Rueda Boroni, F., and Dargent, B. (2015). Nanoscale architecture of the axon initial segment reveals an organized and robust scaffold. *Cell Rep.* 13, 2781–2793. doi: 10.1016/j.celrep.2015.11.051

Longair, M. H., Baker, D. A., and Armstrong, J. D. (2011). Simple neurite tracer: open source software for reconstruction, visualization and analysis of neuronal processes. *Bioinformatics* 27, 2453–2454. doi: 10.1093/bioinformatics/btr390

Moutinho, M., Nunes, M. J., Correia, J. C., Gama, M. J., Castro-Caldas, M., Cedazo-Minguez, A., et al. (2016). Neuronal cholesterol metabolism increases dendritic outgrowth and synaptic markers via a concerted action of GGTase-I and Trk. *Sci. Rep.* 6:30928. doi: 10.1038/srep30928

Mundhara, N., Majumder, A., and Panda, D. (2019). Methyl-beta-cyclodextrin, an actin depolymerizer augments the antiproliferative potential of microtubule-targeting agents. *Sci. Rep.* 9:7638. doi: 10.1038/s41598-019-43947-4

Nair, D., Hosy, E., Petersen, J. D., Constals, A., Giannone, G., Choquet, D., et al. (2013). Super-resolution imaging reveals that AMPA receptors inside synapses are dynamically organized in nanodomains regulated by PSD95. *J. Neurosci.* 33, 13204–13224. doi: 10.1523/JNEUROSCI.2381-12.2013

Nair, D., Kedia, S., and Jose, M. (2020). Does altered probability of real time diffusional collisions of membrane molecules trigger or delay Alzheimers disease. *iScience Notes* 5, 1–4. doi: 10.22580/iSciNoteJ5.5.3

Peake, K. B., and Vance, J. E. (2012). Normalization of cholesterol homeostasis by 2-hydroxypropyl-β-cyclodextrin in neurons and glia from Niemann-Pick C1 (NPC1)-deficient mice. *J. Biol. Chem.* 287, 9290–9298. doi: 10.1074/jbc.M111.326405

Pierrot, N., Tyteca, D., D'auria, L., Dewachter, I., Gailly, P., Hendrickx, A., et al. (2013). Amyloid precursor protein controls cholesterol turnover needed for neuronal activity. *EMBO Mol. Med.* 5, 608–625. doi: 10.1002/emmm.201202215

Porter, F. D., and Herman, G. E. (2011). Malformation syndromes caused by disorders of cholesterol synthesis. *J. Lipid Res.* 52, 6–34. doi: 10.1194/jlr.R009548

Porter, J. A., Young, K. E., and Beachy, P. A. (1996). Cholesterol modification of hedgehog signaling proteins in animal development. *Science* 274, 255–259. doi: 10.1126/science.274.5285.255

Quan, G., Xie, C., Dietschy, J. M., and Turley, S. D. (2003). Ontogenesis and regulation of cholesterol metabolism in the central nervous system of the mouse. *Brain Res. Dev. Brain Res.* 146, 87–98. doi: 10.1016/j.devbrainres.2003.09.015

Ran, F. A., Hsu, P. D., Wright, J., Agarwala, V., Scott, D. A., and Zhang, F. (2013). Genome engineering using the CRISPR-Cas9 system. *Nat. Protoc.* 8, 2281–2308. doi: 10.1038/nprot.2013.143

Rosello-Busquets, C., De La Oliva, N., Martinez-Marmol, R., Hernaiz-Llorens, M., Pascual, M., Muhaisen, A., et al. (2019). Cholesterol depletion regulates axonal growth and enhances central and peripheral nerve regeneration. *Front. Cell Neurosci.* 13:40. doi: 10.3389/fncel.2019.00040

Salikhova, A., Wang, L., Lanahan, A. A., Liu, M., Simons, M., Leenders, W. P., et al. (2008). Vascular endothelial growth factor and semaphorin induce neuropilin-1 endocytosis via separate pathways. *Circ. Res.* 103, e71–e79. doi: 10.1161/CIRCRESAHA.108.183327

Schelski, M., and Bradke, F. (2017). Neuronal polarization: from spatiotemporal signaling to cytoskeletal dynamics. *Mol. Cell Neurosci.* 84, 11–28. doi: 10.1016/j.mcn.2017.03.008

Simons, M., Keller, P., De Strooper, B., Beyreuther, K., Dotti, C. G., and Simons, K. (1998). Cholesterol depletion inhibits the generation of beta-amyloid in hippocampal neurons. *Proc. Natl. Acad. Sci. U S A* 95, 6460–6464. doi: 10.1073/pnas.95.11.6460

Song, A. H., Wang, D., Chen, G., Li, Y., Luo, J., Duan, S., et al. (2009). A selective filter for cytoplasmic transport at the axon initial segment. *Cell* 136, 1148–1160. doi: 10.1016/j.cell.2009.01.016

Spangenberg, E., Severson, P. L., Hohsfield, L. A., Crapser, J., Zhang, J., Burton, E. A., et al. (2019). Sustained microglial depletion with CSF1R inhibitor impairs parenchymal plaque development in an Alzheimer's disease model. *Nat. Commun.* 10:3758. doi: 10.1038/s41467-019-11674-z

Sviridov, D., Mukhamedova, N., and Miller, Y. I. (2020). Lipid rafts as a therapeutic target. *J. Lipid Res.* 61, 687–695. doi: 10.1194/jlr.TR120000658

Takano, T., Funahashi, Y., and Kaibuchi, K. (2019). Neuronal polarity: positive and negative feedback signals. *Front. Cell Dev. Biol.* 7:69. doi: 10.3389/fcell.2019.00069.

Tanwar, M., Kateriya, S., Nair, D., and Jose, M. (2021). Optogenetic modulation of real-time nanoscale dynamics of HCN channels using photoactivated adenylyl cyclases. *RSC Chem. Biol.* 2, 863–875. doi: 10.1039/d0cb00124d

Vance, J. E. (2012). Dysregulation of cholesterol balance in the brain: contribution to neurodegenerative diseases. *Dis. Model Mech.* 5, 746–755. doi: 10.1242/dmm.010124

Vance, J. E., Pan, D., Campenot, R. B., Bussiere, M., and Vance, D. E. (1994). Evidence that the major membrane lipids, except cholesterol, are made in axons

of cultured rat sympathetic neurons. *J. Neurochem.* 62, 329–337. doi: 10.1046/j.1471-4159.1994.62010329.x

Vona, R., Iessi, E., and Matarrese, P. (2021). Role of cholesterol and lipid rafts in cancer signaling: a promising therapeutic opportunity? *Front. Cell Dev. Biol.* 9:622908. doi: 10.3389/fcell.2021.622908

Wang, N., Dhumale, P., Chiang, J., and Puschel, A. W. (2018). The sema3A receptor plexin-A1 suppresses supernumerary axons through rap1 GTPases. *Sci. Rep.* 8:15647. doi: 10.1038/s41598-018-34092-5

Wang, L. J., and Song, B. L. (2012). Niemann-pick C1-like 1 and cholesterol uptake. *Biochim. Biophys. Acta* 1821, 964–972. doi: 10.1016/j.bbalip.2012.03.004

Young, P., Qiu, L., Wang, D., Zhao, S., Gross, J., and Feng, G. (2008). Single-neuron labeling with inducible Cre-mediated knockout in transgenic mice. *Nat. Neurosci.* 11, 721–728. doi: 10.1038/nn.2118

Zhang, J., and Liu, Q. (2015). Cholesterol metabolism and homeostasis in the brain. *Protein Cell* 6, 254–264. doi: 10.1007/s13238-014-0131-3

Conflict of Interest: The authors declare that the research was conducted in the absence of any commercial or financial relationships that could be construed as a potential conflict of interest.

Publisher's Note: All claims expressed in this article are solely those of the authors and do not necessarily represent those of their affiliated organizations, or those of the publisher, the editors and the reviewers. Any product that may be evaluated in this article, or claim that may be made by its manufacturer, is not guaranteed or endorsed by the publisher.

frontiers in Molecular Neuroscience

ORIGINAL RESEARCH
published: 26 November 2021
doi: 10.3389/fnmol.2021.772847

Non-synaptic Cell-Autonomous Mechanisms Underlie Neuronal Hyperactivity in a Genetic Model of *PIK3CA*-Driven Intractable Epilepsy

Achira Roy[1], Victor Z. Han[2,3], Angela M. Bard[2], Devin T. Wehle[2,4], Stephen E. P. Smith[2,5], Jan-Marino Ramirez[2,5,6,7], Franck Kalume[2,6,8] and Kathleen J. Millen[2,5]**

[1] Neuroscience Unit, Jawaharlal Nehru Centre for Advanced Scientific Research (JNCASR), Bengaluru, India, [2] Center for Integrative Brain Research, Seattle Children's Research Institute, Seattle, WA, United States, [3] Department of Biology, University of Washington, Seattle, WA, United States, [4] Graduate Program in Neuroscience, University of Washington, Seattle, WA, United States, [5] Department of Pediatrics, University of Washington, Seattle, WA, United States, [6] Department of Neurological Surgery, University of Washington, Seattle, WA, United States, [7] Department of Physiology and Biophysics, University of Washington, Seattle, WA, United States, [8] Department of Pharmacology, University of Washington, Seattle, WA, United States

OPEN ACCESS

Edited by:
Sumru Bayin,
Memorial Sloan Kettering Cancer Center, United States

Reviewed by:
Benjamin Deneen,
Baylor College of Medicine, United States
Ludovic Tricoire,
Université Pierre et Marie Curie, France

***Correspondence:**
Achira Roy
achira.roy@gmail.com;
achira.roy@jncasr.ac.in
Kathleen J. Millen
kathleen.millen@seattlechildrens.org

Specialty section:
This article was submitted to Methods and Model Organisms, a section of the journal Frontiers in Molecular Neuroscience

Received: 08 September 2021
Accepted: 20 October 2021
Published: 26 November 2021

Citation:
Roy A, Han VZ, Bard AM, Wehle DT, Smith SEP, Ramirez J-M, Kalume F and Millen KJ (2021) Non-synaptic Cell-Autonomous Mechanisms Underlie Neuronal Hyperactivity in a Genetic Model of PIK3CA-Driven Intractable Epilepsy. Front. Mol. Neurosci. 14:772847. doi: 10.3389/fnmol.2021.772847

Patients harboring mutations in the PI3K-AKT-MTOR pathway-encoding genes often develop a spectrum of neurodevelopmental disorders including epilepsy. A significant proportion remains unresponsive to conventional anti-seizure medications. Understanding mutation-specific pathophysiology is thus critical for molecularly targeted therapies. We previously determined that mouse models expressing a patient-related activating mutation in *PIK3CA*, encoding the p110α catalytic subunit of phosphoinositide-3-kinase (PI3K), are epileptic and acutely treatable by PI3K inhibition, irrespective of dysmorphology. Here we report the physiological mechanisms underlying this dysregulated neuronal excitability. *In vivo*, we demonstrate epileptiform events in the *Pik3ca* mutant hippocampus. By *ex vivo* analyses, we show that Pik3ca-driven hyperactivation of hippocampal pyramidal neurons is mediated by changes in multiple non-synaptic, cell-intrinsic properties. Finally, we report that acute inhibition of PI3K or AKT, but not MTOR activity, suppresses the intrinsic hyperactivity of the mutant neurons. These acute mechanisms are distinct from those causing neuronal hyperactivity in other AKT-MTOR epileptic models and define parameters to facilitate the development of new molecularly rational therapeutic interventions for intractable epilepsy.

Keywords: PI3K, epilepsy, mouse model, electrophysiology, hippocampus, BKM120 (buparlisib), RAD001 (everolimus), AZD5363 (PubChem CID: 25227436)

INTRODUCTION

Mutations in the PI3K-AKT-MTOR signaling pathway, long studied for roles in cancer (Yang et al., 2019; Madsen, 2020), also cause clinically important developmental brain overgrowth syndromes. Affected individuals display phenotypes ranging from dysplastic megalencephaly, hemimegalencephaly, and focal cortical dysplasia (FCD), as well as comorbidities including hydrocephalus, autism, and intellectual disability (Bast et al., 2006; Blumcke et al., 2011; Stafstrom and Carmant, 2015; Crino, 2016; Mirzaa et al., 2018; Dobyns and Mirzaa, 2019). These

mutations also cause focal epilepsy, representing 25–50% of all cases of intractable (treatment-resistant) epilepsy in children (Bast et al., 2006; Blumcke et al., 2011; Stafstrom and Carmant, 2015; Mirzaa et al., 2018; Kim and Lee, 2019; Rademacher and Eickholt, 2019; Lee et al., 2021). Most current anti-seizure drugs target single ion channels because they were developed in acute wild-type rodent seizure models (Kehne et al., 2017; Barker-Haliski and White, 2019; Wilcox et al., 2020). These models do not mimic genetic epilepsies in patients; hence the current therapeutics are largely ineffective. Since PI3K pathway mutations are now known to cause intractable epilepsy, repurposing pathway-targeted anti-cancer drugs offers a tantalizing opportunity to fundamentally shift the therapeutic approach toward intractable epilepsy. Presently, the MTOR inhibitor rapamycin and its analogs are the sole pathway-related drugs used clinically to treat epilepsy, primarily in tuberous sclerosis (TSC) patients with rare *TSC1/2* deletion mutations which enhance downstream MTOR signaling (Crino, 2016; Kim and Lee, 2019; Stafstrom, 2019). Yet, these treatments remain effective only to a modest degree, suggesting that MTOR activation may not be the sole arm of this complex signaling pathway accounting for all PI3K pathway-driven epilepsies (Cho, 2011; Meng et al., 2013; Roy et al., 2015; Nguyen and Bordey, 2021).

Mosaic activating mutations of the p110α catalytic subunit of phosphoinositide 3-kinase (*PIK3CA*) in the brain result in a spectrum of segmental overgrowth syndromes including intractable pediatric epilepsy. We have previously generated the first genetic mouse models of patient-related *PIK3CA* mutations that recapitulate brain overgrowth, cortical dysplasia, hydrocephalus, and epilepsy, with phenotypic severity dependent on the mutant allele and its time of activation (Roy et al., 2015, 2019). Moreover, this developmental epilepsy is dissociable from dysmorphology and seizures acutely suppressible by 1-h *in vivo* administration of the pan-PI3K inhibitor BKM120 (Maira et al., 2012; Roy et al., 2015). To assess the underlying acute physiological and pathway mechanisms, here we perform *in vivo* and *ex vivo* electrophysiological studies in our megalencephalic *Nestin-cre;Pik3ca*^{E545K} mouse model, focusing on hippocampal pyramidal neurons. Hippocampal abnormalities are commonly observed in epilepsy patients (Chatzikonstantinou, 2014; Roy et al., 2020). The association between epilepsy and hippocampal pathophysiology is also well established (de Curtis and Gnatkovsky, 2009; Cho, 2011; Berdichevsky et al., 2013; Roy et al., 2015; Mazumder et al., 2019), with some evidence for hippocampal seizure onset in patients with mutations in PI3K pathway (Jansen et al., 2015). Further in this study, we demonstrate clear evidence of hippocampus-initiated seizure activity *in vivo*, which we leverage for more extensive *ex vivo* analyses. We report that *Pik3ca*^{E545K} gain-of-function mutation causes intrinsic changes in neuronal properties leading to hyperactivity. We further establish that this hyperactivity is acutely dependent on PI3K and AKT, but not MTOR, regulation. Our study is the first to define key aspects of acute neuronal dysregulation in this important genetic model of Pik3ca-driven epilepsy, and demonstrates these mechanisms are distinct from synaptic and network-related mechanisms reported in MTOR, TSC, and RHEB epilepsy models (Crino, 2016; Kim and Lee, 2019; Stafstrom, 2019; Hsieh et al., 2020) with PI3K pathway dysregulation.

RESULTS

In vivo Recordings Demonstrate Network Hyperexcitability in Mutant CA1

We investigated *in vivo* changes in the hippocampal CA1 network activity of ∼P70 *Nestin-cre;Pik3ca*^{E545K} mutant mice relative to control littermates using local field potential (LFP) recordings, while simultaneously monitoring cortical surface activity by electrocorticography (ECoG). These recordings showed spontaneous interictal spike activity either restricted to the cortex or the hippocampus exclusively, or concurrent to the two regions in the mutant mice (**Figures 1A–D**). A broad spectrum of spike patterns was observed, consisting of single or groups of interictal spikes, the simplest identifiable unit of epileptiform activity (McCormick and Contreras, 2001), as well as trains of sharp spikes, low-frequency slow waves or high-frequency low-amplitude "brushing events." These epileptiform events were observed exclusively in the mutant mice. Within the mutant group, the event frequency was significantly higher in the hippocampus than in the neocortex. Power spectrum analyses revealed that the mutant hippocampi exhibit significantly higher power in the gamma frequency bands (**Figures 1E–H**), which is often indicative of seizure onset (Lee et al., 2000; Hughes, 2008). There is increasing evidence in the field that elevated EEG gamma activity (20–30 Hz) can serve as a biomarker of pathological tissue involved in seizure generation or at risk of epileptogenesis (Hughes, 2008). Increased gamma activity in the hippocampus has also been associated with seizure generation in animal models (de Curtis and Gnatkovsky, 2009; Jones et al., 2015). In the same way, our data established a clear link between hippocampus and seizures in our model and demonstrated that Pik3ca overactivation caused significant neural hyperexcitation in our mice, predominantly in the hippocampus.

Mutant CA1 and CA3 Pyramidal Neurons Are Hyperactive

To investigate mechanisms driving the mutant epileptiform activity at the cellular level, we used whole-cell patch-clamp recordings from CA1 and CA3 pyramidal neurons in P16–20 control and mutant brains. Silent and spontaneously firing, tonic, and burst-generating neurons were detected in both control and mutant slices (**Figures 2A–C**). However, mutant slices had a significantly higher proportion of burst-generating cells in both regions and lower proportion of tonic-firing cells in mutant CA1 compared to controls. Additionally, we observed significantly higher tonic spike frequencies in mutant CA1 and CA3 and higher burst frequency in mutant CA1, compared to controls (**Figures 2D–G**).

Burst-generating cells demonstrated multiple burst types. Specifically, we identified burst clusters and two types of

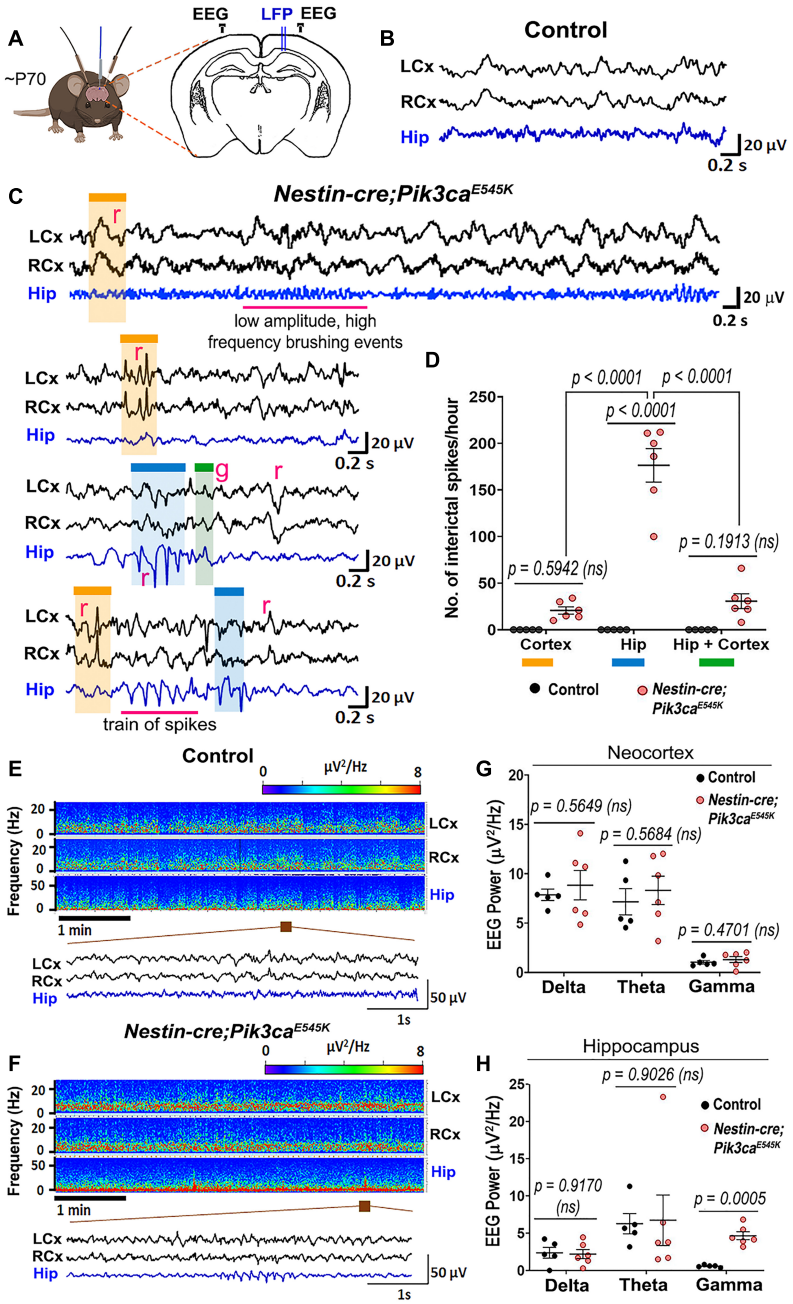

FIGURE 1 | *Nestin-cre;Pik3ca*^{E545K} mutant brains show higher neural excitability. **(A)** Schematic shows electrode placement for EEG-ECoG recordings in ~P70 *Nestin-cre;Pik3ca*^{E545K} and control littermates. LFP, local field potential. **(B,C)** Compared to controls, the mutants showed significantly higher frequency of regional (r) or generalized (g) spikes, train of spikes/polyspikes in neocortex (black traces) and hippocampus (blue traces). Low amplitude, high frequency brushing events were also observed in the hippocampus. **(D)** In the mutant, interictal spike frequency was significantly higher in the hippocampus (blue box), compared to those generated in neocortex (orange box) or generalized in both regions (green box) [F = 46.65, degrees of freedom (df) = 27]. **(E,F)** Power spectrum analysis displayed increased activity in mutants, as emphasized in the representative magnified segments. **(G,H)** Mutant hippocampus demonstrated significantly higher activity in the gamma frequency range (F = 3.932, df = 27; neocortex: F = 26.93, df = 27), where frequency bands as evaluated are: Delta: 0.5–5 Hz, Theta: 5–10 Hz, Gamma: 20–30 Hz. Data is represented as mean ± SEM scatter plots; differences were considered significant at $p < 0.05$; ns, not significant. Scale bars: 0.2 s, 20 μV **(B,C)**; 1 s, 50 μV **(E,F)**.

plateau-bursts: paroxysmal depolarization shift (PDS) and non-PDS waveforms. We defined "burst cluster" as a multi-spike burst activity of random nature without a plateau potential; these were only observed in mutant slices (**Figures 2H,I**). Plateau-bursts with depolarization shift resulting in sodium-spike inactivation were termed as PDS "bursting cells." These

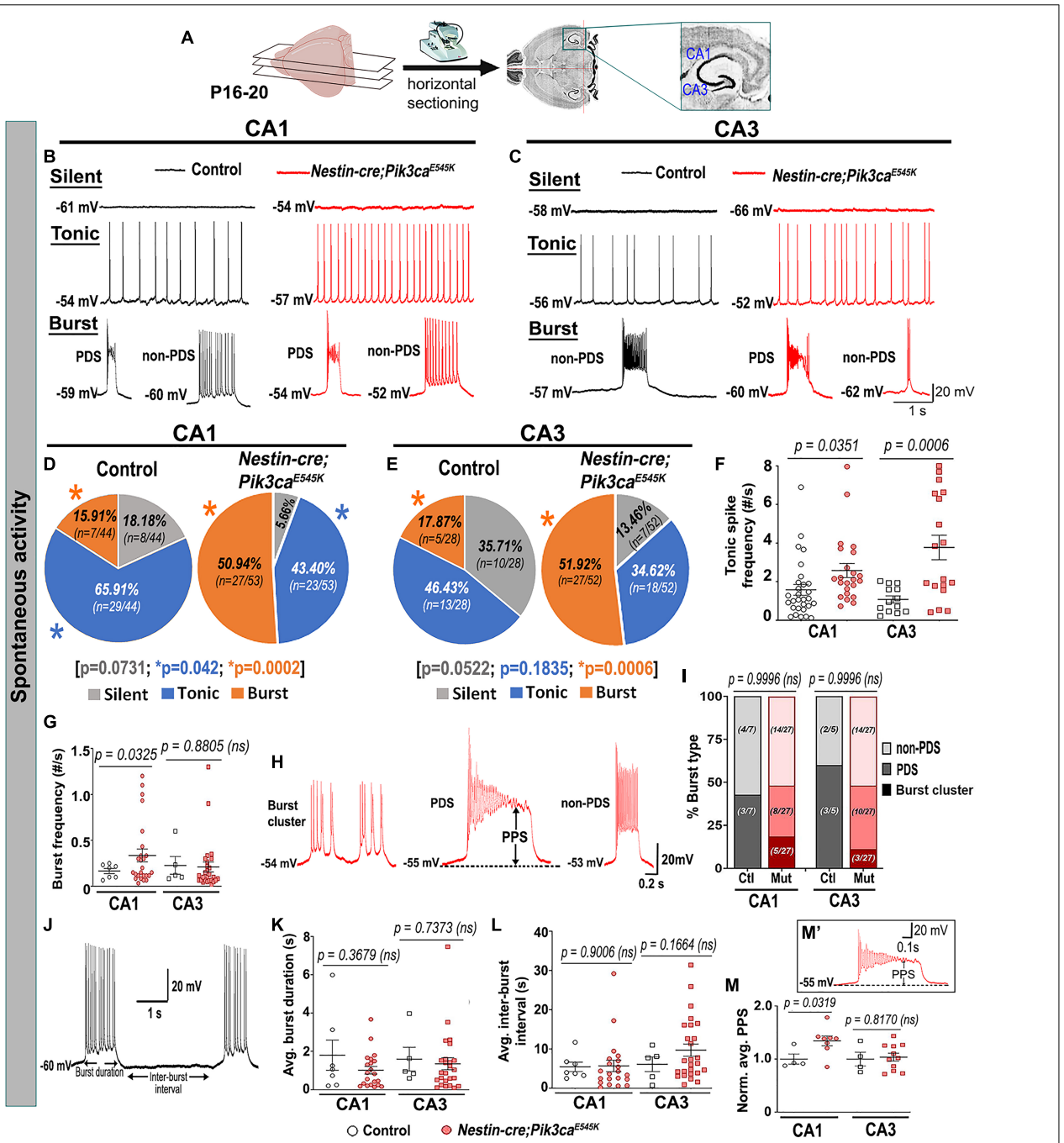

FIGURE 2 | Mutant hippocampal neurons produce increased epileptiform burst activity. **(A)** Flowchart shows acute horizontal brain slicing for whole-cell recording. **(B–E)** Traces represent silent, tonic, and burst categories of CA1 and CA3 neurons based on spontaneous cellular activity; respective pie charts marked proportion of recorded cells. Mutant CA1 and CA3 exhibited significantly higher proportions of burst-firing cells compared to controls. Significantly fewer tonic-firing cells were observed in mutant CA1. **(F,G)** Relative to controls, spontaneous tonic spike frequencies were significantly higher in mutant CA1 (t = 2.175, df = 43.71) and CA3 (t = 4.063, df = 19.78) cells; burst frequency was significantly higher in mutant CA1 (CA1: t = 2.244, df = 29.38; CA3: t = 0.1561, df = 6.754). **(H)** Representative traces for subtypes of burst firing, namely burst cluster, paroxysmal depolarization shift (PDS) and non-PDS plateau bursts. **(I)** Proportion of burst subcategories were not overtly different in control and mutant CA1 and CA3 regions ($F = 7.355e^{-12}$; df = 6); burst clusters were only seen in mutant cells. **(J)** Representative trace demonstrates how burst duration and inter-burst interval were calculated. **(K,L)** In both CA1 and CA3, average (avg.) burst duration (CA1: t = 0.9644, df = 6.793; CA3: t = 0.3508, df = 6.229) and inter-burst interval (CA1: t = 0.1263, df = 22.31; CA3: t = 1.485, df = 10.73) were not significantly different between control and mutant neurons. **(M')** Plateau potential shift (PPS) in mutant bursting cells, as depicted in panel **(M')**, was significantly higher in CA1 (t = 2.586, df = 8.118) but similar in CA3 (t = 0.2436, df = 5.110), compared to respective controls. Data is represented as pie charts, % bar graphs and mean ± SEM scatter plots; differences were considered significant at $p < 0.05$; ns, not significant; PPS, plateau potential shift. Scale bars: 1 s, 20 mV **(B,C,J)**; 0.2 s, 20 mV **(H)**; 0.1 s, 20 mV **(M')**.

depolarization shifts have previously been implicated as the intracellular correlate of *in vivo* interictal spikes (McCormick and Contreras, 2001; Marcuccilli et al., 2010; Kubista et al., 2019; Tryba et al., 2019). We defined non-PDS bursts as those where plateau potential developed in absence of prominent sodium-spike inactivation. No significant differences between control and mutant hippocampal pyramidal cells were observed with respect to average burst duration or inter-burst interval. However, the plateau potential shift (PPS), defined here as the difference of the steady state plateau potential and the resting membrane potential (RMP), was significantly larger in mutant CA1 but not in CA3, relative to respective controls (**Figures 2J–M,M'**). This was despite similar RMP across control and mutant hippocampal neurons (**Table 1**).

The evoked current-clamp recordings further validated the spontaneous activity results, especially by displaying a significantly higher percentage of burst-generating pyramidal neurons in the mutant hippocampus (**Figures 3A–E**). Incidentally, no significant difference in membrane intrinsic properties like input resistance, rheobase current and burst-threshold current, as well as evoked tonic spike frequencies (for the tested 0–90 pA range), was observed between control and mutant cells (**Table 1** and **Figures 3F–H**). But the decay time constant for mutant CA3 neurons was significantly longer than that in mutant CA1 and control groups (**Table 1**). With similar resistance, this implied that mutant CA3 neurons have higher membrane capacitance than other cell groups. Together, these data demonstrate that Pik3ca overactivation results in intracellular neuronal hyperactivity, with some distinct cell type-specific effects.

Pik3ca-Driven Neuronal Hyperactivity Is Not Primarily Dependent on Synaptic Inputs

To determine whether the Pik3ca-related neuronal hyperactivity is driven by altered synaptic interactions or other intrinsic properties, we assessed the effects of channel and receptor blockers on mutant hippocampal physiology. Blocking glutamatergic inputs by extracellular administration of NMDA and non-NMDA receptor-antagonists, 3-[(±)2-carboxypiperazin-4yl] propyl-1-phosphate (CPP) and 6-cyano-7-nitroquinoxaline-2,3-dione (CNQX) respectively, had no overt physiological effect on the majority of mutant hippocampal neurons (**Figures 4A–C,E,F,H–K**). Similarly, blocking inhibitory synaptic inputs with gabazine did not significantly alter the mutant firing patterns, spike frequencies or PPS (**Figures 4A,D,G,L**). The proportion of mutant CA1 neurons affected by these channel blockers was comparatively less than that in CA3. Our data lead to the important conclusion that Pik3ca-driven neuronal hyperactivity is primarily not dependent on synaptic transmission.

In contrast, inhibition of calcium (Ca^{2+})-dependent inward current by extracellular cadmium (Cd^{2+}) attenuated the paroxysmal bursts and reduced burst frequency and PPS (**Figures 5A–D**), indicating a calcium channel-dependent mechanism underlying the Pik3ca-dependent seizure activity. Intracellular cesium blocked potassium channels and related currents, altering the intrinsic firing pattern in both control and mutant hippocampal slices. Specifically, compared to regular baseline recordings, intracellular cesium considerably reduced the proportion of tonic-firing cells in both CA1 and CA3 (**Figures 5E–H**, compare to **Figures 2D,E**). Unlike the spontaneous recordings, intracellular cesium prompted the burst frequency in mutant CA1 to normalize and in mutant CA3 to significantly rise, relative to respective controls (**Figure 5I**, compare to **Figure 2G**). Intracellular cesium also normalized the mutant PPS to control levels (**Figure 5J**, compare to **Figure 2M**). No overt effect on RMP or input resistance was seen in cesium-treated control and mutant cells (**Figures 5K,L**). We conclude that Pik3ca-related epileptiform activity is primarily caused by a complex set of altered non-synaptic cell-intrinsic properties.

Acute Treatment of Neuronal Hyperactivation With PI3K Drugs

The acute *in vivo* suppression of induced seizures in *Nestin-cre;Pik3ca*^{E545K} mice by BKM120 (Roy et al., 2015) prompted us to dissect the downstream pathway dynamics using inhibitors at the cellular level, in order to coarsely determine their mechanistic roles and identify new therapeutic targets to treat intractable epilepsy. Acute extracellular administration of BKM120 or the pan-AKT inhibitor AZD5363 (Davies et al., 2012; **Figures 6A–F,I,I',K,N,N'**) resulted in a large-scale and significant alteration

TABLE 1 | Summary table of intrinsic membrane properties.

#	Intrinsic properties	CA1		CA3	
		Control	Mutant	Control	Mutant
1	Resting membrane potential (RMP; mV)	−55.36 ± 0.58	−54.64 ± 0.64	−56.07 ± 0.82	−56.49 ± 0.92
2	Input resistance (MΩ)	284.27 ± 21.6	262.82 ± 22.72	331.73 ± 23.54	272.99 ± 39.14
3	Time constant (ms)	21.79 ± 1.76	23.58 ± 1.85	32.23 ± 7.33	50.78 ± 3.76
4	Rheobase (pA)	11.54 ± 3.17	18.95 ± 3.66	18.95 ± 3.32	19.33 ± 4.19

Summary of basic intrinsic membrane properties quantitated and compared between control and mutant CA1 and CA3 neurons. No significant differences in resting membrane potential, input resistance and rheobase current (minimum injected current required to elicit the first action potential) were observed between control and mutant neurons, in both CA1 and CA3. Decay time constant of mutant CA3 neurons was significantly longer than that of control CA1 ($p < 0.0001$) and CA3 ($p = 0.0071$) cells, as well as of mutant CA1 neurons ($p < 0.0001$; $F = 31.21$, $df = 33$). Data is represented as mean ± SEM; differences were considered significant at $p < 0.05$.

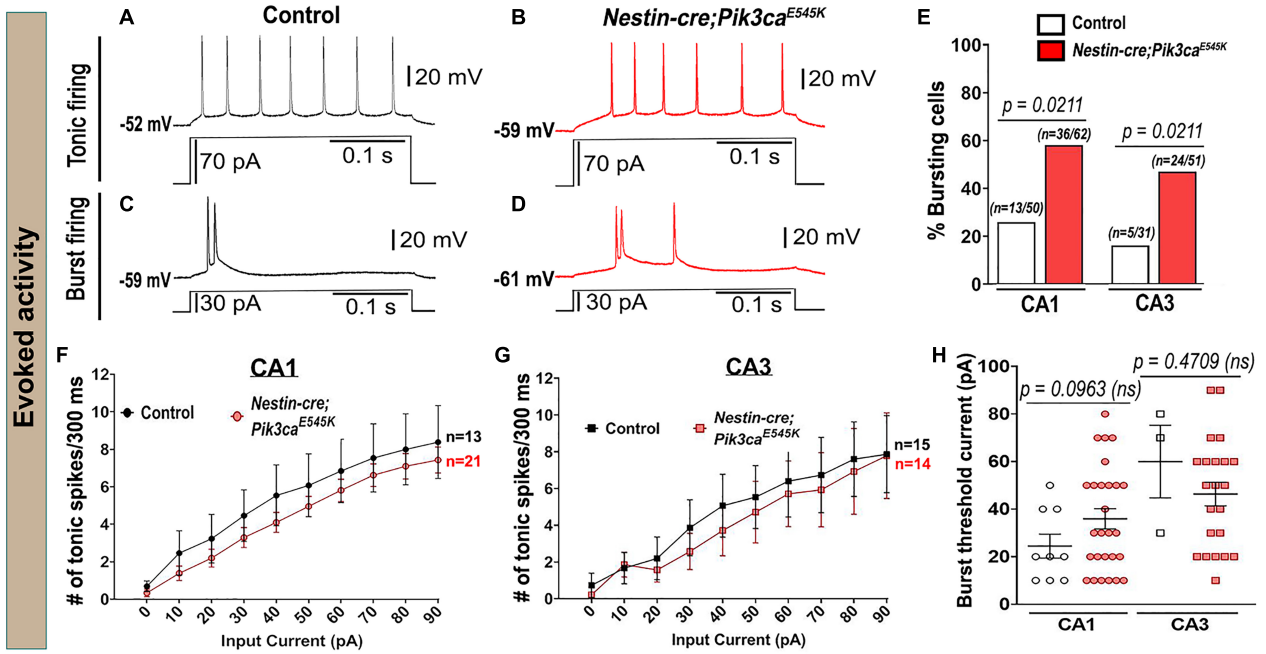

FIGURE 3 | Evoked whole-cell recording shows increased bursting in mutants. **(A–D)** Representative evoked voltage traces of control and mutant showed tonic and burst firing in response to current steps. **(E)** Evoked recording also marked significantly higher bursting cell proportions in the mutant. **(F,G)** No significant differences in evoked tonic spike frequencies were observed in the tested range of input depolarizing current (0–90 pA), between control and mutant CA1 and CA3 neurons (CA1: $F = 13.07$, df = 320; CA3: $F = 4.844$, df = 270). **(H)** No overt differences in the current inducing the first burst were observed between control and mutant (CA1: $t = 1.744$, df = 20.29; CA3: $t = 0.8493$, df = 2.439). Data is represented as bar graphs, mean ± SEM scatter and line plots; differences were considered significant at $p < 0.05$; ns, not significant. Scale bars: 0.1 s, 20 mV **(A–D)**.

of firing pattern, frequencies and a relative reduction of PPS, sometimes leading to gradual silencing of the recorded neurons. In contrast to BKM120, acute AKT downregulation by AZD5363 significantly reduced the mutant burst duration and inter-burst interval (**Figures 6G,H,L,M**). Neither drug had any significant effect on neuronal RMP (pre-BKM120$_{CA1}$: −58.7 ± 1.89 mV, post-BKM120$_{CA1}$: −56.1 ± 1.38 mV; pre-BKM120$_{CA3}$: −59.5 ± 2.07 mV, post-BKM120$_{CA3}$: −58.58 ± 1.70 mV; pre-AZD5363$_{CA1}$: -55.25 ± 2.63 mV, post-AZD5363$_{CA1}$: −52.5 ± 2.18 mV; pre-AZD5363$_{CA3}$: −56.25 ± 2.79 mV, post-AZD5363$_{CA3}$: −54.75 ± 3.95 mV) or tonic rheobase current (**Figures 6J,O**). Further, AZD5363 altered the physiology of all mutant CA3 neurons much faster (∼8 min) than BKM120 (∼32 min); however, both drugs changed the intracellular activity of ∼50% cells within 4 min. AZD5363 also blocked spontaneous bursts in mutant neurons faster than BKM120 (**Figures 6P–R**). Thus, acute regulation of either PI3K or AKT activity directly suppressed *Pik3ca*^{E545K}-driven epileptiform neuronal activity.

In contrast, acute administration of the MTOR inhibitor RAD001 (everolimus) (Krueger et al., 2010; Cho, 2011) showed no overt effect on the mutant RMP (pre-RAD001$_{CA1}$: −59 ± 3.55 mV, post-RAD001$_{CA1}$: −55.6 ± 2.04 mV), tonic or burst firing patterns, frequencies, average PPS, burst duration, inter-burst interval and rheobase current (**Figures 7A–H**). This was despite western blot confirmation that acute treatment of forebrain slices with RAD001 modulated direct downstream targets of MTOR (**Figures 7I–K**). In summary, our study demonstrates that neuronal hyperactivity caused by *Pik3ca* gain-of-function mutation is based on multiple intrinsic electrophysiological characteristics that are acutely modifiable by downregulating PI3K and AKT activity, but not MTOR.

DISCUSSION

Activating mutations in the PI3K-AKT-MTOR pathway commonly cause cortical malformations and pediatric intractable epilepsy (Dobyns and Mirzaa, 2019; Kim and Lee, 2019); yet the underlying mechanisms remain largely undefined. MTOR overactivation and chronic post-transcriptional mechanisms have been widely emphasized as central to these phenotypes (Cho, 2011; Berdichevsky et al., 2013; Meng et al., 2013; Cardamone et al., 2014; Kim and Lee, 2019). However, we have shown that dysmorphology caused by activating *Pik3ca* mutations is distinct from that resulting from MTOR overactivation (Roy et al., 2015). Here we wanted to address if epilepsy mechanisms are also distinct. Using our *Nestin-cre;Pik3ca*^{E545K} model, we establish that Pik3ca-dependent neuronal hyperactivation in hippocampal pyramidal neurons is primarily driven by intrinsic neuronal mechanisms, independent of synaptic inputs. Acute attenuation of seizure activity by inhibiting AKT but not MTOR also reveals a previously unknown role of PI3K signaling in neuronal homeostasis. The

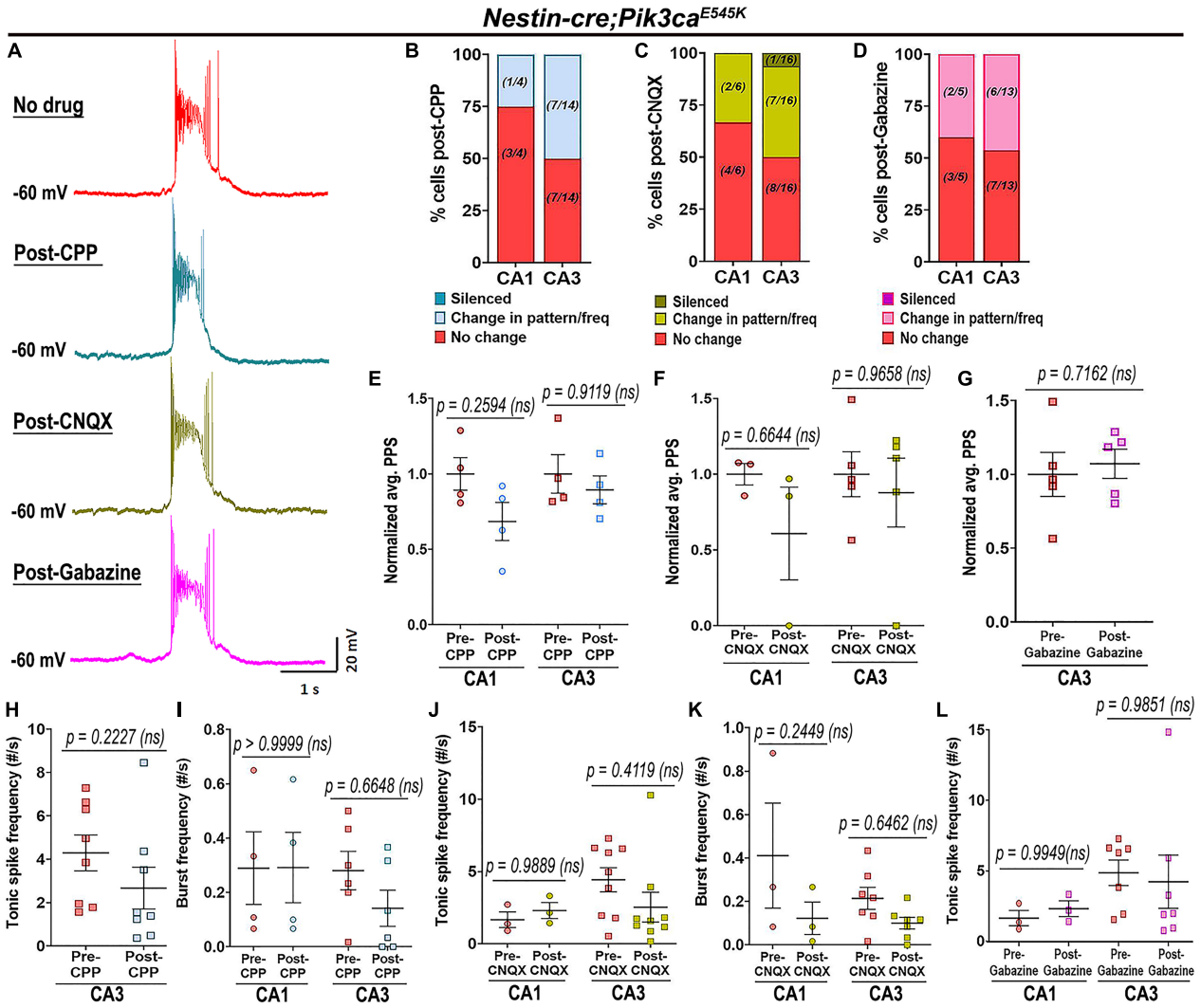

FIGURE 4 | Pik3ca-related epileptiform activity is not dependent on glutamatergic or GABAergic inputs. **(A)** Representative spontaneous mutant trace and traces of the same cell post-treatment with glutamatergic receptor antagonists (CPP, CNQX) and with GABA antagonist gabazine showed no significant change in firing pattern. **(B–D)** Large proportion of mutant cells remained unaffected after being blocked from external glutamatergic or GABAergic inputs. **(E–L)** No significant differences in normalized plateau potential shift (PPS; CPP: $F = 3.391$, df = 12; CNQX: $F = 1.432$, df = 12; Gabazine: $t = 0.3904$, df = 4) or in tonic (CPP: $t = 1.876$, df = 7; CNQX: $F = 0.2766$, df = 20; Gabazine: $F = 0.0001130$, df = 16) and burst frequencies (CPP: $F = 0.5140$, df = 16; CNQX: $F = 5.218$, df = 16) were observed before and after administration of channel blockers. Data is represented as % bar graphs and mean ± SEM scatter plots; differences were considered significant at $p < 0.05$; ns, not significant. Scale bar: 1 s, 20 mV **(A)**.

very short time of action implicates post-translational versus -transcriptional mechanisms.

Epileptiform activity is typically marked by increased tonic depolarizations and/or quasiperiodic bursts, mediated by intrinsic membrane properties, ephaptic or synaptic/circuit-level interactions (Dudek et al., 1998; McCormick and Contreras, 2001). We confirmed enhanced interictal spike frequency and diverse, synchronized epileptiform spike patterns in the mutant brains *in vivo*, predominantly in the hippocampus. This is consistent with studies of *PIK3CA* variants in brain tumors and mouse models with patient-related *Pik3r2* mutations, which are less common causes of intractable epilepsy (Shi et al., 2020; Yu et al., 2020). Our *ex vivo* analyses using acute brain slices revealed intracellular correlates of epileptiform activity and enhanced firing frequencies in the mutant hippocampal pyramidal neurons. Relative to controls, *Pik3ca*^{E545K} neurons exhibited significantly higher proportions of bursting cells and higher heterogeneity in burst patterns, including burst clusters and PDSs. A prior study showed that human neurons from surgically resected neocortical samples of pediatric patients with FCD exhibited remarkably similar burst characteristics (Marcuccilli et al., 2010). These samples were not genotyped; however, since most cases of FCD and epilepsy result from variants in PI3K pathway genes (Mirzaa et al., 2018), such cross-species phenotypic correlation is remarkable and emphasizes the clinical relevance of our mouse model.

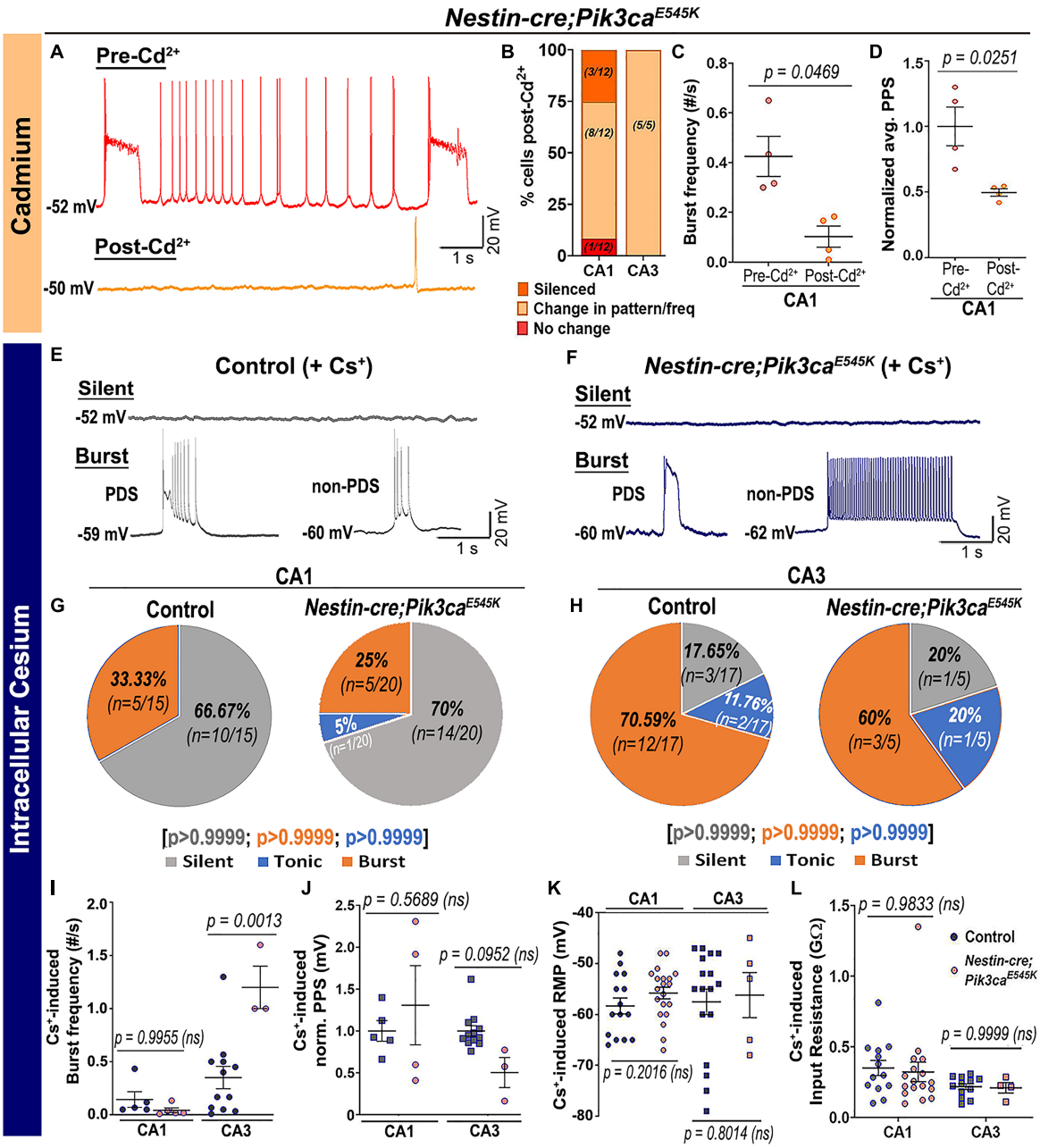

FIGURE 5 | Pik3ca-related burst characteristics are dependent on cell-intrinsic calcium and potassium channel regulation. **(A–D)** Blocking calcium channels by extracellular cadmium (Cd^{2+}) significantly altered the intrinsic bursting pattern of mutant neurons including burst frequency ($t = 3.267$, df = 3) and PPS ($t = 4.172$, df = 3). **(E–H)** Representative traces and respective pie charts show types of cellular activity in control and mutant CA1 and CA3 neurons after administering cesium intracellularly. In response to cesium, tonic firing cells were significantly reduced and original differences in CA1 and CA3 cell proportions between control and mutant were normalized. **(I)** Cs^{+}-induced burst frequency was significantly higher in mutant CA3 than those in respective controls ($F = 26.31$, df = 21); unlike normal spontaneous state, no such difference was observed in CA1. **(J–L)** Intracellular cesium lowered the spontaneously enhanced mutant PPS in CA1 to control levels ($F = 4.003$, df = 20), while having no effect on RMP (CA1: $t = 1.308$, df = 27.32; CA3: $t = 0.2616$, df = 6.816) or input resistance ($F = 2.936$, df = 42) in both control and mutant neurons. Data is represented as pie charts, % bar graphs and mean ± SEM scatter plots; differences were considered significant at $p < 0.05$; ns, not significant. Scale bars: 1 s, 20 mV **(A,E,F)**.

The PI3K-AKT-MTOR pathway is known to influence synaptogenesis and neuronal plasticity (Sanchez-Alegria et al., 2018). For example, neocortical samples from patient and mouse models with *TSC* mutations exhibit synaptic input-mediated epileptogenic hyperexcitability (Wang et al., 2007). However, blocking glutamatergic (NMDA and non-NMDA) or GABAergic synaptic inputs in our mutant brain slices showed no significant effect on the neuronal activity. Thus, our data demonstrate

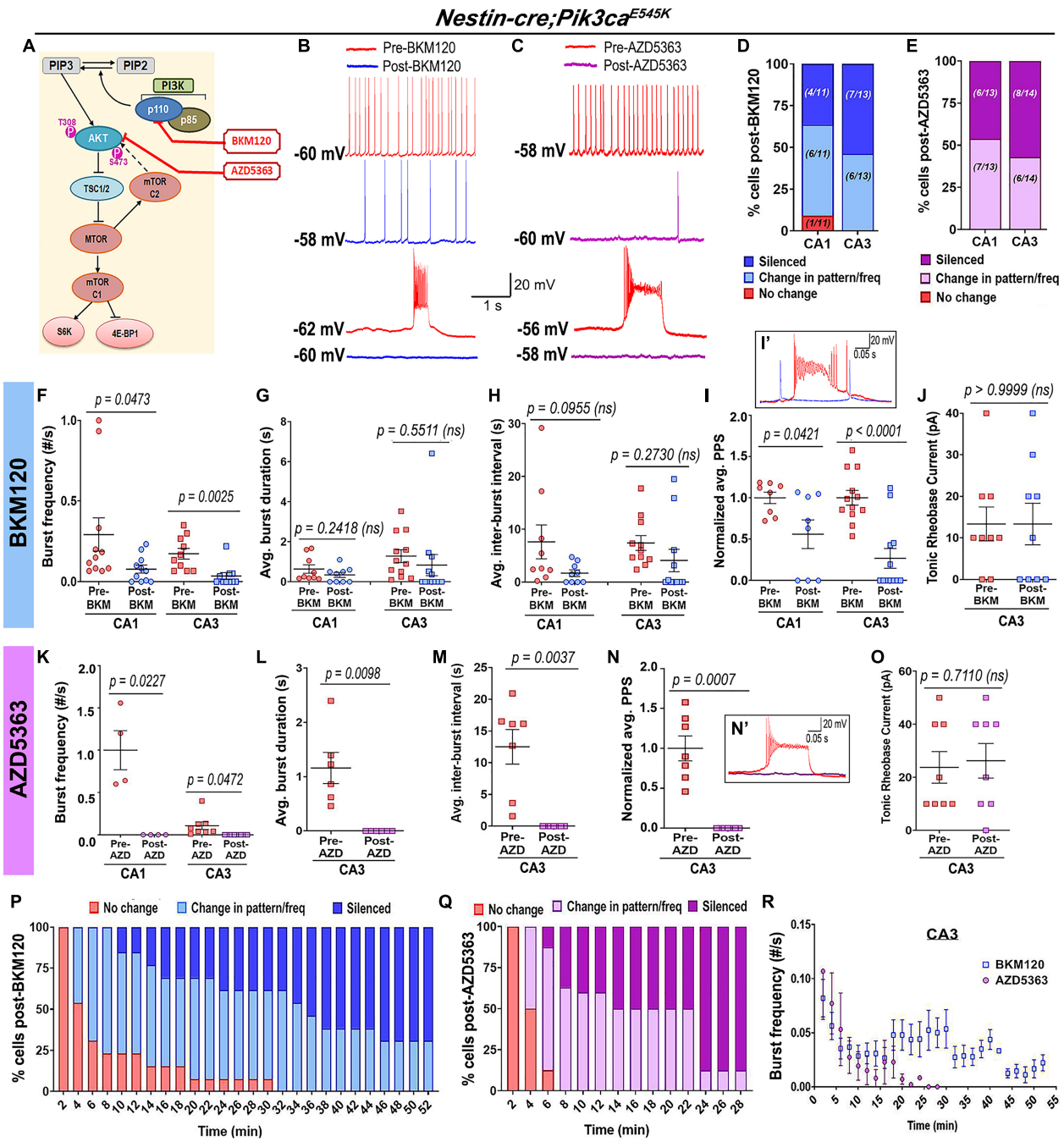

FIGURE 6 | Acute inhibition of Pik3ca or AKT suppresses hyperactivity in mutant neurons. **(A)** Schematic of simplified PI3K-AKT-MTOR pathway, marking targets of action for BKM120, AZD5363, and RAD001. Representative traces demonstrate differential action of BKM120 **(B)** and AZD5363 **(C)** on *Nestin-cre;Pik3ca*^{E545K} hippocampal neurons, ranging from being unaffected to change in frequency/pattern to silencing, as quantitated, respectively, in panels **(D,E)**. **(F–J)** Acute BKM120 treatment in the mutant neurons significantly reduced burst frequency (F = 8.937, df = 38) and PPS (F = 24.39, df = 36) in both CA1 and CA3; but did not significantly affect the average burst duration (t = 1.073, df = 4), inter-burst interval (t = 0.4023, df = 4) or rheobase current (t = 1.000, df = 4). **(K–O)** Acute AKT inhibition in mutant slices by AZD5363 significantly reduced burst frequency (F = 43.50, df = 20), PPS (t = 6.386, df = 6), average burst duration (t = 4.052, df = 5) and inter-burst interval (t = 4.597, df = 6), largely by suppressing bursts or silencing the cells. AZD5363 had no effect on the mutant rheobase current (t = 0.3859, df = 7). **(I',N')** Insets show activity traces of mutant bursting cell before (red) and after BKM120 (blue) or AZD5363 (pink) administration. Plots marked percentage of mutant CA3 "bursting" cells undergoing changes as a function of time, in response to acute administration of BKM120 **(P)** and AZD5363 **(Q)**. **(R)** Mutant plateau frequency significantly dropped as a function of time, where 0 min marked the time of administration of BKM120/AZD5363 onto the brain slice. Data is represented as % bar graphs and mean ± SEM scatter plots; differences were considered significant at $p < 0.05$; ns, not significant. Each pair of pre-drug (spontaneous recording) and post-drug values (from final 5 min recording) were obtained from the same cell **(F–O)**. Scale bars: 1 s, 20 mV **(B,C)**; 0.05 s, 20 mV **(I',N')**.

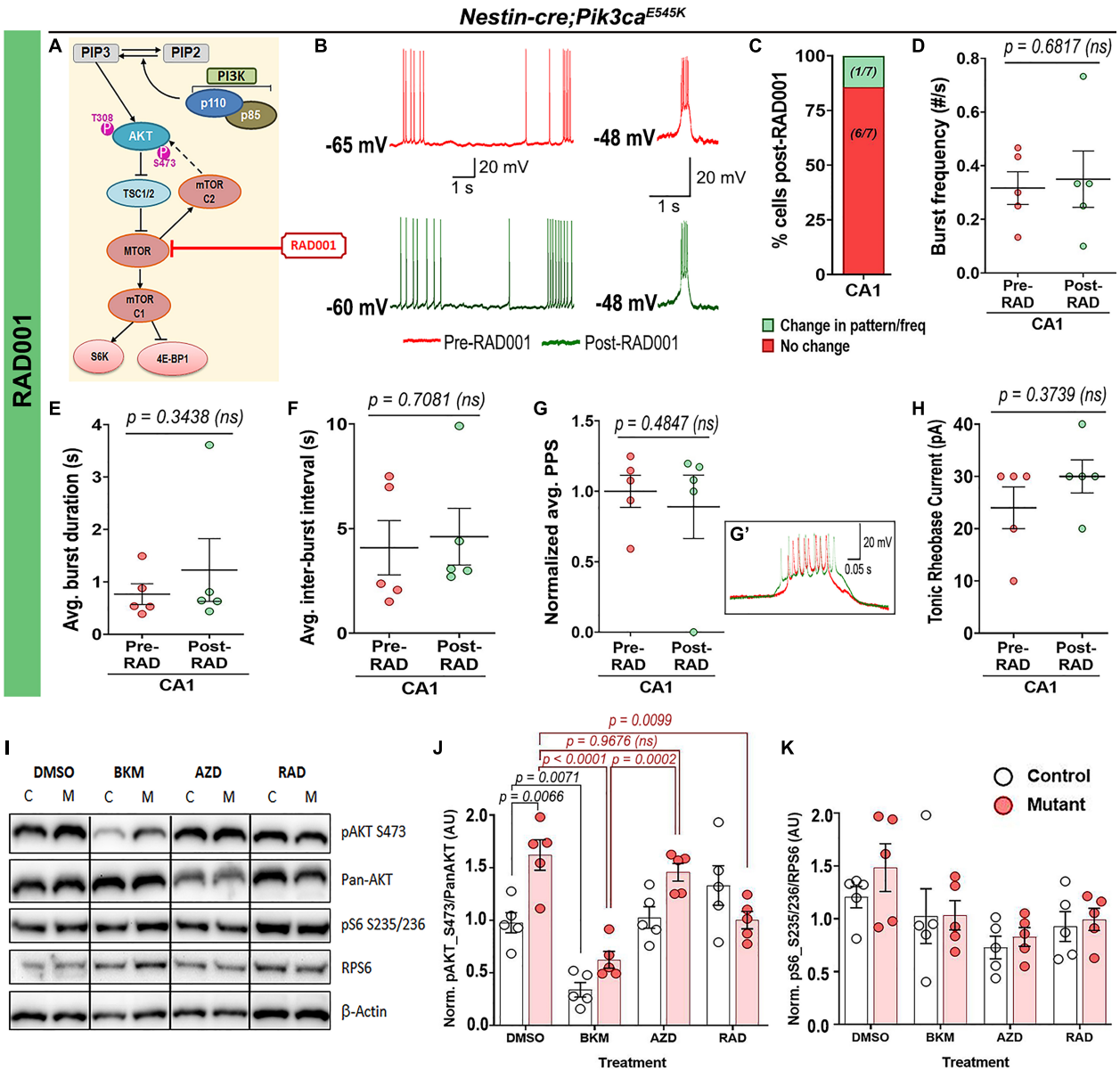

FIGURE 7 | Acute treatment with RAD001 has no overt effect on mutant neuronal physiological properties. **(A)** Schematic of simplified PI3K-AKT-MTOR pathway, marking target of action for RAD001. Representative traces demonstrate action of RAD001 **(B)** on *Nestin-cre;Pik3ca*^{E545K} hippocampal neurons, ranging from being unaffected to change in frequency/pattern to silencing, as quantitated, respectively, in panel **(C)**. **(D–H)** Acute RAD001 treatment had no overt effect on the mutant burst frequency (t = 0.4414, df = 4), average burst duration (t = 1.073, df = 4), inter-burst interval (t = 0.4023, df = 4), rheobase current (t = 1.000, df = 4) or PPS (t = 0.7692, df = 4). **(I)** Representative Western blots bands of pAKT_S473, pan-AKT, pS6-S235/236 and RPS6 (total S6) are demonstrated across different treatment (DMSO, BKM120, AZD5363, and RAD001). **(J,K)** Quantifications of normalized ratios of phosphoproteins over total proteins showed significant reduction of pAKT_S473 in response to acute BKM120 and RAD001 treatment but not post-AZD5363 (F = 22.98, df = 32); pS6_S235/236 in mutant had a decreasing trend in response to all pathway drugs (F = 4.485, df = 32). Data is represented as mean ± SEM scatter plots and bar graphs; differences were considered significant at $p < 0.05$; ns, not significant. Each pair of pre-RAD (spontaneous recording) and post-RAD values (from final 5 min recording) were obtained from the same cell **(D–H)**. Scale bars: 1 s, 20 mV **(B)**; 0.05 s, 20 mV **(G')**.

that altered synaptic interactions are not primary mediators of *Pik3ca*^{E545K}-driven acute hippocampal neuronal hyperactivation. We acknowledge, however, that altered neuronal circuitry are likely contributors to chronic mechanisms driving Pik3ca-mediated epilepsy. Regardless, for the first time, our data indicates that acute seizure mechanisms are distinct and dependent on the location of the mutant protein within the PI3K-AKT-MTOR pathway. This conclusion is further supported by a recent study of a mouse model of MTOR activation, where neuronal hyperexcitation was found be driven by non-cell autonomous mechanisms and not associated with altered intrinsic properties (Koh et al., 2021). Significant reduction of

burst-generating cells, burst frequency and PPS by blocking voltage-dependent calcium or potassium channels indicate that *Pik3ca*^{E545K}-driven hyperactivity is predominantly mediated by multiple altered cell-intrinsic properties. Yet, some cell-intrinsic properties, such as burst frequencies, PPS and time constants, are distinctly different between mutant CA1 and CA3 neurons. Since all neurons do not react uniformly to either pathway overactivation or Cd^{2+}/Cs^{+}-dependent channel inhibition, current anti-seizure drugs that typically target single ion channels cannot address the heterogeneous dysregulation, thus potentially explaining epileptic intractability in this patient population. It is intriguing to note that intercellular signaling heterogeneity involving the PI3K-AKT-MTOR pathway was also reported by a recent quantitative study that highlighted its potential relevance to human disorders, such as insulin resistance (Norris et al., 2021).

PI3K-AKT-MTOR inhibitors developed to treat cancer potentially represent novel anti-seizure therapeutics (Maira et al., 2012; Cardamone et al., 2014; Lindhurst et al., 2015; Venot et al., 2018; Zou et al., 2020; Forde et al., 2021). Rapamycin and its analogs, that are currently in clinical use to treat epilepsy in TSC patients, curbed epileptiform activity in mouse models harboring *TSC1/2*, *RHEB, MTOR*, or *PTEN* mutations when administered long-term (>7-day) (Curatolo and Moavero, 2013; Lasarge and Danzer, 2014; Crino, 2016; Kim and Lee, 2019; Stafstrom, 2019; Hsieh et al., 2020). In contrast, we show acute inhibition of mutant neuronal hyperactivity by BKM120 at cellular level, confirming our previous *in vivo* findings (Roy et al., 2015). We also demonstrate that acute AKT inhibition with AZD5363 has similar effects. This first preclinical study using AZD5363 shows that acute Pik3ca-driven seizure mechanism is predominantly AKT-dependent, limiting roles for other PI3K targets. Intriguingly, rapamycin analog RAD001 had minimal acute effect in our model, yet western analyses demonstrated pathway inhibition with RAD001 was similar to that seen with the other pathway drugs we assessed. While elevated MTOR activity is known to be epileptogenic (Crino, 2016; Kim and Lee, 2019; Koh et al., 2021), our data suggest that alternate PI3K-AKT targets acutely regulate neuronal hyperactivation in PIK3CA-driven epilepsy.

Our study establishes an important foundation to determine active pathway-driven cellular mechanisms in Pik3ca-related epilepsy. The mechanisms are clearly complex. Additional studies will define differential involvement of specific subtypes of Ca^{2+} and K^{+} channels in each type of neuron. However, as a baseline, we have identified specific *ex vivo* parameters to assess the plethora of additional available PI3K pathway inhibitors, to facilitate the development of new molecularly rational therapeutic interventions for intractable epilepsy.

MATERIALS AND METHODS

Mice

The following mouse lines were used: *Nestin-cre* (Jackson Labs, Bar Harbor, ME, United States; Stock #003771, RRID: IMSR_JAX:003771), conditional *Pik3ca*^{E545K} knock-in (Robinson et al., 2012). *Nestin-cre* and *Pik3ca*$^{E545K/+}$ mouse lines were maintained in C57BL/6 and FVB backgrounds, respectively; the progeny mice are of mixed background. The mutant activating *Pik3ca*^{E545K} allele is heterozygous, as in human patients. We have designated *Nestin-cre;Pik3ca*$^{E545K/+}$ conditional mutant mice as "*Pik3ca* mutants" or "mutants" throughout the manuscript.

All mice were housed in Optimice cages with aspen bedding at the Seattle Children's Research Institute's specific pathogen-free (SPF) vivarium facility (light "ON": 6 a.m.–8 p.m.). Noon of the day of vaginal plug was designated as embryonic day 0.5 (E0.5). The day of birth was designated as postnatal day 0 (P0). Genotyping by PCR was done using separate sets of primers for the *Cre* coding region and the *Pik3ca*^{E545K} allele, as previously described (Roy et al., 2015). All mouse procedures were approved and conducted in accordance with the guidelines laid down by the Institutional Animal Care and Use Committees (IACUC) of Seattle Children's Research Institute, Seattle, WA, United States. ARRIVE guidelines have been followed for reporting work involving animal research.

In vivo Electrophysiology

Five control and six *Nestin-cre;Pik3ca*^{E545K} mutant mice (age: ∼P70) were used for *in vivo* regular and depth-electrode electrophysiology experiments. We saw no sex-dependent data correlation (Roy et al., 2015).

Electrode Implantation Surgery

Mice underwent survival surgery to implant ECoG, EMG, and hippocampal depth electrodes under isoflurane anesthesia using similar procedures as reported in our prior work (Roy et al., 2015; Bolea et al., 2019). The ECoG electrodes consisted of silver wire (diameter: 130 μm bare; 180 μm coated) attached to micro-screws. The ECoG electrodes were implanted bilaterally through small cranial burr holes above the somatosensory cortices. A similar reference electrode was placed above the cerebellum following the same procedure. The depth electrodes were made of 2 fine twisted tungsten wires (30 μm nylon coated, California fine wire) and implanted in the hippocampal CA1 region (coordinates: −2.0 mm anteroposterior, 1.5 mm mediolateral, 1.9 mm dorsoventral in reference to bregma) to record LFP. All electrodes were connected to interface connector and fixed to the skull with dental cement (Lang Dental Manufacturing Co., Inc., Wheeling, IL, United States). Mice were allowed to recover from surgery for 2–3 days.

Video, Electroencephalography, and Local Field Potential Recording

Simultaneous video-EEG-LFP recordings were collected from conscious mice on PowerLab 8/35 and 16/30 data acquisition units, using LabChart 7.3.3 software (AD Instruments, Colorado Spring, CO, United States). ∼6 h of baseline ECoG tracings were visually reviewed for the presence of spontaneous epileptiform events, as previously studied (Kalume, 2013; Liautard et al., 2013; Roy et al., 2015). All bioelectrical signals were acquired at a 20 KHz sampling rate. The ECoG signals were processed

with a 1–70 Hz bandpass filter and the LFP signal with a 5 Hz high-pass filter. Interictal spikes were identified as transient, clearly distinguished from background activity, with pointed peak and slow wave. Myoclonic seizures were identified as shock-like muscular jerks on video, associated with a spike or polyspike-wave complex on EEG. Power spectral analysis and visual inspection of the data were conducted to characterize the EEG activity in different frequency bands and identify epileptiform events on the ECoG and local CA1 field recordings. The different frequency bands used in the study (Delta: 0.5–5 Hz, Theta: 5–10 Hz, Gamma: 20–30 Hz) are based on our previously published parameters (Hughes, 2008; Kalume et al., 2015).

Ex vivo Electrophysiology

Slice Preparation

Postnatal (P16–20) pups were anesthetized briefly in a closed chamber by administering isoflurane (5% flow rate) or CO_2 (constant flow rate: 10–30% of chamber vol/min); then perfused transcardially with ice-cold low Na^+-buffer ("slicing solution," which included the following: 252 mM sucrose, 2 mM KCl, 2 mM $MgCl_2$, 2.6 mM $CaCl_2$, 1.2 mM NaH_2PO_4, 26 mM $NaHCO_3$, and 15 mM glucose, with the pH adjusted to 7.4 and the osmolarity to 310 ± 5 mOsm). Brain was dissected out by separating the head and cutting along the skull sutures using fine scissors and forceps. The forebrain was isolated in ice-cold, oxygenated (95% O_2, 5% CO_2) slicing solution. A slanted (∼15° from vertical) agar block was secured on a specimen tray as a support for the brain during slicing. The isolated forebrain was oriented for horizontal slicing, glued to the specimen tray with cyanoacrylate and placed in the vibratome for slicing. Once the hippocampus became visible, acute horizontal slices of ∼250 μm thickness were collected and immediately incubated in the same slicing solution, maintained in a warm bath (28 ± 0.5°C) for recovery. After 30 min, they were transferred into regular artificial cerebrospinal fluid (aCSF), composed of the same components as slicing solution except for the replacement of sucrose with 126 mM NaCl. Slices were then kept at room temperature, continuously superfused with oxygenated aCSF, until recording. Given that *Pik3ca*^{E545K} mutant is megalencephalic, a greater number of hippocampal/forebrain sections were obtained. However, care was taken so that the dorso-ventral plane(s) used for recording was always comparable between control and mutant slices. No randomization was used. Tissue collection was not performed blind since the mice were subjected to genotyping and drug administration.

Recording

Slices were transferred into a recording chamber, continuously superfused with oxygenated aCSF, for *ex vivo* whole-cell recordings. The pClamp software suite (Molecular Devices; RRID: SCR_011323) was used for data acquisition and analysis. Signals were amplified (MultiClamp 700A, Axon Instruments, Molecular Devices, United States), digitized (D1322A, Axon Instruments, Molecular Devices, United States), and stored in a computer for post-hoc analysis. Horizontal hemi-forebrain slices with prominent hippocampus were used for intracellular whole-cell visual patch-clamp experiments. Slices transferred to the recording chamber were maintained at 30–34°C, constantly superfused with oxygenated aCSF Borosilicate glass capillaries/pipettes for patch-clamp recording had electrode resistance (R_e) optimally kept around 5–8 MΩ, after being filled with internal solution containing the following: potassium gluconate (∼132 mM), KCl (5 mM), HEPES (10 mM), EGTA (5 mM), $CaCl_2.H_2O$ (0.5 mM), $MgCl_2$ (2 mM), disodium phosphocreatine (5 mM), disodium-ATP (4 mM), trisodium-GTP (0.5 mM), EGTA (5 mM). Cells were visualized under brightfield optics using the 40X water-immersion objective of an upright microscope (Olympus, BX51WI). The patch electrode was advanced toward the target cells by a micromanipulator (MP-225, Sutter Instrument Company, United States) and 1 GΩ seal was established, typically by a small negative pressure, with the membrane ruptured by gentle suction and/or zap pulses. Whole-cell patch-clamp recording was performed from cell bodies of pyramidal neurons of hippocampal CA1 and CA3, respectively. Following intracellular recording protocols were also used:

(i) Spontaneous cell-attached gapfree recordings in current (I)-clamp: cells were typically tested at resting conditions (without current injection) unless noted otherwise.
(ii) Evoked I-clamp steps protocol: current steps start at −50 pA, incremental 10 pA, duration; 300 ms; 15 steps (−50 to +90 pA) were recorded across experiments.

For the *ex vivo* patch-clamp recording of CA1 and CA3 pyramidal neurons, we used on average 1–2 slices per mouse per genotype and recorded >1 cell per slice. We were meticulous in using similar planar positions of brain slices for our experiments. It is possible there were unconscious sampling biases based on the neuronal position within the CA1 or CA3 pyramidal layer per brain slice.

Acute Chemical Assays

Channel Blockers

Chemicals inhibiting specific ion channels were introduced in the bath/recording buffer to compare different physiological components possibly contributing to the neuronal hyperactivity. To block all fast-synaptic excitatory transmission, 3-[(±)2-carboxypiperazin-4yl] propyl-1-phosphate (CPP, NMDA receptor antagonist, 20 μM; Tocris Bioscience, United Kingdom) and 6-cyano-7-nitroquinoxaline-2,3-dione [CNQX, AMPA/kainate (non-NMDA) receptor antagonist, 20 μM, diluted in DMSO; Alomone Labs, Israel] were introduced in the bath. SR95531 hydrobromide or Gabazine ($GABA_A$ receptor antagonist, 10 μM, Tocris Bioscience, United Kingdom) was used to block inhibitory synaptic transmission. Cd^{2+} ($CdCl_2$, 100 μM; Sigma-Aldrich, United States) was used to depress synaptic transmission and block inward calcium-selective current, isolating the outward K^+ current. To block voltage-dependent K^+ channels, intracellular administration of cesium was done by replacing potassium gluconate with cesium gluconate in the internal solution while maintaining the same osmolarity.

Phosphoinositide-3-Kinase Pathway Drugs

Phosphoinositide-3-kinase pathway inhibitors dissolved in 100% DMSO were added to the circulating recording buffer, thus getting acutely administered in the entire brain slice that is being recorded. For protein analyses, these were added at identical concentration to the brain slices incubated in oxygenated aCSF for ∼1 h. The following inhibitors were used *ex vivo*: pan-PI3K inhibitor BKM120 (Buparlisib; Novartis, Switzerland; working concentration: 3.5 μM); pan-AKT inhibitor AZD5363 (Capivasertib; Selleckchem, United States; working concentration: 0.5 μM); MTOR inhibitor RAD001 (Everolimus, Chem Express Cat# 159351-69-6; working concentration: 0.52 μM). To determine the AZD5363 dose needed to inhibit the AKT isoforms and phosphorylation of AKT in the acute brain slices of our mouse model, we followed the datasheet from https://www.selleckchem.com/products/azd5363.html. A survey of literature demonstrates multiple electrophysiological parameters in wild-type and various mutant (including *TSC2*+/-) mouse brain slice assays with acute drug exposures from 10 nM through 1 μM. The drug concentrations we chose for our study are well within this range (Tang et al., 2002; Ehninger et al., 2008; Olde Engberink et al., 2017; Artinian et al., 2019).

Western Blotting

Horizontal forebrain slices from five control and five mutant mice were obtained and recovered in oxygenated aCSF as detailed above. Slices showing nice hippocampal morphology were selected, treated for 1 h with DMSO, BKM120, AZD5363, and RAD001, respectively, in the same concentrations used for recording. The treated slices were then flash-frozen in liquid nitrogen and stored at −80°C for post-processing. These brain slices were lysed in NP-40 lysis buffer [150 mM NaCl, 50 mM Tris (pH 7.4), 1% NP-40, 10 mM NaF, 2 mM sodium orthovanadate + protease/phosphatase inhibitor cocktails (Sigma, United States)]. Samples were normalized to equal protein concentrations (0.333 mg/ml) using Pierce BCA protein assay (Thermo Fisher Scientific, United States). Standards were made through serial dilutions of 10 mg/ml BSA. Samples were diluted into a final concentration of 1x Laemmli sample buffer and boiled at 95°C for 10 mins. 7.5% 10-well gels were prepared, and samples were run at 120 V for 1.5 h. Gels were transferred onto polyvinylidene difluoride (Millipore) membranes and run either overnight at 25 V or for 2 h at 60 V. Membranes were blocked in 4% milk in TBST (0.05 M Tris, 0.15 M NaCl, pH 7.2, 0.1% (v/v) Tween20) for 1 h at room temperature, and primary antibodies were applied overnight at 4°C in blocking medium. Primary antibodies for western blots were diluted as follows: rabbit anti-Phospho-AKT Ser473 (D9E) (Cell Signaling Technology, United States; RRID: AB_2797780; 1:2,000), mouse anti-Pan-AKT (40D4) (Cell Signaling Technology, United States; Cat# 2920; 1:2,000), rabbit anti-Phospho-S6 Ribosomal Protein Ser235/236 (Cell Signaling Technology, United States; RRID: AB_2721245 , 1:2,000), mouse anti-S6 Ribosomal Protein (54D2) (Cell Signaling Technology, United States; RRID: AB_2238583 , 1:1,000), rabbit anti-beta(β)-Actin (GeneTex, United States; RRID: AB_1949572 , 1:10,000). After washing and probing, respectively, with goat anti-rabbit (RRID: AB_2313567) and anti-mouse (RRID: AB_10015289) horseradish peroxidase (HRP)-conjugated secondary antibodies (1:10,000; Jackson ImmunoResearch Labs, United States), blots were imaged using Femto chemiluminescent detection reagents (Thermo Fisher Scientific, United States; Cat# 34095) in a FluorChem R western blot imaging system (ProteinSimple, Bio-Techne, United States). 8-bit images were used as a representative western blot. 16-bit images were used to quantify the intensity of each band using ImageJ v1.53. Regions of interest were drawn in each sample's lane. After quantifying the lane in a histogram, the peak representing the band of interest was isolated and the area of the region was measured as the band's quantification.

Quantitative and Statistical Analyses

Number of mice used was consistent with previous experiments completed and published by us and other investigators. In whole-cell patch-clamp recording, PPS was calculated by subtracting the baseline potential from the highest plateau/burst potential in a paroxysmal depolarizing event. Burst duration and inter-burst interval were measured as shown in **Figure 2** and averaged across multiple bursts per cell. Burst frequency was calculated as number of burst episodes per time interval. Input resistance was measured from evoked current-clamp recordings by dividing the voltage difference (measured at −10 to −30 pA I-steps) by the current interval of 20 pA. The decay membrane time constant was obtained by recording the membrane response to 20 pA hyperpolarizing current pulses (300 ms duration, 1 Hz) and fitting the response to a single exponential curve. We chose 20 pA of hyperpolarizing current because such a current intensity did not produce sag. Evoked spike frequencies and rheobase current were calculated exclusively from tonic-firing cells. Burst threshold current was calculated from burst-generating cells as the first current step that induced burst. Whole-cell electrophysiological analyses were performed using Clampfit 10.7 and 11 (pClamp, Molecular Devices, United States). For Western Blots, each band intensity was recalculated relative to its respective b-actin band intensity, and then normalized across average intensity per protein lane. Normalized ratios of phosphoproteins over total proteins were thereafter obtained.

Statistical significance was assessed using 2-tailed unpaired *t*-tests with Welch's correction (EEG power analyses, RMP, burst duration, inter-burst interval, Cd^{2+} data), 2-tailed paired *t*-tests (rheobase current, drug-treated analyses) and ANOVA followed by Tukey post-tests (EEG interictal spike frequency, whole-cell tonic spike and burst frequencies, cell proportions, PPS, evoked spike frequency, time constant; Western blots). Normal distribution was assumed for data analyses, as required. For EEG-ECoG-LFP experiments, statistical data analysis was performed in Labchart 8.2 software (AD Instruments) and Igor Pro 6.37 (WaveMetrics Inc., United States); final graphs were made in GraphPad Prism v7.0 (GraphPad Software Inc., San Diego, CA, United States). For the remaining data, statistical analyses and graph plotting were done using GraphPad Prism v7.0 and Microsoft Excel. Differences were considered significant at $p < 0.05$.

DATA AVAILABILITY STATEMENT

The original contributions presented in the study are included in the article/supplementary material, further inquiries can be directed to the corresponding authors.

ETHICS STATEMENT

The animal study was reviewed and approved by Institutional Animal Care and Use Committees (IACUC) of Seattle Children's Research Institute, Seattle, WA, United States.

AUTHOR CONTRIBUTIONS

AR, FK, J-MR, and KJM contributed to the study conception and design and to the overall data interpretation. AR, VH, AMB, DTW, and FK contributed to the data collection. AR and FK contributed to *ex vivo* and *in vivo* data analyses, respectively. DTW and SEPS contributed to western blot data analysis and interpretation. AR, SEPS, FK, and KJM provided the funding resources. AR wrote the first draft of the manuscript and others commented on previous versions of the manuscript. All authors read and approved the final manuscript.

FUNDING

This work was funded by the NIH grants 1R01NS099027 (KJM), R01MH113545 (SEPS), R01NS102796 (FK), CURE Sleep and Epilepsy Grant (FK), Ramalingaswami Re-entry Fellowship from the DBT (Department of Biotechnology, Government of India) (AR), and intramural funding from the Jawaharlal Nehru Centre for Advanced Scientific Research (AR).

ACKNOWLEDGMENTS

We thank Suzanne J. Baker for gifts of mouse lines (*Nestin-cre* and *Pik3ca*^{E545K}); Leon Murphy (Novartis) for BKM120; Rory M. Murphy, Amanda P. Tran Hartman, Nikhil Sahai, and Jiyun Ryu for technical assistance; Aguan D. Wei and Paul Wakenight for discussions.

REFERENCES

Artinian, J., Jordan, A., Khlaifia, A., Honore, E., La Fontaine, A., Racine, A. S., et al. (2019). Regulation of hippocampal memory by mTORC1 in somatostatin interneurons. *J. Neurosci.* 39, 8439–8456. doi: 10.1523/JNEUROSCI.0728-19.2019

Barker-Haliski, M., and White, H. S. (2019). Validated animal models for antiseizure drug (ASD) discovery: advantages and potential pitfalls in ASD screening. *Neuropharmacology* 167:107750. doi: 10.1016/j.neuropharm.2019.107750

Bast, T., Ramantani, G., Seitz, A., and Rating, D. (2006). Focal cortical dysplasia: prevalence, clinical presentation and epilepsy in children and adults. *Acta Neurol. Scand.* 113, 72–81. doi: 10.1111/j.1600-0404.2005.00555.x

Berdichevsky, Y., Dryer, A. M., Saponjian, Y., Mahoney, M. M., Pimentel, C. A., Lucini, C. A., et al. (2013). PI3K-Akt signaling activates mTOR-mediated epileptogenesis in organotypic hippocampal culture model of post-traumatic epilepsy. *J. Neurosci.* 33, 9056–9067. doi: 10.1523/JNEUROSCI.3870-12.2013

Blumcke, I., Thom, M., Aronica, E., Armstrong, D. D., Vinters, H. V., Palmini, A., et al. (2011). The clinicopathologic spectrum of focal cortical dysplasias: a consensus classification proposed by an ad hoc task force of the ILAE diagnostic methods commission. *Epilepsia* 52, 158–174. doi: 10.1111/j.1528-1167.2010.02777.x

Bolea, I., Gella, A., Sanz, E., Prada-Dacasa, P., Menardy, F., Bard, A. M., et al. (2019). Defined neuronal populations drive fatal phenotype in a mouse model of Leigh syndrome. *Elife* 8:e47163. doi: 10.7554/eLife.47163

Cardamone, M., Flanagan, D., Mowat, D., Kennedy, S. E., Chopra, M., and Lawson, J. A. (2014). Mammalian target of rapamycin inhibitors for intractable epilepsy and subependymal giant cell astrocytomas in tuberous sclerosis complex. *J. Pediatr.* 164, 1195–1200. doi: 10.1016/j.jpeds.2013.12.053

Chatzikonstantinou, A. (2014). Epilepsy and the hippocampus. *Front. Neurol. Neurosci.* 34:121–142. doi: 10.1159/000356435

Cho, C. H. (2011). Frontier of epilepsy research–mTOR signaling pathway. *Exp. Mol. Med.* 43, 231–274.

Crino, P. B. (2016). The mTOR signalling cascade: paving new roads to cure neurological disease. *Nat. Rev. Neurol.* 12, 379–392. doi: 10.1038/nrneurol.2016.81

Curatolo, P., and Moavero, R. (2013). mTOR inhibitors as a new therapeutic option for epilepsy. *Expert Rev. Neurother.* 13, 627–638. doi: 10.1586/ern.13.49

Davies, B. R., Greenwood, H., Dudley, P., Crafter, C., Yu, D. H., Zhang, J., et al. (2012). Preclinical pharmacology of AZD5363, an inhibitor of AKT: pharmacodynamics, antitumor activity, and correlation of monotherapy activity with genetic background. *Mol. Cancer Ther.* 11, 873–887. doi: 10.1158/1535-7163.MCT-11-0824-T

de Curtis, M., and Gnatkovsky, V. (2009). Reevaluating the mechanisms of focal ictogenesis: the role of low-voltage fast activity. *Epilepsia* 50, 2514–2525. doi: 10.1111/j.1528-1167.2009.02249.x

Dobyns, W. B., and Mirzaa, G. M. (2019). Megalencephaly syndromes associated with mutations of core components of the PI3K-AKT-MTOR pathway: PIK3CA, PIK3R2, AKT3, and MTOR. *Am. J. Med. Genet. C Semin. Med. Genet.* 181, 582–590. doi: 10.1002/ajmg.c.31736

Dudek, F. E., Yasumura, T., and Rash, J. E. (1998). 'Non-synaptic' mechanisms in seizures and epileptogenesis. *Cell Biol. Int.* 22, 793–805. doi: 10.1006/cbir.1999.0397

Ehninger, D., Han, S., Shilyansky, C., Zhou, Y., Li, W., Kwiatkowski, D. J., et al. (2008). Reversal of learning deficits in a Tsc2+/- mouse model of tuberous sclerosis. *Nat. Med.* 14, 843–848. doi: 10.1038/nm1788

Forde, K., Resta, N., Ranieri, C., Rea, D., Kubassova, O., Hinton, M., et al. (2021). Clinical experience with the AKT1 inhibitor miransertib in two children with PIK3CA-related overgrowth syndrome. *Orphanet J. Rare Dis.* 16:109. doi: 10.1186/s13023-021-01745-0

Hsieh, L. S., Wen, J. H., Nguyen, L. H., Zhang, L., Getz, S. A., Torres-Reveron, J., et al. (2020). Ectopic HCN4 expression drives mTOR-dependent epilepsy in mice. *Sci. Transl. Med.* 12:eabc1492. doi: 10.1126/scitranslmed.abc1492

Hughes, J. R. (2008). Gamma, fast, and ultrafast waves of the brain: their relationships with epilepsy and behavior. *Epilepsy Behav.* 13, 25–31. doi: 10.1016/j.yebeh.2008.01.011

Jansen, L. A., Mirzaa, G. M., Ishak, G. E., O'Roak, B. J., Hiatt, J. B., Roden, W. H., et al. (2015). PI3K/AKT pathway mutations cause a spectrum of brain malformations from megalencephaly to focal cortical dysplasia. *Brain* 138(Pt 6), 1613–1628. doi: 10.1093/brain/awv045

Jones, R. T., Barth, A. M., Ormiston, L. D., and Mody, I. (2015). Evolution of temporal and spectral dynamics of pathologic high-frequency oscillations (pHFOs) during epileptogenesis. *Epilepsia* 56, 1879–1889. doi: 10.1111/epi.13218

Kalume, F. (2013). Sudden unexpected death in Dravet syndrome: respiratory and other physiological dysfunctions. *Respir. Physiol. Neurobiol.* 189, 324–328. doi: 10.1016/j.resp.2013.06.026

Kalume, F., Oakley, J. C., Westenbroek, R. E., Gile, J., de la Iglesia, H. O., Scheuer, T., et al. (2015). Sleep impairment and reduced interneuron excitability in a

mouse model of Dravet Syndrome. *Neurobiol. Dis.* 77, 141–154. doi: 10.1016/j.nbd.2015.02.016

Kehne, J. H., Klein, B. D., Raeissi, S., and Sharma, S. (2017). The National Institute of Neurological Disorders and Stroke (NINDS) Epilepsy Therapy Screening Program (ETSP). *Neurochem. Res.* 42, 1894–1903. doi: 10.1007/s11064-017-2275-z

Kim, J. K., and Lee, J. H. (2019). Mechanistic target of rapamycin pathway in epileptic disorders. *J. Korean Neurosurg. Soc.* 62, 272–287. doi: 10.3340/jkns.2019.0027

Koh, H. Y., Jang, J., Ju, S. H., Kim, R., Cho, G. B., Kim, D. S., et al. (2021). Non-cell autonomous epileptogenesis in focal cortical dysplasia. *Ann. Neurol.* 90, 285–299. doi: 10.1002/ana.26149

Krueger, D. A., Care, M. M., Holland, K., Agricola, K., Tudor, C., Mangeshkar, P., et al. (2010). Everolimus for subependymal giant-cell astrocytomas in tuberous sclerosis. *N. Engl. J. Med.* 363, 1801–1811.

Kubista, H., Boehm, S., and Hotka, M. (2019). the paroxysmal depolarization shift: reconsidering its role in epilepsy, epileptogenesis and beyond. *Int. J. Mol. Sci.* 20:577. doi: 10.3390/ijms20030577

Lasarge, C. L., and Danzer, S. C. (2014). Mechanisms regulating neuronal excitability and seizure development following mTOR pathway hyperactivation. *Front. Mol. Neurosci.* 7:18. doi: 10.3389/fnmol.2014.00018

Lee, S. A., Spencer, D. D., and Spencer, S. S. (2000). Intracranial EEG seizure-onset patterns in neocortical epilepsy. *Epilepsia* 41, 297–307.

Lee, W. S., Baldassari, S., Chipaux, M., dle-Biassette, H. A., Stephenson, S. E. M., Maixner, W., et al. (2021). Gradient of brain mosaic RHEB variants causes a continuum of cortical dysplasia. *Ann. Clin. Transl. Neurol.* 8, 485–490. doi: 10.1002/acn3.51286

Liautard, C., Scalmani, P., Carriero, G., de Curtis, M., Franceschetti, S., and Mantegazza, M. (2013). Hippocampal hyperexcitability and specific epileptiform activity in a mouse model of Dravet syndrome. *Epilepsia* 54, 1251–1261. doi: 10.1111/epi.12213

Lindhurst, M. J., Yourick, M. R., Yu, Y., Savage, R. E., Ferrari, D., and Biesecker, L. G. (2015). Repression of AKT signaling by ARQ 092 in cells and tissues from patients with Proteus syndrome. *Sci. Rep.* 5:17162. doi: 10.1038/srep17162

Madsen, R. R. (2020). PI3K in stemness regulation: from development to cancer. *Biochem. Soc. Trans.* 48, 301–315. doi: 10.1042/bst20190778

Maira, S. M., Pecchi, S., Huang, A., Burger, M., Knapp, M., Sterker, D., et al. (2012). Identification and characterization of NVP-BKM120, an orally available pan-class I PI3-kinase inhibitor. *Mol. Cancer Ther.* 11, 317–328. doi: 10.1158/1535-7163.MCT-11-0474

Marcuccilli, C. J., Tryba, A. K., van Drongelen, W., Koch, H., Viemari, J. C., Pena-Ortega, F., et al. (2010). Neuronal bursting properties in focal and parafocal regions in pediatric neocortical epilepsy stratified by histology. *J. Clin. Neurophysiol.* 27, 387–397. doi: 10.1097/WNP.0b013e3181fe06d8

Mazumder, A. G., Patial, V., and Singh, D. (2019). Mycophenolate mofetil contributes to downregulation of the hippocampal interleukin type 2 and 1beta mediated PI3K/AKT/mTOR pathway hyperactivation and attenuates neurobehavioral comorbidities in a rat model of temporal lobe epilepsy. *Brain Behav. Immun.* 75, 84–93. doi: 10.1016/j.bbi.2018.09.020

McCormick, D. A., and Contreras, D. (2001). On the cellular and network bases of epileptic seizures. *Annu. Rev. Physiol.* 63, 815–846.

Meng, X. F., Yu, J. T., Song, J. H., Chi, S., and Tan, L. (2013). Role of the mTOR signaling pathway in epilepsy. *J. Neurol. Sci.* 332, 4–15.

Mirzaa, G., Roy, A., Dobyns, W. B., Millen, K. J., and Hevner, R. F. (2018). "Hemimegalencephaly and dysplastic megalencephaly," in *Developmental Neuropathology*, eds J. Golden, H. Adle-Biassette, and B. N. Harding (Hoboken, NJ: Wiley Blackwell).

Nguyen, L. H., and Bordey, A. (2021). Convergent and divergent mechanisms of epileptogenesis in mTORopathies. *Front. Neuroanat.* 15:664695. doi: 10.3389/fnana.2021.664695

Norris, D., Yang, P., Shin, S. Y., Kearney, A. L., Kim, H. J., Geddes, T., et al. (2021). Signaling heterogeneity is defined by pathway architecture and intercellular variability in protein expression. *iScience* 24:102118. doi: 10.1016/j.isci.2021.102118

Olde Engberink, A., Hernandez, R., de Graan, P., and Gruol, D. L. (2017). Rapamycin-sensitive late-LTP is enhanced in the hippocampus of IL-6 transgenic mice. *Neuroscience* 367, 200–210.

Rademacher, S., and Eickholt, B. J. (2019). PTEN in autism and neurodevelopmental disorders. *Cold Spring Harb. Perspect. Med.* 9:a036780.

Robinson, G., Parker, M., Kranenburg, T. A., Lu, C., Chen, X., Ding, L., et al. (2012). Novel mutations target distinct subgroups of medulloblastoma. *Nature* 488, 43–48.

Roy, A., Millen, K. J., and Kapur, R. P. (2020). Hippocampal granule cell dispersion: a non-specific finding in pediatric patients with no history of seizures. *Acta Neuropathol. Commun.* 8:54.

Roy, A., Murphy, R. M., Deng, M., MacDonald, J. W., Bammler, T. K., Aldinger, K. A. I, et al. (2019). PI3K-Yap activity drives cortical gyrification and hydrocephalus in mice. *Elife* 8:e45961. doi: 10.7554/eLife.45961

Roy, A., Skibo, J., Kalume, F., Ni, J., Rankin, S., Lu, Y., et al. (2015). Mouse models of human -related brain overgrowth have acutely treatable epilepsy. *Elife* 4:e12703. doi: 10.7554/eLife.12703

Sanchez-Alegria, K., Flores-Leon, M., vila-Munoz, E. A., Rodriguez-Corona, N., and Arias, C. (2018). PI3K signaling in neurons: a central node for the control of multiple functions. *Int. J. Mol. Sci.* 19:3725. doi: 10.3390/ijms19123725

Shi, X., Lim, Y., Myers, A. K., Stallings, B. L., McCoy, A., Zeiger, J., et al. (2020). PIK3R2/Pik3r2 activating mutations result in brain overgrowth and EEG changes. *Ann. Neurol.* 88, 1077–1094. doi: 10.1002/ana.25890

Stafstrom, C. E. (2019). *Developmental Epilepsy–From Clinical Medicine to Neurobiological Mechanisms*. Singapore: World Scientific.

Stafstrom, C. E., and Carmant, L. (2015). Seizures and epilepsy: an overview for neuroscientists. *Cold Spring Harb. Perspect. Med.* 5:a022426. doi: 10.1101/cshperspect.a022426

Tang, S. J., Reis, G., Kang, H., Gingras, A. C., Sonenberg, N., and Schuman, E. M. (2002). A rapamycin-sensitive signaling pathway contributes to long-term synaptic plasticity in the hippocampus. *Proc. Natl. Acad. Sci. U.S.A.* 99, 467–472. doi: 10.1073/pnas.012605299

Tryba, A. K., Merricks, E. M., Lee, S., Pham, T., Cho, S., Nordli, D. R. Jr., et al. (2019). Role of paroxysmal depolarization in focal seizure activity. *J. Neurophysiol.* 122, 1861–1873.

Venot, Q., Blanc, T., Rabia, S. H., Berteloot, L., Ladraa, S., Duong, J. P., et al. (2018). Targeted therapy in patients with PIK3CA-related overgrowth syndrome. *Nature* 558, 540–546.

Wang, Y., Greenwood, J. S., Calcagnotto, M. E., Kirsch, H. E., Barbaro, N. M., and Baraban, S. C. (2007). Neocortical hyperexcitability in a human case of tuberous sclerosis complex and mice lacking neuronal expression of TSC1. *Ann. Neurol.* 61, 139–152. doi: 10.1002/ana.21058

Wilcox, K. S., West, P. J., and Metcalf, C. S. (2020). The current approach of the epilepsy therapy screening program contract site for identifying improved therapies for the treatment of pharmacoresistant seizures in epilepsy. *Neuropharmacology* 166:107811. doi: 10.1016/j.neuropharm.2019.107811

Yang, J., Nie, J., Ma, X., Wei, Y., Peng, Y., and Wei, X. (2019). Targeting PI3K in cancer: mechanisms and advances in clinical trials. *Mol. Cancer* 18:26.

Yu, K., Lin, C. J., Hatcher, A., Lozzi, B., Kong, K., Huang-Hobbs, E., et al. (2020). PIK3CA variants selectively initiate brain hyperactivity during gliomagenesis. *Nature* 578, 166–171. doi: 10.1038/s41586-020-1952-2

Zou, Z., Tao, T., Li, H., and Zhu, X. (2020). mTOR signaling pathway and mTOR inhibitors in cancer: progress and challenges. *Cell Biosci.* 10:31.

Conflict of Interest: The authors declare that the research was conducted in the absence of any commercial or financial relationships that could be construed as a potential conflict of interest.

Publisher's Note: All claims expressed in this article are solely those of the authors and do not necessarily represent those of their affiliated organizations, or those of the publisher, the editors and the reviewers. Any product that may be evaluated in this article, or claim that may be made by its manufacturer, is not guaranteed or endorsed by the publisher.

frontiers in Molecular Neuroscience

ORIGINAL RESEARCH
published: 23 December 2021
doi: 10.3389/fnmol.2021.757646

TALPID3/KIAA0586 Regulates Multiple Aspects of Neuromuscular Patterning During Gastrointestinal Development in Animal Models and Human

Jean Marie Delalande[1,2†], Nandor Nagy[3†], Conor J. McCann[2], Dipa Natarajan[2], Julie E. Cooper[4], Gabriela Carreno[4], David Dora[3], Alison Campbell[5], Nicole Laurent[6], Polychronis Kemos[1], Sophie Thomas[7], Caroline Alby[8], Tania Attié-Bitach[7,8,9], Stanislas Lyonnet[7,8,9], Malcolm P. Logan[10], Allan M. Goldstein[11], Megan G. Davey[12], Robert M. W. Hofstra[13‡], Nikhil Thapar[2,13] and Alan J. Burns[2,14,15]*

[1] Centre for Immunobiology, Barts and The London School of Medicine and Dentistry, Queen Mary University of London, London, United Kingdom, [2] Stem Cells and Regenerative Medicine, Birth Defects Research Centre, UCL Great Ormond Street Institute of Child Health, London, United Kingdom, [3] Department of Anatomy, Histology and Embryology, Semmelweis University, Budapest, Hungary, [4] Developmental Biology and Cancer Program, Birth Defects Research Centre, UCL Great Ormond Street Institute of Child Health, London, United Kingdom, [5] Department of Paediatric Surgery, Christchurch Hospital, Christchurch, New Zealand, [6] Génétique et Anomalies du Développement, Université de Bourgogne, Service d'Anatomie Pathologique, Dijon, France, [7] Laboratory of Embryology and Genetics of Congenital Malformations, INSERM UMR 1163 Institut Imagine, Paris, France, [8] Department of Genetics, Hôpital Necker-Enfants Malades, Assistance Publique Hôpitaux de Paris (AP-HP), Paris, France, [9] Paris Descartes, Sorbonne Paris Cité, Paris, France, [10] Randall Division of Cell and Molecular Biophysics, King's College London, London, United Kingdom, [11] Department of Pediatric Surgery, Massachusetts General Hospital, Harvard Medical School, Boston, MA, United States, [12] Division of Developmental Biology, The Roslin Institute, The University of Edinburgh, Edinburgh, United Kingdom, [13] Department of Clinical Genetics, Erasmus University Medical Center, Rotterdam, Netherlands, [14] Division of Neurogastroenterology and Motility, Department of Gastroenterology, Great Ormond Street Hospital for Children NHS Foundation Trust, London, United Kingdom, [15] Gastrointestinal Drug Discovery Unit, Takeda Pharmaceuticals International, Inc., Cambridge, MA, United States

TALPID3/KIAA0586 is an evolutionary conserved protein, which plays an essential role in protein trafficking. Its role during gastrointestinal (GI) and enteric nervous system (ENS) development has not been studied previously. Here, we analyzed chicken, mouse and human embryonic GI tissues with TALPID3 mutations. The GI tract of TALPID3 chicken embryos was shortened and malformed. Histologically, the gut smooth muscle was mispatterned and enteric neural crest cells were scattered throughout the gut wall. Analysis of the Hedgehog pathway and gut extracellular matrix provided causative reasons for these defects. Interestingly, chicken intra-species grafting experiments and a conditional knockout mouse model showed that ENS formation did not require TALPID3, but was dependent on correct environmental cues. Surprisingly, the lack of TALPID3 in enteric neural crest cells (ENCC) affected smooth muscle and epithelial development in a non-cell-autonomous manner. Analysis of human gut fetal tissues with a *KIAA0586* mutation showed strikingly similar findings compared to the animal models demonstrating conservation of TALPID3 and its necessary role in human GI tract development and patterning.

Keywords: TALPID3, KIAA0586, Sonic Hedgehog, enteric nervous system, neural crest cell, gastrointestinal tract, short-rib polydactyly syndrome, Joubert syndrome

OPEN ACCESS

Edited by:
Parthiv Haldipur, Seattle Children's Research Institute, United States

Reviewed by:
Meryem B. Baghdadi, Institut Curie, France
Joel C. Bornstein, The University of Melbourne, Australia

***Correspondence:**
Alan J. Burns
alan.burns@ucl.ac.uk

† These authors have contributed equally to this work

‡ Deceased

Specialty section:
This article was submitted to Methods and Model Organisms, a section of the journal Frontiers in Molecular Neuroscience

Received: *12 August 2021*
Accepted: *10 November 2021*
Published: *23 December 2021*

Citation:
Delalande JM, Nagy N, McCann CJ, Natarajan D, Cooper JE, Carreno G, Dora D, Campbell A, Laurent N, Kemos P, Thomas S, Alby C, Attié-Bitach T, Lyonnet S, Logan MP, Goldstein AM, Davey MG, Hofstra RMW, Thapar N and Burns AJ (2021) TALPID3/KIAA0586 Regulates Multiple Aspects of Neuromuscular Patterning During Gastrointestinal Development in Animal Models and Human. Front. Mol. Neurosci. 14:757646. doi: 10.3389/fnmol.2021.757646

INTRODUCTION

During embryonic development, normal organogenesis depends on tightly orchestrated interactions between cells of different lineages. In the developing gastrointestinal (GI) tract, such interactions occur between ectoderm-derived neural crest cells (NCC) and the embryonic gut, which is derived from lateral mesoderm and endoderm (Zorn and Wells, 2009; Noah et al., 2011). Interactions between NCC and the developing gut subsequently determine the functional architecture of the enteric nervous system (ENS) by assuring the correct anatomical localization of the enteric neuronal plexuses and the establishment of appropriate interconnections with GI smooth muscle and the mucosa (Sasselli et al., 2012; Goldstein et al., 2013; Rao and Gershon, 2016; Nagy and Goldstein, 2017).

Amongst the numerous proteins that have been shown to be essential for correct vertebrate development is the TALPID3 protein, encoded by the *KIAA0586* gene in human (OMIM 610178). TALPID3 is a ubiquitously expressed protein. Its most recognized function is its requirement for ciliogenesis, as loss of function mutations in the *TALPID3* gene are characterized by a lack of primary cilia in model organisms (Davey et al., 2006, 2007, 2014; Bangs et al., 2011; Ben et al., 2011; Fraser and Davey, 2019; Yan et al., 2020). It has been shown that the TALPID3 protein has an evolutionary conserved intracellular localization at the centrosome, which plays a critical role in ciliogenesis and coordination of ciliary protein trafficking, in particular through functional interactions with Rab8 and Mib1 (Yin et al., 2009; Ben et al., 2011; Mahjoub, 2013; Sung and Leroux, 2013; Villumsen et al., 2013; Kobayashi et al., 2014; Wu et al., 2014; May-Simera et al., 2016; Wang et al., 2016; Li et al., 2017; Naharros et al., 2018). TALPID3 has also been shown to be important for centriole duplication (*via* direct binding to CEP120), as well as centriolar satellite dispersal, centrosome length and orientation, which regulates overall tissue polarity (Wu et al., 2014; Stephen et al., 2015; Tsai et al., 2019). In human, the phenotypic spectrum of *KIAA0586* mutations (the human ortholog of chicken *talpid*^{3}) expands from embryonic lethal ciliopathies to pediatric ciliopathy symptoms including Joubert Syndrome (JBTS) (Akawi et al., 2015; Alby et al., 2015, 2016; Bachmann-Gagescu et al., 2015; Malicdan et al., 2015; Roosing et al., 2015; Stephen et al., 2015). A conditional deletion of *talpid*^{3} in the central nervous system of a mouse model recapitulates the cerebellar phenotype seen in JBTS (Bashford and Subramanian, 2019).

The severe developmental defects caused by the lack of TALPID3 can be linked to the disruption of key developmental signaling pathways, with the strongest association shown to be with the Hedgehog (Hh) pathway (Davey et al., 2006, 2007, 2014; Ben et al., 2011; Ingham, 2016; Matsubara et al., 2016; Fraser and Davey, 2019). Three Hh gene homologs have been described in vertebrates: *Sonic Hedgehog* (*shh*), *Indian Hedgehog* (*ihh*), and *Desert Hedgehog* (*dhh*) (Pathi et al., 2001; Ingham, 2016). At the sub-cellular level, following the binding of Hedgehog ligands to the Patched receptor (PTCH1), the *trans*-membrane transducer Smoothened (SMO) is transported to the primary cilium by anterograde trafficking. Subsequently, GLI proteins located within the cilium tip are processed into activator (GLIA) or repressor (GLIR) isoforms, which are then released in the cytoplasm. The processing of GLI proteins through the cilium establishes the ratio of GLIA to GLIR proteins, which in turn act as transcriptional effectors to control downstream SHH target genes (Kim et al., 2009; Pan et al., 2009; Sasai and Briscoe, 2012; Briscoe and Therond, 2013; Ramsbottom and Pownall, 2016). TALPID3 has been shown to interact and colocalize with the PKA regulatory subunit PKARIIβ at the centrosome. This interaction leads to the phosphorylation of GLI2 and GLI3 and directly links TALPID3 to a functional step in the Hh pathway (Li et al., 2017).

Many studies have demonstrated the central role of the Hh pathway in gut development, physiology and cancer [reviewed in Fukuda and Yasugi (2002); van den Brink (2007), and Merchant (2012)]. Normal gut development has both common and separate requirements for SHH and IHH. In mouse models, mutations in *shh* or *ihh* result in reduced smooth muscle mass, gut malrotation and annular pancreas (Ramalho-Santos et al., 2000). In addition, *shh* mutants exhibit specific defects such as intestinal transformation of the stomach, duodenal stenosis, increased enteric neurons, abnormally distributed ganglia and imperforate anus. On the other hand, *ihh* mutants show reduced epithelial stem cell proliferation and differentiation rate, as well as aganglionic colon (Ramalho-Santos et al., 2000). Interestingly, mutant mice lacking hedgehog-binding protein growth arrest–specific gene 1 (Gas1) or its intracellular messenger Gnaz, have a shortened digestive tract, reduced smooth muscle mass, increased number of enteric neurons and miss-patterned ENS (Kang et al., 2007; Biau et al., 2013). This phenotype has been attributed to a combination of reduced Hh signaling and increased Ret tyrosine kinase signaling (Biau et al., 2013). The Ret tyrosine kinase is essential for ENS development (Natarajan et al., 2002).

Here, we examined the GI tracts of *talpid*^{3} chicken and human fetal gut tissues bearing a homozygous null mutation in *KIAA0586*. We found remarkably similar phenotypes and comparable defects in gut tissues (Schock et al., 2016). We also investigated the role of *TALPID3* in early formation of the ENS, using chicken chimeras and a *talpid*^{3} conditional knock out mouse. We demonstrate that *TALPID3* is not required cell autonomously for ENCC migration and early ENS patterning. Rather, our results demonstrate that *TALPID3* is essential for normal spatial differentiation of smooth muscle and proper expression of ECM components. Our study also reveals that growth and development of both mucosa and smooth muscle are regulated by the ENS *via TALPID3*-mediated signaling.

RESULTS

talpid^3 Chicken Embryos Have Multiple Anatomical Defects Including Gastrointestinal Defects

talpid^3 is a naturally occurring chicken mutant. The *talpid*^{3} mutation is recessive and leads to leaky blood vessels among

other defects. This is causing very high embryonic mortality as reported in both chicken and mouse *Talpid*^{3} models (Davey et al., 2006; Ben et al., 2011). Although limbs and organ defects have been reported in *talpid*^{3} chicken embryos, there has been a lack of detailed analysis of the GI defects in these mutants. As previously described, Buxton et al. (2004) E10.5 *talpid*^{3} chick embryos were smaller than controls, showed generalized edema and displayed a wide range of congenital abnormalities including short ribs, polydactylous paddle shaped limbs, organ defects (lung hypoplasia, liver fibrosis, and cholestasis) and craniofacial abnormalities (hypotelorism, reduction and anterior displacement of the frontonasal process) (**Figure 1A**). At E10.5, the GI tract of *talpid*^{3} chick embryos was significantly reduced in length compared to controls (**Figure 1B**). As previously described, no left right asymmetry or rotation defect was observed in the stomach of *talpid*^{3} chick embryos (Stephen et al., 2014). Transverse sections at the level of the neck showed abnormal connection (fistula) between the esophagus and the trachea or a total absence or narrowing (atresia) of either of the structures (**Figures 1G,O**). Additionally, *talpid*^{3} embryos had an open hindgut (**Figure 1B** – inset-, J,R). Lastly, gut epithelium thickness varied between controls and mutants, as shown in **Figures 1M,Q** insets.

Severe Smooth Muscle and Enteric Nervous System Patterning Defects in *talpid*^{3} Chicken Gastrointestinal Tract

To gain further insight into the GI defects of *talpid*^{3} embryos we performed immunohistochemistry using molecular markers to highlight the neuromuscular organization of the GI tract in controls and *talpid*^{3} mutants. In E8.5 controls, smooth muscle actin (SMA) immunostaining revealed a compact ring of immunopositive cells, corresponding to the presumptive circular muscle layers, encircling the gut epithelium (**Figures 1C–F**). Notably, this muscular ring was located in the outer mesenchyme, with a distinct separation between the muscle and the gut epithelium (**Figures 1C–F**, double arrows). In *talpid*^{3} gut, despite the presence of SMA staining surrounding blood vessels, SMA positive cells were discontinuous or absent around the esophagus (**Figure 1G**). In the stomach and the intestine, the compact muscular ring seen in controls was replaced by diffuse staining that extended across the entire gut mesenchyme, with SMA positive cells abutting the gut epithelium (**Figures 1H,I**, arrowheads). In the colorectum, the circular muscular pattern was disrupted by the open hindgut phenotype (**Figure 1J**). In E8.5 controls, TuJ-1 immunostaining revealed ENCC-derived neurons arranged in characteristic plexuses (**Figures 1K–N**). In the esophagus and the stomach, the presumptive ENS was organized in a single plexus located in the outermost mesenchyme (**Figures 1K,L**, double arrows). In the intestine and colorectum, ENCC were organized in two plexuses: the myenteric plexus (MYP) and the submucosal plexus (SMP) (**Figures 1M,N**). The nerve of Remak (Rem), an avian specific nerve derived from sacral ENCC, was also positively labeled (**Figure 1N**). In E8.5 TALPID3 embryos, ENCC were present throughout the intestine (**Figure 1Q**) and colorectum, although well-defined plexuses were not apparent in the distal gut due to the open hindgut phenotype (**Figure 1R**). Although ENCC were observed alongside the esophagus at E6.5 (data not shown), they were not found around the esophagus at E8.5 and did not form a plexus (**Figure 1O**). At this stage, ENCC were present in the stomach and intestine regions, but they failed to organize in plexuses and were scattered throughout the gut wall (**Figures 1P,Q**). In the colorectum, the nerve of Remak was also smaller in diameter and/or comprised several bundles (**Figures 1Q,R**). The presence of ENCC in distal parts of the GI tract demonstrated that TALPID3 is not required for ENCC migration *per se*. knowing the role of TALPID3 in ciliogenesis, we looked at the presence of primary cilia on migrating ENCC (**Supplementary Figure 1**). In chicken neural tube cultured *in vitro*, primary cilia were readily evident on the neural tube cells. However, we failed to observe them on migrating vagal ENCC, either anatomically by SEM or molecularly using immunofluorescence (**Supplementary Figures 1A–D**). *In vivo*, despite primary cilia being readily detected in E6.5 chicken gut sections, only 11% of HuC$^+$ ENCC showed a detectable primary cilium (**Supplementary Figures 1E,F**). Overall, these results showed regions such as the esophagus being devoid of both ENS and smooth muscle in *talpid*^{3} mutants, whereas regions such as the ventral stomach and the intestine showed scattered ENS and extended regions of smooth muscle differentiation across the mesenchyme.

Hh Signaling Is Disrupted in *talpid*^{3} Gastrointestinal Tract

Due to the well-established functional connection between *TALPID3* and Hh signaling, we investigated changes in this pathway in control and *talpid*^{3} mutants using *in situ* hybridization. *In situ* analysis of *shh* expression in the GI tract of E6.5 control and *talpid*^{3} embryos revealed transcripts in the gut epithelium of both type of tissues, demonstrating expression of the *shh* gene in the *talpid*^{3} mutants (**Figures 2A–H**). Expression of SHH was confirmed in the endoderm of the intestine using an anti-SHH antibody (**Supplementary Figure 2**). To visualize the readout of Hh signaling in the gut wall, mRNA expression of the Hh receptor *PTCH1* was used. In E6.5 control embryos, the pattern of expression of *PTCH1* was composed of one or two concentric gradients surrounding the epithelium (**Figures 2I–L**). In the esophagus, the ventral part of the stomach and the intestine, two concentric gradients were present; the first was located adjacent to the epithelium in the sub-epithelial mesenchyme, and the second more distally located in the outer mesenchyme (**Figures 2I–K**). In the dorsal part of the stomach and the colorectum a single sub-epithelial gradient was present (**Figures 2J,L**). Strikingly, the discrete characteristic gradients of *PTCH1* expression were absent in the GI tract of *talpid*^{3} mutants. Instead a diffuse homogenous expression was observed throughout the gut wall and the epithelium. The same diffuse *PTCH1* pattern was observed at all levels of the GI tract (**Figures 2M–P**). Together these

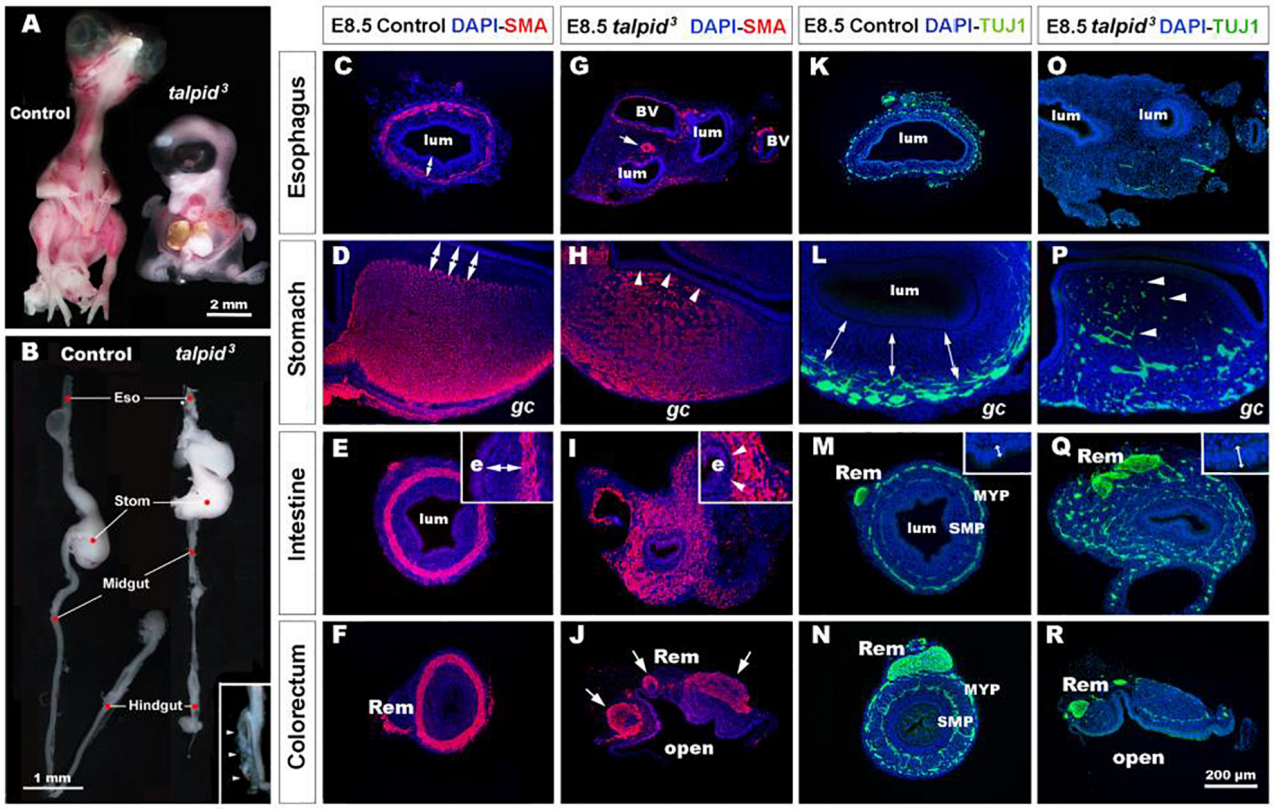

FIGURE 1 | *talpid*^{3} embryos have multiple gastrointestinal defects, including disruption of the neuromuscular patterning of the digestive tract. **(A)** Phenotype of control (left) and *talpid*^{3} (right) embryos at E10.5. *talpid*^{3} mutant embryos have paddle-shaped limbs and hypotelorism. **(B)** Anatomical features of the GI tract along the rostro-caudal axis (esophagus, stomach, intestine, cecum, and colorectum) of E10.5 control embryos (left). In stage-matched *talpid*^{3} embryos (right), all gut regions are apparent, but the esophagus and trachea are malformed, midgut and hindgut are reduced in length, and the terminal hindgut is open. (Inset in **B**) High magnification of an open hindgut (arrowheads). **(C–J)** Expression of smooth muscle actin (SMA) at E8.5 in controls **(C–F)** and **(G–J)** *talpid*^{3} embryos. **(C–F)** In controls, SMA is expressed in the presumptive circular muscle layer in the outer mesenchyme, distant from the epithelium (**C–E**, double arrows). **(G)** In E8.5 *talpid*^{3} embryos, the SMA staining of the esophagus is discontinuous unlike the SMA surrounding blood vessels (arrows). **(H,I)** SMA staining in the stomach and midgut of mutants is widespread throughout the gut wall, with staining extending adjacent to the epithelium (e) and the serosa (s) (**H,I**, arrowheads). **(J)** SMA staining in the colorectum shows disrupted muscle and open hindgut. **(K–R)** Expression of TuJ-1 labeled enteric neural crest at E8.5 in **(K–N)** controls and **(O–R)** *talpid*^{3} embryos. **(K–N)** In E8.5 controls, TuJ-1 staining shows enteric neural crest organized in one **(K)** or two plexuses **(L–N)** clearly separated from the mucosa (double arrows). **(M,N)** The Remak nerve is a single bundle of fibers. **(O–R)** In *talpid*^{3} E8.5 embryos, TuJ-1 staining shows enteric neural crest cells are absent **(O)** or scattered throughout the mesenchyme (**P–R**, arrowhead). The Remak nerve is divided in several bundles **(Q,R)**. Epithelium thickness varies between control and mutant intestine (**M,Q** – inset). e, endoderm; *gc*, greater curvature of the stomach; lum, lumen; m, mucosa; Rem, nerve of Remak; MYP, myenteric plexus; SMP, submucosal plexus; BV, blood vessels. Same scale bar in **(C–R)**.

results showed that, despite epithelial expression of SHH in *talpid*^{3} mutants, the precise integration of the signal in the surrounding mesenchyme was lost, as shown by the aberrant *PTCH1* expression.

Defective Expression of Extracellular Matrix Components in *talpid*^{3} Gut Mesenchyme Leads to the Disappearance of Neural Crest Cells Repellent Cues

In search of a mechanistic explanation for the lack of ENS plexus formation in *talpid*^{3} mutants, we analyzed expression of components of the gut ECM known to influence neuronal behavior (Tennyson et al., 1990; Siebert et al., 2014; Nagy et al., 2016). First, we used the CS-56 antibody, which stains the glycosaminoglycan portion of native chondroitin sulfate proteoglycans (CSPG). CSPG are ECM components regulated by Hh signaling (Nagy et al., 2016). In E6.5 control tissues, CS-56 staining comprised two concentric gradients: the first immediately adjacent to the gut epithelium (sub-epithelial mesenchyme) and the second located in the outer gut wall (outer mesenchyme) (**Figure 3A**). This expression pattern was very similar to *PTCH1* as described above. In E6.5 *talpid*^{3} gut tissues, CS-56 expression was absent from the outer mesenchyme, with only cells adjacent to the epithelium staining positive (**Figure 3F**). Additionally, we examined the expression of Collagen 9 (Coll9), a ECM component expressed in the developing gut, which has been specifically shown to elicit avoidance behavior by neural crest cells *in vitro*

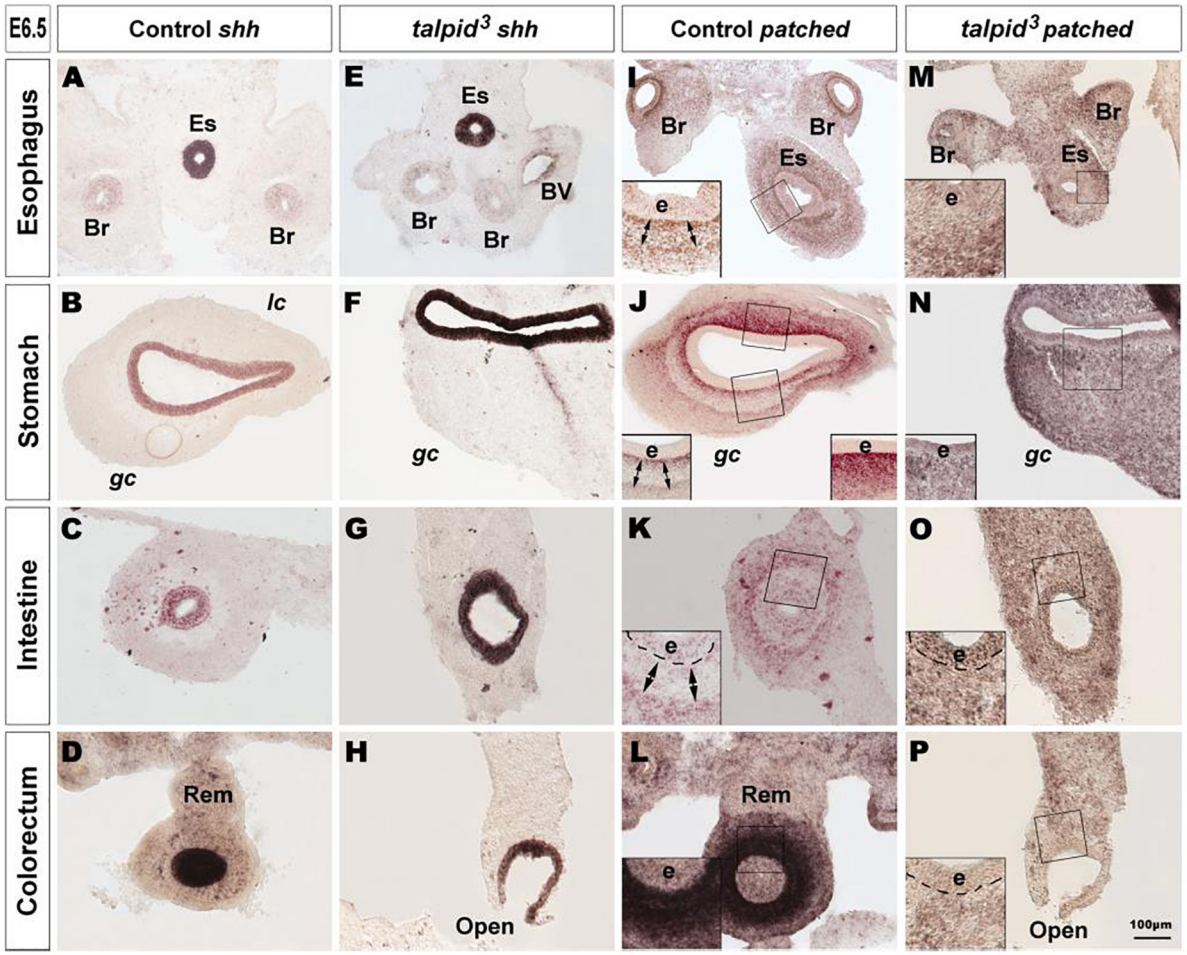

FIGURE 2 | Hh signaling is disrupted in the GI tract of *talpid*^{3} mutants. **(A–P)** *In situ* hybridization for *shh* **(A–H)** and *patched* **(I–P)** in E6.5 control **(A–D,I–L)** and E6.5 *talpid*^{3} mutant **(E–H,M–P)** transverse sections. **(A–H)** In both controls and *talpid*^{3}, *shh* is expressed in the endoderm in all gut regions. **(I–L)** *Patched in situ* in controls shows a discrete pattern of expression with one (**J–L** + insets) or two (**I–K** + Insets) concentric gradients. (**M–P** + insets) In *talpid*^{3} sections the *patched* gradient is replaced by uniform levels of expression. Es, esophagus; Br, bronchus; Rem, nerve of Remak; e, endoderm; *lc*, lesser curvature; *gc*, greater curvature of the stomach. Same scale bar in **(A–P)**.

(Ring et al., 1996; Nagy et al., 2016). Consistent with the CS-56 staining, Coll9 pattern of expression was also composed of two concentric areas, one within the sub-epithelial mesenchyme and one in the outer mesenchyme (**Figures 3B,D**). Interestingly, the Coll9 expression pattern appeared to define exclusion zones for the migrating ENCC, which were only present outside Coll9 positive areas, as shown by N-cadherin (NCadh) staining (**Figures 3B,C**; double arrows). As seen with CS-56, there was no Coll9 expression in the outer mesenchyme of E6.5 *talpid*^{3} gut samples and only the sub-epithelial mesenchyme was stained (**Figures 3G,H**). Interestingly, and in correlation with the lack of outer mesenchyme Coll9 expression, NCadh-positive ENCC were scattered throughout the gut mesenchyme, with some cells located adjacent to the epithelium (**Figures 3G,H**; arrowheads in inset). We also investigated the expression of Coll9 respective to smooth muscle differentiation. We found that SMA and Coll9 have distinct, yet partially overlapping, patterns of expression in control tissues (**Figures 3D,E**). In E6.5 control esophagus, the distal gradient of Coll9 corresponded with the inner boundary of the smooth muscle ring (**Figure 3D**). In the stomach, Coll9 and SMA were mostly mutually exclusive apart from a subdomain in the ventral region where both were co-expressed (**Figure 3E**). In E6.5 *talpid*^{3} esophagus, both the Coll9 distal gradient and the SMA ring were absent (**Figure 3I**). In the *talpid*^{3} stomach, most of the Coll9 expression domain was absent compared to control, while the SMA-positive domain was extended (**Figure 3J**). These results show that expression of CSPG in the gut mesenchyme is regulated by *talpid*^{3} (likely indirectly via the dysregulation of the Hedgehog pathway), as its absence led to significant loss in expression of these ECM components. Moreover, the changes in ECM components expression were concurrent with mislocalization of migrating ENCC.

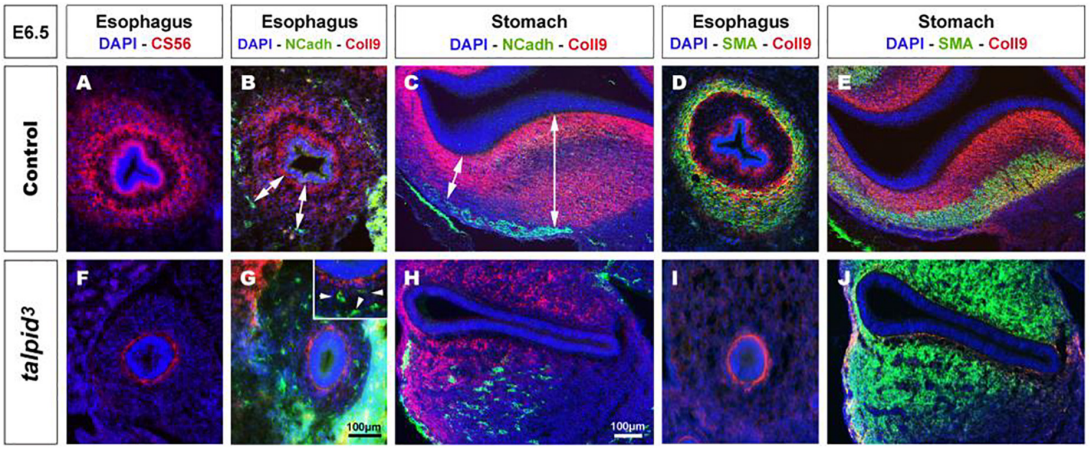

FIGURE 3 | Expression of chondroitin sulfate proteoglycans (CSPG) is altered in *talpid*^{3} gut mesenchyme, causing the disappearance of ENCC repellent cues. **(A–J)** Immunofluorescent staining of esophagus and stomach with CSPG pan marker CS-56 and Coll9, in control **(A–E)** and *talpid*^{3} chicken mutant **(F–J)** at E6.5, **(B,C,G,H)** co-stained with N-Cadherin and **(D,E,I,J)** smooth muscle actin (SMA). **(A,B,D)** In the esophagus, the pattern of two concentric circles of CSPG expression is lost in **(F,G,I)** *talpid*^{3} mutant (**G**-inset, arrowheads) coinciding with scattered ENCC. **(C)** In control stomach, Coll9 expression is widespread and excludes the ENS myenteric plexus whereas in (**H**, double arrows) *talpid*^{3} mutant expression is altered and loss of expression coincides with scattered ENCC. **(D,E)** In control, SMA expression in partially overlapping with Coll9 (yellow merge). **(I,J)** in *talpid*^{3} mutants, Coll9 expression is altered and SMA is either lost **(I)** or extends to ectopic sub-epithelial domains **(J)**. Same scale bar in **(A–J)**.

Transplantation of Wild Type Enteric Neural Crest Cells Does Not Rescue the Formation of Enteric Nervous System Plexuses in a *talpid*^{3} Gut

To investigate the role of *TALPID3* in ENS plexus formation, we attempted to rescue normal ENS patterning in *talpid*^{3} mutants by grafting wild type neural tubes, including neural crest, into *talpid*^{3} host embryos (**Figure 4**). GFP chicken tissues were used as donors for the transplants, so that vagal ENCC had a functional *TALPID3* protein and could also be traced in the chimeric embryos using GFP expression. When compared to GFP > wild type transplanted controls (**Figures 4A–D**) or stage matched *talpid*^{3} embryos (**Figures 4I–L**), transplanted GFP + ENCC behaved similarly to ENCC of *talpid*^{3} embryos and were unable to rescue ENS patterning (**Figures 4E–H**). At the level of the esophagus, instead of surrounding the esophagus in a presumptive circular plexus, as seen in controls (**Figure 4A**), transplanted GFP + ENCC clustered in the dorsal region (**Figure 4E**), in a pattern similar to that seen in *talpid*^{3} embryos (**Figure 4I**). In the stomach and intestine, transplanted GFP + ENCC migrated similar distances along the GI tract as observed in *talpid*^{3} embryos but were scattered throughout the mesenchyme (**Figures 4F,G,J** + inset G) and not arranged in plexuses, as seen in controls (**Figures 4B–D** + inset C). Epithelium and smooth muscle thickness (stained with DAPI and Phalloidin, respectively) in intestine and stomach sections were measured in stage matched GFP > wild type and GFP > *talpid*^{3} chimera, as well as *talpid*^{3} mutants. Measurements from GFP > *talpid*^{3} chimeric tissues and *talpid*^{3} mutant were both statistically ($^{***}p < 0.001$) different from the controls (**Supplementary Figure 3**). The non-parametric Spearman's Rho test was used to measure the correlation between GFP > wild type and GFP > *talpid*^{3} chimera, and *talpid*^{3} mutants measurements. The correlation between GFP > wild type and GFP > *talpid*^{3} transplants was 0.670, whereas the correlation between the GFP > wild type transplant and the *talpid*^{3} mutant was 0.715. Importantly, the correlation between the GFP > *talpid*^{3} and the *talpid*^{3} mutant was 0.942, an extremely high score. The fact that measurements from chimera and mutant clustered together and were statistically different from the control supported histological findings of a lack of rescue. Overall, wild type transplanted vagal ENCC did not rescue ENS plexus formation or the smooth muscle phenotype in a *talpid*^{3} environment.

Lack of TALPID3 in Enteric Neural Crest Cells Does Not Affect Gross Enteric Nervous System Morphology but Affects Smooth Muscle and Mucosa Development in a Non-cell-autonomous Manner

To further assess the role of TALPID3 during ENS development and to test its cell autonomous requirement in ENCC, we performed the converse experiment to that described above, by grafting *talpid*^{3} vagal ENCC into GFP-expressing chick embryos. In the resulting chimeric embryos, the transplanted ENCC were devoid of functional TALPID3 protein and were identified by lack of GFP expression (GFP^{-ve}; **Figure 5** inset). Due to the extremely high mortality of this type of chimera, only one specimen survived to E7.5 for the gut tissues to be analyzed. Surprisingly, transplanted vagal

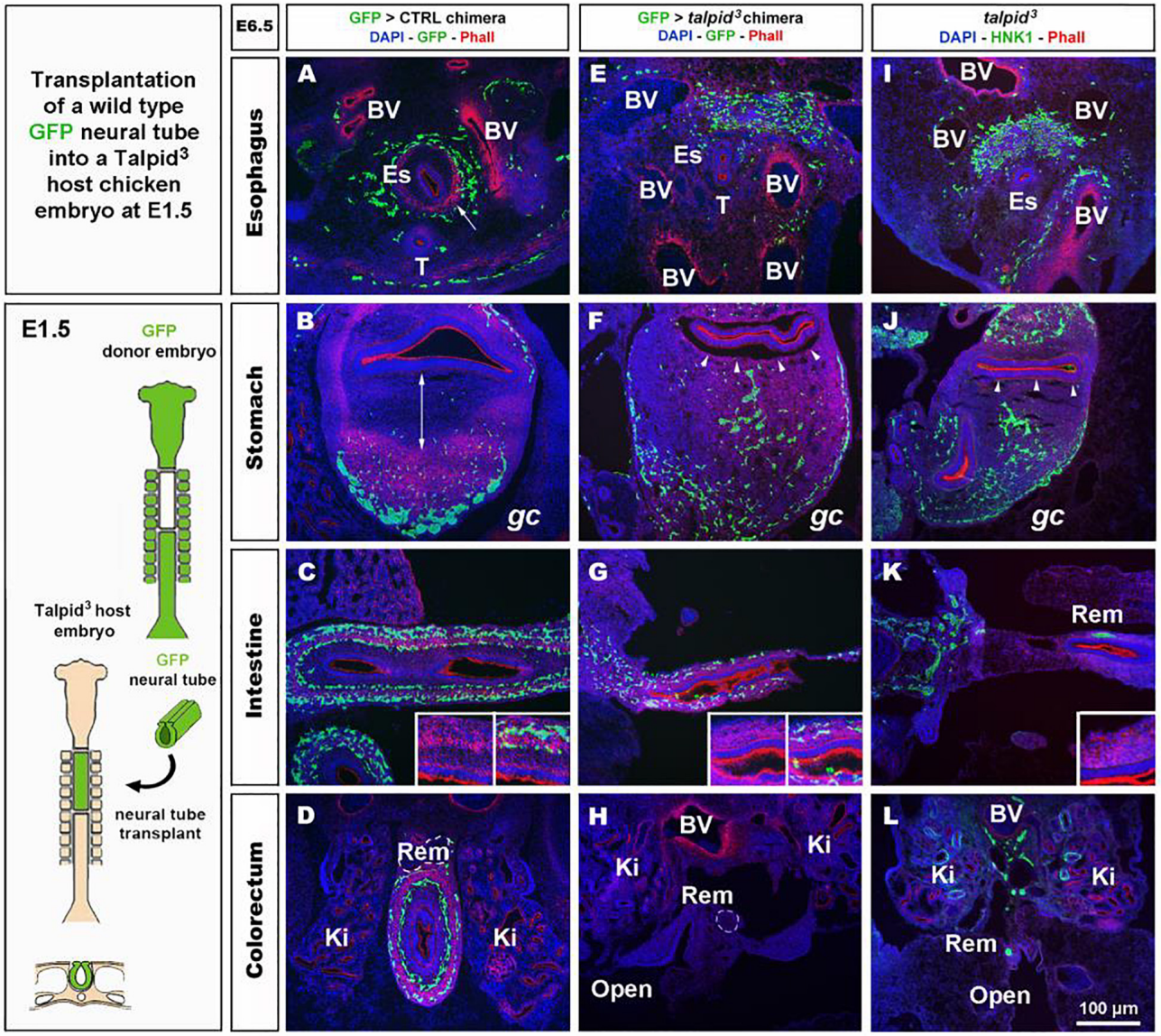

FIGURE 4 | GFP > *talpid*^{3} chimeric embryos show ENS and smooth muscle patterning defects similar to stage matched *talpid*^{3} embryos. **(A–L)** E6.5 chimeric embryos after wild type GFP neural tube transplantation in **(A–D)** GFP > control and **(E–H)** GFP > *talpid*^{3} hosts, compared to **(I–L)** E6.5 *talpid*^{3} embryos. **(A–L)** Immunofluorescent staining for GFP and Phalloidin in **(A–H)** chimeric embryos and **(I–L)** HNK-1 and phalloidin in *talpid*^{3} embryos. (**E–G** + inset) GFP > *talpid*^{3} chimeric embryos have scattered ENCC distribution similar to TALPID3 embryos. **(A–D)** Phalloidin staining shows smooth muscle patterning in control chimera (arrow, double arrow, insets). **(E–H)** Phalloidin staining shows a lack of smooth muscle patterning in the GFP > *talpid*^{3} chimera, similar to the staining found in *talpid*^{3} embryos (**I–L**; arrowheads, inset). BV, blood vessels; Ki, kidneys; Rem, nerve of Remak; Es, esophagus; T, trachea; *gc*, greater curvature of the stomach. Same scale bar in **(A–L)**.

talpid^3 ENCC migrated throughout the GI tract and patterned normally into the characteristic MYP and SMP of the ENS, as shown by HNK1 and GFP staining at E7.5 (**Figures 5A–H**). Importantly, *talpid*^{3}ENCC colonized the entire length of the GI tract and were found in the colorectal region (**Figure 5H** + inset). Here, vagal GFP^{-ve} ENCC (red) were present alongside GFP$^+$ (yellow) ENCC (**Figure 5H** left inset) that were likely sacral ENCC entering the gut prematurely (Burns and Le Douarin, 2001). In contrast to the ENS, which was grossly normal in the chimeric embryo, there were obvious defects in smooth muscle differentiation as revealed by SMA staining: instead of the characteristic SMA$^+$ ring of differentiating smooth muscle cells seen at E7.5 in control chimeras (**Figures 5I–P** + insets J,N), there was thickened and diffuse SMA staining in regions of the esophagus and the stomach, suggesting impaired differentiation (**Figures 5I,J,M,N** double arrows + insets J,N; **Figure 6H**). The characteristic SMA$^+$ ring of cells

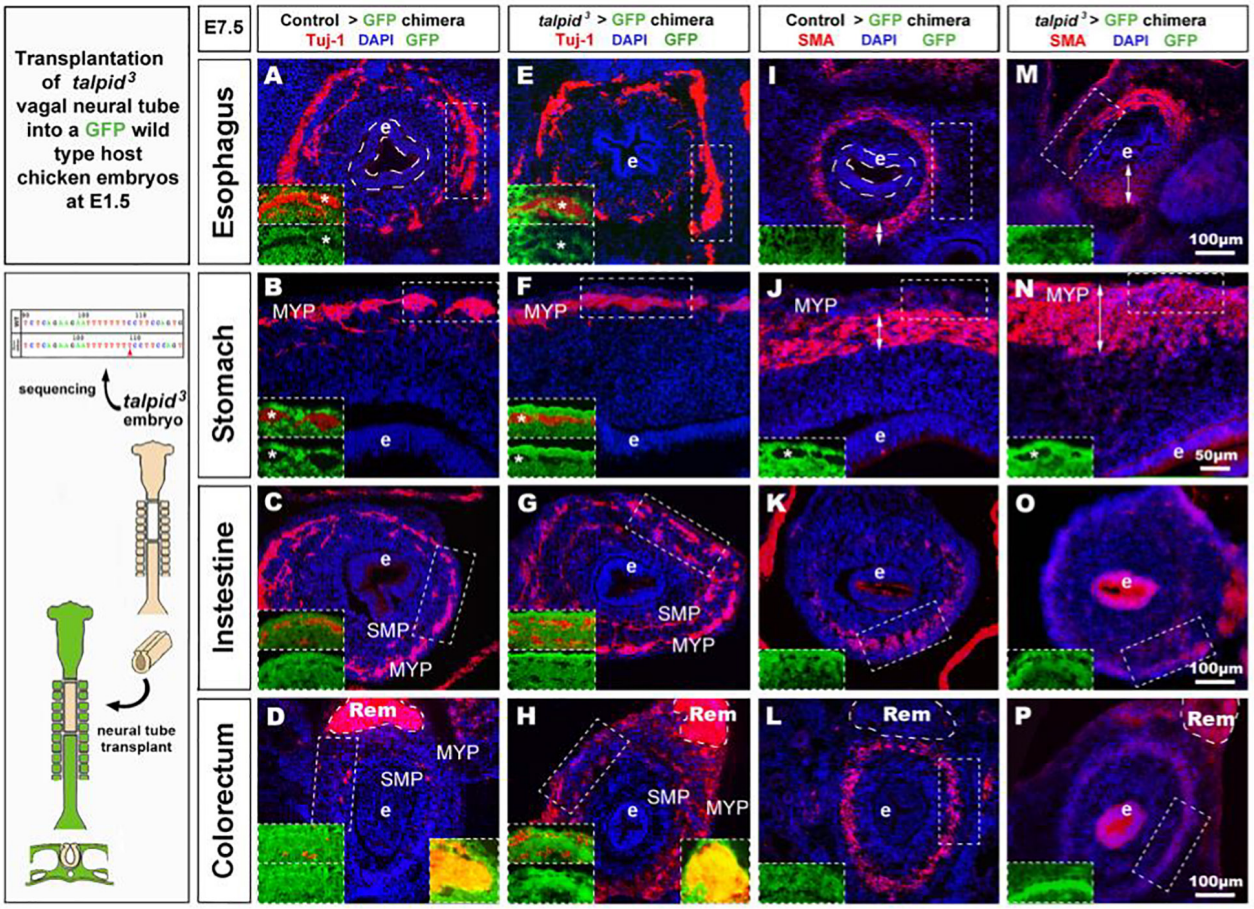

FIGURE 5 | *talpid*^{3} > GFP chimeric embryos have grossly normal ENS but smooth muscle and epithelium defects. **(A–P)** E7.5 chimeric embryos after neural tube transplantation in **(A–D,I,J)** control > GFP and **(B–H,M–P)** *talpid*^{3} > GFP. **(A–P)** Immunofluorescent staining for a TUJ-1+ and GFP [inset] in **(A–H)** and SMA and GFP [inset] in **(I–P)**. Panels **(A–H)** normal ENS patterning is observed in both control > GFP and *talpid*^{3} > GFP. (**D,H** insets) show the presence of (red) vagal TUJ-1+/GFP- ENCC (marked with asterisks *), as well as (yellow) TUJ-1+/GFP+ sacral ENCC in the Remak nerve. **(E–H)** TUJ-1 staining shows grossly normal ENS in *talpid*^{3} > GFP chimera with a more mature/developed appearance of the ENS in the intestine and colon compared to the control chimera. **(I–L)** Well-defined circular SMA staining in control chimera. **(M–P)** Diffuse SMA expression and/or extended SMA domain (double headed arrows) in *talpid*^{3} > GFP chimera. **(O)** SMA staining is almost absent in intestine of *talpid*^{3} > GFP chimera. **(P)** Diffuse, yet circular SMA staining present in colorectum of *talpid*^{3} > GFP chimera. **(A,E,I,M)** The endoderm of *talpid*^{3} > GFP chimera is significantly thinner than controls at the level of the esophagus. e, endoderm; Rem, nerve of Remak; MYP, myenteric plexus; SMP, submucosal plexus. Same scale bar in **(A–P)**.

was also missing in the intestine of the chimeric embryo (**Figure 5O**). Normal SMA staining was observed in some areas around the esophagus and within the colorectum, which coincided with the presence of normal vagal ENCC from the region adjacent to the graft and wild type sacral ENCC, respectively (**Figure 5H** inset). Additionally, the architecture of the mucosa was disrupted in the chimeric embryo, with the esophageal epithelium consisting of a thin folded monolayer, unlike controls where a thickened circular epithelium was present (**Figures 5A,E,I,M** doted lines). Using DAPI, SMA, and TuJ-1 staining, epithelial cells, smooth muscle cells and enteric neurons were counted on stomach sections ($n = 3$ sections minimum, as shown in **Figures 5B,F,J,N**). Numbers were combined with equivalent murine data for chicken/mouse cross-species statistical analysis of chimeric animals where *Talpid3* was knocked down in ENCC, as described below (**Figure 6H**).

Because only one *talpid*^{3} > GFP chicken chimera could be analyzed (due to extremely high mortality) we wished to confirm the chicken results using an alternative approach. For this, we engineered a conditional knock out of the *Talpid3* gene in a mouse model by crossing a *Wnt1:Cre* line (Danielian et al., 1998), with a floxed *Talpid3* knock-out line. Resultant *Wnt1:Cre;Talpid3* $^{flox/flox}$ embryos, which do not express TALPID3 in NCCs, were often embryonic lethal or died at P0, due to presumptive respiratory problems, as their lungs failed to fill with air (**Supplementary Figure 4**). P0 pups showed a craniofacial phenotype characteristic of hypoplastic neural crest derivatives (**Supplementary Figures 3D,F**). In mutants, the GI tract morphology was grossly normal

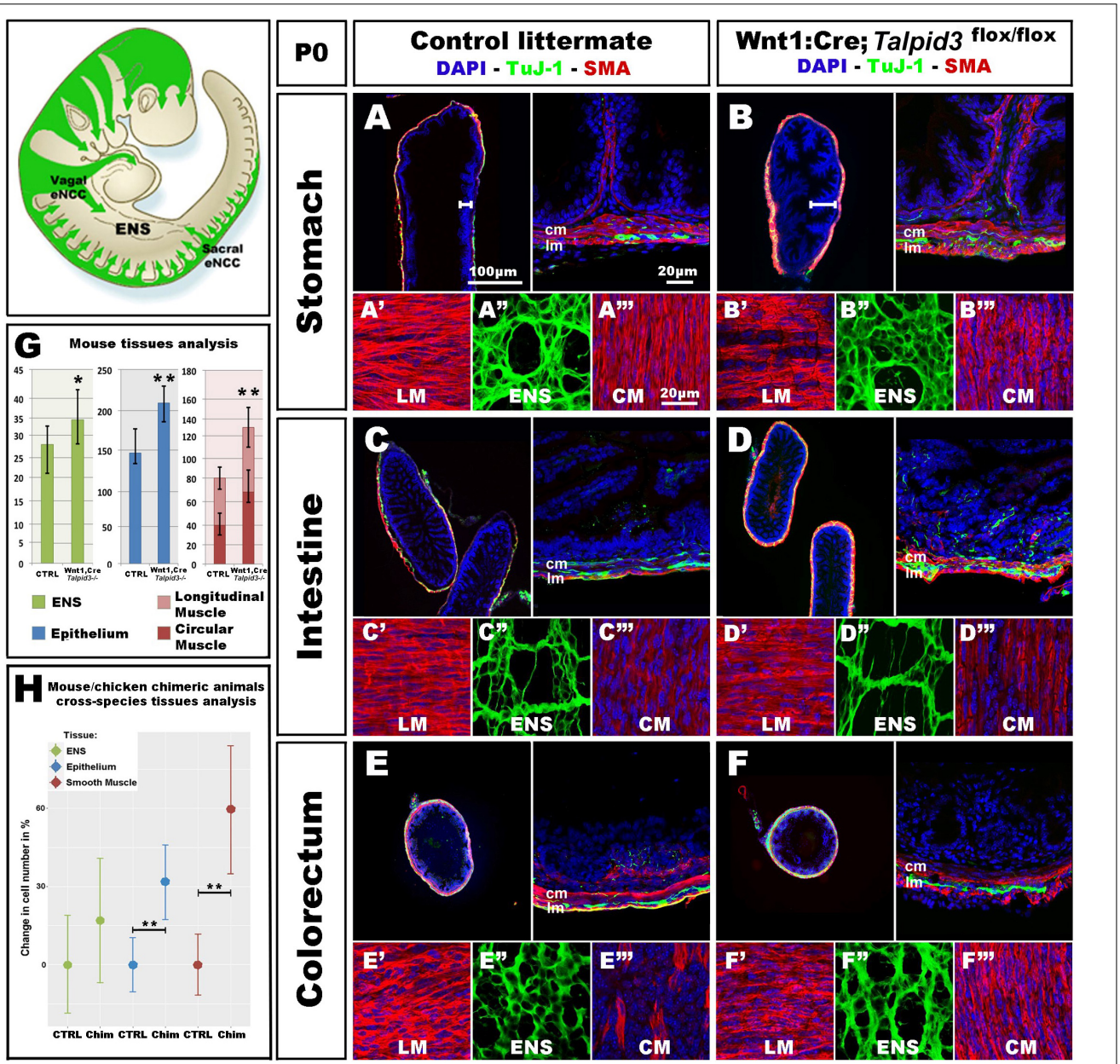

FIGURE 6 | *Wnt1:Cre;Talpid3*$^{flox/flox}$ mice show grossly normal ENS but smooth muscle and epithelium defects. **(A–F)** Immunofluorescent staining for TuJ-1 and SMA at the level of **(A,B)** the stomach, **(C,D)** intestine and **(E,F)** colorectum in control littermate and *Wnt1:Cre;Talpid3*$^{flox/flox}$ P0 pups, respectively. **(A′–A‴,B′–B‴,C′–C‴)** confocal projections at the level of the longitudinal muscle (LM), enteric nervous system (ENS) and circular muscle (CM), respectively. **(G)** Bar graph shows cell counts for ENS, LM, CM and total smooth muscle, as well as epithelium in control littermate versus *Wnt1:Cre;Talpid3*$^{flox/flox}$. In the stomach, the ENS (green) showed a statistically significant (*$p = 0.045$) increase of 29% in the number of ENCC in the mutant, compared to control. Epithelium (blue) showed a statistically significant (**$p = 0.009$) increase of 39% in the mutant, compared to control. Muscle layers (red) showed a highly statistically significant (**$p = 0.002$) increase of 67% in mutant tissue sections compared to control, with 80% increase in the longitudinal muscle (**$p = 0.002$) and 55% increase in the circular muscle (**$p = 0.018$). Difference in epithelium thickness is highlighted in **(A,B)** by white bars. **(H)** Scatter plot shows mouse/chicken cross-species cell counts for ENS, epithelium and smooth muscle in stomach of controls and chimeric animals. Epithelium (blue) showed a statistically significant (**$p = 0.009$) increase of 39% in the mutant, compared to control. Muscle layers (red) showed a highly statistically significant (**$p = 0.002$) increase of 67% in mutant tissue sections compared to control. ctrl, control; chim, chimera; cm, circular muscle; lm, longitudinal muscle. Same scale bars in **(A–A‴–F–F‴)**.

compared to control littermates (**Supplementary Figures 4B,E**). As seen in the chicken model, *Talpid3* ENCC colonized the entire length of the gut and formed an apparently normal ENS all along the GI tract (**Figures 6A–F,A″–F″**). Although the ENS was grossly normal, quantitative analysis of the ENS in the stomach region showed a statistically significant ($p = 0.045$) increase of 29% in the number of ENCC in the mutants ($n = 8$ sections) (**Figure 6G**). Of

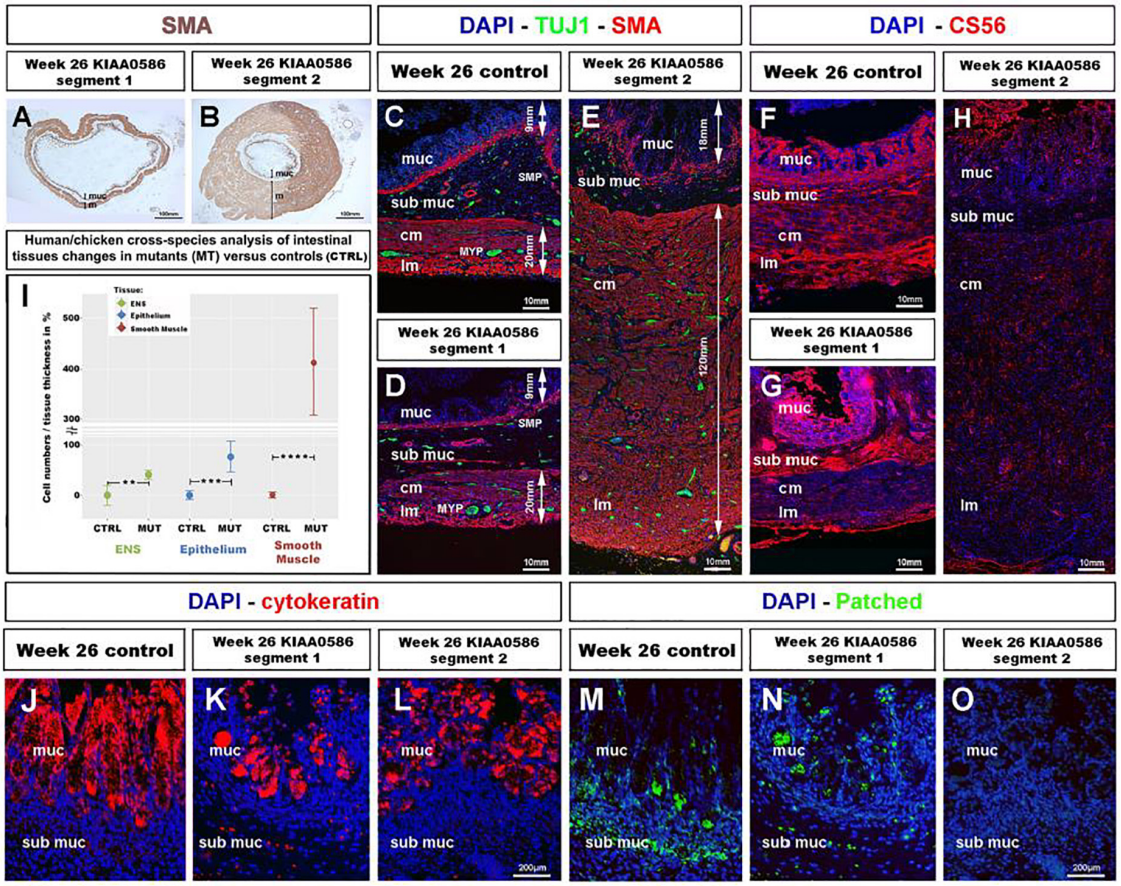

FIGURE 7 | Fetal GI tissues from a 26 weeks human fetus bearing a *KIAA0586* mutation show one gut segment with scattered ENS, mucosa and smooth muscle overgrowth, as well as CS56, Cytokeratin and Patched expression defects. **(A,B)** Low magnification gut sections of a 26 weeks fetus with a *KIAA0596* mutation. SMA immuno-staining reveals grossly normal smooth muscle layers in **(A)** "segment 1" of the intestine and extensive smooth muscle and mucosa overgrowth in **(B)** "segment 2". **(C–E)** Immunofluorescence staining for DAPI (nucleus), TuJ-1 (ENS), and SMA (Smooth Muscle) on intestine sections. **(C)** 26 weeks control intestine with normal ENS patterning and longitudinal and circular smooth muscle layers. Panels **(D,E)** staining in the *KIAA0586* fetus tissue shows grossly normal neuromuscular pattern in **(D)** "segment 1," with well-defined ENS plexuses, normal muscle (∼20 mm) and mucosa (∼6 mm) thickness. **(E)** "segment 2" has scattered ENS with smooth muscle (∼140 mm) and mucosa (∼25 mm) overgrowth. **(F–H)** Immunofluorescence staining for DAPI (nucleus) and CS56 (chondroitin sulfate proteoglycans) on intestine sections. **(F,G)** 26 weeks control intestine and Segment 1" with CS56 expression in the serosa, submucosa and mucosa. **(H)** "Segment 2" shows absence of CS56 staining. **(I)** Human/chicken cross-species analysis of intestinal tissues in *talpid*^{3} and KIAA0586 mutants has statistically significant increase in (i) ENS cells numbers (40.8%,$^{**}p = 0.004$) and (ii) epithelium and smooth muscle tissue thickness (77%,$^{***}p = 0.00006$ and 413%, $^{****}p < 0.0001$, respectively). **(J,K)** Immunofluorescence staining for DAPI (nucleus) and Cytokeratin on mucosal sections. **(J)** 26 weeks control intestine has uniform Cytokeratin staining in the mucosa. **(K,L)** "Segment 1 and 2" show uneven Cytokeratin expression. **(M–O)** Immunofluorescence staining for DAPI (nucleus) and Patched. **(M)** "Segment 1" has reduced submucosal staining and normal mucosal staining compared to 26 weeks control. **(O)** "Segment 2" shows no Patched staining. ctrl, control; muc, mucosa; sub muc, submucosa; cm, circular muscle; lm, longitudinal muscle; MYP, myenteric plexus; SMP, submucosal plexus. Same scale bar in **(J–O)**.

note, and again in accordance with the defects observed in the chicken model, the number of cells in both the epithelium and muscle layers was affected, in a non-cell autonomous manner, by the lack of TALPID3 in the ENCC. Indeed, quantitative analysis of cell numbers in both tissues showed statistically significant 39% increase in the epithelium ($p = 0.009$; $n = 7$ sections) and 67% increase in the muscle layers ($p = 0.002$; $n = 7$ sections), with an 80% increase in the longitudinal muscle ($p = 0.002$) and 55% increase in the circular muscle ($p = 0.018$). Interestingly, the smooth muscle myoblasts appeared misshaped in the conditional *Talpid3* mutant (**Figures 6A′–F′′,A′′–F′′** and **Supplementary Videos 1, 2**). The transgenic mouse measurements were combined with equivalent chicken data from the *talpid*^{3} > GFP transplant for mouse/chicken cross-species analysis. Cell counts for epithelium showed a statistically significant ($^{**}p = 0.009$) increase of 39% in the chimeric animals compared to controls. Smooth muscle cell count showed a highly statistically significant ($^{**}p = 0.002$) increase of 67% in chimeric animals compared to control. The relative increase observed in ENS cell numbers was not statistically significant in this cross-species analysis (**Figure 6H**). Overall, apart

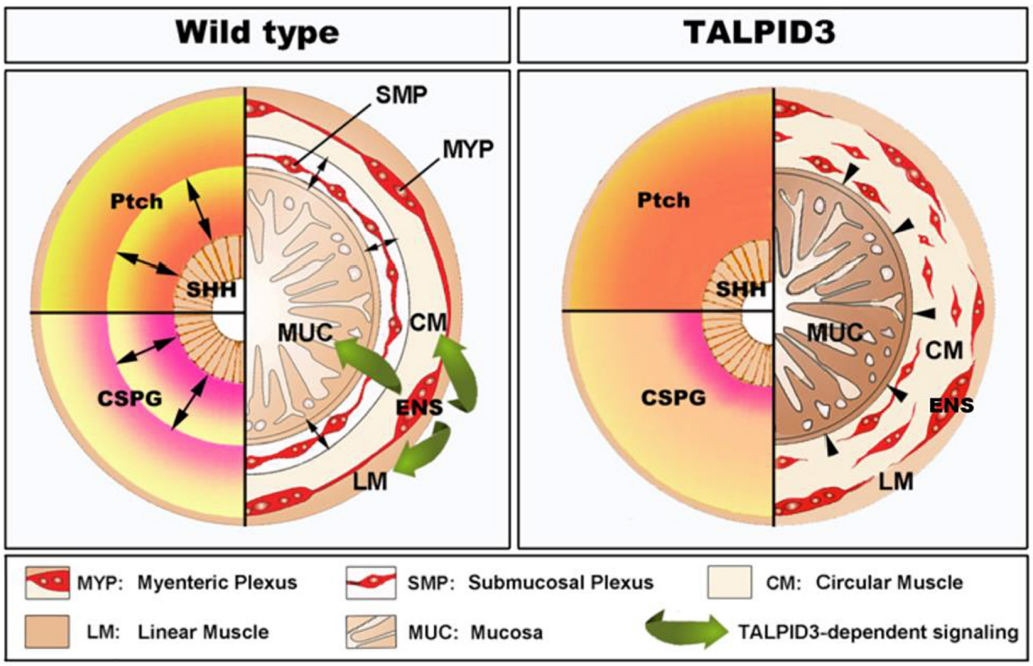

FIGURE 8 | Model of TALPID3-dependent gastrointestinal neuromuscular patterning. During normal gut development **(Left)**, the Sonic Hedgehog (SHH) gradient defines the concentric architecture of the intestine as seen by the discrete PATCHED (Ptch) pattern of expression. SHH readout in the mesenchyme immediately adjacent to the epithelium restricts smooth muscle differentiation to allow the connective tissue of the submucosa to develop. In the absence of a functional TALPID3 protein **(Right)**, the SHH readout is lost, as shown by the diffused *Ptch* expression. Loss of the SHH readout leads to ectopic spread of the smooth muscle differentiation domain adjacent to the epithelium. **(Left – bottom)** During normal gut development, the precise readout of the SHH gradient directs the pattern of CSPG expression, restricting ENCC to the locations where the enteric nervous system (ENS) will form. The ENS regulates smooth muscle and mucosa growth and differentiation *via* a TALPID3-dependent signaling (green arrows). **(Right – bottom)** In the absence of a functional TALPID3 protein, SHH readout is lost, which coincides with a loss of CSPG expression. This loss of expression permits ectopic ENCC migration resulting in scattered ENCC throughout the gut mesenchyme. Loss of TALPID3 also leads to altered growth and differentiation of smooth muscle and mucosal epithelium.

from altered cell numbers, knocking out *talpid*^{3} in ENCC had little effect on early ENS development and patterning in both chicken and mouse models, but it altered growth and differentiation of smooth muscle and mucosa in a non-cell-autonomous manner.

Human Embryonic Tissues Bearing a *KIAA0586* Mutation Recapitulate the Gastrointestinal Defects Observed in TALPID3 Animal Models

To assess whether the role of TALPID3 is conserved throughout evolution and is relevant to human GI tract development and patterning, we examined human fetal GI tissues obtained from a 26 weeks human fetus with a homozygous for a 1815G > A mutation in *KIAA0586*, the human ortholog of *talpid*^{3} *(chicken) and Talpid3 (mouse)*, as previously described (Alby et al., 2015). Previous anatomical description of the fetus listed shortened ribs, micromelia, lingual hamartomas, postaxial and preaxial polydactyly, temporal polymicrogyria and an occipital keyhole defect (Alby et al., 2015; Cocciadiferro et al., 2020). Gross examination of the GI tract revealed an elongated and tubular stomach, but otherwise apparently normal GI tract. Histological analysis showed a portion of the intestine ("segment 1") with grossly normal neuromuscular pattern (**Figures 7A,D,G**) consistent with that observed in a 26 weeks control fetus (**Figure 7C**). However, another portion (designated as "segment 2") showed massive overgrowth of the smooth muscle layers (∼140 mm in the mispatterned "segment 2," compared to ∼20 mm in "segment 1," and 26 weeks control) and the mucosa (∼25 mm in the mispatterned "segment 2," compared to ∼6 mm in "segment 1," and 26 weeks control). The smooth muscle overgrowth in "segment 2" corresponded to an increase in thickness of 6.5 times (**Figures 7B,E,H**). Additionally, immunostaining for TuJ1 showed enteric neurons scattered throughout the gut wall (**Figure 7E**), in a pattern similar to that observed in the *talpid*^{3} chicken model (**Figures 1O–R**). The striking similarities found in histological observations were confirmed by combining equivalent measurements from human and chicken intestinal tissues for human/chicken cross-species analysis. This analysis showed a statistically significant increase in (i) ENS cell numbers (40.8%,$^{**}p = 0.004$) and (ii) epithelium and smooth muscle tissue thickness (77%,$^{***}p = 0.00006$ and 413%, $^{****}p < 0.0001$, respectively) in mutant tissues compared to stage matched controls (**Figure 7I**). We also investigated expression of human chondroitin sulfate proteoglycans using CS56 (**Figures 7F–H**). 19 and 26 weeks controls showed expression of CS56 in

the serosa the submucosa and the mucosa (**Figure 7F** and **Supplementary Figure 5B**). In "segment 1," CS56 expression was also observed in the serosa and the mucosa whereas, strikingly, in "segment 2" no CS56 expression was detected (**Figures 7G,H**). To investigate further the intestinal phenotype of this fetus, we examined the expression of both Patched and Cytokeratin (**Figures 7J–O**). Even though cytokeratin was expressed in the fetus bearing the *KIAA0586* mutation, the staining was not as strong and uniform as in the control. Likewise, Patched staining was reduced in "segment 1" of the fetus bearing the *KIAA0586* mutation compared to the control, whereas "segment 2" showed no staining. The altered *patched* expression was confirmed by *in situ* hybridization (**Supplementary Figures 4C–E**). Both epithelial stainings pointed to delayed/altered gut epithelial differentiation. Overall, the phenotype observed in "segment 2" of the fetus was strikingly similar to that of the *talpid*^{3} chicken model with scattered enteric neurons, smooth muscle and mucosa overgrowth as well as impaired differentiation. Other defects observed in both human and the chicken model included: (i) altered Hh pathway (as shown by a lack of Patched expression and loss of mRNA expression pattern) (ii) impaired epithelium differentiation (as shown by Cytokeratin) and (iii) lack of CSPG components of the ECM.

DISCUSSION

Although TALPID3 has been recognized to have essential functions during embryonic development, its role during GI and ENS development has not, as yet, been studied. Previous investigations have shown that TALPID3 animals are useful to model human birth defects such as short ribs, polydactyly, or craniofacial abnormalities that are attributed to abnormal hedgehog signaling (Davey et al., 2007; Bangs et al., 2011; Ben et al., 2011; Alby et al., 2015). Our findings establish that TALPID3 animal models can also offer insights for congenital human GI defects, such as short gut, tracheoesophageal atresia/fistula, and anorectal abnormalities, i.e., a variety of defects commonly seen in pediatric gastroenterology clinics. Moreover, the striking similarities between the neuromuscular abnormalities described here, in chicken, mouse and human, demonstrate that the function of TALPID3 is well conserved across species and is of importance for normal human gut development.

TALPID3 Is a Regulator of Gastrointestinal Neuromuscular Patterning

We specifically examined the role of TALPID3 in neuromuscular patterning of the developing GI tract, as it was clear from the histological defects in both chicken and human GI tissues that lack of TALPID3 led to severe disruption of this developmental process. Our analysis showed that the lack of TALPID3 consistently affected the neuromuscular patterning of the gut. Interestingly though, the resulting phenotypes varied, depending on the location along the A–P axis of the gut. In the chicken model, lack of TALPID3 in the esophagus led to complete absence of smooth muscle and ENS, whereas in the stomach and the intestine lack of TALPID3 led to ectopic smooth muscle differentiation and misplaced enteric neurons. Likewise, one portion of the human intestine from a fetus bearing a *KIAA0586* mutation showed grossly normal neuromuscular patterning, whereas another had dramatic muscle overgrowth and scattered enteric neurons. These observation, when combined with quantifications of enteric neuronal, smooth muscle and epithelial cell numbers, suggest that, albeit with species differences, TALPID3 is part of a conserved mechanism controlling the appropriate spatial differentiation of smooth muscle and the correct positioning of enteric neurons. Moreover, TALPID3 functions as part of regional-specific mechanisms regulating the correct neuromuscular patterning at different levels of the GI tract. Perhaps this is not surprising since the spatiotemporal development of GI smooth muscle has been shown to have regional-specific differences (Bourret et al., 2017; Graham et al., 2017). Our results are in accordance with recent findings in the related chicken mutant *talpid2* (Brooks et al., 2021).

Disruption of Gastrointestinal Patterning in *talpid*^{3} Mutant Is Linked to Impairment of the Hh Pathway

Our findings add to the body of evidence linking TALPID3 to the Hh signaling pathway (Davey et al., 2007; Bangs et al., 2011; Ben et al., 2011; Alby et al., 2015; Li et al., 2017). The link between TALPID3 and Hh signaling in the gut can be observed in (i) the gross anatomy of the GI tract (ii) the smooth muscle and (iii) ENS defects of the mutants. (i) First, the gross anatomical abnormalities in the TALPID3 chicken GI tract are consistent with a loss of Hh signaling. Severe reduction in GI tract size with normal gross anatomy has been reported using a conditional approach to remove both *Shh* and *Ihh* functions from early mouse gut endoderm (Mao et al., 2010). Likewise, mouse knockouts of *Shh*, *Gli2* and *Gli3* all display tracheo-esophageal atresia/fistula, a phenotype also described here in the TALPID3 chicken mutant (Motoyama et al., 1998; Ramalho-Santos et al., 2000). Additionally, regulation of gut epithelium homeostasis has been linked to the Shh signaling pathway and both *talpid*^{3} chicken and *KIAA0585* human gut tissue showed altered epithelium growth/differentiation (Mao et al., 2010; Ben-Shahar et al., 2019). Lastly, Hedgehog signaling is critical for normal anorectal development and anorectal malformations have been reported in *shh* knockout mice and in humans with polymorphisms in Hedgehog genes (Ramalho-Santos et al., 2000; Gao et al., 2016). The open hindgut phenotype of the *talpid*^{3} chicken model offers an additional model for researching such malformations. (ii) It has been shown that Shh signaling regulates the concentric architecture of the intestine. In particular, SHH affects the mesenchyme immediately adjacent to the epithelium, where it restricts smooth muscle differentiation to allow the connective tissue of the submucosa to develop (van den Brink, 2007; Huycke et al., 2019). The increased domain of smooth muscle differentiation in the stomach and intestine of the *talpid*^{3} chicken suggests that this Hh-dependant

regulation is lost. Moreover, the results from *ptch in situ* hybridization in *talpid*^{3} mutants directly demonstrate that SHH expressed by the endoderm is not correctly integrated throughout the radially surrounding mesenchyme. The lack of PATCHED protein immunostaining in "segment 2" suggests that this part of the gut is unable to respond to SHH signaling. The loss of the proximal SHH readout in the *talpid*^{3} mutants can be directly correlated with the subsequent differentiation of smooth muscle adjacent to the epithelium in the stomach and intestine. This result demonstrates that mesenchymal cells surrounding the epithelium are competent for induction into smooth muscle, but are normally prevented from doing so by the proximal SHH gradient *via* a TALPID3-dependent mechanism. In the esophagus, the lack of TALPID3 does not lead to an extension of the smooth muscle differentiation domain, but rather to a lack of smooth muscle differentiation altogether, pointing to a different region-specific readout of the Hh signal. This failure of smooth muscle differentiation in the esophagus may explain why migrating ENCC do not halt their migration and differentiate into enteric neurons, as they lack target tissue to innervate. Indeed, ENCC were observed at the level of the esophagus at stage E6.5 in the *talpid*^{3} chicken mutant, but no cells were present in this region at E8.5. TALPID3 is therefore necessary for the correct integration of SHH throughout the gut mesenchyme and to define the concentric architecture of the smooth muscle differentiation domain. Our results fit in with a recent study showing that Hedgehog acts through Bmp signaling to inhibit subepithelial smooth muscle and that levels of Hedgehog signaling regulate differentiation of the inner smooth muscle layer (Huycke et al., 2019). This suggests that TALPID3 is part of this regulatory mechanism. (iii) The influence of SHH on NCC migration and proliferation is well established, but many paradoxical results point to a complex role for Hh during ENS development with species and developmental differences, as well as direct and indirect regulatory mechanisms (Ramalho-Santos et al., 2000; Fu et al., 2004; Reichenbach et al., 2008; Biau et al., 2013; Jin et al., 2015). Recent results clearly show, both in chicken and mouse, that the SHH receptor Patched is not expressed by ENCC and point to indirect regulatory mechanisms (Nagy et al., 2016). Our findings are in agreement with an indirect regulation of ENCC by SHH through its role in modifying the gut ECM and thereby the environment through which ENCC migrate, as we discuss below.

Loss of TALPID3 and Hh Signaling Is Associated With ECM Defects and Absence of Environmental Neural Crest Cells Repellent Cues

In search of a mechanistic explanation for the lack of ENS plexus formation in *talpid*^{3} mutants, we analyzed expression of CGPG molecules, which are components of the gut ECM. Expression of ECM components is known to be regulated by both primary cilia and Hh signaling (Seeger-Nukpezah and Golemis, 2012; Nagy et al., 2016), making them good candidates for further investigation. Alterations in ECM expression have also been described in human ciliopathies (Ramalho-Santos et al., 2000; Seeger-Nukpezah and Golemis, 2012). Importantly, CSPG molecules provide guidance cues for neuronal behaviors such as migration, axon outgrowth and axon termination (Ring et al., 1996; Carulli et al., 2005; Siebert et al., 2014). We specifically investigated Coll9, a CSPG expressed in the developing gut, which has been shown to elicit avoidance behavior by NCC *in vitro* (Ring et al., 1996; Nagy et al., 2016). In correlation with the loss of Hh signaling in the GI tract of both the *talpid*^{3} chicken and the fetus bearing a *KIAA0586* mutation, expression of CSPG molecules was lost. Importantly, double staining of CSPG and NCC showed that the disappearance of the CSPG expression correlated tightly with ectopic localization of ENCC, suggesting that the lack of repellent molecules such as Coll9 is a direct mechanism underlying the lack of ENS plexus formation in *talpid*^{3} GI tract. This finding is in agreement with previous studies showing that the regulation of CSPG by SHH in both chicken and mouse models can modify the behavior of ENCC and subsequently ENS patterning (Nagy et al., 2016). To investigate a possible connection between smooth muscle differentiation and the expression of CSPG, we performed double immunofluorescence with SMA and coll9 antibodies. We found that SMA and Coll9 have distinct, yet partially overlapping, patterns of expression. This demonstrates that some myoblasts express Coll9. However, Coll9 is mainly expressed in mesenchymal cells and it is this wider CSPG expression domain, and not the SMA domain, that correlates best with the regional localization of ENCC. Additionally, our chicken transplantation experiments demonstrated the inability of wild type ENCC to rescue ENS formation in a TALPID3-null gut environment. This finding highlights the role of environmental cues in directing ENS formation and shows that ENS plexus development does not rely on self-organizing properties of ENCC. This is in agreement with recent work showing that disruption of the ENCC environment can disrupt ENS patterning (Graham et al., 2017). Our study also demonstrates that TALPID3 expression in the gut is essential for proper expression of guidance cues that direct ENS plexus patterning. Importantly, we also show that this role is conserved during human fetal gut development.

TALPID3 Is Not Required Cell Autonomously for Enteric Nervous System Plexus Formation but Is a Regulator of Neuronal-Mesenchymal-Epithelial Interactions Directing Correct Tissue Growth and Differentiation

We investigated the cell autonomous requirement for TALPID3 during ENCC migration and gut patterning by knocking out *Talpid*^{3} specifically in ENCC, either by neural tube transplantation in chicken or using a *Wnt1-Cre* driven *Talpid*^{3} conditional knockout in mouse. In both models, TALPID3 was found not to be required for ENCC migration or normal ENS plexus formation as the gross morphology of the ENS was unaffected. The only alteration to the ENS in

these conditions was the increase in cell number observed in the chicken model and in the mouse model, which we quantified in stomach sections. Alteration of NCC numbers could be the result of subtle migration or differentiation defects changing the relative number of ENCC in specific locations. Alternatively, it could be linked to a TALPID3-dependent alteration of the SHH pathway and, specifically, the influence of SHH on NCC as a mitogen (Fu et al., 2004; Reichenbach et al., 2008; Roper et al., 2009; Nagy et al., 2016). Remarkably, knocking out *Talpid*^{3} in ENCC led to wider non-cell autonomous defects in other tissues such as smooth muscle and epithelium. Both the mouse and chicken phenotypes revealed a neural crest TALPID3-dependent mechanism controlling growth and differentiation of mesenchyme and epithelium. The most striking effect was alteration of smooth muscle differentiation and increased numbers of myoblasts which we quantified in stomach sections in chicken and mouse. The alteration of smooth muscle differentiation was particularly evident in the stomach region of mice. Variations in epithelium shape and cell numbers were also evident both in mouse, chicken. Mouse/chicken cross-species analysis confirmed that these differences in smooth muscle and epithelial cell numbers were statistically significant when comparing chimeric animals to controls. Interestingly, in addition to its role in smooth muscle development, the Hh pathway also plays an important role in mucosal growth (Mao et al., 2010; Ben-Shahar et al., 2019). Indeed *shh* and *gli3* mutant mice have mucosal hyperplasia in the stomach (Ramalho-Santos et al., 2000; Kim et al., 2005). It has been previously postulated that vagal ENCC could act as a mediator in the mesenchymal-epithelial interactions that control stomach development (Faure et al., 2015). Additionally it has been shown that ENS influences the differentiation and growth of other cell types within the gut, as demonstrated by smooth muscle overgrowth in the aganglionic portion of EdnrB mice, as well as alteration of goblet cell differentiation (Spencer et al., 2007; Thiagarajah et al., 2014). Recent work has also shown that implantation of neural crest cells within tissue-engineered small intestine altered the transcriptome of a wide variety of gastrointestinal cell types, demonstrating the necessity of the neuronal lineage to be able to recapitulate gut organogenesis *in vitro* (Schlieve et al., 2017). Our findings emphasize the importance of the neural component for correct smooth muscle and mucosa development both during embryonic gut development and for regenerative medicine research. Moreover our study shows the central role played by TALPID3 in neuronal-mesenchymal-epithelial interactions necessary for normal GI tract development.

The neural crest specific *talpid*^{3} knockout results described here are in agreement with non-cell autonomous effects seen in other tissues after NCC-specific gene knockout. For example, knocking out the intraflagellar protein Kif3a in NCC led to non-cell autonomous striated muscle defects during tongue development (Millington et al., 2017). Additionally, loss of NCC disrupts the distribution of second heart field cells in the pharyngeal and outflow regions (Bradshaw et al., 2009). Likewise, conditional neural crest Rac1 knockout, using a *Rac1/Wnt1-Cre* line, shows excessive proliferation of SMA+ cell wall around the aortic sac and ventral aorta (Waldo et al., 2005; Thomas et al., 2010). Investigating the gut phenotype of *Rac1/Wnt1-Cre* mutants for smooth muscle defects would be informative. Interestingly, Rac1 is downstream of the non-canonical SHH pathway (Mulligan, 2014). TALPID3 and Rac1 have a comparable function in vesicular trafficking (Stenmark, 2009), centrosome regulation (May et al., 2014) and in cell-matrix interactions (Thomas et al., 2010). Rac1 is also downstream of RET, a tyrosine kinase receptor essential for ENS development (Natarajan et al., 2002; Fu et al., 2010; Mulligan, 2014).

Migrating Enteric Neural Crest Cells Do Not Extend a Prominent Primary Cilia

Having established that TALPID3 was not required cell autonomously for ENCC migration and gross ENS patterning, and considering the role of TALPID3 in ciliogenesis, it follows that primary cilia might not be required for ENCC migration. ENCC are a highly proliferative cell population and it is their mitogenic activity, which is driving their migration and invasiveness (Simpson et al., 2007). It is known that there is a reciprocal regulation of cilia and the cell cycle, so that the primary cilium is dismantled in replicating cells, which makes it unlikely for highly proliferative cells to extend a primary cilium (Ishikawa and Marshall, 2011; Ford et al., 2018). Interestingly, migrating interneurons within the developing murine brain do not show an extended primary cilium (Higginbotham et al., 2012). In our study, we failed to observe primary cilia in migrating chicken vagal ENCC using *in vitro* neural tube culture. Performing Immunohistochemistry on tissue sections at E6.5, migrating ENCC bearing a primary cilium were seldom observed (11% of HuC$^+$ ENCC). It has been shown that differentiated ENS neurons bear a primary cilium (Junquera Escribano et al., 2011; Luesma et al., 2013). Other studies describe primary cilia on YFP+ cranial NCC using the *Wnt1:Cre; Rosa:YFP* transgenic line (Brugmann et al., 2010; Millington et al., 2017). In this transgenic line, YFP is expressed in both the neural tube (which is ciliated) and the neural crest derivatives. This lack of discrimination is problematic to decipher this issue (Cassiman et al., 2006; Murdoch and Copp, 2010). Our study suggests that extending primary cilia mainly happens as ENCC start to differentiate into enteric neurons and might not be required for migration *per se*.

Role of the Human TALPID3 Ortholog *KIAA0586* in Human Gastrointestinal Tract Development

KIAA0586 is the human ortholog of *talpid*^{3}. Some homozygous mutations of *KIAA0586* have been shown to be embryonic lethal and to lead to severe developmental abnormalities such as Hydrolethalus syndrome and short-rib polydactyly (Alby et al., 2015). Here we show that the phenotypic spectrum of *KIAA0586* mutations extends to defects in the GI tract. Apart from a tubular stomach the gross anatomy of the GI tract of the fetus was normal. However, our histological analysis showed severe alteration of the gut patterning with smooth

muscle and mucosa hyperplasia, as well as scattered enteric neurons in a sub-section of the intestine we designated "segment 2." In accordance with the animal models, we show that this phenotype is the consequence of disruption of the Hh pathway and loss of normal ECM expression. Our findings shed light on the central role of KIAA0586 in patterning of the gut during human fetal development. Recently *KIAA0586* mutations have also been identified in Joubert syndrome patients. JBTS is defined by three primary findings: (i) underdevelopment of the brain cerebellar vermis, (ii) brain stem defects giving the appearance of the molar tooth sign (MTS) and (iii) Hypotonia (Abdelhamed et al., 2013; Sanders et al., 2015; Stephen et al., 2015). Importantly also, patients typically have a perturbed respiratory pattern in the neonatal period and severe psychomotor delay. Although very rare, association with Hirschsprung disease and problems with bladder and bowel control (incontinence) have been reported in Joubert patients with milder forms of the disease (Shian et al., 1993; Ozyurek et al., 2008; Akhondian et al., 2013; Purkait et al., 2015). Considering the role of KIAA0586 in tissue patterning our study unfolds, it is also tempting to speculate that other symptoms of JBTS (like psychomotor delay, hypotonia and respiratory difficulties), could be linked to neuronal-mesenchymal-epithelial patterning defects in other parts of the body. Interestingly, in this study, *Wnt1:Cre; Talpid3* $^{fl/fl}$ P0 mutants died at birth from presumed respiratory failure, as their lungs did not appear to inflate. This points to a possible failure in the developmental interactions of neural crest, smooth muscle and epithelium, as lung neural crest cells share developmental origins with ENCC (Burns and Delalande, 2005; Freem et al., 2012). Finally, the ENS is often referred to as the "second brain" and it is possible that brain ECM defects, similar to the ones we describe in this study, could underlie abnormal brain patterning defects, such as cortical heterotopias, commonly seen in Joubert syndrome, but also in Bardet–Biedl syndrome or Meckel–Gruber syndrome (Willaredt et al., 2008; Abdelhamed et al., 2013; Higginbotham et al., 2013). In mice, a large variety of CSPGs represent major components of the ECM in the brain (Horii-Hayashi et al., 2015). In human, defects in ECM, leading to impaired neuronal guidance, could underlie other types of brain function abnormalities. A recent CNS conditional *Talpid*^{3} knockout mouse model for JBTS showed cerebellar defects due to granule cell proliferation, migration and differentiation, three aspects of cellular behavior also affected in our models (Bashford and Subramanian, 2019). This study, however, did not investigate ECM components.

CONCLUSION

Our findings demonstrate a central role for the centrosomal protein TALPID3 in neuromuscular patterning of the developing gastrointestinal tract (summarized in **Figure 8**). We show that the function of TALPID3 during GI neuromuscular patterning is conserved in vertebrates including during human fetal development. Our findings also reveal a new role for the ENS in regulating neuronal-mesenchymal-epithelial interactions necessary for normal GI tract development, and that this regulatory mechanism is TALPID3-dependent. These findings add new understandings to human GI tract developmental mechanisms and have direct implications for regenerative medicine, as they emphasize the importance of the neural component for *in vitro* gut organogenesis.

MATERIALS AND METHODS

Taplid^3 Chicken

Fertile chicken eggs were obtained from commercial sources within the UK. *talpid*^{3} and transgenic (http://topics.sciencedirect.com/topics/page/Green_fluorescent_protein) GFP chicken eggs were obtained from The Roslin Institute, The University of Edinburgh (McGrew et al., 2004; Davey et al., 2006). Eggs were incubated at 37°C and staged according to the embryonic day of development (E), and by using the developmental tables of Hamburger and Hamilton (Hamburger and Hamilton, 1951). The *talpid*^{3} mutation leads to leaky blood vessels causing very high mortality (Davey et al., 2006). This high mortality meant that specimens were collected over more than 10 years. Our study presents oldest time point at which we could reliably analyse gut tissues (E6.5 for most of the study). Beneficial outcrossing of the Talpid flock improved survival over time. It became possible to analyse later time points, when the gut is more developed, as shown in Figure 1 with E8.5 and E10.5 specimens.

Chicken Intraspecies Neural Tube Grafting

For each combination of grafting experiment (chick^{GFP}-*talpid*^{3}; *talpid*^{3}-chick^{GFP}; chick^{GFP}- wild type), the neural tube adjacent to somites 2–6 inclusive (and its associated neural crest) was microsurgically removed from the host embryos at embryonic day E1.5 and replaced with equivalent stage-matched tissue, as previously described (Burns and Le Douarin, 2001; Delalande et al., 2015). Following grafting, eggs were returned to the incubator, and embryos allowed to develop to the appropriate stage. To ascertain the genotype of the Talpid^3 neural tube transplant onto a GFP host embryo, the remaining tissues of the donor were used for DNA extraction, PCR amplification and sequencing of the region flanking the a366 mutation on exon7 using the following primers: Forward: CATTAGCTCTGCCGTCAACA Reverse: GGTAGGCAGACCACTGGAAG (**Figure 5**) (Davey et al., 2006). A total of 30 GFP neural tube grafts into TALPID3 hosts were made, of which 2 homozygote *talpid*^{3} mutant hosts were fixed for analysis at E6.5. After series of "blind" grafting experiments, a total of 5 *talpid*^{3} neural tube grafts onto GFP hosts were identified after genotyping, of which only 1 chimera survived and was fixed for analysis at E7.5.

Mouse Conditional Knockout

Animals used for this study were maintained and the experiments were performed in accordance with local approvals and the United Kingdom Animals (Scientific Procedures) Act, 1986

under license from the Home Office (PPL70/7500). *Talpid3*$^{f/f}$ mice were acquired from Prof. Malcolm Logan (King's College London). *Wnt1-cre;R26R-YFP/YFP* mice (Srinivas et al., 2001; Druckenbrod and Epstein, 2005), in which NCC express yellow fluorescent protein (YFP), were crossed to *Talpid3*$^{f/f}$ to generate a neural crest conditional knockout of *Talpid*^{3}. Subsequent *Wnt1:Cre; Talpid3*$^{flox/flox}$ mouse tissues were examined at postnatal day 0 (P0).

Human Embryonic and Fetal Material

Human material was sourced *via* the Joint MRC/Wellcome Trust Human Developmental Biology Resource (HDBR) under informed ethical consent with Research Tissue Bank ethical approval (08/H0712/34 + 5 and 08/H0906/21 + 5) (Gerrelli et al., 2015). Staging of embryos was carried out according to the Carnegie system. GI tissues from a fetus with Short-rib polydactyly and bearing a homozygous null mutation in *KIAA0586* were obtained from case II:5 family 4, as previously described in Alby et al. (2015). Informed consent was obtained for all participating families, and the study was approved by the ethical committee of Paris Ile de France II.

Tissue Sectioning

Transverse sections were cut from whole embryos and dissected gut segments. Sections were obtained at a thickness of 6 μm from wax blocks and 10–15 μm from frozen blocks. All sections were placed on Superfrost Plus microscope slides (BDH Laboratories).

Immunofluorescence and *in situ* Hybridization

For labeling of chicken and human dissected GI samples, the tissues were cryoprotected in 15% sucrose in PBS and frozen in liquid Nitrogen. Frozen sections were cut at 12 μm using a Leica CM1900 cryostat at −22°C. Briefly, for immunofluorescence, antibody blocking solution (10% sheep serum, 1% Triton-X-100 in PBS) was applied for 1 h at room temperature then samples were rinsed extensively in PBS and incubated primary antibodies (listed in **Table 1**) diluted in antibody blocking solution overnight at 4°C. Samples were then washed three times in PBS for 20 min and incubated with fluorescently tagged secondary antibodies (listed in **Table 2**) for 4 h at room temperature. Samples were washed for 1 h, and stained for 10 min with DAPI, before being mounted under a coverslip using Vectashield mounting medium (Vector Laboratories) as previously described (Wallace and Burns, 2005; Delalande et al., 2014) *in situ* hybridization was performed as previously described (Burns and Delalande, 2005).

Confocal Microscopy, Cell Counting and Statistical Analysis

Tissues were imaged using confocal microscopy (Zeiss LSM 710 confocal microscope). Images of gut sections double immunostained with relevant tissue antibodies and DAPI. Equivalent fields of relevant sections were examined in controls, mutants and/or chimeras (minimum $n = 3$). Cells were counted and tissue thickness measured using the Image-J Fiji cell counter plugin and measuring tool, respectively. Data was plotted to a histogram or interval plot. The results for all samples were normalized to baseline. The outcome was set as the percentage of the difference between the baseline and the experimental conditions. Multiple linear regression was used to study the effects of tissue, species and gene mutation simultaneously (Schneider et al., 2010; Lunt, 2013). This allowed us to assess the relative contribution of each predictor to the total variance that our model explained. Interaction terms were also considered with stricter p-value cut offs. The models were validated using the adjusted R squared and by performing residual analysis. To assess possible tissue rescue in the GFP > *taplid*^{3} transplantation experiment, the non-parametric Spearman's Rho test was used to measure the correlation between control, chimera and mutant. All raw data and statistical analysis calculations are available here: https://datadryad.org/stash/share/xNqbJ7teCQMoatb4CDKgsdbtIPGZ5QH1eGBvz_g-fVY.

Neural Tube Culture and Scanning Electron Microscopy

Migrating vagal NCC for scanning electron microscopy imaging were obtained using *in vitro* neural tube cultures as previously described (Delalande et al., 2008). Samples were then fixed overnight in 2% glutaraldehyde, 2% paraformaldehyde in 0.1 M phosphate buffer, pH7.4, at 4°C, post-fixed in 1% OsO_4/1.5% $K_4Fe(CN)_6$ in 0.1 M phosphate buffer at 3°C for 1.5 h. After rinsing with 0.1 M phosphate buffer and distilled water, specimens were progressively dehydrated to 100% ethanol, then washed once in acetone. The samples were then critical point dried using CO_2 and mounted on aluminum stubs using sticky

TABLE 1 | Primary antibodies for immunohistochemistry studies.

Primary antibody	Concentration	Company
Mouse anti-TuJ1	1:500	Covance (MMS-435P)
Mouse anti-CS56	1:2000	SIGMA (C8350)
Mouse anti-collagen IX	1:2	DSHB (2B9)
Mouse anti-SMA	1:400	Dako (M0851)
Chicken anti-GFP	1:500	Abcam (ab13970)
Chicken anti-Ncad	1:5	DSHB (6B3)
Rabbit anti-SHH	1:400	Santa Cruz (sc-6149)
Rabbit anti-PTCH	1:100	EMD Millipore (06-1102)
Rabbit anti-IFT88	1:400	Thermo Fisher (PA56997)
Pan cytokeratin-488	1:20	eBioscience (53-9003-82)
Rabbit anti-Arl13b	1:50	ProteinTech (17711-1-AP)

TABLE 2 | Secondary antibodies for immunohistochemistry studies.

Secondary antibody	Alexa fluor	Concentration	Company
Goat anti-rabbit	488	1:500	Invitrogen
Goat anti-mouse	488	1:500	Invitrogen
Anti-chicken	488	1:500	Abcam
Anti-mouse	568	1:500	Invitrogen
Anti-rabbit	568	1:500	Invitrogen
Anti-mouse	647	1:500	Invitrogen
Anti-rabbit	647	1:500	Invitrogen

carbon taps. Samples were then coated with a thin layer of Au/Pd (2 nm thick) using a Gatan ion beam coater and imaged with a Jeol JSM-6480LV high-performance, Variable Pressure Analytical Scanning Electron Microscope.

Mouse Skeletal Staining

Wnt1:Cre; Talpid3$^{fl/fl}$ P0 mice and control littermates were fixed in 90% ethanol, then skinned and eviscerated. Staining with Alcian Blue (0.05%) was performed in 70% ethanol with 20% acetic acid, followed by staining with Alizarin Red (0.15%) in 1% KOH. Soft tissue was cleared with 1% KOH with 20% glycerol and skeletons were stored in 80% glycerol.

DATA AVAILABILITY STATEMENT

The datasets presented in this study can be found in online repositories. The names of the repository/repositories and accession number(s) can be found in the article/**Supplementary Material**.

ETHICS STATEMENT

The studies involving human participants were reviewed and approved by MRC/Wellcome Trust Human Developmental Biology Resource (HDBR) under informed ethical consent with Research Tissue Bank ethical approval (08/H0712/34 + 5 and 08/H0906/21 + 5) Ethical Committee of Paris Ile de France II. The patients/participants provided their written informed consent to participate in this study. The animal study was reviewed and approved by local approvals and the United Kingdom Animals (Scientific Procedures) Act 1986 under license from the Home Office (PPL70/7500).

AUTHOR CONTRIBUTIONS

AB, NT, and JD designed the study. AB and JD performed the chicken chimera transplantation experiments. JD, NN, DD, AG, and RH contributed and/or performed the immunohistochemistry analysis. JD, JC, AC, and GC performed *in situ* hybridization experiments. PK performed all the statistical analysis. JD, DN, and CM performed to the mouse experiments. ML provided mouse strains. NL, ST, CA, TA-B, and SL provided human samples. AB, JD, and NN analyzed the data. JD and AB wrote the manuscript with input from all authors. All authors contributed to the article and approved the submitted version.

ACKNOWLEDGMENTS

This article is dedicated to the memory of RH. We would like to thank Dagan Jenkins for the IFT88 antibody, Mark Turmaine for assistance with SEM, Kevin Lee and Erwin Pauws for assistance with cartilage and bone staining as well as help with the phenotype analysis. We also thank Jan Soetaert and Belén Martín-Martín for help with microscopy. MD and the TALPID3 flock are supported by an Institutional Strategic Grant (ISP) to The Roslin Institute from the BBSRC. NN was supported by a Bolyai Fellowship and Hungarian Science Foundation NKFI grant (124740). CM was supported by Guts UK (Derek Butler Fellowship). We are grateful to the French Society of Fetal Pathology (SoFFoet) for participating in the study. We acknowledge the NIHR Great Ormond Street Hospital Biomedical Research Centre which supports all research at Great Ormond Street Hospital NHS Foundation Trust and UCL Great Ormond Street Institute of Child Health. The views expressed are those of the authors and not necessarily those of the NHS, the NIHR or the Department of Health.

SUPPLEMENTARY MATERIAL

The Supplementary Material for this article can be found online at: https://www.frontiersin.org/articles/10.3389/fnmol.2021.757646/full#supplementary-material

Supplementary Figure 1 | Migrating ENCCs do not extend a primary cilium. **(A–C)** Scanning electron microscopy of neural tube culture and migrating vagal neural crest after 18 h culture. **(A)** Low magnification of picture shows neural tube and migrating vagal neural crest spreading out. **(B)** Close up of the neural tube shows primary cilia on cells (pseudocolored in purple, black arrows). **(C)** Close up of migrating vagal NCC shows no primary cilium. **(D)** Immunofluorescent staining for acetylated α-tubulin (green) and intraflagellar transport protein 88 (red) shows colocalization at the centrosome and no primary cilium on migrating vagal NCC (white arrow). **(E)** *In vivo* staining for the primary cilia with Arl13b on E6.5 gut sections shows signal in all mesenchymal gut cells. In migrating HuC^{+} (green) ENCCs, 11% show an extended primary cilium (inset; 10 out of 85 HuC^{+} cells counted, $n = 7$ sections). **(F)** No primary cilia staining is observed in any cell type on *talpid*^{3} E6.5 gut section.

Supplementary Figure 2 | The protein Sonic Hedgehog is expressed in both control and *talpid*^{3} intestine. **(A,B)** Immunofluorescent staining of intestine with SHH and HNK1 in **(A)** E6.5 control and **(B)** *talpid*^{3} mutant embryo. SHH (red) is expressed in the epithelium of both samples. Scattered HNK1 + ENCC (green) are observed in the intestine of *talpid*^{3} mutant embryo.

Supplementary Figure 3 | Transplantation of wild type ENCCs does not rescue the muscle phenotype in GFP > *talpid*^{3} chimeric E6.5 embryo. Measurements of epithelium (DAPI) and smooth muscle (Phalloidin) thickness in stomach and intestine sections were normalized to baseline. At E6.5 there was no statistical difference between the thickness of the epithelium of controls versus GFP > *talpid*^{3} chimera or *talpid*^{3} mutants. Thickness of the smooth muscle, as measured by phalloidin was increased 100% in the chimera and 115% in the mutant compared to GFP > wild type control transplant. Measurements of phalloidin thickness in GFP > *talpid*^{3} chimera and mutant were statistically equivalent and they were both statistically significant from the baseline control (***$p < 0.001$). ctrl, control.

Supplementary Figure 4 | Cranial and GI tract phenotypes of *Wnt1:Cre;Talpid3*$^{fl/fl}$ P0 mice and control littermate. **(A,D)** Gross phenotype of **(A)** control littermate and **(D)** *Wnt1:Cre;Talpid3*$^{fl/fl}$ P0 pups. **(B,E)** Gross morphology of the dissected gastrointestinal tract and lungs of **(B)** control littermate and **(E)** *Wnt1:Cre;Talpid3*$^{fl/fl}$ P0 pups. Mutant littermates show grossly normal GI tract, red colored uninflated lungs as well as craniofacial abnormalities such as cleft pallet, short snot and brachycephaly. **(C,F)** Skeletal staining of the skulls of **(C)** control littermate and **(F)** *Wnt1:Cre;Talpid3*$^{fl/fl}$ P0 pups. Red indicates bone and blue indicates cartilage. **(F)** *Wnt1:Cre;Talpid3*$^{fl/fl}$ skull shows frontonasal hypoplasia, hypoplastic NCC derivatives, micrognathia, facial cleft-partitioning of the nasal cartilage and underdeveloped sagittal suture.

Supplementary Figure 5 | Expression of SMA, Tuj-1, CS56 and *patched* in week 19 control human gut and *patched in situ* hybridization in 26 weeks KIAA0586 gut.

(A,B) Control intestine shows normal neuromuscular patterning and CS56 expression at week 19. **(C–E)** *In situ* hybridization against *patched* in week 19 control and *KIAA0586* mutated tissue. (C + insets) Week 19 control intestine shows strong expression of *patched* in the epithelium, in the myenteric plexus of the ENS and to a lesser extend in the smooth muscle. **(D)** "Segment 1" shows *patched* expression in the myenteric plexus (inset) and the muscle layers. **(E)** "Segment 2" shows a diffuse *patched* expression throughout the section. muc, mucosa; sub muc, submucosa; cm, circular muscle; lm, longitudinal muscle; MYP, myenteric plexus; sero, serosa.

Supplementary Video 1 | Animated confocal *Z* stack of whole mount immunofluorescent staining for SMA smooth muscle actin (red) and TuJ-1 Neuron-specific class III beta-tubulin (green) and DAPI (blue) on stomach of control P0 mice littermate **(Left)** and *Wnt1:Cre;Talpid3*$^{fl/fl}$ **(Right)**.

Supplementary Video 2 | Animated confocal *Z* stack of whole mount immunofluorescent staining for SMA smooth muscle actin (red) and TuJ-1 Neuron-specific class III beta-tubulin (green) and DAPI (blue) on intestine of control P0 mice littermate **(Left)** and *Wnt1:Cre;Talpid3* $^{fl/fl}$ **(Right)**.

REFERENCES

Abdelhamed, Z. A., Wheway, G., Szymanska, K., Natarajan, S., Toomes, C., Inglehearn, C., et al. (2013). Variable expressivity of ciliopathy neurological phenotypes that encompass Meckel-Gruber syndrome and Joubert syndrome is caused by complex de-regulated ciliogenesis, Shh and Wnt signalling defects. *Hum. Mol. Genet.* 22, 1358–1372. doi: 10.1093/hmg/dds546

Akawi, N., McRae, J., Ansari, M., Balasubramanian, M., Blyth, M., Brady, A. F., et al. (2015). Discovery of four recessive developmental disorders using probabilistic genotype and phenotype matching among 4,125 families. *Nat. Genet.* 47, 1363–1369. doi: 10.1038/ng.3410

Akhondian, J., Ashrafzadeh, F., Beiraghi Toosi, M., Moazen, N., Mohammadpoor, T., and Karami, R. (2013). Joubert Syndrome in Three Children in A Family: a Case Series. *Iran. J. Child Neurol.* 7, 39–42.

Alby, C., Malan, V., Boutaud, L., Marangoni, M. A., Bessieres, B., Bonniere, M., et al. (2016). Clinical, genetic and neuropathological findings in a series of 138 fetuses with a corpus callosum malformation. *Birth Defects Res. A Clin. Mol. Teratol.* 106, 36–46. doi: 10.1002/bdra.23472

Alby, C., Piquand, K., Huber, C., Megarbane, A., Ichkou, A., Legendre, M., et al. (2015). Mutations in KIAA0586 Cause Lethal Ciliopathies Ranging from a Hydrolethalus Phenotype to Short-Rib Polydactyly Syndrome. *Am. J. Hum. Genet.* 97, 311–318. doi: 10.1016/j.ajhg.2015.06.003

Bachmann-Gagescu, R., Phelps, I. G., Dempsey, J. C., Sharma, V. A., Ishak, G. E., Boyle, E. A., et al. (2015). KIAA0586 is Mutated in Joubert Syndrome. *Hum. Mutat.* 36, 831–835.

Bangs, F., Antonio, N., Thongnuek, P., Welten, M., Davey, M. G., Briscoe, J., et al. (2011). Generation of mice with functional inactivation of talpid3, a gene first identified in chicken. *Development* 138, 3261–3272. doi: 10.1242/dev.063602

Bashford, A. L., and Subramanian, V. (2019). Mice with a conditional deletion of Talpid3 (KIAA0586) - a model for Joubert syndrome. *J. Pathol.* 248, 396–408. doi: 10.1002/path.5271

Ben, J., Elworthy, S., Ng, A. S., van Eeden, F., and Ingham, P. W. (2011). Targeted mutation of the talpid3 gene in zebrafish reveals its conserved requirement for ciliogenesis and Hedgehog signalling across the vertebrates. *Development* 138, 4969–4978. doi: 10.1242/dev.070862

Ben-Shahar, Y., Pollak, Y., Bitterman, A., Coran, A. G., Bejar, I. N., and Sukhotnik, I. (2019). Sonic hedgehog signaling controls gut epithelium homeostasis following intestinal ischemia-reperfusion in a rat. *Pediatr. Surg. Int.* 35, 255–261. doi: 10.1007/s00383-018-4406-2

Biau, S., Jin, S., and Fan, C.-M. (2013). Gastrointestinal defects of the *Gas1* mutant involve dysregulated Hedgehog and Ret signaling. *Biol. Open* 2, 144–155.

Bourret, A., Chauvet, N., de Santa Barbara, P., and Faure, S. (2017). Colonic mesenchyme differentiates into smooth muscle before its colonization by vagal enteric neural crest-derived cells in the chick embryo. *Cell Tissue Res.* 368, 503–511. doi: 10.1007/s00441-017-2577-0

Bradshaw, L., Chaudhry, B., Hildreth, V., Webb, S., and Henderson, D. J. (2009). Dual role for neural crest cells during outflow tract septation in the neural crest-deficient mutant Splotch2H. *J. Anat.* 214, 245–257. doi: 10.1111/j.1469-7580.2008.01028.x

Briscoe, J., and Therond, P. P. (2013). The mechanisms of Hedgehog signalling and its roles in development and disease. *Nat. Rev. Mol. Cell Biol.* 14, 416–429.

Brooks, E. C., Bonatto Paese, C. L., Carroll, A. H., Struve, J. N., Nagy, N., and Brugmann, S. A. (2021). Mutation in the Ciliary Protein C2CD3 Reveals Organ-Specific Mechanisms of Hedgehog Signal Transduction in Avian Embryos. *J. Dev. Biol.* 9:12. doi: 10.3390/jdb9020012

Brugmann, S. A., Allen, N. C., James, A. W., Mekonnen, Z., Madan, E., and Helms, J. A. (2010). A primary cilia-dependent etiology for midline facial disorders. *Hum. Mol. Genet.* 19, 1577–1592. doi: 10.1093/hmg/ddq030

Burns, A. J., and Delalande, J. M. (2005). Neural crest cell origin for intrinsic ganglia of the developing chicken lung. *Dev. Biol.* 277, 63–79. doi: 10.1016/j.ydbio.2004.09.006

Burns, A. J., and Le Douarin, N. M. (2001). Enteric nervous system development: analysis of the selective developmental potentialities of vagal and sacral neural crest cells using quail-chick chimeras. *Anat. Rec.* 262, 16–28. doi: 10.1002/1097-0185(20010101)262:1<16::AID-AR1007>3.0.CO;2-O

Buxton, P., Davey, M. G., Paton, I. R., Morrice, D. R., Francis-West, P. H., Burt, D. W., et al. (2004). Craniofacial development in the talpid3 chicken mutant. *Differentiation* 72, 348–362.

Carulli, D., Laabs, T., Geller, H. M., and Fawcett, J. W. (2005). Chondroitin sulfate proteoglycans in neural development and regeneration. *Curr. Opin. Neurobiol.* 15, 116–120.

Cassiman, D., Barlow, A., Vander Borght, S., Libbrecht, L., and Pachnis, V. (2006). Hepatic stellate cells do not derive from the neural crest. *J. Hepatol.* 44, 1098–1104.

Cocciadiferro, D., Agolini, E., Digilio, M. C., Sinibaldi, L., Castori, M., Silvestri, E., et al. (2020). The splice c.1815G>A variant in KIAA0586 results in a phenotype bridging short-rib-polydactyly and oral-facial-digital syndrome: a case report and literature review. *Medicine* 99:e19169. doi: 10.1097/MD.0000000000019169

Danielian, P. S., Muccino, D., Rowitch, D. H., Michael, S. K., and McMahon, A. P. (1998). Modification of gene activity in mouse embryos in utero by a tamoxifen-inducible form of Cre recombinase. *Curr. Biol.* 8, 1323–1322.

Davey, M. G., James, J., Paton, I. R., Burt, D. W., and Tickle, C. (2007). Analysis of talpid3 and wild-type chicken embryos reveals roles for Hedgehog signalling in development of the limb bud vasculature. *Dev. Biol.* 301, 155–165. doi: 10.1016/j.ydbio.2006.08.017

Davey, M. G., McTeir, L., Barrie, A. M., Freem, L. J., and Stephen, L. A. (2014). Loss of cilia causes embryonic lung hypoplasia, liver fibrosis, and cholestasis in the talpid3 ciliopathy mutant. *Organogenesis* 10, 177–185. doi: 10.4161/org.28819

Davey, M. G., Paton, I. R., Yin, Y., Schmidt, M., Bangs, F. K., Morrice, D. R., et al. (2006). The chicken talpid3 gene encodes a novel protein essential for Hedgehog signaling. *Genes Dev.* 20, 1365–1377. doi: 10.1101/gad.369106

Delalande, J.-M., Barlow, A. J., Thomas, A. J., Wallace, A. S., Thapar, N., Erickson, C. A., et al. (2008). The receptor tyrosine kinase RET regulates hindgut colonization by sacral neural crest cells. *Dev. Biol.* 313, 279–292. doi: 10.1016/j.ydbio.2007.10.028

Delalande, J.-M., Natarajan, D., Vernay, B., Finlay, M., Ruhrberg, C., Thapar, N., et al. (2014). Vascularisation is not necessary for gut colonisation by enteric neural crest cells. *Dev. Biol.* 385, 220–229.

Delalande, J. M., Thapar, N., and Burns, A. J. (2015). Dual labeling of neural crest cells and blood vessels within chicken embryos using Chick(GFP) neural tube grafting and carbocyanine dye DiI injection. *J. Vis. Exp.* 99:e52514. doi: 10.3791/52514

Druckenbrod, N. R., and Epstein, M. L. (2005). The pattern of neural crest advance in the cecum and colon. *Dev. Biol.* 287, 125–133. doi: 10.1016/j.ydbio.2005.08.040

Faure, S., McKey, J., Sagnol, S., and de Santa Barbara, P. (2015). Enteric neural crest cells regulate vertebrate stomach patterning and differentiation. *Development* 142, 331–342.

Ford, M. J., Yeyati, P. L., Mali, G. R., Keighren, M. A., Waddell, S. H., Mjoseng, H. K., et al. (2018). A Cell/Cilia Cycle Biosensor for Single-Cell Kinetics Reveals Persistence of Cilia after G1/S Transition Is a General Property in Cells and Mice. *Dev. Cell* 47, 509–523.e5. doi: 10.1016/j.devcel.2018.10.027

Fraser, A. M., and Davey, M. G. (2019). TALPID3 in Joubert syndrome and related ciliopathy disorders. *Curr. Opin. Genet. Dev.* 56, 41–48. doi: 10.1016/j.gde.2019.06.010

Freem, L. J., Delalande, J. M., Campbell, A. M., Thapar, N., and Burns, A. J. (2012). Lack of organ specific commitment of vagal neural crest cell derivatives as shown by back-transplantation of GFP chicken tissues. *Int. J. Dev. Biol.* 56, 245–254. doi: 10.1387/ijdb.113438lf

Fu, M., Lui, V. C., Sham, M. H., Pachnis, V., and Tam, P. K. (2004). Sonic hedgehog regulates the proliferation, differentiation, and migration of enteric neural crest cells in gut. *J. Cell Biol.* 166, 673–684.

Fu, M., Sato, Y., Lyons-Warren, A., Zhang, B., Kane, M. A., Napoli, J. L., et al. (2010). Vitamin A facilitates enteric nervous system precursor migration by reducing Pten accumulation. *Development* 137, 631–640. doi: 10.1242/dev.040550

Fukuda, K., and Yasugi, S. (2002). Versatile roles for sonic hedgehog in gut development. *J. Gastroenterol.* 37, 239–246. doi: 10.1007/s005350200030

Gao, H., Wang, D., Bai, Y., Zhang, J., Wu, M., Mi, J., et al. (2016). Hedgehog gene polymorphisms are associated with the risk of Hirschsprung's disease and anorectal malformation in a Chinese population. *Mol. Med. Rep.* 13, 4759–4766. doi: 10.3892/mmr.2016.5139

Gerrelli, D., Lisgo, S., Copp, A. J., and Lindsay, S. (2015). Enabling research with human embryonic and fetal tissue resources. *Development* 142, 3073–3076. doi: 10.1242/dev.122820

Goldstein, A. M., Hofstra, R. M., and Burns, A. J. (2013). Building a brain in the gut: development of the enteric nervous system. *Clin. Genet.* 83, 307–316. doi: 10.1111/cge.12054

Graham, H. K., Maina, I., Goldstein, A. M., and Nagy, N. (2017). Intestinal smooth muscle is required for patterning the enteric nervous system. *J. Anat.* 230, 567–574. doi: 10.1111/joa.12583

Hamburger, V., and Hamilton, H. L. (1951). A series of normal stages in the development of the chick embryo. *J. Morphol.* 88, 49–92. doi: 10.1002/jmor.1050880104

Higginbotham, H., Eom, T. Y., Mariani, L. E., Bachleda, A., Hirt, J., Gukassyan, V., et al. (2012). Arl13b in primary cilia regulates the migration and placement of interneurons in the developing cerebral cortex. *Dev. Cell* 23, 925–938. doi: 10.1016/j.devcel.2012.09.019

Higginbotham, H., Guo, J., Yokota, Y., Umberger, N. L., Su, C. Y., Li, J., et al. (2013). Arl13b-regulated cilia activities are essential for polarized radial glial scaffold formation. *Nat. Neurosci.* 16, 1000–1007. doi: 10.1038/nn.3451

Horii-Hayashi, N., Sasagawa, T., Matsunaga, W., and Nishi, M. (2015). Development and Structural Variety of the Chondroitin Sulfate Proteoglycans-Contained Extracellular Matrix in the Mouse Brain. *Neural Plast.* 2015:256389. doi: 10.1155/2015/256389

Huycke, T. R., Miller, B. M., Gill, H. K., Nerurkar, N. L., Sprinzak, D., Mahadevan, L., et al. (2019). Genetic and Mechanical Regulation of Intestinal Smooth Muscle Development. *Cell* 179, 90–105.e21. doi: 10.1016/j.cell.2019.08.041

Ingham, P. W. (2016). Drosophila Segment Polarity Mutants and the Rediscovery of the Hedgehog Pathway Genes. *Curr. Top. Dev. Biol.* 116, 477–488. doi: 10.1016/bs.ctdb.2016.01.007

Ishikawa, H., and Marshall, W. F. (2011). Ciliogenesis: building the cell's antenna. *Nat. Rev. Mol. Cell Biol.* 12, 222–234. doi: 10.1038/nrm3085

Jin, S., Martinelli, D. C., Zheng, X., Tessier-Lavigne, M., and Fan, C. M. (2015). Gas1 is a receptor for sonic hedgehog to repel enteric axons. *Proc. Natl. Acad. Sci. U. S. A.* 112, E73–E80. doi: 10.1073/pnas.1418629112

Junquera Escribano, C., Cantarero Carmona, I., Luesma Bartolome, M. J., Soriano-Navarro, M., Martinez-Ciriano, C., Castiella Muruzabal, T., et al. (2011). The primary cilium: a relevant characteristic in interstitial cells of rat duodenum enteric plexus. *Histol. Histopathol.* 26, 461–470. doi: 10.14670/HH-26.461

Kang, J.-S., Zhang, W., and Krauss, R. S. (2007). Hedgehog Signaling: cooking with Gas1. *Sci. STKE* 2007:e50. doi: 10.1126/stke.4032007pe50

Kim, J., Kato, M., and Beachy, P. A. (2009). Gli2 trafficking links Hedgehog-dependent activation of Smoothened in the primary cilium to transcriptional activation in the nucleus. *Proc. Natl. Acad. Sci. U. S. A.* 106, 21666–21671. doi: 10.1073/pnas.0912180106

Kim, J. H., Huang, Z., and Mo, R. (2005). Gli3 null mice display glandular overgrowth of the developing stomach. *Dev. Dyn.* 234, 984–991. doi: 10.1002/dvdy.20542

Kobayashi, T., Kim, S., Lin, Y. C., Inoue, T., and Dynlacht, B. D. (2014). The CP110-interacting proteins Talpid3 and Cep290 play overlapping and distinct roles in cilia assembly. *J. Cell Biol.* 204, 215–229. doi: 10.1083/jcb.201304153

Li, J., Wang, C., Wu, C., Cao, T., Xu, G., Meng, Q., et al. (2017). PKA-mediated Gli2 and Gli3 phosphorylation is inhibited by Hedgehog signaling in cilia and reduced in Talpid3 mutant. *Dev. Biol.* 429, 147–157. doi: 10.1016/j.ydbio.2017.06.035

Luesma, M. J., Cantarero, I., Castiella, T., Soriano, M., Garcia-Verdugo, J. M., and Junquera, C. (2013). Enteric neurons show a primary cilium. *J. Cell. Mol. Med.* 17, 147–153. doi: 10.1111/j.1582-4934.2012.01657.x

Lunt, M. (2013). Introduction to statistical modelling 2: categorical variables and interactions in linear regression. *Rheumatology* 54, 1141–1144. doi: 10.1093/rheumatology/ket172

Mahjoub, M. R. (2013). The importance of a single primary cilium. *Organogenesis* 9, 61–69. doi: 10.4161/org.25144

Malicdan, M. C., Vilboux, T., Stephen, J., Maglic, D., Mian, L., Konzman, D., et al. (2015). Mutations in human homologue of chicken talpid3 gene (KIAA0586) cause a hybrid ciliopathy with overlapping features of Jeune and Joubert syndromes. *J. Med. Genet.* 52, 830–839. doi: 10.1136/jmedgenet-2015-103316

Mao, J., Kim, B.-M., Rajurkar, M., Shivdasani, R. A., and McMahon, A. P. (2010). Hedgehog signaling controls mesenchymal growth in the developing mammalian digestive tract. *Development* 137, 1721–1729. doi: 10.1242/dev.044586

Matsubara, Y., Nakano, M., Kawamura, K., Tsudzuki, M., Funahashi, J.-I., Agata, K., et al. (2016). Inactivation of Sonic Hedgehog Signaling and Polydactyly in Limbs of Hereditary Multiple Malformation, a Novel Type of Talpid Mutant. *Front. Cell Dev. Biol.* 4:149. doi: 10.3389/fcell.2016.00149

May, M., Schelle, I., Brakebusch, C., Rottner, K., and Genth, H. (2014). Rac1-dependent recruitment of PAK2 to G2 phase centrosomes and their roles in the regulation of mitotic entry. *Cell Cycle* 13, 2211–2221. doi: 10.4161/cc.29279

May-Simera, H. L., Gumerson, J. D., Gao, C., Campos, M., Cologna, S. M., Beyer, T., et al. (2016). Loss of MACF1 Abolishes Ciliogenesis and Disrupts Apicobasal Polarity Establishment in the Retina. *Cell Rep.* 17, 1399–1413. doi: 10.1016/j.celrep.2016.09.089

McGrew, M. J., Sherman, A., Ellard, F. M., Lillico, S. G., Gilhooley, H. J., Kingsman, A. J., et al. (2004). Efficient production of germline transgenic chickens using lentiviral vectors. *EMBO Rep.* 5, 728–733.

Merchant, J. L. (2012). Hedgehog signalling in gut development, physiology and cancer. *J. Physiol.* 590, 421–432.

Millington, G., Elliott, K. H., Chang, Y.-T., Chang, C.-F., Dlugosz, A., and Brugmann, S. A. (2017). Cilia-dependent GLI processing in neural crest cells is required for tongue development. *Dev. Biol.* 424, 124–137. doi: 10.1016/j.ydbio.2017.02.021

Motoyama, J., Liu, J., Mo, R., Ding, Q., Post, M., and Hui, C. C. (1998). Essential function of Gli2 and Gli3 in the formation of lung, trachea and oesophagus. *Nat. Genet.* 20, 54–57.

Mulligan, L. M. (2014). RET revisited: expanding the oncogenic portfolio. *Nat. Rev. Cancer* 14, 173–186. doi: 10.1038/nrc3680

Murdoch, J. N., and Copp, A. J. (2010). The relationship between Sonic hedgehog signalling, cilia and neural tube defects. *Birth Defects Res. A Clin. Mol. Teratol.* 88, 633–652.

Nagy, N., Barad, C., Graham, H. K., Hotta, R., Cheng, L. S., Fejszak, N., et al. (2016). Sonic hedgehog controls enteric nervous system development by patterning the extracellular matrix. *Development* 143, 264–275. doi: 10.1242/dev.128132

Nagy, N., and Goldstein, A. M. (2017). Enteric nervous system development: a crest cell's journey from neural tube to colon. *Semin. Cell Dev. Biol.* 66, 94–106. doi: 10.1016/j.semcdb.2017.01.006

Naharros, I. O., Cristian, F. B., Zang, J., Gesemann, M., Ingham, P. W., Neuhauss, S. C. F., et al. (2018). The ciliopathy protein TALPID3/KIAA0586 acts upstream of Rab8 activation in zebrafish photoreceptor outer segment formation and maintenance. *Sci. Rep.* 8:2211.

Natarajan, D., Marcos-Gutierrez, C., Pachnis, V., and de Graaff, E. (2002). Requirement of signalling by receptor tyrosine kinase RET for the directed migration of enteric nervous system progenitor cells during mammalian embryogenesis. *Development* 129, 5151–5160. doi: 10.1242/dev.129.22.5151

Noah, T. K., Donahue, B., and Shroyer, N. F. (2011). Intestinal development and differentiation. *Exp. Cell Res.* 317, 2702–2710.

Ozyurek, H., Kayacik, O. E., Gungor, O., and Karagoz, F. (2008). Rare association of Hirschsprung's disease and Joubert syndrome. *Eur. J. Pediatr.* 167, 475–477.

Pan, Y., Wang, C., and Wang, B. (2009). Phosphorylation of Gli2 by protein kinase A is required for Gli2 processing and degradation and the Sonic Hedgehog-regulated mouse development. *Dev. Biol.* 326, 177–189. doi: 10.1016/j.ydbio.2008.11.009

Pathi, S., Pagan-Westphal, S., Baker, D. P., Garber, E. A., Rayhorn, P., Bumcrot, D., et al. (2001). Comparative biological responses to human Sonic, Indian, and Desert hedgehog. *Mech. Dev.* 106, 107–117.

Purkait, R., Basu, R., Das, R., and Chatterjee, U. (2015). Association of Joubert syndrome and Hirschsprung disease. *Indian Pediatr.* 52, 61–62.

Ramalho-Santos, M., Melton, D. A., and McMahon, A. P. (2000). Hedgehog signals regulate multiple aspects of gastrointestinal development. *Development* 127, 2763–2772.

Ramsbottom, S. A., and Pownall, M. E. (2016). Regulation of Hedgehog Signalling Inside and Outside the Cell. *J. Dev. Biol.* 4:23.

Rao, M., and Gershon, M. D. (2016). The bowel and beyond: the enteric nervous system in neurological disorders. *Nat. Rev. Gastroenterol. Hepatol.* 13, 517–528.

Reichenbach, B., Delalande, J. M., Kolmogorova, E., Prier, A., Nguyen, T., Smith, C. M., et al. (2008). Endoderm-derived Sonic hedgehog and mesoderm Hand2 expression are required for enteric nervous system development in zebrafish. *Dev. Biol.* 318, 52–64. doi: 10.1016/j.ydbio.2008.02.061

Ring, C., Hassell, J., and Halfter, W. (1996). Expression pattern of collagen IX and potential role in the segmentation of the peripheral nervous system. *Dev. Biol.* 180, 41–53. doi: 10.1006/dbio.1996.0283

Roosing, S., Hofree, M., Kim, S., Scott, E., Copeland, B., Romani, M., et al. (2015). Functional genome-wide siRNA screen identifies KIAA0586 as mutated in Joubert syndrome. *Elife* 4:e06602. doi: 10.7554/eLife.06602

Roper, R. J., VanHorn, J. F., Cain, C. C., and Reeves, R. H. (2009). A neural crest deficit in Down syndrome mice is associated with deficient mitotic response to Sonic hedgehog. *Mech. Dev.* 126, 212–219. doi: 10.1016/j.mod.2008.11.002

Sanders, A. A., de Vrieze, E., Alazami, A. M., Alzahrani, F., Malarkey, E. B., Sorusch, N., et al. (2015). KIAA0556 is a novel ciliary basal body component mutated in Joubert syndrome. *Genome Biol.* 16:293. doi: 10.1186/s13059-015-0858-z

Sasai, N., and Briscoe, J. (2012). Primary cilia and graded Sonic Hedgehog signaling. *Wiley Interdiscip. Rev. Dev. Biol.* 1, 753–772.

Sasselli, V., Pachnis, V., and Burns, A. J. (2012). The enteric nervous system. *Dev. Biol.* 366, 64–73.

Schlieve, C. R., Fowler, K. L., Thornton, M., Huang, S., Hajjali, I., Hou, X., et al. (2017). Neural Crest Cell Implantation Restores Enteric Nervous System Function and Alters the Gastrointestinal Transcriptome in Human Tissue-Engineered Small Intestine. *Stem Cell Rep.* 9, 883–896. doi: 10.1016/j.stemcr.2017.07.017

Schneider, A., Hommel, G., and Blettner, M. (2010). Linear regression analysis: part 14 of a series on evaluation of scientific publications. *Dtsch. Arztebl. Int.* 107, 776–782. doi: 10.3238/arztebl.2010.0776

Schock, E. N., Chang, C. F., Youngworth, I. A., Davey, M. G., Delany, M. E., and Brugmann, S. A. (2016). Utilizing the chicken as an animal model for human craniofacial ciliopathies. *Dev. Biol.* 415, 326–337. doi: 10.1016/j.ydbio.2015.10.024

Seeger-Nukpezah, T., and Golemis, E. A. (2012). The extracellular matrix and ciliary signaling. *Curr. Opin. Cell Biol.* 24, 652–661.

Shian, W. J., Chi, C. S., Mak, S. C., and Chen, C. H. (1993). Joubert syndrome in Chinese infants and children: a report of four cases. *Zhonghua Yi Xue Za Zhi* 52, 342–345.

Siebert, J. R., Conta Steencken, A., and Osterhout, D. J. (2014). Chondroitin sulfate proteoglycans in the nervous system: inhibitors to repair. *Biomed Res. Int.* 2014:845323.

Simpson, M. J., Zhang, D. C., Mariani, M., Landman, K. A., and Newgreen, D. F. (2007). Cell proliferation drives neural crest cell invasion of the intestine. *Dev. Biol.* 302, 553–568. doi: 10.1016/j.ydbio.2006.10.017

Spencer, N. J., Bayguinov, P., Hennig, G. W., Park, K. J., Lee, H. T., Sanders, K. M., et al. (2007). Activation of neural circuitry and Ca2+ waves in longitudinal and circular muscle during CMMCs and the consequences of rectal aganglionosis in mice. *Am. J. Physiol. Gastrointest. Liver Physiol.* 292, G546–G555. doi: 10.1152/ajpgi.00352.2006

Srinivas, S., Watanabe, T., Lin, C. S., William, C. M., Tanabe, Y., Jessell, T. M., et al. (2001). Cre reporter strains produced by targeted insertion of EYFP and ECFP into the ROSA26 locus. *BMC Dev. Biol.* 1:4. doi: 10.1186/1471-213x-1-4

Stenmark, H. (2009). Rab GTPases as coordinators of vesicle traffic. *Nat. Rev. Mol. Cell Biol.* 10, 513–525. doi: 10.1038/nrm2728

Stephen, L. A., Johnson, E. J., Davis, G. M., McTeir, L., Pinkham, J., Jaberi, N., et al. (2014). The chicken left right organizer has nonmotile cilia which are lost in a stage-dependent manner in the talpid3 ciliopathy. *Genesis* 52, 600–613. doi: 10.1002/dvg.22775

Stephen, L. A., Tawamie, H., Davis, G. M., Tebbe, L., Nurnberg, P., Nurnberg, G., et al. (2015). TALPID3 controls centrosome and cell polarity and the human ortholog KIAA0586 is mutated in Joubert syndrome (JBTS23). *Elife* 4:e08077. doi: 10.7554/eLife.08077

Sung, C.-H., and Leroux, M. R. (2013). The roles of evolutionarily conserved functional modules in cilia-related trafficking. *Nat. Cell Biol.* 15, 1387–1397. doi: 10.1038/ncb2888

Tennyson, V. M., Payette, R. F., Rothman, T. P., and Gershon, M. D. (1990). Distribution of hyaluronic acid and chondroitin sulfate proteoglycans in the presumptive aganglionic terminal bowel of ls/ls fetal mice: an ultrastructural analysis. *J. Comp. Neurol.* 291, 345–362. doi: 10.1002/cne.902910303

Thiagarajah, J. R., Yildiz, H., Carlson, T., Thomas, A. R., Steiger, C., Pieretti, A., et al. (2014). Altered goblet cell differentiation and surface mucus properties in Hirschsprung disease. *PLoS One* 9:e99944. doi: 10.1371/journal.pone.0099944

Thomas, P. S., Kim, J., Nunez, S., Glogauer, M., and Kaartinen, V. (2010). Neural crest cell-specific deletion of Rac1 results in defective cell–matrix interactions and severe craniofacial and cardiovascular malformations. *Dev. Biol.* 340, 613–625. doi: 10.1016/j.ydbio.2010.02.021

Tsai, J. J., Hsu, W. B., Liu, J. H., Chang, C. W., and Tang, T. K. (2019). CEP120 interacts with C2CD3 and Talpid3 and is required for centriole appendage assembly and ciliogenesis. *Sci. Rep.* 9:6037. doi: 10.1038/s41598-019-42577-0

van den Brink, G. R. (2007). Hedgehog signaling in development and homeostasis of the gastrointestinal tract. *Physiol. Rev.* 87, 1343–1375. doi: 10.1152/physrev.00054.2006

Villumsen, B. H., Danielsen, J. R., Povlsen, L., Sylvestersen, K. B., Merdes, A., Beli, P., et al. (2013). A new cellular stress response that triggers centriolar satellite reorganization and ciliogenesis. *EMBO J.* 32, 3029–3040. doi: 10.1038/emboj.2013.223

Waldo, K. L., Hutson, M. R., Stadt, H. A., Zdanowicz, M., Zdanowicz, J., and Kirby, M. L. (2005). Cardiac neural crest is necessary for normal addition of the myocardium to the arterial pole from the secondary heart field. *Dev. Biol.* 281, 66–77. doi: 10.1016/j.ydbio.2005.02.011

Wallace, A. S., and Burns, A. J. (2005). Development of the enteric nervous system, smooth muscle and interstitial cells of Cajal in the human gastrointestinal tract. *Cell Tissue Res.* 319, 367–382. doi: 10.1007/s00441-004-1023-2

Wang, L., Lee, K., Malonis, R., Sanchez, I., and Dynlacht, B. D. (2016). Tethering of an E3 ligase by PCM1 regulates the abundance of centrosomal KIAA0586/Talpid3 and promotes ciliogenesis. *Elife* 5:e12950. doi: 10.7554/eLife.12950

Willaredt, M. A., Hasenpusch-Theil, K., Gardner, H. A., Kitanovic, I., Hirschfeld-Warneken, V. C., Gojak, C. P., et al. (2008). A crucial role for primary cilia in cortical morphogenesis. *J. Neurosci.* 28, 12887–12900. doi: 10.1523/JNEUROSCI.2084-08.2008

Wu, C., Yang, M., Li, J., Wang, C., Cao, T., Tao, K., et al. (2014). Talpid3-binding centrosomal protein Cep120 is required for centriole duplication and proliferation of cerebellar granule neuron progenitors. *PLoS One* 9:e107943. doi: 10.1371/journal.pone.0107943

Yan, H., Chen, C., Chen, H., Hong, H., Huang, Y., Ling, K., et al. (2020). TALPID3 and ANKRD26 selectively orchestrate FBF1 localization and cilia gating. *Nat. Commun.* 11:2196. doi: 10.1038/s41467-020-16042-w

Yin, Y., Bangs, F., Paton, I. R., Prescott, A., James, J., Davey, M. G., et al. (2009). The Talpid3 gene (KIAA0586) encodes a centrosomal protein that is essential for primary cilia formation. *Development* 136, 655–664. doi: 10.1242/dev.028464

Zorn, A. M., and Wells, J. M. (2009). Vertebrate Endoderm Development and Organ Formation. *Annu. Rev. Cell Dev. Biol.* 25, 221–251. doi: 10.1146/annurev.cellbio.042308.113344

Conflict of Interest: AB is currently a full time employee of Takeda Pharmaceuticals International Inc.

The remaining authors declare that the research was conducted in the absence of any commercial or financial relationships that could be construed as a potential conflict of interest.

Publisher's Note: All claims expressed in this article are solely those of the authors and do not necessarily represent those of their affiliated organizations, or those of the publisher, the editors and the reviewers. Any product that may be evaluated in this article, or claim that may be made by its manufacturer, is not guaranteed or endorsed by the publisher.

frontiers | Frontiers in Molecular Neuroscience

CORRECTION
published: 29 April 2022
doi: 10.3389/fnmol.2022.871557

Corrigendum: TALPID3/KIAA0586 Regulates Multiple Aspects of Neuromuscular Patterning During Gastrointestinal Development in Animal Models and Human

Jean Marie Delalande[1,2†], Nandor Nagy[3†], Conor J. McCann[2], Dipa Natarajan[2], Julie E. Cooper[4], Gabriela Carreno[4], David Dora[3], Alison Campbell[5], Nicole Laurent[6], Polychronis Kemos[1], Sophie Thomas[7], Caroline Alby[8], Tania Attié-Bitach[7,8,9], Stanislas Lyonnet[7,8,9], Malcolm P. Logan[10], Allan M. Goldstein[11], Megan G. Davey[12], Robert M. W. Hofstra[13‡], Nikhil Thapar[2,13] and Alan J. Burns[2,14,15]*

[1] Centre for Immunobiology, Barts and The London School of Medicine and Dentistry, Queen Mary University of London, London, United Kingdom, [2] Stem Cells and Regenerative Medicine, Birth Defects Research Centre, UCL Great Ormond Street Institute of Child Health, London, United Kingdom, [3] Department of Anatomy, Histology and Embryology, Semmelweis University, Budapest, Hungary, [4] Developmental Biology and Cancer Program, Birth Defects Research Centre, UCL Great Ormond Street Institute of Child Health, London, United Kingdom, [5] Department of Paediatric Surgery, Christchurch Hospital, Christchurch, New Zealand, [6] Génétique et Anomalies du Développement, Université De Bourgogne, Service d'Anatomie Pathologique, Dijon, France, [7] Laboratory of Embryology and Genetics of Congenital Malformations, INSERM UMR 1163 Institut Imagine, Paris, France, [8] Department of Genetics, Hôpital Necker-Enfants Malades, Assistance Publique Hôpitaux de Paris (AP-HP), Paris, France, [9] Paris Descartes, Sorbonne Paris Cité, Paris, France, [10] Randall Division of Cell and Molecular Biophysics, King's College London, London, United Kingdom, [11] Department of Pediatric Surgery, Massachusetts General Hospital, Harvard Medical School, Boston, MA, United States, [12] Division of Developmental Biology, The Roslin Institute, The University of Edinburgh, Edinburgh, United Kingdom, [13] Department of Clinical Genetics, Erasmus University Medical Center, Rotterdam, Netherlands, [14] Division of Neurogastroenterology and Motility, Department of Gastroenterology, Great Ormond Street Hospital for Children NHS Foundation Trust, London, United Kingdom, [15] Gastrointestinal Drug Discovery Unit, Takeda Pharmaceuticals International, Inc., Cambridge, MA, United States

Keywords: TALPID3, KIAA0586, Sonic Hedgehog, enteric nervous system, neural crest cell, gastrointestinal tract, short-rib polydactyly syndrome, Joubert syndrome

Approved by:
Frontiers Editorial Office, Frontiers Media SA, Switzerland

***Correspondence:**
Alan J. Burns
alan.burns@ucl.ac.uk

†These authors have contributed equally to this work
‡Deceased

Specialty section:
This article was submitted to Methods and Model Organisms, a section of the journal Frontiers in Molecular Neuroscience

Received: *08 February 2022*
Accepted: *30 March 2022*
Published: *29 April 2022*

Citation:
Delalande JM, Nagy N, McCann CJ, Natarajan D, Cooper JE, Carreno G, Dora D, Campbell A, Laurent N, Kemos P, Thomas S, Alby C, Attié-Bitach T, Lyonnet S, Logan MP, Goldstein AM, Davey MG, Hofstra RMW, Thapar N and Burns AJ (2022) Corrigendum: TALPID3/KIAA0586 Regulates Multiple Aspects of Neuromuscular Patterning During Gastrointestinal Development in Animal Models and Human. Front. Mol. Neurosci. 15:871557. doi: 10.3389/fnmol.2022.871557

A Corrigendum on

TALPID3/KIAA0586 Regulates Multiple Aspects of Neuromuscular Patterning During Gastrointestinal Development in Animal Models and Human

by Delalande, J. M., Nagy, N., McCann, C. J., Natarajan, D., Cooper, J. E., Carreno, G., Dora, D., Campbell, A., Laurent, N., Kemos, P., Thomas, S., Alby, C., Attié-Bitach, T., Lyonnet, S., Logan, M. P., Goldstein, A. M., Davey, M. G., Hofstra, R. M. W., Thapar, N., and Burns, A. J. (2021). Front. Mol. Neurosci. 14:757646. doi: 10.3389/fnmol.2021.757646

In the original article, there was an error. Figures 2, 3, 4 and 5 were referenced incorrectly. All references to Figure 5 should have been Figure 2, all references to Figure 4 should have been Figure 3, all references to Figure 3 should have been Figure 4, all references to figure 2 should have been Figure 5.

The authors apologize for this error and state that this does not change the scientific conclusions of the article in any way. The original article has been updated.

Publisher's Note: All claims expressed in this article are solely those of the authors and do not necessarily represent those of their affiliated organizations, or those of the publisher, the editors and the reviewers. Any product that may be evaluated in this article, or claim that may be made by its manufacturer, is not guaranteed or endorsed by the publisher.

frontiers in Molecular Neuroscience

BRIEF RESEARCH REPORT
published: 03 February 2022
doi: 10.3389/fnmol.2022.788301

MicroRNA *miR-155* Activity in Mouse Choline Acetyltransferase-Positive Neurons Is Critical for the Rate of Early and Late Paraplegia After Transient Aortic Cross-Clamping

Hesham Kelani[1], Gerard Nuovo[2], Anna Bratasz[3], Jayanth Rajan[1†], Alexander A. Efanov[1], Jean-Jacques Michaille[4,5], Hamdy Awad[1] and Esmerina Tili[1,5]**

[1] Department of Anesthesiology, Wexner Medical Center, The Ohio State University, Columbus, OH, United States, [2] GNOME, Inc., Powell, OH, United States, [3] Small Animal Imaging Center Shared Resource, Wexner Medical Center, The Ohio State University, Columbus, OH, United States, [4] BioPerox-IL, Faculté des Sciences Gabriel, Université de Bourgogne-Franche Comté, Dijon, France, [5] Department of Cancer Biology and Genetics, Wexner Medical Center, The Ohio State University, Columbus, OH, United States

Aortic aneurism open repair surgery can cause spinal cord (SC) injury with 5–15% of patients developing paraparesis or paraplegia. Using a mouse model of transient aortic cross-clamping (ACC), we have previously found that the expression of proinflammatory microRNA *miR-155* increases in motoneurons (MNs) and endothelial cells (ECs) of ischemic SCs, and that global *miR-155* deletion decreases the percentage of paraplegia by 37.4% at 48-h post-ACC. Here, we investigated the cell-specific contribution of *miR-155* in choline acetyltransferase-positive (ChAT$^+$) neurons (that include all MNs of the SC) and ECs to SC injury after ACC. Mice lacking *miR-155* in ChAT$^+$ neurons (MN-*miR-155*-KO mice) developed 24.6% less paraplegia than control mice at 48-h post-ACC. In contrast, mice lacking *miR-155* in ECs (ECs-*miR-155*-KO mice) experienced the same percentage of paraplegia as control mice, despite presenting smaller central cord edema. Unexpectedly, mice overexpressing *miR-155* in ChAT$^+$ neurons were less likely than control mice to develop early paraplegia during the first day post-ACC, however they reached the same percentage of paraplegia at 48-h. In addition, all mice overexpressing *miR-155* in ECs (ECs-*miR-155*-KI mice) were paraplegic at 48-h post-ACC. Altogether, our results suggest that *miR-155* activity in ChAT$^+$ neurons protects the SC against ischemic injury during the first day post-ACC before becoming deleterious during the second day, which indicates that early and late paraplegias arise from different molecular malfunctions. These results point to the need to develop specific protective therapeutics aimed at inhibiting both the early and late deleterious events after open repair surgery of aortic aneurisms.

Keywords: open repair (OR), aortic cross-clamping, spinal cord injury (SCI), *miR-155*, edema, motoneurons (MNs), endothelial cells (ECs), paraplegia

OPEN ACCESS

Edited by:
Parthiv Haldipur, Seattle Children's Research Institute, United States

Reviewed by:
Zin Khaing, University of Washington, United States
Shyam Gajavelli, University of Florida, United States

****Correspondence:***
Hamdy Awad
Hamdy.Elsayed-Awad@osumc.edu
Esmerina Tili
Esmerina.Tili@osumc.edu

†Present address:
Jayanth Rajan, Lake Erie College of Osteopathic Medicine, Erie, PA, United States

Specialty section:
This article was submitted to Methods and Model Organisms, a section of the journal Frontiers in Molecular Neuroscience

Received: *02 October 2021*
Accepted: *10 January 2022*
Published: *03 February 2022*

Citation:
Kelani H, Nuovo G, Bratasz A, Rajan J, Efanov AA, Michaille J-J, Awad H and Tili E (2022) MicroRNA miR-155 Activity in Mouse Choline Acetyltransferase-Positive Neurons Is Critical for the Rate of Early and Late Paraplegia After Transient Aortic Cross-Clamping. Front. Mol. Neurosci. 15:788301. doi: 10.3389/fnmol.2022.788301

INTRODUCTION

During thoracic-abdominal aortic aneurysm (TAAA) open chest repair (OR) surgery, the transient aortic occlusion due to aortic cross-clamping (ACC) creates a situation of acute hypoxia followed by rapid reperfusion in the spinal cord (SC), thus causing SC injury and paraplegia in about 5–10% of cases depending on the extent of aortic aneurism and duration of the procedure (Coselli et al., 2016, 2019; Moulakakis et al., 2018). The pathophysiology of ACC-induced SC injury, histopathological changes, and molecular mechanisms leading to paraplegia still remains elusive. Specifically, there is currently no preventive intervention given to patients, and cerebral spinal fluid (CSF) drainage and cooling are common practices used to protect TAAA patients from paraplegia (Khachatryan et al., 2021).

In our previously developed mouse model of OR (Awad et al., 2010), ACC-induced hindlimb paraplegia is usually delayed, with the majority of mice undergoing paraplegia approximately 44–48 h following ACC. The SC damage initiates in the gray matter interneurons, and is coupled with neuronal dropout, neuro-inflammation, vascular leakage, and central cord edema, that altogether culminate in paraplegia (Awad et al., 2010, 2018). Of note, the different OR animal models have in common to induce paraplegia within 48-h post-ACC, an observation also made in patients (Kakinohana et al., 2011; Coselli et al., 2016, 2019; Moulakakis et al., 2018; Awad et al., 2021a). We have previously shown that the expression of proinflammatory microRNA *miR-155* (a.k.a. *miR-155-5p*) increases sharply in the SC of wild-type (WT) mice that experience paraplegia after ACC, as compared with non-paraplegic mice (Awad et al., 2018). This upregulation was primarily in motoneurons (MNs) and endothelial cells (ECs) of the SC. Mice with global *miR-155* deletion developed 37.4% less paraplegia than WT mice, had less central cord edema and a better preservation of SC gray matter tissue after ACC (Awad et al., 2018). Hence, we hypothesized that *miR-155* activity in MNs, ECs or a combination of both contributes to paraplegia after ACC. *MiR-155* has been shown to have both, deleterious (Henry et al., 2019; Suofu et al., 2020) and protective (Harrison et al., 2017; Li et al., 2017) effects in animal models of brain traumatic injuries, suggesting that this microRNA plays specific roles in different phases of SC injury, by potentially targeting different sets of transcripts.

To dissociate the specific role of MNs and ECs within the neurovascular unit and the effects that *miR-155* has in both cell types, we developed knock-out (KO) mice that lack the expression of *miR-155* in choline acetyltransferase-positive ($ChAT^+$) neurons, that include all MNs of the SC (MN-*miR-155*-KO), or in ECs (EC-*miR-155*-KO), as well as knock-in (KI) mice that overexpress *miR-155* specifically in $ChAT^+$ neurons (MN-*miR-155*-KI) or ECs (EC-*miR-155*-KI). Using these four *miR-155* mouse genotypes and their littermates expressing *miR-155* normally as controls, we found that overexpressing or deleting *miR-155* in $ChAT^+$ neurons respectively diminishes the percentage of early and late paraplegia post-ACC, while overexpressing *miR-155* in ECs increases the percentage of late paraplegia.

MATERIALS AND METHODS

Animals

The Animal Care and Use Committee at the Ohio State University (OSU) approved all the experiments with animals. This investigation conforms to the Guide for the Care and Use of Laboratory Animals published by the NIH. C57Bl/6 mice were obtained from Jackson Laboratories. To prepare specific *miR-155* KO mice, transgenic *miR-155*$^{fl/fl}$ mice purchased from Jackson Lab were mated to either *ChAT-Cre*$^+$ transgenic mice (Jackson Lab), which provides MN-*miR-155*-KO mice by driving the deletion of *miR-155* in $ChAT^+$ neurons that include all motoneurons of the SC, or to *Tie2-Cre*$^+$ transgenic mice (Jackson Lab), which gives EC-*miR-155*-KO mice by driving the deletion of *miR-155* in ECs. To overexpress *miR-155* in the desired cell types, we used transgenic *Rosa26*$^{lox\text{-}stop\text{-}lox-miR\text{-}155}$ (*Rosa26*$^{\text{LSL-miR-155}}$) mice that were prepared and donated by Dr. Croce (OSU) and will be described in detail in another report. These mice contain a *pri-miR-155* transgene inserted in the *Rosa26* locus, preceded by a *LoxP-Stop-LoxP* cassette that impairs its expression. The expression of the *pri-miR-155* transgene can be induced by expressing the Cre recombinase that removes *LoxP-Stop-LoxP* cassette. *Rosa26*$^{\text{LSL-miR-155}}$ were thus mated to *ChAT-Cre*$^+$ or *Tie2-Cre*$^+$ transgenic mice to drive the expression of *miR-155* in $ChAT^+$ neurons or ECs, respectively. Both male and female mice were used in our study.

Aortic Cross-Clamping

Aortic cross-clamping was conducted the same day for 7.5 min as previously described in detail (Awad et al., 2010, 2018) on both control mice and mice with modified genotype to avoid environmental variations. The procedure is detailed in **Supplementary Materials and Methods**. Following ACC, given the rapidity of development of paraplegia associated with complete impairment of hindlimbs movements, mice were classified as "paraplegic" or "non-paraplegic" upon observation, without further functional testing.

Magnetic Resonance Imaging Analysis

Magnetic resonance imagery (MRIs) were performed blindly at the Small Animal Imaging Core Shared Resource, OSU, using a Bruker BioSpec 94/30USR scanner operating at a field strength of 9.4 T (Bruker BioSpec, Germany). A 4-channels mouse brain phased array receiver-coil and 72 mm volume coil, as a transmitter were used. Anesthetized mice were placed on the holder in prone position, then the spine was gently flatted (when possible) and surface coil was placed over the dorsal side of mice covering upper lumbar and lower thoracic SC. Images were obtained using T2-weighted RARE sequences with the following parameters: TE/TR = 36/3,524 ms, Rare factor = 8, FOV = 15 × 17 mm, slice thickness = 0.5 mm, resolution = 58.6 × 66.4 μm, number of slices = 30, NA = 8. The last rib, and kidneys were used as landmark for conformation. The first slice was placed over the second disc below the last rib and 30 slices (15 mm) anterior have been acquired. The respiratory rate and rectal temperature were monitored through

the experiment with a Small Animal Instrument unit (SAI, Inc., Stonybrook, NY, United States). For volumetric measurements, images were analyzed blindly to the genotype by manually tracing the SC and hyperintense region, which corresponds to edema, using in-house build software. Images and masks of edema has been visualized using open-source ITK-SNAP software[1] (Yushkevich et al., 2006).

Hematoxylin and Eosin Staining

Following euthanasia, mice were perfused, and their SC was collected and fixed in 4% formalin for 2 days, followed by embedding in paraffin. Cross-sections were prepared blindly then stained with hematoxylin and eosin (H&E) at the Mouse Pathology Laboratory at OSU. Sections were then analyzed blindly *vis-à-vis* both the genotype and the pathologic status (paraplegic or non-paraplegic).

RNA Isolation and Quantitative Real-Time PCR

RNAs were extracted using TRIzol (Invitrogen, Carlsbad, CA, United States). The expression of *miR-155* was assessed using TaqMan® 002571 assay. Values were normalized using *snoRNA135*, providing us with a relative level of expression in the different strains.

Statistics

Quantitative real-time PCR tests and other quantitative analyses are presented as mean + SD and were compared using two-tailed Student's *t*-tests. *p*-Values are given in the legends to figures. The percentages of fully paraplegic mice of different genotypes were compared using both a Chi-square test and a Fisher exact test.[2]

RESULTS

Development of Mice That Either Overexpress or Lack *miR-155* in Choline Acetyltransferase-Positive Neurons or in Endothelial Cells

We have previously reported that *miR-155* is primarily upregulated in MNs and ECs of the SC of mice that undergo ACC-induced paraplegia, defined as the complete loss of capability to move their hindlimbs and tail, and that mice with global deletion for *miR-155* showed 37.4% less paraplegia than WT mice (Awad et al., 2018). To elucidate the specific contribution of these two cell types of the neurovascular unit to SC injury and paraplegia after ACC, and to determine how the functions of these cells is affected by the activity of *miR-155*, we developed two KO strains that specifically lack *miR-155* expression either in ChAT$^+$ neurons (MN-*miR-155*-KO), or in ECs (EC-*miR-155*-KO), as well as two KI strains that overexpress *miR-155* specifically in ChAT$^+$ neurons (MN-*miR-155*-KI) or ECs (EC-*miR-155*-KI). Of note, ChAT$^+$ neurons include MNs of the SC plus a number of interneurons. Following genotyping of the offspring of each four crosses, extracts from the cervical SC of control mice and mice of the four above genotypes were analyzed for *miR-155* expression. The offspring of each cross that were either only *miR-155*$^{fl/fl}$, *Rosa26*$^{\text{LSL-miR-155}}$, *ChAT-Cre*$^+$, or *Tie-Cre*$^+$, i.e., that retained normal *miR-155* expression, were used as control mice. As expected, compared with control mice, *miR-155* basal expression was reduced in the SC of both MN-*miR-155*-KO and EC-*miR-155*-KO mice (**Figure 1A**). In contrast, *miR-155* expression was elevated in the SC of both MN-*miR-155*-KI and EC-*miR-155*-KI mice to levels comparable to those of a strong immune response (**Figure 1B**).

The Deletion of *miR-155* in Choline Acetyltransferase-Positive Neurons Decreases the Percentage of Aortic Cross-Clamping -Induced Paraplegia at 48-h

The percentage of paraplegia after ACC surgery of mice of these four genotypes were then compared with that of control mice over a period of 48 h. The percentage of paraplegia at 24 h post-ACC was 11–36% depending on the strain (**Figure 1C** and **Table 1**). It subsequently increased sharply to reach 86.5% for control mice ($n = 37$), 76.9% for MN-*miR-155*-KI ($n = 26$), 90.9% for EC-*miR-155*-KO mice ($n = 11$), and 100% for EC-*miR-155*-KI mice ($n = 10$) at 48-h (**Figure 1C** and **Table 1**). In contrast, the percentage of paraplegia (65.2%) for MN-*miR-155*-KO mice ($n = 23$) was significantly lower (Chi-square: $p = 0.0519$; Fisher exact test: $p = 0.0627$) than that of control mice at 48-h post-ACC, indicating that *miR-155* activity in MNs and other ChAT$^+$ neurons increases the risk of developing paraplegia. Of note, the 24.6% reduction of the percentage of paraplegia obtained by deleting *miR-155* only in ChAT$^+$ neurons represents 65.8% of the reduction (37.4%) given by global *miR-155* deletion (Awad et al., 2018), suggesting that *miR-155* activity in other, non-ChAT$^+$ cells of the SC may add to the deleterious effects of this microRNA after ACC. On the other hand, increasing *miR-155* activity in ECs proved detrimental, as all EC-*miR-155*-KI mice were paraplegic at 48-h, post-ACC. Altogether, these results indicate that *miR-155* activity in ChAT$^+$ neurons is the main driver of SC injury at 48-h post-ACC.

Opposite Effects of *miR-155* Activity in Choline Acetyltransferase-Positive Neurons on Early and Late Paraplegia

Paraplegia after ACC occurs within 2 days in patients as well as in animal models, with a first wave occurring within hours post-ACC (early paraplegia) and a second wave taking place during the second day post-ACC (late paraplegia) (Kakinohana et al., 2011; Coselli et al., 2016, 2019; Moulakakis et al., 2018; Awad et al., 2021a). We therefore looked for *miR-155* effects during these two waves. Unexpectedly, *miR-155* activity protected mice against early paraplegia, for increasing *miR-155* activity in ChAT$^+$ neurons (MN-*miR-155*-KI mice) reduced the percentage of paraplegia at 24-h post-ACC by three times as compared with

[1] http://www.itksnap.org

[2] https://www.socscistatistics.com

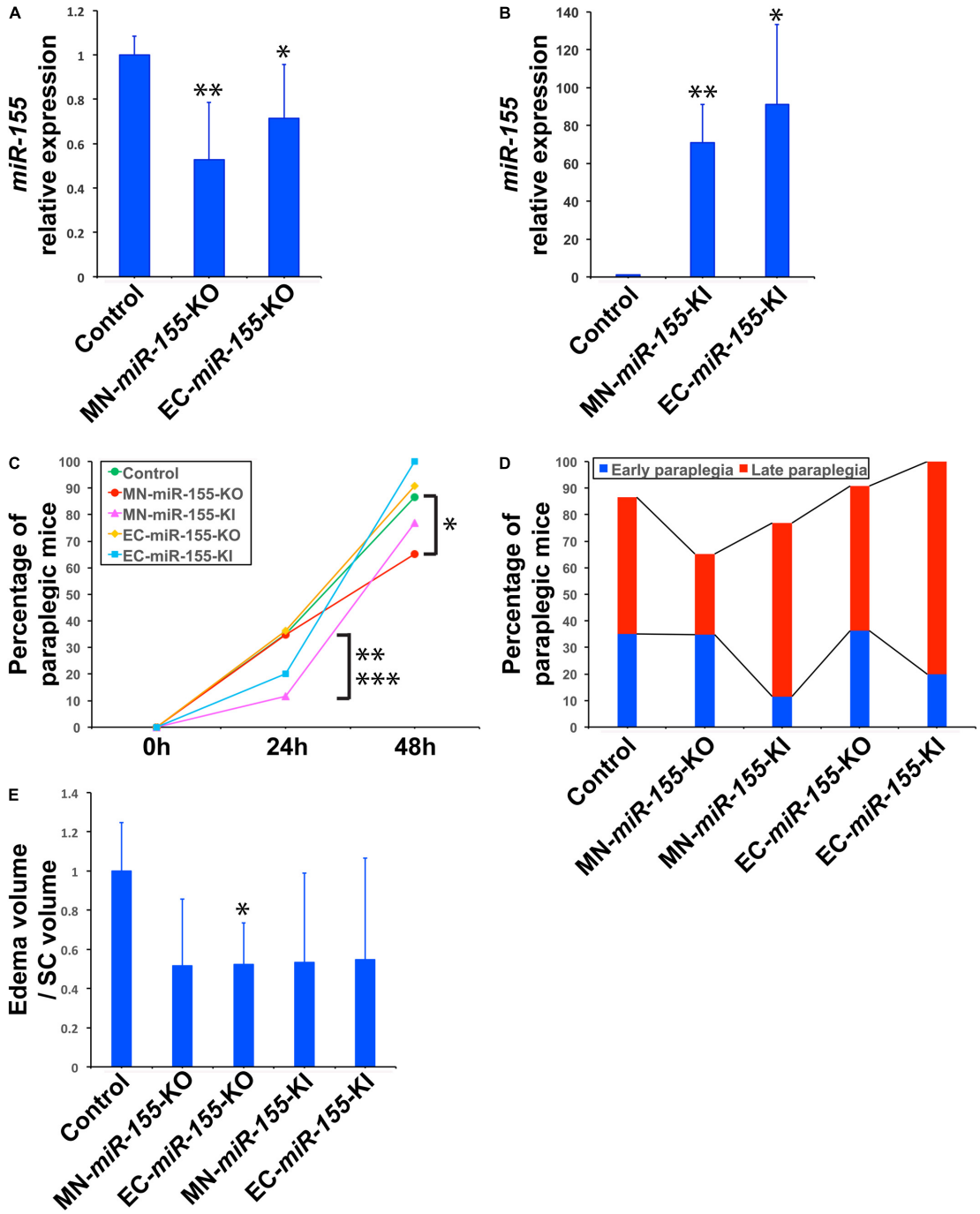

FIGURE 1 | Deletion of *miR-155* in ChAT^{+} neurons protects mice against late paraplegia. **(A)** Real-time PCR analysis showing *miR-155* relative expression in the SC of MN-*miR-155*-KO and EC-*miR-155*-KO mice. $n = 4$ for each group. Values are given as mean ± SD. The mean value for control mice was arbitrarily set to 1. The symbols * and **, significantly different from control. *$p = 0.012$; **$p = 0.055$. **(B)** Real-time PCR analysis showing *miR-155* relative expression in the SC of MN-*miR-155*-KI and EC-*miR-155*-KI mice. $n = 4$ for each group. Values are given as mean ± SD. The mean value for control mice (identical to that in panel **A**) was arbitrarily set to 1. The symbols * and **, significantly different from control. *$p = 0.024$; **$p = 0.0015$. **(C)** Percentages of paraplegic mice at 24- and 48-h post-ACC as indicated for control ($n = 37$), MN-*miR-155*-KO ($n = 23$), EC-*miR-155*-KO ($n = 11$), MN-*miR-155*-KI ($n = 26$), and EC-*miR-155*-KI ($n = 10$) mice. *Significantly lower than control mice, $p = 0.0519$ (Chi-square) or $p = 0.0627$ (Fisher). **Significantly lower than control mice, $p = 0.0342$ (Chi-square) or $p = 0.0426$ (Fisher). ***Significantly lower than MN-*miR-155*-KO mice, $p = 0.0516$ (Chi-square) or $p = 0.0855$ (Fisher). **(D)** Percentages of early and late paraplegia after ACC in control and genetically engineered mice. **(E)** Relative volumes of central cord edema in paraplegic control ($n = 8$), MN-*miR-155*-KO ($n = 3$), EC-*miR-155*-KO ($n = 3$), MN-*miR-155*-KI ($n = 4$), and EC-*miR-155*-KI ($n = 5$) mice at 48-h post-ACC. Edema volume, defined as the volume of increased T2 signal felt to represent central cord edema, was calculated by outlining areas of increased T2 signal. Relative values, calculated as ratios of edema volume/SC volume, are given as mean ± SD. The mean value for control mice was arbitrarily set to 1. *Significantly different from control, $p = 0.031$.

TABLE 1 | Dynamics of paraplegia development post-ACC for the different strains of mice.

Genotypes	Early paraplegia (0–24 h post-ACC)	Late paraplegia (24–48 h post-ACC)	Paraplegic mice at 48-h post-ACC	Non-paraplegic mice at 48-h post-ACC
Control (*n* = 37)	13 (35.1%)	19 (51.4%)	32 (86.5%)	5 (13.5%)
MN-*miR-155*-KO (*n* = 23)	8 (34.8%)	7 (30.4%)	15 (65.2%)	8 (34.8%)
MN-*miR-155*-KI (*n* = 26)	3 (11.5%)	17 (65.4%)	20 (76.9%)	6 (23.1%)
EC-*miR-155*-KO (*n* = 11)	4 (36.4%)	6 (54.5%)	10 (90.9%)	1 (9.1%)
EC-*miR-155*-KI (*n* = 10)	2 (20.0%)	8 (80.0%)	10 (100.0%)	0 (0.0%)

The percentages of mice are given in brackets after the corresponding numbers of paraplegic or non-paraplegic mice.

either control mice (Chi-square: $p = 0.0342$; Fisher exact test: $p = 0.0426$) or MN-*miR-155*-KO mice (Chi-square: $p = 0.0516$; Fisher exact test: $p = 0.0855$) (**Figures 1C,D** and **Table 1**). There also was a possible tendency to reduced early paraplegia of EC-*miR-155*-KI mice, although it did not reach statistical significance. On the other hand, neither *miR-155* deletion in $ChAT^+$ neurons nor in ECs had any measurable effect against early paraplegia (**Figures 1C,D** and **Table 1**). In contrast, the percentage of late paraplegia was lower in MN-*miR-155*-KO mice but higher in MN-*miR-155*-KI mice, indicating that *miR-155* deleterious effects in $ChAT^+$ neurons primarily occur during the second day post-ACC in relation with *miR-155* intraspinal proinflammatory effects (**Figure 1D** and **Table 1**). In addition, overexpressing *miR-155* in ECs (EC-*miR-155*-KI mice) proved highly deleterious during the second day post-ACC, with the remaining 80% of mice developing late paraplegia.

Altogether, these results suggest that: (i) *miR-155* activity in ChAT+ neurons is protective during the first 24 h post-ACC, when the formation of reactive oxygen species causes mitochondrial damage, leading to excitotoxicity followed by cytogenic edema (Juurlink and Paterson, 1998); and (ii) *miR-155* activity in both $ChAT^+$ neurons and ECs increases SC injury during the second day post-ACC, a period marked by the rapid expansion of the central cord (gray matter) edema in relation with increased inflammation and damage to the blood-SC barrier (see hereafter).

The Deletion of *miR-155* in Choline Acetyltransferase-Positive Neurons and Endothelial Cells Is Associated With a Modified Pattern of Central Cord Edema

We have previously reported that ACC leads to the development of central cord edema associated with increased *miR-155* expression at 48-h post-ACC (Awad et al., 2018). We have also reported that the development of central cord edema is somewhat delayed in *miR-155* global KO mice, based on the fact that paraplegic *miR-155* global KO mice showed a reduced volume of edema at 48-h post-ACC as compared with WT mice. As we previously reported (Awad et al., 2018), non-paraplegic control or MN-*miR-155*-KO mice showed minimal edema at 48-h post-ACC, while paraplegic control mice in contrast showed very large edema including both ventral and dorsal horns of the SC and extending from the lumbar toward the cervical region of the SC (**Figure 2** and **Supplementary Figure 1**). Strikingly, the edema in two out of three imaged paraplegic MN-*miR-155*-KO mice was restricted to the lumbar region of the SC (**Figure 2**). The edema in paraplegic EC-*miR-155*-KO also did not extend as far toward the cervical region as in control mice. In contrast, the edema in paraplegic EC-*miR-155*-KI and MN-*miR-155*-KI mice extended anteriorly like in control mice (**Figures 1C**, **2** and **Supplementary Figure 1**).

Volumetric measures showed a tendency toward reduced edema volume in paraplegic mice of all the genetically engineered strains, however this volume reduction reached significance in EC-*miR-155*-KO mice only, possibly due the large variation in edema volume at the time of paraplegia that translated into large standard deviations (**Figure 1E**). Remarkably, while MN-*miR-155*-KO mice had a reduced percentage of paraplegia as compared with control mice at 48-h post-ACC (**Figure 1C**) and developed a central cord edema restricted to the lumbar part of the SC (**Figure 2**), the average volume of their edema was not significantly smaller than that of control mice or of the other genetically engineered mice (**Figure 1E**). This result suggests that *miR-155* deletion in $ChAT^+$ neurons reduces the anterior spreading of the inflammation that develops during the second day after ACC rather than the intensity of the inflammatory response. On the other hand, EC-*miR-155*-KO, whose percentage of paraplegia post-ACC was similar to that of control mice at 48-h (**Figure 1C**), showed an average edema volume approximately 50% smaller than that of control mice (**Figures 1E**, **2** and **Table 1**). This result is not surprising, for ECs are responsible of the maintenance of the stability of the blood-SC barrier. Of note, while all EC-*miR-155*-KI mice were paraplegic at 48-h post-ACC (**Figure 1C**), their average edema volumes was not significantly different from that of control mice (**Figure 1E**). This was possibly due to edema fluid leaking out of the SC, given that EC-*miR-155*-KI mice already showed hemosiderin deposition—a sign of vascular leakage—in different tissue before ACC (not shown). The above results indicate that: (i) there is no direct correlation between either the pattern of edema or the average volume of edema with the percentage of paraplegia at 48-h post-ACC; and (ii) the development and anterior spreading of central cord edema is more likely caused by the inflammation that develops during the second day post-ACC, and whose level is primarily determined by *miR-155* expression in $ChAT^+$ neurons. In agreement with the above conclusion, the lumbar SC of a paraplegic MN-*miR-155*-KO mouse at the time of paraplegia presented with significantly vacuolated gray matter—that contains interneurons and the cell body of MNs—with overall white matter sparing, similar to the SC of paraplegic control mice (**Figure 3**). In contrast, the damage to MNs was

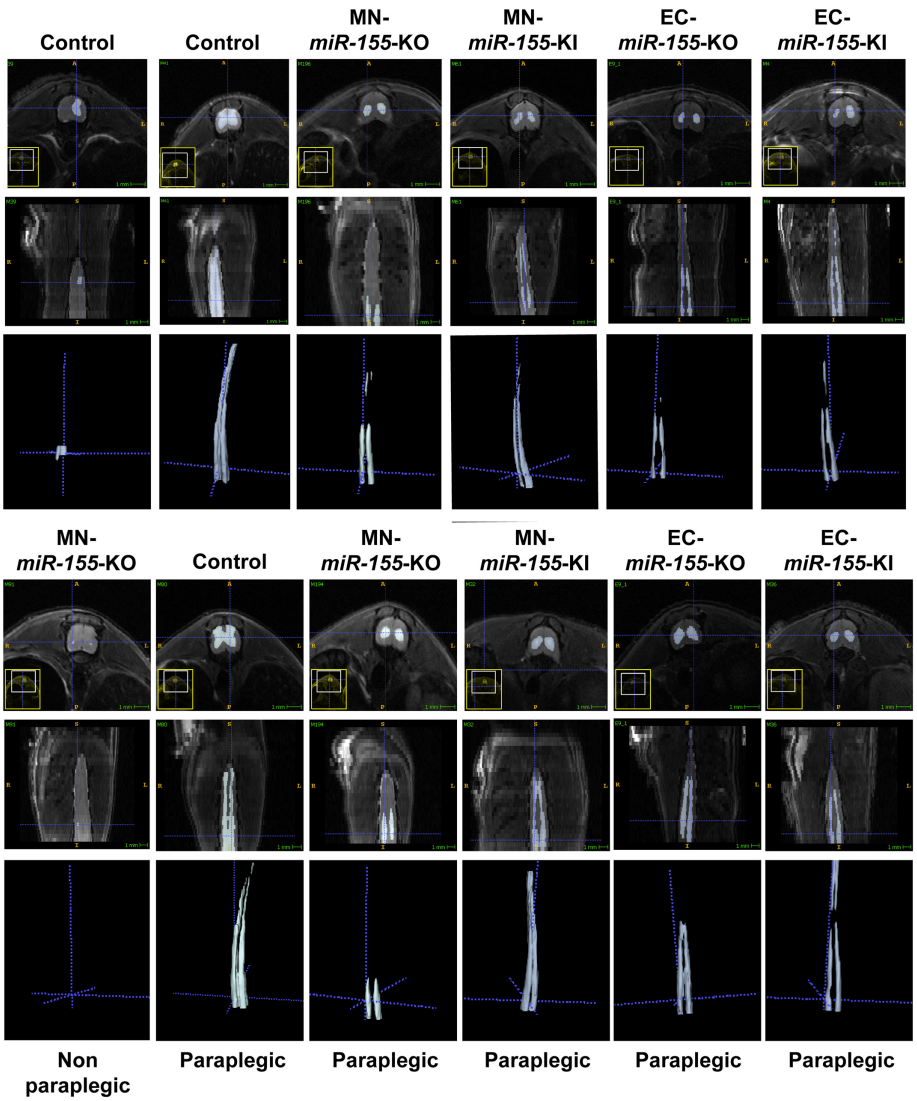

FIGURE 2 | Deletion of *miR-155* in EC modifies the pattern and/or the volume of central cord edema 48-h post-ACC. Representative axial (top rows) and reconstructed coronal (bottom rows) T2-weighted images of thoracic and lumbar SCs from control, MN-*miR-155*-KO, MN-*miR-155*-KI, EC-*miR-155*-KO, and EC-*miR-155*-KI mice as indicated. Mice were either non-paraplegic (first left column) or paraplegic (second to sixth columns).

more limited in the gray matter of a MN-*miR-155*-KI mouse that had a percentage of paraplegia similar to that of control mice.

DISCUSSION

The enlargement of aneurisms of thoracic-abdominal aorta can lead to rupture and death. Currently, two types of TAAA repair surgery are used: OR surgery, that requires ACC to replace the weak and bulging section of the aorta by a graft, and endovascular repair, that consists of stenting the aorta through the femoral artery. We recently developed two dog models that allowed us to compare the pathophysiology of paraplegia after these two surgical procedures, and found that, in contrast to open repair that causes massive gray matter damage and neuronal death as a result of transient, severe ischemia followed by rapid reperfusion, endovascular repair primarily induces white matter damage associated with limited neuronal death as a consequence of extended hypoperfusion (Awad et al., 2021b). As there is presently no preventive pharmaceutical treatment against complications for either procedure, and given the frequency of aortic aneurisms (6–10 per every 100,000 people, with 9,923 deaths recorded in the United States in 2018), it is critical to understand the molecular dysfunctions that lead to similar percentages of paraplegia after these two surgical procedures (Rocha et al., 2020). While the advent of paraplegia after aortic stenting is most often delayed for weeks or even months, OR is especially challenging due to the fast extent of gray matter damage and the very short window of time (2 days) available for preventive intervention before the advent of permanent

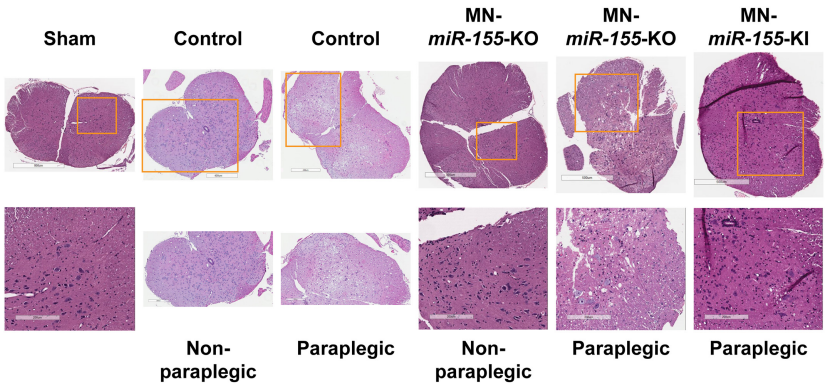

FIGURE 3 | The level of expression of *miR-155* in ChAT$^+$ neurons correlates with the extent of histological damage to the SC gray matter. H&E staining of representative cross-sections of the lumbar SC from sham (surgery procedure without ACC) as well as from control, MN-*miR-155*-KO and MN-*miR-155*-KI ACC-mice, either paraplegic or non-paraplegic, as indicated. Bottom row pictures show enlargements from the respective top row pictures.

paraplegia, in human as well in animal models (Kakinohana et al., 2011; Coselli et al., 2016, 2019; Moulakakis et al., 2018; Awad et al., 2021a). Using our mouse model of transient ACC, we had previously shown that *miR-155* global deletion reduces the risk of developing paraplegia by 37.4% at 48-h (Awad et al., 2018). This result however raised two questions: (i) In which cells of the neurovascular unit are *miR-155* initial, critical deleterious molecular effects are taking place? and (ii) When are deleterious molecular changes leading to paraplegia taking place following ACC?

In the present study, we developed four new types of genetically engineered mice to analyze the effects of *miR-155* activity in ChAT$^+$ neurons and in ECs, that we both previously found to be involved in deleterious events leading to paraplegia (Awad et al., 2018). Our main findings are that: (i) deletion of *miR-155* in ChAT$^+$ neurons, that include the MNs of the SC, reduced the anterior spreading of central cord edema and decreased the percentage of paraplegia at 48-h by 24.6%, primarily by reducing the percentage of late paraplegia (second day post-ACC); (ii) overexpressing *miR-155* in ChAT$^+$ neurons, in contrast, decreased the percentage of early paraplegia (first day post-ACC) without significantly affecting the percentage or paraplegia at 48-h post-ACC; (iii) *miR-155* deletion in ECs remained without measurable effects on the percentage of paraplegia, however it reduced by 50% the volume of central cord edema as well as its anterior spreading; and (iv) overexpressing *miR-155* in ECs led to 100% of mice developing paraplegia.

One critical finding in this study is that *miR-155* activity in ChAT$^+$ neurons was instrumental in molecular malfunctions causing late paraplegia. This is a groundbreaking result, considering the broad literature suggesting that *miR-155* exerts its pro-inflammatory, deleterious effects primarily in cells of the myeloid lineage and that glia-related neuro-inflammation is the main cause of most neuropathologies. Accordingly, a *miR-155* antisense inhibitory RNA reduced brain injury and improved recovery in a mouse model of stroke by distal middle cerebral artery occlusion (Caballero-Garrido et al., 2015). This finding fits well with our results, given that the injection of inhibitory RNAs was conducted for 3 days starting only at 48-h post-occlusion, meaning that the inhibitory RNAs were not interfering with the activity of *miR-155* during the early phase of stroke. Of note, such a delayed intervention would not be possible after ACC, for at 48-h post-ACC mice or patients with severe SC injury are already irreversibly paraplegic.

A second key finding is that *miR-155* activity in ChAT$^+$ neurons in contrast reduced the initial extent of SC damage caused by ischemia/reperfusion. In agreement with this result, *miR-155* had a neuroprotective effect after mouse traumatic brain injury, and mice with global *miR-155* deletion showed increased neuronal degeneration, in particular by decreasing the expression of genes encoding Interferon α2, α4, α5, and β1 (Harrison et al., 2017). In addition, pretreating rats with the flavonoid formonetin before brain traumatic injury increased *miR-155* and *Heme oxygenase-1* expression (Li et al., 2017), the latter through targeting of *Bach1*, a repressor of several genes implicated in protection against oxidative stress. *MiR-155* also increased the survival of cardiomyocyte progenitor cells caused by necrotic cell death during a 16-h oxidative-stress stimulation (Liu et al., 2011). These two findings point to the necessity of distinguishing *miR-155* intrinsic effects on neuron homeostasis and survival at both the early and the late stages after OR. Overall, the findings suggest that *miR-155* targets different sets of transcripts during the early and the late hours after ACC.

In the OR, a short period of ischemia caused by ACC is followed by a wave of reperfusion that induces the formation of reactive oxygen species and mitochondrial damage, and causes excitotoxicity followed by cytogenic edema (Juurlink and Paterson, 1998). Our results suggest that *miR-155* may limit SC injury at this early stage. Later on, an exacerbated inflammatory response leads to the development of vasogenic edema, in particular due to *miR-155* damaging the blood-SC barrier (Lopez-Ramirez et al., 2014). Indeed, vasogenic edema has been shown to be associated with damage to the blood-SC barrier, in particular, due to *miR-155* inhibitory effects on transcripts encoding tight junction protein 1 (TJP1/ZO-1) (Caballero-Garrido et al., 2015). In addition, we have previously associated delayed paraplegia

at 48-h post-ACC with *miR-155* targeting transcripts encoding major facilitator superfamily domain containing 2A (Mfsd2a) (Awad et al., 2018), a transporter implicated in the maintenance of the integrity of the blood-brain barrier (Ben-Zvi et al., 2014) that also delivers docosahexaenoic acid (DHA) to the brain (Nguyen et al., 2014). DHA in particular is a precursor of anti-inflammatory neuroprotectin-D1, that protects the brain and retina against cell injury-induced oxidative stress (Asatryan and Bazan, 2017). Thus, it is not surprising that *miR-155* deletion in ECs reduced the edema at 48-h post-ACC. In this respect, it will be interesting to understand how *miR-155* expression in $ChAT^+$ neurons and ECs can affect the pattern of central cord edema. Finally, the different effects of *miR-155* on neuronal homeostasis at early and late stages are likely to result at least in part from ACC-induced modifications of the neuronal transcriptome and thus of changes in available *miR-155* target transcripts.

A third critical finding in our study is the discovery that the early and late paraplegias induced by ACC are caused by the malfunction of different molecular pathways, and thus that the progression of paraplegia is not linear. Supporting our findings, it has been shown that ACC for 5 min gives rise to neuronal loss and late paraplegia during the second day post-ACC, while ACC for 9 min causes early paraplegia associated with neuronal loss taking place between 8- and 24-h post-ACC (Kakinohana et al., 2011). It was further shown that Caspase 3 activation in neurons was taking place almost exclusively in mice submitted to 5-min of ACC. Strikingly, deleting the gene encoding Caspase 3 protected mice against late paraplegia after 5-min ACC, but not against early paraplegia after 9-min of ACC, indicating that the mechanisms responsible for early and late neuronal death are different (Kakinohana et al., 2011).

On the other hand, *miR-155* is implicated in the production of pro-inflammatory cytokines and chemokines (Tili et al., 2007, 2013). Cytokines and chemokines, produced by microglia, neurons, astrocytes, and ECs, can attract leukocytes such as neutrophils, monocytes, and lymphocytes (Kim et al., 2016). Once activated, these cells participate to further increasing the levels of inflammation and inducing neuronal death (Cartier et al., 2005; Ramesh et al., 2013). Of note, proinflammatory cytokines IL-1β and TNF as well as chemokines KC/IL-8/CXCL8 and MIP1α present a biphasic response to 4-min ACC, with a peak at 6-h and a peak at 36-h post-ACC. In contrast, chemokines MCP1/CCL2, IL-6, and RANTES only peaked at 36-h post-ACC (Smith et al., 2012). In the light of our results, we can speculate that the cytokines and chemokines produced at 6- and 36-h post-ACC play a role in both early and late paraplegia as well as in edema formation, while those produced only at 36-h rather participate to exacerbating inflammation and edema extension and concur to late paraplegia.

As a further complication, *miR-155* has dose-dependent effects, and targets different sets of transcripts when expressed at different doses (Tili et al., 2015; Narayan et al., 2017; Michaille et al., 2019). *MiR-155* expression at 48-h post-ACC is much higher in the SC of paraplegic mice than in the SC of non-paraplegic mice, and is particularly elevated in the MNs of the ventral horns (Awad et al., 2018). It is thus conceivable that both increasing *miR-155* levels at the early stage and impairing its expression or blocking its activity at the later stage post-ACC would be beneficial. It will thus be critical to use massive sequencing along with proteome, Metabolome, and bioinformatics analyses to identify the key miR-155 targets that are responsible the protective and deleterious effects of this microRNA during day-1 and day-2 post-ACC, respectively.

CONCLUSION

In summary, our present findings, in light of previously published reports, define two windows of time during which different molecular deleterious events cause SC injury and paraplegia post-ACC, thus calling for the development of timely targeted preventive therapeutics specifically tailored to prevent neuronal damage during both the early and late phases following ischemia/reperfusion.

DATA AVAILABILITY STATEMENT

The original contributions presented in the study are included in the article/**Supplementary Material**, further inquiries can be directed to the corresponding authors.

ETHICS STATEMENT

The animal study was reviewed and approved by the Animal Care and Use Committee at The Ohio State University.

AUTHOR CONTRIBUTIONS

ET, HA, and J-JM conceived and designed the experiments. HK, GN, AB, JR, and AE performed the experiments. ET, HA, HK, and J-JM analyzed the data and wrote the manuscript. All authors contributed to the article and approved the submitted version.

FUNDING

This work was supported by the National Institutes of Health (R03NS102861 and R21NS113097 to ET, HA, and AB), P30:CA016058 grant to the Small Animal Imaging Core (OSU), and P30:NS104177 grant to the Spinal Cord Injury Facility (OSU).

ACKNOWLEDGMENTS

The authors wish to thank Carlo M. Croce (OSU) for donating *Rosa26*$^{LSL\text{-}miR\text{-}155}$ mice.

SUPPLEMENTARY MATERIAL

The Supplementary Material for this article can be found online at: https://www.frontiersin.org/articles/10.3389/fnmol.2022.788301/full#supplementary-material

REFERENCES

Asatryan, A., and Bazan, N. G. (2017). Molecular mechanisms of signaling via the docosanoid neuroprotectin D1 for cellular homeostasis and neuroprotection. *J. Biol. Chem.* 292, 12390–12397. doi: 10.1074/jbc.R117.783076

Awad, H., Ankeny, D. P., Guan, Z., Wei, P., McTigue, D. M., and Popovich, P. G. (2010). A mouse model of ischemic spinal cord injury with delayed paralysis caused by aortic cross-clamping. *Anesthesiology* 113, 880–891. doi: 10.1097/ALN.0b013e3181ec61ee

Awad, H., Bratasz, A., Nuovo, G., Burry, R., Meng, X., Kelani, H., et al. (2018). MiR-155 deletion reduces ischemia-induced paralysis in an aortic aneurysm repair mouse model: Utility of immunohistochemistry and histopathology in understanding etiology of spinal cord paralysis. *Ann. Diagn. Pathol.* 36, 12–20. doi: 10.1016/j.anndiagpath

Awad, H., Efanov, A., Rajan, J., Denney, A., Gigax, B., Kobalka, P., et al. (2021a). Histological Findings After Aortic Cross-Clamping in Preclinical Animal Models. *J. Neuropathol. Exp. Neurol.* 80, 895–911. doi: 10.1093/jnen/nlab084

Awad, H., Tili, E., Nuovo, G., Kelani, H., Ramadan, M. E., Williams, J., et al. (2021b). Endovascular repair and open repair surgery of thoraco-abdominal aortic aneurysms cause drastically different types of spinal cord injury. *Sci. Rep.* 11:7834. doi: 10.1038/s41598-021-87324-6

Ben-Zvi, A., Lacoste, B., Kur, E., Andreone, B. J., Mayshar, Y., Yan, H., et al. (2014). Mfsd2a is critical for the formation and function of the blood-brain barrier. *Nature* 509, 507–511. doi: 10.1038/nature13324

Caballero-Garrido, E., Pena-Philippides, J. C., Lordkipanidze, T., Bragin, D., Yang, Y., Erhardt, E. B., et al. (2015). In Vivo Inhibition of miR-155 promotes recovery after experimental mouse stroke. *J. Neurosci.* 35, 12446–12464. doi: 10.1523/JNEUROSCI.1641-15.2015

Cartier, L., Hartley, O., Dubois-Dauphin, M., and Krause, K. H. (2005). Chemokine receptors in the central nervous system: role in brain inflammation and neurodegenerative diseases. *Brain Res. Brain Res. Rev.* 48, 16–42. doi: 10.1016/j.brainresrev.2004.07.021

Coselli, J. S., Green, S. Y., Price, M. D., Zhang, Q., Preventza, O., de la Cruz, K. I., et al. (2019). Spinal cord deficit after 1114 extent II open thoracoabdominal aortic aneurysm repairs. *J. Thorac. Cardiovasc. Surg.* 12, S0022–5223(19)30352–6. doi: 10.1016/j.jtcvs.2019.01.120

Coselli, J. S., LeMaire, S. A., Preventza, O., Cruz, K. I., Cooley, D. A., Price, M. D., et al. (2016). Outcomes of 3309 thoracoabdominal aortic aneurysm repairs. *J. Thorac. Cardiovasc. Surg.* 151, 1323–1337. doi: 10.1016/j.jtcvs.2015.12.050

Harrison, E. B., Emanuel, K., Lamberty, B. G., Morsey, B. M., Li, M., Kelso, M. L., et al. (2017). Induction of miR-155 after Brain Injury Promotes Type 1 Interferon and has a Neuroprotective Effect. *Front. Mol. Neurosci.* 10:228. doi: 10.3389/fnmol.2017.00228

Henry, R. J., Doran, S. J., Barrett, J. P., Meadows, V. E., Sabirzhanov, B., Stoica, B. A., et al. (2019). Inhibition of miR-155 Limits Neuroinflammation and Improves Functional Recovery After Experimental Traumatic Brain Injury in Mice. *Neurotherapeutics* 16, 216–230. doi: 10.1007/s13311-018-0665-9

Juurlink, B. H., and Paterson, P. G. (1998). Review of oxidative stress in brain and spinal cord injury: suggestions for pharmacological and nutritional management strategies. *J. Spinal Cord Med.* 21, 309–334. doi: 10.1080/10790268.1998.11719540

Kakinohana, M., Kida, K., Minamishima, S., Atochin, D. N., Huang, P. L., Kaneki, M., et al. (2011). Delayed paraplegia after spinal cord ischemic injury requires caspase-3 activation in mice. *Stroke* 42, 2302–2307. doi: 10.1161/STROKEAHA.110.600429

Khachatryan, Z., Haunschild, J., von Aspern, K., Borger, M. A., and Etz, C. D. (2021). Ischemic spinal cord injury - experimental evidence and evolution of protective measures. *Ann. Thorac. Surg.* 9, S0003–4975(21)00044–8. doi: 10.1016/j.athoracsur.2020.12.028

Kim, J. Y., Park, J., Chang, J. Y., Kim, S. H., and Lee, J. E. (2016). Inflammation after Ischemic Stroke: The Role of Leukocytes and Glial Cells. *Exp. Neurobiol.* 25, 241–251. doi: 10.5607/en.2016.25.5.241

Li, Z., Wang, Y., Zeng, G., Zheng, X., Wang, W., Ling, Y., et al. (2017). Increased miR-155 and heme oxygenase-1 expression is involved in the protective effects of formononetin in traumatic brain injury in rats. *Am. J. Transl. Res.* 9, 5653–5661.

Liu, J., van Mil, A., Vrijsen, K., Zhao, J., Gao, L., Metz, C. H. B. G., et al. (2011). MicroRNA-155 prevents necrotic cell death in human cardiomyocyte progenitor cells via targeting RIP1. *J. Cell. Mol. Med.* 15, 1474–1482. doi: 10.1111/j.1582-4934.2010.01104.x

Lopez-Ramirez, M. A., Wu, D., Pryce, G., Simpson, J. E., Reijerkerk, A., King-Robson, J., et al. (2014). MicroRNA-155 negatively affects blood-brain barrier function during neuroinflammation. *FASEB J.* 28, 2551–2565. doi: 10.1096/fj.13-248880

Michaille, J.-J., Awad, H., Fortman, E. C., Efanov, A. A., and Tili, E. (2019). MiR-155 expression in antitumor immunity: The higher the better? *Genes Chromosomes Cancer* 58, 208–218. doi: 10.1002/gcc.22698

Moulakakis, K. G., Karaolanis, G., Antonopoulos, C. N., Kakisis, J., Klonaris, C., Preventza, O., et al. (2018). Open repair of thoracoabdominal aortic aneurysms in experienced centers. *J. Vasc. Surg.* 68, 634–645.e12. doi: 10.1016/j.jvs.2018.03.410

Narayan, N., Morenos, L., Phipson, B., Willis, S. N., Brumatti, G., Eggers, S., et al. (2017). Functionally distinct roles for different miR-155 expression levels through contrasting effects on gene expression, in acute myeloid leukaemia. *Leukemia* 31, 808–820. doi: 10.1038/leu.2016.279

Nguyen, L. N., Ma, D., Shui, G., Wong, P., Cazenave-Gassiot, A., Zhang, X., et al. (2014). Mfsd2a is a transporter for the essential omega-3 fatty acid docosahexaenoic acid. *Nature* 509, 503–6. doi: 10.1038/nature13241

Ramesh, G., MacLean, A. G., and Philipp, M. T. (2013). Cytokines and chemokines at the crossroads of neuroinflammation, neurodegeneration, and neuropathic pain. *Mediators Inflamm.* 2013:480739. doi: 10.1155/2013/480739

Rocha, R. V., Lindsay, T. F., Friedrich, J. O., Shan, S., Sinha, S., Yanagawa, B., et al. (2020). Systematic review of contemporary outcomes of endovascular and open thoracoabdominal aortic aneurysm repair. *J. Vasc. Surg.* 71, 1396.e–1412.e. doi: 10.1016/j.jvs.2019.06.216

Smith, P. D., Puskas, F., Meng, X., Lee, J. H., Cleveland, J. C. Jr., Weyant, M. J., et al. (2012). The evolution of chemokine release supports a bimodal mechanism of spinal cord ischemia and reperfusion injury. *Circulation* 126, S110–S117.

Suofu, Y., Wang, X., He, Y., Li, F., Zhang, Y., Carlisle, D. L., et al. (2020). Mir-155 knockout protects against ischemia/reperfusion-induced brain injury and hemorrhagic transformation. *Neuroreport* 31, 235–239. doi: 10.1097/WNR.0000000000001382

Tili, E., Chiabai, M., Palmieri, D., Brown, M., Cui, R., Fernandes, C., et al. (2015). Quaking and miR-155 interactions in inflammation and leukemogenesis. *Oncotarget* 6, 24599–24610. doi: 10.18632/oncotarget.5248

Tili, E., Michaille, J.-J., Cimino, A., Costinean, S., Dumitru, C. D., Adair, B., et al. (2007). Modulation of miR-155 and miR-125b levels following lipopolysaccharide/TNF-alpha stimulation and their possible roles in regulating the response to endotoxin shock. *J. Immunol.* 179, 5082–5089. doi: 10.4049/jimmunol.179.8.5082

Tili, E., Michaille, J.-J., and Croce, C. M. (2013). MicroRNAs play a central role in molecular dysfunctions linking inflammation with cancer. *Immunol. Rev.* 253, 167–184. doi: 10.1111/imr.12050

Yushkevich, P. A., Piven, J., Hazlett, H. C., Smith, R. G., Ho, S., Gee, J. C., et al. (2006). User-guided 3D active contour segmentation of anatomical structures: significantly improved efficiency and reliability. *Neuroimage* 31, 1116–1128. doi: 10.1016/j.neuroimage.2006.01.015

Conflict of Interest: GN is employed by GNOME, Inc., Powell, OH, United States.

The remaining authors declare that the research was conducted in the absence of any commercial or financial relationships that could be construed as a potential conflict of interest.

Publisher's Note: All claims expressed in this article are solely those of the authors and do not necessarily represent those of their affiliated organizations, or those of the publisher, the editors and the reviewers. Any product that may be evaluated in this article, or claim that may be made by its manufacturer, is not guaranteed or endorsed by the publisher.

frontiers in Molecular Neuroscience

MINI REVIEW
published: 22 March 2022
doi: 10.3389/fnmol.2022.822917

Early Adversity and Accelerated Brain Aging: A Mini-Review

*Pratik R. Chaudhari†, Aastha Singla† and Vidita A. Vaidya**

Department of Biological Sciences, Tata Institute of Fundamental Research, Mumbai, India

Early adversity is an important risk factor that influences brain aging. Diverse animal models of early adversity, including gestational stress and postnatal paradigms disrupting dam-pup interactions evoke not only persistent neuroendocrine dysfunction and anxio-depressive behaviors, but also perturb the trajectory of healthy brain aging. The process of brain aging is thought to involve hallmark features such as mitochondrial dysfunction and oxidative stress, evoking impairments in neuronal bioenergetics. Furthermore, brain aging is associated with disrupted proteostasis, progressively defective epigenetic and DNA repair mechanisms, the build-up of neuroinflammatory states, thus cumulatively driving cellular senescence, neuronal and cognitive decline. Early adversity is hypothesized to evoke an "allostatic load" *via* an influence on several of the key physiological processes that define the trajectory of healthy brain aging. In this review we discuss the evidence that animal models of early adversity impinge on fundamental mechanisms of brain aging, setting up a substratum that can accelerate and compromise the time-line and nature of brain aging, and increase risk for aging-associated neuropathologies.

Keywords: maternal separation, early stress, hippocampus, proteostasis, mitochondria, neuronal survival, neuroinflammation, cognition

OPEN ACCESS

Edited by:
Parthiv Haldipur, Seattle Children's Research Institute, United States

Reviewed by:
Weiwen Wang, Institute of Psychology (CAS), China

***Correspondence:**
Vidita A. Vaidya
vvaidya@tifr.res.in

†These authors have contributed equally to this work and share first authorship

Specialty section:
This article was submitted to Methods and Model Organisms, a section of the journal Frontiers in Molecular Neuroscience

Received: *26 November 2021*
Accepted: *25 February 2022*
Published: *22 March 2022*

Citation:
Chaudhari PR, Singla A and Vaidya VA (2022) Early Adversity and Accelerated Brain Aging: A Mini-Review. Front. Mol. Neurosci. 15:822917. doi: 10.3389/fnmol.2022.822917

INTRODUCTION

Early adversity is a potent risk factor for adult psychopathology (Gee, 2021; Teicher et al., 2021). Early stressors such as physical, sexual and emotional abuse, parental neglect/loss, parental/caregiver substance abuse and incarceration disrupt physiological and psychological functioning driving maladaptive health outcomes (Brown et al., 2009; Brenhouse et al., 2019). Animal models attempt to capture the molecular, cellular, neuroendocrine, structural, functional and behavioral changes that arise due to early stress, to gain a mechanistic insight into how early adversity programs psychiatric vulnerability (Tzanoulinou and Sandi, 2017; Blaisdell et al., 2019; Torres-Berrío et al., 2019). While the impact of early stress is experienced by multiple physiological systems, the brain remains the central player as a target of stress and in the top-down control over stress-response pathways (McEwen, 2007). Prior reviews have discussed the influence of early stress on anxio-depressive behaviors and disrupted cognition, accompanied by transcriptional, cytoarchitectural, neuroendocrine and functional changes in diverse limbic

Abbreviations: MIA, maternal immune activation; LGABN, licking, grooming, arched back nursing; MD, maternal deprivation; MS, maternal separation; MSUS, maternal separation and unpredictable stress; LBN, limited bedding and nesting; PFC, prefrontal cortex; DNA, Deoxyribonucleic acid; ETC, electron transport chain; ROS, reactive oxygen species; OCR, oxygen consumption rate; ATP, Adenosine triphosphate; UPR, unfolded protein response; GR, glucocorticoid receptor; BDNF, brain derived neurotrophic factor; HPA, Hypothalamo-pituitary-adrenal axis; RNA, Ribonucleic acid.

brain regions (Chen and Baram, 2016; Teicher et al., 2016; Pervanidou and Chrousos, 2018). Amongst the hallmark features of early stress is that it evokes enduring consequences (Miller et al., 2011; Szyf, 2019). Early adversity exacerbates aging-induced telomere erosion, establishing a pathophysiological basis for enhanced morbidity and mortality (Epel and Prather, 2018; Colich et al., 2020). Clinical literature also indicates that individuals exposed to early stress are more likely to suffer a premature death (Brown et al., 2009). In this review, we critically discuss the evidence that early stress accelerates brain aging.

ANIMAL MODELS OF EARLY ADVERSITY

Animal models of early adversity involve stress exposure *in utero*, or during early postnatal time-windows, which can evoke persistent alterations in mood-related behavior, noted long after the cessation of stress (**Figure 1A**; Schmidt et al., 2011). Gestational stress which involves administration of chronic stress to the dam, or exposure to an inflammatory milieu *in utero*, such as in the maternal immune activation (MIA) model, results in persistent changes in anxio-depressive behaviors in the progeny (Brown and Conway, 2019). During the postnatal temporal window, most rodent models of early adversity capitalize on perturbation of dam-pup interactions and fragmented caregiving behavior from the dam (Orso et al., 2019). These include perturbed licking, grooming, and arched back nursing behavior (LGABN), maternal deprivation (MD), maternal separation (MS), maternal separation combined with unpredictable stress to the dam (MSUS), or limited access to bedding and nesting (LBN) (Caldji et al., 2000; Ladd et al., 2000; Molet et al., 2014; Walker et al., 2017). Common across these models are enhanced anxio-depressive behaviors in the progeny, often accompanied by perturbed cognitive, reward and social behavior (Syed and Nemeroff, 2017; Tzanoulinou and Sandi, 2017; Birnie et al., 2020). Juvenile stress models are usually initiated post-weaning from the dam during the peripubertal window, and for the purposes of this review we have restricted our discussion to early adversity models that involve time-windows prior to juvenile life. Early adversity disrupts stress-responsive neuroendocrine pathways, drives neuroinflammatory states, evokes epigenetic changes, and results in structural and functional changes in neurocircuits that regulate anxio-depressive behaviors, including the hippocampus, prefrontal cortex (PFC), amygdala, and the brain-stem monoaminergic nuclei (Babenko et al., 2015; Teicher et al., 2016; Agorastos et al., 2019; Brenhouse et al., 2019). In this review, we discuss the evidence of an altered brain aging trajectory as a consequence of early adversity, focusing predominantly on studies from animal models.

HALLMARK SIGNATURES OF BRAIN AGING

Aging is characterized by a time-dependent loss of molecular, cellular, structural and functional integrity leading to impaired homeostasis (López-Otín et al., 2013). Accompanying the aging-evoked attrition in all organ systems, "brain aging" also exhibits hallmark features with steady and cumulative decrements noted in structure and function, spanning from atrophy-associated cognitive decline to motor deficits (Mattson and Arumugam, 2018; Oschwald et al., 2019). The characteristic signatures of "brain aging" include mitochondrial dysfunction, oxidative stress, compromised neuronal bioenergetics, impaired proteostasis, perturbed DNA repair, altered intracellular signaling, and a cumulative buildup of neuroinflammatory states (Mattson and Arumugam, 2018). Distinct brain regions show individual variation in the extent of their vulnerability to aging-associated neuronal loss, with the hippocampus, cerebral cortex and cerebellum reported to exhibit both synaptic and cellular attrition, accompanied by impaired synaptic plasticity (Fjell and Walhovd, 2010; Morrison and Baxter, 2012; Bartsch and Wulff, 2015; Fan et al., 2018; Mattson and Arumugam, 2018). A key driver of these changes is thought to be aging-associated neuroinflammation, which also appears to differentially impact specific vulnerable cell populations in the brain (Sparkman and Johnson, 2008; Simen et al., 2011; Mattson and Arumugam, 2018). Correlated with these changes is the compromised structural/functional integrity of mitochondria and impaired neuronal bioenergetics, cumulative buildup of dysfunctional proteins and an unfolded protein response, markers of endoplasmic reticulum (ER) stress, failure to effectively scavenge reactive oxygen species (ROS) and oxidative damage, overlaid on a baseline substratum of neuroinflammatory changes, namely a disrupted cytokine milieu and microglial activation (Wyss-Coray, 2016; Mattson and Arumugam, 2018; Webb and Sideris, 2020; Uddin et al., 2021). While these changes overlap and correlate with each other, the causal association between these events still remains unclear. However, several studies highlight that these changes, namely enhanced oxidative stress and neuroinflammatory states, accompanied by impaired DNA repair and mitochondrial dysfunction may play a vital role in driving the synaptic, structural and functional impairments associated with aging (Raz and Rodrigue, 2006; Dröge and Schipper, 2007; Paradies et al., 2011; Regnell et al., 2012; Green and Nolan, 2014; Pluvinage and Wyss-Coray, 2020). While these molecular and cellular changes are vital drivers of determining the aging trajectory, they are further impacted by both genetic background and life-course factors (Yuan et al., 2009; Kõks et al., 2016; Zannas, 2018; Marini et al., 2020; Ancelin et al., 2021). In this review, we focus on the vital life-course factor of early life experience, which can exert a long-lasting impact in determining an organism's aging trajectory and health-span, in particular impacting the quality and nature of brain aging. A working hypothesis suggests that early adversity sets up an underlying "allostatic load" which impacts the physiology of normal aging creating fertile conditions that hasten and compromise the brain aging trajectory (**Figure 1B**; Danese and McEwen, 2012; Epel and Prather, 2018).

Given that most of the literature addressing the impact of early adversity on the brain aging trajectory is based on rodent models, it is worth considering a comparative scale of the equivalent age stages between rodents and humans. We have described in **Figure 1B** the distinct stages of perinatal,

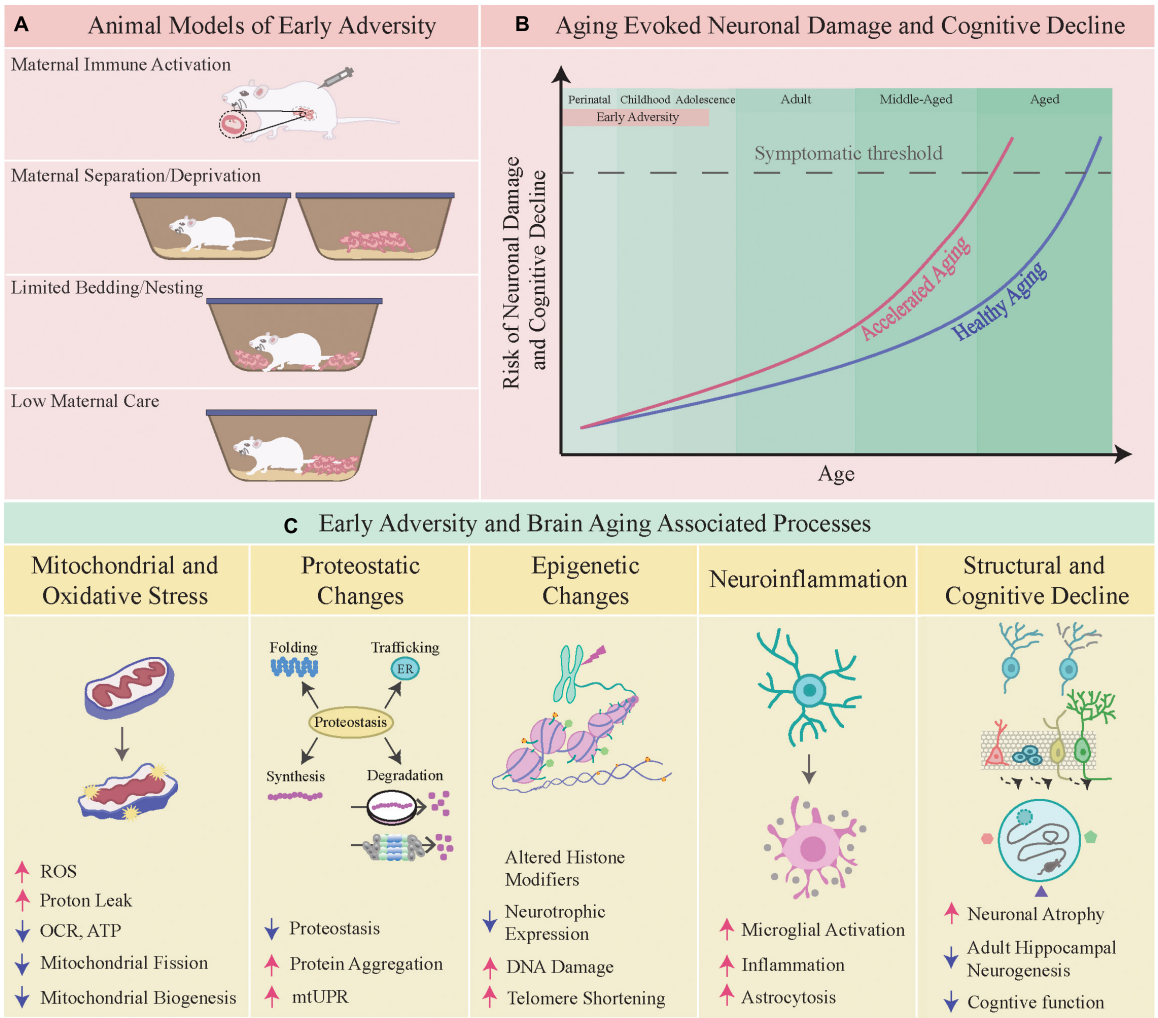

FIGURE 1 | Early adversity and brain aging-associated processes. **(A)** Shown here are specific animal models of early adversity viz. maternal immune activation, maternal separation/deprivation, limited bedding and nesting, and low maternal care. **(B)** The schematic depicts the hastening of brain aging and an earlier onset of neuronal damage and cognitive decline following early adversity. **(C)** Depicted below are some of the aging-associated processes that are perturbed by early adversity, namely the following physiological mechanisms viz. mitochondrial homeostasis, proteostasis, epigenetics, neuroinflammation, structural and cognitive function.

childhood, adolescence, adult, middle-aged and aged, as the major epochs of life. The perinatal stage encompasses the window of life from 23 weeks of gestation onward till about 2 years of human age. While it is challenging to draw direct parallels, the emergence of developmental milestones suggest that postnatal day 1–10 for rodents is equivalent to 23–40 weeks of human gestation, and postnatal day 10–21 is comparable to the window from birth till 3 years of human age. The childhood window comprising of 2–11 years of age for humans is thought to have an equivalence based on developmental indices to postnatal day 20–35 in rodents. The adolescent phase in humans (12–18 years) is thought to be comparable to postnatal day 35–49 in rodent models, with adulthood (20 years onward) compared to rodent models commencing from postnatal day 60 onward. The middle-aged and aged windows are generally thought to commence from 40 and 60 years of age respectively in humans, which has been suggested to compare to 9–15 months for middle-aged and 18 months upward as aged in rodent models (Flurkey et al., 2007; Semple et al., 2013; Dutta and Sengupta, 2016; Agoston, 2017; Wang et al., 2020).

EARLY ADVERSITY, MITOCHONDRIAL DYSFUNCTION AND OXIDATIVE STRESS

Mitochondria are an integrative hub that sense, adapt to and drive cellular stress responses, shaping the homeostatic adaptations to stress (Eisner et al., 2018; Picard et al., 2018). Mitochondria respond dynamically to stress signaling cues and mitokines, adjusting both architecture and function to rapidly adapt to altered energetic demands (Picard et al., 2015; Daniels et al., 2020). This ability of mitochondria to orchestrate effective

cellular stress responses is a key component of the "resilient" phenotype (Hoffmann and Spengler, 2018), and a decline in this buffering capacity is linked to cellular senescence (Correia-Melo et al., 2016; Vasileiou et al., 2019). Early stress is speculated to deteriorate in the stress-buffering capacity of mitochondria, *via* a disrupted mitostasis, and thus accelerate senescence and neuronal damage, a cumulative consequence of brain aging (**Figure 1C**; Tyrka et al., 2016; Hoffmann and Spengler, 2018; Zitkovsky et al., 2021).

Studies using models of fragmented maternal care indicate both short (postnatal day 9) and long-term (10–12 months) changes in mitochondrial function within limbic brain regions and the periphery (Ruigrok et al., 2021). Adult progeny with a history of LBN exhibit perturbed electron transport chain (ETC) activity in the hypothalamus, and altered mitochondrial fusion/fission associated gene expression in the hippocampus upto 1 year of age (Ruigrok et al., 2021). MS evokes dysregulation of mitochondrial sirtuins within the PFC that persist well into middle-aged life (15 months) (Pusalkar et al., 2016), and robust decreases in mitochondrial mass in the periphery, namely the muscle, noted 8 months post the cessation of MS (Ghosh et al., 2016). Further, MS animals exhibit enhanced sensitivity to oxidative stress in peripheral mononuclear cells, noted until 18 months of age, and also reported in gut epithelial cells when examined in adulthood (2 months) in MS animals (Grigoruta et al., 2020; Khorjahani et al., 2020). Impaired calcium homeostasis, enhanced ROS and a decrease in oxygen consumption rate (OCR) or ATP production is also reported in the PFC, raphe and hippocampus of adult (2–6 month) MS animals, suggestive of a broad mitochondrial dysfunction in multiple systems (Della et al., 2013; Amini-Khoei et al., 2017; Masrour et al., 2018; Nold et al., 2019). Proteomic studies in diverse early stress models, spanning analysis from 12–24 weeks of age, indicate a dysregulation of proteins associated with mitochondrial energy metabolism in the PFC and hippocampus (Marais et al., 2009; Mairesse et al., 2012; Föcking et al., 2014; van Zyl et al., 2016; Nold et al., 2019), with a specific study suggesting a temporal variation in these effects noted at postnatal day 21 and 3–4 months following LBN, accompanied by a sex-specific differential expression of the hippocampal proteome at these timepoints (Eagleson et al., 2020). Furthermore, MS regulated glyoxalase enzymatic machinery at around 3 months of age that could result in a build-up of the pro-oxidant, methylglyoxal, which is a precursor of advanced glycation end-products implicated in neurodegeneration (Marais et al., 2009; Allaman et al., 2015). Early stress of MD also reduced superoxide dismutase and catalase activity in the hippocampus and PFC observed as early as postnatal day 20 and persisting into young adulthood (2 months), which could exacerbate oxidative stress in vulnerable limbic neurocircuits (Réus et al., 2017; Talukdar et al., 2020; Abelaira et al., 2021). Collectively, most reports of mitochondrial dysfunction following early stress restrict analysis to young adulthood (2–4 months of age) (Della et al., 2013; Masrour et al., 2018; Eagleson et al., 2020; Lapp et al., 2020), with few exceptions examining the consequences either in early postnatal life or well into middle-aged life ranging from 8–15 months (Ghosh et al., 2016; Pusalkar et al., 2016; Ruigrok et al., 2021). A careful analysis of the impact of early stress on the ontogeny of mitochondria within neuronal circuits, interaction with variables such as sex and genetic background remains to be extensively explored. Such studies are vital because a single-snapshot cannot capture the continuum of mitochondrial functional changes following early adversity, and it is likely that organ systems and brain regions will exhibit distinct timelines with different inflection points when adaptive attempts tip into maladaptive outcomes (Suri and Vaidya, 2015). Thus far the emerging picture raises the intriguing possibility that cumulative mitochondrial allostatic load following early adversity could sow the seeds for the hastening of age-associated impairments (Daniels et al., 2020).

EARLY ADVERSITY, IMPAIRED PROTEOSTASIS AND AUTOPHAGY

Early stress is speculated to alter proteostasis, trigger abnormal unfolded protein responses (UPR), and drive impaired autophagy thus establishing a substrate for aging-associated neuropathology (**Figure 1C**; Pinto et al., 2016; Liu et al., 2018; Criado-Marrero et al., 2019; Saulnier et al., 2021; Sierra-Fonseca et al., 2021). Maintaining effective protein quality is a multistep process spanning from synthesis, appropriate folding and conformational stability to turnover, and is vital in neurons that do not have the scope of cellular replacement to maintain the proteome (Muñoz-Carvajal and Sanhueza, 2020; Giandomenico et al., 2021; Saulnier et al., 2021). The proteostasis network, consisting of proteasome-dependent degradation machinery and autophagic processes is critical to maintaining the integrity of the functional proteome. Aging-dependent progressive decline in the efficiency of the proteostatic network is implicated in the establishment of neurodegeneration (Giandomenico et al., 2021). MS evokes significant disruption in expression of components of both the ubiquitin-proteasome system and the autophagy-lysosomal pathway in the hippocampus with changes noted in young adulthood (3 months), and specific alterations persisting well into middle-aged life (16 months). It is interesting that these changes appear to be restricted to the hippocampus and are not observed in the neocortex, suggesting differential vulnerability of neuronal circuits (Sierra-Fonseca et al., 2021). A recent report indicates that MIA evokes a sex-specific integrated stress response, evoking disrupted proteostasis in the cortex of embryonic 14.5 and 18.5 day old male fetuses, that is linked to the emergence of perturbed social and stereotypic behavior *via* a cytokine-dependent mechanism (Kalish et al., 2021). Early adversity could aggravate the aging-evoked UPR, in particular in the context of mitochondrial proteins, and serve as an early molecular signature that accelerates neuronal impairment (Muñoz-Carvajal and Sanhueza, 2020). Postnatal metabolic stress results in a perturbed UPR in the hippocampus and hypothalamus at 3 months of age, raising the intriguing possibility that the toxic combination of early adversity and metabolic insults could be a potent insult that disrupts healthy brain aging in animals as early as young adulthood (Pinto et al., 2016; Chen et al., 2021). Early adversity is a risk factor for neurodegeneration,

which is linked to a disruption of proteostasis and perturbed amyloidogenic processing in 6–12 month old genetic mouse models of Alzheimer's disease subjected to LBN (Sarter and Bruno, 2004; Dallé and Mabandla, 2018; Lesuis et al., 2018b,a). LBN enhances hippocampal Aβ40 and Aβ42 levels, primary components of amyloid plaques, in 6–12 months old male animals (Lesuis et al., 2018b). Further, gestational stress, MS and LBN enhance plaque burden, hasten cognitive decline noted at 9–12 months of age and shorten life expectancy in genetic mouse models of Alzheimer's disease (Lesuis et al., 2016, 2018b; Hui et al., 2017; Jafari et al., 2019). However, there are also contradictory reports, wherein LBN does not alter the course of cognitive or neurogenic decline in 8–10 month old genetic Alzheimer's disease animal models (Hoeijmakers et al., 2018). Whilst several reports link early adversity to mitochondrial dysfunction, there is still a paucity of detailed reports examining the influence of early adversity on proteostasis, UPR and autophagy in the brain, in particular across the life-span.

EARLY ADVERSITY, EPIGENETIC AND TRANSCRIPTIONAL DYSREGULATION

Amongst the foremost candidates for mediating the persistent effects of early adversity is a perturbed epigenetic landscape, thus driving transcriptional changes that hasten aging-evoked changes (Szyf, 2009; Doherty and Roth, 2018; Zannas, 2019; Palma-Gudiel et al., 2020). In animals exposed to early adversity, cognitive decline emerges as early as 12 months, and has been correlated with an altered epigenome in the hippocampus and PFC (Brunson et al., 2005; McClelland et al., 2011; Suri et al., 2013, 2014; Short et al., 2020). Several studies indicate altered expression of epigenetic machinery and of epigenetic modifications in the promoter regions of stress-responsive genes, such as the glucocorticoid receptor (GR) and brain derived neurotrophic factor (BDNF), with only a few reports examining these changes across the life-span (Roth and Sweatt, 2011; Suri et al., 2013; Pusalkar et al., 2016; Seo et al., 2016, 2020; Liu and Nusslock, 2018; Mourtzi et al., 2021). Several of the epigenetic and transcriptional changes evoked by early adversity are sex-dependent (Parel and Peña, 2022). MS is associated with dysregulated expression of the "writer" and "eraser" class of histone modifying enzymes, as well as DNA modifying enzymes, which in specific cases persist across the life-span, well into middle-aged life (15 months) (Pusalkar et al., 2016). This could contribute to global transcriptional changes in limbic brain regions, in particular within the hippocampus as observed at 15 months of age by Suri et al. (2014) (Marrocco et al., 2019; Peña et al., 2019; Usui et al., 2021). 15 month old MS animals exhibit perturbed expression of genes associated with calcium homeostasis, neuroinflammation, synaptogenesis, autophagy, proteasomal function, and cellular responses to stress (Suri et al., 2014). The nature of transcriptional dysregulation evoked by early adversity varies based on age, highlighting the importance of life-span studies (Suri et al., 2014). Amongst the key genes targeted by early adversity is GR, which plays a key role in mediating stress responses and HPA axis regulation. Diverse models of early adversity exhibit enhanced CpG methylation at the GR promoter in the hippocampus in young adults, driving reduced GR expression and disrupting the negative feedback regulation of the HPA axis (Weaver, 2007; Smart et al., 2015). This would enhance circulating corticosteroid levels, thus impacting neuronal atrophy and cognitive decline (McEwen, 2007). Aging is associated with enhanced circulating corticosteroid that negatively impact hippocampal neuron structure and function (Yau and Seckl, 2012). Following early adversity, animals have enhanced baseline, circadian and stress-evoked corticosteroid levels, compromising hippocampal cytoarchitecture/function and enhancing cognitive decline (McEwen, 2007). GRs and BDNF, both of which are dysregulated by early adversity, profoundly influence mitochondria (Daskalakis et al., 2015). GRs translocate into mitochondria, can regulate oxidative phosphorylation associated nuclear-encoded and mitochondrial gene expression, and influence bioenergetics (Psarra and Sekeris, 2009; Picard et al., 2014). BDNF, which is shown to exhibit a robust decline in the hippocampus and PFC of 15 month old animals subjected to early stress, can influence mitochondrial biogenesis and transport (Roth et al., 2009; Suri et al., 2013; Markham et al., 2014). The disrupted dyad of BDNF-GR signaling could influence cellular changes spanning from altered mitochondrial structure/function to dendritic atrophy, and at the organismal level perturb the neuroendocrine milieu and drive neurodegenerative decline (Rothman and Mattson, 2013; Suri and Vaidya, 2013; Daskalakis et al., 2015). A prior study indicates a marked reduction in expression of genes linked to antioxidant responses and DNA repair in the aging human neocortex after 40 years of age with enhanced oxidative DNA damage associated with the promoters of these downregulated genes likely due to attenuated base-excision repair mechanisms (Lu et al., 2004). Though speculative, one can envisage that early adversity could cumulatively enhance oxidative damage to DNA, RNA, proteins, and lipids (Karanikas et al., 2021). This is supported by evidence of hastened telomere attrition noted in 4–5 year old children that experienced childhood maltreatment, and phenocopied in animal models of early adversity (Drury et al., 2012; Price et al., 2013; Ridout et al., 2018). Amongst the implicated mediators of such DNA damage and telomere shortening following early adversity are the toxic cocktail of glucocorticoid-evoked oxidative stress, mitochondrial dysfunction, enhanced proton leak and neuroinflammation (Swaab et al., 2005; Casagrande et al., 2020).

EARLY ADVERSITY, NEUROINFLAMMATION, STRUCTURAL AND COGNITIVE DECLINE

Early stress triggers neuroimmune responses that drive prolonged, pathological and maladaptive neuroinflammation (Ganguly and Brenhouse, 2015; Nettis et al., 2020). Neuroinflammatory states evoked by early stress have been reviewed extensively, with evidence pointing to an induction of inflammatory cytokines, astrogliosis, and microglial activation (Ganguly and Brenhouse, 2015; Desplats et al., 2020). Most

studies examine consequences of early adversity in postnatal or adult life, and do not address the long-term consequences on neuroinflammation (Delpech et al., 2016; Réus et al., 2019; Desplats et al., 2020; Dutcher et al., 2020; Reshetnikov et al., 2020; Kim et al., 2021). One of the reports indicates that MS increases microglial numbers/activation in 10 month old animals (Criado-Marrero et al., 2020), but few studies have actually followed animals with a history of early adversity across the life-span, to address the temporal and circuit-specific emergence of neuroinflammatory signatures (Ganguly and Brenhouse, 2015; Tay et al., 2018; Andersen, 2022). However, it is noteworthy that in some models of early stress (MIA), neuroinflammatory changes do not appear to contribute to synaptic atrophy and cognitive decline, with no changes reported in microglia or reactive astrocytes in 22 month old animals with a history of MIA (Giovanoli et al., 2015). Adult female, but not male, mice (2–3 months of age) with a life history of being subjected to fragmented maternal care showed deficits in reversal learning, suggesting a sex-specific influence of early adversity on cognition (Goodwill et al., 2018). This raises the possibility that while neuroinflammation is a consequence of early adversity, it remains poorly understood whether it is a causal contributor to accelerated aging-evoked neuronal and functional decline (Merz and Turner, 2021). It also highlights the critical importance of addressing potential sex differences in the pattern, onset and magnitude of neuroinflammatory changes evoked by early adversity, as neurohormones may exert a profound impact in modifying the trajectory of neuroinflammatory signatures (Ganguly and Brenhouse, 2015; González-Pardo et al., 2020).

The aging brain has several hallmark features, including atrophy of vulnerable neuronal populations and marked cognitive impairments (Fjell and Walhovd, 2010). Amongst the brain regions most extensively studied in this regard are the PFC and hippocampus, with dendritic atrophy, reduced spine density, decreased hippocampal neurogenesis, cellular shrinkage and volumetric loss being the key reported features (**Figure 1C**; McEwen and Morrison, 2013; Bartsch and Wulff, 2015). Several of these changes evoked by early adversity have been shown to be sex-dependent. In rats exposed to pre-pubertal stress, adult hippocampal neurogenesis is altered in adulthood in males, but not in females (Brydges et al., 2018). Further, in rats exposed to MS, females exhibit a more elaborate dendritic morphology and reduced thin spine density in infralimbic pyramidal neurons of the mPFC, which is not observed in male rats when examined at postnatal day 40 (Farrell et al., 2016). Several of these changes arise in a milieu associated with enhanced oxidative stress, mitochondrial dysfunction, disrupted proteostasis, neuroinflammatory signatures and an epigenetic milieu that drives reduced growth factor and enhanced inflammatory cytokine expression (Mattson and Arumugam, 2018). Early stress is associated with a long-lasting BDNF dysregulation in the hippocampus and/or PFC noted well into aged life reported at the age of 15 months (Suri et al., 2013) and 22 months (Giovanoli et al., 2015), along with a robust decline in hippocampal neurogenesis reported at the age of 10 months (Ruiz et al., 2018) and 15 months (Suri et al., 2013). The effects of early adversity on neurotransmitters and growth factors are suggested to be sex-dependent, which has been reviewed extensively by Perry et al. (2021). Neural stem cells shift to quiescence with aging, but continue to show similar proliferative capacity upon activation. Early stress is suggested to impair this proliferative capacity in aging neural stem cells, dampening the capacity for repair (Suri et al., 2013; Kalamakis et al., 2019). Several early stress models (MS, LBN, MIA, and MD) exhibit significant cognitive impairments in middle-aged and aged life (Brunson et al., 2005; Sterlemann et al., 2010; Suri et al., 2013; Sousa et al., 2014; Giovanoli et al., 2015; Yajima et al., 2018). The preponderance of literature using early stress models reporting changes at the epigenetic, transcriptional, mitochondrial, proteostatic, neuroinflammatory, cytoarchitectural and behavioral level is at best correlative, but thus far does not provide a clear causal relationship between changes at distinct levels of organization that mechanistically drive the accelerated aging phenotype evoked by early adversity.

CONCLUSION

Early adversity disrupts the functioning of key physiological processes that facilitate adaptive stress responses, setting in motion a cumulative "allostatic load" that alters the nature and time-line of healthy brain aging. Further, early adversity could also impact key neurodevelopmental milestones, which could alter the optimal functioning of neurocircuits thus setting up a substratum for a disruption of the trajectory for brain aging. The interim duration between exposure to early stressors and eventual brain aging outcomes provides a substantial temporal window for interventional approaches, including life-course factors such as exercise, diet, environmental enrichment, epigenetic and pharmacological interventions that may serve to reverse or ameliorate the negative impacts of early adversity on brain aging. Here we have provided an overview of the key brain aging-associated processes targeted by early adversity, and highlighted gaps in knowledge that require future investigation.

AUTHOR CONTRIBUTIONS

PC, AS, and VV jointly wrote the manuscript. All authors contributed to the article and approved the submitted version.

FUNDING

We acknowledge funding to VV from the Sree Ramakrishna Paramahamsa Research Grant for Translational Biomedical Research of the Sree Padmavathi Venkateswara Foundation (SreePVF/G/BS/19/1) and intramural support from the Tata Institute of Fundamental Research and Department of Atomic Energy, Mumbai (Grant reference number: RTI4003). PC received funding support from the India Alliance Early Career Fellowship (IA/E/18/1/504310) from the Department of Biotechnology, Government of India and the Wellcome Trust, United Kingdom.

REFERENCES

Abelaira, H. M., Veron, D. C., de Moura, A. B., Carlessi, A. S., Borba, L. A., Botelho, M. E. M., et al. (2021). Sex differences on the behavior and oxidative stress after ketamine treatment in adult rats subjected to early life stress. *Brain Res. Bull.* 172, 129–138. doi: 10.1016/J.BRAINRESBULL.2021.04.021

Agorastos, A., Pervanidou, P., Chrousos, G. P., and Baker, D. G. (2019). Developmental Trajectories of Early Life Stress and Trauma: a Narrative Review on Neurobiological Aspects Beyond Stress System Dysregulation. *Front. Psychiatry* 10:118. doi: 10.3389/FPSYT.2019.00118

Agoston, D. V. (2017). How to Translate Time? The Temporal Aspect of Human and Rodent Biology. *Front. Neurol.* 8:92. doi: 10.3389/FNEUR.2017.00092

Allaman, I., Bélanger, M., and Magistretti, P. J. (2015). Methylglyoxal, the dark side of glycolysis. *Front. Neurosci.* 9:23. doi: 10.3389/FNINS.2015.00023

Amini-Khoei, H., Mohammadi-Asl, A., Amiri, S., Hosseini, M. J., Momeny, M., Hassanipour, M., et al. (2017). Oxytocin mitigated the depressive-like behaviors of maternal separation stress through modulating mitochondrial function and neuroinflammation. *Prog. Neuropsychopharmacology Biol. Psychiatry* 76, 169–178. doi: 10.1016/J.PNPBP.2017.02.022

Ancelin, M. L., Carrière, I., Artero, S., Maller, J. J., Meslin, C., Dupuy, A. M., et al. (2021). Structural brain alterations in older adults exposed to early-life adversity. *Psychoneuroendocrinology* 129:105272. doi: 10.1016/J.PSYNEUEN.2021.105272

Andersen, S. L. (2022). Neuroinflammation, Early-Life Adversity, and Brain Development. *Harvard Rev. Psychiatry* 30, 24–39. doi: 10.1097/HRP.0000000000000325

Babenko, O., Kovalchuk, I., and Metz, G. A. S. (2015). Stress-induced perinatal and transgenerational epigenetic programming of brain development and mental health. *Neurosci. Biobehav. Rev.* 48, 70–91. doi: 10.1016/J.NEUBIOREV.2014.11.013

Bartsch, T., and Wulff, P. (2015). The hippocampus in aging and disease: from plasticity to vulnerability. *Neuroscience* 309, 1–16. doi: 10.1016/J.NEUROSCIENCE.2015.07.084

Birnie, M. T., Kooiker, C. L., Short, A. K., Bolton, J. L., Chen, Y., and Baram, T. Z. (2020). Plasticity of the Reward Circuitry After Early-Life Adversity: mechanisms and Significance. *Biol. Psychiatry* 87, 875–884. doi: 10.1016/J.BIOPSYCH.2019.12.018

Blaisdell, K. N., Imhof, A. M., and Fisher, P. A. (2019). Early adversity, child neglect, and stress neurobiology: from observations of impact to empirical evaluations of mechanisms. *Int. J. Dev. Neurosci.* 78, 139–146. doi: 10.1016/J.IJDEVNEU.2019.06.008

Brenhouse, H. C., Danese, A., and Grassi-Oliveira, R. (2019). Neuroimmune Impacts of Early-Life Stress on Development and Psychopathology. *Curr. Topics Behav. Neurosci.* 43, 423–447. doi: 10.1007/7854_2018_53

Brown, A. S., and Conway, F. (2019). Maternal Immune Activation and Related Factors in the Risk of Offspring Psychiatric Disorders. *Front. Psychiatry* 10:430. doi: 10.3389/FPSYT.2019.00430

Brown, D. W., Anda, R. F., Tiemeier, H., Felitti, V. J., Edwards, V. J., Croft, J. B., et al. (2009). Adverse childhood experiences and the risk of premature mortality. *Am. J. Prevent. Med.* 37, 389–396. doi: 10.1016/J.AMEPRE.2009.06.021

Brunson, K. L., Kramár, E., Lin, B., Chen, Y., Colgin, L. L., Yanagihara, T. K., et al. (2005). Mechanisms of late-onset cognitive decline after early-life stress. *J. Neurosci:* 25, 9328–9338. doi: 10.1523/JNEUROSCI.2281-05.2005

Brydges, N. M., Moon, A., Rule, L., Watkin, H., Thomas, K. L., and Hall, J. (2018). Sex specific effects of pre-pubertal stress on hippocampal neurogenesis and behaviour. *Trans. Psychiatry* 8:271. doi: 10.1038/S41398-018-0322-4

Caldji, C., Diorio, J., and Meaney, M. J. (2000). Variations in maternal care in infancy regulate the development of stress reactivity. *Biol. Psychiatry* 48, 1164–1174. doi: 10.1016/S0006-3223(00)01084-2

Casagrande, S., Stier, A., Monaghan, P., Loveland, J. L., Boner, W., Lupi, S., et al. (2020). Increased glucocorticoid concentrations in early life cause mitochondrial inefficiency and short telomeres. *J. Exp. Biol.* 223:jeb222513. doi: 10.1242/JEB.222513

Chen, N., Zhang, Y., Wang, M., Lin, X., Li, J., Li, J., et al. (2021). Maternal obesity interrupts the coordination of the unfolded protein response and heat shock response in the postnatal developing hypothalamus of male offspring in mice. *Mol. Cell. Endocrinol.* 527:111218. doi: 10.1016/J.MCE.2021.111218

Chen, Y., and Baram, T. Z. (2016). Toward Understanding How Early-Life Stress Reprograms Cognitive and Emotional Brain Networks. *Neuropsychopharmacology:* 41, 197–206. doi: 10.1038/NPP.2015.181

Colich, N. L., Rosen, M. L., Williams, E. S., and McLaughlin, K. A. (2020). Biological aging in childhood and adolescence following experiences of threat and deprivation: a systematic review and meta-analysis. *Psychol. Bull.* 146, 721–764. doi: 10.1037/BUL0000270

Correia-Melo, C., Marques, F. D., Anderson, R., Hewitt, G., Hewitt, R., Cole, J., et al. (2016). Mitochondria are required for pro-ageing features of the senescent phenotype. *EMBO J.* 35, 724–742. doi: 10.15252/EMBJ.201592862

Criado-Marrero, M., Gebru, N. T., Gould, L. A., Smith, T. M., Kim, S., Blackburn, R. J., et al. (2019). Early Life Stress and High FKBP5 Interact to Increase Anxiety-Like Symptoms through Altered AKT Signaling in the Dorsal Hippocampus. *Int. J. Mol. Sci.* 20:2738. doi: 10.3390/IJMS20112738

Criado-Marrero, M., Smith, T. M., Gould, L. A., Kim, S., Penny, H. J., Sun, Z., et al. (2020). FKBP5 and early life stress affect the hippocampus by an age-dependent mechanism. *Brain Behav. Immun. Health* 9:100143. doi: 10.1016/J.BBIH.2020.100143

Dallé, E., and Mabandla, M. V. (2018). Early Life Stress, Depression And Parkinson's Disease: a New Approach. *Mol. Brain* 11:18. doi: 10.1186/S13041-018-0356-9

Danese, A., and McEwen, B. S. (2012). Adverse childhood experiences, allostasis, allostatic load, and age-related disease. *Physiol. Behav.* 106, 29–39. doi: 10.1016/J.PHYSBEH.2011.08.019

Daniels, T. E., Olsen, E. M., and Tyrka, A. R. (2020). Stress and Psychiatric Disorders: The Role of Mitochondria. *Annu. Rev. Clin. Psychol.* 16, 165–186. doi: 10.1146/ANNUREV-CLINPSY-082719-104030

Daskalakis, N. P., Kloet, E. R., de Yehuda, R., Malaspina, D., and Kranz, T. M. (2015). Early Life Stress Effects on Glucocorticoid-BDNF Interplay in the Hippocampus. *Front. Mol. Neurosci.* 8:68. doi: 10.3389/FNMOL.2015.00068

Della, F. P., Abelaira, H. M., Réus, G. Z., dos Santos, M. A. B., Tomaz, D. B., Antunes, A. R., et al. (2013). Treatment with tianeptine induces antidepressive-like effects and alters the neurotrophin levels, mitochondrial respiratory chain and cycle Krebs enzymes in the brain of maternally deprived adult rats. *Metab. Brain Dis.* 28, 93–105. doi: 10.1007/S11011-012-9375-X

Delpech, J. C., Wei, L., Hao, J., Yu, X., Madore, C., Butovsky, O., et al. (2016). Early life stress perturbs the maturation of microglia in the developing hippocampus. *Brain Behav. Immun.* 57, 79–93. doi: 10.1016/J.BBI.2016.06.006

Desplats, P., Gutierrez, A. M., Antonelli, M. C., and Frasch, M. G. (2020). Microglial memory of early life stress and inflammation: susceptibility to neurodegeneration in adulthood. *Neurosci. Biobehav. Rev.* 117, 232–242. doi: 10.1016/J.NEUBIOREV.2019.10.013

Doherty, T. S., and Roth, T. L. (2018). Epigenetic Landscapes of the Adversity-Exposed Brain. *Prog. Mol. Biol. Trans. Sci.* 157, 1–19. doi: 10.1016/BS.PMBTS.2017.11.025

Dröge, W., and Schipper, H. M. (2007). Oxidative stress and aberrant signaling in aging and cognitive decline. *Aging Cell* 6, 361–370. doi: 10.1111/J.1474-9726.2007.00294.X

Drury, S. S., Theall, K., Gleason, M. M., Smyke, A. T., de Vivo, I., Wong, J. Y. Y., et al. (2012). Telomere length and early severe social deprivation: linking early adversity and cellular aging. *Mol. Psychiatry* 17, 719–727. doi: 10.1038/MP.2011.53

Dutcher, E. G., Pama, E. A. C., Lynall, M.-E., Khan, S., Clatworthy, M. R., Robbins, T. W., et al. (2020). Early-life stress and inflammation: a systematic review of a key experimental approach in rodents. *Brain Neurosci. Adv.* 4:239821282097804. doi: 10.1177/2398212820978049

Dutta, S., and Sengupta, P. (2016). Men and mice: relating their ages. *Life Sci.* 152, 244–248. doi: 10.1016/J.LFS.2015.10.025

Eagleson, K. L., Villaneuva, M., Southern, R. M., and Levitt, P. (2020). Proteomic and mitochondrial adaptations to early-life stress are distinct in juveniles and adults. *Neurobiol. Stress* 13:100251. doi: 10.1016/J.YNSTR.2020.100251

Eisner, V., Picard, M., and Hajnóczky, G. (2018). Mitochondrial dynamics in adaptive and maladaptive cellular stress responses. *Nat. Cell Biol.* 20, 755–765. doi: 10.1038/S41556-018-0133-0

Epel, E. S., and Prather, A. A. (2018). Stress, Telomeres, and Psychopathology: toward a Deeper Understanding of a Triad of Early Aging. *Annu. Rev. Clin. Psychol.* 14, 371–397. doi: 10.1146/ANNUREV-CLINPSY-032816-045054

Fan, W. J., Yan, M. C., Wang, L., Sun, Y. Z., Deng, J. B., and Deng, J. X. (2018). Synaptic aging disrupts synaptic morphology and function in cerebellar Purkinje cells. *Neural Regen. Res.* 13, 1019–1025. doi: 10.4103/1673-5374.233445

Farrell, M. R., Holland, F. H., Shansky, R. M., and Brenhouse, H. C. (2016). Sex-specific effects of early life stress on social interaction and prefrontal cortex dendritic morphology in young rats. *Behav. Brain Res.* 310, 119–125. doi: 10.1016/J.BBR.2016.05.009

Fjell, A. M., and Walhovd, K. B. (2010). Structural brain changes in aging: courses, causes and cognitive consequences. *Rev. Neurosci.* 21, 187–221. doi: 10.1515/REVNEURO.2010.21.3.187

Flurkey, K., Currer, J. M., and Harrison, D. E. (2007). Mouse Models in Aging Research. *Mouse Biomed. Res.* 3, 637–672. doi: 10.1016/B978-012369454-6/50074-1

Föcking, M., Opstelten, R., Prickaerts, J., Steinbusch, H. W. M., Dunn, M. J., van den Hove, D. L. A., et al. (2014). Proteomic investigation of the hippocampus in prenatally stressed mice implicates changes in membrane trafficking, cytoskeletal, and metabolic function. *Dev. Neurosci.* 36, 432–442. doi: 10.1159/000365327

Ganguly, P., and Brenhouse, H. C. (2015). Broken or maladaptive? Altered trajectories in neuroinflammation and behavior after early life adversity. *Dev. Cogn. Neurosci.* 11, 18–30. doi: 10.1016/J.DCN.2014.07.001

Gee, D. G. (2021). Early Adversity and Development: parsing Heterogeneity and Identifying Pathways of Risk and Resilience. *Am. J. Psychiatry* 178, 998–1013. doi: 10.1176/APPI.AJP.2021.21090944

Ghosh, S., Banerjee, K. K., Vaidya, V. A., and Kolthur-Seetharam, U. (2016). Early Stress History Alters Serum Insulin-Like Growth Factor-1 and Impairs Muscle Mitochondrial Function in Adult Male Rats. *J. Neuroendocrinol.* 28, doi: 10.1111/JNE.12397

Giandomenico, S. L., Alvarez-Castelao, B., and Schuman, E. M. (2021). Proteostatic regulation in neuronal compartments. *Trends Neurosci.* 45, 41–52. doi: 10.1016/J.TINS.2021.08.002

Giovanoli, S., Notter, T., Richetto, J., Labouesse, M. A., Vuillermot, S., Riva, M. A., et al. (2015). Late prenatal immune activation causes hippocampal deficits in the absence of persistent inflammation across aging. *J. Neuroinflamm.* 12:221. doi: 10.1186/S12974-015-0437-Y

González-Pardo, H., Arias, J. L., Gómez-Lázaro, E., Taboada, I. L., and Conejo, N. M. (2020). Sex-Specific Effects of Early Life Stress on Brain Mitochondrial Function. *Monoamine Levels Neuroinflamm. Brain Sci.* 10, 1–17. doi: 10.3390/BRAINSCI10070447

Goodwill, H. L., Manzano-Nieves, G., LaChance, P., Teramoto, S., Lin, S., Lopez, C., et al. (2018). Early Life Stress Drives Sex-Selective Impairment in Reversal Learning by Affecting Parvalbumin Interneurons in Orbitofrontal Cortex of Mice. *Cell Rep.* 25, 2299.e–2307.e. doi: 10.1016/J.CELREP.2018.11.010

Green, H. F., and Nolan, Y. M. (2014). Inflammation and the developing brain: consequences for hippocampal neurogenesis and behavior. *Neurosci. Biobehav. Rev.* 40, 20–34. doi: 10.1016/J.NEUBIOREV.2014.01.004

Grigoruta, M., Chavez-Solano, M., Varela-Ramirez, A., Sierra-Fonseca, J. A., Orozco-Lucero, E., Hamdan, J. N., et al. (2020). Maternal separation induces retinal and peripheral blood mononuclear cell alterations across the lifespan of female rats. *Brain Res.* 1749:147117. doi: 10.1016/J.BRAINRES.2020.147117

Hoeijmakers, L., Amelianchik, A., Verhaag, F., Kotah, J., Lucassen, P. J., and Korosi, A. (2018). Early-Life Stress Does Not Aggravate Spatial Memory or the Process of Hippocampal Neurogenesis in Adult and Middle-Aged APP/PS1 Mice. *Front. Aging Neurosci.* 10:61. doi: 10.3389/FNAGI.2018.00061

Hoffmann, A., and Spengler, D. (2018). The Mitochondrion as Potential Interface in Early-Life Stress Brain Programming. *Front. Behav. Neurosci.* 12:306. doi: 10.3389/FNBEH.2018.00306

Hui, J., Feng, G., Zheng, C., Jin, H., and Jia, N. (2017). Maternal separation exacerbates Alzheimer's disease-like behavioral and pathological changes in adult APPswe/PS1dE9 mice. *Behav. Brain Res.* 318, 18–23. doi: 10.1016/J.BBR.2016.10.030

Jafari, Z., Mehla, J., Kolb, B. E., and Mohajerani, M. H. (2019). Gestational Stress Augments Postpartum β-Amyloid Pathology and Cognitive Decline in a Mouse Model of Alzheimer's Disease. *Cereb. Cortex* 29, 3712–3724. doi: 10.1093/CERCOR/BHY251

Kalamakis, G., Brüne, D., Ravichandran, S., Bolz, J., Fan, W., Ziebell, F., et al. (2019). Quiescence Modulates Stem Cell Maintenance and Regenerative Capacity in the Aging Brain. *Cell* 176, 1407.e–1419.e. doi: 10.1016/J.CELL.2019.01.040

Kalish, B. T., Kim, E., Finander, B., Duffy, E. E., Kim, H., Gilman, C. K., et al. (2021). Maternal immune activation in mice disrupts proteostasis in the fetal brain. *Nat. Neurosci.* 24, 204–213. doi: 10.1038/S41593-020-00762-9

Karanikas, E., Daskalakis, N. P., and Agorastos, A. (2021). Oxidative Dysregulation in Early Life Stress and Posttraumatic Stress Disorder: a Comprehensive Review. *Brain Sci.* 11:723. doi: 10.3390/BRAINSCI11060723

Khorjahani, A., Peeri, M., and Azarbayjani, M. A. (2020). The Therapeutic Effect of Exercise on Anxiety and Bowel Oxidative Stress in the Maternal Separation Animal Model. *Basic Clin. Neurosci.* 11, 69–78. doi: 10.32598/BCN.9.10.450

Kim, J., Suh, Y. H., and Chang, K. A. (2021). Interleukin-17 induced by cumulative mild stress promoted depression-like behaviors in young adult mice. *Mol. Brain* 14:11. doi: 10.1186/S13041-020-00726-X

Kōks, S., Dogan, S., Tuna, B. G., González-Navarro, H., Potter, P., and Vandenbroucke, R. E. (2016). Mouse models of ageing and their relevance to disease. *Mech. Ageing Dev.* 160, 41–53. doi: 10.1016/J.MAD.2016.10.001

Ladd, C. O., Huot, R. L., Thrivikraman, K. V., Nemeroff, C. B., Meaney, M. J., and Plotsky, P. M. (2000). Long-term behavioral and neuroendocrine adaptations to adverse early experience. *Prog. Brain Res.* 122, 81–103. doi: 10.1016/S0079-6123(08)62132-9

Lapp, H. E., Mueller, I., and Moore, C. L. (2020). Limited bedding and nesting material changes indices of cellular metabolism and behavioral thermal regulation in Long-Evans rats during the first two weeks of life. *Physiol. Behav.* 222:112957. doi: 10.1016/J.PHYSBEH.2020.112957

Lesuis, S. L., Hoeijmakers, L., Korosi, A., de Rooij, S. R., Swaab, D. F., Kessels, H. W., et al. (2018a). Vulnerability and resilience to Alzheimer's disease: early life conditions modulate neuropathology and determine cognitive reserve. *Alzheimers Res. Ther.* 10:95. doi: 10.1186/S13195-018-0422-7

Lesuis, S. L., Weggen, S., Baches, S., Lucassen, P. J., and Krugers, H. J. (2018b). Targeting glucocorticoid receptors prevents the effects of early life stress on amyloid pathology and cognitive performance in APP/PS1 mice. *Trans. Psychiatry* 8:53. doi: 10.1038/S41398-018-0101-2

Lesuis, S. L., Maurin, H., Borghgraef, P., Lucassen, P. J., van Leuven, F., and Krugers, H. J. (2016). Positive and negative early life experiences differentially modulate long term survival and amyloid protein levels in a mouse model of Alzheimer's disease. *Oncotarget* 7, 39118–39135. doi: 10.18632/ONCOTARGET.9776

Liu, C., Hao, S., Zhu, M., Wang, Y., Zhang, T., and Yang, Z. (2018). Maternal Separation Induces Different Autophagic Responses in the Hippocampus and Prefrontal Cortex of Adult Rats. *Neuroscience* 374, 287–294. doi: 10.1016/J.NEUROSCIENCE.2018.01.043

Liu, P. Z., and Nusslock, R. (2018). How Stress Gets Under the Skin: Early Life Adversity and Glucocorticoid Receptor Epigenetic Regulation. *Curr. Genom.* 19, 653–664. doi: 10.2174/1389202919666171228164350

López-Otín, C., Blasco, M. A., Partridge, L., Serrano, M., and Kroemer, G. (2013). The hallmarks of aging. *Cell* 153:1194. doi: 10.1016/J.CELL.2013.05.039

Lu, T., Pan, Y., Kao, S. Y., Li, C., Kohane, I., Chan, J., et al. (2004). Gene regulation and DNA damage in the ageing human brain. *Nature* 429, 883–891. doi: 10.1038/NATURE02661

Mairesse, J., Vercoutter-Edouart, A. S., Marrocco, J., Zuena, A. R., Giovine, A., Nicoletti, F., et al. (2012). Proteomic characterization in the hippocampus of prenatally stressed rats. *J. Proteom.* 75, 1764–1770. doi: 10.1016/J.JPROT.2011.12.017

Marais, L., Hattingh, S. M., Stein, D. J., and Daniels, W. M. U. (2009). A proteomic analysis of the ventral hippocampus of rats subjected to maternal separation and escitalopram treatment. *Metab. Brain Dis.* 24, 569–586. doi: 10.1007/S11011-009-9156-3

Marini, S., Davis, K. A., Soare, T. W., Zhu, Y., Suderman, M. J., Simpkin, A. J., et al. (2020). Adversity exposure during sensitive periods predicts accelerated epigenetic aging in children. *Psychoneuroendocrinology* 113:104484. doi: 10.1016/J.PSYNEUEN.2019.104484

Markham, A., Bains, R., Franklin, P., and Spedding, M. (2014). Changes in mitochondrial function are pivotal in neurodegenerative and psychiatric

disorders: how important is BDNF? *Br. J. Pharmacol.* 171, 2206–2229. doi: 10.1111/BPH.12531

Marrocco, J., Gray, J. D., Kogan, J. F., Einhorn, N. R., O'Cinneide, E. M., Rubin, T. G., et al. (2019). Early Life Stress Restricts Translational Reactivity in CA3 Neurons Associated With Altered Stress Responses in Adulthood. *Front. Behav. Neurosci.* 13:157. doi: 10.3389/FNBEH.2019.00157

Masrour, F. F., Peeri, M., Azarbayjani, M. A., and Hosseini, M. J. (2018). Voluntary Exercise During Adolescence Mitigated Negative the Effects of Maternal Separation Stress on the Depressive-Like Behaviors of Adult Male Rats: role of NMDA Receptors. *Neurochem. Res.* 43, 1067–1074. doi: 10.1007/s11064-018-2519-6

Mattson, M. P., and Arumugam, T. V. (2018). Hallmarks of Brain Aging: adaptive and Pathological Modification by Metabolic States. *Cell Metab.* 27, 1176–1199. doi: 10.1016/J.CMET.2018.05.011

McClelland, S., Korosi, A., Cope, J., Ivy, A., and Baram, T. Z. (2011). Emerging roles of epigenetic mechanisms in the enduring effects of early-life stress and experience on learning and memory. *Neurobiol. Learn. Memory* 96, 79–88. doi: 10.1016/J.NLM.2011.02.008

McEwen, B. S. (2007). Physiology and neurobiology of stress and adaptation: central role of the brain. *Physiol. Rev.* 87, 873–904. doi: 10.1152/PHYSREV.00041.2006

McEwen, B. S., and Morrison, J. H. (2013). The brain on stress: vulnerability and plasticity of the prefrontal cortex over the life course. *Neuron* 79, 16–29. doi: 10.1016/J.NEURON.2013.06.028

Merz, M. P., and Turner, J. D. (2021). Is early life adversity a trigger towards inflammageing?. *Exp. Gerontol.* 150:111377. doi: 10.1016/J.EXGER.2021.111377

Miller, G. E., Chen, E., and Parker, K. J. (2011). Psychological stress in childhood and susceptibility to the chronic diseases of aging: moving toward a model of behavioral and biological mechanisms. *Psychol. Bull.* 137, 959–997. doi: 10.1037/A0024768

Molet, J., Maras, P. M., Avishai-Eliner, S., and Baram, T. Z. (2014). Naturalistic rodent models of chronic early-life stress. *Dev. Psychobiol.* 56, 1675–1688. doi: 10.1002/DEV.21230

Morrison, J. H., and Baxter, M. G. (2012). The ageing cortical synapse: hallmarks and implications for cognitive decline. *Nat. Rev. Neurosci.* 13, 240–250. doi: 10.1038/NRN3200

Mourtzi, N., Sertedaki, A., and Charmandari, E. (2021). Glucocorticoid Signaling and Epigenetic Alterations in Stress-Related Disorders. *Int. J. Mol. Sci.* 22:5964. doi: 10.3390/IJMS22115964

Muñoz-Carvajal, F., and Sanhueza, M. (2020). The Mitochondrial Unfolded Protein Response: a Hinge Between Healthy and Pathological Aging. *Front. Aging Neurosci.* 12:581849. doi: 10.3389/FNAGI.2020.581849

Nettis, M. A., Pariante, C. M., and Mondelli, V. (2020). Early-Life Adversity, Systemic Inflammation and Comorbid Physical and Psychiatric Illnesses of Adult Life. *Curr. Topics Behav. Neurosci.* 44, 207–225. doi: 10.1007/7854_2019_89

Nold, V., Sweatman, C., Karabatsiakis, A., Böck, C., Bretschneider, T., Lawless, N., et al. (2019). Activation of the kynurenine pathway and mitochondrial respiration to face allostatic load in a double-hit model of stress. *Psychoneuroendocrinology* 107, 148–159. doi: 10.1016/J.PSYNEUEN.2019.04.006

Orso, R., Creutzberg, K. C., Wearick-Silva, L. E., Wendt Viola, T., Tractenberg, S. G., Benetti, F., et al. (2019). How Early Life Stress Impact Maternal Care: a Systematic Review of Rodent Studies. *Front. Behav. Neurosci.* 13:197. doi: 10.3389/FNBEH.2019.00197

Oschwald, J., Guye, S., Liem, F., Rast, P., Willis, S., Röcke, C., et al. (2019). Brain structure and cognitive ability in healthy aging: a review on longitudinal correlated change. *Rev. Neurosci.* 31, 1–57. doi: 10.1515/REVNEURO-2018-0096

Palma-Gudiel, H., Fañanás, L., Horvath, S., and Zannas, A. S. (2020). Psychosocial stress and epigenetic aging. *Int. Rev. Neurobiol.* 150, 107–128. doi: 10.1016/BS.IRN.2019.10.020

Paradies, G., Petrosillo, G., Paradies, V., and Ruggiero, F. M. (2011). Mitochondrial dysfunction in brain aging: role of oxidative stress and cardiolipin. *Neurochem. Int.* 58, 447–457. doi: 10.1016/J.NEUINT.2010.12.016

Parel, S. T., and Peña, C. J. (2022). Genome-wide Signatures of Early-Life Stress: influence of Sex. *Biol. Psychiatry* 91, 36–42. doi: 10.1016/J.BIOPSYCH.2020.12.010

Peña, C. J., Smith, M., Ramakrishnan, A., Cates, H. M., Bagot, R. C., Kronman, H. G., et al. (2019). Early life stress alters transcriptomic patterning across reward circuitry in male and female mice. *Nat. Commun.* 10:5098. doi: 10.1038/S41467-019-13085-6

Perry, C. J., Campbell, E. J., Drummond, K. D., Lum, J. S., and Kim, J. H. (2021). Sex differences in the neurochemistry of frontal cortex: impact of early life stress. *J. Neurochem.* 157, 963–981. doi: 10.1111/JNC.15208

Pervanidou, P., and Chrousos, G. P. (2018). Early-Life Stress: from Neuroendocrine Mechanisms to Stress-Related Disorders. *Horm. Res. Paediatr.* 89, 372–379. doi: 10.1159/000488468

Picard, M., Juster, R. P., and McEwen, B. S. (2014). Mitochondrial allostatic load puts the "gluc" back in glucocorticoids. *Nat. Rev. Endocrinol.* 10, 303–310. doi: 10.1038/NRENDO.2014.22

Picard, M., McEwen, B. S., Epel, E. S., and Sandi, C. (2018). An energetic view of stress: focus on mitochondria. *Front. Neuroendocrinol.* 49:72–85. doi: 10.1016/J.YFRNE.2018.01.001

Picard, M., McManus, M. J., Gray, J. D., Nasca, C., Moffat, C., Kopinski, P. K., et al. (2015). Mitochondrial functions modulate neuroendocrine, metabolic, inflammatory, and transcriptional responses to acute psychological stress. *Proc. Natl. Acad. Sci. U.S.A.* 112, E6614–E6623. doi: 10.1073/PNAS.1515733112

Pinto, B. A. S., Melo, T. M., Flister, K. F. T., França, L. M., Kajihara, D., Tanaka, L. Y., et al. (2016). Early and sustained exposure to high-sucrose diet triggers hippocampal ER stress in young rats. *Metab. Brain Dis.* 31, 917–927. doi: 10.1007/S11011-016-9830-1

Pluvinage, J. V., and Wyss-Coray, T. (2020). Systemic factors as mediators of brain homeostasis, ageing and neurodegeneration. *Nat. Rev. Neurosci.* 21, 93–102. doi: 10.1038/S41583-019-0255-9

Price, L. H., Kao, H. T., Burgers, D. E., Carpenter, L. L., and Tyrka, A. R. (2013). Telomeres and early-life stress: an overview. *Biol. Psychiatry* 73, 15–23. doi: 10.1016/J.BIOPSYCH.2012.06.025

Psarra, A. M. G., and Sekeris, C. E. (2009). Glucocorticoid receptors and other nuclear transcription factors in mitochondria and possible functions. *Biochim. et Biophys. Acta* 1787, 431–436. doi: 10.1016/J.BBABIO.2008.11.011

Pusalkar, M., Suri, D., Kelkar, A., Bhattacharya, A., Galande, S., and Vaidya, V. A. (2016). Early stress evokes dysregulation of histone modifiers in the medial prefrontal cortex across the life span. *Dev. Psychobiol.* 58, 198–210. doi: 10.1002/DEV.21365

Raz, N., and Rodrigue, K. M. (2006). Differential aging of the brain: patterns, cognitive correlates and modifiers. *Neurosci. Biobehav. Rev.* 30, 730–748. doi: 10.1016/J.NEUBIOREV.2006.07.001

Regnell, C. E., Hildrestrand, G. A., Sejersted, Y., Medin, T., Moldestad, O., Rolseth, V., et al. (2012). Hippocampal adult neurogenesis is maintained by Neil3-dependent repair of oxidative DNA lesions in neural progenitor cells. *Cell Rep.* 2, 503–510. doi: 10.1016/J.CELREP.2012.08.008

Reshetnikov, V., Ryabushkina, Y., Kovner, A., Lepeshko, A., and Bondar, N. (2020). Repeated and single maternal separation specifically alter microglial morphology in the prefrontal cortex and neurogenesis in the hippocampus of 15-day-old male mice. *Neuroreport* 31, 1256–1264. doi: 10.1097/WNR.0000000000001544

Réus, G. Z., Fernandes, G. C., de Moura, A. B., Silva, R. H., Darabas, A. C., de Souza, T. G., et al. (2017). Early life experience contributes to the developmental programming of depressive-like behaviour, neuroinflammation and oxidative stress. *J. Psychiatric Res.* 95, 196–207. doi: 10.1016/J.JPSYCHIRES.2017.08.020

Réus, G. Z., Silva, R. H., de Moura, A. B., Presa, J. F., Abelaira, H. M., Abatti, M., et al. (2019). Early Maternal Deprivation Induces Microglial Activation, Alters Glial Fibrillary Acidic Protein Immunoreactivity and Indoleamine 2,3-Dioxygenase during the Development of Offspring Rats. *Mol. Neurobiol.* 56, 1096–1108. doi: 10.1007/S12035-018-1161-2

Ridout, K. K., Levandowski, M., Ridout, S. J., Gantz, L., Goonan, K., Palermo, D., et al. (2018). Early life adversity and telomere length: a meta-analysis. *Mol. Psychiatry* 23, 858–871. doi: 10.1038/MP.2017.26

Roth, T. L., Lubin, F. D., Funk, A. J., and Sweatt, J. D. (2009). Lasting epigenetic influence of early-life adversity on the BDNF gene. *Biol. Psychiatry* 65, 760–769. doi: 10.1016/J.BIOPSYCH.2008.11.028

Roth, T. L., and Sweatt, J. D. (2011). Epigenetic marking of the BDNF gene by early-life adverse experiences. *Horm. Behav.* 59, 315–320. doi: 10.1016/J.YHBEH.2010.05.005

Rothman, S. M., and Mattson, M. P. (2013). Activity-dependent, stress-responsive BDNF signaling and the quest for optimal brain health and resilience throughout the lifespan. *Neuroscience* 239, 228–240. doi: 10.1016/J.NEUROSCIENCE.2012.10.014

Ruigrok, S. R., Yim, K., Emmerzaal, T. L., Geenen, B., Stöberl, N., den Blaauwen, J. L., et al. (2021). Effects of early-life stress on peripheral and central mitochondria in male mice across ages. *Psychoneuroendocrinology* 132:105346. doi: 10.1016/J.PSYNEUEN.2021.105346

Ruiz, R., Roque, A., Pineda, E., Licona-Limón, P., José Valdéz-Alarcón, J., and Lajud, N. (2018). Early life stress accelerates age-induced effects on neurogenesis, depression, and metabolic risk. *Psychoneuroendocrinology* 96, 203–211. doi: 10.1016/J.PSYNEUEN.2018.07.012

Sarter, M., and Bruno, J. P. (2004). Developmental origins of the age-related decline in cortical cholinergic function and associated cognitive abilities. *Neurobiol. Aging* 25, 1127–1139. doi: 10.1016/J.NEUROBIOLAGING.2003.11.011

Saulnier, R. J., Best, C., Kostyniuk, D. J., Gilmour, K. M., and Lamarre, S. G. (2021). Chronic social stress alters protein metabolism in juvenile rainbow trout, Oncorhynchus mykiss. *J. Comp. Physiol. B Biochem. Syst. Environ. Physiol.* 191, 517–530. doi: 10.1007/S00360-021-01340-6

Schmidt, M. V., Wang, X. D., and Meijer, O. C. (2011). Early life stress paradigms in rodents: potential animal models of depression? *Psychopharmacology* 214, 131–140. doi: 10.1007/S00213-010-2096-0

Semple, B. D., Blomgren, K., Gimlin, K., Ferriero, D. M., and Noble-Haeusslein, L. J. (2013). Brain development in rodents and humans: identifying benchmarks of maturation and vulnerability to injury across species. *Prog. Neurobiol.* 10, 1–16. doi: 10.1016/J.PNEUROBIO.2013.04.001

Seo, M. K., Kim, S. G., Seog, D. H., Bahk, W. M., Kim, S. H., Park, S. W., et al. (2020). Effects of Early Life Stress on Epigenetic Changes of the Glucocorticoid Receptor 1 7 Promoter during Adulthood. *Int. J. Mol. Sci.* 21, 1–12. doi: 10.3390/IJMS21176331

Seo, M. K., Ly, N. N., Lee, C. H., Cho, H. Y., Choi, C. M., Nhu, L. H., et al. (2016). Early life stress increases stress vulnerability through BDNF gene epigenetic changes in the rat hippocampus. *Neuropharmacology* 105, 388–397. doi: 10.1016/J.NEUROPHARM.2016.02.009

Short, A. K., Maras, P. M., Pham, A. L., Ivy, A. S., and Baram, T. Z. (2020). Blocking CRH receptors in adults mitigates age-related memory impairments provoked by early-life adversity. *Neuropsychopharmacology* 45, 515–523. doi: 10.1038/S41386-019-0562-X

Sierra-Fonseca, J. A., Hamdan, J. N., Cohen, A. A., Cardenas, S. M., Saucedo, S., Lodoza, G. A., et al. (2021). Neonatal Maternal Separation Modifies Proteostasis Marker Expression in the Adult Hippocampus. *Front. Mol. Neurosci.* 14:661993. doi: 10.3389/FNMOL.2021.661993

Simen, A. A., Bordner, K. A., Martin, M. P., Moy, L. A., and Barry, L. C. (2011). Cognitive dysfunction with aging and the role of inflammation. *Ther. Adv. Chronic Dis.* 2, 175–195. doi: 10.1177/2040622311399145

Smart, C., Strathdee, G., Watson, S., Murgatroyd, C., and McAllister-Williams, R. H. (2015). Early life trauma, depression and the glucocorticoid receptor gene–an epigenetic perspective. *Psychol. Med.* 45, 3393–3410. doi: 10.1017/S0033291715001555

Sousa, V. C., Vital, J., Costenla, A. R., Batalha, V. L., Sebastião, A. M., Ribeiro, J. A., et al. (2014). Maternal separation impairs long term-potentiation in CA1-CA3 synapses and hippocampal-dependent memory in old rats. *Neurobiol. Aging* 35, 1680–1685. doi: 10.1016/J.NEUROBIOLAGING.2014.01.024

Sparkman, N. L., and Johnson, R. W. (2008). Neuroinflammation associated with aging sensitizes the brain to the effects of infection or stress. *Neuroimmunomodulation* 15, 323–330. doi: 10.1159/000156474

Sterlemann, V., Rammes, G., Wolf, M., Liebl, C., Ganea, K., Müller, M. B., et al. (2010). Chronic social stress during adolescence induces cognitive impairment in aged mice. *Hippocampus* 20, 540–549. doi: 10.1002/HIPO.20655

Suri, D., Bhattacharya, A., and Vaidya, V. A. (2014). Early stress evokes temporally distinct consequences on the hippocampal transcriptome, anxiety and cognitive behaviour. *Int. J. Neuropsychopharmacol.* 17, 289–301. doi: 10.1017/S1461145713001004

Suri, D., and Vaidya, V. A. (2013). Glucocorticoid regulation of brain-derived neurotrophic factor: relevance to hippocampal structural and functional plasticity. *Neuroscience* 239, 196–213. doi: 10.1016/J.NEUROSCIENCE.2012.08.065

Suri, D., and Vaidya, V. A. (2015). The adaptive and maladaptive continuum of stress responses - a hippocampal perspective. *Rev. Neurosci.* 26, 415–442. doi: 10.1515/REVNEURO-2014-0083

Suri, D., Veenit, V., Sarkar, A., Thiagarajan, D., Kumar, A., Nestler, E. J., et al. (2013). Early stress evokes age-dependent biphasic changes in hippocampal neurogenesis. *BDNF Express. Cogn. Biol. Psychiatry* 73, 658–666. doi: 10.1016/J.BIOPSYCH.2012.10.023

Swaab, D. F., Bao, A. M., and Lucassen, P. J. (2005). The stress system in the human brain in depression and neurodegeneration. *Ageing Res. Rev.* 4, 141–194. doi: 10.1016/J.ARR.2005.03.003

Syed, S. A., and Nemeroff, C. B. (2017). Early Life Stress, Mood, and Anxiety Disorders. *Chron. Stress* 1:2470547017694461. doi: 10.1177/2470547017694461

Szyf, M. (2009). The early life environment and the epigenome. *Biochim. et Biophys. Acta* 1790, 878–885. doi: 10.1016/J.BBAGEN.2009.01.009

Szyf, M. (2019). The epigenetics of perinatal stress. *Dial. Clin. Neurosci.* 21, 369–378. doi: 10.31887/DCNS.2019.21.4/MSZYF

Talukdar, P. M., Abdul, F., Maes, M., Binu, V., Venkatasubramanian, G., Kutty, B. M., et al. (2020). Maternal Immune Activation Causes Schizophrenia-like Behaviors in the Offspring through Activation of Immune-Inflammatory, Oxidative and Apoptotic Pathways, and Lowered Antioxidant Defenses and Neuroprotection. *Mol. Neurobiol.* 57, 4345–4361. doi: 10.1007/S12035-020-02028-8

Tay, T. L., Béchade, C., D'Andrea, I., St-Pierre, M. K., Henry, M. S., Roumier, A., et al. (2018). Microglia Gone Rogue: impacts on Psychiatric Disorders across the Lifespan. *Front. Mol. Neurosci.* 10:421. doi: 10.3389/FNMOL.2017.00421

Teicher, M. H., Gordon, J. B., and Nemeroff, C. B. (2021). Recognizing the importance of childhood maltreatment as a critical factor in psychiatric diagnoses, treatment, research, prevention, and education. *Mol. Psychiatry* 26, 1–8. doi: 10.1038/S41380-021-01367-9

Teicher, M. H., Samson, J. A., Anderson, C. M., and Ohashi, K. (2016). The effects of childhood maltreatment on brain structure, function and connectivity. *Nat. Rev. Neurosci.* 17, 652–666. doi: 10.1038/NRN.2016.111

Torres-Berrío, A., Issler, O., Parise, E. M., and Nestler, E. J. (2019). Unraveling the epigenetic landscape of depression: focus on early life stress. *Dial. Clin. Neurosci.* 21, 341–357. doi: 10.31887/DCNS.2019.21.4/ENESTLER

Tyrka, A. R., Parade, S. H., Price, L. H., Kao, H. T., Porton, B., Philip, N. S., et al. (2016). Alterations of Mitochondrial DNA Copy Number and Telomere Length With Early Adversity and Psychopathology. *Biol. Psychiatry* 79, 78–86. doi: 10.1016/J.BIOPSYCH.2014.12.025

Tzanoulinou, S., and Sandi, C. (2017). The Programming of the Social Brain by Stress During Childhood and Adolescence: from Rodents to Humans. *Curr. Topics Behav. Neurosci.* 30, 411–429. doi: 10.1007/7854_2015_430

Uddin, M. S., Yu, W. S., and Lim, L. W. (2021). Exploring ER stress response in cellular aging and neuroinflammation in Alzheimer's disease. *Ageing Res. Rev.* 70:101417. doi: 10.1016/J.ARR.2021.101417

Usui, N., Ono, Y., Aramaki, R., Berto, S., Konopka, G., Matsuzaki, H., et al. (2021). Early Life Stress Alters Gene Expression and Cytoarchitecture in the Prefrontal Cortex Leading to Social Impairment and Increased Anxiety. *Front. Genet.* 12:754198. doi: 10.3389/FGENE.2021.754198

van Zyl, P. J., Dimatelis, J. J., and Russell, V. A. (2016). Behavioural and biochemical changes in maternally separated Sprague-Dawley rats exposed to restraint stress. *Metab. Brain Dis.* 31, 121–133. doi: 10.1007/S11011-015-9757-Y

Vasileiou, P., Evangelou, K., Vlasis, K., Fildisis, G., Panayiotidis, M., Chronopoulos, E., et al. (2019). Mitochondrial Homeostasis and Cellular Senescence. *Cells* 8:686. doi: 10.3390/CELLS8070686

Walker, C. D., Bath, K. G., Joels, M., Korosi, A., Larauche, M., Lucassen, P. J., et al. (2017). Chronic early life stress induced by limited bedding and nesting (LBN) material in rodents: critical considerations of methodology, outcomes and translational potential. *Stress* 20, 421–448. doi: 10.1080/10253890.2017.1343296

Wang, S., Lai, X., Deng, Y., and Song, Y. (2020). Correlation between mouse age and human age in anti-tumor research: significance and method establishment. *Life Sci.* 242:117242. doi: 10.1016/J.LFS.2019.117242

Weaver, I. C. G. (2007). Epigenetic programming by maternal behavior and pharmacological intervention. Nature versus nurture: let's call the whole thing off. *Epigenetics* 2, 22–28. doi: 10.4161/EPI.2.1.3881

Webb, M., and Sideris, D. P. (2020). Intimate Relations-Mitochondria and Ageing. *Int. J. Mol. Sci.* 21, 1–48. doi: 10.3390/IJMS2120 7580

Wyss-Coray, T. (2016). Ageing, neurodegeneration and brain rejuvenation. *Nature* 539, 180–186. doi: 10.1038/NATURE20411

Yajima, H., Haijima, A., Khairinisa, M. A., Shimokawa, N., Amano, I., and Takatsuru, Y. (2018). Early-life stress induces cognitive disorder in middle-aged mice. *Neurobiol. Aging* 64, 139–146. doi: 10.1016/J.NEUROBIOLAGING.2017.12.021

Yau, J. L. W., and Seckl, J. R. (2012). Local amplification of glucocorticoids in the aging brain and impaired spatial memory. *Front. Aging Neurosci.* 4:24. doi: 10.3389/FNAGI.2012.00024

Yuan, R., Tsaih, S. W., Petkova, S. B., de Evsikova, C. M., Xing, S., Marion, M. A., et al. (2009). Aging in inbred strains of mice: study design and interim report on median lifespans and circulating IGF1 levels. *Aging Cell* 8, 277–287. doi: 10.1111/J.1474-9726.2009.00478.X

Zannas, A. S. (2018). Gene-environment Interactions in Late Life: linking Psychosocial Stress with Brain Aging. *Curr. Neuropharmacol.* 16, 327–333. doi: 10.2174/1570159X15666171109121452

Zannas, A. S. (2019). Epigenetics as a key link between psychosocial stress and aging: concepts, evidence, mechanisms. *Dial. Clin. Neurosci.* 21, 389–396. doi: 10.31887/DCNS.2019.21.4/AZANNAS

Zitkovsky, E. K., Daniels, T. E., and Tyrka, A. R. (2021). Mitochondria and early-life adversity. *Mitochondrion* 57, 213–221. doi: 10.1016/J.MITO.2021.01.005

Conflict of Interest: The authors declare that the research was conducted in the absence of any commercial or financial relationships that could be construed as a potential conflict of interest.

Publisher's Note: All claims expressed in this article are solely those of the authors and do not necessarily represent those of their affiliated organizations, or those of the publisher, the editors and the reviewers. Any product that may be evaluated in this article, or claim that may be made by its manufacturer, is not guaranteed or endorsed by the publisher.

frontiers in Molecular Neuroscience

REVIEW
published: 31 March 2022
doi: 10.3389/fnmol.2022.858582

AUTS2 Syndrome: Molecular Mechanisms and Model Systems

Alecia Biel[1], Anthony S. Castanza[2], Ryan Rutherford[1], Summer R. Fair[1], Lincoln Chifamba[1], Jason C. Wester[3], Mark E. Hester[1,3,4] and Robert F. Hevner[2]**

[1] The Steve and Cindy Rasmussen Institute for Genomic Medicine, Abigail Wexner Research Institute at Nationwide Children's Hospital, Columbus, OH, United States, [2] Department of Pathology, University of California, San Diego, San Diego, CA, United States, [3] Department of Neuroscience, The Ohio State University College of Medicine, Columbus, OH, United States, [4] Department of Pediatrics, The Ohio State University College of Medicine, Columbus, OH, United States

OPEN ACCESS

Edited by:
Sumru Bayin,
Memorial Sloan Kettering Cancer Center, United States

Reviewed by:
Esther B. E. Becker,
University of Oxford, United Kingdom
Ashwin S. Shetty,
Harvard University, United States

***Correspondence:**
Mark E. Hester
Mark.Hester@NationwideChildrens.org
Robert F. Hevner
rhevner@health.ucsd.edu;
rhevner@ucsd.edu

Specialty section:
This article was submitted to Methods and Model Organisms, a section of the journal Frontiers in Molecular Neuroscience

Received: 20 January 2022
Accepted: 01 March 2022
Published: 31 March 2022

Citation:
Biel A, Castanza AS, Rutherford R, Fair SR, Chifamba L, Wester JC, Hester ME and Hevner RF (2022) AUTS2 Syndrome: Molecular Mechanisms and Model Systems. Front. Mol. Neurosci. 15:858582. doi: 10.3389/fnmol.2022.858582

AUTS2 syndrome is a genetic disorder that causes intellectual disability, microcephaly, and other phenotypes. Syndrome severity is worse when mutations involve 3' regions (exons 9-19) of the *AUTS2* gene. Human AUTS2 protein has two major isoforms, full-length (1259 aa) and C-terminal (711 aa), the latter produced from an alternative transcription start site in exon 9. Structurally, AUTS2 contains the putative "AUTS2 domain" (~200 aa) conserved among AUTS2 and its ohnologs, fibrosin, and fibrosin-like-1. Also, AUTS2 contains extensive low-complexity sequences and intrinsically disordered regions, features typical of RNA-binding proteins. During development, *AUTS2* is expressed by specific progenitor cell and neuron types, including pyramidal neurons and Purkinje cells. AUTS2 localizes mainly in cell nuclei, where it regulates transcription and RNA metabolism. Some studies have detected AUTS2 in neurites, where it may regulate cytoskeletal dynamics. Neurodevelopmental functions of AUTS2 have been studied in diverse model systems. In zebrafish, *auts2a* morphants displayed microcephaly. In mice, excision of different *Auts2* exons (7, 8, or 15) caused distinct phenotypes, variously including neonatal breathing abnormalities, cerebellar hypoplasia, dentate gyrus hypoplasia, EEG abnormalities, and behavioral changes. In mouse embryonic stem cells, AUTS2 could promote or delay neuronal differentiation. Cerebral organoids, derived from an AUTS2 syndrome patient containing a pathogenic missense variant in exon 9, exhibited neocortical growth defects. Emerging technologies for analysis of human cerebral organoids will be increasingly useful for understanding mechanisms underlying AUTS2 syndrome. Questions for future research include whether AUTS2 binds RNA directly, how AUTS2 regulates neurogenesis, and how AUTS2 modulates neural circuit formation.

Keywords: intellectual disability, microcephaly, RNA-binding protein, AUTS2 syndrome, FBRSL1, dentate gyrus hypoplasia, cerebellar hypoplasia, cerebral organoids

INTRODUCTION TO AUTS2 SYNDROME

The *AUTS2* gene (autism-susceptibility-gene-2) was first identified in humans by genetic analysis of monozygotic twins with autism and chromosomal translocation *t*(7;20) (Sultana et al., 2002). Human *AUTS2* was further revealed as a 1.2-Mb gene on chromosome 7q11.22, which encodes a 1259-aa full-length protein, and a 711-aa C-terminal isoform (Beunders et al., 2013). Sequence analysis of AUTS2 detected motifs such as proline-rich regions and histidine repeats, but no recognizable structural domains. As of 2021, more than 60 patients with pathogenic *AUTS2* variants have been reported, and the AUTS2 syndrome has been well characterized as a neurodevelopmental and somatic malformation disorder with diverse phenotypes. The most common phenotypes are intellectual disability (ID) and microcephaly (Beunders et al., 2016).

Although the *AUTS2* gene was named for autism susceptibility, many AUTS2 syndrome patients have an outgoing personality in childhood (Beunders et al., 2016). Rather, the most frequent trait is ID (or developmental delay), mild to severe, in virtually all patients. The major traits and their frequency are ID (98%), microcephaly (65%), feeding difficulties (62%), attention deficit hyperactivity disorder (ADHD) (54%), and autistic traits (52%) (Beunders et al., 2013, 2016; Sanchez-Jimeno et al., 2021). Hypotonia (38%) and spasticity (37%), inverse disorders of neuromuscular reflexes, are also relatively frequent. A small minority have epilepsy (7%). As observed by neuroimaging, structural brain anomalies occur in 27% of *AUTS2* patients (Sanchez-Jimeno et al., 2021). The reported brain malformations include corpus callosum hypoplasia, cerebellar hypoplasia, small posterior fossa, and Chiari malformation type 1 (Liu et al., 2021; Fair et al., 2022). Somatic developmental problems are also numerous in AUTS2 syndrome. These include growth defects, such as low birth weight (20%) and short stature (43%); musculoskeletal anomalies, such as kyphosis/scoliosis (24%) and tight heel cords (37%); and facial dysmorphisms, such as hypertelorism (44%) and micrognathia/retrognathia (36%). Thus, in the most severe cases, AUTS2 syndrome can affect many organs.

As a gauge of overall severity, an "AUTS2 syndrome severity score" representing the sum of 32 traits was formulated (Beunders et al., 2013). Interestingly, the severity scores were observed more severe in patients with whole gene deletions or C-terminal mutations (exons 9–19), and less severe in patients with N-terminal mutations (exons 1–8) (Beunders et al., 2013; Sanchez-Jimeno et al., 2021). The hypothesis that the C-terminal part of the protein mediates major AUTS2 functions was further supported by *Auts2a* knockdown experiments in zebrafish, in which expression of the C-terminal isoform rescued the microcephaly phenotype (Beunders et al., 2013). The C-terminal isoform is comprised of a proline-rich region (exons 9–13), the putative "AUTS2 domain" of ∼200 aa (exons 14–19), and disordered regions (exon 19), but does not include the HX repeat encoded by the first part of exon 9 (described in more detail below). Indeed, the alternative tss, corresponding to position 1,597 of full-length *AUTS2* cDNA (Beunders et al., 2013), lies within the HX repeat encoded by cDNA positions 1,575–1,626. The translation start site for AUTS2-C corresponds to position 1,666 of full-length cDNA, and thus does not include the HX repeat.

AUTS2 syndrome exhibits phenotypic overlap with several other genetic causes of ID, including Rubinstein-Taybi syndrome (*CREBBP* or *EP300*) (Fergelot et al., 2016), NONO syndrome (Sewani et al., 2020), TBR1 syndrome (Nambot et al., 2020), and FBRSL1 syndrome (Ufartes et al., 2020). The similarities among these disorders reflect their related roles in genetic pathways and binding interactions. Specifically, expression of *Auts2* is regulated by transcription factor TBR1 (Bedogni et al., 2010); AUTS2 protein interacts with NONO protein (Castanza et al., 2021); AUTS2 binds and regulates *EP300* mRNA (Castanza et al., 2021); and FBRSL1, an RNA-binding protein (Baltz et al., 2012), is the closest homolog of AUTS2 in the genome (Sellers et al., 2020).

THE *AUTS2* GENE FAMILY AND FUNCTIONS

When *AUTS2* was first described, its functions could not be predicted on the basis of homology to known proteins. Indeed, only partial sequence homology was found to two genes with unknown functions, designated CG9056 and FLJ11618 (Sultana et al., 2002). Subsequent research identified CG9056 as Drosophila tay bridge (*tay*), and FLJ11618 as human fibrosin (*FBRS*). Both genes, it is now known, indeed belong to the same diversified superfamily of genes as *AUTS2* (Sellers et al., 2020).

More narrowly, the "*AUTS2* gene family" consists of the three most closely related genes, *AUTS2, FBRSL1*, and *FBRS*. These genes are ohnologs—defined as paralogs produced by two-rounds of gene duplication from a single ancestral gene during the evolution of jawed vertebrates ∼450 million years ago (Sacerdot et al., 2018; Sellers et al., 2020). Accordingly, *AUTS2, FBRSL1*, and *FBRS* genes are found in all vertebrates. By sequence analysis, *AUTS2* appears most closely related to the ancestral *AUTS2* precursor (*aAUTS2p*) gene; also, *AUTS2* and *FBRSL1* are closer to each other than to FBRS (Sellers et al., 2020).

The ancestral *aAUTS2p* gene arose in early bilaterian animals ∼650 million years ago, and its derivatives are found in the *Nephrozoa* clade (Sellers et al., 2020). Thus, non-Chordate bilaterians, such as flies and amphioxus, contain only one *AUTS2*-related gene. In Drosophila, that gene is *tay* (tay bridge), which regulates neuronal development in the protocerebral bridge and motoneurons (Poeck et al., 2008; Molnar and de Celis, 2013; Molnar et al., 2018). However, *tay* is relatively divergent from *aAUTS2p*, and shows only patchy homology to mammalian *AUTS2* (Sellers et al., 2020). The most highly conserved sequence in AUTS2-related proteins from diverse vertebrate and invertebrate species aligns with exon 14 of human *AUTS2*, which encodes part of the predicted "AUTS2 domain." Also highly conserved is the "HX repeat" or "HQHT repeat" region encoded in the first half of *AUTS2* exon 9.

While much progress has been made comprehending evolution of the *AUTS2* gene family, no consensus conserved functions of the proteins have been determined. Several AUTS2

superfamily members localize in cell nuclei, including AUTS2 (Bedogni et al., 2010), FBRSL1 (Ufartes et al., 2020), and tay bridge (Molnar and de Celis, 2013). Among these, FBRSL1 was previously identified as an mRNA binding protein (Baltz et al., 2012). Further studies of the *AUTS2* gene family and superfamily will be necessary to shed light on conserved and divergent functions of these proteins.

STRUCTURE OF THE HUMAN *AUTS2* GENE, TRANSCRIPTS, AND PROTEIN ISOFORMS

Human *AUTS2* spans 1,195,032 base pairs on chromosome 7q11.22 (UCSD Genome Browser, assembly hg38[1]). Exons 1–7 are separated by long introns (16–301 kb), while exons 7–19 have shorter introns (∼1–3 kb) (**Figure 1A** and **Supplementary Table 1**). Full-length AUTS2 cDNA (NCBI CCDS5539.1) encodes a protein of 1259 amino acids (NP_056385.1), here designated isoform AUTS2-FL (**Figure 1B**). Many variant transcripts have been annotated from sequencing projects, but the best documented variant is generated from an in-frame alternative transcription start site (tss) in exon 9, to produce the C-terminal isoform of AUTS2 (Beunders et al., 2013), here designated AUTS2-C (**Figures 1A,B**). The AUTS2-C transcript also utilizes an alternative splice junction between exons 9–10 to incorporate an additional 7 amino acids, totaling 711 aa. Both AUTS2-FL and AUTS2-C are highly basic (pI = 9.41).

Sequence analysis has revealed several features of AUTS2 protein that suggest possible functions (**Figure 1B**). Among the most salient features of AUTS2 are its high contents of predicted intrinsically disordered regions (IDRs) and low complexity sequences (LCSs). One recent analysis found that predicted IDRs comprise 64.4% of AUTS2-FL (Sellers et al., 2020). Among LCSs, AUTS2 contains two proline-rich regions (PRRs), two histidine-rich regions (HRRs), and one serine-rich region (SRR) (Sultana et al., 2002; and Expasy ScanProsite) (**Figure 1B**). HRR1 contains an HX (HQ and HT) repeat (aa 525–542), while HRR2 contains an 8-aa stretch of only histidines. Together, putative IDRs and LCSs cover ∼74.2% of AUTS2-FL. This is significant because IDRs and short repetitive amino acid motifs are typical features of mRNA-binding proteins (Castello et al., 2012; Hentze et al., 2018). Consistent with this analysis, AUTS2 was recently found to bind RNA-protein complexes, and possibly RNA directly (Castanza et al., 2021).

Sequence analysis also indicates that AUTS2 is likely to be localized in cell nuclei. AUTS2-FL has multiple nuclear localization sequences (NLSs) in the 5′ region, and NucPred indicates 100% likelihood of intranuclear localization. AUTS2-C does not have discrete NLSs, but its overall sequence predicts 70% likelihood of intranuclear localization (NucPred). In addition, AUTS2-FL, but not AUTS2-C, contains a PY motif (PPPY), which may bind WW-domains to interact with other proteins. PY motifs interact with Nedd4 family E3 ubiquitin ligases for proteolysis (Hatstat et al., 2021), and with other proteins for signal transduction or transcription (Lin et al., 2019).

The domain structure of AUTS2 is unknown. The protein contains no recognized structural domain sequences, and its structure has not been studied experimentally. Previous studies have used bioinformatics to propose AUTS2-FL structures with three domains (Sellers et al., 2020) or five domains (Castanza et al., 2021), but these remain speculative. Sequence analysis of AUTS2 using NCBI Conserved Domains Database identifies an ∼200-aa "AUTS2 domain" (pfam15336), predicted on the basis of sequence conservation across the *AUTS2* gene family (*AUTS2, FBRSL1*, and *FBRS*) (Castanza et al., 2021). The AUTS2 domain is present in both AUTS2-FL and AUTS2-C isoforms (**Figure 1B**). Sequence analysis of AUTS2-FL with ProDom identified six possible domains, three of which are also found in FBRSL1 (**Supplementary Figure 1** and **Supplementary Table 2**). All of the putative domains identified by ProDom are annotated as likely poly(A)-RNA binding proteins. Finally, comparison of AUTS2 and FBRSL1 identifies a highly conserved 46 aa sequence (73.9% identity, no gaps) in the N-terminal part of AUTS2-FL, here designated the AUTS2/FBRSL1 short homology (AFsh) region (**Figure 1B**, **Supplementary Figure 1B**, and **Supplementary Table 3**).

Other interesting features of *AUTS2* include two blocs of exons, ExB1 and ExB2 (comprised of exons 6–9 and 15–19, respectively), each connected by splice junctions that encode amino acids across the junctions; as well as several exons that encode non-integer numbers of amino acids (**Figure 1B**). These features imply reduced likelihood of alternative splicing involving those exons and may indicate important functions for the encoded protein sequences. Indeed, ExB1 encodes PRR1, SRR, and IDR regions, potentially for RNA binding; ExB2 encodes part of the AUTS2 domain. Interestingly, ExB1 and ExB2 are conserved in FBRSL1 as exons 6–9 and 13–17 of that gene (**Supplementary Figure 1** and **Supplementary Table 3**). For ExB1, the encoded protein sequences are relatively divergent between AUTS2 and FBRSL1, mostly due to insertions and deletions involving PRR1. In contrast, ExB2 is better conserved at the protein level, and encodes most of the putative AUTS2 domain in both FBRSL1 and AUTS2.

To further explore potential AUTS2 protein structures, we used RoseTTAfold[2] (Baek et al., 2021) to computationally predict structures of AUTS2, FBRSL1, and the AUTS2 domains of each protein (**Supplementary Figures 2–5**). None of the RoseTTAfold models yielded high-confidence results, most likely because no known structures are available for proteins of similar sequence. However, all of the models showed extensive stretches of disordered, open structure. Indeed, one possibility is that outside the putative AUTS2 domain, AUTS2 and FBRSL1 lack classic well-structured domains, and instead utilize disordered sequences for RNA binding. Putting all features together, both AUTS2 and FBRSL1 are seen as proteins with extensive IDRs and LCSs, punctuated by conserved motifs and the putative AUTS2 domain (**Figure 1C** and **Supplementary Figure 1C**).

[1]https://genome.ucsc.edu

[2]https://robetta.bakerlab.org

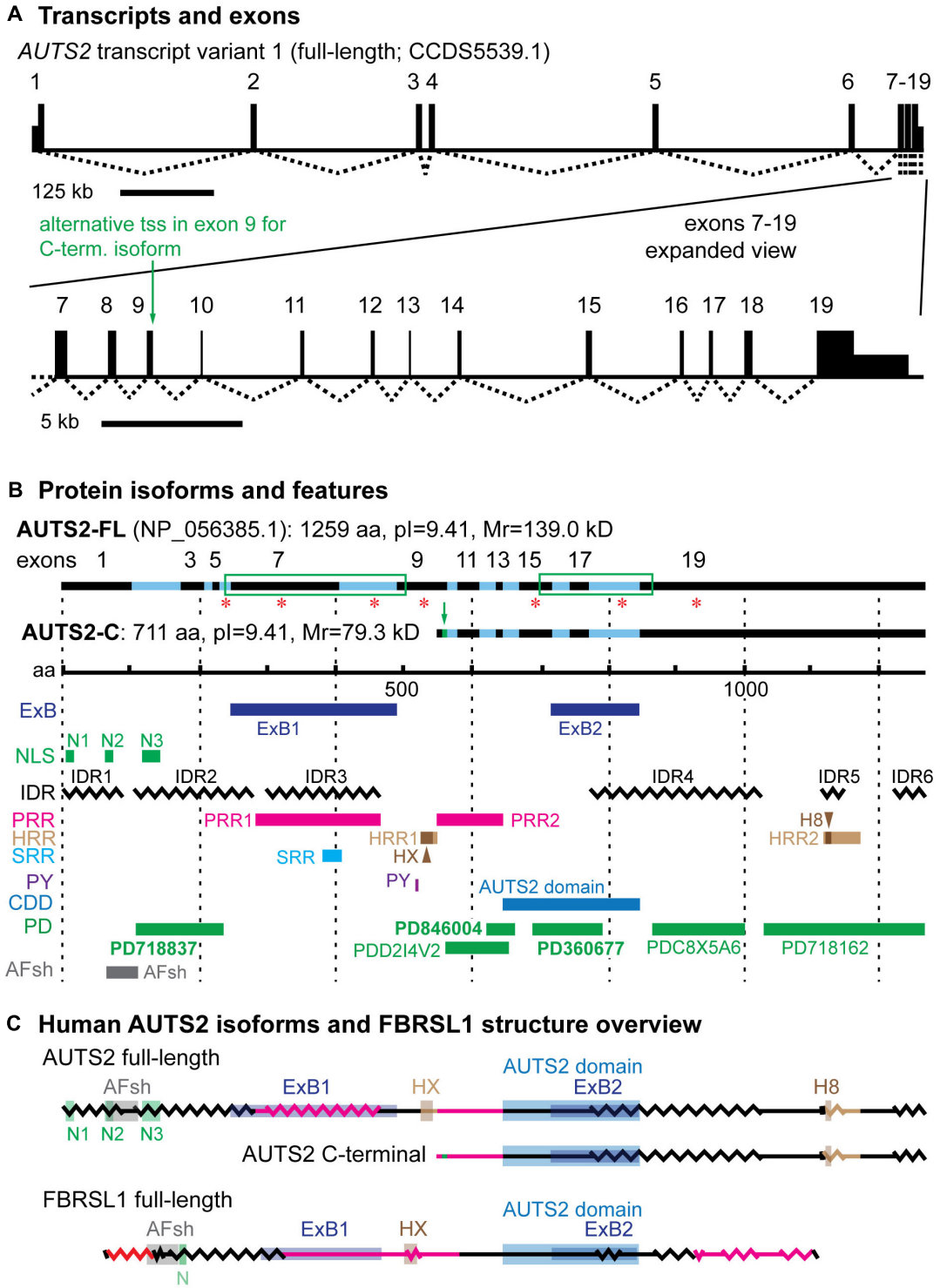

FIGURE 1 | *AUTS2* transcripts and protein isoforms. **(A)** The full-length *AUTS2* transcript has 19 exons. An alternative transcription start site (tss) in exon 9 produces mRNA for the C-terminal protein isoform. **(B)** The full-length and C-terminal isoforms are indicated with source exons in black (odd) and blue (even). Green boxes enclose splice junctions in which amino acids were encoded across the junctions, comprising exon blocs. Red asterisks indicate source exons that encoded a non-integer number of amino acids. Features mapped from protein sequence: ExB, exon bloc; NLS, nuclear localization sequence; IDR, intrinsically disordered region; PRR, Pro-rich repeat; HRR, His-rich repeat; HX, HX repeat; H8, polyhistidine (8×) repeat; SRR, Ser-rich repeat; PY, PY protein binding motif; CDD, conserved domain database; PD, ProDom predicted domains (domain names in bold also identified in FBRSL1); AFsh, AUTS2-FBRSL1 short homology region. **(C)** Both major AUTS2 isoforms have a high content of IDRs (zigzag lines) and regions enriched in amino acids Pro, His, or Ser (red lines). The C-terminal isoform includes the AUTS2 domain, but lacks N-terminal features such as the HX repeat.

AUTS2 EXPRESSION PATTERNS AND INTRACELLULAR LOCALIZATION

The expression of *AUTS2* mRNA and protein isoforms has been studied in multiple tissues and cell types (**Table 1**). In humans, *AUTS2* mRNA is expressed at relatively high levels in fetal and adult brain, skeletal muscle, and kidney; and at lower levels in several other tissues (Sultana et al., 2002). In mice, *Auts2* mRNA is expressed in many areas of the developing brain and spinal cord (**Figure 2A**) (Bedogni et al., 2010). In developing cerebral cortex, *Auts2* is expressed mainly in the cortical plate, where postmitotic neurons are located, although lower levels of mRNA are also detected in progenitor compartments (ventricular zone and subventricular zone) (Bedogni et al., 2010). Moreover, AUTS2 protein has been detected in neurogenic cortical progenitor cells (Castanza et al., 2021). From E16.5 to the first postnatal week in mice, *Auts2* mRNA is expressed in an intracortical gradient from high rostral to low caudal, suggesting a possible role in cortical patterning (Bedogni et al., 2010). AUTS2 protein is localized mainly in the nuclei of neurons, but not glial cells; in cerebral cortex, AUTS2 is expressed by pyramidal neurons, but not GABAergic interneurons (Bedogni et al., 2010; Gao et al., 2014; Castanza et al., 2021). AUTS2 protein may additionally be present in neuronal cytoplasm, including neurites and growth cones (Hori et al., 2014). In postnatal mouse cerebellum, AUTS2 protein is detected at high levels in Purkinje cells and Golgi neurons (**Figures 2B,C**) (Yamashiro et al., 2020).

Recently, the open Marmoset Gene Atlas[3] has published *AUTS2* expression results in the developing and adult non-human primate brain. As shown by *in situ* hybridization, *AUTS2* mRNA is expressed in many regions of the developing marmoset brain, with particularly high levels in the amygdala (**Figure 2D**). In adult marmosets, *AUTS2* mRNA levels remain high in the amygdala, and in granule neurons of the hippocampal dentate gyrus (**Figures 2E,F**).

MOLECULAR FUNCTIONS AND INTERACTIONS OF AUTS2 PROTEIN

Transcriptional Activation

Molecular functions of AUTS2 have been elucidated in the context of AUTS2 interacting molecules, complexes, and chromatin (**Figure 3**). The first proposed function of AUTS2, as a transcriptional activator, was determined on the basis of its interactions with other regulators of transcription, and its distribution in active open chromatin. In human embryonic kidney (HEK) cells induced to express AUTS2, AUTS2 associated with non-canonical forms of polycomb repressive complex 1

[3]https://gene-atlas.brainminds.riken.jp/

TABLE 1 | AUTS2 expression in developing brain and cultured cells.

Tissue/cell type	Auts2 gene expression	AUTS2 isoform expression	References
Embryonic stem cells	Before differentiation (D0)	Long only	Monderer-Rothkoff et al., 2021
	Differentiation day 6 (D6)	Short only	
	D12 (corresponding to ∼E12)	Long and short	
Whole brain	mRNA Peaks at E16, decreases until reaching low levels at P21	Short > long; Both decrease throughout early development	Bedogni et al., 2010; Hori et al., 2014; Hori et al., 2020; Liu et al., 2021
	Early embryonic stages, mRNA strongest expression in neocortex, hippocampus, and cerebellum		
Cerebral cortex	Rostral (high expression)-caudal (low expression) gradient	Short predominate; Low levels of Long	Bedogni et al., 2010; Hori et al., 2014; Castanza et al., 2021
Hippocampus	From E14 onward: dentate gyrus (DG), CA1, and CA3	Predominantly short	Bedogni et al., 2010; Castanza et al., 2021
	P21: granule cell layer and subgranular zone		Bedogni et al., 2010
Cerebellum	Early stages: granule neurons, precursor of Purkinje cells, and some deep nuclei	Long > short	Bedogni et al., 2010; Castanza et al., 2021
	P21: Purkinje cells and Golgi neurons		Bedogni et al., 2010; Yamashiro et al., 2020; Castanza et al., 2021
Thalamus	E14: dorsal thalamus		Bedogni et al., 2010
	P21: anterior thalamic nuclei and ventrolateral/ventromedial nuclei only	Unknown	Bedogni et al., 2010
Fetal brain	8 weeks: frontal, parietal, and temporal lobes of the neocortex, telencephalon, ganglionic eminence, caudate nucleus, putamen nuclei, and cerebellum	Short predominate in early stages (8–24 weeks), both transcripts are expressed in similar low levels in adult brain	Oksenberg et al., 2013; Pinto et al., 2020; Monderer-Rothkoff et al., 2021
	23 weeks: dentate gyrus, CA1 and CA3 pyramidal cell subregions, the ganglionic eminence, caudate nucleus, and putamen nuclei; neocortex and prefrontal cortex		

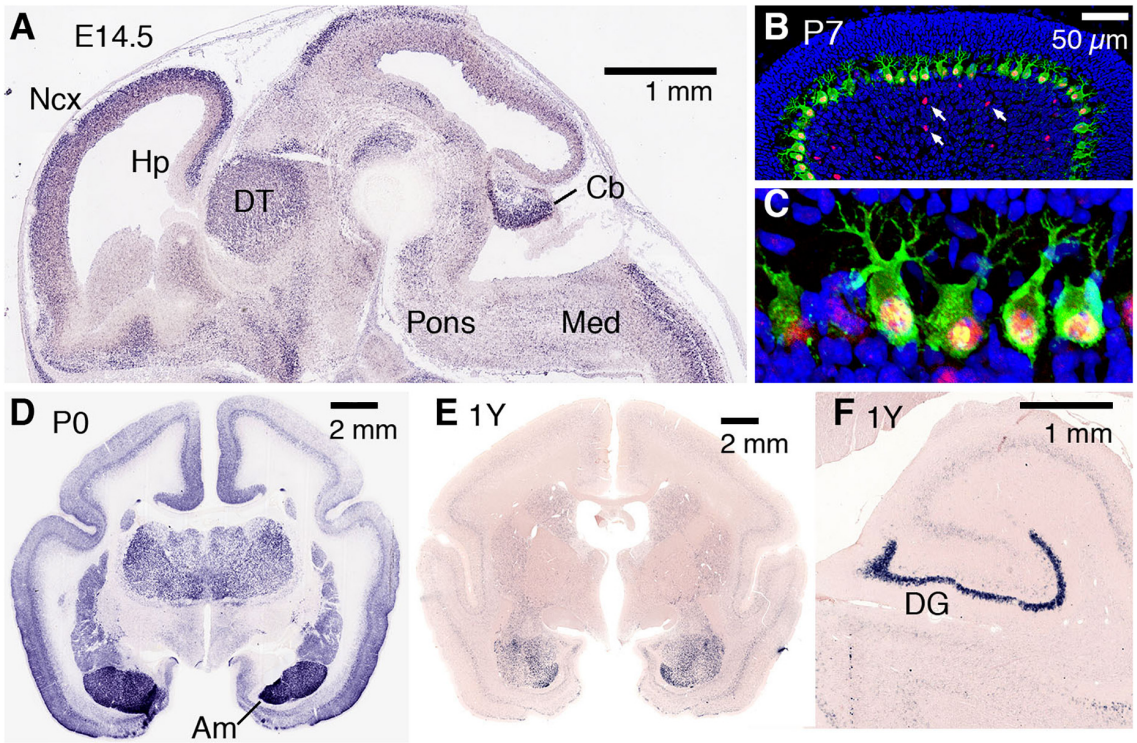

FIGURE 2 | AUTS2 expression in developing mouse and marmoset brain. **(A)** By *in situ* hybridization, Auts2 expression is observed in multiple areas of E14.5 mouse brain, including cerebral neocortex (Ncx), hippocampus (Hp), dorsal thalamus (DT), pons, cerebellum (Cb), and medulla (Med). Sagittal section from Genepaint (https://gp3.mpg.de/). **(B,C)** In P7 mouse cerebellum, AUTS2 protein (red) localizes in the nuclei of calbindin + (green) Purkinje cells, and in scattered Golgi neurons (arrows). Panel **(C)** magnified 5× from **(B)**. **(D)** In neonatal marmosets, AUTS2 is expressed in many brain regions, with highest levels in amygdala (Am). **(E,F)** In 1-year-old (young adult) marmosets, AUTS2 levels remain high in amygdala and dentate gyrus (DG). Data for panels **(D–F)** from the Marmoset Gene Atlas (https://gene-atlas.brainminds.riken.jp/).

(PRC1), which is a complex that contains PCGF3/5, RING1A/B, and RYBP/YAF2, but no CBX proteins (Gao et al., 2014). Canonical PRC1 is an epigenetic repressor that ubiquitinates histones. In contrast, non-canonical PRC1 (ncPRC1) was found to activate gene expression via AUTS2-mediated recruitment of P300, a histone lysine acetyltransferase (**Figure 3A**) (Gao et al., 2014). Consistent with this function, ChIP-seq indicated that in developing brain, AUTS2 localizes to actively transcribed chromatin, usually within ±5 kb of transcriptional start sites (Gao et al., 2014; Oksenberg et al., 2014; Liu et al., 2021). Subsequently, WDR68 was identified as an additional component of the AUTS2-containing ncPRC1 complex (Wang et al., 2018). On the other hand, two groups have reported that AUTS2-FL interacts with ncPRC1, but AUTS2-C does not (Geng et al., 2021; Monderer-Rothkoff et al., 2021). In a study of mutations in AUTS2 syndrome, the interaction of AUTS2 with P300 in HEK 293 cells was found to be disrupted by mutations involving the HX repeat (Liu et al., 2021). Importantly, the HX repeat encompasses the alternative tss for AUTS2-C, and indeed a small deletion in the HX repeat was found to eliminate expression of AUTS2-C (Martinez-Delgado et al., 2021). Significantly, most of the above-mentioned AUTS2-protein interactions and disruptions were studied in HEK cells after AUTS2 overexpression (Gao et al., 2014; Wang et al., 2018; Geng et al., 2021), or in yeast two-hybrid assays (Monderer-Rothkoff et al., 2021). Further studies are needed to confirm that AUTS2 interacts with proteins such as PCGF3/5, RING1B, and P300 at physiological levels in cortical neurons *in vivo*.

RNA Metabolism

Another proposed intranuclear function of AUTS2 is to regulate RNA metabolism by associating with RNA-binding protein (RBP) complexes, and possibly with RNA directly. Immunoprecipitation (IP) of AUTS2 from developing mouse cortex followed by mass spectrometry (IP-MS) revealed that AUTS2 interacts with multiple RBPs *in vivo*, including scaffolds NONO and SFPQ, splicing factors such as SRSF3/7, and RNA helicases DDX5/17 (**Figure 3A**) (Castanza et al., 2021). Also, in yeast two-hybrid assays, AUTS2 was reported to interact with splicing factor SF3B1 (Monderer-Rothkoff et al., 2021). In neonatal mouse neocortex, AUTS2 IP followed by RNA sequencing (RIP-seq) detected abundant transcripts, including many, such as *Ep300*, that are dysregulated in *Auts2* conditional mutant mice (described below) (Castanza et al., 2021). The hypothesis that AUTS2 may bind RNA directly is further supported by its high content of IDRs and LCSs, characteristic of RBPs (Castello et al., 2012; Hentze et al., 2018) (**Figure 1**). Furthermore, FBRSL1—the closest homolog

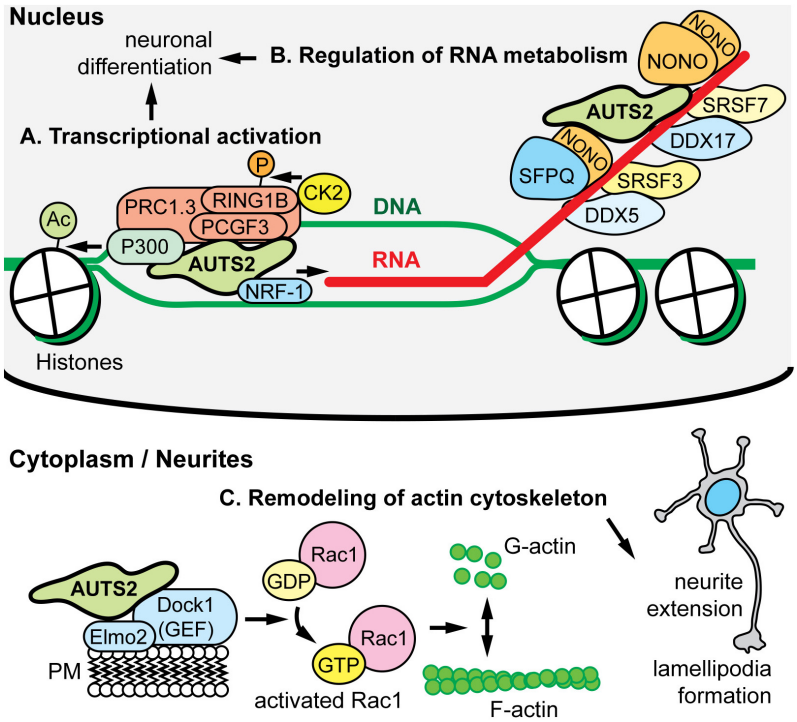

FIGURE 3 | AUTS2 molecular functions and interactions. **(A)** In HEK293 cells, AUTS2 associates with variant forms of polycomb repressive complex 1 (vPRC1), which also contains PCGF3/5, RING1B, and other PRC1 subunits (PMID: 25519132). In turn, AUTS2 recruits P300, a histone acetyltransferase that opens chromatin, and binds NRF1, a transcriptional activator (PMID: 34637754). Also, vPRC1 recruits CK2, a protein kinase that phosphorylates and inactivates RING1B, a ubiquitin ligase and core subunit of PRC1 for chromatin inactivation. The net effect of AUTS2 is to convert PRC1 from a repressor to an activator of transcription. **(B)** In developing cerebral cortex, AUTS2 associates with multiple RNA-binding proteins (RBPs), including the scaffolds NONO and SFPQ; splicing factors SRSF3 and SRSF7; and RNA helicases DDX5 and DDX7 (PMID: 34013328). Also, AUTS2 co-immunoprecipitated multiple RNA species, suggesting that AUTS2 binds RNA directly or indirectly. **(C)** In HEK293 cells, AUTS2 associates with a guanine nucleotide exchange factor (GEF) complex containing DOCK1 (also known as DOCK180) and ELMO2 (PMID: 25533347). Through this interaction, AUTS2 is thought to cause activation of Rac1 (a small G protein), remodeling of the cytoskeleton, neurite elongation, and lamellipodia formation. AUTS2 was also found to interact with another GEF, P-REX1; and may regulate multiple small G proteins.

(ohnolog) of AUTS2—has been identified as a poly(A)-RBP (Baltz et al., 2012). More studies of RNA regulation by AUTS2 are needed to determine if AUTS2 interacts directly with RNA, or only indirectly through protein complexes.

Cytoskeletal Dynamics

Outside the nucleus, AUTS2-FL was found to interact with guanine nucleotide exchange factors (GEFs) such as P-Rex1 and the Dock1/Elmo2 complex (**Figure 3B**) (Hori et al., 2014). These GEFs activate Rac1, a small G protein "molecular switch" that controls cytoskeletal organization. By interacting with GEFs, AUTS2 was proposed to enhance Rac1 activation and thus control neurite outgrowth, cell migration, and the formation of lamellipodia and filopodia (Hori et al., 2014). For future studies, it would be useful to see if these AUTS2-GEF interactions, found in HEK cells after overexpression, also occur under physiologic conditions in neurons *in vivo*.

Inhibition of BMP Signaling to Promote Neuronal Differentiation

In HEK cells and in mESCs differentiated to radial glia-like neuronal progenitor cells, both AUTS2-FL and AUTS2-C interacted with WDR68 and SKI to form a novel AUTS2-WDR68-SKI (AWS) complex (Geng et al., 2021). The AWS complex recruited CUL4, a ubiquitin E3 ligase, to mediate proteolytic degradation of phosphorylated SMAD1/5/9, and thereby inhibit BMP pathway signaling to promote neuronal differentiation (Geng et al., 2021). Further studies of this proposed mechanism are needed to evaluate its relevance to cortical neuron differentiation *in vivo*, since the aforementioned studies were done in cultured HEK cells or mESCs, after overexpression of AUTS2 or proposed interacting molecules.

NEURODEVELOPMENTAL FUNCTIONS OF AUTS2 IN ANIMAL MODEL SYSTEMS

Zebrafish

The first animal studies of AUTS2 neurodevelopmental functions were conducted in zebrafish, using splice-blocking and translation-blocking morpholinos to knock down *auts2a* (Beunders et al., 2013; Oksenberg et al., 2013). In *auts2a* morphants, AUTS2 deficiency resulted in microcephaly, decreased neurogenesis, and other growth defects (**Table 2**).

TABLE 2 | Animal models of *AUTS2* syndrome.

Species	Perturbation	Phenotypes	Rescue	References
Zebrafish	sb-morpholinos against *auts2a*	Microcephaly. Micrognathia. Retrognathia. Decreased neurogenesis. Decreased proliferation.	AUTS2-FL AUTS2-C	Beunders et al., 2013
Zebrafish	tb- and sb-morpholinos against *auts2a*	Microcephaly. Microphthalmia. Decreased neurogenesis. Increased proliferation. Increased apoptosis. Fewer spinal motoneurons. Fewer spinal sensory neurons. Increased axon branching.	AUTS2-FL	Oksenberg et al., 2013
Mouse	*Auts2*$^{del7/del7}$ (*Nes*-Cre)	No brain abnormalities decreased body growth. Impaired righting reflex. Decreased USVs. Impaired negative geotaxis.		Gao et al., 2014
Mouse	*Auts2*$^{del8/del8}$ (whole organism)	No brain abnormalities (P0)neonatal lethal. AUTS2-C upregulated.		Hori et al., 2014
Mouse	*Auts2*$^{neo/+}$ (∼50% reduced AUTS2-FL and AUTS2-C)	Decreased anxiety. Decreased exploratory behav. Impaired novel object recog. Impaired cued assoc. memory Increased nociceptive resp. Altered acoustic startle		Hori et al., 2015
Mouse	*Auts2*$^{del8/del8}$ (*Emx1*-Cre or *CaMKIIa*-CreER^{T2}) *Auts2*$^{del8/+}$	Increased dendritic spines. Increased mEPSCs. Decreased social interactions. Decreased exploratory behav. Decreased fear of heights. Impaired novel object recog. Increased nociceptive resp. Decreased prepulse inhibition. Altered acoustic startle Decreased USVs		Hori et al., 2020
Mouse	*Auts2*$^{del8/del8}$ (*En1*-Cre)	Cerebellum small, malformed. Decreased Purkinje cells. Decreased MB DA neurons. AUTS2-C upregulated. Impaired motor learning. Decreased male USVs.		Yamashiro et al., 2020
Mouse	*Auts2*$^{del15/del15}$ (*Nes*-Cre) *Auts2*$^{del15/del15}$ (*Emx1*-Cre)	Neonatal lethal. Abnormal breathing rhythms. Dentate gyrus small. Abnormal EEG.		Castanza et al., 2021

These phenotypes were rescued by expression of either AUTS2-FL or AUTS2-C, indicating that important AUTS2 functions are retained in the C-terminal region (Beunders et al., 2013). Interestingly, one study in zebrafish observed micrognathia/retrognathia in *auts2a* morphants, replicating a phenotype observed in humans (Beunders et al., 2013). Jaw growth may potentially be a conserved function of AUTS2, related to the evolutionary amplification of *AUTS2* ohnologs in gnathostomes (Sellers et al., 2020). However, since zebrafish lack laminated cerebral cortex, and morphants often exhibit off-target effects (Vogan, 2015), the utility of zebrafish for studying human brain development is very limited. Moreover, zebrafish have a second gene, *auts2b*, also expressed in developing brain (Kondrychyn et al., 2017).

Mice

Several mouse models of AUTS2 deficiency have been produced by gene targeting of different *Auts2* exons (**Table 2**). The structure of the *Auts2* gene in mice (1.1 Mb, chromosome 5) is similar as in humans, and likewise comprises 19 exons (Castanza et al., 2021). The alternative TSS in exon 9 is active in mice and produces a C-terminal AUTS2 isoform similar to that in humans (Hori et al., 2014). In addition, mice have another alternative TSS in exon 7, which uses a translational start site in exon 8 and produces a slightly longer C-terminal isoform (Hori et al., 2014). Analyses of protein and RNA indicate that AUTS2-FL and AUTS2-C isoforms are both expressed in developing mouse brain, with AUTS2-C isoforms predominating in embryonic cerebral cortex, and AUTS2-FL in cerebellum

(Gao et al., 2014; Hori et al., 2014; Molyneaux et al., 2015; Castanza et al., 2021).

In mice lacking *Auts2* exon 7 (*Auts2*$^{del7/del7}$) in the nervous system (*Nes*-Cre), mutants had normal birth weight but grew more slowly than controls postnatally, and exhibited behavioral abnormalities such as decreased ultrasonic vocalizations (**Table 2**) (Gao et al., 2014). No structural brain defects were reported, and only one gene (*Dynll1*) was significantly dysregulated among a panel of 9 candidate *Auts2* target genes assayed by RT-PCR. Importantly, excision of exon 7 did not disrupt the exon 9 TSS, and AUTS2-C was presumably still expressed, although this was not tested (Gao et al., 2014). Thus, this model likely caused only partial loss of AUTS2 function, related to the full-length isoform.

In another mouse model, mutants lacking *Auts2* exon 8 (*Auts2*$^{del8/del8}$) throughout the organism died in the neonatal period (**Table 2**) (Hori et al., 2014). The neonatal brains showed no abnormalities by macroscopic examination or histology. In this model, the alternative TSS in exon 9 was again undisturbed, and AUTS2-C protein was actually increased in the cerebral cortex of *Auts2*$^{del8/del8}$ mice, possibly as a compensatory response to AUTS2-FL depletion (Hori et al., 2014). Conditional excision of exon 8 in cerebral cortex pyramidal neurons during development (*Emx1*-Cre) or adulthood (*CaMKIIa*-CreERT2) permitted longer postnatal survival and additional studies (Hori et al., 2020). In these models, increased numbers of dendritic spines were observed on pyramidal neurons in the hippocampus (CA1) and neocortical layers 2–3 of mutant mice, along with increased numbers of miniature excitatory postsynaptic currents (mEPSCs), as well as behavioral abnormalities (Hori et al., 2020). Conditional deletion of *Auts2* exon 8 in the developing cerebellum and caudal midbrain (*En1*-Cre) caused cerebellar hypoplasia, with defects of Purkinje cell maturation and synaptogenesis, plus behavioral abnormalities (Yamashiro et al., 2020). The latter results accord with previous evidence that AUTS2-FL is the main isoform in developing cerebellum (Castanza et al., 2021). Importantly, the cerebellar hypoplasia in mice (Yamashiro et al., 2020) recapitulates the cerebellar hypoplasia seen in some AUTS2 syndrome patients with missense or microdeletion variants in exon 9 (Liu et al., 2021; Fair et al., 2022).

In the course of producing *Auts2*^{del8}, an unexpected loss-of-function allele (*Auts2*^{neo}) that reduces both AUTS2-FL and AUTS2-C was also produced (**Table 2**) (Hori et al., 2014). Like *Auts2*$^{del8/del8}$, the *Auts2*$^{neo/neo}$ genotype caused neonatal lethality. Heterozygous *Auts2*$^{neo/+}$ mice, reported to have ∼50% reduction of AUTS2-FL and AUTS2-C isoforms, showed behavioral abnormalities (Hori et al., 2015). Since human AUTS2 mutations are heterozygous (Beunders et al., 2013; Sanchez-Jimeno et al., 2021), *Auts2*$^{neo/+}$ mice model the human AUTS2 syndrome in this regard.

Recently, a conditional exon 15 allele (*Auts2*^{del15}) was produced to interfere with expression of both AUTS2-FL and AUTS2-C isoforms (**Table 2**) (Castanza et al., 2021). Mice lacking exon 15 (*Auts2*$^{del15/del15}$) throughout the CNS (*Nes*-Cre) died neonatally with severe breathing abnormalities, documented by plethysmography. The erratic breathing implicated abnormal development of brainstem respiratory centers and raised the possibility that *AUTS2* might be a vulnerability gene for sudden infant death syndrome. Excision of exon 15 only in the developing cortex (*Emx1*-Cre) allowed for survival to adulthood, and revealed defects of cortical structure, function, and gene expression (Castanza et al., 2021). Notably, the dentate gyrus (DG) of hippocampus was hypoplastic, with virtual absence of hilar mossy neurons and reduced numbers of granule neurons. Also, EEG recordings showed abnormal spiking activity. While the neocortex appeared structurally intact, genes involved in neocortical patterning (such as *Tshz2*) and laminar identity (such as *Wnt7b* and *Pcdh20*) were significantly dysregulated, as determined by RNA-seq. Significantly, many RNA transcripts that interacted with AUTS2 in normal neocortex (by RIP-seq) were also dysregulated in *Auts2*$^{del15/del15}$ mutant neocortex (by RNA-seq). Indeed, mRNA dysregulation correlated more strongly with binding of the RNA to AUTS2 protein (RIP-seq), than with binding of AUTS2 to cognate genes in chromatin (ChIP-seq). These distinctions support the hypothesis that AUTS2 regulates gene expression mainly by modulating RNA metabolism.

Interestingly, the transcriptome analysis of *Auts2*$^{del15/del15}$ neocortex (Castanza et al., 2021) revealed dysregulation of mRNAs for proteins that were previously reported to interact with AUTS2 protein. Specifically, transcripts *Ep300* and *Prex1* not only bound AUTS2, but also were significantly decreased in *Auts2*$^{del15/del15}$ neocortex. *Ep300* and *Prex1* encode P300 and P-Rex1, respectively, both of which reportedly interacted with AUTS2 upon overexpression in HEK cells (Gao et al., 2014; Hori et al., 2014). These findings suggest that overexpression of AUTS2 might induce elevated levels of *Ep300* and *Prex1* mRNA, and consequently, likewise elevated levels of P300 and P-Rex1 proteins. Overexpression of P300 and P-Rex1 with AUTS2 might lead to non-physiologic interactions in HEK cells, which are extremely different from neurons in cerebral cortex. Similarly, the activation of Rac1 observed after AUTS2 overexpression in N1E-115 mouse neuroblastoma cells (the "AUTS2-Rac1 pathway") may also be explained, at least in part, by AUTS2 regulation of transcripts *Prex1* and *Rasgrf2*, which were significantly reduced in *Auts2*$^{del15/del15}$ neocortex. Both *Prex1* and *Rasgrf2* encode GEFs that activate Rac1 (Yoshizawa et al., 2005; Li et al., 2006). Thus, AUTS2 overexpression in HEK cells might indirectly induce elevated levels of GEFs via RNA regulation, and thereby activate Rac1.

Finally, a novel mouse *Auts2* allele with conditional excision of exon 9 (*Auts2*^{del9}) was recently described (Geng et al., 2021). Excision of exon 9 was reported to deplete both AUTS2-FL and AUTS2-C, although no details of the generation of these mice, nor documentation of the protein depletion, were provided. Homozygous excision of exon 9 (*Auts2*$^{del9/del9}$) in the central nervous system (*Nes*-Cre) was reported to cause early embryonic lethality. Heterozygous exon 9 excision was found to impair neuronal gene expression, as determined by RT-PCR of cultured neocortical cells (Geng et al., 2021). No brain abnormalities were reported. Further studies are needed to validate this model.

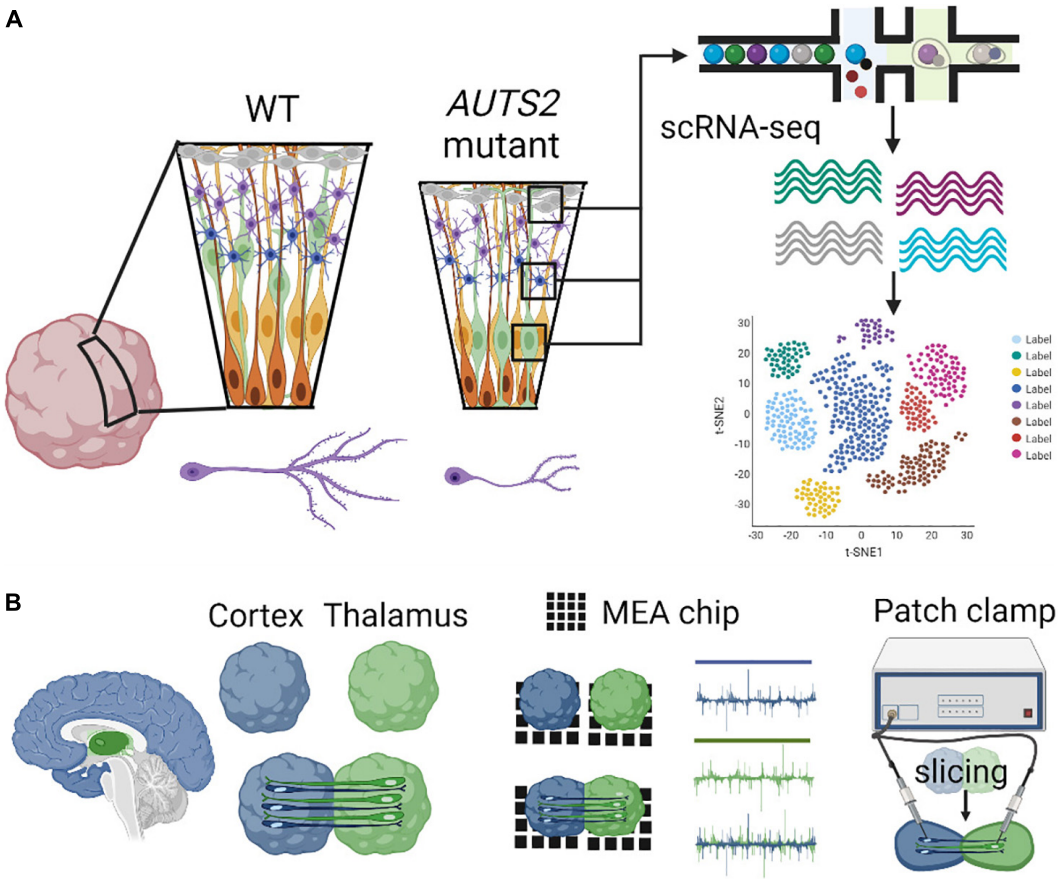

FIGURE 4 | Modeling AUTS2 syndrome using cerebral organoids. **(A)** *AUTS2* mutant cerebral organoids have proliferative deficits in neural progenitor cells and impaired neuritogenesis in cortical neurons (left). Utilization of scRNA-seq to determine cell type specific changes in gene expression within diverse progenitor, neuronal, and glial cell populations (right). **(B)** Generation of assembloids through the fusion of brain region specific organoids (cortical-thalamic assembloid shown, left) investigating neural circuitry using MEA and patch-clamp electrophysiology (right).

MOUSE EMBRYONIC STEM CELL MODELS

The question of whether AUTS2 regulates neurogenesis has also been studied using mouse embryonic stem cells (mESCs) treated with *in vitro* differentiation protocols. One group reported that AUTS2 fosters the differentiation of mESCs to motor neurons (MNs) (Liu et al., 2021). Interestingly, a reduction of spinal MNs was reported in *auts2a* morphant zebrafish (Oksenberg et al., 2013); however, no MN defects have been reported in human *AUTS2* patients or mouse models. In another study, AUTS2 was found necessary for the differentiation of mESCs to mixed neuron types (Russo et al., 2018). For cortical-type neurons, AUTS2 facilitated the differentiation of mESCs to cortical neurons in one study (Geng et al., 2021), but delayed mESC differentiation to cortical neurons in another (Monderer-Rothkoff et al., 2021). WDR68, implicated as an essential binding partner for transcriptional activation by AUTS2, also appeared necessary for the differentiation of mESCs to cortical neurons (Wang et al., 2018). While defects of neurogenesis presumably cause microcephaly in human AUTS2 syndrome, mESCs have so far shown variable results and limited utility for understanding AUTS2 syndrome phenotypes.

CEREBRAL ORGANOIDS AS A MODEL TO INVESTIGATE MOLECULAR MECHANISMS UNDERLYING AUTS2 SYNDROME

Mouse models of AUTS2 deficiency have furthered our understanding of AUTS2 functions during neurodevelopment. However, the role of AUTS2 during human cortical development, which involves a greater expansion of radial glia cell and neuronal diversity compared to mice, has not been investigated until recently with cerebral organoids (COs) (Fair et al., 2022). COs, derived from human pluripotent stem cells, are three-dimensional *in vitro* models that can be utilized to investigate the complex and human-specific features of early brain development (Lancaster et al., 2013; Di Lullo and Kriegstein, 2017; Pasca, 2018; Pollen et al., 2019; Qian et al., 2019; Setia and Muotri, 2019). As COs have been

extensively reviewed elsewhere, we will focus on how COs can be used to investigate the mechanisms of aberrant human corticogenesis underlying various neurodevelopmental disorders (NDs), emphasizing studies relevant to AUTS2 syndrome.

Recently, the first COs derived from an AUTS2 syndrome patient, with a pathogenic missense variant in exon 9, were generated and studied (Fair et al., 2022). Patient COs displayed reduced growth analogous to microcephaly, deficits in neural progenitor cell (NPC) proliferation, and abnormal neuronal differentiation, which were rescued by CRISPR-Cas9 gene editing of the variant to the wild-type allele (**Figure 4**). These data highlight essential roles for AUTS2 during early human cortical development as well as identified proliferative deficits and reduced WNT-β-Catenin signaling in NPCs, which may underlie microcephaly in AUTS2 syndrome. Gene expression signatures of defective neuritogenesis were also observed, similar findings which are consistent with previous mouse studies. Future investigation is necessary to understand how AUTS2 functions in various progenitor cells (e.g., apical, intermediate, and basal), how it regulates neuronal differentiation, and how it controls the formation of neuronal circuits. The development and comparison of additional brain region-specific COs coupled with advanced technological tools to investigate various patient *AUTS2* variants can start to uncover neurobiological functions that contribute to the clinical heterogeneity observed in AUTS2 syndrome patients (**Figure 4**).

INVESTIGATING MECHANISMS UNDERLYING ABERRANT CORTICOGENESIS IN AUTS2 DEFICIENT CEREBRAL ORGANOIDS

Disruptions in the *AUTS2* gene are associated with microcephaly in human patients (Beunders et al., 2013; Sanchez-Jimeno et al., 2021). However, current mouse models of Auts2 deficiency have not been able to recapitulate a microcephalic phenotype (Gao et al., 2014; Hori et al., 2014; Castanza et al., 2021). Understanding the etiology of microcephaly in AUTS2 and other neurodevelopmental disorders has been limited by the primary use of mouse models which do not adequately recapitulate the manner and severity in which microcephaly arises (Gabriel et al., 2020; Nieto-Estevez and Hsieh, 2020). A major developmental difference occurs during neurogenesis between humans and mice, particularly in the generation of the subventricular zone (SVZ). Although both humans and rodents undergo extensive SVZ growth, humans have a more complex, organized, and expansive SVZ subdivided into the outer and inner SVZ (Borrell and Gotz, 2014; Florio and Huttner, 2014; Florio et al., 2018). This compartmentalization allows for a more heterogeneous population of neural precursor cells with dynamic proliferative capabilities (such as cell cycle length and mode of division). Subsequently, the cortical plate is massively expanded in humans and becomes highly folded (undergoes gyrification) whereas the mouse brain is smooth (lissencephalic) (Kelava and Lancaster, 2016; Gabriel et al., 2020). Thus, major variations exist between human and rodent brain development resulting in dramatic differences in brain composition, size, and complexity.

As a complementary system to mouse models, COs can be used to dissect the underlying mechanisms of microcephaly while also helping to elucidate the fundamental mechanism of normal human brain development (Gopalakrishnan, 2019; Setia and Muotri, 2019; Gabriel et al., 2020). Microcephaly is thought to arise from a common disease mechanism ultimately owing to dysregulation of the cell cycle that disrupts the timing of this carefully orchestrated neurogenesis (Jean et al., 2020). It is hypothesized that human brain development occurs in distinct stages of cell proliferation and subsequent differentiation, whereas mice may undergo both proliferation and differentiation simultaneously (Geschwind and Rakic, 2013; Florio and Huttner, 2014; Gabriel et al., 2020). Furthermore, mouse models of candidate microcephaly genes typically require homozygous inactivation of the causal gene or significant mutant gene overexpression in order to induce a phenotype. However, primary microcephaly in humans is caused predominately by gene point mutations and truncations (Barrera et al., 2010; Buchman et al., 2010; Lizarraga et al., 2010; Alkuraya et al., 2011; McIntyre et al., 2012; Insolera et al., 2014). For example, mouse models of microcephaly associated CDK5RAP2 disease requires a complete knockout of *CDK5RAP2* and result in apoptosis as the primary cause of neuronal progenitor cell depletion and microcephaly (Barrera et al., 2010; Buchman et al., 2010; Lizarraga et al., 2010). Conversely, a patient-derived CO model containing a heterozygous truncating mutation in the *CDK5RAP2* gene recapitulated severe microcephaly and resulted in fewer neurons and smaller progenitor zones (Lancaster et al., 2013). Further investigation of radial glial spindle orientations revealed that patient COs displayed a greater percentage of oblique and vertical divisions compared to controls. This observation in patient COs correlated with premature neural differentiation, which was further supported by increased BrdU+/doublecortin positive cells.

Similarly, a recent study modeling a pathogenic *AUTS2* missense variant in COs revealed significantly reduced organoid growth (Fair et al., 2022). AUTS2 mutant COs showed dysregulated cell cycle control and reduced symmetrical (horizontal) cellular division, which correlated with premature neuronal differentiation in comparison to control COs. Increased asymmetrical progenitor divisions and premature neuronal differentiation are also common features observed in other CO models containing mutant microcephaly genes (Gabriel et al., 2020). These data support the role of AUTS2 in regulating the highly intricate transcriptional program of neuronal differentiation and perturbations in this process could underlie cognitive deficits in patients.

Although mice do not have an OSVZ, both OSVZ formation and DG morphogenesis involve extensive cell migration and proliferation (Molnár et al., 2019; Nelson et al., 2020). Castanza et al. (2021) used a conditional knock-out model to inactivate *Auts2* specifically in the cerebral cortex and found that the dentate gyrus had a reduced size that was associated with decreased neurogenesis, a common feature of AUTS2-associated microcephaly. It is possible that similar molecular mechanisms

that perturbs DG neurogenesis in AUTS2 deficient mice, may contribute to neocortical growth defects in human AUTS2 syndrome patients.

GENOMICS TECHNOLOGIES TO STUDY MOLECULAR FEATURES OF AUTS2 DEFICIENCY IN CEREBRAL ORGANOIDS

Single cell (sc) RNA-seq, combined with immunohistochemical, spatial transcriptomics, and chromatin immunoprecipitation techniques can provide important morphological context to reconstruct the organization of disease-related expression patterns (Rao et al., 2021). Early rosette structures in COs represent ventricular zone (VZ)-like structures that are comprised of stratified progenitors, which undergo distinct stromal translocations critical to their progression through the cell cycle. Apical neural progenitors divide symmetrically within VZ-like structures in COs, and at the onset of neurogenesis, they shift to asymmetric divisions forming another apical neural progenitor and either a neuron or an intermediate progenitor (IP) cell, which is a type of basal neural progenitor. Although apical neural progenitors can directly give rise to neurons, most neurogenesis in the human neocortex occurs indirectly through subsequent IP division and neural differentiation (Pebworth et al., 2021). In contrast to rodents, humans and larger mammals contain an abundant type of basal progenitor called outer radial glial (ORG) cells, which also give rise to IP cells and are formed in the OSVZ. COs are invaluable models of human brain development since they contain an outer subventricular zone (oSVZ), which are abundant in ORG (Kadoshima et al., 2013; Lancaster et al., 2013) (**Figure 4**).

Recent work identified altered morphological and functional properties of apical neural progenitors in AUTS2 deficient COs (Fair et al., 2022). Further investigation of AUTS2 function using immunofluorescence techniques and sc-RNA seq will provide deeper understanding for the role of AUTS in IP and ORG populations in human corticogenesis and in AUTS2 syndrome. Correlating spatial progenitor zone context with cell type specific transcriptomic signatures may provide further mechanistic insight into whether downstream targets of AUTS2 are affected in specific progenitor zone populations in COs. Additionally, combining sc and epigenetic sequencing methods may also provide critical insights into altered regions of chromatin accessibility leading to deficits in transcriptional control caused by AUTS2 deficiency.

Although ChIP-seq is a widely used method to evaluate global active and repressed chromatin states, it is limited by low signal-to-noise ratios and is not compatible with low cellular input–a potentially significant challenge for organoid applications (Lewis et al., 2021). However, newer chromatin mapping methods such as CUT&RUN and CUT&Tag can be combined with scRNA-seq to target and profile specific chromatin signatures with single cell resolution (Kaya-Okur et al., 2019; Yu et al., 2022). Single-cell chromatin profiling of AUTS2 syndrome organoid models could extend our understanding for the role of the PRC1-AUTS2 complex in epigenetically heterogeneous cell populations. Such studies could also be valuable to understand the function of *AUTS2* variants in regard to cell-type specific regulatory elements, especially those related to cell cycle control, cell fate inheritance, and timing of neuronal differentiation.

Recently, sc-RNA seq and ATAC-seq analyses uncovered a dynamic period of chromatin remodeling during the development of human forebrain organoids (Trevino et al., 2020). Dynamic epigenetic changes were identified within these organoids during human cortical neurogenesis, driven by specific transcription factors (particularly those associated with astrocyte maturation and interneuron specification). Furthermore, direct comparisons with human tissue confirmed that *in vivo* forebrain regulatory programs largely map with those seen in forebrain organoids cultured for over 20 months. Interestingly, during forebrain organoid development, 81% of Simons Foundation Autism Research Initiative (SFARI) genes were found to be expressed (Trevino et al., 2020). Further analysis identified SFARI genes as significantly enriched for enhancer-gene linkages predominantly in glial progenitor and mature neural cell types. These data provide a foundation for future investigation of potential disease mechanisms in ASD and hold implications for understanding molecular and cellular mechanisms underlying AUTS2 syndrome.

ELECTROPHYSIOLOGICAL TOOLS TO INVESTIGATE THE ROLE OF AUTS2 IN SYNAPTIC TRANSMISSION

Several studies have shown that loss of *Auts2* results in dysregulated regional and laminar neuronal differentiation in mouse models (Hori et al., 2020; Castanza et al., 2021; Monderer-Rothkoff et al., 2021) and more recently in COs (Fair et al., 2022). However, the neurodevelopmental impact of altered differentiation on synaptic physiology and how loss of AUTS2 leads to epilepsy in AUTS2 syndrome remains unclear. One study showed that the elimination of dendritic spines was impaired in *Auts2*-knocked-down hippocampal neurons (Hori et al., 2020). As a result, an excess of dendritic spines was observed and was suggested to drive the increase of excitatory inputs within Auts2 mutant hippocampal slices as demonstrated through electrophysiological experiments (Hori et al., 2020). Further studies revealed alterations in synaptic gene regulation in both *Auts2* mutant mouse hippocampus and frontal cortex (Hori et al., 2020; Castanza et al., 2021), and in a CO model containing an *AUTS2* pathogenic variant (Fair et al., 2022). All of these studies suggest AUTS2 functions at excitatory synapses, however, the mechanisms of AUTS2 in establishing synaptic maturation and regulating synaptic homeostasis during neurodevelopment remains largely unknown.

To investigate synaptic functions *in vitro*, conventional patch-clamp recording techniques remain the gold standard for providing high temporal resolution of electrical activities in neurons. Whole-cell voltage-clamp recordings on acute hippocampal slices from conditional AUTS2 deficient ($Auts2^{del8/del8}$; *Emx1*-Cre) mice (P33–P44) revealed an increased frequency of miniature excitatory postsynaptic currents (mEPSCs) with no change in amplitude, suggesting an increase of functional excitatory synapses (**Table 2**). Further investigations

at earlier developmental time points and across different regions in Auts2 deficient brains would provide a more complete understanding of Auts2 function in synaptic transmission.

Although patch-clamp techniques offer multiple advantages to probe synaptic function in neuronal cultures, its limited throughput nature does not allow for probing neuronal connectivity and investigating neural network dynamics. To address this limitation, multi-electrode array (MEA) platforms have been extensively utilized to record extracellular field potentials from a diverse and large number of neurons *in vitro* to investigate neural network properties. The application of MEAs in studying the effects of AUTS2 deficiency on neuronal network dynamics has not been explored, and thus would provide further mechanistic understanding of AUTS2 function in synaptic transmission (**Figure 4**).

Several studies have investigated electrical properties and neuronal connectivity within CO models (Quadrato et al., 2017; Trujillo et al., 2019; Fair et al., 2020). MEAs provide the unique advantage of non-invasively measuring electrical activity of neuronal networks within developing COs, although their utilization to study mechanisms underlie ASD is underexplored. Thus, investigation of spontaneous electrical activities and potential alterations in neural network properties in AUTS2 deficient COs would lead to greater understanding of mechanisms underlying epilepsy in AUTS2 syndrome.

GENERATION OF BRAIN REGION-SPECIFIC CEREBRAL ORGANOIDS AND ASSEMBLOIDS TO UNDERSTAND THE ROLE OF AUTS2 DURING NEURODEVELOPMENT

Animal studies have shown that *Auts2* is dynamically regulated during brain development and is expressed from a gradient in a high rostral to low caudal pattern within the developing neocortex (Bedogni et al., 2010). As previously described, two main AUTS2 isoforms are differentially regulated during brain development, although the regulatory mechanisms and functions of these isoforms are not well established (**Table 1**). Owing to this complex and heterogenous expression profile, it is important to understand the precise role of these isoforms within different brain regions throughout development. Numerous protocols exist to generate either brain region specific or whole brain organoids. In this section, we will discuss application of brain region specific organoid and assembloid models that can be leveraged to investigate Auts2 function during neurodevelopment.

Postnatal AUTS2 expression includes high expression levels frontal cortex, cerebellum, and hippocampus (**Figure 2**). However, it is unclear whether postnatal AUTS2 expression is essential to maintain proper function within these brain regions (**Table 1**). One hypothesis is that AUTS2 deficiency within the developing hippocampus may underlie ID in AUTS2 syndrome patients. Hippocampal organoids serve as *in vitro* models for investigating human hippocampus development and hippocampus-related diseases and consist of hippocampal granule- and pyramidal-like neurons that form a functional electrical network (Sakaguchi et al., 2015; Pomeshchik et al., 2020). Recently used to model Alzheimer's disease (Sakaguchi et al., 2015; Pomeshchik et al., 2020), hippocampal organoids can also be applied to understand the role of AUTS2 during hippocampus development. As previously described, Castanza et al. (2021) showed dentate gyrus hypoplasia in *Emx1*-Cre $Auts2^{del15/del15}$ mice. Utilization of hippocampal organoids can yield important mechanistic insights into the role of AUTS2 in progenitor proliferation, migration, and differentiation within human hippocampal development.

Cerebellar organoids can also be leveraged to understand the role of AUTS2 during cerebellar development. Mouse models of AUTS2 deficiency show cerebellar hypoplasia, impaired dendrite maturation in Purkinje cells, increased parallel fiber synapse formation, and decreased number of excitatory presynaptic synapses from climbing fiber innervations (Yamashiro et al., 2020). Previous work utilizing a polarized cerebellar organoid model identified similarities in human cerebellar ontogenesis regarding the layered neural-tube-like structure with dorsoventral and apicobasal polarities (Muguruma et al., 2015; Silva et al., 2020; Nayler et al., 2021). Cerebellar organoids derived from AUTS2 syndrome patients could be generated to further understand multiple aspects of cerebellar development, such as cellular differentiation, gene expression changes within specific cell types (i.e., sc RNA-seq focusing on Purkinje cells, granular cells, etc.), and investigating E/I balance in the cerebellum utilizing MEA or patch clamp electrophysiology (**Figure 4**).

Though the development of *in vitro* tools to model and study long-range human brain circuits has remained a challenging endeavor, novel platforms are emerging based on the fusion of regionally-specified brain organoids called assembloids. For instance, the neural circuitry between the human thalamus and cerebral cortex can be mimicked and studied in a cortico-thalamic assembloid (Gobbo et al., 2021) (**Figure 4**). Assembloids are becoming increasingly important, serving as a functional tool to investigate the underlying causes of synaptic deficits underlying neurodevelopmental disorders. A variety of assembloids are being developed to investigate multi-synaptic circuitry in human models, such as cortico-thalamic, cortico-striatal, cortico-cortico assembloids (Xiang et al., 2019; Andersen et al., 2020; Chen et al., 2020; Marton and Pasca, 2020). Cortico-thalamic and cortico-striatal dysfunction has been associated with neurodevelopmental disorders and associated co-morbidities such as epilepsy (Shepherd, 2013; He et al., 2021). AUTS2 is highly expressed in the dorsal thalamus and in the striatum (Bedogni et al., 2010), to study neural circuitry between the frontal cortex and these brain regions. To investigate the role of AUTS2 within the prefrontal-thalamic circuit, an assembloid model could be recapitulated between forebrain and thalamic organoids, and several methodologies such as patch clamping or MEAs could be used to investigate alterations in synaptic transmission occurring in assembloid circuits (**Figure 4**).

The utilization of patient *AUTS2* variant iPSCs to create assembloids and brain region specific organoids, such as hippocampal and cerebellar organoids, will provide invaluable tools to understand mechanisms underlying AUTS2 syndrome

at multiple levels of analysis including molecular, cellular, and functional levels, as well as provide a novel screening platform for developing therapeutics.

MOLECULAR TOOLS FOR ANALYZING THE ROLE OF AUTS2 IN NEURAL CIRCUIT DEVELOPMENT AND MAINTENANCE

Auts2 conditional knockout mouse models are invaluable for dissecting the circuit mechanisms that may contribute to phenotypes observed in AUTS2 syndrome. As noted above, mouse models for Auts2 deficiency do not demonstrate microcephaly (Castanza et al., 2021). However, loss of *Auts2* causes changes in molecular expression that suggest disrupted neuronal differentiation, which should lead to altered circuit architecture (Castanza et al., 2021; Monderer-Rothkoff et al., 2021). Indeed, in some models, the density of dendritic spines on excitatory neocortical and hippocampal pyramidal cells is abnormally high, with a concomitant increase in the frequency of miniature excitatory postsynaptic currents (mEPSCs) (Hori et al., 2020). This suggests there may be an imbalance in the ratio of excitation to inhibition (E/I) within neural circuits of *Auts2* mouse models. Congruent with this hypothesis, abnormal voltage spikes similar to epileptic interictal discharges occur spontaneously in the hippocampi of *Auts2* cKO mice (Castanza et al., 2021). Disruptions in E/I balance are commonly observed across several animal models of neurodevelopmental disorders (Sohal and Rubenstein, 2019). However, it is important to determine how loss of *Auts2* alters the developmental trajectory of specific neuronal subtypes and circuits, to guide precision therapeutic approaches.

In mouse neocortex, AUTS2 is largely restricted to excitatory projection neurons (Castanza et al., 2021). These cells can be parsed into three major subclasses based on their long-range axonal targets: (1) intratelencephalic (IT) that project across the corpus callosum, (2) pyramidal tract (PT) that project to subcortical structures, and (3) corticothalamic (CT) that project to thalamic nuclei (Harris and Shepherd, 2015). In mice, these three subclasses form unique local circuits among each other and with neighboring inhibitory interneurons (Lee S.H. et al., 2014; Harris and Shepherd, 2015; Wester et al., 2019). Thus, it is important to determine if specific subtypes of projection neurons are uniquely susceptible to loss of *Auts2*.

Based on molecular expression data, current evidence suggests AUTS2 may be involved in development of all 3 cortical projection neuron types. First, AUTS2 is strongly expressed in superficial cortical layers (Bedogni et al., 2010; Castanza et al., 2021), which are populated exclusively by IT-type cells. Second, AUTS2 is also expressed in layer 5, which contains PT-type neurons (Castanza et al., 2021). Third, *Auts2* expression is activated by Tbr1 (Bedogni et al., 2010), which is a transcription factor that promotes the differentiation of IT-, CT-, and PT-type neurons (Hevner et al., 2002; Han et al., 2011; McKenna et al., 2011; Srinivasan et al., 2012). Fourth, AUTS2 can also be co-expressed with CTIP2 (Bedogni et al., 2010), which is a transcription factor prominently associated with PT-type cells. However, a subset of IT-type neurons does express CTIP2 (Harb et al., 2016), which may account for this observation.

Current tools in mice can directly test how loss of *Auts2* differentially alters neocortical circuits involving IT-, CT-, and PT-type neurons. The *Emx1*-Cre mouse line expresses Cre recombinase in progenitors of neocortical and hippocampal projection neurons as early as embryonic day (E) 10.5 (Gorski et al., 2002) and is a powerful strategy to eliminate *Auts2* expression from the forebrain when crossed to *Auts2* floxed mice (Castanza et al., 2021). On this genetic background, IT-, CT-, and PT-type cells can be identified by injecting retrograde tracers or viral vectors into non-overlapping target structures. Using this strategy, it will be possible to determine which subtypes receive abnormally high excitatory synaptic input, and if it originates from neighboring projection neurons in local circuits or from long-range afferents outside of cortex, such as thalamus. Furthermore, *Auts2* can be conditionally deleted from specific subclasses. For example, to target CT-type cells, the *Ntsr1*-Cre line can be used to express Cre in these neurons as early as embryonic day 16.5 (Gong et al., 2007). Superficial IT-type neurons can be targeted by *in utero* electroporation of a plasmid encoding Cre into *Auts2* floxed mice after E14.5. Several tools exist to investigate if loss of *Auts2* from projection neurons alters their synaptic connectivity with neighboring inhibitory interneurons. For example, conditional *Auts2* knockout mice can be crossed to those expressing fluorescent reporters in specific interneuron subtypes (e.g., the *PV*-tdTomato mouse line (Kaiser et al., 2016). Alternatively, AAV vectors are available that encode fluorophores and channelrhodopsin (ChR2) under the control of an inhibitory interneuron-specific promoter [e.g., AAV-m*Dlx*-NLS-mRuby (Chan et al., 2017)].

In the hippocampus, AUTS2 is expressed throughout the canonical tri-synaptic circuit that includes the entorhinal cortex, dentate gyrus, CA3, and CA1 (Bedogni et al., 2010; Castanza et al., 2021). Thus, loss of *Auts2* may disrupt information processing at multiple stages within this structure. In the dentate gyrus, AUTS2 is expressed in two different populations of excitatory projection neurons: granule cells (GCs) and hilar mossy neurons (HMNs). Importantly, forebrain knockout of *Auts2* leads to a significant reduction in the number of HMNs (Castanza et al., 2021). HMNs project within the dentate gyrus both ipsilaterally and contralaterally to regulate the output of GCs, which in turn target region CA3 (Scharfman and Myers, 2016; Danielson et al., 2017). Although HMNs provide excitatory synaptic input to CGs, their primary role may be to disynaptically inhibit GCs via their input to a diverse set of inhibitory interneurons (Jinde et al., 2012; Scharfman and Myers, 2016). Indeed, loss of HMNs is common in temporal lobe epilepsy (Bui et al., 2018) and may be responsible for the interictal-like events observed by Castanza et al. (2021). Several tools are available to study how loss of *Auts2* alters circuits in the dentate gyrus, perhaps leading to disinhibition and hyperexcitability. HMNs can be selectively targeted for expression of fluorophores and ChR2 by injection of retrograde viral vectors into the contralateral dentate gyrus (Danielson et al., 2017). Furthermore, as described above, local inhibitory interneurons can also be selectively targeted using transgenic and viral strategies. Combining these

tools should allow the investigation of synaptic connections among HMNs, GCs, and interneurons on the background of conditional forebrain knockout of *Auts2*. An alternative strategy to selectively target HMNs is to use *Crlr*-Cre or *Drd2*-Cre mouse lines (Gangarossa et al., 2012; Jinde et al., 2012), however, the temporal expression patterns of Cre are not well characterized and may not allow for conditional knockout of *Auts2* during early developmental periods. Finally, loss of *Auts2* may lead to hippocampal hyperexcitability via increases in excitatory synapse formation onto CA1 projection neurons (Hori et al., 2020). The laminar structure of the hippocampus should allow future studies to determine if increased excitatory drive to CA1 originates primarily from CA3 or extrahippocampal inputs (entorhinal cortex or thalamus). This can be accomplished by stimulating axonal projections traveling through either the stratum radiatum or the stratum lacunosum moleculare, respectively.

Finally, mouse models offer an opportunity to investigate if communication among different brain structures is affected by loss of *Auts2*. Indeed, several brain structures that prominently express AUTS2 directly target each other for synaptic connections. These include the prefrontal cortex (PFC), ventrolateral/ventromedial (VL/VM) thalamic nuclei, cerebellum, and hippocampus (Bedogni et al., 2010; Castanza et al., 2021). For example, deep cerebellar nuclei project to directly to VL/VM thalamus (Gornati et al., 2018), which in turn projects to the PFC (Collins et al., 2018). Furthermore, CT- and PT-type projection neurons in PFC provide feedback synaptic input to VM thalamus (Collins et al., 2018). Finally, excitatory hippocampal CA1 projection neurons directly target the PFC (Lee A.T. et al., 2014). An important open question is whether loss of *Auts2* alters the afferent input strength of these connections. This can be addressed by injecting AAVs encoding ChR2 into each of these structures to assess synaptic connectivity and physiology via optogenetic assisted circuit mapping (Petreanu et al., 2007; Collins et al., 2018).

FUTURE DIRECTIONS AND KEY QUESTIONS

As this review has illustrated, multiple functions have been proposed for AUTS2 (**Figure 3**) on the basis of studies in multiple model systems (**Table 2**). Other members of the *AUTS2* gene family (*FBRSL1, FBRS*) and superfamily (such as *tay*) likewise appear to have overlapping, but diversified functions. Importantly, many AUTS2 functions and interactions with other proteins remain to be confirmed, or have been studied in heterologous cell types (such as HEK cells). Considering these caveats, a paramount future goal will be to better define the functions and binding partners of AUTS2 in neurons from cerebral organoids. With several lines of evidence suggesting that AUTS2 is an RNA-binding protein, this possibility can be investigated using methods such as eCLIP. With the advent of methods to produce human COs and assembloids, future studies can go beyond animal models to evaluate AUTS2 molecular functions, binding partners, and neurodevelopmental roles in developing human neural tissues.

AUTHOR CONTRIBUTIONS

RH and AB produced figures and supplementary figures. All authors wrote and edited the manuscript.

FUNDING

This work was supported by NINDS grants R01NS085081 and R01NS092339 (RH), by the Nationwide Foundation Pediatric Innovation Fund (MH), and by NIMH grant R01MH124870 and SFARI Pilot Award #724187 (JW).

ACKNOWLEDGMENTS

Figure 4 contains schematics that were created with BioRender.com.

SUPPLEMENTARY MATERIAL

The Supplementary Material for this article can be found online at: https://www.frontiersin.org/articles/10.3389/fnmol.2022.858582/full#supplementary-material

Supplementary Figure 1 | *FBRSL1* transcript and protein. **(A)** The full-length FBRSL1 transcript has 17 exons. **(B)** Protein source exons are indicated in black (odd) and blue (even). Green boxes enclose splice junctions in which amino acids were encoded across the junctions, comprising exon blocs. Red asterisks indicate source exons that encoded a non-integer number of amino acids. Features mapped from protein sequence: ExB, exon bloc; NLS, nuclear localization sequence; IDR, intrinsically disordered region; PRR, Pro-rich repeat; HRR, His-rich repeat; HX, HX repeat; RRR, Arg-rich repeat; CDD, conserved domain database; PD, ProDom predicted domains (domain names in bold also identified in AUTS2); AFsh, AUTS2-FBRSL1 short homology region. **(C)** FBRSL has a high content of IDRs (zigzag lines) and regions enriched in amino acids Pro, His, or Arg (red lines).

Supplementary Figure 2 | Predictive modeling of AUTS2 (1–1,199) secondary and tertiary structure. The AUTS2 protein sequence (aa 1–1,199) was modeled using RoseTTAfold. (The C-terminal aa 1,200–1,259 were omitted because only sequences up to 1,199 aa can be analyzed). Left panels show predicted structures, and right panels show error estimates for each aa position, for models 1–5. Overall confidence was low (0.19 on scale 0–1), most likely because no structures of similar sequences were available. All of the models show multiple long stretches of disordered secondary structure (most obvious in model 5), with intervening alpha helices. Models not shown to the same scale.

Supplementary Figure 3 | Predictive modeling of FBRSL1 secondary and tertiary structure. The complete FBRSL1 protein sequence (aa 1–1,045) was modeled using RoseTTAfold. Left panels show predicted structures, and right panels show error estimates for each aa position, for models 1–5. Overall confidence was low (0.17 on scale 0–1), most likely because no structures of similar sequences were available. All of the models show multiple long stretches of disordered secondary structure (most obvious in model 4), with intervening alpha helices. Models not shown to the same scale.

Supplementary Figure 4 | Predictive modeling of the AUTS2 domain of AUTS2 protein. The AUTS2 domain of AUTS2 protein (aa 645–844) was modeled using RoseTTAfold. Left panels show predicted structures, and right panels show error estimates for each aa position, for models 1–5. Overall confidence was low (0.45 on scale 0–1), most likely because no structures of similar sequences were available. All of the models show stretches of disordered secondary structure with intervening alpha helices. Models not shown to the same scale.

Supplementary Figure 5 | Predictive modeling of the AUTS2 domain of FBRSL1 protein. The AUTS2 domain of FBRSL1 protein (aa 587–784) was modeled using RoseTTAfold. Left panels show predicted structures, and right panels show error estimates for each aa position, for models 1–5. Overall confidence was low (0.42 on scale 0–1), most likely because no structures of similar sequences were available. All of the models show stretches of disordered secondary structure with intervening alpha helices. Models not shown to the same scale.

Supplementary Table 1 | *AUTS2* cDNA and protein features. Human *AUTS2* cDNA (CCDS5539.1) and AUTS2 protein (NP_056385.1) features.

Supplementary Table 2 | *FBRSL1* cDNA and protein features. Human *FBRSL1* cDNA (CCDS45010.1) and FBRSL1 protein (NP_001136113.1) features.

Supplementary Table 3 | Comparison of *AUTS2* and *FBRSL1* cDNA and protein features. Exon homologies, amino acid sequence homologies, and contents of IDRs and LCSs.

REFERENCES

Alkuraya, F. S., Cai, X., Emery, C., Mochida, G. H., Al-Dosari, M. S., Felie, J. M., et al. (2011). Human mutations in NDE1 cause extreme microcephaly with lissencephaly [corrected]. *Am. J. Hum. Genet.* 88, 536–547. doi: 10.1016/j.ajhg.2011.04.003

Andersen, J., Revah, O., Miura, Y., Thom, N., Amin, N. D., Kelley, K. W., et al. (2020). Generation of functional human 3D Cortico-motor assembloids. *Cell* 183, 1913–1929.e26. doi: 10.1016/j.cell.2020.11.017

Baek, M., DiMaio, F., Anishchenko, I., Dauparas, J., Ovchinnikov, S., Lee, G. R., et al. (2021). Accurate prediction of protein structures and interactions using a three-track neural network. *Science* 373, 871–876. doi: 10.1126/science.abj8754

Baltz, A. G., Munschauer, M., Schwanhausser, B., Vasile, A., Murakawa, Y., Schueler, M., et al. (2012). The mRNA-bound proteome and its global occupancy profile on protein-coding transcripts. *Mol. Cell* 46, 674–690. doi: 10.1016/j.molcel.2012.05.021

Barrera, J. A., Kao, L. R., Hammer, R. E., Seemann, J., Fuchs, J. L., and Megraw, T. L. (2010). CDK5RAP2 regulates centriole engagement and cohesion in mice. *Dev. Cell* 18, 913–926. doi: 10.1016/j.devcel.2010.05.017

Bedogni, F., Hodge, R. D., Nelson, B. R., Frederick, E. A., Shiba, N., Daza, R. A., et al. (2010). Autism susceptibility candidate 2 (Auts2) encodes a nuclear protein expressed in developing brain regions implicated in autism neuropathology. *Gene Expr. Patterns* 10, 9–15. doi: 10.1016/j.gep.2009.11.005

Beunders, G., van de Kamp, J., Vasudevan, P., Morton, J., Smets, K., Kleefstra, T., et al. (2016). A detailed clinical analysis of 13 patients with AUTS2 syndrome further delineates the phenotypic spectrum and underscores the behavioural phenotype. *J. Med. Genet.* 53, 523–532. doi: 10.1136/jmedgenet-2015-103601

Beunders, G., Voorhoeve, E., Golzio, C., Pardo, L. M., Rosenfeld, J. A., Talkowski, M. E., et al. (2013). Exonic deletions in AUTS2 cause a syndromic form of intellectual disability and suggest a critical role for the C terminus. *Am. J. Hum. Genet.* 92, 210–220. doi: 10.1016/j.ajhg.2012.12.011

Borrell, V., and Gotz, M. (2014). Role of radial glial cells in cerebral cortex folding. *Curr. Opin. Neurobiol.* 27, 39–46. doi: 10.1016/j.conb.2014.02.007

Buchman, J. J., Tseng, H. C., Zhou, Y., Frank, C. L., Xie, Z., and Tsai, L. H. (2010). Cdk5rap2 interacts with pericentrin to maintain the neural progenitor pool in the developing neocortex. *Neuron* 66, 386–402. doi: 10.1016/j.neuron.2010.03.036

Bui, A. D., Nguyen, T. M., Limouse, C., Kim, H. K., Szabo, G. G., Felong, S., et al. (2018). Dentate gyrus mossy cells control spontaneous convulsive seizures and spatial memory. *Science* 359, 787–790. doi: 10.1126/science.aan4074

Castanza, A. S., Ramirez, S., Tripathi, P. P., Daza, R. A. M., Kalume, F. K., Ramirez, J. M., et al. (2021). AUTS2 regulates RNA metabolism and dentate gyrus development in mice. *Cereb. Cortex* 26, 4808–4824. doi: 10.1093/cercor/bhab124

Castello, A., Fischer, B., Eichelbaum, K., Horos, R., Beckmann, B. M., Strein, C., et al. (2012). Insights into RNA biology from an atlas of mammalian mRNA-binding proteins. *Cell* 149, 1393–1406. doi: 10.1016/j.cell.2012.04.031

Chan, K. Y., Jang, M. J., Yoo, B. B., Greenbaum, A., Ravi, N., Wu, W. L., et al. (2017). Engineered AAVs for efficient noninvasive gene delivery to the central and peripheral nervous systems. *Nat. Neurosci.* 20, 1172–1179. doi: 10.1038/nn.4593

Chen, A., Guo, Z., Fang, L., and Bian, S. (2020). Application of fused organoid models to study human brain development and neural disorders. *Front. Cell. Neurosci.* 14:133. doi: 10.3389/fncel.2020.00133

Collins, D. P., Anastasiades, P. G., Marlin, J. J., and Carter, A. G. (2018). Reciprocal circuits linking the prefrontal cortex with dorsal and ventral thalamic nuclei. *Neuron* 98, 366–379.e4. doi: 10.1016/j.neuron.2018.03.024

Danielson, N. B., Turi, G. F., Ladow, M., Chavlis, S., Petrantonakis, P. C., Poirazi, P., et al. (2017). *In vivo* imaging of dentate gyrus mossy cells in behaving mice. *Neuron* 93, 552–559.e4. doi: 10.1016/j.neuron.2016.12.019

Di Lullo, E., and Kriegstein, A. R. (2017). The use of brain organoids to investigate neural development and disease. *Nat. Rev. Neurosci.* 18, 573–584. doi: 10.1038/nrn.2017.107

Fair, S. R., Julian, D., Hartlaub, A. M., Pusuluri, S. T., Malik, G., Summerfied, T. L., et al. (2020). Electrophysiological maturation of cerebral organoids correlates with dynamic morphological and cellular development. *Stem Cell Rep.* 15, 855–868. doi: 10.1016/j.stemcr.2020.08.017

Fair, S. R., Schwind, W., Julian, D., Biel, A., Ramadesikan, S., Westfall, J., et al. (2022). Cerebral organoids containing an AUTS2 missense variant model microcephaly. *medRxiv* [Preprint]. doi: 10.1101/2022.02.23.22271091

Fergelot, P., Van Belzen, M., Van Gils, J., Afenjar, A., Armour, C. M., Arveiler, B., et al. (2016). Phenotype and genotype in 52 patients with Rubinstein-Taybi syndrome caused by EP300 mutations. *Am. J. Med. Genet. A* 170, 3069–3082. doi: 10.1002/ajmg.a.37940

Florio, M., Heide, M., Pinson, A., Brandl, H., Albert, M., Winkler, S., et al. (2018). Evolution and cell-type specificity of human-specific genes preferentially expressed in progenitors of fetal neocortex. *eLife* 7:e32332. doi: 10.7554/eLife.32332

Florio, M., and Huttner, W. B. (2014). Neural progenitors, neurogenesis and the evolution of the neocortex. *Development* 141, 2182–2194. doi: 10.1242/dev.090571

Gabriel, E., Ramani, A., Altinisik, N., and Gopalakrishnan, J. (2020). Human brain organoids to decode mechanisms of microcephaly. *Front. Cell. Neurosci.* 14:115. doi: 10.3389/fncel.2020.00115

Gangarossa, G., Longueville, S., De Bundel, D., Perroy, J., Herve, D., Girault, J. A., et al. (2012). Characterization of dopamine D1 and D2 receptor-expressing neurons in the mouse hippocampus. *Hippocampus* 22, 2199–2207. doi: 10.1002/hipo.22044

Gao, Z., Lee, P., Stafford, J. M., von Schimmelmann, M., Schaefer, A., and Reinberg, D. (2014). An AUTS2-Polycomb complex activates gene expression in the CNS. *Nature* 516, 349–354. doi: 10.1038/nature13921

Geng, Z., Wang, Q., Miao, W., Wolf, T., Chavez, J., Giddings, E., et al. (2021). AUTS2 controls neuronal lineage choice through a novel PRC1-independent complex and BMP inhibition. *bioRxiv* [Preprint]. doi: 10.1101/2021.06.29.450402

Geschwind, D. H., and Rakic, P. (2013). Cortical evolution: judge the brain by its cover. *Neuron* 80, 633–647. doi: 10.1016/j.neuron.2013.10.045

Gobbo, D., Scheller, A., and Kirchhoff, F. (2021). From physiology to pathology of cortico-thalamo-cortical oscillations: astroglia as a target for further research. *Front. Neurol.* 12:661408. doi: 10.3389/fneur.2021.661408

Gong, S., Doughty, M., Harbaugh, C. R., Cummins, A., Hatten, M. E., Heintz, N., et al. (2007). Targeting Cre recombinase to specific neuron populations with bacterial artificial chromosome constructs. *J. Neurosci.* 27, 9817–9823. doi: 10.1523/JNEUROSCI.2707-07.2007

Gopalakrishnan, J. (2019). The emergence of stem cell-based brain organoids: trends and challenges. *Bioessays* 41:e1900011. doi: 10.1002/bies.201900011

Gornati, S. V., Schafer, C. B., Eelkman Rooda, O. H. J., Nigg, A. L., De Zeeuw, C. I., and Hoebeek, F. E. (2018). Differentiating cerebellar impact on thalamic nuclei. *Cell Rep.* 23, 2690–2704. doi: 10.1016/j.celrep.2018.04.098

Gorski, J. A., Talley, T., Qiu, M., Puelles, L., Rubenstein, J. L., and Jones, K. R. (2002). Cortical excitatory neurons and glia, but not GABAergic neurons, are produced in the Emx1-expressing lineage. *J. Neurosci.* 22, 6309–6314. doi: 10.1523/JNEUROSCI.22-15-06309.2002

Han, W., Kwan, K. Y., Shim, S., Lam, M. M., Shin, Y., Xu, X., et al. (2011). TBR1 directly represses Fezf2 to control the laminar origin and development

of the corticospinal tract. *Proc. Natl. Acad. Sci. U.S.A.* 108, 3041–3046. doi: 10.1073/pnas.1016723108

Harb, K., Magrinelli, E., Nicolas, C. S., Lukianets, N., Frangeul, L., Pietri, M., et al. (2016). Area-specific development of distinct projection neuron subclasses is regulated by postnatal epigenetic modifications. *eLife* 5:e09531. doi: 10.7554/eLife.09531

Harris, K. D., and Shepherd, G. M. (2015). The neocortical circuit: themes and variations. *Nat. Neurosci.* 18, 170–181. doi: 10.1038/nn.3917

Hatstat, A. K., Ahrendt, H. D., Foster, M. W., Mayne, L., Moseley, M. A., Englander, S. W., et al. (2021). Characterization of small-molecule-induced changes in Parkinson's-Related Trafficking via the Nedd4 Ubiquitin Signaling Cascade. *Cell Chem. Biol.* 28, 14–25.e9. doi: 10.1016/j.chembiol.2020.10.008

He, C., Cortes, J. M., Kang, X., Cao, J., Chen, H., Guo, X., et al. (2021). Individual-based morphological brain network organization and its association with autistic symptoms in young children with autism spectrum disorder. *Hum. Brain Mapp.* 42, 3282–3294. doi: 10.1002/hbm.25434

Hentze, M. W., Castello, A., Schwarzl, T., and Preiss, T. (2018). A brave new world of RNA-binding proteins. *Nat. Rev. Mol. Cell Biol.* 19, 327–341. doi: 10.1038/nrm.2017.130

Hevner, R. F., Miyashita-Lin, E., and Rubenstein, J. L. (2002). Cortical and thalamic axon pathfinding defects in Tbr1, Gbx2, and Pax6 mutant mice: evidence that cortical and thalamic axons interact and guide each other. *J. Comp. Neurol.* 447, 8–17. doi: 10.1002/cne.10219

Hori, K., Nagai, T., Shan, W., Sakamoto, A., Abe, M., Yamazaki, M., et al. (2015). Heterozygous Disruption of Autism susceptibility candidate 2 Causes impaired emotional control and cognitive memory. *PLoS One* 10:e0145979. doi: 10.1371/journal.pone.0145979

Hori, K., Nagai, T., Shan, W., Sakamoto, A., Taya, S., Hashimoto, R., et al. (2014). Cytoskeletal regulation by AUTS2 in neuronal migration and neuritogenesis. *Cell Rep.* 9, 2166–2179. doi: 10.1016/j.celrep.2014.11.045

Hori, K., Yamashiro, K., Nagai, T., Shan, W., Egusa, S. F., Shimaoka, K., et al. (2020). AUTS2 regulation of synapses for proper synaptic inputs and social communication. *iScience* 23, 101183. doi: 10.1016/j.isci.2020.101183

Insolera, R., Bazzi, H., Shao, W., Anderson, K. V., and Shi, S. H. (2014). Cortical neurogenesis in the absence of centrioles. *Nat. Neurosci.* 17, 1528–1535. doi: 10.1038/nn.3831

Jean, F., Stuart, A., and Tarailo-Graovac, M. (2020). Dissecting the genetic and etiological causes of primary microcephaly. *Front. Neurol.* 11:570830. doi: 10.3389/fneur.2020.570830

Jinde, S., Zsiros, V., Jiang, Z., Nakao, K., Pickel, J., Kohno, K., et al. (2012). Hilar mossy cell degeneration causes transient dentate granule cell hyperexcitability and impaired pattern separation. *Neuron* 76, 1189–1200. doi: 10.1016/j.neuron.2012.10.036

Kadoshima, T., Sakaguchi, H., Nakano, T., Soen, M., Ando, S., Eiraku, M., et al. (2013). Self-organization of axial polarity, inside-out layer pattern, and species-specific progenitor dynamics in human ES cell-derived neocortex. *Proc. Natl. Acad. Sci. U.S.A.* 110, 20284–20289. doi: 10.1073/pnas.1315710110

Kaiser, T., Ting, J. T., Monteiro, P., and Feng, G. (2016). Transgenic labeling of parvalbumin-expressing neurons with tdTomato. *Neuroscience* 321, 236–245. doi: 10.1016/j.neuroscience.2015.08.036

Kaya-Okur, H. S., Wu, S. J., Codomo, C. A., Pledger, E. S., Bryson, T. D., Henikoff, J. G., et al. (2019). CUT&Tag for efficient epigenomic profiling of small samples and single cells. *Nat. Commun.* 10:1930. doi: 10.1038/s41467-019-09982-5

Kelava, I., and Lancaster, M. A. (2016). Stem cell models of human brain development. *Cell Stem Cell* 18, 736–748. doi: 10.1016/j.stem.2016.05.022

Kondrychyn, I., Robra, L., and Thirumalai, V. (2017). Transcriptional complexity and distinct expression patterns of auts2 Paralogs in *Danio rerio*. *G3* 2577–2593. doi: 10.1534/g3.117.042622

Lancaster, M. A., Renner, M., Martin, C. A., Wenzel, D., Bicknell, L. S., Hurles, M. E., et al. (2013). Cerebral organoids model human brain development and microcephaly. *Nature* 501, 373–379. doi: 10.1038/nature12517

Lee, S. H., Kwan, A. C., and Dan, Y. (2014). Interneuron subtypes and orientation tuning. *Nature* 508, E1–E2. doi: 10.1038/nature13128

Lee, A. T., Vogt, D., Rubenstein, J. L., and Sohal, V. S. (2014). A class of GABAergic neurons in the prefrontal cortex sends long-range projections to the nucleus accumbens and elicits acute avoidance behavior. *J. Neurosci.* 34, 11519–11525. doi: 10.1523/JNEUROSCI.1157-14.2014

Lewis, E., Kaushik, K., Sandoval, L., Antony, I., Dietmann, S., and Kroll, K. (2021). Epigenetic regulation during human cortical development: seq-ing answers from the brain to the organoid. *Neurochem. Int.* 147:105039. doi: 10.1016/j.neuint.2021.105039

Li, S., Tian, X., Hartley, D. M., and Feig, L. A. (2006). Distinct roles for Ras-guanine nucleotide-releasing factor 1 (Ras-GRF1) and Ras-GRF2 in the induction of long-term potentiation and long-term depression. *J. Neurosci.* 26, 1721–1729. doi: 10.1523/JNEUROSCI.3990-05.2006

Lin, Z., Yang, Z., Xie, R., Ji, Z., Guan, K., and Zhang, M. (2019). Decoding WW domain tandem-mediated target recognitions in tissue growth and cell polarity. *eLife* 8:e49439. doi: 10.7554/eLife.49439

Liu, S., Aldinger, K. A., Cheng, C. V., Kiyama, T., Dave, M., McNamara, H. K., et al. (2021). NRF1 association with AUTS2-Polycomb mediates specific gene activation in the brain. *Mol. Cell* 81:4757. doi: 10.1016/j.molcel.2021.10.023

Lizarraga, S. B., Margossian, S. P., Harris, M. H., Campagna, D. R., Han, A. P., Blevins, S., et al. (2010). Cdk5rap2 regulates centrosome function and chromosome segregation in neuronal progenitors. *Development* 137, 1907–1917. doi: 10.1242/dev.040410

Martinez-Delgado, B., Lopez-Martin, E., Lara-Herguedas, J., Monzon, S., Cuesta, I., Juliá, M., et al. (2021). De novo small deletion affecting transcription start site of short isoform of AUTS2 gene in a patient with syndromic neurodevelopmental defects. *Am. J. Med. Genet. A* 185, 877–883. doi: 10.1002/ajmg.a.62017

Marton, R. M., and Pasca, S. P. (2020). Organoid and assembloid technologies for investigating cellular crosstalk in human brain development and disease. *Trends Cell Biol.* 30, 133–143. doi: 10.1016/j.tcb.2019.11.004

McIntyre, R. E., Lakshminarasimhan Chavali, P., Ismail, O., Carragher, D. M., Sanchez-Andrade, G., Forment, J. V., et al. (2012). Disruption of mouse Cenpj, a regulator of centriole biogenesis, phenocopies Seckel syndrome. *PLoS Genet.* 8:e1003022. doi: 10.1371/journal.pgen.1003022

McKenna, W. L., Betancourt, J., Larkin, K. A., Abrams, B., Guo, C., Rubenstein, J. L., et al. (2011). Tbr1 and Fezf2 regulate alternate corticofugal neuronal identities during neocortical development. *J. Neurosci.* 31, 549–564. doi: 10.1523/JNEUROSCI.4131-10.2011

Molnar, C., and de Celis, J. F. (2013). Tay bridge is a negative regulator of EGFR signalling and interacts with Erk and Mkp3 in the Drosophila melanogaster wing. *PLoS Genet.* 9:e1003982. doi: 10.1371/journal.pgen.1003982

Molnar, C., Estrada, B., and de Celis, J. F. (2018). Tay bridge and extracellular-regulated kinase activity are required for motoneuron function in the Drosophila neural system. *Genes Brain Behav.* 17:e12470. doi: 10.1111/gbb.12470

Molnár, Z., Clowry, G. J., Sestan, N., Alzu'bi, A., Bakken, T., Hevner, R. F., et al. (2019). New insights into the development of the human cerebral cortex. *J. Anat.* 235, 432–451. doi: 10.1111/joa.13055

Molyneaux, B. J., Goff, L. A., Brettler, A. C., Chen, H. H., Hrvatin, S., Rinn, J. L., et al. (2015). DeCoN: genome-wide analysis of in vivo transcriptional dynamics during pyramidal neuron fate selection in neocortex. *Neuron* 85, 275–288. doi: 10.1016/j.neuron.2014.12.024

Monderer-Rothkoff, G., Tal, N., Risman, M., Shani, O., Nissim-Rafinia, M., Malki-Feldman, L., et al. (2021). AUTS2 isoforms control neuronal differentiation. *Mol. Psychiatry* 26, 666–681. doi: 10.1038/s41380-019-0409-1

Muguruma, K., Nishiyama, A., Kawakami, H., Hashimoto, K., and Sasai, Y. (2015). Self-organization of polarized cerebellar tissue in 3D culture of human pluripotent stem cells. *Cell Rep.* 10, 537–550. doi: 10.1016/j.celrep.2014.12.051

Nambot, S., Faivre, L., Mirzaa, G., Thevenon, J., Bruel, A. L., Mosca-Boidron, A. L., et al. (2020). De novo TBR1 variants cause a neurocognitive phenotype with ID and autistic traits: report of 25 new individuals and review of the literature. *Eur. J. Hum. Genet.* 28, 770–782. doi: 10.1038/s41431-020-0571-6

Nayler, S., Agarwal, D., Curion, F., Bowden, R., and Becker, E. B. E. (2021). High-resolution transcriptional landscape of xeno-free human induced pluripotent stem cell-derived cerebellar organoids. *Sci. Rep.* 11:12959. doi: 10.1038/s41598-021-91846-4

Nelson, B. R., Hodge, R. D., Daza, R. A., Tripathi, P. P., Arnold, S. J., Millen, K. J., et al. (2020). Intermediate progenitors support migration of neural stem cells into dentate gyrus outer neurogenic niches. *eLife* 9:e53777. doi: 10.7554/eLife.53777

Nieto-Estevez, V., and Hsieh, J. (2020). Human brain organoid models of developmental epilepsies. *Epilepsy Curr.* 20, 282–290. doi: 10.1177/1535759720949254

Oksenberg, N., Haliburton, G. D., Eckalbar, W. L., Oren, I., Nishizaki, S., Murphy, K., et al. (2014). Genome-wide distribution of Auts2 binding localizes with active neurodevelopmental genes. *Transl. Psychiatry* 4:e431. doi: 10.1038/tp.2014.78

Oksenberg, N., Stevison, L., Wall, J. D., and Ahituv, N. (2013). Function and regulation of AUTS2, a gene implicated in autism and human evolution. *PLoS Genet*. 9:e1003221. doi: 10.1371/journal.pgen.1003221

Pasca, S. P. (2018). The rise of three-dimensional human brain cultures. *Nature* 553, 437–445. doi: 10.1038/nature25032

Pebworth, M. P., Ross, J., Andrews, M., Bhaduri, A., and Kriegstein, A. R. (2021). Human intermediate progenitor diversity during cortical development. *Proc. Natl. Acad. Sci. U.S.A.* 118, e2019415118. doi: 10.1073/pnas.2019415118

Petreanu, L., Huber, D., Sobczyk, A., and Svoboda, K. (2007). Channelrhodopsin-2-assisted circuit mapping of long-range callosal projections. *Nat. Neurosci.* 10, 663–668. doi: 10.1038/nn1891

Pinto, D., Pagnamenta, A., Klei, L., Anney, R., Merico, D., Regan, R., et al. (2020). Functional impact of global rare copy number variation in autism spectrum disorders. *Nature* 466, 368–372. doi: 10.1038/nature09146

Poeck, B., Triphan, T., Neuser, K., and Strauss, R. (2008). Locomotor control by the central complex in Drosophila-An analysis of the tay bridge mutant. *Dev. Neurobiol.* 68, 1046–1058. doi: 10.1002/dneu.20643

Pollen, A. A., Bhaduri, A., Andrews, M. G., Nowakowski, T. J., Meyerson, O. S., Mostajo-Radji, M. A., et al. (2019). Establishing cerebral organoids as models of human-specific brain evolution. *Cell* 176, 743–756.e17. doi: 10.1016/j.cell.2019.01.017

Pomeshchik, Y., Klementieva, O., Gil, J., Martinsson, I., Hansen, M. G., de Vries, T., et al. (2020). Human iPSC-derived hippocampal spheroids: an innovative tool for stratifying Alzheimer disease patient-specific cellular phenotypes and developing therapies. *Stem Cell Rep.* 15, 256–273. doi: 10.1016/j.stemcr.2020.06.001

Qian, X., Song, H., and Ming, G. L. (2019). Brain organoids: advances, applications and challenges. *Development* 146:dev166074. doi: 10.1242/dev.166074

Quadrato, G., Nguyen, T., Macosko, E. Z., Sherwood, J. L., Min Yang, S., Berger, D. R., et al. (2017). Cell diversity and network dynamics in photosensitive human brain organoids. *Nature* 545, 48–53. doi: 10.1038/nature22047

Rao, A., Barkley, D., França, G. S., and Yanai, I. (2021). Exploring tissue architecture using spatial transcriptomics. *Nature* 596, 211–220. doi: 10.1038/s41586-021-03634-9

Russo, D., Della Ragione, F., Rizzo, R., Sugiyama, E., Scalabri, F., Hori, K., et al. (2018). Glycosphingolipid metabolic reprogramming drives neural differentiation. *EMBO J.* 37:e97674. doi: 10.15252/embj.201797674

Sacerdot, C., Louis, A., Bon, C., Berthelot, C., and Roest Crollius, H. (2018). Chromosome evolution at the origin of the ancestral vertebrate genome. *Genome Biol.* 19:166. doi: 10.1186/s13059-018-1559-1

Sakaguchi, H., Kadoshima, T., Soen, M., Narii, N., Ishida, Y., Ohgushi, M., et al. (2015). Generation of functional hippocampal neurons from self-organizing human embryonic stem cell-derived dorsomedial telencephalic tissue. *Nat. Commun.* 6:8896. doi: 10.1038/ncomms9896

Sanchez-Jimeno, C., Blanco-Kelly, F., Lopez-Grondona, F., Losada-Del Pozo, R., Moreno, B., Rodrigo-Moreno, M., et al. (2021). Attention deficit hyperactivity and autism spectrum disorders as the core symptoms of AUTS2 syndrome: description of five new patients and update of the frequency of manifestations and genotype-phenotype correlation. *Genes* 12:1360. doi: 10.3390/genes12091360

Scharfman, H. E., and Myers, C. E. (2016). Corruption of the dentate gyrus by "dominant" granule cells: implications for dentate gyrus function in health and disease. *Neurobiol. Learn. Mem.* 129, 69–82. doi: 10.1016/j.nlm.2015.09.005

Sellers, R. A., Robertson, D. L., and Tassabehji, M. (2020). Ancestry of the AUTS2 family-A novel group of polycomb-complex proteins involved in human neurological disease. *PLoS One* 15:e0232101. doi: 10.1371/journal.pone.0232101

Setia, H., and Muotri, A. R. (2019). Brain organoids as a model system for human neurodevelopment and disease. *Semin. Cell Dev. Biol.* 95, 93–97. doi: 10.1016/j.semcdb.2019.03.002

Sewani, M., Nugent, K., Blackburn, P. R., Tarnowski, J. M., Hernandez-Garcia, A., Amiel, J., et al. (2020). Further delineation of the phenotypic spectrum associated with hemizygous loss-of-function variants in NONO. *Am. J. Med. Genet. A* 182, 652–658. doi: 10.1002/ajmg.a.61466

Shepherd, G. M. (2013). Corticostriatal connectivity and its role in disease. *Nat. Rev. Neurosci.* 14, 278–291. doi: 10.1038/nrn3469

Silva, T. P., Fernandes, T. G., Nogueira, D. E. S., Rodrigues, C. A. V., Bekman, E. P., Hashimura, Y., et al. (2020). Scalable generation of mature cerebellar organoids from human pluripotent stem cells and characterization by immunostaining. *J. Vis. Exp.* 160:e61143. doi: 10.3791/61143

Sohal, V. S., and Rubenstein, J. L. R. (2019). Excitation-inhibition balance as a framework for investigating mechanisms in neuropsychiatric disorders. *Mol. Psychiatry* 24, 1248–1257. doi: 10.1038/s41380-019-0426-0

Srinivasan, K., Leone, D. P., Bateson, R. K., Dobreva, G., Kohwi, Y., Kohwi-Shigematsu, T., et al. (2012). A network of genetic repression and derepression specifies projection fates in the developing neocortex. *Proc. Natl. Acad. Sci. U.S.A.* 109, 19071–19078. doi: 10.1073/pnas.1216793109

Sultana, R., Yu, C. E., Yu, J., Munson, J., Chen, D., Hua, W., et al. (2002). Identification of a novel gene on chromosome 7q11.2 interrupted by a translocation breakpoint in a pair of autistic twins. *Genomics* 80, 129–134. doi: 10.1006/geno.2002.6810

Trevino, A. E., Sinnott-Armstrong, N., Andersen, J., Yoon, S. J., Huber, N., Pritchard, J. K., et al. (2020). Chromatin accessibility dynamics in a model of human forebrain development. *Science* 367:eaay1645. doi: 10.1126/science.aay1645

Trujillo, C. A., Gao, R., Negraes, P. D., Gu, J., Buchanan, J., Preissl, S., et al. (2019). Complex oscillatory waves emerging from cortical organoids model early human brain network development. *Cell Stem Cell* 25, 558–569.e7. doi: 10.1016/j.stem.2019.08.002

Ufartes, R., Berger, H., Till, K., Salinas, G., Sturm, M., Altmuller, J., et al. (2020). De novo mutations in FBRSL1 cause a novel recognizable malformation and intellectual disability syndrome. *Hum. Genet.* 139, 1363–1379. doi: 10.1007/s00439-020-02175-x

Vogan, K. (2015). Zebrafish mutants versus morphants. *Nat. Genet.* 47:105. doi: 10.1038/ng.3208

Wang, Q., Geng, Z., Gong, Y., Warren, K., Zheng, H., Imamura, Y., et al. (2018). WDR68 is essential for the transcriptional activation of the PRC1-AUTS2 complex and neuronal differentiation of mouse embryonic stem cells. *Stem Cell Res.* 33, 206–214. doi: 10.1016/j.scr.2018.10.023

Wester, J. C., Mahadevan, V., Rhodes, C. T., Calvigioni, D., Venkatesh, S., Maric, D., et al. (2019). Neocortical projection neurons instruct inhibitory interneuron circuit development in a lineage-dependent manner. *Neuron* 102, 960–975.e6. doi: 10.1016/j.neuron.2019.03.036

Xiang, Y., Tanaka, Y., Cakir, B., Patterson, B., Kim, K. Y., Sun, P., et al. (2019). hESC-derived thalamic organoids form reciprocal projections when fused with cortical organoids. *Cell Stem Cell* 24, 487–497.e7. doi: 10.1016/j.stem.2018.12.015

Yamashiro, K., Hori, K., Lai, E. S. K., Aoki, R., Shimaoka, K., Arimura, N., et al. (2020). AUTS2 governs cerebellar development, purkinje cell maturation, motor function and social communication. *iScience* 23:101820. doi: 10.1016/j.isci.2020.101820

Yoshizawa, M., Kawauchi, T., Sone, M., Nishimura, Y. V., Terao, M., Chihama, K., et al. (2005). Involvement of a Rac activator,P-Rex1, in neurotrophin-derived signaling and neuronal migration. *J. Neurosci.* 25, 4406–4419. doi: 10.1523/JNEUROSCI.4955-04.2005

Yu, F., Sankaran, V. G., and Yuan, G. C. (2022). CUT&RUNTools 2.0: a pipeline for single-cell and bulk-level CUT&RUN and CUT&Tag data analysis. *Bioinformatics* 38, 252–254. doi: 10.1093/bioinformatics/btab507

Conflict of Interest: The authors declare that the research was conducted in the absence of any commercial or financial relationships that could be construed as a potential conflict of interest.

Publisher's Note: All claims expressed in this article are solely those of the authors and do not necessarily represent those of their affiliated organizations, or those of the publisher, the editors and the reviewers. Any product that may be evaluated in this article, or claim that may be made by its manufacturer, is not guaranteed or endorsed by the publisher.

frontiers | Frontiers in Molecular Neuroscience

REVIEW
published: 14 April 2022
doi: 10.3389/fnmol.2022.867010

A Model of Discovery: The Role of Imaging Established and Emerging Non-mammalian Models in Neuroscience

Elizabeth M. Haynes[1,2]*, *Tyler K. Ulland*[3] and *Kevin W. Eliceiri*[1,2,4,5]

[1] Morgridge Institute for Research, Madison, WI, United States, [2] Center for Quantitative Cell Imaging, University of Wisconsin-Madison, Madison, WI, United States, [3] Department of Pathology, University of Wisconsin-Madison, Madison, WI, United States, [4] Department of Biomedical Engineering, University of Wisconsin-Madison, Madison, WI, United States, [5] Department of Medical Physics, University of Wisconsin-Madison, Madison, WI, United States

OPEN ACCESS

Edited by:
Sumru Bayin,
Memorial Sloan Kettering Cancer Center, United States

Reviewed by:
Matthew B. Veldman,
Medical College of Wisconsin, United States
Jake Hines,
Winona State University, United States
Sarah Ackerman,
University of Oregon, United States

***Correspondence:**
Elizabeth M. Haynes
ehaynes2@wisc.edu

Specialty section:
This article was submitted to Methods and Model Organisms, a section of the journal Frontiers in Molecular Neuroscience

Received: 31 January 2022
Accepted: 18 March 2022
Published: 14 April 2022

Citation:
Haynes EM, Ulland TK and Eliceiri KW (2022) A Model of Discovery: The Role of Imaging Established and Emerging Non-mammalian Models in Neuroscience. Front. Mol. Neurosci. 15:867010. doi: 10.3389/fnmol.2022.867010

Rodents have been the dominant animal models in neurobiology and neurological disease research over the past 60 years. The prevalent use of rats and mice in neuroscience research has been driven by several key attributes including their organ physiology being more similar to humans, the availability of a broad variety of behavioral tests and genetic tools, and widely accessible reagents. However, despite the many advances in understanding neurobiology that have been achieved using rodent models, there remain key limitations in the questions that can be addressed in these and other mammalian models. In particular, *in vivo* imaging in mammals at the cell-resolution level remains technically difficult and demands large investments in time and cost. The simpler nervous systems of many non-mammalian models allow for precise mapping of circuits and even the whole brain with impressive subcellular resolution. The types of non-mammalian neuroscience models available spans vertebrates and non-vertebrates, so that an appropriate model for most cell biological questions in neurodegenerative disease likely exists. A push to diversify the models used in neuroscience research could help address current gaps in knowledge, complement existing rodent-based bodies of work, and bring new insight into our understanding of human disease. Moreover, there are inherent aspects of many non-mammalian models such as lifespan and tissue transparency that can make them specifically advantageous for neuroscience studies. Crispr/Cas9 gene editing and decreased cost of genome sequencing combined with advances in optical microscopy enhances the utility of new animal models to address specific questions. This review seeks to synthesize current knowledge of established and emerging non-mammalian model organisms with advances in cellular-resolution *in vivo* imaging techniques to suggest new approaches to understand neurodegeneration and neurobiological processes. We will summarize current tools and *in vivo* imaging approaches at the single cell scale that could help lead to increased consideration of non-mammalian models in neuroscience research.

Keywords: microscopy, model organisms, neurodegeneration, zebrafish, zebra finch, *Danionella*, emerging model organisms, intravital imaging

INTRODUCTION

The Historical Combined Power of Observation and Animal Models in Neuroscience

The earliest roots of modern neuroscience were born out of careful observation of neurons in animal models. Ramón y Cajal used light microscopy and sparse neuronal labeling in various mammalian and non-mammalian animal models to identify structures like growth cones and dendritic spines and propose theories of how the brain functioned. The power of basic observation combined with light microscopy and animal models has not become less important since: experiments in chicken embryos and frogs were essential to our early understanding of the rules that governed neurodevelopment (Hamburger, 1934; Levi-Montalcini and Levi, 1943; Gaze, 1959; Erdogan et al., 2016), *Caenorhabditis elegans* gave us the first connectome of an organism (White et al., 1986), and the use of fruit flies, chicken embryos, and rodents helped improve our understanding of the genetic pathways and ligands that control axon guidance (Letourneau, 1975; Seeger et al., 1993; Halloran and Kalil, 1994; Tessier-Lavigne, 1994; Polleux et al., 1998). The diffraction limited resolution of light microscopy initially constrained the study of ultrastructure of the neuron–the organization of organelles and cytoskeletal structures–to be accessible only through electron microscopy (Palay, 1954). However, fluorescence labeling and eventually super-resolution microscopy advanced the study of the neuronal cytoskeleton and its supporting organelles by enabling cell-level imaging with temporal resolution that is not possible with electron microscopy. The use of fluorescence light microscopy also allows for individual proteins and structures to be followed over time at a relatively high spatial (sub-cellular) resolution. This allowed microscopy data to rapidly move away from being solely pictures illustrating observed phenomena, and instead become quantifiable data that can reveal biological changes with mechanistic significance.

The close relationship between microscopy and neuroscience has not been one-sided: the use of animal models to study the function and anatomy of the nervous system has also been a tremendous technology driver for the development of new imaging methods and reagents. There are continuous efforts in the bioimaging community for developing optical imaging technologies capable of imaging faster at a higher resolution and deeper into tissues. To prove the effectiveness of new imaging tools or analysis methods, test models are needed. While *ex vivo* imaging phantoms have utility in testing new methods, *in vivo* imaging, especially of the brain, is often used as a gold standard for the success of a new optical imaging technology. For example, after the development of the modern laser scanning confocal in 1986 (Amos and White, 2003), a range of specimens including chick, *C. elegans* and *Drosophila* were used to demonstrate its ability to optically section complex samples (White et al., 1987). The advent of the laser scanning confocal was followed by 2-photon microscopy in order to overcome the problems of scattering and diffraction that hindered deep tissue imaging (Denk et al., 1990). 2-photon was promptly applied to image neurons in brain slices (Yuste and Denk, 1995; Svoboda et al., 1996), and expression of green fluorescent protein (GFP) in the brain of larval Drosophila (Potter et al., 1996).

The use of small, accessible models to benchmark new technology demonstrates another important concept: cutting edge technology should be paired with the most compatible samples to fully leverage its potential. While imaging in human tissues has been critical in the past for understanding neurodegenerative disease pathology, primary human tissue cannot be genetically manipulated and is generally not compatible with live optical imaging, reducing the utility of most advanced microscopy methods. Additionally, most available human tissue often reflects advanced stages of disease, making it difficult to understand the early processes driving neurodegeneration. While brain organoids are easier to image and can be manipulated in more ways, they lack the physiological context and organization of brain tissue. To comprehensively dissect mechanisms of brain function and disease it is necessary to use intravital imaging and animal models (Bellen et al., 2010; Dawson et al., 2018; Fontana et al., 2018; Rapti, 2020).

Opportunities and Challenges of *in vivo* Observation

Human and non-human primates have large and complex brains, ranging in size from the ∼86 billion neurons of humans to the 634 million neurons of the marmoset (Herculano-Houzel, 2009). An advantage of non-primate models are their more compact nervous systems, which are easier to manipulate and image. *C. elegans* famously has only 302 total neurons (White et al., 1986), making early attempts at circuit-tracing possible. Comparatively, the brain of *Drosophila* has ∼100,000 neurons (Scheffer et al., 2020), an adult zebrafish brain has ∼10 million neurons (Hinsch and Zupanc, 2007), and a mouse brain has ∼70 million neurons (Herculano-Houzel et al., 2006). A drawback to the use of invertebrates are the anatomical and cellular dissimilarities between invertebrate nervous systems and human nervous systems. This can make it difficult to study diseases affecting specific areas of the human brain, as many neurodegenerative diseases do. Compared to invertebrates, brain anatomy and function are generally similar across vertebrates and comparable to humans, even in lower vertebrates like fish (**Figure 1**). Ideally, a scientist should select the least complex model organism that possesses all components necessary to model the aspect(s) of a disease they are interested in.

In many cases, the least complex animal best capable of answering fundamental questions on neurodegenerative disease is still a vertebrate. However, imaging the brain and nervous system in vertebrate animals presents unique challenges for optical imaging: (1) The brain is dense and hidden away behind a skull and skin that promotes scattering, (2) Individual neurons are small, with structures like synapses requiring super-resolution techniques to resolve them, (3) But axons and dendrites form complex architectures that span large areas. Addressing these challenges for mammalian models such as non-human primates and rodents commonly requires extracting and manipulating

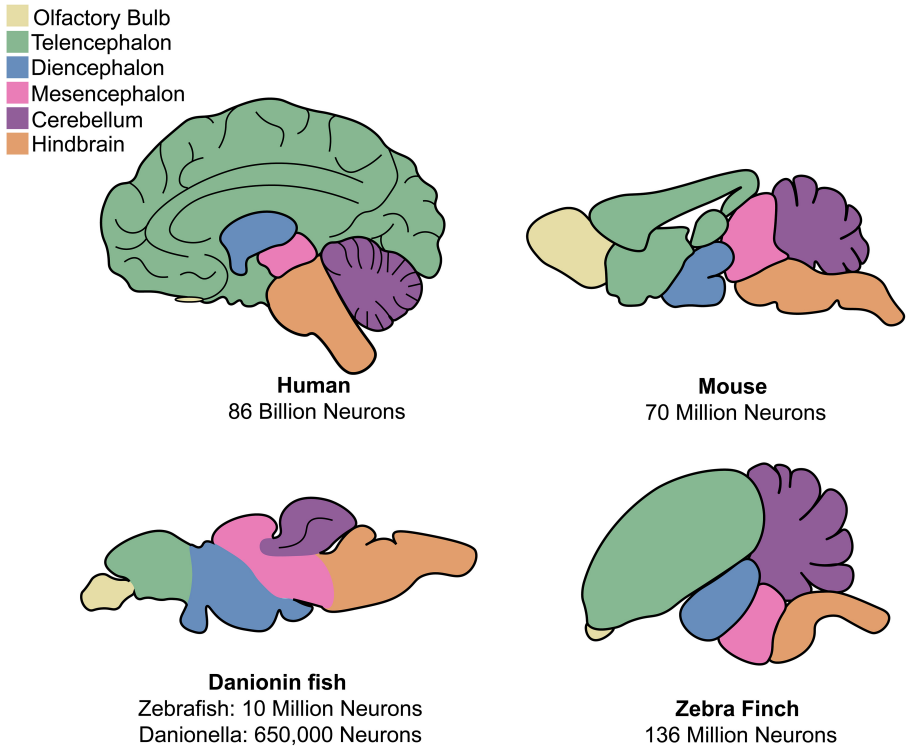

FIGURE 1 | Comparison of anatomy for mammalian and discussed non-mammalian vertebrates. Both mammalian and non-mammalian vertebrates share similar brain anatomy, though region size and organization varies greatly between species.

tissues–sectioning brains, culturing neurons, or clearing whole tissues. To image neurons *in vivo* in mammals, an approach known as intravital microscopy, surgery must be performed to increase access to the brain. A cranial window can be installed, where a portion of skull is removed and replaced with a coverslip (Levasseur et al., 1975; Svoboda et al., 1997; Cramer et al., 2021). Cranial windows have allowed for unprecedented intravital imaging in rodent and non-human primate (NHP) models but can also drastically change the local environment where they are installed. Cranial windows can induce inflammatory responses, alter cortical activity and hemodynamics, and result in temperature fluctuations at the site of the window (Bacskai et al., 2001; Kalmbach and Waters, 2012; Guo et al., 2017; Park et al., 2019; Cramer et al., 2021). Thinning of the skull is less invasive and can be preferable to installation of a cranial window but is technically difficult and can require periodic re-thinning over repeated imaging sessions (Christie et al., 2001; Cramer et al., 2021). Despite improvements in cranial window technology and technique, intravital imaging in mammalian models still requires compromise: lower resolution, smaller fields of view, shorter imaging periods and increased costs overall. Due to the difficulty in achieving high temporal and spatial resolution in intravital imaging in mammals, studies often focus on lower-resolution types of functional imaging (such as use of calcium sensors), or information about neuron density or morphology.

Cellular and sub-cellular phenomena that require very high temporal and spatial resolution to observe are largely outside the reach of intravital imaging. However, these cell-level dynamics are exceedingly important to understanding neuronal health and function. This includes organelle distribution, cytoskeletal organization, movement of cargos by molecular motors, interactions between neurons and glia, and metabolic state (Dubey et al., 2015; Sweeney et al., 2018; Borst et al., 2019; Qin et al., 2021; Wilson and Metzakopian, 2021). A push for broader use of non-mammalian models can help to bridge current gaps in spatial and temporal sampling, such as imaging at the single-cell level, where imaging is impossible or impractical in mammalian models.

Non-mammalian models can be selected for advantages like small size and accessible nervous systems, as well as useful properties such as increased optical clarity that make *in vivo* imaging easier and less invasive (**Table 1**). Non-mammalian models are also less expensive to use, and their smaller size makes it easier to cover large fields of view faster. Their short life cycles and quick time to maturity makes generation of mutant or transgenic animals faster and can speed up research studies. Lastly without the need for invasive surgery, use of non-mammalian vertebrates also faces lower regulatory barriers.

The power of optical imaging technologies like 2-photon (Denk et al., 1990) and light sheet microscopy (LSFM) (Huisken et al., 2004) have brought revolutionary improvements to our ability to observe cellular level dynamics *in vivo*, while specialized microenvironment sensitive imaging techniques such as fluorescent lifetime imaging (FLIM) and use of biosensors

TABLE 1 | Comparative summary of a selection of common and emerging vertebrate models.

Species	Human Tissue (*Homo sapiens*)	Macaque (*Macaca mulatta*)	Mouse (*Mus musculus*)	Zebra Finch (*Taeniopygia guttata*)	Zebrafish (*Danio rerio*)	Danionella (*Danionella cerebrum*)	Killifish (*Nothobranchius furzeri*)	Western Clawed Frog (*Xenopus tropicalis*)	Axolotl (*Ambystoma mexicanus*)
Lifespan	70-100 years	25-40 years	2-3 years	5-7 years	3-4 years	3-4 years	4-8 months	n/a, likely similar to X. laevis (15-20 years)	10-15 years
Ages Studied	adult-advanced age	adult	embryo-adult	adult	embryo-adult	embryo-adult	adult	embryo-adult	embryo-adult
Neurons in Adult	86 billion (Herculano-Houzel, 2009)	6.4 billion (Herculano-Houzel, 2009)	70 million (Herculano-Houzel et al., 2006)	136 million (Olkowicz et al., 2016)	10 million (Hinsch and Zupanc, 2007)	650,000	n/a	n/a	n/a
Skull thickness	6.5-8mm depending on area (Li et al., 2007)	2-4mm depending on area (Nie et al., 2011)	310-340μm (Soleimanzad et al., 2017)	~300μm (Abi-Haidar and Olivier, 2009)	~20-25μm (Castranova et al., 2021)	no skull roof	n/a	n/a	n/a
Ex-vivo cultures	uncommon	uncommon	yes	yes	yes	no	no	yes	yes
Live Optical Imaging	–	+	+	+	++	+++	–	–	–
Genetics	–	+	+++	+	+++	++	++	+	+
Behavior	–	Broad array of behaviors including social, learning, memory, and exploration.	Broad array of behaviors including social, learning, memory, and exploration.	Most notable for vocal learning and sexual dimorphism in vocal behavior.	Broad array of behaviors in adults and larvae, including predator avoidance, social behavior, learning, memory, and exploration.	Broad array of behaviors in adults, including vocalization, social behavior, and learning, memory and exploration.	Broad array of behaviors in adults, including social behavior, learning, memory, and exploration.	Adult vocalization and tadpole swimming have been studied.	No reported studies of stereotyped behavior.
Regenerative	–	–	–	+	++	not reported, but likely	++	+	+++
Useful Features	High relevance to disease. Necessary for initial characterization of pathologies and genes associated with a disease.	Primate with ~92% genetic conservation to humans and high physiological relevance to human disease.	Mammal with high physiological relevance to human disease. Highly established protocols.	More closely models human vocalization and vocal learning than other available models.	Small vertebrate, transparent in the embryonic and larval stages. Pigmentless mutants available for adults. Well established model with many resources.	Small transparent vertebrate with the smallest known brain of any vertebrate. Amenable to genetic techniques used in most teleost fish.	Short-lived fish that displays aging-associated cognitive defects, neurodegeneration and muscular degeneration. Embryos can suspend aging during "diapause" for months to years.	Smaller Xenopus species with a compact diploid genome that reaches maturity faster than X. laevis. Useful for cell and developmental biology and genetics.	Extreme ability to regenerate brain and peripheral nervous system.

(Continued)

TABLE 1 | (Continued)

Species	Human Tissue (*Homo sapiens*)	Macaque (*Macaca mulatta*)	Mouse (*Mus musculus*)	Zebra Finch (*Taeniopygia guttata*)	Zebrafish (*Danio rerio*)	Danionella (*Danionella cerebrum*)	Killifish (*Nothobranchius furzeri*)	Western Clawed Frog (*Xenopus tropicalis*)	Axolotl (*Ambystoma mexicanus*)
Drawbacks	Limited tissue availability, no temporal context available, usually limited to histopathology.	Expensive, prolonged time to maturity. Difficult to image due to skull, skin, and fur. Ethical concerns.	Generation of mutants takes a long time. Does not recapitulate all human disease phenotypes. Difficult to image due to skull, skin, and fur.	There is no reliable way to generate transgenic animals.	Limited working antibodies. Genetic duplications in teleosts can make gene editing challenging.	Produces relatively few embryos. Neotenic traits may complicate use as disease model.	Few resources currently available. Male-male aggression complicates housing.	Pigmented tissue makes imaging impractical, though albino strains exist and mutants lacking yellow pigment have been made (Nakajima et al., 2021).	Excessively large genome size, no true pigmentless mutant, neotenic traits may complicate use as disease model

Signs denote ease or ability to use the model for a particular purpose. -, difficult or not possible; +, possible; ++, easily possible; +++, very easy, model is well suited to this purpose.

(Leopold et al., 2019; Datta et al., 2020) can tell us more about dynamics within *in vivo* sub-cellular domains. With the notable exception of LSFM, many advanced imaging techniques have been under-utilized in non-mammalian models. What would it take to expand the repertoire of advanced imaging techniques in non-mammalian vertebrates?

A New Age for Non-mammalian Models

Approximately 45% of neurobiology papers published in the last decade have relied on the use of rat and mouse models, compared to 2% for NHP and 6% for other common vertebrate and non-vertebrate models.[1] There are many reasons for the extensive use of rodents in the field, mostly related to the availability of tools and reagents, sequenced genome, and physiological similarities to humans. It is unquestionable that rodent models represent many important aspects of human disease, but what biological opportunities do researchers leave on the table by optimizing only the technological approaches without addressing their choice of animal model as well? Given the rapid expansion of genomic, transcriptomic, and microscopy tools available to the average neurobiologist, it is possible to select models for biological qualities that help address specific neurobiological questions, instead of for their generalist versatility.

Calls for the diversification of model organisms in neurobiological research are hardly new (Manger et al., 2008; Keifer and Summers, 2016; Russell et al., 2017; Yartsev, 2017; Żakowski, 2020). The arguments for introducing new model systems can vary depending on need: for some, it is necessary to find animals that mirror aspects of complex human behavior such as vocal learning or social dynamics, for others, it is enough for an animal to have some special characteristic that allows for new experimental flexibility. *C. elegans* was initially proposed for connectome mapping by 2002 Nobel laureate Sydney Brenner in part because the *Drosophila* brain was too large for the project (Emmons, 2015). Serendipitously, 2008 Nobel laureate Martin Chalfie credits his work with Brenner and *C. elegans* for his decision to utilize GFP to visualize biological structures: "[. . .] if I had not worked on *C. elegans* and constantly told people that one of its advantages was that it was transparent, I am convinced I would have ignored GFP when I first heard of it" (Chalfie, 2009). The use of diverse model organisms can inform new scientific thinking and inspire innovation.

To best understand how to encourage re-evaluation of model choice and awareness of new model systems for neuroscience research, we must first ask what has contributed to the lack of diversity in the animal models widely used for neuroscience research. One key factor is that initially there were limited ways in which to manipulate animals biologically, and so scientists had to rely on what biology was available to study through natural diversity. As powerful new tools for genetic manipulation were developed, the field began to condense into a handful of models that had sequenced genomes, and well-defined protocols for housing, breeding, and experimental manipulation. This has generally been a boon for research, enabling researchers across the world to speak in a shared language of standardized experimental approaches and reagents. Today, though, it is easier than ever to sequence and edit an organism's genome. CRISPR has proven to be easily adaptable to many different model systems, and there is a plethora of tools for next generation sequencing and transcriptomics. The pace at which reagents, protocols, and knowledge can be disseminated to create a "shared language" within a field has also increased, fueled by initiatives like protocol-focused websites and journals, preprints, social media, and organism-dedicated societies.

We therefore propose that any animal can become a useful model for neurobiological disease research if it meets the following conditions: (1) The model represents a useful structure, system, or behavior related to neurobiology, (2) It is easily acquired, maintained, and bred in a lab environment, (3) It can be genetically manipulated, and (4) There is a way to measure perturbations to the nervous system through behavioral output,

[1]Non-human primates considered include marmoset, macaque, squirrel monkey, vervet monkey, and mouse lemur. Other common models considered include: *C. elegans*, chick, Drosophila, zebrafish, Xenopus, and zebra finch. Results were generated from PubMed searches for the name of the model organism + "neurobiology".

imaging, or other measurements. For the purposes of this review, we will focus on three rising non-mammalian vertebrates–Zebrafish (*Danio rerio*), *Danionella* species, and zebra finch (*Taeniopygia guttata*)–that are both amenable to cutting-edge optical imaging techniques at a cellular-level resolution and well-suited to serve as models of neurodegenerative disease. We will also discuss the cellular targets that would benefit from study in non-mammalian vertebrates. We will briefly describe some of the advanced imaging and cell labeling techniques that have been successfully used to look at neurobiological disease in non-mammalian models, give an overview of some of the current gaps in tools and knowledge, and discuss additional emerging models and ways in which the field could expand and grow.

Targets of Imaging at Cellular and Sub-Cellular Resolution *in vivo*

Emerging questions in neurodegenerative disease are increasingly focused on the interplay of multiple systems within the brain during disease progression–and microscopy is perfectly suited to interrogate how multiple cellular systems interact in a temporal and spatial manner. Fluorescence labeling and endogenous signals (such as second harmonic generation of fibrillar collagen and intrinsic metabolic fluorescence) allow tracking of several structures or cell types simultaneously in living animals. Using imaging techniques with high temporal and spatial resolution, we can also assess cells not as a single homogenous unit, but as dynamic structures with regions that react and respond to their local environment. In addition, the use of genetically encoded biosensors can inform us of how cell-cell or cell-environment interactions can change intracellular calcium, membrane voltage, redox potential, and more (Yano et al., 2010; Bando et al., 2019; Zhang Y. et al., 2021).

Some of the major features that can be examined through imaging are the contribution of the "neurovascular unit" (NVU) and the brain's immune cells, microglia, in neurodegenerative disease. The NVU is defined as the multiple interacting elements, both cellular and extracellular, that regulate blood flow and blood brain barrier function. This includes not only the neurons and the vasculature itself, but also the microglia, pericytes, and astrocytes that provide support and help maintain cerebral homeostasis (Iadecola, 2017; Sweeney et al., 2018; Schaeffer and Iadecola, 2021). Though previously the study of neurodegeneration and cerebrovascular disease were considered distinct, the theory of the NVU has been a fruitful subject of research since its conception (Iadecola, 2017). Defects in cerebrovascular blood flow have been found in Alzheimer's disease (AD) and other dementias, Huntington's disease (HD), Parkinson's disease (PD), amyotrophic lateral sclerosis, and other neurodegenerative diseases (Rule et al., 2010; Melzer et al., 2011; Chen J. J. et al., 2012; Murphy et al., 2012; van de Haar et al., 2016; Leeuwis et al., 2017; Leijenaar et al., 2017; Sweeney et al., 2018).

Microglia, resident phagocytic glia in the brain, have been an implicated in the pathogenesis of Alzheimer's disease and other neurodegenerative diseases (Srinivasan et al., 2016; Wang et al., 2016; Füger et al., 2017; Huang et al., 2017; Masuda et al., 2019; Prinz et al., 2019; Tejera and Heneka, 2019). Microglia are not only responsible for clearing debris and pathogens from the central nervous system (CNS), but also function in synaptic remodeling and secrete signaling factors that contribute to immune response and tissue repair (Davalos et al., 2005; Nimmerjahn et al., 2005; Paolicelli et al., 2011; Schafer et al., 2012; Miyamoto et al., 2016; Weinhard et al., 2018; Davies et al., 2019). Like macrophages, they are dynamic and migratory cells that have different morphological phenotypes and close interactions with other cells in the brain. Studying microglia requires the ability to image a wide field of view (due to their migratory nature), deep into tissue at a high temporal and spatial resolution which is difficult to achieve in larger mammalian brains. Microglia are present in both mammalian and non-mammalian vertebrates, and microglia-like cells have been extensively described in invertebrate annelids (Sharma et al., 2021). The existence of distinct microglia in other invertebrates, such as *Drosophila*, is less clear and suggests they may have arisen convergently in annelids (Hartenstein and Giangrande, 2018). Study of microglia in small non-mammalian vertebrates, and comparative study of annelid and vertebrate microglia could improve our overall understanding of microglia function in CNS homeostasis and disease.

Astrocytes are another glial component of the NVU that mediate connections between neurons and the vasculature to provide synaptic support and control cerebral blood flow (Braun and Iliff, 2020). Astrocytes accomplish this through physically contacting synapses and vasculature, forming an incredibly complex morphology with up to 80% of the cell's membrane being used in fine processes (Ventura and Harris, 1999; Ogata and Kosaka, 2002; Mathiisen et al., 2010; Reeves et al., 2011; Khakh and Sofroniew, 2015). The complex morphology of astrocytes, alongside their complex role in connecting multiple cell types, makes them excellent candidates for microscopic study with increased spatial and temporal resolution.

Underlying the cellular-level phenomenon we can observe are the sub-micron structures that facilitate cellular behavior. The neuronal cytoskeleton drives neuronal development but must also be maintained throughout the life of an organism. Defects in the neuronal cytoskeleton can cause cell death through signaling cascades as well as failure in cargo trafficking (Dubey et al., 2015). Mitochondria produce the ATP necessary for cells to function, but also play a role in calcium buffering and generation of reactive oxygen species. Multiple neurodegenerative diseases are known to induce defects in the neuronal cytoskeleton and mitochondria (Dubey et al., 2015; Mandal et al., 2018), but the relationship between this damage, disease progression, and neuronal death are still unclear. Additionally, other sub-micron structures such as endoplasmic reticulum-mitochondria contact sites, endosomes, and lysosomes are relevant for the study of neuronal function and disease (Mandal et al., 2018; Peng et al., 2019; Wilson and Metzakopian, 2021). Imaging of these structures is technically challenging and typically requires targeting superficial neurons and sparse labeling techniques, coupled to sensitive, high-resolution microscopes capable of rapid acquisition speeds.

Neuroimaging Tools for *in vivo* Applications

There have been multiple comprehensive reviews recently published on microscopy techniques in neuroscience (Choquet et al., 2021; Werner et al., 2021) and on LSFM specifically (Power and Huisken, 2017; Fiolka, 2019; Hillman et al., 2019; Lemon and McDole, 2020; Stelzer et al., 2021). Therefore, these techniques will only be reviewed in brief in the context of their usefulness for addressing problems in neurodegenerative disease.

Confocal Imaging

Laser-scanning and spinning disk confocal imaging are among the most commonly used techniques in neurobiological imaging (Tanaami et al., 2002; Amos and White, 2003). Confocal microscopes can be in upright or inverted configuration and are suited for use with traditional slides and coverslips. Confocal microscopy generates optical sectioning by its use of a pinhole to reject light from outside the desired focal plane. The rejection of light produces high signal to noise (SNR) imaging, however, exposure of the sample to laser light is still a viability concern. Since regions of the sample outside of the plane of focus are still in the cone of illumination, excess light is delivered to the sample and living samples are at risk of increased phototoxicity and photobleaching. Scanning confocal microscopes are also typically slow, making them best suited to fixed samples or live samples that do not require high temporal resolution views.

Spinning-disk confocal microscopes trade a fixed pinhole (single point scanning) for an array of pinholes on a mechanically spinning disk (multi-point scanning). These pinhole arrays allow for parallel illumination of the sample. Parallelization of illumination and detection reduces the amount of light the sample is exposed to and increases the speed of imaging. This makes spinning-disk confocal typically more suitable than scanning confocal for fast *in vivo* imaging of cellular and sub-cellular phenomenon (Fuseler et al., 2018).

Additional gains in scan speed can be achieved through swept field confocal technology and similar approaches (Castellano-Muñoz et al., 2012). In this technique, the mechanical spinning disk is jettisoned in favor of a fixed aperture plate. Light from the aperture plate is "swept" over the sample by galvanometric and piezo-mirrors which can reach faster scan speeds than spinning disk or laser scanning technology. The high speeds of swept field confocal are useful for imaging cellular and sub-cellular dynamics *in vivo* (Castellano-Muñoz et al., 2012).

All confocal techniques suffer difficulties with penetration depth in complex animal tissues due to scattering and diffraction of light, and so are best suited to imaging of flattened tissues or superficial structures. Confocal microscopes are generally used with laser lines between 400 and 600 nm.

2-Photon and 3-Photon Microscopy

Multiphoton microscopy, which includes 2- and 3-photon microscopy, relies on the principle that a fluorophore can be excited by 1-photon at its exact excitation wavelength, but it can also be excited by two or three simultaneous (<1 femtosecond apart) photons which are two to three times the wavelength of its normal excitation, respectively. For example, a fluorophore could be excited with one photon at 488 nm, two photons at 976 nm, or three photons at 1464 nm. Both 2-photon and 3-photon microscopy benefit from the deeper penetration afforded by longer wavelengths of light, and thus are the choice for many *in vivo* neuroimaging applications (Denk and Svoboda, 1997; So et al., 2000). 2-photon microscopes use lasers in the 700–1000 nm wavelengths, while 3-photon microscopes tend to use lasers between 1300 and 1700 nm wavelengths. In addition to depth, the long wavelength used for excitation can provide better viability when compared to traditional brightfield or confocal microscopy. 3-photon microscopy can be hindered by the currently limited range of fluorophores that are capable of being excited by its longer infrared wavelengths.

Light Sheet Fluorescence Microscopy

Light sheet fluorescence microscopy, also known as selective plane illumination microscopy (SPIM), is a technique in which a cylindrical lens is used to shape a laser beam into a thin gaussian sheet of light (Huisken et al., 2004). The light sheet constrains illumination of the sample only on the focal plane of interest, allowing optical sectioning without the need to reject any out of focus light. This avoids delivery of excess laser light to the sample which reduces photobleaching and phototoxicity. In addition, the use of high-speed scientific cameras reduces the time it takes to acquire a volume, further reducing laser exposure and enabling high-volume, long-term imaging while limiting damage to the sample. LSFM systems are generally highly adaptable and can be built around the requirements of the sample, making them well-suited to a diverse range of model systems (Power and Huisken, 2017).

Light sheet fluorescence microscopy tends to be hindered by tissue-induced scattering, which deforms the light sheet itself and causes striping and deterioration in the resulting image. This can be combatted by using multi-view systems that allow for illumination and imaging from two sides of the sample (Huisken and Stainier, 2007; Krzic et al., 2012). A final image can be reconstructed by piecing together the two halves of the image. This increases the time required for acquisition and the amount of light the sample is exposed to, so it is not a universal solution.

Alternative beam strategies for LSFM have also been developed, notably 2-photon, Bessel beam, lattice, and Airy light sheets, as well as the recent field synthesis method (Planchon et al., 2011; Truong et al., 2011; Chen et al., 2014; Vettenburg et al., 2014; Liu et al., 2018; Chang et al., 2019). These alternative beams combat the diffraction and scattering of a traditional light sheet and can create thinner and more uniform light sheets which improve resolution and image quality.

Single Objective Light Sheet Microscopy

Traditional LSFM set-ups utilize two objectives oriented at an orthogonal angle to each other, resulting in spatial constraints regarding the size and angle of the objective's nose cone. This limited LSFM to lower numerical aperture (NA) lenses until single-objective LSFM solutions were introduced (Botcherby et al., 2007; Dunsby, 2008; Bouchard et al., 2015; Fadero et al., 2018; Kim et al., 2019; Yang et al., 2019; Sapoznik et al., 2020).

The continued evolution of single-objective light sheet systems could lead to the wide-spread adoption of these microscopes for high-speed, long-term *in vivo* cellular and sub-cellular imaging.

Super-Resolution Techniques

Limited super-resolution techniques have been applied to neurons *in vivo*. Stimulated emission depletion microscopy (STED) has been used to image dendritic spines and even synaptic structures in a living mouse (Ter Veer et al., 2017; Wegner et al., 2017, 2018; Masch et al., 2018). Single-molecule STORM using an oblique plane strategy was introduced in 2019, allowing for tissue-scale super-resolution imaging in Drosophila and stickleback fish (Kim et al., 2019). Though limited to fixed tissues, cleared tissue and expansion microscopy techniques also allow for high-resolution tissue-scale imaging (Chen et al., 2015; Wassie et al., 2019; Porter and Morton, 2020; Weiss et al., 2021).

"Smart" Microscopy and Image Analysis

Smart, adaptive microscopy techniques alongside of other advanced image processing routines such as deconvolution and machine learning can yield additional insights from collected data and reduce the burden of large datasets through improved visualization and automation. This is critically important for brain imaging, where computational solutions are needed for challenges including low signal-to-noise ratio, areas of divergent image quality, and extremely fast recording times (as in imaging of calcium dynamics or voltage sensors). Smart microscopy, where images are computational analyzed in real-time, has been successfully applied in LSFM to automatically rotate the sample for improved imaging based on detected image quality (He and Huisken, 2020). Adaptive focus imaging has also been applied alongside light sheet imaging to keep embryos in focus despite dramatic changes in shape over development (Royer et al., 2016, 2018; Ji, 2017; McDole et al., 2018). Improvements in image quality for lower-resolution or lower signal-to-noise ration images can be obtained through deconvolution and denoising tools. Deconvolution is a relatively standard technique for fluorescent microscopy, but new strategies for deconvolution such as super-resolution radial fluctuations (SRRF) are being developed (Gustafsson et al., 2016; Culley et al., 2018). Deconvolution can also be coupled to machine learning to improve the resolution of low-quality images by training a neural network on higher quality images (Weigert et al., 2018; Krull et al., 2019). Machine learning techniques have been widely used in modern fluorescent microscopy for denoising and image quality improvement as well as segmentation of images. There are many open source machine learning tools available that give biologists the option to train deep-learning models based on their own datasets, or utilize publicly accessible pre-trained models (Moen et al., 2019; Weigert et al., 2020; Stringer et al., 2021; von Chamier et al., 2021). The importance of such open access computational tools, including widely used open source image processing platforms such as ImageJ (Schindelin et al., 2012), will keep growing as the limits of light microscopy continue to be pushed. Advances in computational imaging have great opportunity to enable new capabilities in established and emerging animal models.

Rising Non-mammalian Vertebrate Models for the Study of Neurodegenerative Disease

Zebrafish

Background and Genetic Tools

Danio rerio, the zebrafish, has been a rising star within neuroscience since it was championed by George Streisinger starting in the 1970s (Varga, 2018). Though it was just one of many bony fish models used at the time, it has left the world of "emerging model organisms" to become an example of successful widespread adoption of a "new" model. The optical clarity of zebrafish during embryonic and larval stages offers unprecedented access to imaging for a vertebrate, and its reduced size means that imaging whole brain volumes is increasingly achievable. Their potential as a disease model is good, with 82% of human disease genes have a zebrafish ortholog (Howe et al., 2013). Zebrafish spawn in large clutches of ∼100 embryos, making them popular for large scale pharmacological, genetic, and behavioral screening. To this end, multiple well-established methods exist for genetic manipulation in zebrafish, including CRISPR/cas9 editing and transgenesis *via* Tol2 mediated insertion (Kawakami, 2005; Kwan et al., 2007; Don et al., 2017; Liu et al., 2019). However, it is worth noting that zebrafish have ∼30% of their genome duplicated, which can complicate the creation of mutant or knockout animals as multiple genes may need to be targeted (Woods et al., 2000, 2005; Howe et al., 2013). Existing zebrafish mutants and transgenic lines can be acquired easily through an international repository (ZIRC), and a large library of phenotypically interesting mutants already exist thanks to an important large scale ENU mutagenesis effort (Driever et al., 1996).

Aiding in their utility as a genetic model, zebrafish are quick to develop. They reach juvenile status at 30 days post-fertilization and become sexually mature adults at ∼90 days post-fertilization. Mice, in comparison, reach sexual maturity at ∼55 days post-fertilization, making them slightly faster to mature but relatively comparable. Zebrafish are generally kept for 2 years in lab housing facilities but can survive for as long as 5 years. Their lifespan along with detectable aging-associated changes make them a model with great potential for addressing neurodegenerative and aging-associated diseases (Keller and Murtha, 2004; Kishi, 2004; Adams and Kafaligonul, 2018).

Zebrafish have already proven useful models for neuroscience because of their small and accessible brains. The structure and composition of the zebrafish nervous system shares much in common with that of humans, including a general architecture of a spinal cord, hindbrain, midbrain, and forebrain and predominantly similar neurochemical components (**Figure 1**; Kimmel, 1993; Bae et al., 2009; Panula et al., 2010). One notable anatomical difference between mammalian and teleost fish brain structure is that fish lack a cerebral cortex. All mammalian CNS glial cell types are also found

in zebrafish, namely, oligodendrocytes, astrocytes, and microglia (Kawai et al., 2001; Yoshida and Macklin, 2005; Avila et al., 2007; Lyons and Talbot, 2014; Xu et al., 2015; Chen et al., 2020).

In addition to brains that are largely comparable to mammals, adult zebrafish also have a host of complex behaviors that parallel many established murine tests of learning and memory, anxiety, and social preference (Orger and de Polavieja, 2017). The similarities between zebrafish and mouse behavioral assays allow comparisons to be made between the substantial body of literature in mice and new work in zebrafish.

Imaging Neuronal Function During Behavior

Pairing behavioral assays with live imaging has immense potential for the study of neurological disease, especially neurodegenerative diseases that are known to cause motor, learning, and memory deficits. These kinds of experiments are increasingly common, though technical challenges limit their widespread adoption. One such caveat is that imaging behaving larvae generally requires stabilization, either through mounting or paralysis through genetic or chemical means. This stabilization reduces much of the natural feedback received by the fish while enacting the behavior. Stabilized or partially stabilized larvae have been used with multiphoton and LSFM microscopy to image genetically encoded calcium indicators (GECIs) in opto-motor control, auditory and visual response, olfaction, and prey-capture decisions (Förster et al., 2020; Wang et al., 2020; Bruzzone et al., 2021; Herrera et al., 2021). The introduction of adaptive imaging techniques and real-time correction for movement allow for reduced levels of restraint while improving image quality (Wang et al., 2014; Rodríguez and Ji, 2018; Griffiths et al., 2020). This leaves the ability to image reaction to virtual stimuli, but without natural feedback from the environment or sensory systems such as the lateral line or vestibular system. Real-time virtual feedback stimulation can be provided in response to active behaving (Portugues and Engert, 2011; Ahrens et al., 2013; Trivedi and Bollmann, 2013; Bianco and Engert, 2015; Jouary et al., 2016; Kawashima et al., 2016; Naumann et al., 2016; Huang et al., 2020), but great interest still remains in functional neuronal imaging of freely swimming fish.

Currently, multiple solutions for imaging of freely behaving larvae exist, most with widefield fluorescence illumination and detection combined with methods to perform tracking and predictive adjustments of optical elements (Cong et al., 2017; Kim et al., 2017; Symvoulidis et al., 2017). 2-photon and LSFM solutions to image true freely behaving larvae are technically difficult to implement as they require precise direction of the illumination area. Despite their relative speed compared to other techniques, acquiring whole brain volumes using 2-photon or LSFM takes additional time compared to a single widefield acquisition, making it slow in comparison to the speed of a moving larva. Light field microscopy presents an alternative approach, providing speed at the sacrifice of spatial resolution (Levoy et al., 2006). Confocal light field microscopy has recently been implemented to improve resolution for volumetric imaging of neuronal GECIs in freely swimming larvae (Zhang Z. et al., 2021).

Imaging Cellular Dynamics

Both scanning and spinning disk confocal microscopy have been standard methods in the field for imaging cellular dynamics in development and disease in the zebrafish. Since its introduction in 2004, however, LSFM has revolutionized imaging cellular dynamics in embryonic and larval zebrafish, particularly during development. The use of mounting methods that preserve the 3D integrity of the sample is an important principle in LSFM, and zebrafish embryos can be mounted for LSFM imaging purely in water using FEP tubes and an agarose plug (Power and Huisken, 2017). The ability to mount and image without using a constrictive mounting medium allows for a much more natural progression of shape change and morphogenesis during development. This can be combined with adaptive imaging techniques to keep embryos in focus and within the field of view over many hours or days of development (McDole et al., 2018; Daetwyler et al., 2019; He and Huisken, 2020). Little work has been done specifically using LSFM to look at cell-scale phenomenon, like glia and the NVU in neurodegenerative disease in zebrafish. However, foundational work has been completed in characterizing lymphatics, vasculature, astrocytes, and microglia in the zebrafish brain using both LSFM and standard confocal microscopy.

Vascular imaging in zebrafish is a relatively mature field with established transgenic lines and existing protocols for the segmentation and quantification of complex vascular networks, including cerebellar vasculature (Chen Q. et al., 2012; Daetwyler et al., 2019; Kugler et al., 2020, 2021). A newly published zebrafish transgenic line marking astrocytes will prove a valuable resource to illuminating the role of astrocytes in development and disease (Chen et al., 2020) and could be combined with existing transgenic lines (Lawson and Weinstein, 2002) marking vasculature to better understand interplay between vascular systems and glia in the NVU.

Use of the zebrafish model has also enabled imaging of the glymphatic network of the CNS, a traditionally difficult imaging subject due to its complexity and location. Castranova et al. (2021) achieved live imaging of immune cells within meningeal lymphatics in larval and juvenile zebrafish brain. Zebrafish have thin skulls, and when coupled to a pigmentless strain they were able to image the meningeal lymphatics in intact animals through the skull using spinning disk confocal. This work shows the promise of non-invasive cellular-level imaging in the intact juvenile zebrafish, and positions zebrafish as a model to understand the interplay of the glymphatic network with neurodegenerative diseases.

Microglia in zebrafish are a rapidly expanding topic of interest–more papers have been published between 2019 and 2021 on microglia in zebrafish that in the preceding 12 years combined. Zebrafish microglia are generated in two waves, with a primitive wave derived from the primitive macrophages in

the yolk sac, and a second wave that replaces the original population and originates from the hematopoietic stem cells of the dorsal aorta (Xu et al., 2015; Ferrero et al., 2018; Wu et al., 2020; Silva et al., 2021). Zebrafish microglia share a core transcriptional signature with mammalian microglia and are morphologically and functionally similar to microglia of other species (Oosterhof et al., 2017; Geirsdottir et al., 2019). Imaging studies in zebrafish have been used to show cross talk between neuronal activity and microglial morphology, phagocytosis of myelin sheaths and dying neurons, and response to long-range signaling cues (Peri and Nüsslein-Volhard, 2008; Li et al., 2012; Sieger et al., 2012; Mazaheri et al., 2014; Hughes and Appel, 2020). Two populations of zebrafish microglia have been observed: ameboid microglia, which have a higher capacity for phagocytosis, and the white-matter enriched ramified microglia, which actively remodel their protrusions and may play a more regulatory role (Wu et al., 2020). This is an interesting distinction because humans have heterogenous microglia populations, while other studied model organisms have been found to have more homogeneous microglia populations (Böttcher et al., 2019; Geirsdottir et al., 2019; Masuda et al., 2019; Sharma et al., 2021). If zebrafish microglia more closely resemble the heterogeneity of human microglia, they could fill an important niche in our understanding of microglia in human disease.

Sub-Cellular Dynamics

Embryonic and larval zebrafish have multiple subtypes of neuron with axons that grow superficially enough to allow for detailed imaging of sub-cellular structures at excellent resolution. The posterior lateral line (pLL) axons and the Rohon-Beard (RB) sensory neurons are two such commonly imaged populations. Imaging of microtubules (Stepanova et al., 2003; Asakawa and Kawakami, 2010; Lee et al., 2017; Haynes et al., 2021), mitochondria (Plucińska et al., 2012; Campbell et al., 2014; Paquet et al., 2014; Auer et al., 2015; Drerup et al., 2017; Mandal et al., 2018), ER-Mitochondria contact sites (Cieri et al., 2018; Vallese et al., 2020), endosomes (Clark et al., 2011; Ponomareva et al., 2014, 2016), and lysosomes (Drerup and Nechiporuk, 2013) is common in these superficial neurons in zebrafish embryos and larvae. When paired with genetic manipulation of disease-associated genes, zebrafish are an excellent tool to discern the molecular mechanisms behind basic disease processes.

Spinning disk and swept-field confocal microscopes have traditionally been the tool of choice to image fast-moving sub-cellular structures like microtubule comets and organelles. Zebrafish sensory axons, for example, can have axon arbors spread through a volume of 20–50 μm. That volume must be obtained in seconds or less to achieve adequate speed for measuring sub-cellular dynamics. However, progressive improvements in high NA light-sheet microscopes are enabling them to break into the sub-cellular niche. Lattice light sheet is difficult to implement but able to resolve objects of 200 nm, meaning that structures like Golgi and ER were able to be resolved in the brain of a living zebrafish embryo (Liu et al., 2018). Single objective light sheet as well as super-resolution techniques like STED have yet to be applied for sub-cellular imaging in zebrafish, however, the potential for their utility is high.

Disease Models

With an array of tools and techniques available for multiple ages, zebrafish are growing into their potential as an excellent model for neurodegenerative disease research. Disease-relevant mutations can be easily introduced through CRISPR/Cas9 editing or transgenic insertion, allowing the study of both the native function of the mutated gene as well as the disease-relevant consequences of its loss or mutation. Numerous disease models for neurodegenerative disorders including PD, AD, and hereditary spastic paraplegia (HSP) have been generated in zebrafish through genetic or non-genetic means (Fontana et al., 2018; Vaz et al., 2018; Naef et al., 2019; Wang and Cao, 2021).

Many of these diseases are complex and polygenic, making them difficult to model. For example, there are multiple genes associated with familial risk for PD, though most cases are spontaneous. In humans, PD results in neurodegeneration of the dopaminergic neurons and is accompanied by aggregation of the protein α-synuclein. PD can be modeled in the zebrafish through drug treatments that decrease dopamine levels or numbers of dopaminergic neurons or through genetic knockdown or knockout (Vaz et al., 2018). The role of synuclein genes and other PD associated genes have been studied in zebrafish and have been associated with defects in the dopaminergic system, mitochondrial dysfunction, and neurodegeneration (Milanese et al., 2012; O'Donnell et al., 2014; Vaz et al., 2018).

Alzheimer's disease has been more difficult to model in zebrafish. A standard model of AD in mice is the 5xFAD mouse, which uses transgenic insertion of amyloid precursor protein (APP) and presenilin1 (PSEN1) with a constellation of 5 mutations associated with human familial AD (Oakley et al., 2006). An equivalent to this model has not been generated in zebrafish, though perturbation of presenilin-1 and −2 genes and zebrafish APP genes *appa* and *appb* have been widely used to test the role of these genes in development and disease (Kaiser et al., 2012; Luna et al., 2013; Fontana et al., 2018; Banote et al., 2020). Aβ peptide, the product of APP cleavage, has also been used directly in zebrafish to study the role of different length Aβ on biological processes and Aβ toxicity. Cerebroventricular injection of Aβ-42 showed AD-like phenotypes including neuronal cell death and microglial activation in both young and aged animals (Bhattarai et al., 2016, 2017). Microglia have been implicated in pathways controlling neuroproliferation in the zebrafish in response to Aβ injection (Bhattarai et al., 2020), though no live cell imaging of glia or neuronal cell interaction with plaques have been performed in zebrafish to date.

A strength of the zebrafish model is the ability to correlate phenotypes at the cellular and sub-cellular resolution with adult behavior and pathology. For example, a genetic zebrafish model of the progressive neurodegenerative disease hereditary spastic paraplegia showed defects in microtubule dynamics and axon stability during development as well as adult behavioral defects, demonstrating the ability to link early onset phenotypes to adult outcomes (Haynes et al., 2021). Further work to follow the consequences of genetic disruption of neurodegenerative disease

risk genes from the sub-cellular level to specific circuits to whole-animal behavioral phenotypes could establish zebrafish as a revolutionary disease model.

Danionella

Background and Genetic Tools

Danionella are a genus of danionin fish species related to zebrafish, but smaller in size and with the peculiar advantage of being nearly completely transparent as adults. This remarkable characteristic is owed in part to their neoteny, or retention of juvenile traits. *Danionella* species range in length from 11 to 18 mm, which is roughly comparable to an older zebrafish larvae/a young juvenile (∼12 mm) (Conway et al., 2021). Many previously published papers on *Danionella* have stated the species used in their work is *Danionella translucida*. However, recently published morphological and molecular analysis showed that the widely used species in current research is *not D. translucida*, but a new species currently designated as *Danionella cerebrum* (Britz et al., 2021). Thus, we will use the designation *D. cerebrum* to discuss the species used in Penalva et al. (2018), Schulze et al. (2018), and Kadobianskyi et al. (2019). *Danionella cerebrum* possess the smallest adult vertebrate brain known, only eight times larger than a *Drosophila* brain (Schulze et al., 2018). Both *D. cerebrum* and *Danionella dracula* lack a bony roof on the top of the skull, making them highly amenable to brain imaging (Schulze et al., 2018; Conway et al., 2021). This allows the study of more established and mature circuits and brain regions with excellent resolution and relatively unobstructed field of view. Danionella cerebrum reach sexual maturity at 6–8 weeks, and spawn in clutches of around 12 eggs per female (Rajan et al., 2022). *Danionella* can be raised and maintained similarly to zebrafish, and their embryos develop at similar rates, making comparative studies between zebrafish larvae and *Danionella* adults straightforward, and avoiding additional investment in equipment (Penalva et al., 2018). Transgenesis in *Danionella* uses the same techniques applicable to zebrafish and other teleosts. Transgene insertion using Tol2 to express GCaMP6f and CRISPR/Cas9 mutagenesis of the *tyr* gene are both demonstrated successfully in Schulze et al. (2018). While the same tools for zebrafish transgene insertion can be used with *Danionella*, CRISPR gRNAs must be designed to be specific to available sequence for *Danionella* genes (Schulze et al., 2018; Kadobianskyi et al., 2019). Currently, no demonstration of genetic mutation of human-disease associated genes has been published.

Behavior

Danionella exhibit measurable social behavior and socially reinforced learning and have an additional surprising characteristic: males of both *D. translucida* and *D. dracula* species can vocalize. These vocalizations are short multi-pulse bursts and made primarily during displays of male-directed aggression (Penalva et al., 2018; Schulze et al., 2018; Tatarsky et al., 2021). Vocalization is not known to occur in zebrafish, so study of vocalization represents new possibilities in neurobiological research with this model. The ability to pair behavior with adult imaging, as discussed previously, is a huge strength of the fish systems presented here. Adult Danionella can be mounted and imaged in agarose as long as their gills remain exposed, unlike zebrafish larvae which do not yet depend on their gills for oxygenation (Schulze et al., 2018). This opens the possibility of live-imaging of neuronal calcium indicators in vocalizing fish presented with a visual cue of an intruding male, an exciting new way to assess behavioral circuits and sex differences in the brain (as females do not vocalize).

Sub-Cellular and Cellular Imaging

Danionella have immense potential for visualization of cellular and sub-cellular structures at high resolution within the brain of an adult animal. Though efforts have only begun recently, mosaic expression of GFP driven by the pan-neuronal promotor *elavl3* has been demonstrated to visualize sparsely labeled neurons in 5 days post-fertilization larval *D. cerebrum* using 2-photon microscopy. A region of the brain of a living adult *D. cerebrum* has been imaged from its dorsal surface to a depth of 376 μm, corresponding to the ventral surface (Penalva et al., 2018), and the brain vasculature of an adult *D. dracula* has been imaged to a depth of ∼800 μm using 2 and 3-photon microscopy (Akbari et al., 2021). These studies combined indicate that whole-brain live imaging is achievable in an adult vertebrate species.

The lack of a skull roof also means that these fish are likely amenable to both LSFM and confocal microscopy for shallow to mid-range depths, though neither technique has been thoroughly explored in *Danionella* species. It is unknown how well these animals tolerate long-term imaging, or whether they could be successfully intubated for long-term experiments. The ability to image fast events such as calcium dynamics, as well as longer-term events such as neurodegenerative processes, glia-neuron interactions, or neuronal development would increase their attractiveness as a model. Though additional work remains to establish protocols and best practices for imaging in *Danionella* species, the ease of imaging *Danionella* at both the larval and adult stages enables previously impossible or impractical longitudinal studies of development, aging, and neurological disease. This underscores their importance as an emerging vertebrate model.

Zebra Finch

Background

A well-established animal model with largely unexplored imaging potential is the zebra finch, *T. guttata*. Zebra finches are a songbird species from Australia that are easy to breed and reach sexual maturity in 70–80 days, making them one of the fastest maturing bird species. The greatest potential of the zebra finch for modeling neurobiology is its song: Finches and other songbirds reflect human speech patterns in their capacity to learn, recall, and perform complex songs. The circuits directing songbird vocalization have been used to investigate the neurobiology behind practice and performance, sexual differences in vocal learning, motor control of speech, and the interplay between motor control and vocal learning.

Behavior

Juvenile male finches learn their song from a male tutor, typically the father, and their vocal learning shares much in common with

human vocal learning. The subsong produced by young zebra finch parallels human infant "babbling," where both generate random syllables to dial in the correct notes that will eventually form their adult song or speech (Aronov et al., 2008). The adult song is highly stereotyped, though differences between individuals exist, making it easy to quantify changes in song pattern (Mello, 2014).

Many neurological diseases such as Huntington's, Parkinson's, and Fragile X syndrome result in changes in speech. Yet, the underlying mechanisms behind loss of normal speech patterns in neurological disease cannot be truly mirrored by any of the dominant research organisms outside of zebra finch. Rodents can vocalize, including audible squeaks and ultrasonic vocalizations (USVs), but are not known to imitate sounds or learn vocalizations. This can lead to unclear results when studying genes known to affect vocal learning, such as *Foxp2*. Global *Foxp2* knockdown has been accomplished in mouse, and area-specific *Foxp2* knockdown has been performed in mouse and zebra finch (Haesler et al., 2007; French and Fisher, 2014; Norton et al., 2019; Urbanus et al., 2020). In mice, results for whether USVs were affected in *Foxp2* global heterozygous knockout pups was inconsistent, and region-specific knockouts in the cortex, striatum, or cerebellum did not produce a deficit in USVs (French and Fisher, 2014; Urbanus et al., 2020). In zebra finch, region-specific knockdown of *Foxp2* using lentiviral shRNA in a region known to be important for song production (Area X) impaired the ability of young male finches to copy their tutor's song (Haesler et al., 2007). This defect in song learning reflects the developmental vocal dyspraxia shown by humans with mutation of FoxP2 (Lai et al., 2001).

Genetics and Disease Models

Currently, the relative lack of genetic tools in birds has been a hinderance for their use as models of neurological disease. Great efforts have been made to interrogate why traditional virus-mediated transfection and primordial germ cell (PGC) editing are more difficult in zebra finch compared to other birds like the chicken. Recent studies have shown that divergence in the low-density lipoprotein receptor of zebra finches is one of the factors behind inefficient lentiviral transfection, as it is the main receptor for the VSV G protein component of the lentiviral system (Velho et al., 2021). Significant differences exist between zebra finch and chicken PGCs, including different distribution and developmental gene-expression programs, which may further underly difficulties in transgenesis (Jung et al., 2019). Alternative strategies, such as electroporation and lentiviral injection into the brain have been successful at producing tissue-targeted zebra finch knockdowns and transgenics (Haesler et al., 2007; Ahmadiantehrani and London, 2017; Norton et al., 2019).

Germ line transgenesis of zebra finches have been achieved, but with low-efficiency (Agate et al., 2009; Abe et al., 2015; Liu et al., 2015). Recent reports have improved efficacy of transgenesis by direct lentiviral infection of cultured PGCs (Gessara et al., 2021), resulting in transgenic songbirds expressing eGFP in various tissues including neurons in the song circuits. CRISPR/Cas9 editing has been achieved in quail and chicken, and adenovirus-mediated CRISPR/Cas9 delivery has been used to edit zebra finch PGCs, but no adult mutant has yet been generated in zebra finch (Lee et al., 2019; Xu et al., 2020; Jung et al., 2021). Successful use of CRISPR/Cas9 in zebra finch would be a great leap forward in the tractability of this model for the study of neurodegenerative diseases.

Even with the current difficulty of transgenesis, a transgenic models for Huntington's disease has been produced (Liu et al., 2015). Parkinson's has also been modeled in the finch through reduction of presynaptic dopamine input to Area X of the finch brain using 6-hydroxydopamine injection (Miller et al., 2015). HD model finches had severe defects in song learning and adult song maintenance, as well as other pathology associated with human HD-like loss of striatal neurons and HTT protein aggregates (Liu et al., 2015). The dopamine-reduction PD model resulted in changes to normal vocal variability (Miller et al., 2015).

Microscopy in the Zebra Finch Model

Current studies in finch mostly rely on electrophysiology and examination of the song pattern to understand how changes in neuronal function led to changes in song. Most imaging studies in finches are done in fixed tissue using confocal or widefield detection, and fluorescent markers or antibodies. A host of validated antibodies and their localization in the brain can be found at the Zebra Finch Expression Brain Atlas.[2] Recently, both expansion microscopy and LSFM have been used to image neurons and vasculature in the zebrafish brain, though use of LSFM in adult finch brains requires tissue clearing to reduce scattering. There remain some hurdles with tissue clearing in finch since existing clearing protocols have been primarily optimized for murine brain tissue. Rocha et al. (2019) report successful use of iDISCO+ and CUBIC clearing protocols in zebra finch adult brains and were able to visualize anatomical landmarks and the song systems of the finch *via* LSFM. Düring et al. (2019) have also used Expansion Microscopy to resolve individual neurons and their dendritic spines within the zebra finch brain using LSFM.

Fixed and sectioned tissues, rather than entire brains, still dominate studies of zebra finch song system projections. Though not a new technique in itself, organotypic brain slices have been recently used to image the finch brain at a higher resolution, including functional imaging using calcium sensors (Shen et al., 2017). The use of brain slices allows better access to tissues for specific labeling of structures and may prove useful for introducing other biosensors or looking at glial function. The initial use of biosensors and optogenetic tools has been successful in the zebra finch *in vivo*. Optogenetic control of song circuits using channel rhodopsin (hChR2-YFP) *in vivo* has been used to test mechanisms controlling song patterning and learning (Roberts et al., 2012). 2-photon microscopy with an installed cranial window has been used with head-fixed male zebra finches to record GECIs during female-directed song

[2]http://www.zebrafinchatlas.org/

(Picardo et al., 2016), and to look at the differential response of GECI expressing high vocal center neurons and astrocytes during playback of the bird's own song (Graber et al., 2013). Head-fixed 2-photon imaging has been successful in generating some higher-resolution data as well, notably to measure dendritic spine size in the high vocal center before and after a pupil bird listens to a tutor bird sing (Roberts et al., 2012). Further work to expand the toolkit for *in vivo* imaging with multi-photon and cranial window or thinned skull techniques would enhance the zebra finch's potential as a major brain disease model. Additional ways to differentially label multiple cell types within the living zebra finch could also expand our understanding of how supporting cells like glia contribute to successful vocal learning and memory. Imaging at the level of cellular resolution can help to further refine our understanding projections within the song system, and how neurological disease processes can lead to changes in vocal learning and speech function.

Other Emerging Models

"For such a large number of problems there will be some animal of choice, or a few such animals, on which it can be most conveniently studied." Krogh et al. (1929)

The models listed above are a limited selection of useful models that have already demonstrated great promise for neurobiological disease research, but this list is not comprehensive and does not represent the full landscape of all established and emerging model systems in neuroscience. Invertebrate models will continue to be important players in understanding human disease due to their simpler nervous systems and their comparatively scaled-down number of genes and transcripts. C. elegans and Drosophila have been immensely productive models for neuroscience for decades (Kimble and Nüsslein-Volhard, 2022). Both animals have detailed maps of their nervous systems available, and well-understood circuits that can be optogenetically probed thanks to the ease of genetic manipulations in both species (White et al., 1986; Schroll et al., 2006; Zimmermann et al., 2009; Leifer et al., 2011; Inagaki et al., 2014; Shipley et al., 2014; Scheffer et al., 2020). Many fundamental neuronal genes have been discovered in *C. elegans* and *Drosophila*. In Drosophila, these include the important neurodevelopmental genes *hedgehog* and *notch*, as well as the first identified learning mutants *dunce* (cAMP phosphodiesterase) and *rutabaga* (adenylate cyclase) (Dudai et al., 1976; Lehmann et al., 1981; Jürgens et al., 1984; Livingstone et al., 1984; Wieschaus et al., 1984; Fuccillo et al., 2006; Louvi and Artavanis-Tsakonas, 2006; Le Gall et al., 2008; de Bivort et al., 2009; Bellen et al., 2010). *C. elegans* research led to the discovery of the axon guidance protein netrin (UNC-6 and its receptors UNC-5 and UNC-40) (Hedgecock et al., 1990; Leung-Hagesteijn et al., 1992; Leonardo et al., 1997), and the identification of the circuits controlling touch sensation (Chalfie et al., 1985) among other important work. This foundation of established knowledge of circuits and molecular machinery in the nervous system of *Drosophila* and *C. elegans* now allows for very precise questions to be asked about complex circuit function, learning and memory, and *Drosophila*'s smaller size allows for whole-brain live imaging during behavior (Lemon et al., 2015; Huang et al., 2018; Aimon et al., 2019; Mann et al., 2021).

Invertebrates have the potential to be much more than vessels for cell biological studies as they possess useful behavioral traits that can inform the study of genes in neurobiological disease. To continue to use classical invertebrates as an example: *C. elegans* sleep, react to attractive and repulsive cues, and search for food and mates and *Drosophila* perform elaborate courtship dances, show aggression to compete for resources, and are capable of olfactory and visual learning. Since *C. elegans* and *Drosophila* are both members of the same group, Ecdysozoa, an additional argument can be made for expanding into other invertebrate models to add additional breadth to comparative studies. Emerging invertebrate models include cephalopods, hydra, chordates, rotifers, and planaria. These models share a commonality of maintained regenerative capacity throughout life and have gained traction as potential models of aging and mechanisms of regeneration (Austad, 2009; Murthy and Ram, 2015; Voskoboynik and Weissman, 2015; Gribble and Mark Welch, 2017). Both aging and regeneration are of broad interest for neurodegenerative disease: to understand and prevent the risk of neurodegenerative disease associated with aging (Hou et al., 2019; Azam et al., 2021), and to help recover cognitive function in patients suffering from neurodegeneration.

There are also alternative vertebrate models of interest in aging and regeneration (**Table 1**). Since lifespan varies broadly among organisms, it is possible to select animals that age at different rates to investigate the impacts of slower or faster aging on neurobiological processes. The African turquoise killifish, *Notobranchius furzeri*, is a short-lived (∼4–8 months) vertebrate that reaches maturity in as little as 2 weeks and displays aging-associated disease phenotypes (Harel and Brunet, 2015; Russell et al., 2017; Vrtílek et al., 2018). Its lifespan is considerably shorter than other vertebrates used to study aging, such as mouse and zebrafish (3.5- and 4-year maximal lifespans, respectively), greatly accelerating the pace at which experiments can be performed.

Multiple vertebrates are capable of at least some level of regeneration or increased neuroplasticity. Ground squirrels and birds are known to go through seasonal remodeling of their brains. Ground squirrels reversibly remodel their retinas and associated synapses during winter torpor (Merriman et al., 2016) while food-storing birds show seasonal changes in hippocampus size and neuronal recruitment into the hippocampus (Sherry and MacDougall-Shackleton, 2015; Pozner et al., 2018). Amphibians like *Xenopus* and axolotls are also highly regenerative, however, unlike *Xenopus*, axolotls and other salamanders retain their neuroregenerative abilities after metamorphosis (Filoni et al., 1977; Bosco, 1979; Joven et al., 2019; Phipps et al., 2020). Comparative analysis of genes involved in regenerative processes across species, and between regenerative and non-regenerative species, will help us understand the pathways involved in regeneration and provide potential druggable targets and new therapeutics for neurodegenerative disease, stroke, and traumatic injury.

Many of the models discussed in this section have not yet been used in imaging studies. Building the reagents and protocols necessary for fixed tissue imaging, let alone live imaging, is non-trivial and not every model will be suited for microscopy approaches. However, successful strategies for tackling stubborn transgenesis or imaging in one model inform approaches for how to solve similar problems in subsequent models. For example, both axolotls and *Xenopus* contain the same three types of pigment as zebrafish (Masselink and Tanaka, 2021). Indeed, albino strains of both *Xenopus* and Axolotl already exist, but retain some pigmentation (Frost and Malacinski, 1979; Woodcock et al., 2017; Fukuzawa, 2021). Forward genetic screens to create pigmentless Axolotls would be impossible, but since pigment-producing genes have been identified and targeted in zebrafish, CRISPR/cas9 mutagenesis could be used to edit these genes in amphibians to produce transparent models more suited to imaging A *Xenopus* mutant lacking yellow pigment has been recently generated, and further targeting of known pigment-related genes could lead to the production of completely pigmentless amphibians (Nakajima et al., 2021).

DISCUSSION

Modeling neurodegenerative diseases largely falls into the categories of "modeling known components," such as genes and pathologies, and "uncovering unknown etiologies of disease"– these could be genes, cells, tissues, or extracellular factors involved. The introduction of new model organisms into the field of neurodegenerative disease research could help answer questions in both categories. Comparative studies of how different species react to the pathological and genetic drivers of neurodegenerative disease can help us understand the pathways that mediate disease, discover new genes involved, and develop potential therapeutics.

For a model to be widely utilized, it must fill a required niche. The non-mammalian vertebrate models discussed in this review all complement existing mammalian research and fill in the gaps of what cannot be done in mammals or invertebrates. To succeed, the model must also be supported by an enthusiastic and invested community. For example, *C. elegans*, *Drosophila*, and zebrafish have all benefitted greatly from a strong community and wide sharing of resources among labs. It is essential for information on husbandry, basic protocols, genome sequence, and anatomical descriptions to be easily available and disseminated. Therefore model organism databases such as FlyBase, WormBase, and ZFIN serve as irreplaceable resources for researchers working on model organisms. Community advocacy is also an important factor in normalizing the use of new models and advocating for funding. New models often face steep challenges associated with obtaining funding and acceptance of a model's relevance to a research topic.

To push neuroimaging forward in these emerging models, a solid base of genetic tools is needed. A method of genetic editing is needed to create disease-specific models and tag endogenous proteins. CRISPR/cas9 is generally successful in a variety of animals, but as demonstrated in zebra finch, the road to genetic editing is not always straightforward. Imaging of specific neurons or areas of the brain *in vivo* requires the development of techniques to generate transgenic animals and the identification of tissue-specific promotors to control expression of fluorescent proteins.

To visualize labeled tissues it is useful to generate animals devoid of pigment or develop protocols for installation of cranial windows. Cranial window are an area of active development with newly designed windows for rodent models that are flexible and easier to work with (Cramer et al., 2021). Still the use of animal models that do not require cranial windows is an important biological consideration given the concerns of wound healing responses to the window surgery itself. Imaging technology continues to evolve as well with new infrared laser sources and adaptive optics for imaging deep into specimens, computational optics-based systems that enable smart microscopy to image more selectively, and technical efforts that continue to push the spatial and temporal resolution of modern optical imaging. One important aspect seen in both modern imaging technology and animal model work is the key role of community. As discussed previously, community directly drives animal model research: the strong *Drosophila*, zebrafish, and *C. elegans* communities are great examples of this with their own genetic repositories, data websites, technical newsletters, and research conferences. These communities embrace open access science with free sharing of reagents, methods, and specimens. The imaging community is also rapidly embracing this concept of open access with not only well established open source software such as the widely adopted ImageJ but the increasing trend toward open hardware systems such as OpenSPIM (Pitrone et al., 2013). This open sharing of both the model itself and all the tools utilized not only helps in established models but will aid in the discovery and adoption of new research models of important neuroscience problems. Modern neuroscience needs a range of models and tools to solve its mysteries and open science greatly drives this. The tandem of imaging and animal models exemplifies this community approach, and this will continue to drive great innovation in both biological systems and the tools used to study them.

AUTHOR CONTRIBUTIONS

The project was first conceptualized by EMH. All authors wrote the manuscript, contributed to the article, and approved the submitted version.

FUNDING

This work was funded by a Morgridge Institute for Research postdoctoral fellowship to EMH. We also acknowledge funding from NIH P30-AG534255 UWADRCDP (TKU and KWE), NIH R01AG070973 (TKU), and NIH R01HL142752-03S1 (TKU).

ACKNOWLEDGMENTS

We would like to acknowledge all the important work that we were not able to include in this review.

REFERENCES

Abe, K., Matsui, S., and Watanabe, D. (2015). Transgenic songbirds with suppressed or enhanced activity of CREB transcription factor. *Proc. Natl. Acad. Sci. U.S.A.* 112, 7599–7604. doi: 10.1073/pnas.1413484112

Abi-Haidar, D., and Olivier, T. (2009). Confocal reflectance and two-photon microscopy studies of a songbird skull for preparation of transcranial imaging. *J. Biomed. Opt.* 14:034038. doi: 10.1117/1.3155522

Adams, M. M., and Kafaligonul, H. (2018). Zebrafish-a model organism for studying the neurobiological mechanisms underlying cognitive brain aging and use of potential interventions. *Front. Cell Dev. Biol.* 6:135. doi: 10.3389/fcell.2018.00135

Agate, R. J., Scott, B. B., Haripal, B., Lois, C., and Nottebohm, F. (2009). Transgenic songbirds offer an opportunity to develop a genetic model for vocal learning. *Proc. Natl. Acad. Sci. U.S.A.* 106, 17963–17967. doi: 10.1073/pnas.0909139106

Ahmadiantehrani, S., and London, S. E. (2017). A reliable and flexible gene manipulation strategy in posthatch zebra finch brain. *Sci. Rep.* 7:43244. doi: 10.1038/srep43244

Ahrens, M. B., Orger, M. B., Robson, D. N., Li, J. M., and Keller, P. J. (2013). Whole-brain functional imaging at cellular resolution using light-sheet microscopy. *Nat. Methods* 10, 413–420. doi: 10.1038/nmeth.2434

Aimon, S., Katsuki, T., Jia, T., Grosenick, L., Broxton, M., Deisseroth, K., et al. (2019). Fast near-whole-brain imaging in adult *Drosophila* during responses to stimuli and behavior. *PLoS Biol.* 17:e2006732. doi: 10.1371/journal.pbio.2006732

Akbari, N., Tatarsky, R. L., Bass, A. H., and Xu, C. (2021). Whole-brain optical access in small adult vertebrates with two- and three-photon microscopy. *bioRxiv* [Preprint] bioRxiv: 2021.12.09.471956, doi: 10.1101/2021.12.09.471956

Amos, W. B., and White, J. G. (2003). How the confocal laser scanning microscope entered biological research. *Biol. Cell* 95, 335–342. doi: 10.1016/s0248-4900(03)00078-9

Aronov, D., Andalman, A. S., and Fee, M. S. (2008). A specialized forebrain circuit for vocal babbling in the juvenile songbird. *Science* 320, 630–634. doi: 10.1126/science.1155140

Asakawa, K., and Kawakami, K. (2010). A transgenic zebrafish for monitoring *in vivo* microtubule structures. *Dev. Dyn.* 239, 2695–2699. doi: 10.1002/dvdy.22400

Auer, T. O., Xiao, T., Bercier, V., Gebhardt, C., Duroure, K., Concordet, J.-P., et al. (2015). Deletion of a kinesin I motor unmasks a mechanism of homeostatic branching control by neurotrophin-3. *Elife* 4, e05061. doi: 10.7554/eLife.05061

Austad, S. N. (2009). Is there a role for new invertebrate models for aging research? *J. Gerontol. A Biol. Sci. Med. Sci.* 64, 192–194. doi: 10.1093/gerona/gln059

Avila, R. L., Tevlin, B. R., Lees, J. P. B., Inouye, H., and Kirschner, D. A. (2007). Myelin structure and composition in zebrafish. *Neurochem. Res.* 32, 197–209. doi: 10.1007/s11064-006-9136-5

Azam, S., Haque, M. E., Balakrishnan, R., Kim, I.-S., and Choi, D.-K. (2021). The ageing brain: molecular and cellular basis of neurodegeneration. *Front. Cell Dev. Biol.* 9:683459. doi: 10.3389/fcell.2021.683459

Bacskai, B. J., Kajdasz, S. T., Christie, R. H., Carter, C., Games, D., Seubert, P., et al. (2001). Imaging of amyloid-beta deposits in brains of living mice permits direct observation of clearance of plaques with immunotherapy. *Nat. Med.* 7, 369–372. doi: 10.1038/85525

Bae, Y.-K., Kani, S., Shimizu, T., Tanabe, K., Nojima, H., Kimura, Y., et al. (2009). Anatomy of zebrafish cerebellum and screen for mutations affecting its development. *Dev. Biol.* 330, 406–426. doi: 10.1016/j.ydbio.2009.04.013

Bando, Y., Grimm, C., Cornejo, V. H., and Yuste, R. (2019). Genetic voltage indicators. *BMC Biol.* 17:71. doi: 10.1186/s12915-019-0682-0

Banote, R. K., Chebli, J., Şatır, T. M., Varshney, G. K., Camacho, R., Ledin, J., et al. (2020). Amyloid precursor protein-b facilitates cell adhesion during early development in zebrafish. *Sci. Rep.* 10:10127. doi: 10.1038/s41598-020-66584-8

Bellen, H. J., Tong, C., and Tsuda, H. (2010). 100 years of *Drosophila* research and its impact on vertebrate neuroscience: a history lesson for the future. *Nat. Rev. Neurosci.* 11, 514–522. doi: 10.1038/nrn2839

Bhattarai, P., Cosacak, M. I., Mashkaryan, V., Demir, S., Popova, S. D., Govindarajan, N., et al. (2020). Neuron-glia interaction through Serotonin-BDNF-NGFR axis enables regenerative neurogenesis in Alzheimer's model of adult zebrafish brain. *PLoS Biol.* 18:e3000585. doi: 10.1371/journal.pbio.3000585

Bhattarai, P., Thomas, A. K., Cosacak, M. I., Papadimitriou, C., Mashkaryan, V., Froc, C., et al. (2016). IL4/STAT6 signaling activates neural stem cell proliferation and neurogenesis upon Amyloid-β42 aggregation in adult zebrafish brain. *Cell Rep.* 17, 941–948. doi: 10.1016/j.celrep.2016.09.075

Bhattarai, P., Thomas, A. K., Zhang, Y., and Kizil, C. (2017). The effects of aging on Amyloid-β42-induced neurodegeneration and regeneration in adult zebrafish brain. *Neurogenesis (Austin)* 4:e1322666. doi: 10.1080/23262133.2017.1322666

Bianco, I. H., and Engert, F. (2015). Visuomotor transformations underlying hunting behavior in zebrafish. *Curr. Biol.* 25, 831–846. doi: 10.1016/j.cub.2015.01.042

Borst, K., Schwabenland, M., and Prinz, M. (2019). Microglia metabolism in health and disease. *Neurochem. Int.* 130:104331. doi: 10.1016/j.neuint.2018.11.006

Bosco, L. (1979). Expression of regenerative capacity of caudal spinal cord during the larval development of *Xenopus laevis*. *Acta Embryol. Exp.* 3, 275–285.

Botcherby, E. J., Juskaitis, R., Booth, M. J., and Wilson, T. (2007). Aberration-free optical refocusing in high numerical aperture microscopy. *Opt. Lett.* 32, 2007–2009. doi: 10.1364/ol.32.002007

Böttcher, C., Schlickeiser, S., Sneeboer, M. A. M., Kunkel, D., Knop, A., Paza, E., et al. (2019). Human microglia regional heterogeneity and phenotypes determined by multiplexed single-cell mass cytometry. *Nat. Neurosci.* 22, 78–90. doi: 10.1038/s41593-018-0290-2

Bouchard, M. B., Voleti, V., Mendes, C. S., Lacefield, C., Grueber, W. B., Mann, R. S., et al. (2015). Swept confocally-aligned planar excitation (SCAPE) microscopy for high speed volumetric imaging of behaving organisms. *Nat. Photonics* 9, 113–119. doi: 10.1038/nphoton.2014.323

Braun, M., and Iliff, J. J. (2020). "Chapter Fifteen – The impact of neurovascular, blood-brain barrier, and glymphatic dysfunction in neurodegenerative and metabolic diseases," in *International Review of Neurobiology*, eds G. Söderbom, R. Esterline, J. Oscarsson, and M. P. Mattson (Cambridge, MA: Academic Press), 413–436. doi: 10.1016/bs.irn.2020.02.006

Britz, R., Conway, K. W., and Rüber, L. (2021). The emerging vertebrate model species for neurophysiological studies is *Danionella cerebrum*, new species (Teleostei: Cyprinidae). *Sci. Rep.* 11:18942. doi: 10.1038/s41598-021-97600-0

Bruzzone, M., Chiarello, E., Albanesi, M., Miletto Petrazzini, M. E., Megighian, A., Lodovichi, C., et al. (2021). Whole brain functional recordings at cellular resolution in zebrafish larvae with 3D scanning multiphoton microscopy. *Sci. Rep.* 11:11048. doi: 10.1038/s41598-021-90335-y

Campbell, P. D., Shen, K., Sapio, M. R., Glenn, T. D., Talbot, W. S., and Marlow, F. L. (2014). Unique function of Kinesin Kif5A in localization of mitochondria in axons. *J. Neurosci.* 34, 14717–14732. doi: 10.1523/JNEUROSCI.2770-14.2014

Castellano-Muñoz, M., Peng, A. W., Salles, F. T., and Ricci, A. J. (2012). Swept field laser confocal microscopy for enhanced spatial and temporal resolution in live-cell imaging. *Microsc. Microanal.* 18, 753–760. doi: 10.1017/S1431927612000542

Castranova, D., Samasa, B., Venero Galanternik, M., Jung, H. M., Pham, V. N., and Weinstein, B. M. (2021). Live imaging of intracranial lymphatics in the zebrafish. *Circ. Res.* 128, 42–58. doi: 10.1161/CIRCRESAHA.120.317372

Chalfie, M. (2009). GFP: lighting up life. *Proc. Natl. Acad. Sci. U.S.A.* 106, 10073–10080. doi: 10.1073/pnas.0904061106

Chalfie, M., Sulston, J. E., White, J. G., Southgate, E., Thomson, J. N., and Brenner, S. (1985). The neural circuit for touch sensitivity in *Caenorhabditis elegans*. *J. Neurosci.* 5, 956–964. doi: 10.1523/JNEUROSCI.05-04-00956.1985

Chang, B.-J., Kittisopikul, M., Dean, K. M., Roudot, P., Welf, E. S., and Fiolka, R. (2019). Universal light-sheet generation with field synthesis. *Nat. Methods* 16, 235–238. doi: 10.1038/s41592-019-0327-9

Chen, B.-C., Legant, W. R., Wang, K., Shao, L., Milkie, D. E., Davidson, M. W., et al. (2014). Lattice light-sheet microscopy: imaging molecules to embryos at high spatiotemporal resolution. *Science* 346:1257998. doi: 10.1126/science.1257998

Chen, F., Tillberg, P. W., and Boyden, E. S. (2015). Expansion microscopy. *Science* 347, 543–548. doi: 10.1126/science.1260088

Chen, J. J., Salat, D. H., and Rosas, H. D. (2012). Complex relationships between cerebral blood flow and brain atrophy in early Huntington's disease. *Neuroimage* 59, 1043–1051. doi: 10.1016/j.neuroimage.2011.08.112

Chen, J., Poskanzer, K. E., Freeman, M. R., and Monk, K. R. (2020). Live-imaging of astrocyte morphogenesis and function in zebrafish neural circuits. *Nat. Neurosci.* 23, 1297–1306. doi: 10.1038/s41593-020-0703-x

Chen, Q., Jiang, L., Li, C., Hu, D., Bu, J.-W., Cai, D., et al. (2012). Haemodynamics-driven developmental pruning of brain vasculature in zebrafish. *PLoS Biol.* 10:e1001374. doi: 10.1371/journal.pbio.1001374

Choquet, D., Sainlos, M., and Sibarita, J.-B. (2021). Advanced imaging and labelling methods to decipher brain cell organization and function. *Nat. Rev. Neurosci.* 22, 237–255. doi: 10.1038/s41583-021-00441-z

Christie, R. H., Bacskai, B. J., Zipfel, W. R., Williams, R. M., Kajdasz, S. T., Webb, W. W., et al. (2001). Growth arrest of individual senile plaques in a model of Alzheimer's disease observed by *in vivo* multiphoton microscopy. *J. Neurosci.* 21, 858–864. doi: 10.1523/JNEUROSCI.21-03-00858.2001

Cieri, D., Vicario, M., Giacomello, M., Vallese, F., Filadi, R., Wagner, T., et al. (2018). SPLICS: a split green fluorescent protein-based contact site sensor for narrow and wide heterotypic organelle juxtaposition. *Cell Death Differ.* 25, 1131–1145. doi: 10.1038/s41418-017-0033-z

Clark, B. S., Winter, M., Cohen, A. R., and Link, B. A. (2011). Generation of Rab-based transgenic lines for *in vivo* studies of endosome biology in zebrafish. *Dev. Dyn.* 240, 2452–2465. doi: 10.1002/dvdy.22758

Cong, L., Wang, Z., Chai, Y., Hang, W., Shang, C., Yang, W., et al. (2017). Rapid whole brain imaging of neural activity in freely behaving larval zebrafish (*Danio rerio*). *Elife* 6:e28158. doi: 10.7554/eLife.28158

Conway, K. W., Kubicek, K. M., and Britz, R. (2021). Extreme evolutionary shifts in developmental timing establish the miniature *Danionella* as a novel model in the neurosciences. *Dev. Dyn.* 250, 601–611. doi: 10.1002/dvdy.280

Cramer, S. W., Carter, R. E., Aronson, J. D., Kodandaramaiah, S. B., Ebner, T. J., and Chen, C. C. (2021). Through the looking glass: a review of cranial window technology for optical access to the brain. *J. Neurosci. Methods* 354:109100. doi: 10.1016/j.jneumeth.2021.109100

Culley, S., Tosheva, K. L., Matos Pereira, P., and Henriques, R. (2018). SRRF: universal live-cell super-resolution microscopy. *Int. J. Biochem. Cell Biol.* 101, 74–79. doi: 10.1016/j.biocel.2018.05.014

Daetwyler, S., Günther, U., Modes, C. D., Harrington, K., and Huisken, J. (2019). Multi-sample SPIM image acquisition, processing and analysis of vascular growth in zebrafish. *Development* 146:dev173757. doi: 10.1242/dev.173757

Datta, R., Heaster, T. M., Sharick, J. T., Gillette, A. A., and Skala, M. C. (2020). Fluorescence lifetime imaging microscopy: fundamentals and advances in instrumentation, analysis, and applications. *J. Biomed. Opt.* 25, 1–43. doi: 10.1117/1.JBO.25.7.071203

Davalos, D., Grutzendler, J., Yang, G., Kim, J. V., Zuo, Y., Jung, S., et al. (2005). ATP mediates rapid microglial response to local brain injury *in vivo*. *Nat. Neurosci.* 8, 752–758. doi: 10.1038/nn1472

Davies, C. L., Patir, A., and McColl, B. W. (2019). Myeloid cell and transcriptome signatures associated with inflammation resolution in a model of self-limiting acute brain inflammation. *Front. Immunol.* 10:1048. doi: 10.3389/fimmu.2019.01048

Dawson, T. M., Golde, T. E., and Lagier-Tourenne, C. (2018). Animal models of neurodegenerative diseases. *Nat. Neurosci.* 21, 1370–1379.

de Bivort, B. L., Guo, H.-F., and Zhong, Y. (2009). Notch signaling is required for activity-dependent synaptic plasticity at the *Drosophila* neuromuscular junction. *J. Neurogenet.* 23, 395–404. doi: 10.3109/01677060902878481

Denk, W., and Svoboda, K. (1997). Photon upmanship: why multiphoton imaging is more than a gimmick. *Neuron* 18, 351–357. doi: 10.1016/s0896-6273(00)81237-4

Denk, W., Strickler, J. H., and Webb, W. W. (1990). Two-photon laser scanning fluorescence microscopy. *Science* 248, 73–76. doi: 10.1126/science.2321027

Don, E. K., Formella, I., Badrock, A. P., Hall, T. E., Morsch, M., Hortle, E., et al. (2017). A Tol2 gateway-compatible toolbox for the study of the nervous system and neurodegenerative disease. *Zebrafish* 14, 69–72. doi: 10.1089/zeb.2016.1321

Drerup, C. M., and Nechiporuk, A. V. (2013). JNK-interacting protein 3 mediates the retrograde transport of activated c-Jun N-terminal kinase and lysosomes. *PLoS Genet.* 9:e1003303. doi: 10.1371/journal.pgen.1003303

Drerup, C. M., Herbert, A. L., Monk, K. R., and Nechiporuk, A. V. (2017). Regulation of mitochondria-dynactin interaction and mitochondrial retrograde transport in axons. *Elife* 6:e22234. doi: 10.7554/eLife.22234

Driever, W., Solnica-Krezel, L., Schier, A. F., Neuhauss, S. C., Malicki, J., Stemple, D. L., et al. (1996). A genetic screen for mutations affecting embryogenesis in zebrafish. *Development* 123, 37–46. doi: 10.1242/dev.123.1.37

Dubey, J., Ratnakaran, N., and Koushika, S. P. (2015). Neurodegeneration and microtubule dynamics: death by a thousand cuts. *Front. Cell. Neurosci.* 9:343. doi: 10.3389/fncel.2015.00343

Dudai, Y., Jan, Y. N., Byers, D., Quinn, W. G., and Benzer, S. (1976). dunce, a mutant of *Drosophila* deficient in learning. *Proc. Natl. Acad. Sci. U.S.A.* 73, 1684–1688. doi: 10.1073/pnas.73.5.1684

Dunsby, C. (2008). Optically sectioned imaging by oblique plane microscopy. *Opt. Express* 16, 20306–20316. doi: 10.1364/oe.16.020306

Düring, D. N., Rocha, M. D., Dittrich, F., Gahr, M., and Hahnloser, R. H. R. (2019). Expansion light sheet microscopy resolves subcellular structures in large portions of the songbird Brain. *Front. Neuroanat.* 13:2. doi: 10.3389/fnana.2019.00002

Emmons, S. W. (2015). The beginning of connectomics: a commentary on White et al. (1986) "The structure of the nervous system of the nematode *Caenorhabditis elegans*.". *Philos. Trans. R. Soc. Lond. B Biol. Sci.* 370:20140309. doi: 10.1098/rstb.2014.0309

Erdogan, B., Ebbert, P. T., and Lowery, L. A. (2016). Using Xenopus laevis retinal and spinal neurons to study mechanisms of axon guidance *in vivo* and *in vitro*. *Semin. Cell Dev. Biol.* 51, 64–72. doi: 10.1016/j.semcdb.2016.02.003

Fadero, T. C., Gerbich, T. M., Rana, K., Suzuki, A., DiSalvo, M., Schaefer, K. N., et al. (2018). LITE microscopy: tilted light-sheet excitation of model organisms offers high resolution and low photobleaching. *J. Cell Biol.* 217, 1869–1882. doi: 10.1083/jcb.201710087

Ferrero, G., Mahony, C. B., Dupuis, E., Yvernogeau, L., Di Ruggiero, E., Miserocchi, M., et al. (2018). Embryonic microglia derive from primitive macrophages and are replaced by cmyb-dependent definitive microglia in zebrafish. *Cell Rep.* 24, 130–141. doi: 10.1016/j.celrep.2018.05.066

Filoni, S., Bosco, L., and Carlizzi, C. (1977). La rigenerazione del midollo spinale della coda di larve di *Xenopus laevis* operate negli stadi tardivi. *Atti Accad. Naz. Lincei Cl. Sci. Fis. Mat. Nat. Rend.* 63, 440–446.

Fiolka, R. (2019). Resolution upgrades for light-sheet microscopy. *Nat. Methods* 16, 813–814. doi: 10.1038/s41592-019-0542-4

Fontana, B. D., Mezzomo, N. J., Kalueff, A. V., and Rosemberg, D. B. (2018). The developing utility of zebrafish models of neurological and neuropsychiatric disorders: a critical review. *Exp. Neurol.* 299, 157–171. doi: 10.1016/j.expneurol.2017.10.004

Förster, D., Helmbrecht, T. O., Mearns, D. S., Jordan, L., Mokayes, N., and Baier, H. (2020). Retinotectal circuitry of larval zebrafish is adapted to detection and pursuit of prey. *Elife* 9:e58596. doi: 10.7554/eLife.58596

French, C. A., and Fisher, S. E. (2014). What can mice tell us about Foxp2 function? *Curr. Opin. Neurobiol.* 28, 72–79. doi: 10.1016/j.conb.2014.07.003

Frost, S. K., and Malacinski, G. M. (1979). The developmental genetics of pigment mutants in the *Mexican axolotl*. *Dev. Genet.* 1, 271–294. doi: 10.1002/dvg.1020010402

Fuccillo, M., Joyner, A. L., and Fishell, G. (2006). Morphogen to mitogen: the multiple roles of hedgehog signalling in vertebrate neural development. *Nat. Rev. Neurosci.* 7, 772–783. doi: 10.1038/nrn1990

Füger, P., Hefendehl, J. K., Veeraraghavalu, K., Wendeln, A.-C., Schlosser, C., Obermüller, U., et al. (2017). Microglia turnover with aging and in an Alzheimer's model via long-term *in vivo* single-cell imaging. *Nat. Neurosci.* 20, 1371–1376. doi: 10.1038/nn.4631

Fukuzawa, T. (2021). Periodic albinism of a widely used albino mutant of *Xenopus laevis* caused by deletion of two exons in the Hermansky-Pudlak syndrome type 4 gene. *Genes Cells* 26, 31–39. doi: 10.1111/gtc.12818

Fuseler, J., Jerome, W. G., and Price, R. L. (2018). "Types of confocal instruments: basic principles and advantages and disadvantages," in *Basic Confocal Microscopy*, eds W. G. Jerome and R. L. Price (Cham: Springer International Publishing), 187–213. doi: 10.1007/978-3-319-97454-5_8

Gaze, R. M. (1959). Regeneration of the optic nerve in Xenopus laevis. *Q. J. Exp. Physiol. Cogn. Med. Sci.* 44, 290–308.

Geirsdottir, L., David, E., Keren-Shaul, H., Weiner, A., Bohlen, S. C., Neuber, J., et al. (2019). Cross-species single-cell analysis reveals divergence of the primate microglia program. *Cell* 179, 1609–1622.e16.

Gessara, I., Dittrich, F., Hertel, M., Hildebrand, S., Pfeifer, A., Frankl-Vilches, C., et al. (2021). Highly efficient genome modification of cultured primordial germ

cells with lentiviral vectors to generate transgenic songbirds. *Stem Cell Rep.* 16, 784–796. doi: 10.1016/j.stemcr.2021.02.015

Graber, M. H., Helmchen, F., and Hahnloser, R. H. R. (2013). Activity in a premotor cortical nucleus of zebra finches is locally organized and exhibits auditory selectivity in neurons but not in glia. *PLoS One* 8:e81177. doi: 10.1371/journal.pone.0081177

Gribble, K. E., and Mark Welch, D. B. (2017). Genome-wide transcriptomics of aging in the rotifer *Brachionus manjavacas*, an emerging model system. *BMC Genomics* 18:217. doi: 10.1186/s12864-017-3540-x

Griffiths, V. A., Valera, A. M., Lau, J. Y., Roš, H., Younts, T. J., Marin, B., et al. (2020). Real-time 3D movement correction for two-photon imaging in behaving animals. *Nat. Methods* 17, 741–748. doi: 10.1038/s41592-020-0851-7

Guo, D., Zou, J., Rensing, N., and Wong, M. (2017). *in vivo* two-photon imaging of astrocytes in GFAP-GFP transgenic mice. *PLoS One* 12:e0170005. doi: 10.1371/journal.pone.0170005

Gustafsson, N., Culley, S., Ashdown, G., Owen, D. M., Pereira, P. M., and Henriques, R. (2016). Fast live-cell conventional fluorophore nanoscopy with ImageJ through super-resolution radial fluctuations. *Nat. Commun.* 7:12471.

Haesler, S., Rochefort, C., Georgi, B., Licznerski, P., Osten, P., and Scharff, C. (2007). Incomplete and inaccurate vocal imitation after knockdown of FoxP2 in songbird basal ganglia nucleus Area X. *PLoS Biol.* 5:e321. doi: 10.1371/journal.pbio.0050321

Halloran, M. C., and Kalil, K. (1994). Dynamic behaviors of growth cones extending in the corpus callosum of living cortical brain slices observed with video microscopy. *J. Neurosci.* 14, 2161–2177. doi: 10.1523/JNEUROSCI.14-04-02161.1994

Hamburger, V. (1934). The effects of wing bud extirpation on the development of the central nervous system in chick embryos. *J. Exp. Zool.* 68, 449–494. doi: 10.1002/jez.1400680305

Harel, I., and Brunet, A. (2015). The african turquoise killifish: a model for exploring vertebrate aging and diseases in the fast lane. *Cold Spring Harb. Symp. Quant. Biol.* 80, 275–279. doi: 10.1101/sqb.2015.80.027524

Hartenstein, V., and Giangrande, A. (2018). Connecting the nervous and the immune systems in evolution. *Commun. Biol.* 1:64. doi: 10.1038/s42003-018-0070-2

Haynes, E. M., He, J. H., Jean-Pierre, M., Jarzyna, M., Eliceiri, K. W., Huisken, J., et al. (2021). KLC4 shapes axon arbors during development and mediates adult behavior. *bioRxiv* [Preprint] bioRxiv: 2021.09.26.461872, doi: 10.1101/2021.09.26.461872

He, J., and Huisken, J. (2020). Image quality guided smart rotation improves coverage in microscopy. *Nat. Commun.* 11:150. doi: 10.1038/s41467-019-13821-y

Hedgecock, E. M., Culotti, J. G., and Hall, D. H. (1990). The unc-5, unc-6, and unc-40 genes guide circumferential migrations of pioneer axons and mesodermal cells on the epidermis in *C. elegans*. *Neuron* 4, 61–85. doi: 10.1016/0896-6273(90)90444-k

Herculano-Houzel, S. (2009). The human brain in numbers: a linearly scaled-up primate brain. *Front. Hum. Neurosci.* 3:31. doi: 10.3389/neuro.09.031.2009

Herculano-Houzel, S., Mota, B., and Lent, R. (2006). Cellular scaling rules for rodent brains. *Proc. Natl. Acad. Sci. U.S.A.* 103, 12138–12143. doi: 10.1073/pnas.0604911103

Herrera, K. J., Panier, T., Guggiana-Nilo, D., and Engert, F. (2021). Larval zebrafish use olfactory detection of sodium and chloride to avoid salt water. *Curr. Biol.* 31, 782–793.e3. doi: 10.1016/j.cub.2020.11.051

Hillman, E. M. C., Voleti, V., Li, W., and Yu, H. (2019). Light-sheet microscopy in neuroscience. *Annu. Rev. Neurosci.* 42, 295–313. doi: 10.1146/annurev-neuro-070918-050357

Hinsch, K., and Zupanc, G. K. H. (2007). Generation and long-term persistence of new neurons in the adult zebrafish brain: a quantitative analysis. *Neuroscience* 146, 679–696. doi: 10.1016/j.neuroscience.2007.01.071

Hou, Y., Dan, X., Babbar, M., Wei, Y., Hasselbalch, S. G., Croteau, D. L., et al. (2019). Ageing as a risk factor for neurodegenerative disease. *Nat. Rev. Neurol.* 15, 565–581. doi: 10.1038/s41582-019-0244-7

Howe, K., Clark, M. D., Torroja, C. F., Torrance, J., Berthelot, C., Muffato, M., et al. (2013). The zebrafish reference genome sequence and its relationship to the human genome. *Nature* 496, 498–503. doi: 10.1038/nature12111

Huang, C., Maxey, J. R., Sinha, S., Savall, J., Gong, Y., and Schnitzer, M. J. (2018). Long-term optical brain imaging in live adult fruit flies. *Nat. Commun.* 9:872. doi: 10.1038/s41467-018-02873-1

Huang, K.-H., Rupprecht, P., Frank, T., Kawakami, K., Bouwmeester, T., and Friedrich, R. W. (2020). A virtual reality system to analyze neural activity and behavior in adult zebrafish. *Nat. Methods* 17, 343–351. doi: 10.1038/s41592-020-0759-2

Huang, K.-L., Marcora, E., Pimenova, A. A., Di Narzo, A. F., Kapoor, M., Jin, S. C., et al. (2017). A common haplotype lowers PU.1 expression in myeloid cells and delays onset of Alzheimer's disease. *Nat. Neurosci.* 20, 1052–1061. doi: 10.1038/nn.4587

Hughes, A. N., and Appel, B. (2020). Microglia phagocytose myelin sheaths to modify developmental myelination. *Nat. Neurosci.* 23, 1055–1066. doi: 10.1038/s41593-020-0654-2

Huisken, J., and Stainier, D. Y. R. (2007). Even fluorescence excitation by multidirectional selective plane illumination microscopy (mSPIM). *Opt. Lett.* 32, 2608–2610. doi: 10.1364/ol.32.002608

Huisken, J., Swoger, J., Del Bene, F., Wittbrodt, J., and Stelzer, E. H. K. (2004). Optical sectioning deep inside live embryos by selective plane illumination microscopy. *Science* 305, 1007–1009. doi: 10.1126/science.1100035

Iadecola, C. (2017). The neurovascular unit coming of age: a journey through neurovascular coupling in health and disease. *Neuron* 96, 17–42. doi: 10.1016/j.neuron.2017.07.030

Inagaki, H. K., Jung, Y., Hoopfer, E. D., Wong, A. M., Mishra, N., Lin, J. Y., et al. (2014). Optogenetic control of *Drosophila* using a red-shifted channelrhodopsin reveals experience-dependent influences on courtship. *Nat. Methods* 11, 325–332. doi: 10.1038/nmeth.2765

Ji, N. (2017). Adaptive optical fluorescence microscopy. *Nat. Methods* 14, 374–380. doi: 10.1038/nmeth.4218

Jouary, A., Haudrechy, M., Candelier, R., and Sumbre, G. (2016). A 2D virtual reality system for visual goal-driven navigation in zebrafish larvae. *Sci. Rep.* 6:34015. doi: 10.1038/srep34015

Joven, A., Elewa, A., and Simon, A. (2019). Model systems for regeneration: salamanders. *Development* 146:dev167700. doi: 10.1242/dev.167700

Jung, K. M., Kim, Y. M., Keyte, A. L., Biegler, M. T., Rengaraj, D., Lee, H. J., et al. (2019). Identification and characterization of primordial germ cells in a vocal learning *Neoaves* species, the zebra finch. *FASEB J.* 33, 13825–13836. doi: 10.1096/fj.201900760RR

Jung, K. M., Kim, Y. M., Kim, J. L., and Han, J. Y. (2021). Efficient gene transfer into zebra finch germline-competent stem cells using an adenoviral vector system. *Sci. Rep.* 11:14746. doi: 10.1038/s41598-021-94229-x

Jürgens, G., Wieschaus, E., Nüsslein-Volhard, C., and Kluding, H. (1984). Mutations affecting the pattern of the larval cuticle *in Drosophila melanogaster* : II. Zygotic loci on the third chromosome. *Wilehm Roux Arch. Dev. Biol.* 193, 283–295. doi: 10.1007/BF00848157

Kadobianskyi, M., Schulze, L., Schuelke, M., and Judkewitz, B. (2019). Hybrid genome assembly and annotation of *Danionella translucida*. *Sci. Data* 6:156. doi: 10.1038/s41597-019-0161-z

Kaiser, D. M., Acharya, M., Leighton, P. L. A., Wang, H., Daude, N., Wohlgemuth, S., et al. (2012). Amyloid beta precursor protein and prion protein have a conserved interaction affecting cell adhesion and CNS development. *PLoS One* 7:e51305. doi: 10.1371/journal.pone.0051305

Kalmbach, A. S., and Waters, J. (2012). Brain surface temperature under a craniotomy. *J. Neurophysiol.* 108, 3138–3146. doi: 10.1152/jn.00557.2012

Kawai, H., Arata, N., and Nakayasu, H. (2001). Three-dimensional distribution of astrocytes in zebrafish spinal cord. *Glia* 36, 406–413. doi: 10.1002/glia.1126

Kawakami, K. (2005). Transposon tools and methods in zebrafish. *Dev. Dyn.* 234, 244–254. doi: 10.1002/dvdy.20516

Kawashima, T., Zwart, M. F., Yang, C.-T., Mensh, B. D., and Ahrens, M. B. (2016). The serotonergic system tracks the outcomes of actions to mediate short-term motor learning. *Cell* 167, 933–946.e20. doi: 10.1016/j.cell.2016.09.055

Keifer, J., and Summers, C. H. (2016). Putting the "biology" back into "neurobiology": the strength of diversity in animal model systems for neuroscience research. *Front. Syst. Neurosci.* 10:69. doi: 10.3389/fnsys.2016.00069

Keller, E. T., and Murtha, J. M. (2004). The use of mature zebrafish (*Danio rerio*) as a model for human aging and disease. *Comp. Biochem. Physiol. C Toxicol. Pharmacol.* 138, 335–341. doi: 10.1016/j.cca.2004.04.001

Khakh, B. S., and Sofroniew, M. V. (2015). Diversity of astrocyte functions and phenotypes in neural circuits. *Nat. Neurosci.* 18, 942–952. doi: 10.1038/nn.4043

Kim, D. H., Kim, J., Marques, J. C., Grama, A., Hildebrand, D. G. C., Gu, W., et al. (2017). Pan-neuronal calcium imaging with cellular resolution in freely swimming zebrafish. *Nat. Methods* 14, 1107–1114. doi: 10.1038/nmeth.4429

Kim, J., Wojcik, M., Wang, Y., Moon, S., Zin, E. A., Marnani, N., et al. (2019). Oblique-plane single-molecule localization microscopy for tissues and small intact animals. *Nat. Methods* 16, 853–857. doi: 10.1038/s41592-019-0510-z

Kimble, J., and Nüsslein-Volhard, C. (2022). The great small organisms of developmental genetics: *Caenorhabditis elegans* and *Drosophila melanogaster*. *Dev. Biol.* 485, 93–122. doi: 10.1016/j.ydbio.2022.02.013

Kimmel, C. B. (1993). Patterning the brain of the zebrafish embryo. *Annu. Rev. Neurosci.* 16, 707–732. doi: 10.1146/annurev.ne.16.030193.003423

Kishi, S. (2004). Functional aging and gradual senescence in zebrafish. *Ann. N. Y. Acad. Sci.* 1019, 521–526. doi: 10.1196/annals.1297.097

Krogh, A. (1929). The progress of physiology. *Science* 70, 200–204. doi: 10.1126/science.70.1809.200

Krull, A., Buchholz, T.-O., and Jug, F. (2019). "Noise2void-learning denoising from single noisy images," in *Proceedings of the IEEE/CVF Conference on Computer Vision and Pattern Recognition (openaccess.thecvf.com)*, Long Beach, CA, 2129–2137.

Krzic, U., Gunther, S., Saunders, T. E., Streichan, S. J., and Hufnagel, L. (2012). Multiview light-sheet microscope for rapid in toto imaging. *Nat. Methods* 9, 730–733. doi: 10.1038/nmeth.2064

Kugler, E., Chico, T., and Armitage, P. A. (2020). "Validating Segmentation of the Zebrafish Vasculature," in *Medical Image Understanding and Analysis*, eds Y. Zheng, B. M. Williams, and K. Chen (Cham: Springer International Publishing), 270–281. doi: 10.1016/S1474-4422(16)00102-2

Kugler, E., Snodgrass, R., Bowley, G., Plant, K., Serbanovic-Canic, J., Hamilton, N., et al. (2021). The effect of absent blood flow on the zebrafish cerebral and trunk vasculature. *Vasc. Biol.* 3, 1–16. doi: 10.1530/VB-21-0009

Kwan, K. M., Fujimoto, E., Grabher, C., Mangum, B. D., Hardy, M. E., Campbell, D. S., et al. (2007). The Tol2kit: a multisite gateway-based construction kit for Tol2 transposon transgenesis constructs. *Dev. Dyn.* 236, 3088–3099. doi: 10.1002/dvdy.21343

Lai, C. S., Fisher, S. E., Hurst, J. A., Vargha-Khadem, F., and Monaco, A. P. (2001). A forkhead-domain gene is mutated in a severe speech and language disorder. *Nature* 413, 519–523. doi: 10.1038/35097076

Lawson, N. D., and Weinstein, B. M. (2002). *in vivo* imaging of embryonic vascular development using transgenic zebrafish. *Dev. Biol.* 248, 307–318. doi: 10.1006/dbio.2002.0711

Le Gall, M., De Mattei, C., and Giniger, E. (2008). Molecular separation of two signaling pathways for the receptor. *Notch. Dev. Biol.* 313, 556–567. doi: 10.1016/j.ydbio.2007.10.030

Lee, J., Ma, J., and Lee, K. (2019). Direct delivery of adenoviral CRISPR/Cas9 vector into the blastoderm for generation of targeted gene knockout in quail. *Proc. Natl. Acad. Sci. U.S.A.* 116, 13288–13292. doi: 10.1073/pnas.1903230116

Lee, T. J., Lee, J. W., Haynes, E. M., Eliceiri, K. W., and Halloran, M. C. (2017). The kinesin adaptor Calsyntenin-1 organizes microtubule polarity and regulates dynamics during sensory axon arbor development. *Front. Cell. Neurosci.* 11:107. doi: 10.3389/fncel.2017.00107

Leeuwis, A. E., Benedictus, M. R., Kuijer, J. P. A., Binnewijzend, M. A. A., Hooghiemstra, A. M., Verfaillie, S. C. J., et al. (2017). Lower cerebral blood flow is associated with impairment in multiple cognitive domains in Alzheimer's disease. *Alzheimers Dement.* 13, 531–540. doi: 10.1016/j.jalz.2016.08.013

Lehmann, R., Dietrich, U., Jiménez, F., and Campos-Ortega, J. A. (1981). Mutations of early neurogenesis in *Drosophila*. *Wilehm Roux Arch. Dev. Biol.* 190, 226–229.

Leifer, A. M., Fang-Yen, C., Gershow, M., Alkema, M. J., and Samuel, A. D. T. (2011). Optogenetic manipulation of neural activity in freely moving *Caenorhabditis elegans*. *Nat. Methods* 8, 147–152. doi: 10.1038/nmeth.1554

Leijenaar, J. F., van Maurik, I. S., Kuijer, J. P. A., van der Flier, W. M., Scheltens, P., Barkhof, F., et al. (2017). Lower cerebral blood flow in subjects with Alzheimer's dementia, mild cognitive impairment, and subjective cognitive decline using two-dimensional phase-contrast magnetic resonance imaging. *Alzheimers Dement.* 9, 76–83. doi: 10.1016/j.dadm.2017.10.001

Lemon, W. C., and McDole, K. (2020). Live-cell imaging in the era of too many microscopes. *Curr. Opin. Cell Biol.* 66, 34–42. doi: 10.1016/j.ceb.2020.04.008

Lemon, W. C., Pulver, S. R., Höckendorf, B., McDole, K., Branson, K., Freeman, J., et al. (2015). Whole-central nervous system functional imaging in larval *Drosophila*. *Nat. Commun.* 6:7924. doi: 10.1038/ncomms8924

Leonardo, E. D., Hinck, L., Masu, M., Keino-Masu, K., Ackerman, S. L., and Tessier-Lavigne, M. (1997). Vertebrate homologues of *C. elegans* UNC-5 are candidate netrin receptors. *Nature* 386, 833–838. doi: 10.1038/386833a0

Leopold, A. V., Shcherbakova, D. M., and Verkhusha, V. V. (2019). Fluorescent biosensors for neurotransmission and neuromodulation: engineering and applications. *Front. Cell. Neurosci.* 13:474. doi: 10.3389/fncel.2019.00474

Letourneau, P. C. (1975). Cell-to-substratum adhesion and guidance of axonal elongation. *Dev. Biol.* 44, 92–101. doi: 10.1016/0012-1606(75)90379-6

Leung-Hagesteijn, C., Spence, A. M., Stern, B. D., Zhou, Y., Su, M. W., Hedgecock, E. M., et al. (1992). UNC-5, a transmembrane protein with immunoglobulin and thrombospondin type 1 domains, guides cell and pioneer axon migrations in *C. elegans*. *Cell* 71, 289–299. doi: 10.1016/0092-8674(92)90357-i

Levasseur, J. E., Wei, E. P., Raper, A. J., Kontos, H. A., and Patterson, J. L. (1975). Detailed description of a cranial window technique for acute and chronic experiments. *Stroke* 6, 308–317. doi: 10.1161/01.str.6.3.308

Levi-Montalcini, R., and Levi, G. (1943). Recherches quantitatives sur la marche du processus de différenciation des neurones dans les ganglions spinaux de l'embryon de poulet. *Arch. Biol.* 54, 189–206.

Levoy, M., Ng, R., Adams, A., and Footer, M. (2006). "Light field microscopy," in *Proceedings of the ACM SIGGRAPH 2006*, Vol. 25 (New York, NY: ACM), 924–934. doi: 10.1145/1179352.1141976

Li, H., Ruan, J., Xie, Z., Wang, H., and Liu, W. (2007). Investigation of the critical geometric characteristics of living human skulls utilising medical image analysis techniques. *Int. J. Veh. Saf.* 2, 345–367. doi: 10.1504/ijvs.2007.016747

Li, Y., Du, X.-F., Liu, C.-S., Wen, Z.-L., and Du, J.-L. (2012). Reciprocal regulation between resting microglial dynamics and neuronal activity *in vivo*. *Dev. Cell* 23, 1189–1202. doi: 10.1016/j.devcel.2012.10.027

Liu, K., Petree, C., Requena, T., Varshney, P., and Varshney, G. K. (2019). Expanding the CRISPR toolbox in zebrafish for studying development and disease. *Front. Cell Dev. Biol.* 7:13. doi: 10.3389/fcell.2019.00013

Liu, T.-L., Upadhyayula, S., Milkie, D. E., Singh, V., Wang, K., Swinburne, I. A., et al. (2018). Observing the cell in its native state: imaging subcellular dynamics in multicellular organisms. *Science* 360:eaaq1392. doi: 10.1126/science.aaq1392

Liu, W.-C., Kohn, J., Szwed, S. K., Pariser, E., Sepe, S., Haripal, B., et al. (2015). Human mutant huntingtin disrupts vocal learning in transgenic songbirds. *Nat. Neurosci.* 18, 1617–1622. doi: 10.1038/nn.4133

Livingstone, M. S., Sziber, P. P., and Quinn, W. G. (1984). Loss of calcium/calmodulin responsiveness in adenylate cyclase of rutabaga, a *Drosophila* learning mutant. *Cell* 37, 205–215. doi: 10.1016/0092-8674(84)90316-7

Louvi, A., and Artavanis-Tsakonas, S. (2006). Notch signalling in vertebrate neural development. *Nat. Rev. Neurosci.* 7, 93–102. doi: 10.1038/nrn1847

Luna, S., Cameron, D. J., and Ethell, D. W. (2013). Amyloid-β and APP deficiencies cause severe cerebrovascular defects: important work for an old villain. *PLoS One* 8:e75052. doi: 10.1371/journal.pone.0075052

Lyons, D. A., and Talbot, W. S. (2014). Glial cell development and function in zebrafish. *Cold Spring Harb. Perspect. Biol.* 7:a020586. doi: 10.1101/cshperspect.a020586

Mandal, A., Pinter, K., and Drerup, C. M. (2018). Analyzing neuronal mitochondria *in vivo* using fluorescent reporters in zebrafish. *Front. Cell Dev. Biol.* 6:144. doi: 10.3389/fcell.2018.00144

Manger, P. R., Cort, J., Ebrahim, N., Goodman, A., Henning, J., Karolia, M., et al. (2008). Is 21st century neuroscience too focussed on the rat/mouse model of brain function and dysfunction? *Front. Neuroanat.* 2:5. doi: 10.3389/neuro.05.005.2008

Mann, K., Deny, S., Ganguli, S., and Clandinin, T. R. (2021). Coupling of activity, metabolism and behaviour across the *Drosophila* brain. *Nature* 593, 244–248. doi: 10.1038/s41586-021-03497-0

Masch, J.-M., Steffens, H., Fischer, J., Engelhardt, J., Hubrich, J., Keller-Findeisen, J., et al. (2018). Robust nanoscopy of a synaptic protein in living mice by organic-fluorophore labeling. *Proc. Natl. Acad. Sci. U.S.A.* 115, E8047–E8056. doi: 10.1073/pnas.1807104115

Masselink, W., and Tanaka, E. M. (2021). Toward whole tissue imaging of axolotl regeneration. *Dev. Dyn.* 250, 800–806. doi: 10.1002/dvdy.282

Masuda, T., Sankowski, R., Staszewski, O., Böttcher, C., Amann, L., Sagar, et al. (2019). Spatial and temporal heterogeneity of mouse and human microglia at single-cell resolution. *Nature* 566, 388–392. doi: 10.1038/s41586-019-0924-x

Mathiisen, T. M., Lehre, K. P., Danbolt, N. C., and Ottersen, O. P. (2010). The perivascular astroglial sheath provides a complete covering of the brain microvessels: an electron microscopic 3D reconstruction. *Glia* 58, 1094–1103. doi: 10.1002/glia.20990

Mazaheri, F., Breus, O., Durdu, S., Haas, P., Wittbrodt, J., Gilmour, D., et al. (2014). Distinct roles for BAI1 and TIM-4 in the engulfment of dying neurons by microglia. *Nat. Commun.* 5:4046. doi: 10.1038/ncomms5046

McDole, K., Guignard, L., Amat, F., Berger, A., Malandain, G., Royer, L. A., et al. (2018). In toto imaging and reconstruction of post-implantation mouse development at the single-cell level. *Cell* 175, 859–876.e33. doi: 10.1016/j.cell.2018.09.031

Mello, C. V. (2014). The zebra finch, *Taeniopygia guttata*: an avian model for investigating the neurobiological basis of vocal learning. *Cold Spring Harb. Protoc.* 2014, 1237–1242. doi: 10.1101/pdb.emo084574

Melzer, T. R., Watts, R., MacAskill, M. R., Pearson, J. F., Rüeger, S., Pitcher, T. L., et al. (2011). Arterial spin labelling reveals an abnormal cerebral perfusion pattern in Parkinson's disease. *Brain* 134, 845–855. doi: 10.1093/brain/awq377

Merriman, D. K., Sajdak, B. S., Li, W., and Jones, B. W. (2016). Seasonal and post-trauma remodeling in cone-dominant ground squirrel retina. *Exp. Eye Res.* 150, 90–105. doi: 10.1016/j.exer.2016.01.011

Milanese, C., Sager, J. J., Bai, Q., Farrell, T. C., Cannon, J. R., Greenamyre, J. T., et al. (2012). Hypokinesia and reduced dopamine levels in zebrafish lacking β- and γ1-synucleins. *J. Biol. Chem.* 287, 2971–2983. doi: 10.1074/jbc.M111.308312

Miller, J. E., Hafzalla, G. W., Burkett, Z. D., Fox, C. M., and White, S. A. (2015). Reduced vocal variability in a zebra finch model of dopamine depletion: implications for Parkinson disease. *Physiol Rep* 3, e12599. doi: 10.14814/phy2.12599

Miyamoto, A., Wake, H., Ishikawa, A. W., Eto, K., Shibata, K., Murakoshi, H., et al. (2016). Microglia contact induces synapse formation in developing somatosensory cortex. *Nat. Commun.* 7:12540. doi: 10.1038/ncomms12540

Moen, E., Bannon, D., Kudo, T., Graf, W., Covert, M., and Van Valen, D. (2019). Deep learning for cellular image analysis. *Nat. Methods* 16, 1233–1246.

Murphy, M. J., Grace, G. M., Tartaglia, M. C., Orange, J. B., Chen, X., Rowe, A., et al. (2012). Widespread cerebral haemodynamics disturbances occur early in amyotrophic lateral sclerosis. *Amyotroph. Lateral Scler.* 13, 202–209. doi: 10.3109/17482968.2011.625569

Murthy, M., and Ram, J. L. (2015). Invertebrates as model organisms for research on aging biology. *Invertebr. Reprod. Dev.* 59, 1–4. doi: 10.1080/07924259.2014.970002

Naef, V., Mero, S., Fichi, G., D'Amore, A., Ogi, A., Gemignani, F., et al. (2019). Swimming in deep water: zebrafish modeling of complicated forms of hereditary spastic paraplegia and spastic ataxia. *Front. Neurosci.* 13:1311. doi: 10.3389/fnins.2019.01311

Nakajima, K., Shimamura, M., and Furuno, N. (2021). Generation of no-yellow-pigment *Xenopus tropicalis* by slc2a7 gene knockout. *Dev. Dyn.* 250, 1420–1431. doi: 10.1002/dvdy.334

Naumann, E. A., Fitzgerald, J. E., Dunn, T. W., Rihel, J., Sompolinsky, H., and Engert, F. (2016). From whole-brain data to functional circuit models: the zebrafish optomotor response. *Cell* 167, 947–960.e20. doi: 10.1016/j.cell.2016.10.019

Nie, L., Guo, Z., and Wang, L. V. (2011). Photoacoustic tomography of monkey brain using virtual point ultrasonic transducers. *J. Biomed. Opt.* 16:076005. doi: 10.1117/1.3595842

Nimmerjahn, A., Kirchhoff, F., and Helmchen, F. (2005). Resting microglial cells are highly dynamic surveillants of brain parenchyma *in vivo*. *eNeuroforum* 11, 95–95. doi: 10.1126/science.1110647

Norton, P., Barschke, P., Scharff, C., and Mendoza, E. (2019). Differential song deficits after lentivirus-mediated knockdown of foxp1, foxp2, or foxp4 in area x of juvenile zebra finches. *J. Neurosci.* 39, 9782–9796. doi: 10.1523/JNEUROSCI.1250-19.2019

O'Donnell, K. C., Lulla, A., Stahl, M. C., Wheat, N. D., Bronstein, J. M., and Sagasti, A. (2014). Axon degeneration and PGC-1α-mediated protection in a zebrafish model of α-synuclein toxicity. *Dis. Model. Mech.* 7, 571–582.

Oakley, H., Cole, S. L., Logan, S., Maus, E., Shao, P., Craft, J., et al. (2006). Intraneuronal beta-amyloid aggregates, neurodegeneration, and neuron loss in transgenic mice with five familial Alzheimer's disease mutations: potential factors in amyloid plaque formation. *J. Neurosci.* 26, 10129–10140. doi: 10.1523/JNEUROSCI.1202-06.2006

Ogata, K., and Kosaka, T. (2002). Structural and quantitative analysis of astrocytes in the mouse hippocampus. *Neuroscience* 113, 221–233. doi: 10.1016/s0306-4522(02)00041-6

Olkowicz, S., Kocourek, M., Luèan, R. K., Porteš, M., Fitch, W. T., Herculano-Houzel, S., et al. (2016). Birds have primate-like numbers of neurons in the forebrain. *Proc. Natl. Acad. Sci. U.S.A.* 113, 7255–7260. doi: 10.1073/pnas.1517131113

Oosterhof, N., Holtman, I. R., Kuil, L. E., van der Linde, H. C., Boddeke, E. W. G. M., Eggen, B. J. L., et al. (2017). Identification of a conserved and acute neurodegeneration-specific microglial transcriptome in the zebrafish. *Glia* 65, 138–149. doi: 10.1002/glia.23083

Orger, M. B., and de Polavieja, G. G. (2017). Zebrafish behavior: opportunities and challenges. *Annu. Rev. Neurosci.* 40, 125–147. doi: 10.1146/annurev-neuro-071714-033857

Palay, S. L. (1954). "Electron microscope study of the cytoplasm of neurons," in *Anatomical Record*, ed. H. F. Smith (New York, NY: Wiley-Liss Div John Wiley & Sons Inc), 336–336. doi: 10.1016/0014-4886(72)90028-3

Panula, P., Chen, Y.-C., Priyadarshini, M., Kudo, H., Semenova, S., Sundvik, M., et al. (2010). The comparative neuroanatomy and neurochemistry of zebrafish CNS systems of relevance to human neuropsychiatric diseases. *Neurobiol. Dis.* 40, 46–57. doi: 10.1016/j.nbd.2010.05.010

Paolicelli, R. C., Bolasco, G., Pagani, F., Maggi, L., Scianni, M., Panzanelli, P., et al. (2011). Synaptic pruning by microglia is necessary for normal brain development. *Science* 333, 1456–1458. doi: 10.1126/science.1202529

Paquet, D., Plucińska, G., and Misgeld, T. (2014). *in vivo* imaging of mitochondria in intact zebrafish larvae. *Methods Enzymol.* 547, 151–164. doi: 10.1016/B978-0-12-801415-8.00009-6

Park, H., You, N., Lee, J., and Suh, M. (2019). Longitudinal study of hemodynamics and dendritic membrane potential changes in the mouse cortex following a soft cranial window installation. *Neurophotonics* 6, 015006. doi: 10.1117/1.NPh.6.1.015006

Penalva, A., Bedke, J., Cook, E. S. B., Barrios, J. P., Bertram, E. P. L., and Douglass, A. D. (2018). Establishment of the miniature fish species *Danionella translucida* as a genetically and optically tractable neuroscience model. *bioRxiv* [Preprint] bioRxiv: 444026, doi: 10.1101/444026

Peng, W., Minakaki, G., Nguyen, M., and Krainc, D. (2019). Preserving lysosomal function in the aging brain: insights from neurodegeneration. *Neurotherapeutics* 16, 611–634. doi: 10.1007/s13311-019-00742-3

Peri, F., and Nüsslein-Volhard, C. (2008). Live imaging of neuronal degradation by microglia reveals a role for v0-ATPase a1 in phagosomal fusion *in vivo*. *Cell* 133, 916–927. doi: 10.1016/j.cell.2008.04.037

Phipps, L. S., Marshall, L., Dorey, K., and Amaya, E. (2020). Model systems for regeneration: *Xenopus*. *Development* 147:dev180844. doi: 10.1242/dev.180844

Picardo, M. A., Merel, J., Katlowitz, K. A., Vallentin, D., Okobi, D. E., Benezra, S. E., et al. (2016). Population-level representation of a temporal sequence underlying song production in the zebra finch. *Neuron* 90, 866–876. doi: 10.1016/j.neuron.2016.02.016

Pitrone, P. G., Schindelin, J., Stuyvenberg, L., Preibisch, S., Weber, M., Eliceiri, K. W., et al. (2013). OpenSPIM: an open-access light-sheet microscopy platform. *Nat. Methods* 10, 598–599. doi: 10.1038/nmeth.2507

Planchon, T. A., Gao, L., Milkie, D. E., Davidson, M. W., Galbraith, J. A., Galbraith, C. G., et al. (2011). Rapid three-dimensional isotropic imaging of living cells using Bessel beam plane illumination. *Nat. Methods* 8, 417–423. doi: 10.1038/nmeth.1586

Plucińska, G., Paquet, D., Hruscha, A., Godinho, L., Haass, C., Schmid, B., et al. (2012). *in vivo* imaging of disease-related mitochondrial dynamics in a vertebrate model system. *J. Neurosci.* 32, 16203–16212. doi: 10.1523/JNEUROSCI.1327-12.2012

Polleux, F., Giger, R. J., Ginty, D. D., Kolodkin, A. L., and Ghosh, A. (1998). Patterning of cortical efferent projections by semaphorin-neuropilin interactions. *Science* 282, 1904–1906. doi: 10.1126/science.282.5395.1904

Ponomareva, O. Y., Eliceiri, K. W., and Halloran, M. C. (2016). Charcot-Marie-Tooth 2b associated Rab7 mutations cause axon growth and guidance defects

during vertebrate sensory neuron development. *Neural Dev.* 11:2. doi: 10.1186/s13064-016-0058-x

Ponomareva, O. Y., Holmen, I. C., Sperry, A. J., Eliceiri, K. W., and Halloran, M. C. (2014). Calsyntenin-1 regulates axon branching and endosomal trafficking during sensory neuron development *in vivo*. *J. Neurosci.* 34, 9235–9248. doi: 10.1523/JNEUROSCI.0561-14.2014

Porter, D. D. L., and Morton, P. D. (2020). Clearing techniques for visualizing the nervous system in development, injury, and disease. *J. Neurosci. Methods* 334:108594. doi: 10.1016/j.jneumeth.2020.108594

Portugues, R., and Engert, F. (2011). Adaptive locomotor behavior in larval zebrafish. *Front. Syst. Neurosci.* 5:72. doi: 10.3389/fnsys.2011.00072

Potter, S. M., Wang, C. M., Garrity, P. A., and Fraser, S. E. (1996). Intravital imaging of green fluorescent protein using two-photon laser-scanning microscopy. *Gene* 173, 25–31. doi: 10.1016/0378-1119(95)00681-8

Power, R. M., and Huisken, J. (2017). A guide to light-sheet fluorescence microscopy for multiscale imaging. *Nat. Methods* 14, 360–373. doi: 10.1038/nmeth.4224

Pozner, T., Vistoropsky, Y., Moaraf, S., Heiblum, R., and Barnea, A. (2018). Questioning seasonality of neuronal plasticity in the adult avian brain. *Sci. Rep.* 8:11289. doi: 10.1038/s41598-018-29532-1

Prinz, M., Jung, S., and Priller, J. (2019). Microglia biology: one century of evolving concepts. *Cell* 179, 292–311. doi: 10.1016/j.cell.2019.08.053

Qin, Q., Teng, Z., Liu, C., Li, Q., Yin, Y., and Tang, Y. (2021). TREM2, microglia, and Alzheimer's disease. *Mech. Ageing Dev.* 195:111438. doi: 10.1016/j.mad.2021.111438

Rajan, G., Duroure, K., and Del Bene, F. (2022). "Chapter 16 – *Danionella translucida*, a tankful of new opportunities," in *Laboratory Fish in Biomedical Research*, eds L. D'Angelo and P. de Girolamo (Cambridge, MA: Academic Press), 409–418. doi: 10.1016/b978-0-12-821099-4.00017-1

Rapti, G. (2020). A perspective on *C. elegans* neurodevelopment: from early visionaries to a booming neuroscience research. *J. Neurogenet.* 34, 259–272. doi: 10.1080/01677063.2020.1837799

Reeves, A. M. B., Shigetomi, E., and Khakh, B. S. (2011). Bulk loading of calcium indicator dyes to study astrocyte physiology: key limitations and improvements using morphological maps. *J. Neurosci.* 31, 9353–9358. doi: 10.1523/JNEUROSCI.0127-11.2011

Roberts, T. F., Gobes, S. M. H., Murugan, M., Ölveczky, B. P., and Mooney, R. (2012). Motor circuits are required to encode a sensory model for imitative learning. *Nat. Neurosci.* 15, 1454–1459. doi: 10.1038/nn.3206

Rocha, M. D., Düring, D. N., Bethge, P., Voigt, F. F., Hildebrand, S., Helmchen, F., et al. (2019). Tissue clearing and light sheet microscopy: imaging the unsectioned adult zebra finch brain at cellular resolution. *Front. Neuroanat.* 13:13. doi: 10.3389/fnana.2019.00013

Rodríguez, C., and Ji, N. (2018). Adaptive optical microscopy for neurobiology. *Curr. Opin. Neurobiol.* 50, 83–91. doi: 10.1016/j.conb.2018.01.011

Royer, L. A., Lemon, W. C., Chhetri, R. K., and Keller, P. J. (2018). A practical guide to adaptive light-sheet microscopy. *Nat. Protoc.* 13, 2462–2500. doi: 10.1038/s41596-018-0043-4

Royer, L. A., Lemon, W. C., Chhetri, R. K., Wan, Y., Coleman, M., Myers, E. W., et al. (2016). Adaptive light-sheet microscopy for long-term, high-resolution imaging in living organisms. *Nat. Biotechnol.* 34, 1267–1278. doi: 10.1038/nbt.3708

Rule, R. R., Schuff, N., Miller, R. G., and Weiner, M. W. (2010). Gray matter perfusion correlates with disease severity in ALS. *Neurology* 74, 821–827. doi: 10.1212/WNL.0b013e3181d3e2dd

Russell, J. J., Theriot, J. A., Sood, P., Marshall, W. F., Landweber, L. F., Fritz-Laylin, L., et al. (2017). Non-model model organisms. *BMC Biol.* 15:55. doi: 10.1186/s12915-017-0391-5

Sapoznik, E., Chang, B.-J., Huh, J., Ju, R. J., Azarova, E. V., Pohlkamp, T., et al. (2020). A versatile oblique plane microscope for large-scale and high-resolution imaging of subcellular dynamics. *Elife* 9:e57681. doi: 10.7554/eLife.57681

Schaeffer, S., and Iadecola, C. (2021). Revisiting the neurovascular unit. *Nat. Neurosci.* 24, 1198–1209. doi: 10.1038/s41593-021-00904-7

Schafer, D. P., Lehrman, E. K., Kautzman, A. G., Koyama, R., Mardinly, A. R., Yamasaki, R., et al. (2012). Microglia sculpt postnatal neural circuits in an activity and complement-dependent manner. *Neuron* 74, 691–705. doi: 10.1016/j.neuron.2012.03.026

Scheffer, L. K., Xu, C. S., Januszewski, M., Lu, Z., Takemura, S.-Y., Hayworth, K. J., et al. (2020). A connectome and analysis of the adult *Drosophila* central brain. *Elife* 9:e57443. doi: 10.7554/eLife.57443

Schindelin, J., Arganda-Carreras, I., Frise, E., Kaynig, V., Longair, M., Pietzsch, T., et al. (2012). Fiji: an open-source platform for biological-image analysis. *Nat. Methods* 9, 676–682. doi: 10.1038/nmeth.2019

Schroll, C., Riemensperger, T., Bucher, D., Ehmer, J., Völler, T., Erbguth, K., et al. (2006). Light-induced activation of distinct modulatory neurons triggers appetitive or aversive learning in *Drosophila larvae*. *Curr. Biol.* 16, 1741–1747. doi: 10.1016/j.cub.2006.07.023

Schulze, L., Henninger, J., Kadobianskyi, M., Chaigne, T., Faustino, A. I., Hakiy, N., et al. (2018). Transparent *Danionella translucida* as a genetically tractable vertebrate brain model. *Nat. Methods* 15, 977–983. doi: 10.1038/s41592-018-0144-6

Seeger, M., Tear, G., Ferres-Marco, D., and Goodman, C. S. (1993). Mutations affecting growth cone guidance in *Drosophila*: genes necessary for guidance toward or away from the midline. *Neuron* 10, 409–426. doi: 10.1016/0896-6273(93)90330-t

Sharma, K., Bisht, K., and Eyo, U. B. (2021). A comparative biology of microglia across species. *Front. Cell Dev. Biol.* 9:652748. doi: 10.3389/fcell.2021.652748

Shen, J., Blute, T. A., Liberti, W. A., Yen, W., Liberti, D. C., Kotten, D. N., et al. (2017). Songbird organotypic culture as an *in vitro* model for interrogating sparse sequencing networks. *bioRxiv* [Preprint] bioRxiv: 164228, doi: 10.1101/164228

Sherry, D. F., and MacDougall-Shackleton, S. A. (2015). Seasonal change in the avian hippocampus. *Front. Neuroendocrinol.* 37:158–167. doi: 10.1016/j.yfrne.2014.11.008

Shipley, F. B., Clark, C. M., Alkema, M. J., and Leifer, A. M. (2014). Simultaneous optogenetic manipulation and calcium imaging in freely moving C. elegans. *Front. Neural Circuits* 8:28. doi: 10.3389/fncir.2014.00028

Sieger, D., Moritz, C., Ziegenhals, T., Prykhozhij, S., and Peri, F. (2012). Long-range Ca2+ waves transmit brain-damage signals to microglia. *Dev. Cell* 22, 1138–1148. doi: 10.1016/j.devcel.2012.04.012

Silva, N. J., Dorman, L. C., Vainchtein, I. D., Horneck, N. C., and Molofsky, A. V. (2021). In situ and transcriptomic identification of synapse-associated microglia in the developing zebrafish brain. *bioRxiv* [Preprint] bioRxiv: 2021.05.08.443268, doi: 10.1101/2021.05.08.443268

So, P. T., Dong, C. Y., Masters, B. R., and Berland, K. M. (2000). Two-photon excitation fluorescence microscopy. *Annu. Rev. Biomed. Eng.* 2, 399–429.

Soleimanzad, H., Gurden, H., and Pain, F. (2017). Optical properties of mice skull bone in the 455- to 705-nm range. *JBO* 22:010503. doi: 10.1117/1.jbo.22.1.010503

Srinivasan, K., Friedman, B. A., Larson, J. L., Lauffer, B. E., Goldstein, L. D., Appling, L. L., et al. (2016). Untangling the brain's neuroinflammatory and neurodegenerative transcriptional responses. *Nat. Commun.* 7:11295. doi: 10.1038/ncomms11295

Stelzer, E. H. K., Strobl, F., Chang, B.-J., Preusser, F., Preibisch, S., McDole, K., et al. (2021). Light sheet fluorescence microscopy. *Nat. Rev. Methods Primers* 1, 1–25. doi: 10.1063/9780735423398_006

Stepanova, T., Slemmer, J., Hoogenraad, C. C., Lansbergen, G., Dortland, B., De Zeeuw, C. I., et al. (2003). Visualization of microtubule growth in cultured neurons via the use of EB3-GFP (end-binding protein 3-green fluorescent protein). *J. Neurosci.* 23, 2655–2664. doi: 10.1523/JNEUROSCI.23-07-02655.2003

Stringer, C., Wang, T., Michaelos, M., and Pachitariu, M. (2021). Cellpose: a generalist algorithm for cellular segmentation. *Nat. Methods* 18, 100–106. doi: 10.1038/s41592-020-01018-x

Svoboda, K., Denk, W., Kleinfeld, D., and Tank, D. W. (1997). *in vivo* dendritic calcium dynamics in neocortical pyramidal neurons. *Nature* 385, 161–165. doi: 10.1038/385161a0

Svoboda, K., Tank, D. W., and Denk, W. (1996). Direct measurement of coupling between dendritic spines and shafts. *Science* 272, 716–719. doi: 10.1126/science.272.5262.716

Sweeney, M. D., Kisler, K., Montagne, A., Toga, A. W., and Zlokovic, B. V. (2018). The role of brain vasculature in neurodegenerative disorders. *Nat. Neurosci.* 21, 1318–1331. doi: 10.1038/s41593-018-0234-x

Symvoulidis, P., Lauri, A., Stefanoiu, A., Cappetta, M., Schneider, S., Jia, H., et al. (2017). NeuBtracker-imaging neurobehavioral dynamics in freely behaving fish. *Nat. Methods* 14, 1079–1082. doi: 10.1038/nmeth.4459

Tanaami, T., Otsuki, S., Tomosada, N., Kosugi, Y., Shimizu, M., and Ishida, H. (2002). High-speed 1-frame/ms scanning confocal microscope with a microlens and Nipkow disks. *Appl. Opt.* 41, 4704–4708. doi: 10.1364/ao.41.004704

Tatarsky, R. L., Guo, Z., Campbell, S. C., Kim, H., Fang, W., Perelmuter, J. T., et al. (2021). Acoustic and postural displays in a miniature and transparent teleost fish, *Danionella dracula*. *bioRxiv* [Preprint] bioRxiv: 2021.11.10.468077, doi: 10.1101/2021.11.10.468077

Tejera, D., and Heneka, M. T. (2019). "Microglia in neurodegenerative disorders," in *Microglia: Methods and Protocols*, eds O. Garaschuk and A. Verkhratsky (New York, NY: Springer), 57–67. doi: 10.1007/978-1-4939-9658-2_5

Ter Veer, M. J. T., Pfeiffer, T., and Nägerl, U. V. (2017). Two-photon STED microscopy for nanoscale imaging of neural morphology *in vivo*. *Methods Mol. Biol.* 1663, 45–64. doi: 10.1007/978-1-4939-7265-4_5

Tessier-Lavigne, M. (1994). Axon guidance by diffusible repellants and attractants. *Curr. Opin. Genet. Dev.* 4, 596–601. doi: 10.1016/0959-437x(94)90078-h

Trivedi, C. A., and Bollmann, J. H. (2013). Visually driven chaining of elementary swim patterns into a goal-directed motor sequence: a virtual reality study of zebrafish prey capture. *Front. Neural Circuits* 7:86. doi: 10.3389/fncir.2013.00086

Truong, T. V., Supatto, W., Koos, D. S., Choi, J. M., and Fraser, S. E. (2011). Deep and fast live imaging with two-photon scanned light-sheet microscopy. *Nat. Methods* 8, 757–760. doi: 10.1038/nmeth.1652

Urbanus, B. H. A., Peter, S., Fisher, S. E., and De Zeeuw, C. I. (2020). Region-specific Foxp2 deletions in cortex, striatum or cerebellum cannot explain vocalization deficits observed in spontaneous global knockouts. *Sci. Rep.* 10:21631. doi: 10.1038/s41598-020-78531-8

Vallese, F., Catoni, C., Cieri, D., Barazzuol, L., Ramirez, O., Calore, V., et al. (2020). An expanded palette of improved SPLICS reporters detects multiple organelle contacts *in vitro* and *in vivo*. *Nat. Commun.* 11:6069. doi: 10.1038/s41467-020-19892-6

van de Haar, H. J., Jansen, J. F. A., van Osch, M. J. P., van Buchem, M. A., Muller, M., Wong, S. M., et al. (2016). Neurovascular unit impairment in early Alzheimer's disease measured with magnetic resonance imaging. *Neurobiol. Aging* 45, 190–196. doi: 10.1016/j.neurobiolaging.2016.06.006

Varga, M. (2018). The doctor of delayed publications: the remarkable life of george streisinger (1927-1984). *Zebrafish* 15, 314–319. doi: 10.1089/zeb.2017.1531

Vaz, R. L., Outeiro, T. F., and Ferreira, J. J. (2018). Zebrafish as an animal model for drug discovery in parkinson's disease and other movement disorders: a systematic review. *Front. Neurol.* 9:347. doi: 10.3389/fneur.2018.00347

Velho, T. A. F., Lovell, P. V., Friedrich, S. R., Olson, C. R., Miles, J., Mueller, P. A., et al. (2021). Divergent low-density lipoprotein receptor (LDLR) linked to low VSV G-dependent viral infectivity and unique serum lipid profile in zebra finches. *Proc. Natl. Acad. Sci. U.S.A.* 118:e2025167118. doi: 10.1073/pnas.2025167118

Ventura, R., and Harris, K. M. (1999). Three-dimensional relationships between hippocampal synapses and astrocytes. *J. Neurosci.* 19, 6897–6906. doi: 10.1523/JNEUROSCI.19-16-06897.1999

Vettenburg, T., Dalgarno, H. I. C., Nylk, J., Coll-Lladó, C., Ferrier, D. E. K., Èižmár, T., et al. (2014). Light-sheet microscopy using an Airy beam. *Nat. Methods* 11, 541–544. doi: 10.1038/nmeth.2922

von Chamier, L., Laine, R. F., Jukkala, J., Spahn, C., Krentzel, D., Nehme, E., et al. (2021). Democratising deep learning for microscopy with ZeroCostDL4Mic. *Nat. Commun.* 12:2276. doi: 10.1038/s41467-021-22518-0

Voskoboynik, A., and Weissman, I. L. (2015). Botryllus schlosseri, an emerging model for the study of aging, stem cells, and mechanisms of regeneration. *Invertebr. Reprod. Dev.* 59, 33–38. doi: 10.1080/07924259.2014.944673

Vrtílek, M., Žák, J., Polaèik, M., Blažek, R., and Reichard, M. (2018). Longitudinal demographic study of wild populations of African annual killifish. *Sci. Rep.* 8:4774. doi: 10.1038/s41598-018-22878-6

Wang, J., and Cao, H. (2021). Zebrafish and medaka: important animal models for human neurodegenerative diseases. *Int. J. Mol. Sci.* 22:10766. doi: 10.3390/ijms221910766

Wang, K., Hinz, J., Zhang, Y., Thiele, T. R., and Arrenberg, A. B. (2020). Parallel channels for motion feature extraction in the pretectum and tectum of larval zebrafish. *Cell Rep.* 30, 442–453.e6. doi: 10.1016/j.celrep.2019.12.031

Wang, K., Milkie, D. E., Saxena, A., Engerer, P., Misgeld, T., Bronner, M. E., et al. (2014). Rapid adaptive optical recovery of optimal resolution over large volumes. *Nat. Methods* 11, 625–628. doi: 10.1038/nmeth.2925

Wang, Y., Ulland, T. K., Ulrich, J. D., Song, W., Tzaferis, J. A., Hole, J. T., et al. (2016). TREM2-mediated early microglial response limits diffusion and toxicity of amyloid plaques. *J. Exp. Med.* 213, 667–675. doi: 10.1084/jem.20151948

Wassie, A. T., Zhao, Y., and Boyden, E. S. (2019). Expansion microscopy: principles and uses in biological research. *Nat. Methods* 16, 33–41.

Wegner, W., Ilgen, P., Gregor, C., van Dort, J., Mott, A. C., Steffens, H., et al. (2017). *in vivo* mouse and live cell STED microscopy of neuronal actin plasticity using far-red emitting fluorescent proteins. *Sci. Rep.* 7:11781. doi: 10.1038/s41598-017-11827-4

Wegner, W., Mott, A. C., Grant, S. G. N., Steffens, H., and Willig, K. I. (2018). *in vivo* STED microscopy visualizes PSD95 sub-structures and morphological changes over several hours in the mouse visual cortex. *Sci. Rep.* 8:219. doi: 10.1038/s41598-017-18640-z

Weigert, M., Schmidt, U., Boothe, T., Müller, A., Dibrov, A., Jain, A., et al. (2018). Content-aware image restoration: pushing the limits of fluorescence microscopy. *Nat. Methods* 15, 1090–1097. doi: 10.1038/s41592-018-0216-7

Weigert, M., Schmidt, U., Haase, R., Sugawara, K., and Myers, G. (2020). "Star-convex polyhedra for 3D object detection and segmentation in microscopy," in *Proceedings of the 2020 IEEE Winter Conference on Applications of Computer Vision (WACV)*, Snowmass, CO, 3655–3662. doi: 10.1109/WACV45572.2020.9093435

Weinhard, L., di Bartolomei, G., Bolasco, G., Machado, P., Schieber, N. L., Neniskyte, U., et al. (2018). Microglia remodel synapses by presynaptic trogocytosis and spine head filopodia induction. *Nat. Commun.* 9:1228. doi: 10.1038/s41467-018-03566-5

Weiss, K. R., Voigt, F. F., Shepherd, D. P., and Huisken, J. (2021). Tutorial: practical considerations for tissue clearing and imaging. *Nat. Protoc.* 16, 2732–2748. doi: 10.1038/s41596-021-00502-8

Werner, C., Sauer, M., and Geis, C. (2021). Super-resolving microscopy in neuroscience. *Chem. Rev.* 121, 11971–12015. doi: 10.1021/acs.chemrev.0c01174

White, J. G., Amos, W. B., and Fordham, M. (1987). An evaluation of confocal versus conventional imaging of biological structures by fluorescence light microscopy. *J. Cell Biol.* 105, 41–48. doi: 10.1083/jcb.105.1.41

White, J. G., Southgate, E., Thomson, J. N., and Brenner, S. (1986). The structure of the nervous system of the nematode *Caenorhabditis elegans*. *Philos. Trans. R. Soc. Lond. B Biol. Sci.* 314, 1–340.

Wieschaus, E., Nüsslein-Volhard, C., and Jürgens, G. (1984). Mutations affecting the pattern of the larval cuticle in *Drosophila melanogaster* : III. Zygotic loci on the X-chromosome and fourth chromosome. *Wilehm Roux Arch. Dev. Biol.* 193, 296–307. doi: 10.1007/BF00848158

Wilson, E. L., and Metzakopian, E. (2021). ER-mitochondria contact sites in neurodegeneration: genetic screening approaches to investigate novel disease mechanisms. *Cell Death Differ.* 28, 1804–1821.

Woodcock, M. R., Vaughn-Wolfe, J., Elias, A., Kump, D. K., Kendall, K. D., Timoshevskaya, N., et al. (2017). Identification of mutant genes and introgressed tiger salamander DNA in the laboratory axolotl, *Ambystoma mexicanum*. *Sci. Rep.* 7:6. doi: 10.1038/s41598-017-00059-1

Woods, I. G., Kelly, P. D., Chu, F., Ngo-Hazelett, P., Yan, Y. L., Huang, H., et al. (2000). A comparative map of the zebrafish genome. *Genome Res.* 10, 1903–1914. doi: 10.1101/gr.10.12.1903

Woods, I. G., Wilson, C., Friedlander, B., Chang, P., Reyes, D. K., Nix, R., et al. (2005). The zebrafish gene map defines ancestral vertebrate chromosomes. *Genome Res.* 15, 1307–1314. doi: 10.1101/gr.4134305

Wu, S., Nguyen, L. T. M., Pan, H., Hassan, S., Dai, Y., Xu, J., et al. (2020). Two phenotypically and functionally distinct microglial populations in adult zebrafish. *Sci. Adv.* 6:eabd1160. doi: 10.1126/sciadv.abd1160

Xu, J., Zhu, L., He, S., Wu, Y., Jin, W., Yu, T., et al. (2015). Temporal-spatial resolution fate mapping reveals distinct origins for embryonic and adult microglia in zebrafish. *Dev. Cell* 34, 632–641. doi: 10.1016/j.devcel.2015.08.018

Xu, K., Han, C. X., Zhou, H., Ding, J. M., Xu, Z., Yang, L. Y., et al. (2020). Effective MSTN gene knockout by AdV-delivered CRISPR/Cas9 in postnatal chick leg muscle. *Int. J. Mol. Sci.* 21:2584. doi: 10.3390/ijms21072584

Yang, B., Chen, X., Wang, Y., Feng, S., Pessino, V., Stuurman, N., et al. (2019). Epi-illumination SPIM for volumetric imaging with high spatial-temporal resolution. *Nat. Methods* 16, 501–504. doi: 10.1038/s41592-019-0401-3

Yano, T., Oku, M., Akeyama, N., Itoyama, A., Yurimoto, H., Kuge, S., et al. (2010). A novel fluorescent sensor protein for visualization of redox states in the cytoplasm and in peroxisomes. *Mol. Cell. Biol.* 30, 3758–3766. doi: 10.1128/MCB.00121-10

Yartsev, M. M. (2017). The emperor's new wardrobe: rebalancing diversity of animal models in neuroscience research. *Science* 358, 466–469. doi: 10.1126/science.aan8865

Yoshida, M., and Macklin, W. B. (2005). Oligodendrocyte development and myelination in GFP-transgenic zebrafish. *J. Neurosci. Res.* 81, 1–8. doi: 10.1002/jnr.20516

Yuste, R., and Denk, W. (1995). Dendritic spines as basic functional units of neuronal integration. *Nature* 375, 682–684. doi: 10.1038/375682a0

Żakowski, W. (2020). Animal use in neurobiological research. *Neuroscience* 433, 1–10. doi: 10.1016/j.neuroscience.2020.02.049

Zhang, Y., Rózsa, M., Liang, Y., Bushey, D., Wei, Z., Zheng, J., et al. (2021). Fast and sensitive GCaMP calcium indicators for imaging neural populations. *bioRxiv* [Preprint] bioRxiv: 2021.11.08.467793, doi: 10.1101/2021.11.08.467793

Zhang, Z., Bai, L., Cong, L., Yu, P., Zhang, T., Shi, W., et al. (2021). Imaging volumetric dynamics at high speed in mouse and zebrafish brain with confocal light field microscopy. *Nat. Biotechnol.* 39, 74–83. doi: 10.1038/s41587-020-0628-7

Zimmermann, G., Wang, L.-P., Vaughan, A. G., Manoli, D. S., Zhang, F., Deisseroth, K., et al. (2009). Manipulation of an innate escape response in *Drosophila*: photoexcitation of acj6 neurons induces the escape response. *PLoS One* 4:e5100. doi: 10.1371/journal.pone.0005100

Conflict of Interest: The authors declare that the research was conducted in the absence of any commercial or financial relationships that could be construed as a potential conflict of interest.

Publisher's Note: All claims expressed in this article are solely those of the authors and do not necessarily represent those of their affiliated organizations, or those of the publisher, the editors and the reviewers. Any product that may be evaluated in this article, or claim that may be made by its manufacturer, is not guaranteed or endorsed by the publisher.

frontiers | Frontiers in Molecular Neuroscience

MINI REVIEW
published: 04 May 2022
doi: 10.3389/fnmol.2022.829666

Neuronal Polarity Pathways as Central Integrators of Cell-Extrinsic Information During Interactions of Neural Progenitors With Germinal Niches

*David J. Solecki**

Department of Developmental Neurobiology, St. Jude Children's Research Hospital, Memphis, TN, United States

Germinal niche interactions and their effect on developing neurons have become the subject of intense investigation. Dissecting the complex interplay of cell-extrinsic and cell-intrinsic factors at the heart of these interactions reveals the critical basic mechanisms of neural development and how it goes awry in pediatric neurologic disorders. A full accounting of how developing neurons navigate their niches to mature and integrate into a developing neural circuit requires a combination of genetic characterization of and physical access to neurons and their supporting cell types plus transformative imaging to determine the cell biological and gene-regulatory responses to niche cues. The mouse cerebellar cortex is a prototypical experimental system meeting all of these criteria. The lessons learned therein have been scaled to other model systems and brain regions to stimulate discoveries of how developing neurons make many developmental decisions. This review focuses on how mouse cerebellar granule neuron progenitors interact with signals in their germinal niche and how that affects the neuronal differentiation and cell polarization programs that underpin lamination of the developing cerebellum. We show how modeling of these mechanisms in other systems has added to the growing evidence of how defective neuronal polarity contributes to developmental disease.

Keywords: germinal zone, niche, morphogen, cell polarity, Pard complex

OPEN ACCESS

Edited by:
Parthiv Haldipur, Seattle Children's Research Institute, United States

Reviewed by:
Toma Adachi, National Center of Neurology and Psychiatry, Japan

***Correspondence:**
David J. Solecki
david.solecki@stjude.org

Specialty section:
This article was submitted to Methods and Model Organisms, a section of the journal Frontiers in Molecular Neuroscience

Received: *06 December 2021*
Accepted: *15 March 2022*
Published: *04 May 2022*

Citation:
Solecki DJ (2022) Neuronal Polarity Pathways as Central Integrators of Cell-Extrinsic Information During Interactions of Neural Progenitors With Germinal Niches. Front. Mol. Neurosci. 15:829666. doi: 10.3389/fnmol.2022.829666

GENERAL GERMINAL ZONE CONSIDERATIONS

Neuronal progenitor cells and neural stem cells residing in germinal zones (GZs) throughout the central nervous system face a bewildering array of extracellular signals that are critical to controlling decisions such as how many more progeny to produce or when to exit the cell cycle and terminally differentiate (Choi et al., 2005; Corbin et al., 2008; Bjornsson et al., 2015; Dehay et al., 2015; Ortega et al., 2018). Among these signals, diverse secreted morphogens, such as hedgehogs and Wnts or extracellular matrix (ECM) molecules, are made in an autocrine or paracrine manner by progenitors and neural stem cells themselves or by supporting cells such as glia or endothelia in niche environments (Borello and Pierani, 2010; Kazanis and ffrench-Constant, 2011; Tiberi et al., 2012; Barros et al., 2020). Moreover, homotypic and heterotypic cell-to-cell contacts have dual

roles, being involved in quorum sensing between cell types and serving as critical anchor points for migration or cell sorting events (Marthiens et al., 2010; Solecki, 2012; Famulski and Solecki, 2013; Morante-Redolat and Porlan, 2019).

Each GZ and niche environment has a unique complement of these genetically encoded secreted proteins or cell-recognition mechanisms that corresponds precisely to the required output of that particular niche. For example, the rapid development of the mouse cerebral cortex corresponds to a GZ extrinsic code that promotes the rapid elaboration of the neurons that populate each layer of the cortical plate with pyramidal neurons (Qian et al., 1998, 2000; Corbin et al., 2008; Uzquiano et al., 2018), whereas the adult subventricular zone (SVZ) vascular niche favors the maintenance of quiescent stem cells that sporadically produce new neurons throughout the life of the rodent (Shen et al., 2008; Tavazoie et al., 2008). Each decision made by the cells in these specialized niches involves an intricate balance between the reception of extrinsic morphogen signals and the cell-intrinsic mechanisms by which the signals are interpreted to transform morphogenic information into executable cell biological programs that ultimately underlie circuit formation. Despite our progress in identifying genetically encoded morphogens and the fundamental decisions they control, how cell-intrinsic machinery translates morphogen information into consolidated cell biological programs remains one of the most elusive aspects of neural development because of the difficulties in determining how cells integrate diverse pathways in time and space.

THE EARLY POSTNATAL CEREBELLAR GERMINAL ZONE AND LAMINATION

Cerebellar granule neurons (CGNs) are prototypical model systems that have enabled researchers to make inroads into understanding how signals are integrated with cell biological programs, especially in the context of signaling cascades that control GZ exit and the onset of neuronal differentiation (Hatten and Roussel, 2011; Singh and Solecki, 2015; Leto et al., 2016; Iulianella et al., 2019; Consalez et al., 2020). The GZ of the developing mouse cerebellum, particularly the external germinal layer (EGL), which gives rise to granule neurons, is unique among brain regions in that (1) the nearly crystalline structure of the developing cerebellar layers and their cellular composition has been exhaustively examined at both the light and electron microscopy levels and (2) cerebellar investigators have unprecedented access to almost unlimited numbers of granule neurons for *in vivo*, *ex vivo*, and *in vitro* experimentation at both the tissue and single-cell levels. This combination of the fundamental ground truth of how the GZ is structured and deep access to cerebellar granule neuron manipulation has led to the mouse cerebellar GZ being one of the best characterized GZs in the central nervous system.

After arising from radial glial neural stem cells of the rhombic lip, CGN progenitors (GNPs) migrate to the EGL secondary GZ on the surface of the cerebellar anlage (Ryder and Cepko, 1994; Wingate and Hatten, 1999). Massive GNP proliferation in the EGL *via* mostly symmetric cell divisions, with cell cycles faster than those of cell lines dividing *in vitro*, creates a cohort of CGNs that not only account for approximately 85% of all cerebellar neurons but also represent the most abundant neuronal type in the entire brain (Fujita, 1967; Espinosa and Luo, 2008; Roussel and Hatten, 2011). After GNP terminal differentiation, newly formed CGNs are displaced slightly inward from the outermost layer of the EGL (oEGL) to the inner EGL (iEGL), where they extend parallel fibers, migrate tangentially along the axons of CGNs that have already differentiated, and fasciculate with their differentiated neighbors. Approximately 36 h after the final division of their GNP parent cell, CGNs are ready to move to their final destination in the internal granule layer (IGL) by radially migrating as single cells along Bergmann glial fibers past the Purkinje cell layer.

NICHE FACTORS PROMOTING GNP PROLIFERATION AND DIFFERENTIATION

This section summarizes the molecular participants in cell-to-cell communication events that control the output of GNP proliferative decisions and the elaboration of the CGN differentiation programs during the critical steps in CGN development. Pioneering studies by Gao and Hatten using a GNP and CGN culture system showed that growth factors such as IGF1, bFGF, and EGF, which are potent mitogens, sensed by receptor tyrosine kinases, for neural stem cells throughout the brain, elicit only minimal enhancement of GNP proliferation (Gao et al., 1991). In contrast, GNPs grown in culture at high density in cellular reaggregates stimulated proliferation that was nearly 10-fold higher than that seen in control cultures, implying that GNP homotypic interactions among progenitor cells are essential to maintain progenitor cell divisions within the densely packed EGL. Paracrine interactions are also critical modulators of GNP neurogenesis in the oEGL niche. Now-classic experiments showed that Purkinje cells secrete the Sonic hedgehog (Shh) morphogen, which diffuses over long distances to GNPs residing in the oEGL and is the most potent mitogen discovered for these cells to date (Dahmane and Ruiz i Altaba, 1999; Wallace, 1999; Wechsler-Reya and Scott, 1999; Lewis et al., 2004). Shh control of GNP proliferation is evolutionarily conserved, as genetic lesions that activate the Shh pathway in both humans and mice lead to transformation of GNPs and ultimately to the formation of medulloblastoma tumors. The oEGL niche contains undefined constituents that support Shh-induced GNP neurogenesis, as GNPs seeded onto thick cerebellar slices in an overlay assay respond to Shh only when they settle in the oEGL (Choi et al., 2005). In addition to Purkinje cells, the meningeal fibroblasts that overlie the oEGL also provide short-range paracrine signals that modulate GNP proliferation. Early electron microscopy studies demonstrated that GNPs maintain contact with the basal lamina produced by meningeal fibroblasts (Hausmann and Sievers, 1985), and chemical ablation of the meninges leads to reduced GNP proliferation (von Knebel Doeberitz et al., 1986). The meninges express several molecules that are arrayed near the

oEGL niche and can directly affect GNP proliferative outcomes. One of these molecules is Jagged1, which activates GNP Notch2 receptors, ultimately initiating a transcriptional cascade that maintains GNPs in the undifferentiated state (Solecki et al., 2001). Meningeal fibroblasts also produce stromal-derived factor 1 (SDF-1) (Zou et al., 1998; Zhu et al., 2002), which synergizes with Shh at the level of GNP proliferation (Klein et al., 2001). Finally, as discussed in detail below, the meningeal secreted extracellular matrix, the main constituent of the basal lamina contacted by GNPs, also modulates GNP responsiveness to Shh.

Like GNP proliferation, CGN differentiation is controlled by a combination of autocrine or paracrine interactions in the niche that drive progenitors to the postmitotic state. Co-culture assays with highly purified populations of CGNs and cerebellar glia showed that interactions between GNPs and CGNs or between GNPs and Bergmann glia drive progenitors into the postmitotic state (Gao et al., 1991). Follow-up studies showed that CGNs drive GNP differentiation via surface expression of vitronectin (Pons et al., 2001), an ECM component in the iEGL, and secretion of bone morphogenic proteins 2 and 4 (Bmp2/4) (Rios et al., 2004). Both factors inhibit GNP Shh signaling. Cerebellar glia produces basic fibroblast growth factor (bFGF), which stimulates CGN axon extension (Hatten et al., 1988), and N-cadherin, which facilitates CGN migration, two processes concurrent with CGN differentiation (Horn et al., 2018). Finally, Purkinje cells produce at least three secreted signals that promote CGN maturation: brain-derived neurotrophic factor (BDNF) (Schwartz et al., 1997), Wnt3 (Anne et al., 2013), and pituitary adenylate cyclase–activating peptide (PACAP) (Nicot et al., 2002; Niewiadomski et al., 2013). Wnt3 and PACAP both act by inhibiting Shh-dependent GNP proliferation to drive CGNs into the postmitotic state.

CELL POLARITY AND THE INTRINSIC MACHINERY THAT INTERPRETS GERMINAL NICHE SIGNALS

Despite the discovery of the extensive array of molecules that activate the signaling cascades modulating GNP proliferation and CGN differentiation, few cell-intrinsic mechanisms for integrating the reception of such signals with the cell biological mechanisms elaborated during differentiation have been characterized. Cell polarity represents a promising cell-intrinsic mechanism by which to coordinate tissue information with the internal organization of the cell during a morphogenic program (Singh and Solecki, 2015; Laumonnerie and Solecki, 2018). In the classic example of epithelial cells, polarity signaling cascades such as the partitioning-defective (Pard) signaling complex and planar cell polarity signaling cascades consistently orient cells in the tissue so that the polarity axes align (Goldstein and Macara, 2007; Baum and Georgiou, 2011; Campanale et al., 2017). In the case of apical–basal polarity, polarity signaling enforcement of a consistent epithelial orientation synchronizes the transport function of epithelial cells across epithelial tissues and ensures tissue function. Polarity signaling similarly coordinates the structure and function of neural tissues. For example, the apical–basal polarity of radial glial cells ensures the appropriate lamination of cortical regions of the brain (Chou et al., 2018), whereas the axodendritic polarity of neurons controls proper information flow in neuronal circuits (Barnes et al., 2008). Polarity signaling from the Pard complex also plays critical roles in the early stages of neuronal differentiation, such as the timing of GNPs becoming postmitotic and the onset of CGN GZ exit in the developing cerebellum (Laumonnerie and Solecki, 2018). Three main components of the Pard complex, Pard3, Pard6α, and Prkcz, are expressed at low levels in GNPs, increase their expression dramatically in differentiating CGNs, and are necessary for CGN differentiation (Famulski et al., 2010; Singh et al., 2016). Pard3 and Pard6α gain of function in GNPs, which generally express low levels of these proteins, stimulates terminal differentiation and GZ exit by encouraging differentiation-specific cytoskeletal organization and junctional adhesion molecule C (JAM-C) adhesion to differentiated CGNs and Bergmann glia. Low levels of Pard3 and Pard6α expression in GNPs represent an active developmental cell polarity switch, because GNPs express an E3 ubiquitin ligase, seven *in absentia* homolog 2 (Siah2) (Famulski et al., 2010), and a transcriptional repressor, zinc finger E-box–binding homeobox 1 (Zeb1), that act as complementary Pard complex inhibitors that enforce GNP GZ occupancy (Singh et al., 2016). As GNPs differentiate, Siah2 and Zeb1 expression recedes, leading to enhanced Pard complex–driven cytoskeletal organization and JAM-C adhesion that drives GZ exit and radial migration initiation.

Recent studies have expanded our knowledge of the role of the Pard complex in mediating key integrative steps in the response of GNPs and CGNs to niche conditions to organize cell biological pathways responsible for differentiation. Ong et al. (2020) used sophisticated imaging technologies to reveal how the Pard complex participates in a coincidence detection circuit between the pial ECM and Shh signaling at the level of GNP ciliogenesis (**Figure 1**). Pioneering studies by Mueller and colleagues showed that Shh signaling required beta 1 integrin receptors to modulate GNP proliferation effectively; however, the mechanism by which this occurred was unclear (Blaess et al., 2004). Ong et al. showed that Ras signaling stimulated by integrin receptor binding to pial secreted laminin activates the expression of Siah2 in a manner that requires Shh signaling, which ultimately maintains GNPs in the proliferative state.

How do niche signals cooperate to regulate GNP proliferation? Cutting-edge three-dimensional electron microscopy that enabled full volumetric reconstruction of single cells within the intact oEGL and iEGL niche environments showed that GNPs are more ciliated than are CGNs. Cilia containing the Patched and Smoothened receptors are the primary sites within Shh-responsive cells that transduce the signaling cascade for this morphogen (Huangfu and Anderson, 2005; Caspary et al., 2007; Rohatgi et al., 2007). Complex epistasis experiments involving Siah2, Ras, and integrin receptors revealed the molecular basis for this difference in ciliation. Siah2 regulates GNP Shh responsiveness in a feed-forward fashion by maintaining GNP primary cilia in an integrin-dependent and Ras-dependent manner (Ong et al., 2020). Analysis of Siah2 ubiquitination targets defined a novel role for the Pard complex in promoting

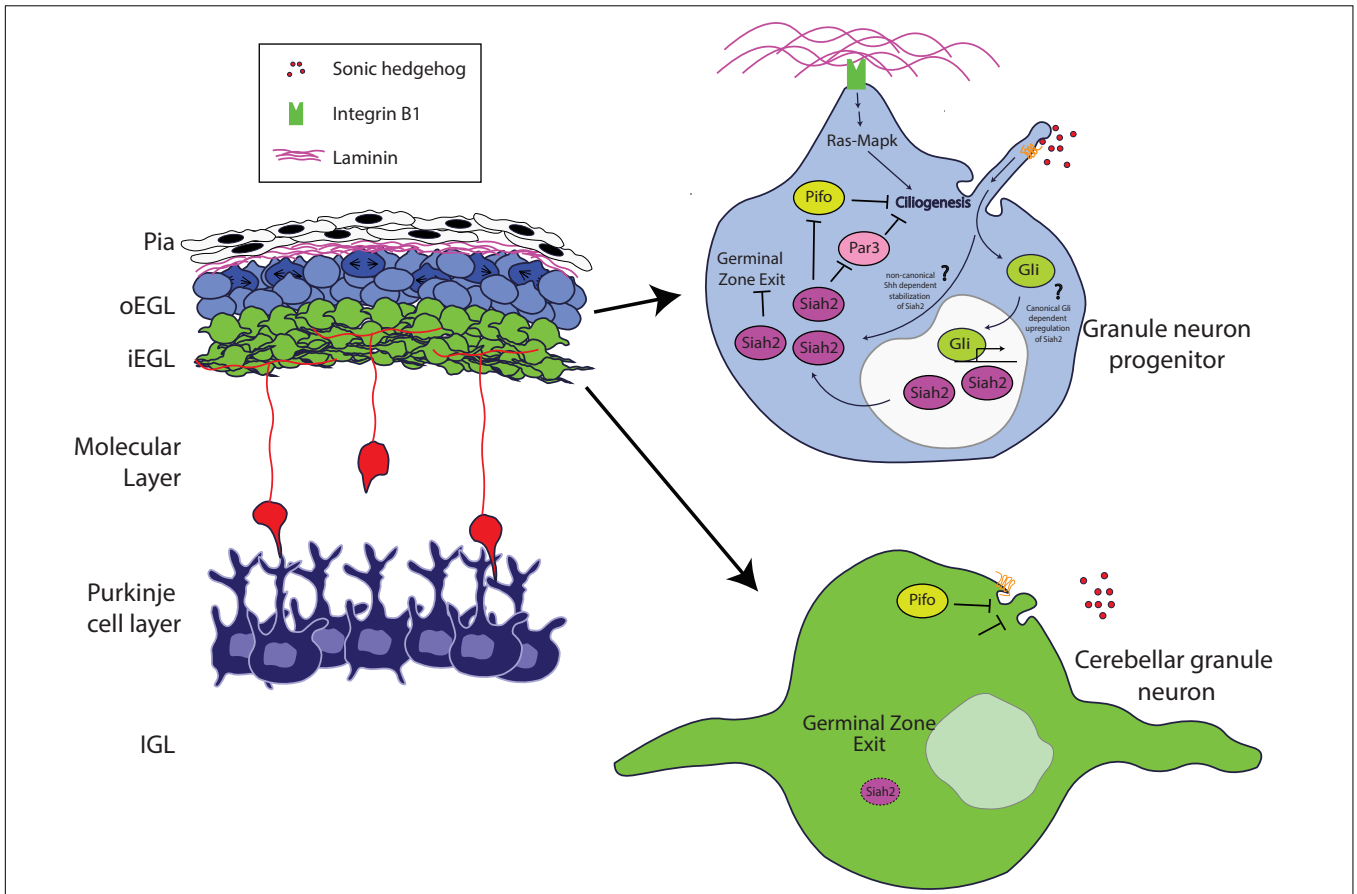

FIGURE 1 | Schematic of how Siah2 is regulated in developing CGNs. The laminin-rich basement membrane surrounding the oEGL in a developing cerebellum promotes Shh signaling driven primary ciliogenesis in GNPs via Integrin β1—Ras/Mapk signaling. The primary cilium allows GNPs to sense the Shh mitogen and activate the Shh pathway to maintain Siah2 expression which in turn promotes GZ occupancy by inhibiting GZ exit. Siah2 acts in a feed-forward mechanism to maintain mitogen sensitivity by promoting primary ciliogenesis through the antagonism of a key cilia disassembly proteins Pifo and Dbn, and the polarity inducer Pard3. As GNPs leave the oEGL, the lack of trophic support leads to the disassembly of the primary cilium and loss of sensitivity to Shh, which promotes CGN differentiation.

GNP differentiation. By using Siah2 gain of function as the basis for a live cell–imaging target rescue screen that is possible only with the large number of GNPs present in the developing cerebellum, Ong and colleagues revealed that Pard3 expression causes cilia retraction. Therefore, when coincidence detection between ECM and Shh signals in the oEGL niche predominates, the resulting Ras-dependent Siah2 activity diminishes the ability of Pard3 to facilitate cilia retraction, leading to the maintenance of Shh responsiveness. However, when Pard3 expression is elevated in the iEGL, a cell biological program promoting cilia retraction is favored, leading GNPs to be less sensitive to the Shh mitogen and allowing their transition to the differentiated CGN state.

Kullmann et al. (2020) used an array of advanced light-sheet imaging techniques to demonstrate a unique interaction between the Pard complex and oxygen tension, a non-genetically encoded niche condition that controls the timing of GNP differentiation (**Figure 2**). Macro light-sheet imaging and machine learning quantitation of the vasculature of iDISCO-cleared developing cerebellum revealed an interesting correlation with CGN differentiation. The EGL and molecular layer of postnatal day 7 cerebella are poorly vascularized when compared with the IGL, where differentiated CGNs reside, and with neighboring regions of the brain, where neurons differentiate earlier than in the cerebellum, suggesting that the cerebellar niche is an oxygen-poor environment. This hypothesis was bolstered by high hypoxyprobe staining of these layers in the developing cerebellum and high levels of hypoxia-inducible factor 1 alpha (Hif1α) in GNPs during the stages of cerebellar development with low vascularization. Hif1α, which is negatively regulated in normoxia by the von Hippel–Lindau (VHL) tumor suppressor protein, a component of an E3 ubiquitin ligase complex (Gossage et al., 2015), is not only a marker for hypoxia but also an evolutionarily conserved transcription factor that activates the expression of genes that are activated in response to hypoxia (Kaelin and Ratcliffe, 2008; Ivan and Kaelin, 2017). Genetic deletion of Hif1α and VHL *in vivo* revealed that the Hif1α pathway enforces GNP occupancy with the EGL niche and delays the timing of CGN migration initiation. Hif1α binds to the *Zeb1* gene promoter

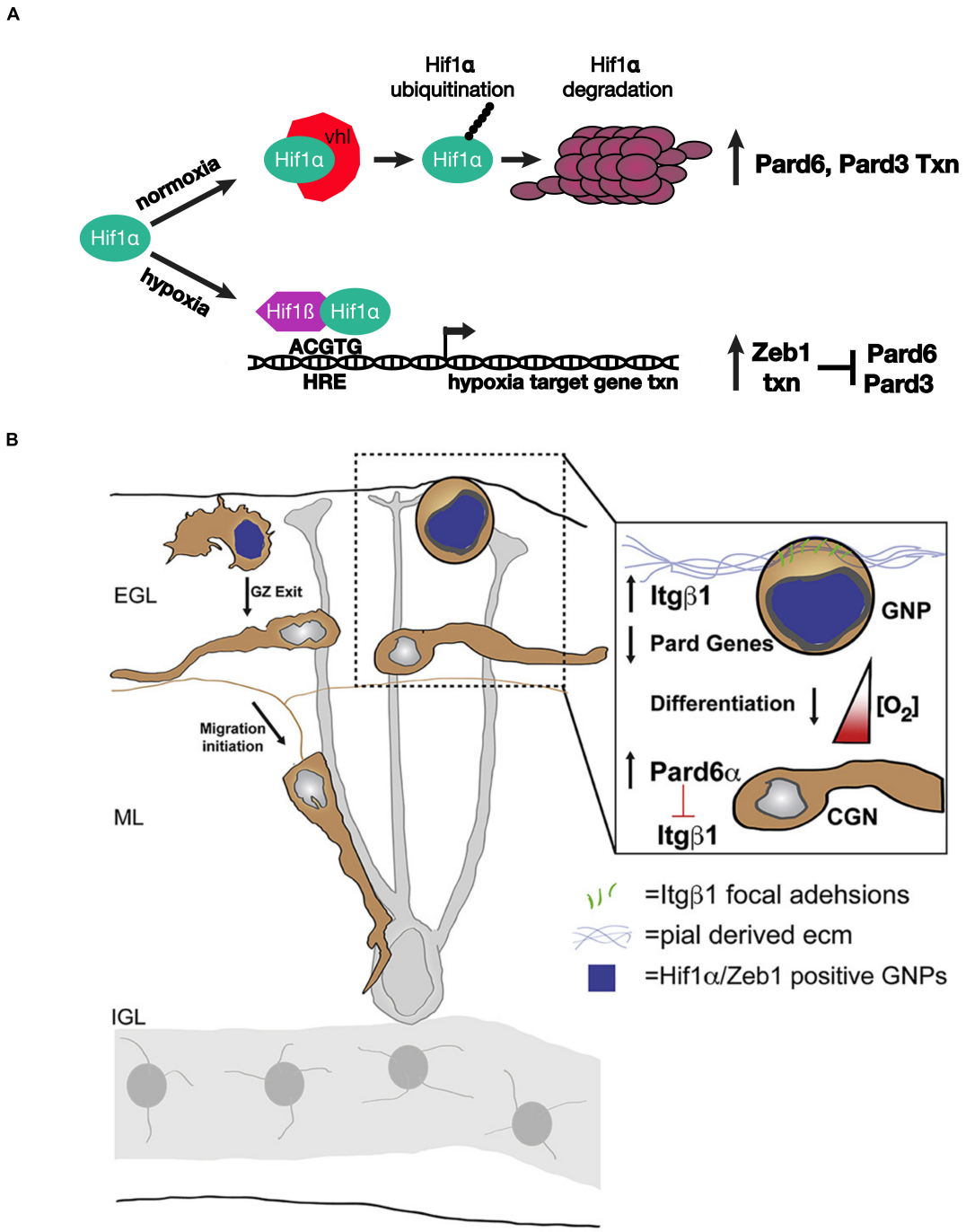

FIGURE 2 | Schematic of how oxygen tension regulates neuronal polarity in developing CGNs. **(A)** Model for the genetic interactions between Hif1α, Zeb1, and the Pard proteins in hypoxia or normoxia. **(B)** The laminin-rich basement membrane surrounding the oEGL in a developing cerebellum. GNPs expressing Hif1α and Zeb1 (blue nuclei) have lower level of Pard6α gene expression. As oxygen levels increase during development Pard6α gene expression increases which loosen Itgβ1 adhesion to the pial basal lamina. Images adapted from Kullmann et al. (2020) with permission from (Elsevier).

and activates Zeb1 mRNA expression. As Zeb1 transcriptionally represses Pard3 and Pard6α mRNA expression in GNPs, epistasis studies were needed to determine whether hypoxia or the Hif1α pathway enforced GZ occupancy by inhibiting the Pard complex gene expression. GZ occupancy stimulated by Hif1α gain of function, or hypoxia, could be rescued equally by Zeb1 loss of function and by Pard complex gain of function, showing for the first time that oxygen tension in the EGL regulates the onset of CGN polarization directly via Pard3 and Pard6a expression.

How does Hif1α - Zeb1 antagonism of Pard complex function enforce GZ occupancy? Lattice light-sheet structured illumination microscopy (LLSM-SIM) was instrumental in determining the precise cellular mechanism (Chen et al., 2014). Electron microscopic studies showed that GNPs maintain contact with the basal lamina during their time in the GZ niche (Hausmann and Sievers, 1985); however, imaging of GNP focal adhesion to pial ECM was not possible with conventional light microscopy because of the poor signal ratio and resolution. LLSM-SIM revealed that GNPs maintained in the undifferentiated state by over-expressing Hif1α or Zeb1 have numerous ECM focal adhesions and that Pard6α expression potently diminishes these adhesions, probably at the transcriptional level. Integrin receptors are a central component of the focal adhesions that recognize ECM. Not only does deleting beta 1 integrin rescue hypoxia-induced GZ occupancy, but elevating beta 1 integrin expression maintains GNPs in their germinal niche. Taken together, these findings show that the environmental niche conditions modulate how GNPs interact with ECM landmarks within the niche via Hif1α or Zeb1 inhibition of neuronal polarization. Moreover, the two studies highlight how Siah2-dependent post-translation regulation of the Pard complex converges upon the same integrin receptors that are regulated by the Hif1α and Zeb1 pathways in response to oxygen tension.

RELEVANCE TO OTHER MODELS AND TO NEURODEVELOPMENTAL DISEASE

Polarity regulation mechanisms discovered in the mouse cerebellum may have relevance to the mouse cerebral cortex. For example, Zeb1 has been found to regulate cortical neuron differentiation *via* polarity gene expression in a manner similar to that reported in CGNs (Jiang et al., 2018; Liu et al., 2019; Wang et al., 2019). In the case of the cortex, Zeb1 must bind to CTBP2 to suppress NeuroD1 expression at the developmental stage between radial glia and intermediate progenitors, which suggests that the NeuroD1 basic helix–loop–helix (bHLH) transcription may be upstream of polarity gene expression. Interestingly, prolonged Zeb1 expression in the cerebral cortex leads to subcortical band heterotopia, suggesting that the Zeb1 polarity gene regulatory pathways are involved in neuronal migration disorders distinct from those induced by defective cytoskeletal genes.

Although few mutations in polarity genes have been observed in human neurodevelopmental disorders, there is growing evidence that polarity pathways are, nevertheless, perturbed in human disease. In humans, medulloblastoma comprises a spectrum of pediatric brain tumors derived from the transformation of progenitor cells in the major GZs of the cerebellum. GNPs have been shown definitively to be the cell type of origin for Shh-class medulloblastomas (Goodrich et al., 1997; Kim et al., 2003; Oliver et al., 2005; Rohatgi et al., 2007; Yang et al., 2008). These tumors express elevated levels of Zeb1 and Siah2 and low levels of Pard complex (Singh et al., 2016; Ong et al., 2020), consistent with the polarity trajectories described for mouse GNPs. Genetic deletion of the Patched1 Shh receptor, which stimulates Shh medulloblastoma formation in humans, creates a cohort of GNPs that do not leave the EGL GZ in mouse models of Shh medulloblastoma. In these mouse models, manipulating polarity pathways in pre-tumorigenic GNPs revealed that elevating the level of Pard complex or reducing Zeb1 or Siah2 expression restores appropriate GZ exit and CGN differentiation. Therefore, differentiative therapy of pediatric brain tumors by promoting neuronal polarization may be a promising treatment strategy.

The Zeb1–Hif1α–Pard complex pathway may also be relevant for neurodevelopmental disorders related to prenatal health problems. Intrauterine growth restriction (IUGR) affects many pregnancies, leading to hypoxia in developing brain tissue that ultimately causes motor and cognitive defects in affected children. Among the more prominent features associated with IUGR is defective cerebellar development. A recent study using a porcine model of human neurodevelopment linked Pard complex defects directly to IUGR (Iskusnykh et al., 2021). IUGR in piglets leads to an enlarged EGL and defective GZ exit of GNPs, as assayed by *ex vivo* slice preparations of postnatal pig cerebella. Prominent reductions in Pard3 and Jam-C mRNA expression in the cerebella of piglets with IUGR suggested that GZ exit defects were due to defective neuronal polarization. Indeed, an *ex vivo* GZ exit assay like those developed with the mouse cerebellum showed that restoring Pard3 and Jam-C expression rescued GZ exit in IUGR cerebella to control levels. Interestingly, that study showed that Pard3 and Jam-C are also required for appropriate survival of differentiated CGNs, suggesting functions for neuronal polarity beyond the migration step in cerebellar development. Although the study did not link elevated prenatal hypoxia to defective GZ occupancy, the findings of Kullmann et al. (2020) suggest that the hypoxia associated with IUGR positions Hif1α and Zeb1 as central mediators of the reduced polarity gene expression observed when uterine insufficiency leads to prenatal hypoxia. These findings raise the tantalizing possibility of elevated polarity signaling having therapeutic benefits for two unrelated classes of neurological disorders: pediatric cancers and defects in brain development associated with prenatal hypoxia.

AUTHOR CONTRIBUTIONS

The author confirms being the sole contributor of this work and has approved it for publication.

FUNDING

The DS laboratory was funded by the American Lebanese Syrian Associated Charities (ALSAC) and by grants 1R01NS066936 and R01NS104029 from the National Institute of Neurological Disorders (NINDS).

ACKNOWLEDGMENTS

I thank Keith A. Laycock, Ph.D., ELS for editing the manuscript.

REFERENCES

Anne, S. L., Govek, E. E., Ayrault, O., Kim, J. H., Zhu, X., Murphy, D. A., et al. (2013). WNT3 inhibits cerebellar granule neuron progenitor proliferation and medulloblastoma formation via MAPK activation. *PLoS One* 8:e81769. doi: 10.1371/journal.pone.0081769

Barnes, A. P., Solecki, D., and Polleux, F. (2008). New insights into the molecular mechanisms specifying neuronal polarity in vivo. *Curr. Opin. Neurobiol.* 18, 44–52. doi: 10.1016/j.conb.2008.05.003

Barros, D. I., Amaral, F., and Pego, A. P. (2020). Laminin-Inspired cell-instructive microenvironments for neural stem cells. *Biomacromolecules* 21, 276–293. doi: 10.1021/acs.biomac.9b01319

Baum, B., and Georgiou, M. (2011). Dynamics of adherens junctions in epithelial establishment, maintenance, and remodeling. *J. Cell Biol.* 192, 907–917. doi: 10.1083/jcb.201009141

Bjornsson, C. S., Apostolopoulou, M., Tian, Y., and Temple, S. (2015). It takes a village: constructing the neurogenic niche. *Dev. Cell* 32, 435–446. doi: 10.1016/j.devcel.2015.01.010

Blaess, S., Graus-Porta, D., Belvindrah, R., Radakovits, R., Pons, S., Littlewood-Evans, A., et al. (2004). Beta1-integrins are critical for cerebellar granule cell precursor proliferation. *J. Neurosci.* 24, 3402–3412. doi: 10.1523/JNEUROSCI.5241-03.2004

Borello, U., and Pierani, A. (2010). Patterning the cerebral cortex: traveling with morphogens. *Curr. Opin. Genet. Dev.* 20, 408–415. doi: 10.1016/j.gde.2010.05.003

Campanale, J. P., Sun, T. Y., and Montell, D. J. (2017). Development and dynamics of cell polarity at a glance. *J. Cell Sci.* 130, 1201–1207. doi: 10.1242/jcs.188599

Caspary, T., Larkins, C. E., and Anderson, K. V. (2007). The graded response to Sonic Hedgehog depends on cilia architecture. *Dev. Cell* 12, 767–778. doi: 10.1016/j.devcel.2007.03.004

Chen, B. C., Legant, W. R., Wang, K., Shao, L., Milkie, D. E., Davidson, M. W., et al. (2014). Lattice light-sheet microscopy: imaging molecules to embryos at high spatiotemporal resolution. *Science* 346:1257998. doi: 10.1126/science.1257998

Choi, Y., Borghesani, P. R., Chan, J. A., and Segal, R. A. (2005). Migration from a mitogenic niche promotes cell-cycle exit. *J. Neurosci.* 25, 10437–10445. doi: 10.1523/JNEUROSCI.1559-05.2005

Chou, F. S., Li, R., and Wang, P. S. (2018). Molecular components and polarity of radial glial cells during cerebral cortex development. *Cell Mol. Life Sci.* 75, 1027–1041. doi: 10.1007/s00018-017-2680-0

Consalez, G. G., Goldowitz, D., Casoni, F., and Hawkes, R. (2020). Origins, development, and compartmentation of the granule cells of the cerebellum. *Front. Neural Circuits* 14:611841. doi: 10.3389/fncir.2020.611841

Corbin, J. G., Gaiano, N., Juliano, S. L., Poluch, S., Stancik, E., and Haydar, T. F. (2008). Regulation of neural progenitor cell development in the nervous system. *J. Neurochem.* 106, 2272–2287. doi: 10.1111/j.1471-4159.2008.05522.x

Dahmane, N., and Ruiz i Altaba, A. (1999). Sonic hedgehog regulates the growth and patterning of the cerebellum. *Development* 126, 3089–3100. doi: 10.1242/dev.126.14.3089

Dehay, C., Kennedy, H., and Kosik, K. S. (2015). The outer subventricular zone and primate-specific cortical complexification. *Neuron* 85, 683–694. doi: 10.1016/j.neuron.2014.12.060

Espinosa, J. S., and Luo, L. (2008). Timing neurogenesis and differentiation: insights from quantitative clonal analyses of cerebellar granule cells. *J. Neurosci.* 28, 2301–2312. doi: 10.1523/JNEUROSCI.5157-07.2008

Famulski, J. K., and Solecki, D. J. (2013). New spin on an old transition: epithelial parallels in neuronal adhesion control. *Trends Neurosci.* 36, 163–173. doi: 10.1016/j.tins.2012.10.002

Famulski, J. K., Trivedi, N., Howell, D., Yang, Y., Tong, Y., Gilbertson, R., et al. (2010). Siah regulation of Pard3A controls neuronal cell adhesion during germinal zone exit. *Science* 330, 1834–1838. doi: 10.1126/science.1198480

Fujita, S. (1967). Quantitative analysis of cell proliferation and differentiation in the cortex of the postnatal mouse cerebellum. *J. Cell Biol.* 32, 277–287. doi: 10.1083/jcb.32.2.277

Gao, W. O., Heintz, N., and Hatten, M. E. (1991). Cerebellar granule cell neurogenesis is regulated by cell-cell interactions in vitro. *Neuron* 6, 705–715. doi: 10.1016/0896-6273(91)90168-y

Goldstein, B., and Macara, I. G. (2007). The PAR proteins: fundamental players in animal cell polarization. *Dev. Cell* 13, 609–622. doi: 10.1016/j.devcel.2007.10.007

Goodrich, L. V., Milenkovic, L., Higgins, K. M., and Scott, M. P. (1997). Altered neural cell fates and medulloblastoma in mouse patched mutants. *Science* 277, 1109–1113. doi: 10.1126/science.277.5329.1109

Gossage, L., Eisen, T., and Maher, E. R. (2015). VHL, the story of a tumour suppressor gene. *Nat. Rev. Cancer* 15, 55–64. doi: 10.1038/nrc3844

Hatten, M. E., and Roussel, M. F. (2011). Development and cancer of the cerebellum. *Trends Neurosci.* 34, 134–142. doi: 10.1016/j.tins.2011.01.002

Hatten, M. E., Lynch, M., Rydel, R. E., Sanchez, J., Joseph-Silverstein, J., Moscatelli, D., et al. (1988). In vitro neurite extension by granule neurons is dependent upon astroglial-derived fibroblast growth factor. *Dev. Biol.* 125, 280–289. doi: 10.1016/0012-1606(88)90211-4

Hausmann, B., and Sievers, J. (1985). Cerebellar external granule cells are attached to the basal lamina from the onset of migration up to the end of their proliferative activity. *J. Comp. Neurol.* 241, 50–62. doi: 10.1002/cne.902410105

Horn, Z., Behesti, H., and Hatten, M. E. (2018). N-cadherin provides a cis and trans ligand for astrotactin that functions in glial-guided neuronal migration. *Proc. Natl. Acad. Sci. U.S.A.* 115, 10556–10563. doi: 10.1073/pnas.1811100115

Huangfu, D., and Anderson, K. V. (2005). Cilia and Hedgehog responsiveness in the mouse. *Proc. Natl. Acad. Sci. U.S.A.* 102, 11325–11330. doi: 10.1073/pnas.0505328102

Iskusnykh, I. Y., Fattakhov, N., Buddington, R. K., and Chizhikov, V. V. (2021). Intrauterine growth restriction compromises cerebellar development by affecting radial migration of granule cells via the JamC/Pard3a molecular pathway. *Exp. Neurol.* 336:113537. doi: 10.1016/j.expneurol.2020.113537

Iulianella, A., Wingate, R. J., Moens, C. B., and Capaldo, E. (2019). The generation of granule cells during the development and evolution of the cerebellum. *Dev. Dyn.* 248, 506–513. doi: 10.1002/dvdy.64

Ivan, M., and Kaelin, W. G. Jr. (2017). The EGLN-HIF O2-Sensing system: multiple inputs and feedbacks. *Mol. Cell* 66, 772–779. doi: 10.1016/j.molcel.2017.06.002

Jiang, Y., Yan, L., Xia, L., Lu, X., Zhu, W., Ding, D., et al. (2018). Zinc finger E-box-binding homeobox 1 (ZEB1) is required for neural differentiation of human embryonic stem cells. *J. Biol. Chem.* 293, 19317–19329. doi: 10.1074/jbc.RA118.005498

Kaelin, W. G. Jr., and Ratcliffe, P. J. (2008). Oxygen sensing by metazoans: the central role of the HIF hydroxylase pathway. *Mol. Cell* 30, 393–402. doi: 10.1016/j.molcel.2008.04.009

Kazanis, I., and ffrench-Constant, C. (2011). Extracellular matrix and the neural stem cell niche. *Dev. Neurobiol.* 71, 1006–1017. doi: 10.1002/dneu.20970

Kim, J. Y., Nelson, A. L., Algon, S. A., Graves, O., Sturla, L. M., Goumnerova, L. C., et al. (2003). *Medulloblastoma tumorigenesis* diverges from cerebellar granule cell differentiation in patched heterozygous mice. *Dev. Biol.* 263, 50–66. doi: 10.1016/s0012-1606(03)00434-2

Klein, R. S., Rubin, J. B., Gibson, H. D., DeHaan, E. N., Alvarez-Hernandez, X., Segal, R. A., et al. (2001). SDF-1 alpha induces chemotaxis and enhances Sonic hedgehog-induced proliferation of cerebellar granule cells. *Development* 128, 1971–1981. doi: 10.1242/dev.128.11.1971

Kullmann, J. A., Trivedi, N., Howell, D., Laumonnerie, C., Nguyen, V., Banerjee, S. S., et al. (2020). Oxygen tension and the VHL-Hif1α pathway determine onset of neuronal polarization and cerebellar germinal zone exit. *Neuron* 106:e605. doi: 10.1016/j.neuron.2020.02.025

Laumonnerie, C., and Solecki, D. J. (2018). Regulation of polarity protein levels in the developing central nervous system. *J. Mol. Biol.* 430, 3472–3480. doi: 10.1016/j.jmb.2018.05.036

Leto, K., Arancillo, M., Becker, E. B., Buffo, A., Chiang, C., Ding, B., et al. (2016). Consensus paper: cerebellar development. *Cerebellum* 15, 789–828. doi: 10.1007/s12311-015-0724-2

Lewis, P. M., Gritli-Linde, A., Smeyne, R., Kottmann, A., and McMahon, A. P. (2004). Sonic hedgehog signaling is required for expansion of granule neuron precursors and patterning of the mouse cerebellum. *Dev. Biol.* 270, 393–410. doi: 10.1016/j.ydbio.2004.03.007

Liu, J., Liu, Y., Shao, J., Li, Y., Qin, L., Shen, H., et al. (2019). Zeb1 is important for proper cleavage plane orientation of dividing progenitors and neuronal migration in the mouse neocortex. *Cell Death Differ.* 26, 2479–2492. doi: 10.1038/s41418-019-0314-9

Marthiens, V., Kazanis, I., Moss, L., Long, K., and Ffrench-Constant, C. (2010). Adhesion molecules in the stem cell niche–more than just staying in shape? *J. Cell Sci.* 123(Pt 10), 1613–1622. doi: 10.1242/jcs.054312

Morante-Redolat, J. M., and Porlan, E. (2019). Neural stem cell regulation by adhesion molecules within the subependymal niche. *Front. Cell Dev. Biol.* 7:102. doi: 10.3389/fcell.2019.00102

Nicot, A., Lelievre, V., Tam, J., Waschek, J. A., and DiCicco-Bloom, E. (2002). Pituitary adenylate cyclase-activating polypeptide and sonic hedgehog interact to control cerebellar granule precursor cell proliferation. *J. Neurosci.* 22, 9244–9254. doi: 10.1523/JNEUROSCI.22-21-09244.2002

Niewiadomski, P., Zhujiang, A., Youssef, M., and Waschek, J. A. (2013). Interaction of PACAP with Sonic hedgehog reveals complex regulation of the hedgehog pathway by PKA. *Cell Signal.* 25, 2222–2230. doi: 10.1016/j.cellsig.2013.07.012

Oliver, T. G., Read, T. A., Kessler, J. D., Mehmeti, A., Wells, J. F., Huynh, T. T., et al. (2005). Loss of patched and disruption of granule cell development in a pre-neoplastic stage of medulloblastoma. *Development* 132, 2425–2439. doi: 10.1242/dev.01793

Ong, T., Trivedi, N., Wakefield, R., Frase, S., and Solecki, D. J. (2020). Siah2 integrates mitogenic and extracellular matrix signals linking neuronal progenitor ciliogenesis with germinal zone occupancy. *Nat. Commun.* 11:5312. doi: 10.1038/s41467-020-19063-7

Ortega, J. A., Memi, F., Radonjic, N., Filipovic, R., Bagasrawala, I., Zecevic, N., et al. (2018). The subventricular zone: a key player in human neocortical development. *Neuroscientist* 24, 156–170. doi: 10.1177/1073858417691009

Pons, S., Trejo, J. L., Martinez-Morales, J. R., and Marti, E. (2001). Vitronectin regulates Sonic hedgehog activity during cerebellum development through CREB phosphorylation. *Development* 128, 1481–1492. doi: 10.1242/dev.128.9.1481

Qian, X., Goderie, S. K., Shen, Q., Stern, J. H., and Temple, S. (1998). Intrinsic programs of patterned cell lineages in isolated vertebrate CNS ventricular zone cells. *Development* 125, 3143–3152. doi: 10.1242/dev.125.16.3143

Qian, X., Shen, Q., Goderie, S. K., He, W., Capela, A., Davis, A. A., et al. (2000). Timing of CNS cell generation: a programmed sequence of neuron and glial cell production from isolated murine cortical stem cells. *Neuron* 28, 69–80. doi: 10.1016/s0896-6273(00)00086-6

Rios, I., Alvarez-Rodriguez, R., Marti, E., and Pons, S. (2004). Bmp2 antagonizes sonic hedgehog-mediated proliferation of cerebellar granule neurones through Smad5 signalling. *Development* 131, 3159–3168. doi: 10.1242/dev.01188

Rohatgi, R., Milenkovic, L., and Scott, M. P. (2007). Patched1 regulates hedgehog signaling at the primary cilium. *Science* 317, 372–376. doi: 10.1126/science.1139740

Roussel, M. F., and Hatten, M. E. (2011). Cerebellum development and medulloblastoma. *Curr. Top. Dev. Biol.* 94, 235–282.

Ryder, E. F., and Cepko, C. L. (1994). Migration patterns of clonally related granule cells and their progenitors in the developing chick cerebellum. *Neuron* 12, 1011–1028. doi: 10.1016/0896-6273(94)90310-7

Schwartz, P. M., Borghesani, P. R., Levy, R. L., Pomeroy, S. L., and Segal, R. A. (1997). Abnormal cerebellar development and foliation in BDNF-/- mice reveals a role for neurotrophins in CNS patterning. *Neuron* 19, 269–281. doi: 10.1016/s0896-6273(00)80938-1

Shen, Q., Wang, Y., Kokovay, E., Lin, G., Chuang, S. M., Goderie, S. K., et al. (2008). Adult SVZ stem cells lie in a vascular niche: a quantitative analysis of niche cell-cell interactions. *Cell Stem Cell* 3, 289–300. doi: 10.1016/j.stem.2008.07.026

Singh, S., and Solecki, D. J. (2015). Polarity transitions during neurogenesis and germinal zone exit in the developing central nervous system. *Front. Cell Neurosci.* 9:62. doi: 10.3389/fncel.2015.00062

Singh, S., Howell, D., Trivedi, N., Kessler, K., Ong, T., Rosmaninho, P., et al. (2016). Zeb1 controls neuron differentiation and germinal zone exit by a mesenchymal-epithelial-like transition. *Elife* 5:e12717. doi: 10.7554/eLife.12717

Solecki, D. J. (2012). Sticky situations: recent advances in control of cell adhesion during neuronal migration. *Curr. Opin. Neurobiol.* 22, 791–798. doi: 10.1016/j.conb.2012.04.010

Solecki, D. J., Liu, X. L., Tomoda, T., Fang, Y., and Hatten, M. E. (2001). Activated Notch2 signaling inhibits differentiation of cerebellar granule neuron precursors by maintaining proliferation. *Neuron* 31, 557–568. doi: 10.1016/s0896-6273(01)00395-6

Tavazoie, M., Van der Veken, L., Silva-Vargas, V., Louissaint, M., Colonna, L., Zaidi, B., et al. (2008). A specialized vascular niche for adult neural stem cells. *Cell Stem Cell* 3, 279–288. doi: 10.1016/j.stem.2008.07.025

Tiberi, L., Vanderhaeghen, P., and van den Ameele, J. (2012). Cortical neurogenesis and morphogens: diversity of cues, sources and functions. *Curr. Opin. Cell Biol.* 24, 269–276. doi: 10.1016/j.ceb.2012.01.010

Uzquiano, A., Gladwyn-Ng, I., Nguyen, L., Reiner, O., Gotz, M., Matsuzaki, F., et al. (2018). Cortical progenitor biology: key features mediating proliferation versus differentiation. *J. Neurochem.* 146, 500–525. doi: 10.1111/jnc.14338

von Knebel Doeberitz, C., Sievers, J., Sadler, M., Pehlemann, F. W., Berry, M., and Halliwell, P. (1986). Destruction of meningeal cells over the newborn hamster cerebellum with 6-hydroxydopamine prevents foliation and lamination in the rostral cerebellum. *Neuroscience* 17, 409–426. doi: 10.1016/0306-4522(86)90256-3

Wallace, V. A. (1999). Purkinje-cell-derived Sonic hedgehog regulates granule neuron precursor cell proliferation in the developing mouse cerebellum. *Curr. Biol.* 9, 445–448. doi: 10.1016/s0960-9822(99)80195-x

Wang, H., Xiao, Z., Zheng, J., Wu, J., Hu, X. L., Yang, X., et al. (2019). ZEB1 represses neural differentiation and cooperates with CTBP2 to dynamically regulate cell migration during neocortex development. *Cell Rep.* 27, 2333–2336. doi: 10.1016/j.celrep.2019.04.081

Wechsler-Reya, R. J., and Scott, M. P. (1999). Control of neuronal precursor proliferation in the cerebellum by Sonic Hedgehog. *Neuron* 22, 103–114. doi: 10.1016/s0896-6273(00)80682-0

Wingate, R. J., and Hatten, M. E. (1999). The role of the rhombic lip in avian cerebellum development. *Development* 126, 4395–4404. doi: 10.1242/dev.126.20.4395

Yang, Z. J., Ellis, T., Markant, S. L., Read, T. A., Kessler, J. D., Bourboulas, M., et al. (2008). Medulloblastoma can be initiated by deletion of Patched in lineage-restricted progenitors or stem cells. *Cancer Cell* 14, 135–145. doi: 10.1016/j.ccr.2008.07.003

Zhu, Y., Yu, T., Zhang, X. C., Nagasawa, T., Wu, J. Y., and Rao, Y. (2002). Role of the chemokine SDF-1 as the meningeal attractant for embryonic cerebellar neurons. *Nat. Neurosci.* 5, 719–720. doi: 10.1038/nn881

Zou, Y. R., Kottmann, A. H., Kuroda, M., Taniuchi, I., and Littman, D. R. (1998). Function of the chemokine receptor CXCR4 in haematopoiesis and in cerebellar development. *Nature* 393, 595–599.

Conflict of Interest: The author declares that the research was conducted in the absence of any commercial or financial relationships that could be construed as a potential conflict of interest.

frontiers | Frontiers in Molecular Neuroscience

ORIGINAL RESEARCH
published: 27 May 2022
doi: 10.3389/fnmol.2022.832317

Multiple Roles of Ret Signalling During Enteric Neurogenesis

Dipa Natarajan[1,2], Conor McCann[2], Justine Dattani[3], Vassilis Pachnis[1,4]*† and Nikhil Thapar[1,2,5,6,7]*†*

[1] Division of Molecular Neurobiology, MRC National Institute for Medical Research, London, United Kingdom, [2] Birth Defects Research Centre, Great Ormond Street Institute of Child Health, University College London, London, United Kingdom, [3] Department of Mathematical Sciences, University of Bath, Bath, United Kingdom, [4] The Francis Crick Institute, London, United Kingdom, [5] Department of Gastroenterology, Hepatology and Liver Transplant, Queensland Children's Hospital, Brisbane, QLD, Australia, [6] Faculty of Medicine, University of Queensland, Brisbane, QLD, Australia, [7] Woolworths Centre for Child Nutrition Research, Queensland University of Technology, Brisbane, QLD, Australia

OPEN ACCESS

Edited by:
Sumru Bayin, Memorial Sloan Kettering Cancer Center, United States

Reviewed by:
Marlene M. Hao, The University of Melbourne, Australia
Artur Kania, Montreal Clinical Research Institute (IRCM), Canada

***Correspondence:**
Dipa Natarajan
dipanatarajan@gmail.com
Vassilis Pachnis
Vassilis.Pachnis@crick.ac.uk
Nikhil Thapar
Nikhil.Thapar@health.qld.gov.au

† These authors have contributed equally to this work

Specialty section:
This article was submitted to Methods and Model Organisms, a section of the journal Frontiers in Molecular Neuroscience

Received: *09 December 2021*
Accepted: *15 March 2022*
Published: *27 May 2022*

Citation:
Natarajan D, McCann C, Dattani J, Pachnis V and Thapar N (2022) Multiple Roles of Ret Signalling During Enteric Neurogenesis. Front. Mol. Neurosci. 15:832317. doi: 10.3389/fnmol.2022.832317

The majority of the enteric nervous system is formed by vagal neural crest cells which enter the foregut and migrate rostrocaudally to colonise the entire length of the gastrointestinal tract. Absence of enteric ganglia from the distal colon are the hallmark of Hirschsprung disease, a congenital disorder characterised by severe intestinal dysmotility. Mutations in the receptor tyrosine kinase RET have been identified in approximately 50% of familial cases of Hirschsprung disease but the cellular processes misregulated in this condition remain unclear. By lineage tracing neural crest cells in mice homozygous for a knock-in allele of *Ret* (*Ret*$^{51/51}$), we demonstrate that normal activity of this receptor is required *in vivo* for the migration of enteric nervous system progenitors throughout the gut. In mutant mice, progenitors of enteric neurons fail to colonise the distal colon, indicating that failure of colonisation of the distal intestine is a major contributing factor for the pathogenesis of Hirschsprung disease. Enteric nervous system progenitors in the ganglionic proximal guts of mutant mice are also characterised by reduced proliferation and differentiation. These findings suggest that the functional abnormalities in Hirschsprung disease result from a combination of colonic aganglionosis and deficits in neuronal circuitry of more proximal gut segments. The reduced neurogenesis in the gut of *Ret*$^{51/51}$ mutants was reproduced in the multilineage enteric nervous system progenitors isolated from these animals. Correction of the molecular defects of such progenitors fully restored their neurogenic potential in culture. These observations enhance our understanding of the pathogenesis of Hirschsprung disease and highlight potential approaches for its treatment.

Keywords: enteric nervous system, neural crest cells, Hirschsprung disease, colonic aganglionosis, normoganglionic gut, ENS progenitor cells, isoforms

HIGHLIGHTS

- Normal *Ret* activity is required for migration, proliferation and neuronal differentiation of neural crest cells (NCC).
- The $Ret^{51/51}$ mouse line (homozygous for a knock-in mutation expressing only the Ret^{51} isoform) is an established animal model of human Hirschsprung Disease.
- Ret^{51}/YFP line generated to lineage trace NCC in these animals.
- Neuronal circuitry is affected in the proximal "normoganglionic" region of $Ret^{51/51}$ gut as shown by DiI labelling of the nerve plexuses.
- ENS progenitor cells (EPCs) derived from the ganglionic segment of $Ret^{51/51}$ guts exhibit defects *in vitro*.
- $Ret^{51/51}$ EPCs can be rescued by introducing the Ret^{9} isoform.
- Proximal segments of $Ret^{51/51}$ gut may phenocopy the dysfunction commonly observed in the proximal ganglionated bowel in Hirschsprung Disease.
- Study enhances our understanding of Hirschsprung disease and highlights potential treatment approaches.

INTRODUCTION

The enteric nervous system (ENS) is composed of a large number of neurons and glia which form interconnected ganglia that control the peristalsis, blood flow and secretions of the gut wall (Furness, 2006). In mice, most progenitors of the ENS originate at embryonic day (E) 8.5–8.75 from the vagal neural crest (NC) and migrate ventrolaterally to reach the dorsal aorta. These pre-enteric NC cells (pENCCs) invade the foregut mesenchyme and (thereafter called enteric NC cells-ENCCs) initiate their rostrocaudal migration to colonise, uniformly, the entire length of the gastrointestinal tract (Kapur et al., 1992; Lo and Anderson, 1995; Durbec P. et al., 1996; Durbec P. L. et al., 1996; Pattyn et al., 1999; Young et al., 2001; Burns, 2005). During migration, ENCCs receive signals that allow them to survive, proliferate extensively and differentiate into enteric neurons and glia (Heanue and Pachnis, 2007; Laranjeira et al., 2011; Sasselli et al., 2012; Akbareian et al., 2013).

Hirschsprung disease (HSCR) is a congenital condition characterized by a failure of the ENS to complete development along the length of the gastrointestinal (GI) tract, which results in the absence of enteric ganglia in the most distal segment of the large intestine, variably extending more proximally. This leads to tonic muscle contraction of the affected part resulting in functional intestinal obstruction and, if left untreated, toxic megacolon and death (Amiel et al., 2008). Surgical resection of the aganglionic gut segment remains the treatment of choice for HSCR patients as it alleviates the life-threatening consequences of obstruction (Haricharan and Georgeson, 2008). However, a significant proportion, if not the majority, of HSCR patients are characterised post-operatively by high levels of morbidity (Metzger et al., 2009) although it is currently unclear whether this results from the primary pathology (aganglionosis) and the necessary surgical intervention or from additional deficits in the maturation and function of neuronal networks in more proximal and apparently "normoganglionic" gut segments.

Intestinal aganglionosis is caused by molecular defects in extracellular signals and their receptors, intracellular molecular cascades and diverse classes of transcription factors (Heanue and Pachnis, 2007). The receptor tyrosine kinase (RTK) Ret, in association with the GPI-anchored co-receptors GFRα1-4, forms signalling receptor complexes that are activated by the GDNF family of ligands (GFLs) (Airaksinen et al., 1999; Baloh et al., 2000). *Ret*, *Gfrα1* and *Gdnf* are critical for the development of the mammalian ENS since deletion of each of these genes results in total intestinal aganglionosis (Schuchardt et al., 1994; Moore et al., 1996; Pichel et al., 1996; Sanchez et al., 1996; Enomoto et al., 1998). Consistent with the role of *Ret* in mouse ENS development, mutations in the human homologue have been identified in approximately 50% of familial cases of HSCR (Amiel et al., 2008; Emison et al., 2010). Although no changes in the coding sequence of *RET* can be identified in the remaining familial cases, reduced expression of this gene is thought to be a contributing factor in most cases of HSCR (Grice et al., 2005; Miao et al., 2010).

In mouse embryos, *Ret* is not expressed during the early stages of vagal NC migration but the gene is induced in pENCCs as they approach the dorsal aorta (Durbec P. L. et al., 1996). During colonisation of the gut by ENCCs *Ret* expression is maintained in undifferentiated progenitors and in enteric neurons, but the gene is down-regulated in glial cells (Hao and Young, 2009; Laranjeira and Pachnis, 2009). Analysis of the phenotype of mutant mice has demonstrated that Ret signalling is necessary for the survival of the early progenitors of the ENS within the foregut, while *in vitro* and organ culture studies have suggested that Ret promotes the proliferation and migration of ENCCs (Taraviras et al., 1999; Young and Newgreen, 2001; Natarajan et al., 2002; Gianino et al., 2003). The role of Ret signalling in the differentiation of enteric neurons and the formation of functional neuronal circuits within the gut has been described by Lasrado et al. (2017). However, the elimination of the majority of early ENS progenitors upon *Ret* deletion has prevented the *in vivo* analysis of the role of this signalling pathway on the proliferation and migration of ENCCs at later stages of embryogenesis. These studies require the generation and analysis of hypomorphic and conditional mutant alleles of *Ret* which can by-pass the early requirement of this gene for the survival of early ENS progenitors (Uesaka et al., 2008; Uesaka and Enomoto, 2010).

c-Ret is expressed in two main isoforms Ret^{9} and Ret^{51}, which differ in their C-terminal tail sequence from residue 1062 (Y1062): with Ret^{9} containing 9 downstream amino acids versus 51 different amino acids in Ret^{51}. Both isoforms have been shown to be important in ENS development. In order to provide critical insights into the role of Ret in ENS development we have previously generated the monoisoformic alleles Ret^{9} and Ret^{51}, which express one of the two main Ret isoforms, Ret^{9}, Ret^{51}, respectively (de Graaff et al., 2001). Using targeted mutagenesis in embryonic stem cells, monoisoformic mouse lines were generated expressing either Ret^{51} or Ret^{9} isoforms. Mice expressing only Ret^{9} isoform were phenotypically normal and displayed a normal ENS. However, mice homozygous for

the Ret^{51} isoform (i.e., expressing only Ret^{51} and no Ret^{9}) lack enteric ganglia from the distal 2/3 of the colon and show intestinal obstruction and megacolon, cardinal features of HSCR (de Graaff et al., 2001). Ret and other signalling pathways such as EDNRB as well as transcription factors such as Sox10 have been shown to be important for ENS development (Barlow et al., 2003; Bondurand et al., 2006). The binding of ligands (Durbec P. et al., 1996; Trupp et al., 1996) activates the Ret receptor and triggers multiple transduction pathways through different adaptor proteins. It has been hypothesised that altered adapter protein binding, to isoform-specific carboxyl-terminal sequences, mediates downstream signalling activation and the developmental functions of each isoform (Wong et al., 2005; Jain et al., 2010). However, the molecular mechanisms underlying the differing functions of the individual isoforms remain unclear. Therefore, to better understand the consequences of *Ret* mutations in ENS development, we have analysed the phenotype of $Ret^{51/51}$ homozygous animals during embryogenesis and explored the mechanisms by which *Ret* mutations lead to aganglionosis. These experiments suggest that normal *Ret* activity is required *in vivo* for the efficient migration of ENCCs throughout the gastrointestinal tract and for their normal proliferation and neuronal differentiation. Moreover, we demonstrate that enteric neurons in $Ret^{51/51}$ homozygous mice have defective axonogenesis and thus abnormal neuronal circuits within the gut wall. We also show that the neuronal deficit in the gut of $Ret^{51/51}$ mutants can be reproduced in clonogenic cultures of multilineage ENS progenitors isolated from embryonic gut and that this deficit can be rescued by expression of the missing Ret^{9} isoform. Based on these findings, we suggest that abnormal intestinal function in HSCR patients is not restricted to the aganglionic hindgut but is likely to involve more proximal "normoganglionic" gut segments. Our data also argue that the neurogenic deficit of multilineage ENS progenitors from HSCR patients is not irreversible and can be restored by correcting the relevant molecular defect.

MATERIALS AND METHODS

Animals

The generation of the Ret^{51} (de Graaff et al., 2001) and $Rosa26^{stopYFP}$ (MGI:2449038) (Srinivas et al., 2001) alleles and the $Tg^{Wnt1Cre}$ (MGI:2386570) transgene have been described previously (Danielian et al., 1997). Since the *Rosa26* (MGI:104735) and *Ret* (MGI:97902) loci are linked on mouse chromosome 6[1], and the Ret^{51} and $Rosa26^{stopYFP}$ alleles have been generated independently, we devised a breeding strategy to generate a recombinant chromosome that carries both alleles. More specifically, we first crossed $Ret^{+/+}$;$Rosa26^{+/StopYFP}$ and $Ret^{+/51}$;$Rosa26^{+/+}$ animals to generate mice heterozygous for both the Ret^{51} and $Rosa26^{StopYFP}$ alleles. These mice were then crossed to wild-type animals and their progeny were screened for co-transmission of Ret^{51} and $R26^{StopYFP}$. Approximately 2% (1/50) of these mice were positive for both alleles suggesting that meiotic recombination generated a recombinant chromosome carrying both alleles (YFP and Ret^{51} knocked-in alleles). This was subsequently confirmed by further breeding of these animals to wild-type mice and genotyping of their progeny. The day of vaginal plug detection was considered to be E0.5. Mouse studies were carried out under the authority of a UK Home Office Project License in a Home Office designated facility.

[1]www.ensembl.org

Immunostaining

Immunostaining on whole mount gut preparations was performed as described previously (Bondurand et al., 2006). Briefly, dissected guts were fixed for 2 h in 4% PFA at 4°C, washed in PBT (PBS + 0.1% Triton X100) and incubated in PBT containing 10% heat-inactivated sheep serum (PBT-HISS) at room temperature (RT) for a minimum of 1 hour. The specimens were then incubated overnight (O/N) at 4°C with either rabbit anti-GFP (Molecular Probes; 1:1000) or the mouse anti-b-Tubulin III, TuJ1 (Covance, United Kingdom; 1:1000) diluted in PBT-HISS. After washing, secondary antibody (in PBT-HISS) was applied for 2-3 h at RT or O/N at 4^{o}C (anti-rabbit Alexa Fluor 488 or anti-mouse Alexa Fluor 568 (both Molecular Probes, 1:1000). After several washes in PBT, samples were photographed using a Leica GFP microscope and documented using OpenLab software.

Fixed and cryoprotected embryos were frozen in OCT compound and sections were cut at 12 μm thickness using a MICROM HM 560 cryostat. For immunolabelling, sections were postfixed with 4%PFA, washed with PBS + 0.1% Triton X100 (PBT), and blocked for 30 min using blocking solution (1%BSA, 0.15% glycine in PBT). All primary antibodies were diluted using the blocking solution and were applied O/N. Secondary antibodies were applied for 1–4 h at RT. Slides were mounted using anti-fade mountant (Vectashield + Dapi; Vector Laboratories).

Short term cultures were fixed for 10 min at RT with 4% PFA, washed with PBT and treated with primary and secondary antibodies as described above.

The antibodies used were as follows: TuJ1 (Covance, United Kingdom 1:1000); GFP (anti-mouse or anti-rabbit Molecular Probes, 1:1000); GFAP (rabbit; DAKO, United States, 1:400); B-FABP (rabbit; kind gift from Thomas Muller, 1:1000); SOX10 (mouse; cell line kindly provided by Dr. David Anderson, 1:1), anti-HuC&D (mouse, Molecular Probes, 1:300); anti-BrdU antibody (rat; Oxford Biotechnology, 1:500), anti-phospho-histone 3 (PH3, rabbit; Chemicon, 1:500). Secondary antibodies used were anti-mouse Alexa Fluor 488 or 568, anti-rabbit Alexa Fluor 488 or 568, anti-rat Alexa Fluor 568 (all Molecular Probes, 1:1000 dilution).

Immunostaining of gut short term cultures or sections from embryos exposed to BrdU were performed as follows. Following incubation with primary and secondary antibodies as above, cell/sections were post-fixed in 4% PFA for 10 min, washed with PBT and then incubated in freshly prepared 2 M HCl in PBT at RT for 15 min. After washing with 1x PBS for 2 × 5 min at RT, cells/sections were incubated with primary and secondary antibodies (rat anti-BrdU followed by anti-rat Alexa Fluor 568). Cells/sections were washed and mounted in Vectashield + Dapi.

BrdU Incorporation

BrdU (Sigma-Aldrich, Feltham, United Kingdom) stock solution (10 mg/ml made in 0.9% NaCl) was injected intraperitoneally (10 μl/gm) into pregnant mice and embryos were harvested 1 h after the BrdU injection. Embryos were processed for sectioning as described above.

Short Term Enteric Nervous System Cultures

Short term cultures were performed as described previously (Bondurand et al., 2006). Guts were dissected from E11.5 or E14.5 embryos in L15 medium (PAA Laboratories, Yeovil, United Kingdom), washed 2x in Ca^{2+} and Mg^{2+} free PBS (Phosphate Buffered Saline; Roche) and incubated with dispase/collagenase (Roche, 0.5 mg/ml in PBS) for 3 min at RT (E11.5) or 45 min at 37^{o}C (E14.5). The tissue was then washed in 1xPBS, dissociated into single cells by pipetting and plated onto fibronectin-coated (20 μg/ml, Sigma) 8-well permanox slide wells (VWR, Leicestershire, United Kingdom) in OptiMEM (Gibco, Invitrogen, Horsham and Loughborough, United Kingdom) supplemented with L-glutamine (1 mM; Gibco Invitrogen, Horsham and Loughborough, United Kingdom) and 1% penicillin/streptomycin (Gibco Invitrogen, Horsham and Loughborough, United Kingdom). These cultures were maintained for 2–3 h in a 37^{o}C incubator with 5%CO_2, and then processed for immunostaining.

To establish short term ENS cultures from perinatal animals, guts were incubated in L15 medium on ice for 20–30 min. The outer muscle layers containing myenteric plexus was peeled, rinsed in 1xPBS and digested with 1mg/ml of Collagenase, Type IV (Sigma-Aldrich, Feltham, United Kingdom) for 1 h at 37^{o}C. The tissue was washed with PBS, resuspended in OptiMEM, supplemented with L-glutamine (1 mM; Gibco Invitrogen, Horsham and Loughborough, United Kingdom) and 1% penicillin/streptomycin (Gibco Invitrogen, Horsham and Loughborough, United Kingdom) and plated onto fibronectin coated dishes and cultured 2–3 h.

Neuronal Outgrowth

For neuronal outgrowth assays, E11.5 guts from +/*Ret*^{51} x + /*Ret*^{51} heterozygous crosses were dissociated individually as mentioned above and plated sparsely onto dishes coated with 1 mg/ml poly-D-lysine hydrobromide (Sigma-Aldrich, Feltham, United Kingdom) and 100 mg/ml Laminin (Sigma-Aldrich, Feltham, United Kingdom) in Neurobasal medium (Invitrogen, United Kingdom) with N2 and B27 supplements (Invitrogen, United Kingdom), 1% penicillin/streptomycin (Gibco Invitrogen, Horsham and Loughborough, United Kingdom) and 1 mM Glutamine (Gibco Invitrogen, Horsham and Loughborough, United Kingdom). The cultures were maintained for 6 days in an incubator at 37^{o}C with 5% CO_2. Cultures were then fixed and processed for immunolabelling with TuJ1 antibody. Neuronal outgrowths were measured using the Neuronal outgrowth programme (Metamorph) on an Axiophot fluorescence microscope.

DiI Labelling of Postnatal Guts and Estimation of Neurite Length

Guts isolated from postnatal animals from +/*Ret*^{51} x + /*Ret*^{51} heterozygous crosses were fixed in 4% PFA for 20 min at RT. A small crystal of DiI (1,1′-didodecyl 3,3,3′,3′-indocarbocyanine perchlorate, Cell Tracker, Molecular Probes) was placed at 2 different locations on the midgut and the colon. Organs were then placed in 4% PFA for 6 days in a 37^{o}C incubator, washed with PBS and mounted onto glass slides for photography. The axons which projected furthest at P1, in both the oral and aboral directions from the DiI crystal placed in the midgut, were measured using the Neurite outgrowth programme (Metamorph). 10–12 axons from 6 control (*Ret*$^{+/+}$) and mutant *Ret*$^{51/51}$ guts, obtained from 4 independent litters, were measured both orally and aborally in control and mutant genotypes.

Generation and Analysis of Enteric Nervous System Progenitor Cells From *Ret*$^{51/51}$ Guts

Retroviruses expressing *Ret*^{9} or *Ret*^{51} were generated by cloning human cDNA for *Ret*^{9} or *Ret*^{51} into the Not1 site of the pMX-IRES-GFP vector. Isolation of EPCs, analysis of clonal cultures and pMX-IRES-GFP-retroviral transductions have been described previously (Bondurand et al., 2003). Briefly, guts were isolated individually from +/*Ret*^{51} x + /*Ret*^{51} heterozygous crosses, enzymatically dissociated and cultured until neurophere-like bodies formed at approximately day 7. Genotypes were pooled and transduced with the retroviruses for either 7 h (embryonic cells) or O/N (for postnatal cells) and FACS sorted for GFP. GFP + EPCs were plated at "clonal" density (i.e., about 200–300 cells per well of 6 well dish) and cultured for 7–10 days. Colonies were then immunostained and analysed as described above (36). Efficiency of transduction varied with the batch of retrovirus (i.e., control GFP RV vs. Ret^9 RV vs. Ret^{51} RV). However, with an MOI of 2–3, the efficiency was found to be approximately 5% in embryonic gut cells versus 1% in postnatal gut cells. For all EPCs experiments, 3 independent litters were used. In each litter, cells of the same genotype were pooled. Post FACS, 6–11 colonies with 50–100 cells were counted in each experiment.

Imaging

All samples were analysed using either an Axiophot epifluorescence microscope (Zeiss), or an Axiovert microscope (Zeiss). Whole mounts guts were analysed using an Olympus/Leica stereoscope. All figures were compiled using Adobe Photoshop software.

Statistical Analysis

Data are expressed as mean ± standard error of the mean. Statistical analysis was performed using GraphPad Prism software (GraphPad). Intergroup differences were evaluated by Welch's *t*-test, in addition to ANOVA in **Figure 6**. In cases where sample sizes were small, we further applied Mann–Whitney *U* tests which validated the results obtained via *t*-test analysis. Statistical differences were considered to be significant if *p*-value was less than 0.05.

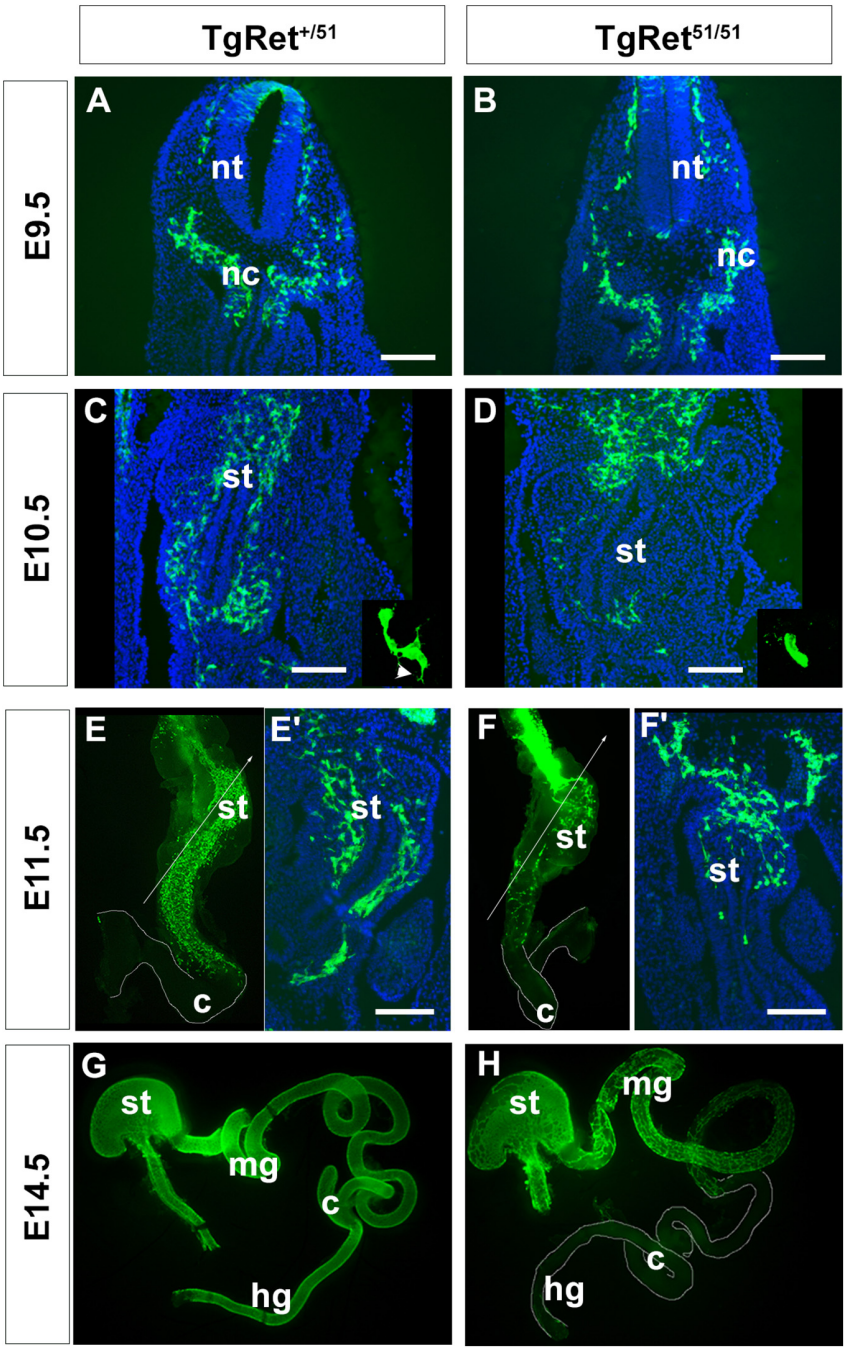

FIGURE 1 | Delayed migration of ENS progenitors along the gut of *Ret*$^{51/51}$ mutant embryos. **(A,B)** Immunostaining of representative cryosections through the foregut of control (Tg*Ret*$^{+/51}$) and Tg*Ret*$^{51/51}$ E9.5 embryos with GFP-specific antibodies. At this stage no difference was detected in the distribution of GFP-labelled vagal neural crest cells (nc) and pENCCs between control and mutant embryos. **(C,D)** GFP immunostaining of sections through the foregut of E10.5 control (Tg*Ret*$^{+/51}$) and Tg*Ret*$^{51/51}$ embryos. In control (Tg*Ret*$^{+/51}$) embryos, ENCCS are distributed throughout the foregut mesenchyme but in Tg*Ret*$^{51/51}$ mutants they fail to migrate much beyond the gastroesophageal junction. Insets show high power images of isolated GFP^{+} cells from control (Tg*Ret*$^{+/51}$) and mutant embryos, respectively. Arrowhead in inset **(C)** shows projections in control ENCC. **(E,F)** Whole mount preparations of gut dissected from control (Tg*Ret*$^{+/51}$) and Tg*Ret*$^{51/51}$ E11.5 embryos, immunostained for GFP showing that migration of Tg*Ret*$^{51/51}$ ENCCs is delayed relative to control Tg*Ret*$^{+/51}$ cells. **(E',F')** Sections through the foregut of control Tg*Ret*$^{+/51}$ and Tg*Ret*$^{51/51}$ embryos that correspond to the lines shown respectively in **(E,F)**. **(G,H)** Whole mount preparations of gut dissected from control Tg*Ret*$^{+/51}$ and Tg*Ret*$^{51/51}$ E14.5 embryos immunostained for GFP. Control ENS progenitors have colonized the entire gut but *Ret*$^{51/51}$ progenitors have colonized only the foregut and the proximal half of the small intestine. Embryos from 3 litters per stage were used (approximately 4–6 per genotype). The embryos were isolated, genotyped individually and analyzed separately using immunolabelling. Scale bar: 200 μm. nc, neural crest; nt, neural tube; st, stomach; mg, midgut; c, caecum; hg, hindgut. Tg*Ret*$^{+/51}$ represents cells or embryos from genotype *Wnt1*$^{cre/+}$;*R26R*$^{stop/YFP}$;*Ret*$^{+/51}$ and Tg*Ret*$^{51/51}$ represents cells or embryos from genotype *Wnt1*$^{cre/+}$;*R26R*$^{stop/YFP}$;*Ret*$^{51/51}$.

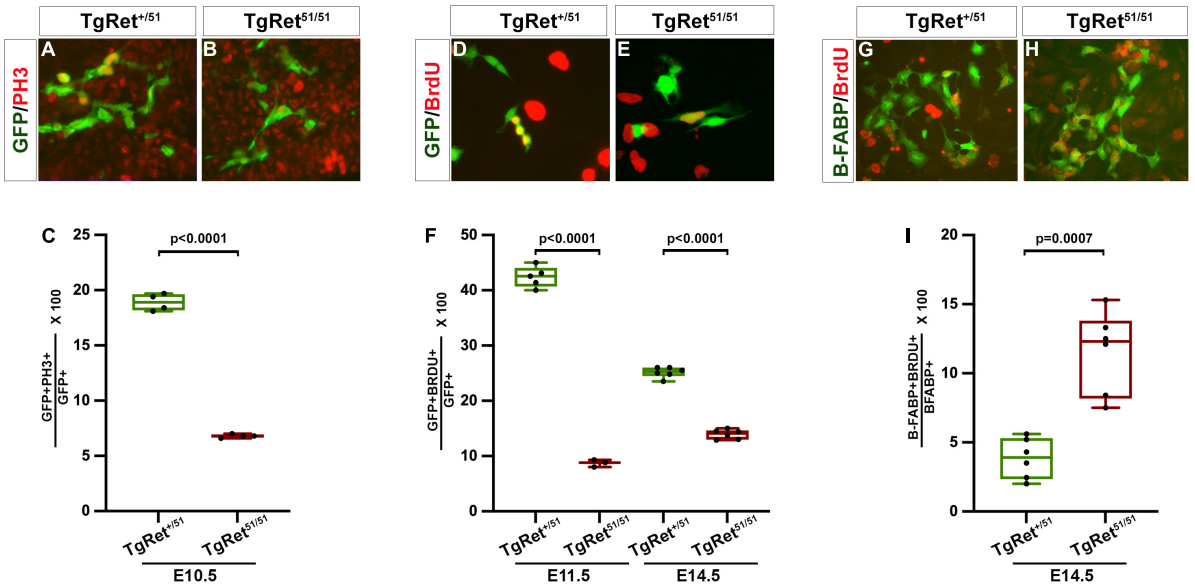

FIGURE 2 | Reduced proliferation of ENCCs homozygous for the *Ret*$^{51/51}$ mutation. **(A,B)** Short term cultures of dissociated gut from control (Tg*Ret*$^{+/51}$) and Tg*Ret*$^{51/51}$ E10.5 embryos immunostained for GFP and PH3. **(C)** Quantification of the percentage of double positive cells (GFP^{+}PH3^{+} {green/red}) in the two genotypes $n = 4$. **(D,E)** Short term cultures established from dissociated guts from control (Tg*Ret*$^{+/51}$) and Tg*Ret*$^{51/51}$ embryos that had previously been exposed to BrdU. **(F)** The fraction of GFP^{+}BrdU^{+} {green/red} cells was quantified for E11.5 and E14.5 embryos ($n = 5, 6$ resp). **(G,H)** Short term cultures of dissociated gut from control (Tg*Ret*$^{+/51}$) and Tg*Ret*$^{51/51}$ E14.5 embryos immunostained form B-FABP (green) and BrdU (red) $n = 6$. **(I)** Quantification of the percentage of B-FABP^{+}BrdU^{+} double immunostained cells. GFP (green), BrdU (red). Statistical analysis performed by Welch's *t*-test. Tg*Ret*$^{+/51}$ represents cells or embryos from genotype *Wnt1*$^{cre/+}$;*R26R*$^{stop/YFP}$;*Ret*$^{+/51}$ and Tg*Ret*$^{51/51}$ represents cells or embryos from genotype *Wnt1*$^{cre/+}$;*R26R*$^{stop/YFP}$;*Ret*$^{51/51}$.

RESULTS

Delayed Colonisation of the Gut by *Ret*$^{51/51}$ Homozygous Neural Crest Cells

To explore the mechanisms of aganglionosis in HSCR cases resulting from *RET* mutations we compared the development of the ENS in embryos in which NC cells were either heterozygous or homozygous for the *Ret*^{51} mutation. To facilitate these studies, we lineally marked early NC cells by generating, via breeding, a recombinant chromosome carrying both alleles (*R26*^{StopYFP}*Ret*^{51}; for breeding strategy see section "Materials and Methods"). Enteric neurogenesis was then compared in *Tg*$^{Wnt1-cre}$ transgenics that were either heterozygous *R26*^{StopYFP}*Ret*$^{+/51}$ (hereafter called control; Tg*Ret*$^{+/51}$) or homozygous for the *R26*^{StopYFP}*Ret*$^{51/51}$ mutant allele (hereafter called Tg*Ret*$^{51/51}$). Embryos from 3 litters per stage were used. The embryos were isolated genotyped individually and analysed separately using immunolabelling. In E9.0-9.5 control Tg*Ret*$^{+/51}$ embryos, YFP^{+} vagal NC cells were present lateral to the neural tube and ventrolaterally to the dorsal aorta (**Figure 1A**). A similar distribution of YFP^{+} cells was observed in equivalent sections from Tg*Ret*$^{51/51}$ embryos (**Figure 1B**), indicating that the pre-enteric stages of vagal NC cell migration remain unaffected by the *Ret*^{51} mutation. In E10.5 control (Tg*Ret*$^{+/51}$) embryos a large number of YFP^{+} cells were found scattered throughout the mesenchyme of the foregut, from the ventral side of the dorsal aorta (**Figure 1C** top), through the wall of the stomach and up to the duodenum (**Figure 1C** bottom). In mutant littermates however, YFP^{+} cells were present in the mesenchyme of the gastroesophageal junction (**Figure 1D**) with very few cells found in more distal foregut regions. Consistent with their migratory behaviour, in control (Tg*Ret*$^{+/51}$) embryos, YFP^{+} cells projected prominent cellular processes into the surrounding mesenchyme but such processes were conspicuously absent from mutant (Tg*Ret*$^{51/51}$) YFP^{+} cells (compare insets in **Figures 1C,D** and arrowhead in **Figure 1C**).

As expected, in E11.5 control (Tg*Ret*$^{+/51}$) embryos YFP^{+} cells had colonised the foregut and most of the small intestine with the front of NC cell migration approaching the caecum (**Figures 1E,E'**). In contrast, noticeably fewer YFP^{+} cells were present in the stomach and the small intestine of mutant littermates and the front of migration was located at more proximal gut regions (**Figures 1F,F'**). In addition to their reduced number and delayed migration, mutant ENCCs and their progeny were tightly packed and only occupied a small sector of the intestinal radial axis (data not shown).

In control (Tg*Ret*$^{+/51}$) embryos colonisation of the gastrointestinal tract by ENCCs was completed by E14.5 (**Figure 1G**; Young et al., 1998; Bondurand et al., 2006). However, in similar stage mutant embryos (Tg*Ret*$^{51/51}$), the front of migration of YFP^{+} cells were still within the small intestine (**Figure 1H**). Eventually, ENCCs colonised the entire small intestine and the proximal colon of Tg*Ret*$^{51/51}$ animals but no colonisation of the distal 2/3 of the colon was observed at any stage. Taken together, these data indicate that despite the timely invasion of the foregut mesenchyme by *Ret*$^{51/51}$

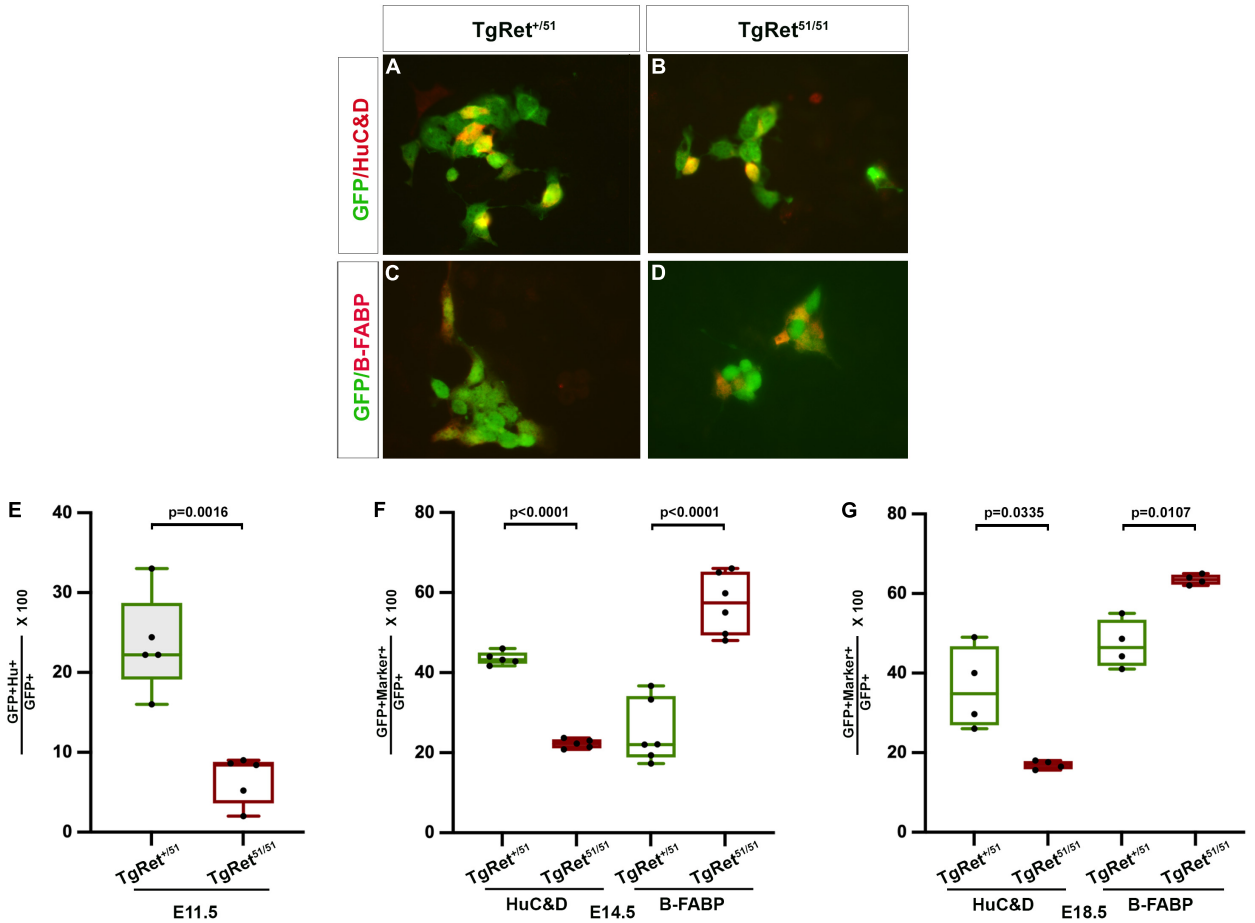

FIGURE 3 | Normal *Ret* activity is required for enteric neuron differentiation. **(A,B)** Short term cultures of dissociated gut from control Tg*Ret*$^{+/51}$ **(A)** and Tg*Ret*$^{51/51}$ **(B)** E11.5 embryos showing the co-expression of GFP (green) with a neuronal marker HuC/D (red). **(C,D)** Short term cultures of gut from control Tg*Ret*$^{+/51}$ **(C)** and Tg*Ret*$^{51/51}$ **(D)** E14.5 embryos showing co-expression of GFP (green) and a glial marker B-FABP (red). **(E–G)** Quantification of the percentage of GFP cells co-expressing either HuC/D or B-FABP at various time points. Graph showing percentage of GFP co-expressing HuC/D at E11.5 **(E)**. A significantly smaller fraction of *Ret*$^{51/51}$ GFP^{+} cells have differentiated into neurons. Quantification of the percentage of GFP cells co-expressing HuC/D or B-FABP in short-term cultures of dissociated gut from control, Tg*Ret*$^{+/51}$ and Tg *Ret*$^{51/51}$ E14.5 embryos **(F)**. Quantification of percentage of GFP cells co-expressing HuC/D or B-FABP from whole mount of myenteric plexus of E18.5 **(G)** from control Tg*Ret*$^{+/51}$ and Tg*Ret*$^{51/51}$ embryos. Although the fraction of *Ret*$^{51/51}$ GFP^{+} cells that have differentiated into neurons is reduced, the fraction expressing glial markers is increased at both E14.5 and E18.5. Embryos from 4 litters were used for analysis. Statistical analysis performed by Welch's *t*-test. Tg*Ret*$^{+/51}$ represents cells or embryos from genotype *Wnt1*$^{cre/+}$;*R26R*$^{stop/YFP}$;*Ret*$^{+/51}$ and Tg*Ret*$^{51/51}$ represents cells or embryos from genotype *Wnt1*$^{cre/+}$;*R26R*$^{stop/YFP}$;*Ret*$^{51/51}$.

ENCCs, the subsequent rostrocaudal migration of these cells is severely compromised. Such migratory deficit is evident throughout the period of colonisation of the gut by ENS progenitors and results in failure of arrival of ENCCs in the distal colon.

Reduced Proliferation of *Ret*$^{51/51}$ Homozygous Enteric Neural Crest Cells

The reduction in the number of ENCCs in the gut of Tg*Ret*$^{51/51}$ embryos (**Figure 1**) raised the possibility that normal *Ret* activity is required *in vivo* for the proliferation of ENS precursors. To examine this possibility, appropriate sections from embryos, obtained from 3 litters, that had been exposed to a short pulse of bromodeoxyuridine (BrdU) prior to harvesting (to mark cells in the S-phase) were double immunostained for YFP and BrdU. In addition, untreated embryos, from 3 litters, were also immunostained for YFP and pH3 (to mark cells in mitosis). No significant difference was observed in the fraction of BrdU-labelled YFP^{+} pENCCS present in sections of control (Tg*Ret*$^{+/51}$) and mutant (Tg*Ret*$^{51/51}$) E9.0-9.5 embryos (data not shown). In contrast, the fraction of pH3^{+}GFP^{+} cells in the gut of E10.5 mutant embryos (6.8 $\pm$ 0.1%; n = 4) was significantly reduced relative to control (Tg*Ret*$^{+/51}$) littermates (18.9 $\pm$ 0.4%; $p < 0.0001$; n = 4) (**Figures 2A,B** and graph **Figure 2C**). Consistent with these results, BrdU incorporation was also reduced in ENS progenitors of E10.5 mutant embryos relative to controls.

To examine the potential role of *Ret* in the proliferation of ENS progenitors at later stages of gut colonisation, the guts

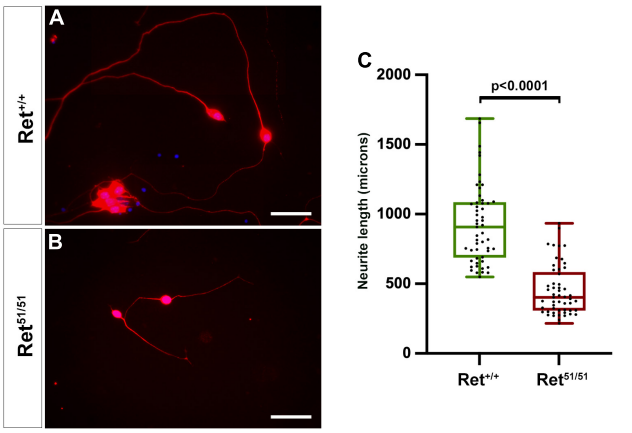

FIGURE 4 | Neuritogenesis is compromised in *Ret*$^{51/51}$ neurons maintained in culture. **(A,B)** Cultures of enteric neurons from gut of control (*Ret*$^{+/+}$) and *Ret*$^{51/51}$ embryos immunostained for TuJ1 (red). **(C)** Graph showing the average neurite length of control (*Ret*$^{+/+}$) and *Ret*$^{51/51}$ neurons from gut cultured for 6 days. *Ret*$^{51/51}$ neurons have significantly shorter processes. Embryos from 3 litters of E11.5 *Ret*$^{+/51}$ heterozygous crosses were analysed. (n = 6 for each genotype; 53 axons each). Scale bar: 200 μm. Statistical analysis performed by Welch's t-test.

of individual BrdU-treated embryos were dissociated into a single cell suspension and plated onto fibronectin-coated tissue culture dishes. Two hours after plating these short-term cultures were fixed and double immunostained for YFP and BrdU. In cultures from E11.5 control (Tg*Ret*$^{+/51}$) embryos, 42.4 ± 0.8% of YFP$^+$ cells were also positive for BrdU (n = 5) but only 8.7 ± 0.4% of *TgRet*$^{51/51}$ YFP$^+$ cells were double labelled (YFP$^+$BrdU$^+$; n = 3, p < 0.0001) (**Figures 2D,E** and graph **Figure 2F**). A significant reduction in the fraction of BrdU$^+$YFP$^+$ cells was also observed in E14.5 Tg*Ret*$^{51/51}$ embryos (control, Tg*Ret*$^{+/51}$,25.1 ± 0.4%; Tg*Ret*$^{51/51}$mutant, 13.9 ± 0.4; n = 6 each, p < 0.0001) (**Figure 2F**) although at this stage the difference in the proliferation rate of YFP$^+$ cells from the two genotypes was less pronounced, suggesting that the capacity of ENS progenitors to proliferate recovers partially at later embryonic stages. To explore the cellular basis of such recovery, we examined BrdU incorporation specifically in BFABP$^+$ cells which appear in the gut of mouse embryos at around E14.5 and represent progenitors of enteric glia. This analysis showed a significant increase in the proliferation of the BFABP-expressing glial progenitors in the gut of E14.5 Tg*Ret*$^{51/51}$ embryos relative to their control (Tg*Ret*$^{+/51}$) littermates (11.5 ± 1.2% in Tg*Ret*$^{51/51}$ homozygous guts compared to 3.8 ± 0.6% in control (Tg*Ret*$^{+/51}$) guts; n = 6 each, p = 0.0007; **Figures 2G,H** and graph **Figure 2I**). Together, these experiments show that normal *Ret* activity is required to maintain the appropriate levels of proliferation of ENS progenitors during gut colonisation.

Neuronal Differentiation Is Compromised in the Gut of *Ret*$^{51/51}$ Embryos

The gut dysmotility observed in HSCR patients is thought to result mainly from the lack of enteric ganglia in the distal colon (Amiel et al., 2008) but the potential effect of *RET* mutations on the differentiation or connectivity of enteric neurons in more proximal "normoganglionic" gut segments is unknown. To begin addressing this issue, we compared neuronal and glial differentiation in the gut of control Tg*Ret*$^{+/51}$ and Tg*Ret*$^{51/51}$ embryos. For this, short-term cultures of dissociated gut from individual YFP-expressing embryos were double immunostained for YFP and either pan-neuronal (TuJ1 or HuC/D) or glial (B-FABP or GFAP) markers. At E11.5, 23.6 ± 2.7% of YFP$^+$ cells from the gut of control (Tg*Ret*$^{+/51}$) embryos co-expressed HuC/D while only 6.6 ± 1.3% of YFP$^+$ cells from mutant (Tg*Ret*$^{51/51}$) littermates were positive for this marker (p = 0.0016; n = 5 each; **Figures 3A,B** and graph **Figure 3E**). Similar results were obtained using the pan-neuronal marker TuJ1 (34.4 ± 0.2% of YFP-expressing cells were positive for TuJ1 in control (Tg*Ret*$^{+/51}$) embryos vs. 19.7 ± 0.31% in Tg*Ret*$^{51/51}$ embryos; p < 0.0001, n = 6, **Supplementary Figure 1**). Reduced neuronal differentiation was also observed in the gut of E14.5 Tg*Ret*$^{51/51}$ embryos (22.2 ± 0.5% of YFP$^+$ cells co-expressed HuC/D in the gut of Tg*Ret*$^{51/51}$ animals compared to 43.5 ± 0.7% in control Tg*Ret*$^{+/51}$ littermates; p < 0.0001; n = 5 each; **Figure 3F**). Interestingly at this stage, the percentage of YFP$^+$ cells co-expressing the glial marker B-FABP in the gut of Tg*Ret*$^{51/51}$ embryos was increased (57.3 ± 3.1%) relative to heterozygous (Tg*Ret*$^{+/51}$) controls (25.1 ± 3.2%; p < 0.0001, n = 6; **Figures 3C,D** and graph **Figure 3F**). Additionally, the percentage of YFP$^+$ cells co-expressing GFAP was similar to B-FABP (35.6 ± 1.1% in control Tg*Ret*$^{+/51}$ embryos versus 57.9 ± 1.2% in Tg*Ret*$^{51/51}$ embryos p < 0.0001, n = 4; **Supplementary Figure 1**). Consistent with this observation, the fraction of YFP$^+$ cells co-expressing *Sox10* [which marks both undifferentiated progenitors and glial cells (Paratore et al., 2001) was also increased (63.2 ± 1.0% in Tg*Ret*$^{51/51}$ animals vs. 38.4 ± 2.4% in controls (Tg*Ret*$^{+/51}$); p = 0.0007, **Supplementary Figure 1**)]. A reduced number of neurons and increased number of glial cells was also observed in whole mount preparations of myenteric plexus from Tg*Ret*$^{51/51}$ E18.5 animals [HuC/D: 36.2 ± 5.2% in controls (Tg*Ret*$^{+/51}$) versus 16.9 ± 0.5% in Tg*Ret*$^{51/51}$ mutants, p = 0.0335 and B-FABP: 47.2 ± 3.0% in controls (Tg*Ret*$^{+/51}$) versus 63.5 ± 0.6% in Tg*Ret*$^{51/51}$; p = 0.0107; n = 4; **Figure 3G**]. Taken together, these studies reveal a specific deficit in neuronal differentiation in the gut of mutant Tg*Ret*$^{51/51}$ homozygous animals.

Axonal Defects of Enteric Neurons in *Ret*$^{51/51}$ Embryos

Normal development of neuronal circuitry within the gut wall is critical for the peristaltic and secretomotor activity of the intestine (Sasselli et al., 2013) and, as expected, both functions are severely compromised within aganglionic gut segments of HSCR patients (Furness, 2006). To begin addressing the state of neuronal circuits in more proximal "normoganglionic" gut segments in an HSCR animal model, we initially compared neurite development in cultured enteric neurons from control (*Ret*$^{+/+}$) and *Ret*$^{51/51}$ embryos. For this, individually dissociated guts from 3 litters of E11.5 embryos were cultured under

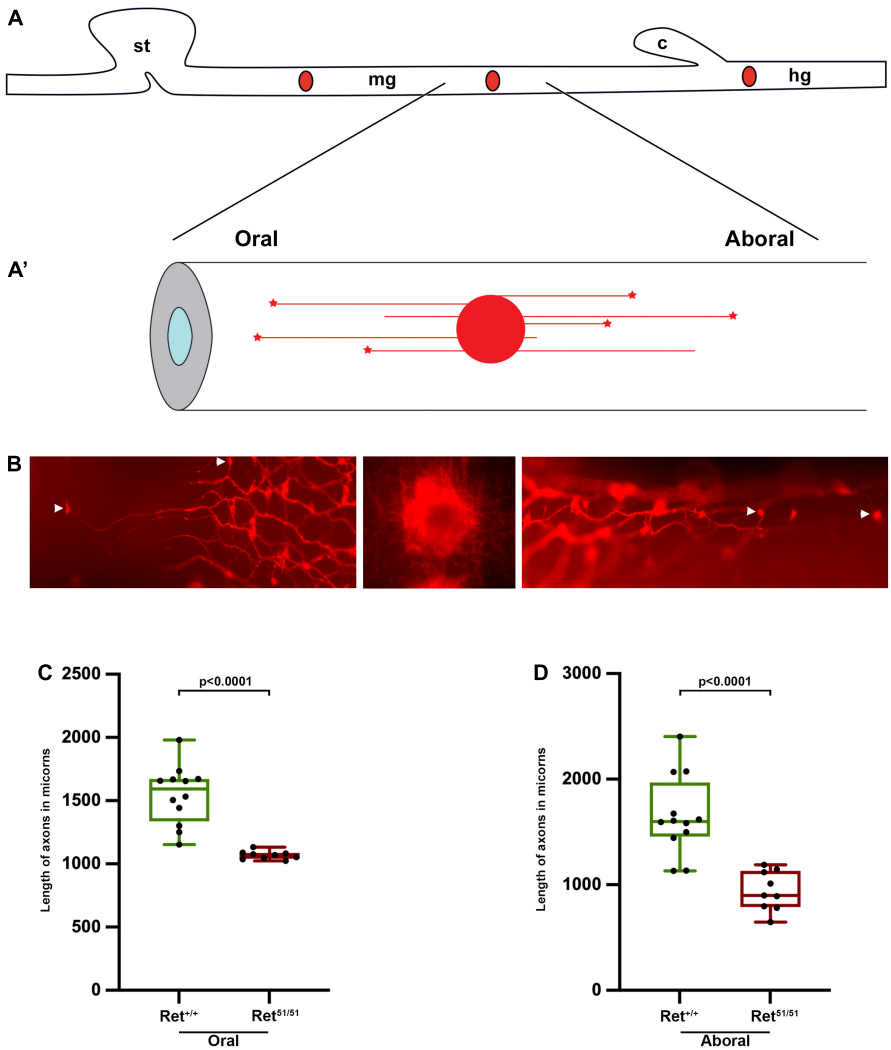

FIGURE 5 | Reduced neurite length of *Ret*$^{51/51}$ enteric neurons **(A,A')** Schematic representation of DiI labelling and retrograde DiI labelling of individual enteric neurons and their processes. **(B)** Fluorescent images of DiI labelled enteric neurons in the gut of perinatal animals. Middle panel shows the site of DiI crystal, left and right panels show individually labelled oral and aboral enteric neurons respectively. Arrowheads point to the cell body showing length of processes of control (*Ret*$^{+/+}$) and *Ret*$^{51/51}$ orally **(C)** and aborally projecting **(D)** neurons in the gut of perinatal animals. P1 pups (n = 6 for each genotype) from 4 litters were used for analysis; 9–12 axons were measured in the oral and aboral directions. Statistical analysis performed by Welch's t-test.

conditions that allow robust neurite outgrowth and several days later enteric neurons were fixed and immunolabelled with TuJ1 to highlight their processes. Enteric neurons from control (*Ret*$^{+/+}$) embryos extended neurites that were significantly longer compared to those from *Ret*$^{51/51}$ animals [control (*Ret*$^{+/+}$): 930.4 ± 39.1 μm versus *Ret*$^{51/51}$ mutant, 451.8 ± 24.8 μm; $p < 0.0001$; $n = 53$ axons from 6 embryos/genotype; **Figures 4A,B** and graph **Figure 4C**). These findings suggest that axonogenesis of *Ret*$^{51/51}$ homozygous enteric neurons is compromised, raising the possibility that the organisation of neuronal circuits in the ganglionated gut segments of *Ret*$^{51/51}$ animals is defective.

To further explore this possibility *in vivo*, we compared neurite length in intact guts from control (*Ret*$^{+/+}$) and *Ret*$^{51/51}$ newborn mice. Due to the complexity of the enteric plexus at this stage (Furness, 2006) we were unable to measure the length or follow the trajectory of individual axons using standard immunostaining procedures. To bypass this limitation, we applied the lipophilic dye DiI (1,1′-didodecyl 3,3,3′,3′-indocarbocyanine perchlorate) to specific locations along fixed whole-mount gut preparations with the aim of labelling retrogradely the neurites and the corresponding cell bodies of individual enteric neurons (schematic diagram in **Figures 5A,A'**; Porter et al., 1997; Sasselli et al., 2013). P1 pups were obtained from 4 independent litters and the axons that extended farthest from a DiI crystal place in the midgut, adjacent to the caecum, were measured. As anticipated, DiI labelled both orally- and aborally-projecting axons which happened to cross the point of DiI application (**Figure 5B**). Interestingly, in control (*Ret*$^{+/+}$) guts the mean distance of the two furthest away orally or anally projecting neurons was significantly longer

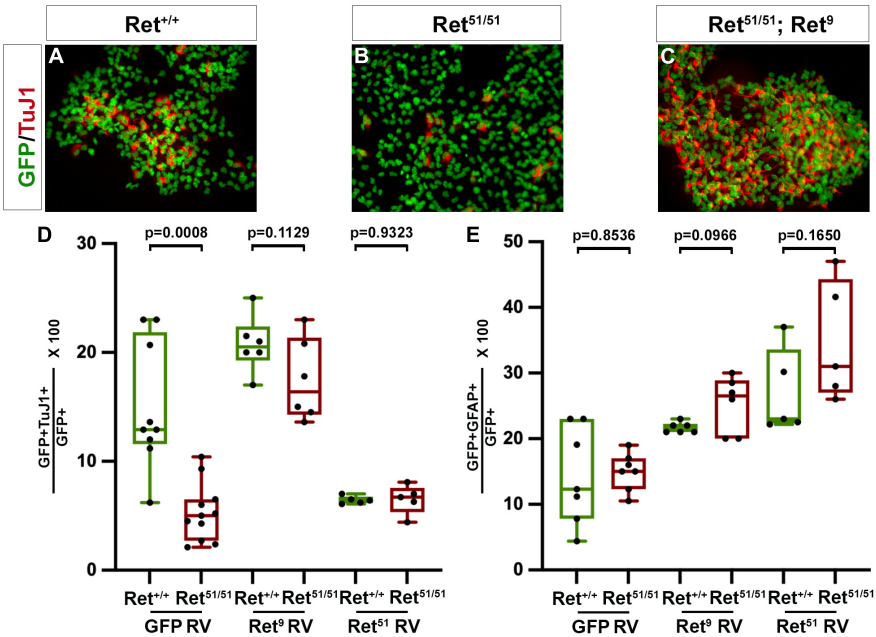

FIGURE 6 | *Ret* activity is critical for neuronal differentiation of multilineage ENS progenitors. **(A,B)** Colonies established from control ($Ret^{+/+}$) and $Ret^{51/51}$ EPCs were immunostained for GFP (green) and TuJ1 (red). Neuronal differentiation was dramatically reduced in the $Ret^{51/51}$ colony. **(C)** Expression of Ret^{9} isoform in colonies from $Ret^{51/51}$ EPCs rescues their neuronal differentiation deficit. Graph **(D)** shows quantification of neuronal differentiation in control ($Ret^{+/+}$) and $Ret^{51/51}$ EPC colonies after transduction with control GFP, Ret^{9} and Ret^{51} retroviruses (GFP RV, Ret^{9} RV and Ret^{51} RV). **(E)** Quantification of glial differentiation in control ($Ret^{+/+}$) and $Ret^{51/51}$ EPC colonies after transduction with control GFP, Ret^{9} and Ret^{51} retroviruses (GFP RV, Ret^{9} RV and Ret^{51} RV). Neuronal differentiation was rescued on expressing the Ret^{9} isoform but this was reduced when Ret^{51} isoform was expressed in control ($Ret^{+/+}$) EPCs. EPCs were isolated from 3 independent Litters. genotypes were pooled and 6–11 colonies counted post transduction, FACS and culture. Statistical analysis performed by Welch's *t*-test. ANOVA (and multiple comparison) analysis of equivalent colonies transduced with either control GFP, Ret^{9} or Ret^{51} retroviruses in shown in **Supplementary Table 1**.

relative to their $Ret^{51/51}$ mutant counterparts (**Figures 5C,D**). In control ($Ret^{+/+}$) animals, orally projecting axons were observed at 1545.8 ± 67.0 mm versus 1067.9 ± 10.9 mm $Ret^{51/51}$ guts ($p < 0.0001$; $n = 6$ each). Similarly, anally projecting axons were measured at 1649.6 ± 107.7 mm in control ($Ret^{+/+}$) gut compared to 941.7 ± 62.1 mm ($p < 0.0001$; $n = 6$ each) in $Ret^{51/51}$ guts. Taken together with our analysis of enteric neurons in culture, these studies further support the idea that *Ret* activity is required for normal axonogenesis of enteric neurons and the formation of functional neuronal circuits in the mammalian intestine.

Multilineage Enteric Nervous System Progenitors From $Ret^{51/51}$ Animals Show Reduced Neuronal Differentiation in Clonogenic Cultures

We and others have previously suggested that multi-lineage progenitors of enteric neurons and glia derived from ganglionated gut segments of HSCR patients could be autotransplanted to the aganglionic colon to restore peristaltic activity (Young et al., 2005; Bondurand et al., 2006). However, our present findings suggest that in addition to the absence of enteric ganglia from the aganglionic gut segments, the ganglionated proximal intestine of HSCR patients is characterised by neuronal deficits, such as a relative reduction in the number of enteric neurons and defective axonogenesis of at least a fraction of enteric neurons. This raises the possibility that upon transplantation into aganglionic gut segments, autologous enteric neural progenitors from "HSCR" patients expressing mutant forms of *Ret* are likely to generate enteric neurons and form ganglia with deficits similar to those detected in the ganglia of origin. To begin addressing this issue we compared neuronal and glial differentiation in clonal cultures of ENS Progenitor Cells (EPCs) isolated from the small intestine of control ($Ret^{+/+}$) and $Ret^{51/51}$ newborn mice (Bondurand et al., 2003). Our previous studies have shown that EPCs can be isolated efficiently from the gut of $Ret^{51/51}$ mutants (Bondurand et al., 2003) but the extent to which embryonic $Ret^{51/51}$ EPCs differentiate *in vitro* was not examined in these studies. To address the differentiation capacity of multi-lineage ENS progenitors from $Ret^{51/51}$ gut, EPCs were isolated from embryonic guts from 3 independent litters from + /Ret^{51} x + /Ret^{51} heterozygous crosses. From each litter, cells of the same genotype (i.e., $Ret^{+/+}$ or $Ret^{51/51}$) were pooled and cultured till NLBs were formed (see section "Materials and Methods"). These were transduced using either a control GFP or Ret^{9} or Ret^{51} containing retrovirus (RV) and after FACS, were allowed to form colonies for 7 days followed by immunostaining with antibodies for pan-neuronal (TuJ1) and glial (GFAP) markers. 6–11 colonies with 50–100 cells were counted and analysed. A significant fraction of cells in control ($Ret^{+/+}$) colonies transduced with GFP RV had differentiated into $TuJ1^{+}$

or GFAP$^+$ cells (on average 15.1 ± 1.9% neurons; n = 9 and 14.4 ± 2.8% glial cells; n = 7; **Figures 6A,D,E**). A similar fraction of glial cells was also present in EPC colonies from *Ret*$^{51/51}$ mutant guts (14.8 ± 1.1%; n = 7; p = 0.8536; **Figure 6E**). In contrast, the percentage of TuJ1$^+$ cells in mutant colonies was significantly reduced (5.31 ± 0.8%, p = 0.0008; **Figures 6B,D**). Moreover, the axonal length of neurons generated from *Ret*$^{51/51}$ EPCs was significantly shorter relative to their control (*Ret*$^{+/+}$) counterparts. These findings are consistent with our *in vivo* analysis of *Ret*$^{51/51}$ guts and suggest that ENS progenitors from these animals do not differentiate efficiently into neurons.

Similar experiments were conducted using postnatal (P1) guts from control (*Ret*$^{+/+}$) and *Ret*$^{51/51}$ embryos. Here, the outer myenteric plexus was isolated as peels, dissociated and cultured until NLBs formed, infected with a GFP containing retrovirus and EPCs plated at clonal densities after FACS. We found that colonies from postnatal EPCs took longer to grow even though the number of colonies formed were not dissimilar between the two genotypes, and as a consequence, differentiation took longer. Therefore, at day 5, differentiation into neurons and glia was minimal in both control (*Ret*$^{+/+}$) and *Ret*$^{51/51}$ EPC colonies, therefore analysis was performed at Day 10. However, even at this stage, the neuronal differentiation in *Ret*$^{51/51}$ EPCs was reduced compared to control (*Ret*$^{+/+}$) EPCs [6.1 ± 1.2% of EPCs in *Ret*$^{51/51}$ colonies versus 12.8 ± 1.5% in control (*Ret*$^{+/+}$) colonies (n = 3 each; p = 0.0265; **Supplementary Figure 2**)]. Expression of earlier markers such as Mash1 and Phox2b however seemed to be similar in both genotypes and appeared at the correct time during differentiation (data not shown). Glial cell differentiation also was not significantly different between the two genotypes. On culturing these colonies for longer periods of time (up to 15 days) more neurons were observed in *Ret*$^{51/51}$ EPC colonies but this was still not comparable to equivalent control (*Ret*$^{+/+}$) EPC colonies. Thus far, all our results indicate that the ability of EPCs from *Ret*$^{51/51}$ gut are compromised in their ability to form neurons from early embryonic to postnatal stages.

Expression of the *Ret*^{9} Isoform Rescues the Differentiation Deficit of *Ret*$^{51/51}$ Mutant Enteric Nervous System Progenitor Cells

The previous findings argue that ENS progenitors originating from proximal gut segments of HSCR patients and grafted into distal aganglionic gut regions are likely to have reduced neurogenic capacity. A potential means of addressing this limitation would be to genetically modify the grafted cells by expressing a wild-type form of the receptor. To explore the feasibility of this approach, we attempted to correct the genetic deficit of *Ret*$^{51/51}$ mutant EPCs by expressing the missing *Ret*^{9} isoform (*Ret*$^{51/51}$;*Ret*^{9}) using retroviral transduction (Bondurand et al., 2003) and examined the effect of this genetic modification on neuronal differentiation in clonal cultures. Importantly, the expression of the *Ret*^{9} isoform in *Ret*$^{51/51}$ EPCs efficiently rescues the neurogenic deficit of mutant EPCs shown by expression of neuronal marker TuJI (20.8 ± 1.1% in control *Ret*$^{+/+}$ EPCs versus 17.5 ± 1.5% in *Ret*$^{51/51}$;*Ret*^{9} cells, n = 6 each, p = 0.1129; **Figure 6C** and graph **Figure 6D**). Interestingly, no discernible effect on gliogenic differentiation was observed (21.7 ± 0.3% in control *Ret*$^{+/+}$ EPCs versus 25.2 ± 1.8% in *Ret*$^{51/51}$;*Ret*^{9} EPCs, p = 0.0966; n = 6 each; **Figure 6E**). These finding suggest that correction of the genetic deficit of EPCs prior to auto-transplantation into aganglionic gut segments is likely to improve their ability to generate appropriate neuronal networks in the gut wall.

Preliminary data from experiments with postnatal EPCs infected with *Ret*^{9} retrovirus indicate that the neuronal differentiation is rescued as in the embryonic EPCs. However, further work needs to be done to analyse their general morphology and neuronal outgrowths.

It was clear from the above experiments that introducing the *Ret*^{9} isoform into *Ret*$^{51/51}$ EPCs, rescued the neurogenic potential. We also wanted to investigate the effect of introducing the *Ret*^{51} isoform into control (*Ret*$^{+/+}$) and *Ret*$^{51/51}$ EPCs. For this, a retrovirus expressing Ret^{51} was transduced into *Ret*$^{51/51}$ EPCs as well as control (*Ret*$^{+/+}$) EPCs and the resulting clonal colonies were analysed as above. There was no significant difference in the percentage of glial cells (27.0 ± 2.9% in control *Ret*$^{+/+}$ versus 34.7 ± 4.1% in *Ret*$^{51/51}$;*Ret*^{51} EPC colonies, n = 5 each; p = 0.1650, **Figure 6E**). The same was true for the neurogenic differentiation in *Ret*$^{51/51}$ EPCs (6.5 ± 0.6%; n = 5) suggesting that introducing the *Ret*^{51} isoform did not rescue the neuronal defect (**Supplementary Table 1**). However, intriguingly, we found that following introduction of the *Ret*^{51} isoform in control (*Ret*$^{+/+}$) EPCs, in the resulting colonies, neurogenic differentiation was reduced (6.4 ± 0.2%, n = 5) similar to the *Ret*$^{51/51}$ (p = 0.9323) (**Figure 6D**).

These results support the hypothesis that *Ret*^{9} and *Ret*^{51} represent functionally distinct isoforms which can affect differentiation. The significance of this result is still not clear and more work needs to be done to fully support this finding such as studying the time course of expression, of both isoforms in EPCs, and the effects on differentiation over a longer developmental period.

DISCUSSION

Linage Tracing of Neural Crest Cells Shows That Migration Is Delayed in *Ret*^{5151} Embryos

The critical role of the RTK Ret in the development of the mammalian ENS has been well established, and the cellular mechanisms controlled by this signalling pathway *in vivo* are becoming clearer (Lasrado et al., 2017; McCallum et al., 2020). The almost complete elimination of early ENS progenitors in *Ret* null mice (Taraviras et al., 1999) has precluded the analysis of the role of the receptor at later stages of enteric neurogenesis *in vivo* and much of our understanding of its role in ENS development so far has been explored using explant and cell culture assays. However, the role of *Ret* signalling in ENS development using a conditional *Ret* allele inactivated at relatively late stages of embryogenesis has been examined (Uesaka et al., 2007, 2008; Uesaka and Enomoto, 2010). These authors demonstrated that, in addition to promoting survival of early ENCCs, *Ret* signalling

is also required for neuronal survival in the colon and suggested that at least some cases of HSCR disease result from a region- and stage-specific elimination of postmigratory and postmitotic enteric neurons. In addition, it was reported that a novel hypomorphic allele of *Ret* results in delayed migration of ENCCs (Uesaka et al., 2008). Notwithstanding these studies, a systematic analysis of the effects of reduced *Ret* signalling throughout enteric neurogenesis is lacking.

Here we have used a genetic lineage tracing system, which marks all NC cells and their derivatives, to analyse enteric neurogenesis in mice in which ENS progenitors are homozygous for Ret^{51}. Although previous reports had established that $Ret^{51/51}$ homozygous mice lack enteric ganglia from the distal part of the hindgut (de Graaff et al., 2001), a cardinal feature of HSCR, it was unclear whether the observed colonic aganglionosis in these mice reflected a generalised migratory deficit of ENS progenitors or was due to a hindgut-specific elimination of postmigratory enteric neurons, as suggested previously (Uesaka et al., 2008). Our findings show that pENCCs only expressing Ret^{51} were capable of invading the mesenchyme of the proximal foregut but contrary to their Ret-deficient counterparts did not undergo apoptosis. These findings argue that signalling by Ret^{51} is sufficient to support survival of ENCCs within the foregut thus bypassing the early apoptotic block in ENS development observed in *Ret* null mice (Taraviras et al., 1999). However, shortly after entering the foregut, ENS progenitors in $Ret^{51/51}$ mutants showed characteristic deficits in migration, proliferation and differentiation. These studies establish that the cellular outputs of *Ret* signalling during ENS histogenesis are multiple and dose-dependent and reinforce a regulatory role for this receptor in co-ordinating and integrating overlapping cellular processes. Since the initial number of ENCCs that invade the foregut is similar between control and $Ret^{51/51}$ embryos, we suggest that the ensuing delay in the colonisation of the proximal gastrointestinal tract in the latter is unlikely to result simply from reduced "population pressure" (Landman et al., 2007) but rather suggests a direct role of Ret signalling on ENCC migration. This view is consistent with the disparate morphologies of individual ENCCs, which in control embryos show characteristic migratory features (such as cellular processes that invade the surrounding mesenchyme) that are absent from their mutant counterparts. A potential molecular basis for the population pressure in NC, namely that these cells tend to migrate away from each other upon contact and thus are directed toward less densely populated spaces has been shown by Carmona-Fontaine et al. (2008). Such contact inhibition is likely to be mediated by the Wnt5a planar cell polarity pathway and members of the Rho GTPase family, such as RhoA and Rac1 (Carmona-Fontaine et al., 2008). In a manner perhaps analogous to contact inhibition, explants of embryonic gut already populated by intrinsic ENCCs failed to be colonised by extrinsic NC cells; in contrast, similar stage explants from aganglionic gut were readily colonised by extrinsic NC cells (Hotta et al., 2009). Moreover, *Wnt5a* is known to be expressed at high levels within the intestinal mesenchyme during gut organogenesis (Lickert et al., 2001) while Rac GTPases have a role in Ret signalling and the normal colonisation of the gut by ENS progenitors (Fukuda et al., 2002; Fuchs et al., 2009; Sasselli et al., 2013). Irrespective of the mechanisms, these findings suggest that Ret signalling is required for the repulsive behaviour of ENS progenitors that facilitates the colonisation of the gastrointestinal tract by NC cells during embryogenesis.

Colonisation of Gut by pENCCS Is Delayed in $Ret^{51/51}$ Mutants

The apparently normal invasion of the foregut by pENCCS in $Ret^{51/51}$ homozygous animals is in stark contrast to the profound delay in the colonisation of the rest of the gastrointestinal tube in these mutants, and provides evidence that multiple and genetically distinct mechanisms operate for the colonisation of different gut regions by NC cells. We have previously suggested that GDNF, which during the early stages of gut colonisation is expressed in the mesenchyme of the stomach, ahead of ENCCs, functions as a chemoattractant for a subset of Ret-expressing NC cells that arrive in the dorsal aorta and directs them into the foregut mesenchyme (Young and Newgreen, 2001; Natarajan et al., 2002). It is possible that the complementary expression of RET and GDNF in pENCCs and the stomach, respectively (Natarajan et al., 2002) guarantee the colonisation of the foregut mesenchyme by sufficient numbers of NC cells which, once within the confines of the developing gut, migrate rostrocaudally by directed dispersion as a result of contact inhibition.

Irrespective of the migratory mechanisms that are controlled by the Ret receptor, our data indicate that the colonic aganglionosis of $Ret^{51/51}$ mutants results from failure of colonisation of the colon by ENS progenitors, as opposed to the elimination of postmigratory cells that have entered the colon. This conclusion is based on two main findings: first, at no point were we able to detect YFP-expressing cells in the distal colon of mutant embryos and, second, we have failed to detect apoptotic cells in the enteric lineages of these mutants. Although it is possible that non-apoptotic mechanisms mediate the death of such cells in distal colon, as suggested previously (Uesaka et al., 2007, 2008) our data suggest that delayed migration of ENCCs is a significant contributing factor for the pathogenesis of at least some cases of HSCR. Moreover, these findings, together with reports by Uesaka et al. (2007, 2008) argue that multiple and complex pathogenetic mechanisms underlie the development of HSCR.

Ret Signalling Is Important for Neuronal Differentiation

In addition to its role in ENCC migration, our data also provide strong evidence that Ret signalling is required *in vivo* for enteric neuron differentiation. Our suggestion is currently based on the reduced expression of pan-neuronal markers in the gut of $Ret^{51/51}$ animals. However, the mammalian gut contains a large number of neuronal subtypes that can be distinguished by molecular or functional criteria (Qu et al., 2008; Hao and Young, 2009; Lasrado et al., 2017). Given the widespread expression of *Ret* in undifferentiated ENS progenitors (Durbec P. et al., 1996; Durbec P. L. et al., 1996; Young et al., 1999), it suggests that most, if not all, neuronal subtypes would be underrepresented in the gut of $Ret^{51/51}$ animals. Reduced neuronal differentiation in the gut of $Ret^{51/51}$ animals is associated with an increase in the fraction of cells expressing glial markers (**Figure 3**). This effect could reflect

a potential role of Ret signalling in the choice between neuronal and glial cell identities in the mammalian ENS. McCallum et al. (2020) have shown in zebrafish that a high proportion of enteric glia proliferate and can differentiate into neurons. Laranjeira et al. (2011) showed that glial cells dedifferentiated and could give rise to neurons at sites of injury.

Our experiments whereby Ret^{51} was expressed in $Ret^{51/51}$ EPCs using retroviruses perhaps shed light on this fact. Expressing Ret^{51} in $Ret^{51/51}$ EPCs with the hypothesis that it could perhaps increase the levels of proteins did not rescue neuronal differentiation. However, intriguingly expressing Ret^{51} in wild-type EPCs caused a drastic reduction in the neuronal differentiation of the wild-type EPCs. This may suggest that Ret^{51} is expressed more in progenitor cells which are glial-like and requires Ret^{9} to initiate neuronal differentiation. Hickey et al. (2009) have shown, using RNA isolation and microarray analyses, that genes were differentially induced in response to Ret^{9} and Ret^{51} isoforms suggesting that they have different biological roles. Alternative studies have also suggested that these isoforms may perform different functions; Jain et al. (2010) have shown that various tyrosines in Ret^{9} and Ret^{51} are docking sites for several adaptors and that mutating Y1062 in $Ret^{51/51}$ caused distal aganglionosis. RET^{51} transcripts have also been shown to be increased in human MEN2 tumours suggesting their role in tumour formation (Le Hir et al., 2000). Previous work, where Y1062 was mutated to phenylalanine in monoisoformic $Ret^{9/9}$ mice, showed that the signalling from Y1062 was a critical regulator for development of ENS and kidneys (Wong et al., 2005). Moreover, replacing Y1062 in a Ret^{51} context did not fully rescue the phenotype suggesting that amino acid residues around Y1062, in both isoforms, perhaps determined their function. In these studies, Ret^{51} expression delays neuronal differentiation but not glial differentiation. As in the CNS, where neural stem cells are similar to astrocytes and glia-like, perhaps Ret^{51}-expressing NCC are more stem cell like. *In vivo* studies are limited as the $Ret^{51/51}$ animals do not survive more than P2 due to the added defects in kidney development as well. As ENS development involves many molecules and factors along with RET, more work is needed to fully understand the specific roles of the isoforms and the effect of other factors on their functions.

Rescue of Neuronal Differentiation Deficits Maybe Relevant for Cell Based Therapies for Hirschsprung Disease

One of the fundamental issues in the treatment of HSCR disease is the postoperative outcome of the (usually) young patients, which is often poor and characterised by continued severe dysmotility of the gut (Thapar, 2009; vans-Barns et al., 2021). Our analysis of $Ret^{51/51}$ homozygous mice suggests that defects in the organisation and function of neuronal circuits in proximal "normoganglionic" gut segments could at least partly be responsible for the functional abnormalities of the gut prior, and subsequent, to the surgical resection of the obstructed gut segment. Reduced neuronal numbers, reduced length of neuronal processes seen both in EPCs and in newborn gut are likely to result in reproducible changes in the organisation and function of neuronal circuitry in the gut and provide a potential explanation for the functional abnormalities observed throughout the gut of HSCR patients. Moreover, these observations draw attention to the fact that removal of the aganglionic part of the colon in HSCR patients is not likely to eliminate all potential causes of gut dysmotility and malfunction in postoperative life.

Our current observations are also relevant to efforts to rescue the aganglionic phenotype of HSCR patients or animal models of this condition. We and others have previously suggested that self-renewing multilineage ENS progenitors (such as EPCs) isolated from proximal gut segments of HSCR patients could be expanded *in vitro* and used to colonise distal aganglionic gut segments (Kruger et al., 2002; Bondurand et al., 2003; Young et al., 2005). It is currently unknown to what extent, in such auto-transplantation models, the grafted stem cells would maintain a "memory" of the neuronal deficit present in the segments of origin. Tsai et al. (2011), engrafted prospectively selected enteric neural crest stem cells into a rat model of HSCR disease and found that they differentiated into neurons and glia even though the engraftment was diffuse throughout gut. Lindley et al. (2008) transplanted mouse and human neurospheres into aganglionic hindguts of embryonic mouse and showed that neurons and glia were formed, as were synapses. Human gut mucosal tissue was cultured to form NLBs and transplanted into aganglionic chick and foetal human hindgut *in vitro* to produce ganglia like structures containing enteric neurons and glia (Metzger et al., 2009). These transplantations have been performed using wild-type cells with un-colonised gut serving as aganglionic recipients. Our current data show that progenitors originating from ganglionated gut segment of a HSCR animal model maintain the differentiation deficit in culture, suggesting that ENS stem cells from HSCR patients maintain their genetic characteristics. Importantly, our ability to rescue the differentiation deficit of mutant ENS progenitors, by restoring expression of the missing Ret isoform, establishes the genetic manipulation of ENS stem cells as an approach which, in principle, could restore the ability of these cells to generate efficiently enteric neurons upon transplantation into the gut of HSCR patients.

DATA AVAILABILITY STATEMENT

The datasets presented in this study can be found in online repositories. The names of the repository/repositories and accession number(s) can be found in the article/**Supplementary Material**.

ETHICS STATEMENT

The animal study was reviewed and approved by United Kingdom Home Office. Mouse studies were carried out under the authority of a UK Home Office Project License in a Home Office designated facility.

AUTHOR CONTRIBUTIONS

DN, NT, and VP designed and planned the experiments. DN and NT conducted the study, collected the data, and along with VP interpreted the data, and drafted the manuscript. CM gave valuable comments, helped in editing manuscript and figures and helped with expression studies. JD helped in analysing data as well as gave advice on statistical analyses. All authors have read and agreed to the version of the manuscript.

FUNDING

This work was supported by the UK Medical Research Council and the Francis Crick Institute, which received its core funding from Cancer Research UK (FC001128 and FC001159), the UK Medical Research Council (FC001128 and FC001159), and the Wellcome Trust (FC001128 and FC001159). VP acknowledges additional funding from BBSRC (BB/L022974) and the Wellcome Trust (212300/Z/18/Z).

ACKNOWLEDGMENTS

We would like to acknowledge the late Graham Preece for help with the FACS facility. We would also like to thank Benjamin Jevans for contributing to **Figure 5A**. We acknowledge all grant and funding bodies for their support in enabling this research and publication.

SUPPLEMENTARY MATERIAL

The Supplementary Material for this article can be found online at: https://www.frontiersin.org/articles/10.3389/fnmol.2022.832317/full#supplementary-material

Supplementary Figure 1 | Short term cultures of dissociated guts from control Tg*Ret*$^{+/51}$ and Tg*Ret*$^{51/51}$ embryos were immunostained for different markers. Graph shows the quantification of percentage of GFP cells co-expressing TuJI at E11.5 in Tg*Ret*$^{+/51}$ control (green box) and Tg*Ret*$^{51/51}$ (red box) embryos $n = 6$. This was similar to the neuronal marker HuC/D where a significantly smaller fraction of Tg*Ret*$^{51/51}$ GFP^{+} cells have differentiated into neurons. Quantification of GFP cells co-expressing either GFAP ($n = 4$) or Sox10 ($n = 4$) in E14.5 control Tg*Ret*$^{+/51}$ versus mutant Tg*Ret*$^{51/51}$ embryos also showed that GFAP expression was similar to B-FABP whereby the percentage was higher in mutant versus control. This is also shown with Sox10 expression which labels both undifferentiated cells as well as glial cells. The fraction of Tg*Ret*$^{51/51}$ GFP^{+} cells that have differentiated into neurons is reduced at E11.5 and the fraction expressing glial markers is increased at E14.5. Statistical analysis performed by Welch's *t*-test. Tg*Ret*$^{+/51}$ represents cells or embryos from genotype *Wnt1*$^{cre/+}$;*R26R*$^{stop/YFP}$;*Ret*$^{+/51}$ and Tg*Ret*$^{51/51}$ represents cells or embryos from genotype *Wnt1*$^{cre/+}$;*R26R*$^{stop/YFP}$;*Ret*$^{51/51}$.

Supplementary Figure 2 | Reduced neuronal differentiation in *Ret*$^{51/51}$ EPC from postnatal gut myenteric peels. EPCs cultured after transduction of P1 control (*Ret*$^{+/+}$) or *Ret*$^{51/51}$ guts using a GFP retrovirus, and labelled with GFP (green) to mark all infected cells and TuJ1 (red), a pan neuronal marker to label all neurons. **(A)** Colony from control (*Ret*$^{+/+}$) EPC showed normal neuronal differentiation. **(B)** Colony from *Ret*$^{51/51}$ EPC showed reduced neuronal differentiation. **(C)** Quantification of neuronal differentiation in colonies. $n = 3$ for each genotype. Statistical analysis performed by Welch's *t*-test.

REFERENCES

Airaksinen, M. S., Titievsky, A., and Saarma, M. (1999). GDNF family neurotrophic factor signaling: four masters, one servant? *Mol. Cell. Neurosci.* 13, 313–325. doi: 10.1006/mcne.1999.0754

Akbareian, S. E., Nagy, N., Steiger, C. E., Mably, J. D., Miller, S. A., Hotta, R., et al. (2013). Enteric neural crest-derived cells promote their migration by modifying their microenvironment through tenascin-C production. *Dev. Biol.* 382, 446–456. doi: 10.1016/j.ydbio.2013.08.006

Amiel, J., Sproat-Emison, E., Garcia-Barcelo, M., Lantieri, F., Burzynski, G., Borrego, S., et al. (2008). Hirschsprung disease, associated syndromes and genetics: a review. *J. Med. Genet.* 45, 1–14. doi: 10.1136/jmg.2007.053959

Baloh, R. H., Enomoto, H., Johnson, E. M. Jr., and Milbrandt, J. (2000). The GDNF family ligands and receptors - implications for neural development. *Curr. Opin. Neurobiol.* 10, 103–110. doi: 10.1016/s0959-4388(99)00048-3

Barlow, A., de Graaff, E., and Pachnis, V. (2003). Enteric nervous system progenitors are coordinately controlled by the G protein-coupled receptor EDNRB and the receptor tyrosine kinase RET. *Neuron* 40, 905–916. doi: 10.1016/s0896-6273(03)00730-x

Bondurand, N., Natarajan, D., Barlow, A., Thapar, N., and Pachnis, V. (2006). Maintenance of mammalian enteric nervous system progenitors by SOX10 and endothelin 3 signalling. *Development* 133, 2075–2086. doi: 10.1242/dev.02375

Bondurand, N., Natarajan, D., Thapar, N., Atkins, C., and Pachnis, V. (2003). Neuron and glia generating progenitors of the mammalian enteric nervous system isolated from foetal and postnatal gut cultures. *Development* 130, 6387–6400. doi: 10.1242/dev.00857

Burns, A. J. (2005). Migration of neural crest-derived enteric nervous system precursor cells to and within the gastrointestinal tract. *Int. J. Dev. Biol.* 49, 143–150. doi: 10.1387/ijdb.041935ab

Carmona-Fontaine, C., Matthews, H. K., Kuriyama, S., Moreno, M., Dunn, G. A., Parsons, M., et al. (2008). Contact inhibition of locomotion in vivo controls neural crest directional migration. *Nature* 456, 957–961. doi: 10.1038/nature07441

Danielian, P. S., Echelard, Y., Vassileva, G., and McMahon, A. P. (1997). A 5.5-kb enhancer is both necessary and sufficient for regulation of Wnt-1 transcription in vivo. *Dev. Biol.* 192, 300–309. doi: 10.1006/dbio.1997.8762

de Graaff, E., Srinivas, S., Kilkenny, C., D'Agati, V., Mankoo, B. S., Costantini, F., et al. (2001). Differential activities of the RET tyrosine kinase receptor isoforms during mammalian embryogenesis. *Genes Dev.* 15, 2433–2444. doi: 10.1101/gad.205001

Durbec, P., Marcos-Gutierrez, C. V., Kilkenny, C., Grigoriou, M., Wartiowaara, K., Suvanto, P., et al. (1996). GDNF signalling through the Ret receptor tyrosine kinase. *Nature* 381, 789–793. doi: 10.1038/381789a0

Durbec, P. L., Larsson-Blomberg, L. B., Schuchardt, A., Costantini, F., and Pachnis, V. (1996). Common origin and developmental dependence on c-ret of subsets of enteric and sympathetic neuroblasts. *Development* 122, 349–358. doi: 10.1242/dev.122.1.349

Emison, E. S., Garcia-Barcelo, M., Grice, E. A., Lantieri, F., Amiel, J., Burzynski, G., et al. (2010). Differential contributions of rare and common, coding and noncoding Ret mutations to multifactorial Hirschsprung disease liability. *Am. J. Hum. Genet.* 87, 60–74. doi: 10.1016/j.ajhg.2010.06.007

Enomoto, H., Araki, T., Jackman, A., Heuckeroth, R. O., Snider, W. D., Johnson, E. M. Jr., et al. (1998). GFR alpha1-deficient mice have deficits in the enteric nervous system and kidneys. *Neuron* 21, 317–324. doi: 10.1016/s0896-6273(00)80541-3

Fuchs, S., Herzog, D., Sumara, G., Buchmann-Moller, S., Civenni, G., Wu, X., et al. (2009). Stage-specific control of neural crest stem cell proliferation by the small rho GTPases Cdc42 and Rac1. *Cell Stem Cell* 4, 236–247. doi: 10.1016/j.stem.2009.01.017

Fukuda, T., Kiuchi, K., and Takahashi, M. (2002). Novel mechanism of regulation of Rac activity and lamellipodia formation by RET tyrosine kinase. *J. Biol. Chem.* 277, 19114–19121. doi: 10.1074/jbc.M200643200

Furness, J. B. (2006). The organisation of the autonomic nervous system: peripheral connections. *Auton. Neurosci.* 130, 1–5. doi: 10.1016/j.autneu.2006.05.003

Gianino, S., Grider, J. R., Cresswell, J., Enomoto, H., and Heuckeroth, R. O. (2003). GDNF availability determines enteric neuron number by controlling precursor proliferation. *Development* 130, 2187–2198. doi: 10.1242/dev.00433

Grice, E. A., Rochelle, E. S., Green, E. D., Chakravarti, A., and McCallion, A. S. (2005). Evaluation of the RET regulatory landscape reveals the biological relevance of a HSCR-implicated enhancer. *Hum. Mol. Genet.* 14, 3837–3845. doi: 10.1093/hmg/ddi408

Hao, M. M., and Young, H. M. (2009). Development of enteric neuron diversity. *J. Cell. Mol. Med.* 13, 1193–1210. doi: 10.1111/j.1582-4934.2009.00813.x

Haricharan, R. N., and Georgeson, K. E. (2008). Hirschsprung disease. *Semin. Pediatr. Surg.* 17, 266–275.

Heanue, T. A., and Pachnis, V. (2007). Enteric nervous system development and Hirschsprung's disease: advances in genetic and stem cell studies. *Nat. Rev. Neurosci.* 8, 466–479. doi: 10.1038/nrn2137

Hickey, J. G., Myers, S. M., Tian, X., Zhu, S. J., Jl, V. S., Andrew, S. D., et al. (2009). RET-mediated gene expression pattern is affected by isoform but not oncogenic mutation. *Genes Chromosomes Cancer* 48, 429–440. doi: 10.1002/gcc.20653

Hotta, R., Pepdjonovic, L., Anderson, R. B., Zhang, D., Bergner, A. J., Leung, J., et al. (2009). Small-molecule induction of neural crest-like cells derived from human neural progenitors. *Stem Cells* 27, 2896–2905. doi: 10.1002/stem.208

Jain, S., Knoten, A., Hoshi, M., Wang, H., Vohra, B., Heuckeroth, R. O., et al. (2010). Organotypic specificity of key RET adaptor-docking sites in the pathogenesis of neurocristopathies and renal malformations in mice. *J. Clin. Invest.* 120, 778–790. doi: 10.1172/JCI41619

Kapur, R. P., Yost, C., and Palmiter, R. D. (1992). A transgenic model for studying development of the enteric nervous system in normal and aganglionic mice. *Development* 116, 167–175. doi: 10.1242/dev.116.Supplement.167

Kruger, G. M., Mosher, J. T., Bixby, S., Joseph, N., Iwashita, T., and Morrison, S. J. (2002). Neural crest stem cells persist in the adult gut but undergo changes in self-renewal, neuronal subtype potential, and factor responsiveness. *Neuron* 35, 657–669. doi: 10.1016/s0896-6273(02)00827-9

Landman, K. A., Simpson, M. J., and Newgreen, D. F. (2007). Mathematical and experimental insights into the development of the enteric nervous system and Hirschsprung's disease. *Dev. Growth Differ.* 49, 277–286. doi: 10.1111/j.1440-169X.2007.00929.x

Laranjeira, C., and Pachnis, V. (2009). Enteric nervous system development: recent progress and future challenges. *Auton. Neurosci.* 151, 61–69. doi: 10.1016/j.autneu.2009.09.001

Laranjeira, C., Sandgren, K., Kessaris, N., Richardson, W., Potocnik, A., Vanden Berghe, P., et al. (2011). Glial cells in the mouse enteric nervous system can undergo neurogenesis in response to injury. *J. Clin. Invest.* 121, 3412–3424. doi: 10.1172/JCI58200

Lasrado, R., Boesmans, W., Kleinjung, J., Pin, C., Bell, D., Bhaw, L., et al. (2017). Lineage-dependent spatial and functional organization of the mammalian enteric nervous system. *Science* 356, 722–726. doi: 10.1126/science.aam7511

Le Hir, H., Charlet-Berguerand, N., Gimenez-Roqueplo, A., Mannelli, M., Plouin, P., de Franciscis, V., et al. (2000). Relative expression of the RET9 and RET51 isoforms in human pheochromocytomas. *Oncology* 58, 311–318. doi: 10.1159/000012118

Lickert, H., Kispert, A., Kutsch, S., and Kemler, R. (2001). Expression patterns of Wnt genes in mouse gut development. *Mech. Dev.* 105, 181–184. doi: 10.1016/s0925-4773(01)00390-2

Lindley, R. M., Hawcutt, D. B., Connell, M. G., Almond, S. L., Vannucchi, M. G., Faussone-Pellegrini, M. S., et al. (2008). Human and mouse enteric nervous system neurosphere transplants regulate the function of aganglionic embryonic distal colon. *Gastroenterology* 135, 205–216e6. doi: 10.1053/j.gastro.2008.03.035

Lo, L., and Anderson, D. J. (1995). Postmigratory neural crest cells expressing c-RET display restricted developmental and proliferative capacities. *Neuron* 15, 527–539. doi: 10.1016/0896-6273(95)90142-6

McCallum, S., Obata, Y., Fourli, E., Boeing, S., Peddie, C. J., Xu, Q., et al. (2020). Enteric glia as a source of neural progenitors in adult zebrafish. *eLife* 9:e56086. doi: 10.7554/eLife.56086

Metzger, M., Caldwell, C., Barlow, A. J., Burns, A. J., and Thapar, N. (2009). Enteric nervous system stem cells derived from human gut mucosa for the treatment of aganglionic gut disorders. *Gastroenterology* 136, 2214–2225.e1–e3. doi: 10.1053/j.gastro.2009.02.048

Miao, X., Leon, T. Y., Ngan, E. S., So, M. T., Yuan, Z. W., Lui, V. C., et al. (2010). Reduced RET expression in gut tissue of individuals carrying risk alleles of Hirschsprung's disease. *Hum. Mol. Genet.* 19, 1461–1467. doi: 10.1093/hmg/ddq020

Moore, M. W., Klein, R. D., Farinas, I., Sauer, H., Armanini, M., Phillips, H., et al. (1996). Renal and neuronal abnormalities in mice lacking GDNF. *Nature* 382, 76–79. doi: 10.1038/382076a0

Natarajan, D., Marcos-Gutierrez, C., Pachnis, V., and de Graaff, E. (2002). Requirement of signalling by receptor tyrosine kinase RET for the directed migration of enteric nervous system progenitor cells during mammalian embryogenesis. *Development* 129, 5151–5160. doi: 10.1242/dev.129.22.5151

Paratore, C., Goerich, D. E., Suter, U., Wegner, M., and Sommer, L. (2001). Survival and glial fate acquisition of neural crest cells are regulated by an interplay between the transcription factor Sox10 and extrinsic combinatorial signaling. *Development* 128, 3949–3961. doi: 10.1242/dev.128.20.3949

Pattyn, A., Morin, X., Cremer, H., Goridis, C., and Brunet, J. F. (1999). The homeobox gene Phox2b is essential for the development of autonomic neural crest derivatives. *Nature* 399, 366–370. doi: 10.1038/20700

Pichel, J. G., Shen, L., Sheng, H. Z., Granholm, A. C., Drago, J., Grinberg, A., et al. (1996). Defects in enteric innervation and kidney development in mice lacking GDNF. *Nature* 382, 73–76. doi: 10.1038/382073a0

Porter, A. J., Wattchow, D. A., Brookes, S. J., and Costa, M. (1997). The neurochemical coding and projections of circular muscle motor neurons in the human colon. *Gastroenterology* 113, 1916–1923. doi: 10.1016/s0016-5085(97)70011-8

Qu, Z. D., Thacker, M., Castelucci, P., Bagyanszki, M., Epstein, M. L., and Furness, J. B. (2008). Immunohistochemical analysis of neuron types in the mouse small intestine. *Cell Tissue Res.* 334, 147–161. doi: 10.1007/s00441-008-0684-7

Sanchez, M. P., Silos-Santiago, I., Frisen, J., He, B., Lira, S. A., and Barbacid, M. (1996). Renal agenesis and the absence of enteric neurons in mice lacking GDNF. *Nature* 382, 70–73. doi: 10.1038/382070a0

Sasselli, V., Boesmans, W., Vanden Berghe, P., Tissir, F., Goffinet, A. M., and Pachnis, V. (2013). Planar cell polarity genes control the connectivity of enteric neurons. *J. Clin. Invest.* 123, 1763–1772. doi: 10.1172/JCI66759

Sasselli, V., Pachnis, V., and Burns, A. J. (2012). The enteric nervous system. *Dev. Biol.* 366, 64–73.

Schuchardt, A., D'Agati, V., Larsson-Blomberg, L., Costantini, F., and Pachnis, V. (1994). Defects in the kidney and enteric nervous system of mice lacking the tyrosine kinase receptor Ret. *Nature* 367, 380–383. doi: 10.1038/367380a0

Srinivas, S., Watanabe, T., Lin, C. S., William, C. M., Tanabe, Y., Jessell, T. M., et al. (2001). Cre reporter strains produced by targeted insertion of EYFP and ECFP into the ROSA26 locus. *BMC Dev. Biol.* 1:4. doi: 10.1186/1471-213x-1-4

Taraviras, S., Marcos-Gutierrez, C. V., Durbec, P., Jani, H., Grigoriou, M., Sukumaran, M., et al. (1999). Signalling by the RET receptor tyrosine kinase and its role in the development of the mammalian enteric nervous system. *Development* 126, 2785–2797. doi: 10.1242/dev.126.12.2785

Thapar, N. (2009). New frontiers in the treatment of Hirschsprung disease. *J. Pediatr. Gastroenterol. Nutr.* 48(Suppl. 2), S92–S94. doi: 10.1097/MPG.0b013e3181a15d62

Trupp, M., Arenas, E., Fainzilber, M., Nilsson, A. S., Sieber, B. A., Grigoriou, M., et al. (1996). Functional receptor for GDNF encoded by the c-ret proto-oncogene. *Nature* 381, 785–789. doi: 10.1038/381785a0

Tsai, Y. H., Murakami, N., and Gariepy, C. E. (2011). Postnatal intestinal engraftment of prospectively selected enteric neural crest stem cells in a rat model of Hirschsprung disease. *Neurogastroenterol. Motil.* 23, 362–369. doi: 10.1111/j.1365-2982.2010.01656.x

Uesaka, T., and Enomoto, H. (2010). Neural precursor death is central to the pathogenesis of intestinal aganglionosis in Ret hypomorphic mice. *J. Neurosci.* 30, 5211–5218. doi: 10.1523/JNEUROSCI.6244-09.2010

Uesaka, T., Jain, S., Yonemura, S., Uchiyama, Y., Milbrandt, J., and Enomoto, H. (2007). Conditional ablation of GFRalpha1 in postmigratory enteric neurons triggers unconventional neuronal death in the colon and causes a Hirschsprung's disease phenotype. *Development* 134, 2171–2181. doi: 10.1242/dev.001388

Uesaka, T., Nagashimada, M., Yonemura, S., and Enomoto, H. (2008). Diminished Ret expression compromises neuronal survival in the colon and causes intestinal aganglionosis in mice. *J. Clin. Invest.* 118, 1890–1898. doi: 10.1172/JCI34425

vans-Barns, H. M. E. E., Swannjo, J., Trajanovska, M., Safe, M., Hutson, J. M., Teague, W. J., et al. (2021). Post-operative colonic manometry in children with Hirschsprung disease: a systematic review. *Neurogastroenterol. Motil.* 33:e14201. doi: 10.1111/nmo.14201

Wong, A., Bogni, S., Kotka, P., de Graaff, E., D'Agati, V., Costantini, F., et al. (2005). Phosphotyrosine 1062 is critical for the in vivo activity of the Ret9 receptor tyrosine kinase isoform. *Mol. Cell. Biol.* 25, 9661–9673. doi: 10.1128/MCB.25.21.9661-9673.2005

Young, H. M., Ciampoli, D., Hsuan, J., and Canty, A. J. (1999). Expression of Ret-, p75(NTR)-, Phox2a-, Phox2b-, and tyrosine hydroxylase-immunoreactivity by undifferentiated neural crest-derived cells and different classes of enteric neurons in the embryonic mouse gut. *Dev. Dyn.* 216, 137–152. doi: 10.1002/(SICI)1097-0177(199910)216:2<137::AID-DVDY5>3.0.CO;2-6

Young, H. M., Hearn, C. J., Ciampoli, D., Southwell, B. R., Brunet, J. F., and Newgreen, D. F. (1998). A single rostrocaudal colonization of the rodent intestine by enteric neuron precursors is revealed by the expression of Phox2b, Ret, and p75 and by explants grown under the kidney capsule or in organ culture. *Dev. Biol.* 202, 67–84. doi: 10.1006/dbio.1998.8987

Young, H. M., Hearn, C. J., Farlie, P. G., Canty, A. J., Thomas, P. Q., and Newgreen, D. F. (2001). GDNF is a chemoattractant for enteric neural cells. *Dev. Biol.* 229, 503–516. doi: 10.1006/dbio.2000.0100

Young, H. M., and Newgreen, D. (2001). Enteric neural crest-derived cells: origin, identification, migration, and differentiation. *Anat. Rec.* 262, 1–15. doi: 10.1002/1097-0185(20010101)262:1<1::AID-AR1006>3.0.CO;2-2

Young, H. M., Turner, K. N., and Bergner, A. J. (2005). The location and phenotype of proliferating neural-crest-derived cells in the developing mouse gut. *Cell Tissue Res.* 320, 1–9. doi: 10.1007/s00441-004-1057-5

Conflict of Interest: The authors declare that the research was conducted in the absence of any commercial or financial relationships that could be construed as a potential conflict of interest.

Publisher's Note: All claims expressed in this article are solely those of the authors and do not necessarily represent those of their affiliated organizations, or those of the publisher, the editors and the reviewers. Any product that may be evaluated in this article, or claim that may be made by its manufacturer, is not guaranteed or endorsed by the publisher.

frontiers | Frontiers in Molecular Neuroscience

REVIEW
published: 30 May 2022
doi: 10.3389/fnmol.2022.818696

Modeling Brain Tumors: A Perspective Overview of *in vivo* and Organoid Models

Francesco Antonica[1†], Giuseppe Aiello[1†], Alessia Soldano[2†], Luana Abballe[3], Evelina Miele[3] and Luca Tiberi[1]*

[1] *Armenise-Harvard Laboratory of Brain Disorders and Cancer, Department of Cellular, Computational and Integrative Biology (CIBIO), University of Trento, Trento, Italy,* [2] *Laboratory of Translational Genomics, Department of Cellular, Computational and Integrative Biology (CIBIO), University of Trento, Trento, Italy,* [3] *Department of Pediatric Hematology/Oncology and Cellular and Gene Therapy, Bambino Gesù Children's Hospital, Scientific Institute for Research, Hospitalization and Healthcare (IRCCS), Rome, Italy*

Brain tumors are a large and heterogeneous group of neoplasms that affect the central nervous system and include some of the deadliest cancers. Almost all the conventional and new treatments fail to hinder tumoral growth of the most malignant brain tumors. This is due to multiple factors, such as intra-tumor heterogeneity, the microenvironmental properties of the human brain, and the lack of reliable models to test new therapies. Therefore, creating faithful models for each tumor and discovering tailored treatments pose great challenges in the fight against brain cancer. Over the years, different types of models have been generated, and, in this review, we investigated the advantages and disadvantages of the models currently used.

Keywords: organoid, mouse, *Drosophila*, xenograft, model, cancer, zebrafish

OPEN ACCESS

Edited by:
Parthiv Haldipur, Seattle Children's Research Institute, United States

Reviewed by:
Massimo Zollo, University of Naples Federico II, Italy
Roberta Azzarelli, University of Cambridge, United Kingdom

***Correspondence:**
Luca Tiberi
luca.tiberi@unitn.it

[†] These authors have contributed equally to this work and share first authorship

Specialty section:
This article was submitted to Methods and Model Organisms, a section of the journal Frontiers in Molecular Neuroscience

Received: *19 November 2021*
Accepted: *23 March 2022*
Published: *30 May 2022*

Citation:
Antonica F, Aiello G, Soldano A, Abballe L, Miele E and Tiberi L (2022) Modeling Brain Tumors: A Perspective Overview of in vivo and Organoid Models. Front. Mol. Neurosci. 15:818696. doi: 10.3389/fnmol.2022.818696

INTRODUCTION

Primary malignant brain tumors remain among the deadliest form of cancers despite the deeper understanding of their tumorigenic processes, acquired during the recent years, and the multimodality therapeutic approach (Aldape et al., 2019). Brain tumors are also the most common solid tumor in children and are the leading cause of cancer-related morbidity and mortality in this population. An important shared feature of this heterogeneous group of diseases is the unique biology of the brain and its microenvironment, which represents a further degree of complexity in understanding the underlying biological mechanisms and in generating and delivering effective therapies. To this end, genetically engineered mouse models (GEMM) have been widely used in the field of cancer research as they allow to study mechanisms of tumorigenesis and tumor biology in a physiological context (Li and Langhans, 2021). However, most of these models cannot fully recapitulate the human tumor heterogeneity and show great limitations for preclinical drug testing (Gould et al., 2015; Aldape et al., 2019). Patient-derived xenografts (PDX) have been generated to overcome these limitations and to resemble human cancer more closely. These models retain patient mutational heterogeneity and, to date, have been considered one of the most reliable models for preclinical tests (Brabetz et al., 2018; Smith et al., 2020). However, PDXs cannot be used to address mechanisms of tumorigenesis, as they are already derived from tumor tissue. Human-induced pluripotent stem cell (hiPSC)-derived organoids solve the latter limit and represent a great advance for the understanding of tumorigenesis and for the development of new therapeutic strategies (Bian et al., 2018; Ogawa et al., 2018; Ballabio et al., 2020). In this review, our aim is to describe the advantages and disadvantages of current and developing models for brain tumors with

the highest incidence (meningiomas) or morbidity and mortality (gliomas, medulloblastoma, and ependymomas) in adulthood and childhood that could lead to new therapeutic strategies (**Figure 1**).

GLIOMAS

Gliomas are a large family of brain tumors affecting adult as well as pediatric patients. Gliomas can be subdivided into two wide categories, low- and high-grade gliomas, based on their aggressiveness (Omuro and DeAngelis, 2013). The low-grade tumors (LGGs, Grades I and II according to the World Health Organization – WHO) are characterized by slower growth and infiltration compared with the high-grade (WHO Grades III and IV) (Louis et al., 2021). Nevertheless, the proper grade and the classification of the different gliomas rely not only on their histological features but also on the molecular characteristics such as genes found altered (i.e., *IDH1, ATRX, TP53, CDK2A, BRAF, FGFR1*, and *PDGFRA*) and on the methylation profile. In 2021, an updated edition of the WHO Classification of Tumors of the Central Nervous System was published that redefined all the pre-existing tumor classification (i.e., subclassification in adult vs. pediatric) and added new entities (i.e., diffuse glioma G34-mutant) (Louis et al., 2021). While LGGs show a better prognosis due to their low proliferation rate and infiltration, high-grade gliomas (HGGs) remain very challenging to cure with a median survival of less than 15 months in the case of the more aggressive glioblastoma multiforme (GBM), and diffuse midline glioma, H3 K27-altered in pediatrics. Indeed, the invasive nature of GBM makes surgical resection difficult; relapse occurs rapidly after treatments, and the high intra-tumor heterogeneity

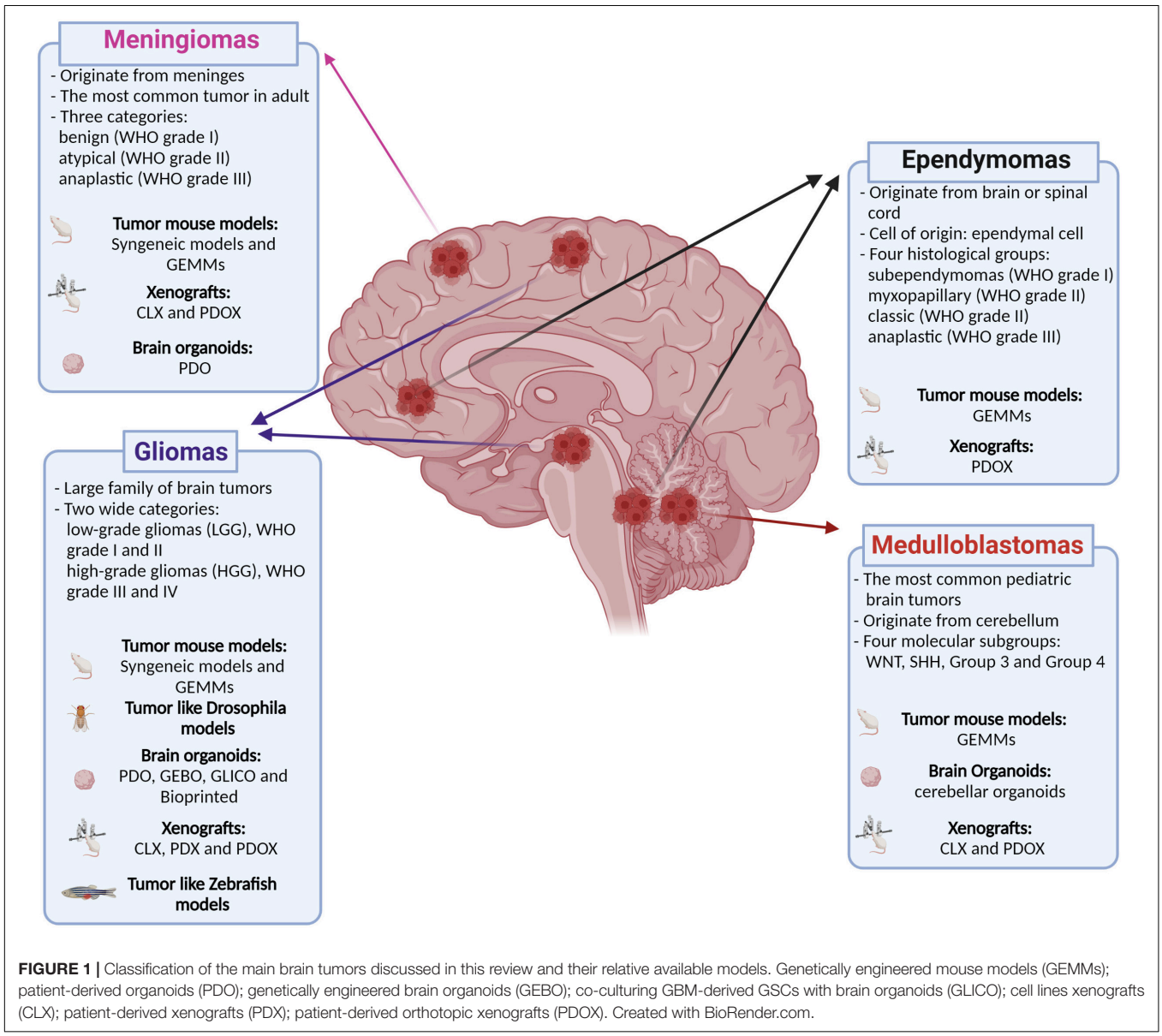

FIGURE 1 | Classification of the main brain tumors discussed in this review and their relative available models. Genetically engineered mouse models (GEMMs); patient-derived organoids (PDO); genetically engineered brain organoids (GEBO); co-culturing GBM-derived GSCs with brain organoids (GLICO); cell lines xenografts (CLX); patient-derived xenografts (PDX); patient-derived orthotopic xenografts (PDOX). Created with BioRender.com.

increases the difficulties in establishing effective drugs. The heterogeneity within GBM tumors has been identified at several levels, such as genetic, transcriptional, and DNA methylation. Since 2010, GBM has begun to be classified into 4 subtypes: proneural, neural, classical, and mesenchymal (Verhaak et al., 2010). This classification relied on peculiar aberrations and gene expression on specific genes, such as PDGFRA/IDH1, EGFR, and NF1. Afterwards, the improvement of high-throughput sequencing as well as the development of new profiling method (i.e., DNA methylation) has allowed to better stratify all the 4 canonical GBM subtypes (Zhang et al., 2020). In addition, it was shown how the prognosis can be closely correlated with the molecular subtype; for example, the proneural GBM has been shown to have a better prognosis than mesenchymal GBM (Phillips et al., 2006). The poorest prognosis of mesenchymal GBM is characterized by over-expression of genes related to angiogenesis and cell invasion (Phillips et al., 2006). Finally, using scRNA-seq technique has been defined that GBM has a peculiar feature of intra-tumoral heterogeneity. Indeed, several studies have shown that the different GBM molecular subtypes can co-exist within the same tumor (Patel et al., 2014; Darmanis et al., 2017; Neftel et al., 2019). This last aspect makes challenging to define which therapy would be more appropriate for each patient. Due to the inner complexity and aggressiveness, the development of reliable models for HGGs and GBM remains a crucial challenge in the tumor biology field, and several efforts have been conducted to generate *in vitro* and *in vivo* models, aiming to set up the best experimental strategy for investigating new therapeutic approaches (Ho et al., 2014; Hicks et al., 2021). On the other hand, low-grade gliomas, due to their low proliferative features, make challenging to culture them, as cell lines or organoids or to have a proper tumor growth in a reasonable period in a mouse model, and, for these reasons, are less investigated. Finally, the recent fine re-classification of the different glioma based on their genetic should be taken in consideration, for example, for the future creation of new genetic models.

Mouse Models of Glioma

In the context of gliomas, different types of *in vivo* models have been generated until now: xenografts including CLX (cell lines xenografts) and PDX (patient-derived xenografts), syngeneic, GEMM, and *Drosophila melanogaster*.

Xenografts (Cell Lines Xenografts and Patient-Derived Xenografts)

Xenograft models have been generated by injecting patient-derived cells or established cell lines into the mouse brain (i.e., U251, U87, A172, and T98G) (**Table 1**) (Fareh et al., 2012; Jandial et al., 2018; Hicks et al., 2021). Nevertheless, all the models based on cell lines lack the heterogeneity present in the human tumor due to the selection occurring in cells when cultured. A further step was taken when glioma stem-like cells (GSC) were isolated and maintained *in vitro* in 2D or in spheroid culture conditions. Indeed, CD133/PROMININ-1 positive cells can be isolated from primary tumors, cultured and propagated as spheres, and finally grafted in mice (Singh et al., 2004; Yi et al., 2016). Xenograft models can also be obtained by primary tumors (Sasaki et al., 2001; Joo et al., 2013; Kerstetter-Fogle et al., 2020) (**Figure 2A** and **Table 1**). These models, called PDX, have the enormous advantage of being directly generated from tumor cells, thus maintaining the features of the original neoplasm, including its cellular composition that will grow in the murine microenvironment (Shu et al., 2008). Although xenograft models are considered a reliable scenario and, in some cases, the closest to humans, they have the important weakness of being devoid of the host's immune system, as they are generated in immune-compromised mice. More in detail, depending on the immunocompromised mouse strain used, the lack of adaptive or innate immune system does not allow investigating the interaction between tumor and immune system. A possible solution has been recently proposed by xenografting tumor cells into the telencephalon ventricle of wild-type mouse embryos, where tumors persist in postnatal life (Hoffmann et al., 2020). Furthermore, the growth of GBM cells in the brain of nude mice, coupled with the possibility of genetically labeling them with barcodes, has provided a novel approach to trace different tumor clones *in vivo*. Indeed, Lan et al. (2017) using the patient-derived orthotopic xenografts (PDOX)-based approach showed the contribution of the different cancer cells in tumor formation, aggression, and therapy response. The possibility to track patient-derived GBM cell behavior *in vivo* with the barcoding approach has suggested the existence of a proliferative hierarchy, contributing to the tumor re-growth with a slow-cycling cancer stem cell subpopulation at its apex (Lan et al., 2017). On the other hand, PDXs have been also shown to be a valid approach for *in vivo* biobanking of pediatric brain tumors. Indeed, the xenografted tumor tissue closely recapitulated the histology, genetics, and drug sensitivity of the original tumor (Brabetz et al., 2018; Smith et al., 2020). Finally, orthotopic xenografts represent a valuable system to test the tumorigenicity of glioma-related mutations. In particular, the introduction of H3.3-K27M mutation in neural stem cells (NSCs) makes such cells capable to induce tumors formation upon transplantation in the mouse brain (Haag et al., 2021). Furthermore, distinct mutations in H3.3 trigger a tumoral phenotype, depending whether the NSCs derived from forebrain or brainstem modeling the possible different origins of pediatric high-grade glioma (Bressan et al., 2021).

Syngeneic Models

Several years ago, an interesting approach of inducing brain cancer in mice was developed, which consists of injecting ethyl-nitrosourea into the placenta of pregnant females between E15 and E18 (Thomas et al., 1994), or injecting methylcholantrene directly in the brain (Seligman et al., 1939). Both treatments with carcinogens lead to the formation of GBM-like tumors, from which cell lines are derived and, in turn, used to generate syngeneic allograft serially grafting (Ausman et al., 1970; Kaye et al., 1986). These models, contrary to PDOX where immunocompromised mice are used, allow to study the interaction between tumor-immune microenvironment and give the possibility to test immunotherapies. On the other

TABLE 1 | An example of different types of brain tumor models and their relative features.

Glioma models			
Brain tumor	**Type of model**	**Features**	**References**
HGG	CLX	Glioma cell-lines T98 and U87 xenograft	Jandial et al., 2018
HGG	CLX	Glioma cell-lines TG1 xenograft	Fareh et al., 2012
HGG	CLX/syngeneic	Syngeneic glioma cell lines GL261 xenograft	Ausman et al., 1970
HGG	PDX/PDOX	Xenograft of patient-derived GBM cells/neurospheres	Sasaki et al., 2001; Joo et al., 2013; Kerstetter-Fogle et al., 2020
Pediatric tumors	PDOX	Xenograft of patient-derived tumor cells (from different type of pediatric glioma)	Brabetz et al., 2018; Smith et al., 2020
HGG	GEMM	*Pdgfb* OE, $Trp53^{-/-}$	Hede et al., 2009
HGG	GEMM	*Pdgfb* OE, $Ink4a/Arf^{-/-}$, $Trp53^{-/-}$, $Pten^{-/-}$	Hambardzumyan et al., 2009
HGG	GEMM	*K-Ras* OE, $Ink4a/Arf^{-/-}$	Uhrbom et al., 2005
HGG	GEMM	*EGFRvIII* OE, $Ink4a/Arf^{-/-}$, $Pten^{-/-}$	Zhu et al., 2009
HGG	GEMM	*EGFRvIII* OE, *V12-Ras*, $Pten^{-/-}$	Wei et al., 2006
HGG	GEMM	$Nf1^{+/-}$, $Trp53^{+/-}$, $Pten^{+/-}$	Kwon et al., 2008
HGG	GEMM	*H-Ras-V12* OE, *Akt* OE, $Trp53^{+/-}$	Marumoto et al., 2009
LGG	GEMM	$Nras^{G12V}$ OE, $Idh1^{R132H}$ *OE*, sh*Atrx*, sh*Trp53*	Núñez et al., 2019
HGG	GEBO	*EGFRvIII* OE, *EGFR* OE, $CDKN2A^{-/-}/CDKN2B^{-/-}$ or $NF1^{-/-}$, $TP53^{-/-}$, $PTEN^{-/-}$	Bian et al., 2018
HGG	GEBO	$H\text{-}Ras^{G12V}$ OE, $TP53^{-/-}$	Ogawa et al., 2018
GBM	PDO	Patient-derived organoid	Jacob et al., 2020
	Drosophila		
GBM	Transgenic	*dEGFRλ*, *dp110CAAX*, *dPTEN*, $dRas85D^{N17}$, $dRas85D^{V12}$, $dRaf^{GOF}$ OE, dPTEN dsRNA	Read et al., 2009, 2013
GBM	Transgenic	$dRaf^{GOF}$, *hFGFR3-hTACC3*, $dEGFR^{ACT}$, $dPI3K^{ACT}$	Chen et al., 2018
	Zebrafish		
GBM	Transgenic	$HRAS^{G12V}$, $KRAS^{G12V}$*EGFRvIII*, $BRAF^{V600E}$ OE	Mayrhofer et al., 2017
Glioma	Transgenic	$KRAS^{G12V}$ OE	Ju et al., 2015
Glioma	Transgenic	*DAAkt1*, *DARac1* OE	Jung et al., 2013
HGG/MPNSTs	Knockout	$nf1a^{+/-}$; $nf1b^{-/-}$; $tp53^{e7/e7}$	Shin et al., 2012
GBM	CLX	Glioblastoma cell line U373-MG with shRacs or Racs OE Xenograft	Lai et al., 2017
GBM	CLX	Glioblastoma cell line U87 and its derived cancer stem cells Xenograft	Yang et al., 2013a
GBM	CLX	Glioblastoma cell lines U87 and U373 Xenotransplantation alone or with Mesenchymal stem cells	Breznik et al., 2017
GBM	PDX	Primary GBM-derived cells xenografts	Rampazzo et al., 2013
GBM	PDX	glioblastoma GBM9 cells xenografts into $prkdc^{-/-}$, $il2rga^{-/-}$	Yan et al., 2019
Medulloblastoma models			
MB subgroup	**Type of model**	**Features**	**References**
WNT	GEMM	$Ctnnb1^{+/-}$; $TP53^{-/-}$	Gibson et al., 2010
WNT	PDOX	Xenograft of patient-derived tumor cells	Brabetz et al., 2018; Smith et al., 2020
SHH	GEMM	$Ptch1^{+/-}$	Goodrich et al., 1997
SHH	GEMM	$Ptch1^{+/-}$, $Trp53^{-/-}$	Wetmore et al., 2001
SHH	GEMM	$Ptch1^{+/-}$, $Cdkn2c^{-/-}$	Uziel et al., 2005
SHH	GEMM	*SmoA2* OE	Dey et al., 2012
SHH	GEMM	$Sufu^{+/-}$, $Trp53^{-/-}$	Lee et al., 2007
SHH	GEMM	$Trp53^{-/-}$ with *gPtch1.1*/Cas9	Zuckermann et al., 2015
Adult SHH	GEMM	*SmoM2* OE, *truncated BRPF1* OE	Aiello et al., 2019
SHH	Orthotopic xenograft	*MYCN* OE in NES	Huang et al., 2019
SHH	Orthotopic xenograft	Orthotropic xenograft of iPSC-derived NES from a Gorlin patient with a germline *PTCH1* mutation	Susanto et al., 2020
SHH	PDOX	Xenograft of patient-derived tumor cells	Brabetz et al., 2018; Smith et al., 2020
Group 3	GEMM	*Mycn* OE, $Trp53^{-/-}$	Swartling et al., 2010
Group 3	GEMM	GTML $Trp53^{KI/KI}$ $p53ER^{TAM}$	Hill et al., 2015
Group 3	GEMM	$Mll4^{-/-}$	Dhar et al., 2018
Group 3	GEMM	*Gfi1* OE + *c-MYC* OE/*Otx2* OE + *c-MYC* OE	Ballabio et al., 2020
Group 3	Orthotopic xenograft	*Myc* OE, $Trp53^{-/-}$	Kawauchi et al., 2012; Pei et al., 2012
Group 3	Orthotopic xenograft	Myc^{T58A} OE, *Trp53* DN	Pei et al., 2012

(Continued)

TABLE 1 | (Continued)

Glioma models

Brain tumor	Type of model	Features	References
Group 3	Orthotopic xenograft	*Myc* OE, *Gfi1b* OE	Northcott et al., 2014
Group 3	PDOX	Xenograft of patient-derived tumor cells	Brabetz et al., 2018; Smith et al., 2020
Group 3	Organoid model	*Gfi1* OE + *c-MYC* OE/*Otx2* OE + *c-MYC* OE	Ballabio et al., 2020, 2021
Group 4	GEMM	Activated SRC OE, *Tp53* DN	Forget et al., 2018
Group 4	PDOX	Xenograft of patient-derived tumor cells	Brabetz et al., 2018; Smith et al., 2020

Ependymoma models

Brain tumor	Type of model	Features	References
Ependymoma	GEMM	*RELAFUS1*	Ozawa et al., 2018
Ependymoma	GEMM	YAP1-MAMLD1	Pajtler et al., 2019
Ependymoma	GEMM	*nlsYAP5SA* or *Lats1*$^{-/-}$ and *Lats2*$^{-/-}$	Eder et al., 2020
Ependymoma	PDOX	Xenograft of patient-derived tumor cells	Brabetz et al., 2018; Smith et al., 2020

Meningioma models

Brain tumor	Type of model	Features	References
Meningioma	CLX	BenMen1, Me3TSC cell line xenograft	Püttmann et al., 2005; Cargioli et al., 2007
Meningioma	CLX	CH-157-MN cell line xenograft	Ragel et al., 2008
Meningioma	CLX	IOMM-Lee cell line xenograft	McCutcheon et al., 2000
Meningioma	PDOX	Xenograft of patient-derived tumor cells	McCutcheon et al., 2000
Meningioma	GEMM	*Nf2*$^{-/-}$	Kalamarides et al., 2002
Meningioma	GEMM	*PDGFB* OE + *Nf2*$^{-/-}$ + *Cdkn2ab*$^{-/-}$	Peyre et al., 2015
Meningioma	GEMM	*SmoM2* OE	Boetto et al., 2018
Meningioma	GEMM	*Nf2*$^{-/-}$ + *Ink4a*$^{-/-}$	Kalamarides et al., 2011
Meningioma	PDO	Patient-derived organoids	Chan et al., 2021; Yamazaki et al., 2021

hand, these models do not recapitulate several aspects of HGGs and GBMs, such as infiltration and histology. Recently, injection of engineered NSCs (*Nf1* and *Pten* KO + *EGFRvIII* overexpression) into immunocompetent syngeneic mouse strain has been used to propose an epigenetic-driven mechanism exploited by GBM stem cells to evade immune system (Gangoso et al., 2021).

Genetically Engineered Mouse Model

The genetically engineered mouse model (GEMM) represents one of the most reliable *in vivo* models to study whether specific genetic alterations are responsible for tumor initiation and progression (**Figure 2B**). The analysis of the genetic landscape of HGG and GBM led to the identification of the most frequently mutated or amplified genes, and specific GEMMs have been created based on this knowledge. Such genetic alterations include gene amplification (i.e., *PDGFA*/*B*), gain-of-function activating mutations (i.e., *KRAS*, *HRAS*, *EGFR*, *NRAS*, and *PDGFRA*) and loss-of-function mutations/gene deletions (i.e., *TP53*, *CDKN2A*, *PTEN*, *NF1*, *ATRX*, *AKT*, *IDH1*, *H3F3A*, and *INK4a*) (**Table 1**) (Uhrbom et al., 2005; Wei et al., 2006; Kwon et al., 2008; Hambardzumyan et al., 2009; Hede et al., 2009; Marumoto et al., 2009; Zhu et al., 2009; Núñez et al., 2019; Akter et al., 2021; Hicks et al., 2021). However, GEMMs also have several limitations. They are time-consuming and tumors do not always recapitulate the intra-tumor heterogeneity observed in patients (Reilly, 2009; Day et al., 2015).

Cre-Lox

Cre-lox is a gene-editing technology that allows site-specific recombination between sequences called Lox sites using the enzyme Cre recombinase. The action of Cre can be spatio-temporally controlled by driving its expression in certain cell types *via* specific promoters or Tamoxifen administration (when Cre is fused to ER^{T2}). For example, this system has been used to generate mice that develop tumors by the introduction of the *EGFRvIII* genetic variant (Zhu et al., 2009), shedding light on the impact on GBM tumorigenesis of wild type and mutant forms of EGFR. The genetic knocking out of *Nf1, Trp53*, and *Pten* is also able to induce glioma in the mouse brain. Furthermore, the Cre-Lox approach helps to investigate the putative cell of origin by selective gene loss in specific lineage using peculiar promoters (Llaguno et al., 2009, 2015, 2019). The penetrance of brain tumor formation changes with the differentiation state of the cell, as observed in transgenic mice where tamoxifen-inducible Cre was expressed in neural stem cells (i.e.,

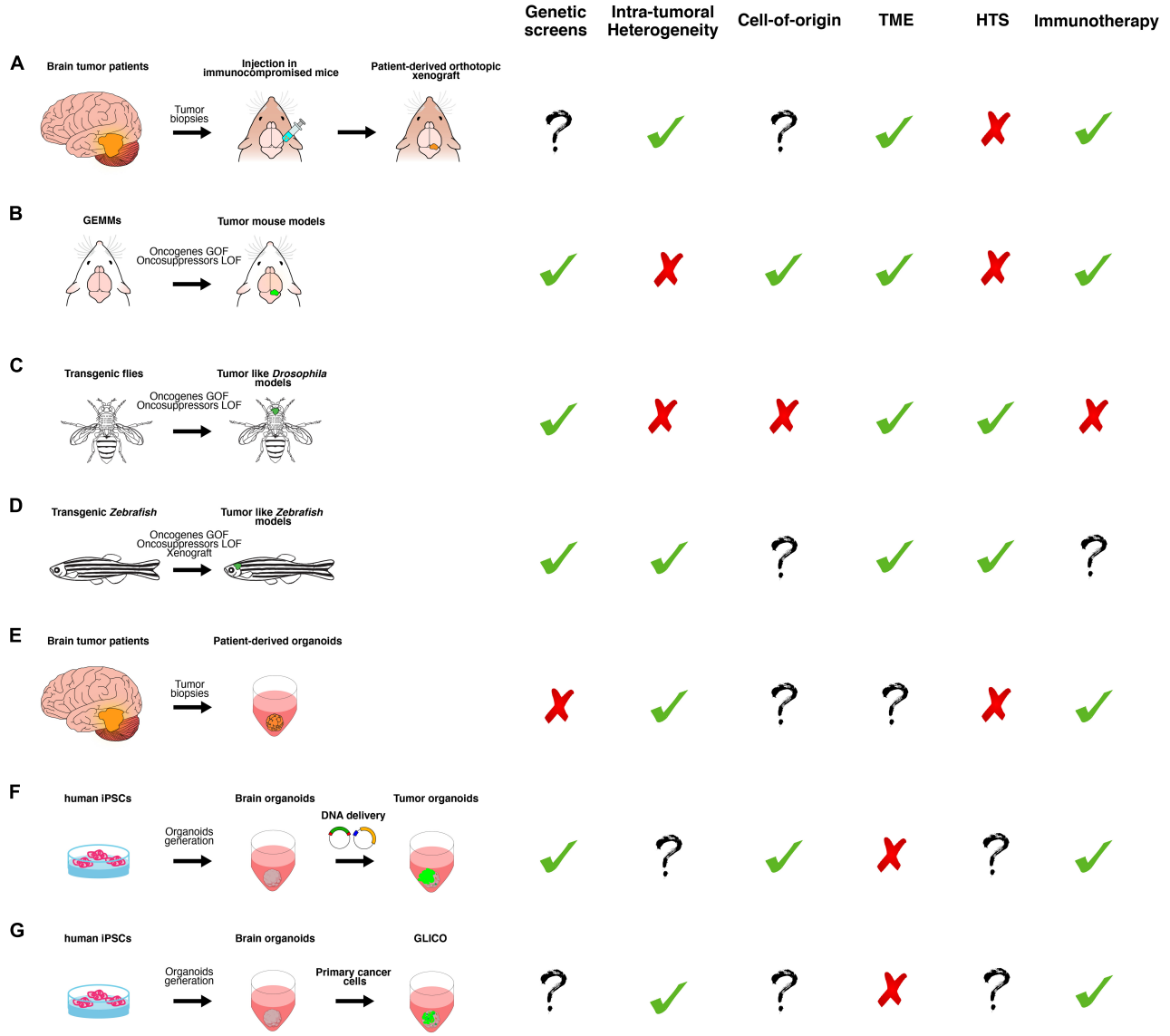

FIGURE 2 | A schematic overview of the main classes of *in vitro* and *in vivo* preclinical brain cancer models and their relative applications. **(A)** Brain cancer tissue surgically resected from patients is directly transplanted in the brain of immunocompromised mice, producing patient-derived orthotopic xenograft models (PDOX). **(B)** Genetically engineered mouse models (GEMMs) in which the tumor formation is induced by gain or loss of function of oncogenes or oncosuppressors, respectively. They can be generated by breeding animals that carry germline mutations or injecting virus or plasmids, harboring the gene of interest. **(C)** Transgenic flies in which the tumor-like phenotype is determined by gain or loss of function of oncogenes or oncosuppressors, respectively, in a time- and tissue-specific manner. **(D)** Transgenic Zebrafish in which the tumor-like phenotype is determined by gain or loss of function of oncogenes or oncosuppressors, respectively, in a time- and tissue-specific manner. Xenotransplantation of human glioma cells in zebrafish. **(E)** Brain cancer tissue surgically resected from patients is directly cultured in 3D culture as patient-derived organoids (PDO). **(F)** Tumor organoids can be generated by gain or loss of function of oncogenes or oncosuppressors, respectively, in cerebral or cerebellar organoids derived from human-induced pluripotent stem cells (iPSCs). **(G)** GLICO can be generated by co-culturing primary cancer cells with cerebral organoids. Based on published works, we summarized the possible usages of each class of the models in the following applications: genetic screens (i.e., testing the function of new genes in tumor formation, progression and aggressiveness); investigation of intra-tumoral heterogeneity, cell of origin and tumor microenvironment (TME); high-throughput screening (HTS) of new chemotherapeutic drugs and, finally, for testing new immunotherapy approaches.

Nestin-CreER^{T2}) (Llaguno et al., 2009), bipotential progenitors (i.e., *Ascl1-CreER*TM), oligodendrocyte progenitors (i.e., *NG2-creER*TM) (Llaguno et al., 2015) and immature (*NeuroD1-creER*^{T2}) or post-mitotic neurons (*CamKIIα-creER*TM) (Llaguno et al., 2019). Indeed, only neuronal stem cells (Nestin^{+} or GFAP^{+} cells) and early progenitors (Ascl1^{+} or NG2^{+} cells) that are at the top of the differentiation hierarchy are susceptible to cancer formation, while tumorigenesis is abolished in immature or post-mitotic neurons (NeuroD1^{+} or CamKIIα^{+} cells). Such an experimental model can be easily applied to the study of other tumors such as medulloblastoma and organoid models (described in the next sections).

Transposon System

Another method to generate GEMMs that overexpress or inactivate/silence the genes responsible for gliomagenesis is to insert the transgenes of interest into the genome, using the transposon system. The sleeping beauty (SB) transposon-based glioma mouse model was created, overexpressing *PDGF-A* and silencing *Nf1* and *Trp53* (Sumiyoshi et al., 2018). The same approach was used to test the role of *Atrx* silencing in brain tumors induced by overexpression of *Nras* and *Trp53* silencing (Koschmann et al., 2016). The possibility to integrate different constructs and deliver the DNA in the newborn mouse brain offers the advantage to test the tumor-inducing function of several genes in a less costly and time-consuming way.

RCAS-TVA

One of the most popular systems to generate GEMM to induce brain tumors is the RCAS-TVA method. RCAS-TVA is an efficient viral gene delivery system, consisting of RCAS (replication-competent avian sarcoma) viruses that carry the genes of interest and can only infect cells expressing the receptor TVA (tumor virus A). These cells were, indeed, previously engineered to express the tTA receptor under the control of specific cell lineage promoters, such as *Nestin*, *Gfap* (Holland et al., 1998), and *CNPase* (Lindberg et al., 2009). This allows studying whether specific oncogenes can induce tumor in a defined population and different anatomical regions. Of note, the RCAS-TVA approach has revealed how GBM can be induced by the *EGFR* mutant with loss of *Ink4a* or *Trp53* and that they arise more easily from *Nestin* cells than *Gfap* ones (Lindberg et al., 2009). The same approach has been used to model the low-grade brain tumor pilocytic astrocytoma (Gronych et al., 2011).

Globally, the GEMMs have the advantage to model GBM and HGG in mice with an intact immune system, allowing to test immunotherapies and to investigate the interaction between neoplastic and immune cells. Furthermore, GEMMs allow studying the impact of the different mutations on tumor progression and response to treatments. On the other hand, GEMMs have also serious and important pitfalls such as the lack of intra-tumor heterogeneity and the diversity of blood–brain barrier (BBB) in the mouse brain compared to the human one (Aday et al., 2016), thus affecting the treatment delivery.

Drosophila melanogaster

Drosophila melanogaster is a powerful genetic model that can be successfully used to study cancer biology (**Figure 2C** and **Table 1**). Its intrinsic peculiarity allows overcoming the downsides of other models, such as tissue cultures and mice. In fact, the signalings involved in cancer are conserved in *Drosophila* (Reiter et al., 2001; Yamamoto et al., 2014), and a wide range of genetic tools exists to perform large-scale genetic screens. *Drosophila* represents also a powerful platform to perform pharmacological screens; in fact, compared to cell or organoid cultures, it represents a whole animal system that allows testing of a large number of compounds simultaneously in a high throughput fashion (Bell et al., 2009; Willoughby et al., 2013). Compared to the different techniques used to generate mouse models of brain tumors, fly gliomas have been studied by producing genetically modified *Drosophila* strains that carry alterations in the key pathways affected in human patients.

Drosophila Model of Glioma Obtained by Perturbation of EGFR-PI3K Signaling: A Tool to Understand Gliomagenesis

Many of the key signalings perturbed in GBM, such as EGFR signaling and the phosphatidyl-inositol-3-kinase (PI3K) pathway (Brennan et al., 2013), are conserved in *Drosophila.* Moreover, single functional orthologs exist for most of these genes, such as *EGFR* (*dEGFR*), *PIK3CA* (*dp110*), *PTEN* (*dPTEN*), *RAS* (*dRas*), *RAF* (*dRaf*), and *AKT* (*dAkt*). Glia-specific co-activation of EGFR and PI3K signaling in the fruit fly results in diffuse glial neoplasia in the larva (Read et al., 2009, 2013). This model has been used to perform a kinome-wide genetic screen that identified new genes involved in glioma development (Read et al., 2013). Interestingly, most of the modifiers have orthologs previously connected to GBM, while 16 appeared to be new modifiers, such as *dRIOK1* and *dRIOK2*. Overexpression of mutant *dEGFR* and *dp110* in precise time windows during adult life (Chi et al., 2018) also leads to brain enlargement and extensive glial expansion that ultimately results in a shorter lifespan and defective neural behaviors. Chen et al. (2018) established both high- and low-grade glioma models in the fruit fly by expressing constitutively active *Drosophila* Raf ($dRaf^{GOF}$), human *FGFR3-TACC3* fusion gene, or constitutively active *Drosophila* EGFR and PI3K ($dEGFR^{ACT}$; $dPI3K^{ACT}$) in glia. Interestingly, the gliomas exhibited an increase of tissue stiffness compared with non-transformed brains, similar to the gradual tissue stiffening observed in human LGGs compared to HGGs (Miroshnikova et al., 2016) mediated by the Ion Channel dPiezo (Chen et al., 2018). The importance of tissue stiffness in glioma has also been demonstrated by Kim et al. (2014); through a genetic screening, they identified Lox, a Lysyl oxidase involved in extracellular matrix stiffness, as a potential mediator of neoplastic glial migration dependent on the pan-glial PDGF receptor (Pvr).

Drosophila Model of Glioma Obtained by Perturbation of EGFR-PI3K Signaling: A Tool to Understand the Cancer Stem Cells Role in Tumorigenesis

Drosophila has largely contributed to the understanding of the molecular mechanism underlying asymmetric cell division, an intrinsic property of cancer stem cells, leading to the first discoveries connecting this process to tumorigenesis (Caussinus and Gonzalez, 2005; Gómez-López et al., 2013). The previously described *Drosophila* GBM models driven by RTK-Ras have been used to identify and study transcription factors altered in GSCs. For example, Cheng et al. (2016) described the role of the transcription factor FOXD1 and of its target ALDH14A3, whose expression is altered in patient-derived GSCs. Another example of a transcription factor whose expression is altered in patient-derived GSCs is the Achaete-scute homolog 1 (ASCL1), an ortholog of the *Drosophila* achaete. Using the *Drosophila* GBM model described before (Read et al., 2009), it has been demonstrated that overexpression of fly Achaete or human *ASCL1* reduced tumor size and proliferation, and induced a

switch from glial to neuronal fate (Park et al., 2017). Interestingly, the ASCL1 role is evolutionarily conserved; in fact, ASCL1 overexpression efficiently reduces growth capacity of proneural human cancer stem cells-derived models of GBM and promotes a lineage switch, activating the neuronal fate and repressing the glial one (Narayanan et al., 2019; Azzarelli et al., 2022).

Therefore, Park et al. (2017) showed the usefulness of *Drosophila* GBM models for understanding how transcription factors involved in differentiation processes can affect GBM formation and gliomagenesis. YAP (yes-associated protein, also known as YAP1) and TAZ (transcriptional co-activator with PDZ-binding motif) are Hippo pathway effectors involved in the control of stem cells fate (proliferation/differentiation). Using the previously described Pten-RNAi/RASV12 overexpression-induced GBM model (Cheng et al., 2016), Minata et al. (2019) demonstrated that Tep1 (CD109 in mammals) loss in glioma cells reduces Yki (the *Drosophila* YAP/TAZ ortholog) and attenuates gliomagenesis. High levels of CD109 have been reported in GBM samples, and this work clarified its role in clonogenicity, tumor initiation, and radio-resistance of GBM. The data obtained both in human and *Drosophila* samples (Gangwani et al., 2020) suggest a conserved oncogenic signaling of CD109 through the YAP/TAZ pathway. Understanding the role of this signaling in *Drosophila* is extremely relevant to human pathology as YAP/TAZ have been shown to be required for GSCs plasticity and for GBM initiation due to their ability to prevent GSC differentiation. Finally, Hakes and Brand (2020) clarified the contribution of neural lineages to GBM by studying the orphan nuclear receptor TLX, which correlates with a poor prognosis in patients with GBM (Park et al., 2010). TLX is required for a linage-specific (Type II) NSCs identity and progression during development and, when overexpressed, can induce tumor formation by inducing a switch in NSC identity, a block of differentiation and reversion of intermediate neural progenitors (INP)s to NSC fate.

In conclusion, *Drosophila* has been proved very helpful in studying the signaling pathway, and the molecular mechanisms underlying GBM development and the finding obtained using this model are of great relevance for the understanding of human pathogenesis. However, *Drosophila* still maintains many limitations in mimicking the human microenvironment. Indeed, the absence of an adaptive immune system as well as the differences in the ability of the immune cells to infiltrate the brain tissues limits the possibility to study the immune-tumor interaction. Moreover, due to the differences between humans and *Drosophila* development, this model does not allow to fully recapitulate human brain tumor heterogeneity and pathology.

Zebrafish (*Danio rerio*)

Zebrafish is a well-established and robust model for studying cancer pathology and its fit for rapid and efficient screening of new treatments. Thanks to its short embryonic developmental time, small size, and its transparency, coupled with conservation of genetic mechanisms underlying biological processes and the possibility to transplant human cells; it represents an important model for gliomas studies (**Figure 2D** and **Table 1**). Compared to *Drosophila*, where modeling of brain tumor is achieved solely by production of transgenic models, zebrafish models of glioma are produced using different techniques.

Transgenic Models of Glioma

Gliomas can be induced in zebrafish by activation of the EGFR/RAS/ERK/AKT pathway *via* overexpression (a zic4 enhancer) of several oncogenes, such as $KRAS^{V12}$, $EGFR^{vIII}$, among others (Mayrhofer et al., 2017). Analysis of global RNA expression established that obtained brain tumors resemble GBMs of the mesenchymal subtype, with a strong YAP component. Similarly, overexpression of $KRAS^{G12V}$ in a putative neural stem and/or progenitor cells induced brain tumorigenesis (Ju et al., 2015) and overexpression of dominant-active human Akt1 (*DAAkt1*) or Rac1G12V (*DARac1*) (Ptf1a promoter)-induced gliomas of various histological grades, frequently infiltrated (Jung et al., 2013). Different tumor-initiating cells affect the tumor type; in fact, overexpression of $KRAS^{G12V}$ under the control of the krt5 gene promoter induced low frequency brain tumors in the ventricular zones (VZ) that resemble malignant peripheral nerve sheath tumors (MPNSTs) (Ju et al., 2015). In contrast, overexpression of $KRAS^{G12V}$ under the control of the *gfap* gene promoter induced brain tumors characterized by prominent activation of the canonical RAS-RAF-ERK pathway in both VZs and brain parenchyma at higher frequency (Ju et al., 2015). This study demonstrated that zebrafish could be explored to study cellular origins and molecular mechanisms. Ju et al. (2014) also developed the first animal model of gliomagenesis driven by Sonic Hedgehog (Shh) by overexpressing Smoothened (Smoa1) under the krt5 neural promoter. Transgenic zebrafish models have also been used to study the macrophage infiltration and contribution to tumor growth. Two publications clarified that expression of the human AKT1 oncogene in neural cells leads to tumor formation and significant increase in the macrophage and microglia populations that showed tumor-promoting functions (Chia et al., 2018). In particular, this is due to infiltration of macrophages from the peripheral area into the brain mediated *via* Sdf1b-Cxcr4b signaling. Cancer cells exploit the mechanisms used to mediating neuro-microglial *via* P2ry12 activation to promote their own proliferation (Chia et al., 2019). Finally, several transgenic models expressing IDH1 mutations were used to evaluate their roles in tumor development, but none of them led to glioma development, suggesting that further mutations are required (Gao et al., 2018).

Knockout Models

Several strategies have been used to produce knock out models to study the involvement of endogenous genes in glioma formation. Shin et al. (2012) used targeting-induced local lesions in genomes (TILLING) strategy to generate several null alleles of *nf1a* and *nf1b*. Thanks to these transgenic strains - they demonstrated that loss of nf1 is involved in tumorigenesis; in fact, adult $nf1a^{+/-}$; $nf1b^{-/-}$; $tp53^{e7/e7}$ animals show an earlier onset and increased penetrance of HGGs and MPNSTs (Shin et al., 2012). The same group also induced the CRISPR/Cas9-mediated knockout of *atrx*, a known tumor suppressor gene in sarcomas, in the *nf1/p53*-deficient zebrafish, to study its contribution to malignant growth

(Oppel et al., 2019). Moreover, knock out models have also been used in combination with transgenesis to study the connection between the immune system and tumor growth, as described above (Chia et al., 2019).

Knockdown With Morpholinos

The MO are antisense oligonucleotides that bind to complementary target mRNAs and block their translation, acting similarly to small interfering RNAs (siRNAs) and short hairpin RNAs (shRNAs), or alter the pre-mRNA splicing. Gliomas and, in particular, glioblastomas are tumors characterized by a high level of vascularization, and their growth depends on the formation of new blood vessels (Ahir et al., 2020). MO have been used in zebrafish to study the role of genes in angiogenesis and their contribution to GBM growth. For example, this has been done with *Ephrin-B3* (*ephrinb3-like* in zebrafish), highly expressed in GBM and acting as a survival factor (Royet et al., 2017) and with *PlexA*, also highly expressed in GBM and in tumor-associated blood vessels in patient biopsies (Jacob et al., 2016).

Xenotransplantation of Cancer Cells

Xenotransplantation of human glioma cells in zebrafish is a powerful technique to study tumor growth and invasion. In fact, the transplanted cells not only survive but are also able to migrate and interact with the host environment. Zebrafish offers several advantages over other xenograft models: firstly, it lacks an adaptive immune system in early stages of life (before 30 days post-fertilization, pfs) (Lam et al., 2004); therefore, no use of immunocompromised animals is needed at these stages. Moreover, the presence of many genetic tools, together with the small size and the transparency of zebrafish, allows live and high-resolution imaging of the transplanted cells (Pudelko et al., 2018; Vargas-Patron et al., 2019). Xenotransplantation can be performed at different injection sites: glioma/glioblastoma cell lines as U87 and U373T have been injected in the yolk sack at the stage 48-h pfs and analyzed for several parameters such as survival, proliferation, and invasion (Yang et al., 2013a; Lai et al., 2017). These studies led to the characterization of the role of genes such as Rac, MMP-9 in glioma aggressiveness/invasiveness, or the role of TGF-β1 in enhancing tumor-induced angiogenesis (Yang et al., 2013b).

Injections have also been performed in the zebrafish brain, ranging between 48- and 72-h pfs. Two studies used modified U-87 glioma cells lines to characterize the role of the KMT2A-NOTCH regulatory cascade (Huang et al., 2017) and of RECQ1 Helicase (Vittori et al., 2017) in glioma proliferation. Other groups used xenografts injection in the brain to study microenvironment and tumor migration/invasion; Breznik et al. (2017) investigated the role of mesenchymal stem cells (MSCs) in modulation of glioblastoma cells invasion by xenotransplantation of a mixture of MSC and U87 and U373 GBM cells. Xenotransplant into the brain (7 days pfs) was used to study differentiation of primary GBM cells induced by treatment with Wnt ligands, or overexpression of β-catenin (Rampazzo et al., 2013). Recently, it has been reported an optically clear mutant zebrafish (*prkdc−/−, il2rga−/−*) that lacks adaptive and natural killer immune cells that have been used to graft GBM9 glioblastoma cells intraperitoneally at 2 months old, and seems to be a promising model for developing personalized therapeutic approaches (Yan et al., 2019).

In conclusion, zebrafish overcomes many drawbacks of murine models, in terms of tumor live visualization, late development of the immune response, and presence of many genetic tools for manipulation and of the *Drosophila* models, especially thanks to the higher degree of physiological similarity to the mammalian models. However, open questions remain on pharmacokinetic studies for accurate drug delivery, dosing, and metabolism in zebrafish due to the divergent physiological features (such as body temperature and organ systems) (Kirchberger et al., 2017; Casey and Stewart, 2020).

3D Organoid-Based Models for Glioma

Organoid models represent the most advanced approach, combining the most recent techniques of 3D culturing, 3D printing, and bioengineering (Rodrigues et al., 2021). There are two main cellular sources for deriving tumor organoids: the patient tumor biopsies (**Figure 2E** and **Table 1**) and pluripotent stem cells derived brain organoids (**Figure 2F** and **Table 1**).

Patient-Derived Organoids

The first glioblastoma organoids were generated by Hubert et al. in 2016. Contrary to the classical spheroids formed by one cell type, they created more complex organoids starting from xenografts, GEMMs, and patient biopsies (Hubert et al., 2016). They observed that such cells cultured using Matrigel-based 3D culture methods formed organoids, recapitulating many GBM features, including a hypoxic gradient and resistance to radiation. Recently, Jacob et al. (2020) have established a growth factors-free chemically defined medium-based protocol to derive, expand, and cryopreserve GBM organoids, starting from tumor biopsies, so called PDOs (patient-derived glioblastoma organoids). The cellular composition, as well as the transcriptional profiling, confirmed the high similarity between PDOs and the original tumor. Such similarities were also observed in the response to treatment with radiations and temozolomide, and the infiltrative nature was observed upon xenograft in nude mice. Organoids were also generated from glioma of different grades (Grades II, III, and IV) but, despite some of the original tumor features, are retained; they survive in culture for a limited time, making the biobanking and expansion quite challenging. Nevertheless, Golebiewska et al. (2020) were able to successfully generate a living collection of PDOs that maintains most of the genetic, molecular, and phenotypical features of the primary tumor and a similar response to therapy. They also analyzed the DNA methylation patterns, currently considered the gold standard for the correct brain tumor diagnosis and subtyping, which revealed a good correlation between primary tumor and the respective-derived PDO. Finally, PDOs have been shown to maintain some of the immune cells (i.e., microglia and T-cell) during the 1st weeks in culture, opening the possibility to study their interaction with tumor cells (Jacob et al., 2020). Nevertheless, culture conditions need to be improved to ensure a stable expansion of the immune compartment in long-term culture.

Genetically Engineered Brain Organoids

Few years ago, two independent studies showed how genetically modified brain cancer models can also be generated *in vitro*. Using the same *in vivo* approach of genes in human gliomas (i.e., $HRAS^{G12V}$ and $TP53^{-/-}$; *cMYC* overexpression; *EGFRvIII* and *EGFR* overexpression and $CDKN2A^{-/-}$; $NF1^{-/-}$ and $PTEN^{-/-}$ and $TP53^{-/-}$), cerebral organoids derived from human-induced pluripotent stem cells (hiPSCs) were modified in order to induce neoplastic organoids (Bian et al., 2018; Ogawa et al., 2018) (**Figure 2F** and **Table 1**). The addition of fluorescent reporter genes allows to specifically track the modified cells and as they grew. Such neoplastic organoids exhibited a transcriptional profile partially similar to human gliomas, and their aggressiveness was confirmed *in vivo* upon orthotopic injection into nude mice. However, they did not show strong molecular similarity to patients, and it was not clearly shown whether they also retain intra-tumoral heterogeneity. This represents the major weakness for making this model suitable to investigate the intra-tumoral heterogeneity. On the other hand, these models have a great potential in drug screening by providing "unlimited" mini tumor organoids. They can be genetically modified in a less time-consuming and more cost-effective way than mouse models, allowing for the screening of new genes involved in tumor formation before testing them *in vivo*. Finally, GEBOs might be a valid model to investigate the cell of origin of glioma as already shown to be feasible for Group 3 Medulloblastoma (Ballabio et al., 2021). Generation of cerebellar as well as cerebral organoids from hiPSCs relies on well-established protocols (Muguruma et al., 2015; Velasco et al., 2019) that generate structures resembling fetal cerebellum or brain also from molecular points of view (Velasco et al., 2019; Nayler et al., 2021).

GLICO

Cerebral organoids have been also recently used for studying the behavior and invasion of GBM cells. The first approach consisted of co-culturing GBM spheroids with mouse ESC-derived brain organoids, proving the potential of modeling GBM invasion with organoids (da Silva et al., 2018). Similarly, Linkous et al. (2019) described a model of co-culturing GBM-derived GSCs with brain organoids, called GLICO (**Figure 2G**). With this approach, they were able to detect GBM cells invading normal brain organoids using microtubule structure, similar to what is observed in the GBM cells invading human brain parenchyma (Osswald et al., 2015). Additional studies have shown that this model can be successfully used to investigate invasion (Goranci-Buzhala et al., 2020; Krieger et al., 2020). Furthermore, when GSCs were co-cultured in 3D with organoids starting to differentiate, allowing also to recapitulate the lineage heterogeneity of cancer cells (Pine et al., 2020; Azzarelli et al., 2021). Nevertheless, this phenomenon seemed to be also dependent on the organoid media composition (Azzarelli et al., 2021). The pitfalls of GLICO are those related to being based on cell lines that do not allow investigating cancer in a context where original cell types and microenvironment are maintained (Jacob et al., 2020). Nevertheless, GLICO represents an excellent and valid model for studying cell behavior, such as invasion and cellular plasticity of GSCs.

Bioprinted Glioblastoma Organoids

The concept of bioprinting GBM organoids consists of putting together different cell types to recreate the different tumor regions. For example, it is possible to print freshly dissociated GBM cells on a chip together with vascular endothelial cells using a porcine ECM as "bioink" (Yi et al., 2019). This GBM-on-a-chip approach also allows recreating the hypoxic gradient and the infiltrating region. To increase complexity, GBM stem cells have been bioprinted together with neural stem cells (NSCs), astrocytes, and macrophage. The presence of immune cells allows to study their interaction and effect on the growth and invasion of cancer cells (Tang et al., 2020). Despite these models are very promising, the approach is still in its infancy and, therefore, presents some pitfalls, such as the technology is not yet precise and requires the use of specialized equipment and skilled researchers that, in turn, require significant investments.

To summarize, as for the other models, organoid-based systems have advantages and disadvantages. As an *in vitro* model, the usage of organoids allows to perform a drug screen and a test for immunotherapy; in addition, organoids can be used for an invasion assay and for testing the function of genes for inducing tumors. On the other hand, such models have disadvantages such as lack of vascular network. In the future, the possibility to induce cancer in "vascularized" brain cancer organoids might overcome this limitation and being used to study *in vitro* the interaction between cancer cells and blood vessels (Shi et al., 2020; Matsui et al., 2021). Concerning the intra-tumoral heterogeneity, this can be observed only when organoids are generated from tumor biopsies (Jacob et al., 2020). Finally, another challenge in the field remains to create brain cancer organoid with proper tumor microenvironment such as an immune compartment. Indeed, it would be worth establishing co-culture of brain cancer organoids (i.e., PDO) with different types of immune cells derived from patient peripheral blood or tumor biopsies (i.e., tumor infiltrating lymphocytes or tumor-associated macrophages/microglia). Alternatively, following a hiPSC-based approach, GEBOs might be co-cultured with iPSC-derived microglia (Xu et al., 2021).

MEDULLOBLASTOMA

Medulloblastoma (MB) is the most common malignant brain tumor in childhood that specifically arises in the cerebellum. The highest peak of incidence is during the first decades of life, even though this disease can occur throughout adulthood (Louis et al., 2016). Nowadays, an effective and definitive treatment has not yet been found, and 40% of affected children experience tumor recurrence, while 30% die from MB (Jones et al., 2012). Next-generation techniques have been applied to analyze MB molecular features/profiles. Genome-sequencing and array-based transcriptional profiling allowed the classification of MB into four main molecular subgroups: WNT, SHH, Group 3, and Group 4 (Taylor et al., 2012). The classification depends on a broad variety of macro and micro-genetic aberrations, which define specific cytogenetics, mutational patterns, gene expression signatures, and patient outcomes. Because of its molecular subtyping, here,

we give an overview of the different models developed for each MB subgroup.

Mouse Models of Medulloblastoma

WNT Medulloblastoma

The gold GEMM of WNT MB comes from the efforts of Gibson et al. (2010), hypothesizing, for the first time, the cell of origin of the tumor. Human WNT MB are distributed within the IV ventricle and infiltrate the brainstem. Indeed, genes marking human WNT MB are more frequently expressed in the lower rhombic lip (LRL) and embryonic dorsal brainstem. For this reason, Gibson and collaborators generated *Blbp-Cre*$^{+}$; *Ctnnb1*$^{+/lox(ex3)}$; *Tp53*$^{flx/flx}$ mice, characterized by a dominant mutation of the beta-catenin gene and loss of the tumor suppressor *Tp53* in *Blbp*$^{+}$ cells, which are Olig3^{+} progenitor cells in the LRL and progenitor cell populations across the hindbrain (including the cerebellar ventricular zone) (Gibson et al., 2010) (**Figure 2B** and **Table 1**). *Blbp-Cre*$^{+}$; *Ctnnb1*$^{+/lox(ex3)}$; *Tp53*$^{flx/flx}$ mice developed MB, recapitulating the anatomy and gene expression profiles of human WNT MB, as well as the aberrant vasculature that interferes in the blood brain barrier formation. A damaged blood brain barrier could increase the drug's efficacy, thus explaining the good prognosis and excellent response to chemotherapy compared to the other MB subgroups. These data indicate the similarities between the GEMMs and the human patients, showing their importance in defining new therapeutic approaches (Phoenix et al., 2016). A tumor suppressor role has been recently hypothesized for *DDX3X* (Patmore et al., 2020), often found mutated in WNT MB. DDX3X regulates hindbrain patterning, and its loss removes lineage restriction toward tumor formation, allowing for the onset of WNT MB from either lower or upper rhombic lips.

SHH Medulloblastoma

The first GEMM for SHH MB was a *Ptch1*$^{+/-}$ model, where aberrant SHH pathway activation leads to uncontrolled proliferation of cerebellar granule neuron progenitors (CGNPs) (Goodrich et al., 1997). Indeed, granule lineage identity is a prerequisite for the SHH MB onset, as it has been demonstrated by the conditional *Ptch1* knockout in unipotent (*Math1*$^{+}$) CGNPs (Schüller et al., 2008; Yang et al., 2008) and through the deregulation of different effectors of the SHH pathway, such as Smoothened and Sufu (Lee et al., 2007; Dey et al., 2012) (**Figure 2B** and **Table 1**). Based on mutations found in human SHH MB, a plethora of GEMMs have been generated using different approaches (Wetmore et al., 2001; Uziel et al., 2005) (listed in **Table 1**). A subgroup of patients with SHH MB shows somatic loss-of-function mutations of the transcriptional corepressor *BCOR*. Interestingly, *BCOR* is involved in MB formation (Tiberi et al., 2014; Kutscher et al., 2020) with possible therapeutic implications in *BCOR* mutant SHH MB. Zuckermann et al. (2015) have shown an interesting method to validate the oncogenic role of mutations found in human patients by performing postnatal somatic CRISPR/Cas-mediated deletion of tumor suppressor genes using a polyethylenimines-mediated *in vivo* transfection into the mouse neonatal cerebellum. Indeed, *Ptch1* CRISPR/Cas-mediated deletion in mice characterized by homozygous deletion of *Trp53* recapitulates MB (Zuckermann et al., 2015). SHH MB can be obtained by different cell types, other than CGNPs, such as cochlear granule neuron progenitors (CNPs) (Grammel et al., 2012). Recently, we have proposed postmitotic granule neurons as a possible origin for the human adult SHH MB. These cells can be reprogramed and give rise to tumors in the cerebellum of mice resembling human adult SHH MB (Aiello et al., 2019). In particular, the co-expression of mutant *Brfp1* and *SmoM2* alters chromatin accessibility of stem/progenitor-related genes, thus reprogramming the precursor cell properties and favoring the adult SHH MB tumorigenesis. However, whether the de-differentiation process of granule neurons is a key event in *BRPF1*-mutated SHH MB is still unknown and needs further investigation. Additionally, SHH GEMMs were brought to the discoveries of new important pathological features. Indeed, single-cell RNA sequencing on murine Shh MB treated with vismodegib (a Smo inhibitor) revealed some cell types (*Sox2*$^{+}$ and *Myod1*$^{+}$) resistant to treatment (Ocasio et al., 2019). A rare Sox2^{+} quiescent cell population, enriched after antimitotic chemotherapy, and Smoothened inhibition are thought to be responsible for tumor relapse (Vanner et al., 2014). Furthermore, the tumor sustains itself by shaping its surroundings to make it conducive to growth (Yao et al., 2020). CGNPs are, indeed, able to *trans*-differentiate into tumor astrocytes that sustain tumor progression by activating microglia *via* IL-4 production. Microglia, in turn, produce IGF-1 that promotes tumor progression. Among the mechanisms driving tumor resistance to conventional therapies and relapse, it has been shown the presence of a stem cell niche within SHH MB, namely cancer stem cells (CSCs), which express the stemness marker Nanog under Hh/Gli transcriptional regulation (Po et al., 2010; Miele et al., 2017; Abballe and Miele, 2021).

Group 3 Medulloblastoma

Modeling of Group 3 MB is more challenging due to the intratumoral heterogeneity and the similarities to Group 4 in the mutational profile. For years, the GTML mouse model has been considered as the golden standard model for Group 3 MB. This transgenic mouse is characterized by a Tet system that allows the expression of both *MYCN* and *Luciferase* under the control of the Glutamate transporter 1 (Glt1) promoter, reported to be expressed in hindbrain progenitors (Swartling et al., 2010). Since several high-risk Group 3 human patients showing relapse after treatment are characterized by *MYC* amplification and *TP53* inactivating mutation, this model was exploited to verify the interaction between *P53* and MYCN. *GTML/Trp53*$^{KI/KI}$ mice produce a more aggressive tumor that recapitulates the human large cell/anaplastic (LCA) histology and relapse (Hill et al., 2015). However, GTML-derived MB neurospheres show, in a small percentage, SHH-dependent features, thus not fully recapitulating the Group 3 MB human scenario (Swartling et al., 2012).

Due to the high diversity in the mutational landscape of Group 3 MB, we developed an *in vivo* screen approach to

test putative tumor driver mutations among hits identified by exome sequencing and microarray data of human Group 3 patients with MB.

Either overexpressing oncogenes with the PiggyBac transposon system or by CRISPR/Cas9-mediated deletion of tumor suppressor genes, we found that *Gfi1* + *c-MYC* and *Otx2* + *c-MYC* genes overexpressions were able to mimic the histological and transcriptional profile of human Group 3 MB (Ballabio et al., 2020) (**Figure 2B** and **Table 1**). Moreover, the *Otx2* + *c-MYC* combination of genes generated metastasis, recapitulating the malignancy of the tumor. Chromatin modifiers such as *MLL4* (alias for *KMT2D*) are often mutated in Group 3 patients with MB, as already mentioned, and whether these could have a causative role in tumor formation has been tested. *Nestin-cre; Mll4*$^{flox/flox}$ mice lead to the downregulation of several tumor suppressors, such as *Dnmt3* and *Bcl6*, and to Group 3 MB formation (Dhar et al., 2018). Despite the extensive genomic characterization, it is still unknown what the developmental origins of Group 3 MB are. We have hypothesized a critical role of Notch1 in tumor formation, claiming that its expression level in different progenitor cells impairs their competence in inducing MB. In particular, *S100b*$^{+}$ cells show a higher level of Notch1 compared to *Math1*$^{+}$ progenitor cells, and are able to initiate Group 3 MB upon *Gfi1* + *c-MYC* overexpression, while *Math1*$^{+}$ and *Sox2*$^{+}$ cells do not initiate tumorigenesis (Ballabio et al., 2021). The overexpression of *MYC* in isolated *TP53*$^{-/-}$ CGNPs and their following orthotopic transplantation in nude mice is able to mimic some of the Group 3 MB clinical features, strongly suggesting their cooperation in determining a more aggressive behavior (Kawauchi et al., 2012; Pei et al., 2012). However, Group 3 MB features can be also obtained by passing the *TP53* loss that is not often found within Group 3 tumors. Indeed, it has been shown that the overexpression of *c-Myc*, together with *GFI1*/*GFI1B* activation, allows to recapitulate Group 3 MB tumorigenesis (Northcott et al., 2014; Vo et al., 2017). A list of G3 GEMMs is presented in **Table 1**.

Group 4 Medulloblastoma

The Group 4 MB is the least explored and understood among the subgroups. A comparative analysis of protein phosphorylation levels between Group 3 and Group 4 leads to hypothesize a role of the receptor tyrosine kinase (RTK) pathway in the Group 4 MB onset; these findings were validated by the enrichment at the mRNA level of *ERBB4*, a well-established RTK member (Forget et al., 2018). SRC is a key regulator of the RTK pathway and was found upregulated at both mRNA and protein levels in Group 4. Moreover, *in utero* electroporation in the fourth ventricle of E13.5 mouse embryos of the active form of SRC, together with a dominant negative form of TP53, leads to Group 4 MB formation (**Figure 2B** and **Table 1**). However, *TP53* seems not to be mutated in Group 4 MB, but iso-chromosome 17q is frequently present in these patients. SRC-driven tumors present distinct molecular features from MYC-derived tumors. Since ERBB4 and SRC were detectable in the nuclear transitory zone (NTZ) on embryonic Day 13.5 (E13.5), Forget et al. (2018) speculated that their expression could reflect Group 4 developmental origin. ScRNAseq analysis on human Group 4 MB indicated an enrichment of markers involved in neuronal differentiation, such as *ENO2*, *SYT11*, *TUBB3*, and *MAP2*, or in glutamatergic lineage specification, such as *EOMES* and *LMX1A*. These factors have been implicated in defining neuronal fates of unipolar brush cells (UBC) and glutamatergic cerebellar nuclei (GluCN) in the embryonic upper rhombic lip (Englund et al., 2006; Chizhikov et al., 2010; Hovestadt et al., 2019). Lin et al. (2016) found enrichment of super-enhancer activation of LMX1A, TBR2, and LHX2, which could support origin from progenitors in the embryonic upper rhombic lip. However, the developmental origin of Group 4 is still an open question, and further studies must be conducted to clarify the involvement of UBC, GluCN, or other cell types in the Group 4 MB onset. The identification of the cell of origin is a crucial step for the development of faithful and proper models for Group 4 MB.

Patient-Derived Xenograft and Patient-Derived Organoids Xenograft

As previously stated, mouse models show some limitations due to the different biological contexts and cannot fully recapitulate the complexity of human tumors (Gould et al., 2015). For this reason, PDX models emerged as an important tool to investigate subtype specific features of different pediatric brain tumors. A study conducted by the Children's Oncology Group set the generation of 30 orthotopic pediatric brain tumor PDX models (Brabetz et al., 2018). An important effort in generating PDX models has been also achieved by the St. Jude Children's Research Hospital by the generation of 37 novel orthotopic PDX models derived from patients with pediatric brain tumor (Smith et al., 2020). These new models include all the four MB subgroups (WNT, SHH, Group 3, and Group 4) that have been shown to maintain histological features of the original tumors and to genetically match the patients' tumors. DNA methylation, transcriptional and histological analyses at early and late passages demonstrated the reliability of PDX models, providing a useful and valid resource to study cancer biology and to test novel and tailored therapeutic approaches.

Recently, it has been generated a humanized mouse model based on the orthotopic transplantation of human neuroepithelial stem cells (NES) (Huang et al., 2019). NES are multipotent stem cells able to differentiate into neurons with hindbrain identity. Orthotopic transplantation of NES transduced with *MYCN* leads to the formation of a human cancer phenotype as a powerful tool to dissect the processes of tumorigenesis. An alternative method to model SHH MB using human cells was described by Susanto et al. (2020) that performed an orthotopic transplantation of iPSC-derived NES from a Gorlin patient with a germline *PTCH1* mutation. They followed tumor development by re-transplanting tumor-isolated NES (tNES) cells in nude mice and identifying *LGALS1* as a putative new therapeutic target.

3D Organoid-Based Models for Medulloblastoma

Similar to gliomas, 3D cerebellar organoid models have been shown to be an emerging important tool to study human

medulloblastoma. Taking advantage of already-available exome sequencing data and after adapting a previously developed protocol for cerebellar organoid generation (Muguruma et al., 2015; Ballabio et al., 2020), the first organoid model of Group 3 MB has been generated by overexpressing a combination of *Gfi1* + *c-MYC* and *Otx2* + *c-MYC oncogenes*, identified previously as candidate driver genes in the same study by an *in vivo* mutagenesis screen. These Group 3 MB organoid models more closely mimic the histological, transcriptional, and DNA methylation profile of human Group 3 MB (Ballabio et al., 2020, 2021) (**Figure 2B** and **Table 1**), suggesting that they could be a more suitable platform for high-throughput drug testing and development of personalized therapies (Qian et al., 2019). Future studies could be done to develop models for the other MB subtypes by mutagenesis or by engraftment of patient-derived tumor cells. These could then allow us to study with more precision the mechanisms at the origin of the tumor formation and how the mutations found in the patients' tumors drive tumorigenesis with unprecedented details in a human tissue. This could then lead to the identification of new potential targets for therapies and for diseases that, to date, cannot be tackled. It is, indeed, also possible that the human brain, due to its species-specific differences, could have different susceptibility to disease and brain tumors (Watanabe et al., 2017; Kanton et al., 2019; Eichmüller et al., 2022), a reason why studying mechanisms of tumorigenesis in human tissue becomes essential.

EPENDYMOMA

Ependymoma can originate in the brain or spinal cord. In the brain, ependymomas are thought to originate from ependymal cells lining in the ventricles. Histologically, ependymomas are classified into four groups: subependymoma (WHO Grade I), myxopapillary ependymoma and classic ependymoma (WHO Grade II), and anaplastic ependymoma (WHO Grade III), of which classic and anaplastic ependymoma are the most common subtypes in children (**Figure 1**). Over 90% of pediatric ependymomas arise in the infratentorial and supratentorial regions. Supratentorial (ST) ependymomas in children have two major subgroups: *RELA* fusion-positive ependymoma and *YAP1* fusion-positive ependymoma. Ependymoma mouse models have been generated by *RELAFUS1* fusion gene expression in $Nestin^+$, $Gfap^+$ or $Blbp^+$ cells in the mouse brain. These tumors recapitulate some of the histology and the transcriptome panel of human ependymomas (Ozawa et al., 2018). The *YAP1-MAMLD1* fusion gene delivered to mice by *in utero* electroporation drives tumor formation, and tumors share histological and molecular characteristics of human ependymoma (Pajtler et al., 2019). Recently, Eder et al. (2020) have reported that ectopic expression of active nuclear YAP1 (nlsYAP5SA) or conditional deletion of YAP1's negative regulators *Lats1* and *Lats2* kinases in neural progenitor cells of the ventricular zone also induced tumors with molecular characteristics of human ependymoma. PDXs derived from pediatric ependymoma showed to maintain a genetic, molecular, and histological similarity to the parental tumors, opening the possibility to have an additional model for investigating and treating such a disease (Brabetz et al., 2018; Smith et al., 2020). No organoid-based models have been reported for human ependymoma (**Table 1**).

MENINGIOMAS

Meningioma is another common type of tumors located in the brain, which originates from the meninges. Meningiomas, representing the most frequent tumor in the adult, are generally benign (WHO Grade I) with a lower percentage classified as atypical (WHO Grade II) and rarely anaplastic (WHO Grade III) (Boetto et al., 2021). The genomic profile of a large cohort of meningiomas has identified alteration in the genes encoding for NF2, SMARCB1, SMARCE1, TRAF7, KLF4, POLR2A, BAP1, and members of the PI3K and Hedgehog pathways (Youngblood et al., 2019). The mouse model of meningiomas consisted in xenograft of immortalized cell lines or patient-derived tumor cells (McCutcheon et al., 2000; Püttmann et al., 2005; Cargioli et al., 2007; Ragel et al., 2008), GEMMs (Kalamarides et al., 2002, 2011; Peyre et al., 2013, 2015; Boetto et al., 2018, 2021) and syngeneic allogenic graft (Boetto et al., 2021) (**Table 1**). Meningiomas can be induced in GEMMs overexpressing *PDGFB* in a context of loss of function of *Nf2*, *Cdkn2ab* or *p16Ink4a* or over-expressing only *SmoM2* $PGDS^+$ arachnoid cells. Recently, PDO has been generated also from meningioma biopsies (Chan et al., 2021; Yamazaki et al., 2021). Its histological and molecular characterizations positively confirmed the high similarity between the parental tumor and PDOs (Yamazaki et al., 2021).

TRANSLATION IN CLINICAL PRACTICE OF MODEL-BASED KNOWLEDGE AND DISCOVERIES

The main goal of the different models is to be used for the design of new therapeutical approaches and then being translated into clinical practice for glioma treatments. Concerning high-grade glioma (including GBM), the standard chemotherapeutic treatment is based on temozolomide, while lower grade gliomas relies on procarbazine, lomustine, and vincristine or temozolomide. Despite the enormous number of pre-clinical *in vivo* and *in vitro* models, the drugs used for treating gliomas (from Grade II to Grade IV) have remained the same over the last decades. Indeed, this negative and low progression of developing new drugs against glioma has also pushed the field to test already approved drugs originally designed for other diseases (Lyne and Yamini, 2021). This approach, called drug repositioning, has the advantage to have drugs already being tested for their safety, making eventually the path to a clinical trial to be faster. Furthermore, this approach could be coupled to the possibility to generate, expand, and Biobank organoids derived from histologically and molecularly different tumors (Golebiewska et al., 2020; Jacob et al., 2020) in order to have a more "personalized" and specific drug screen.

Current treatment for MB consists of surgery, radio- and chemotherapy; nevertheless, after surgery, patients suffer from severe psychosocial, neurocognitive, and neuro-endocrine deficits. Present studies are focused on the development of target therapies that take into account the molecular differences among the subgroups (Northcott et al., 2019; Thompson et al., 2020). In the scenario, the development of *in vitro* and *in vivo* models is crucial. In general, despite the models developed for brain cancer are increasing in terms of numbers, complexity, and the degree of similarity to the original tumor, the drugs available for treating the disease are always the same. What has really improved tough is the knowledge of the genetics and biology of the different types of brain cancer. This could be considered the starting point for rethinking about new pharmacological, immunological, and genetic therapies.

CONCLUSION

Genomic, transcriptomic, and proteomic analyses on human brain tumor patients have greatly increased our knowledge and understanding of the signaling pathways regulating the different cancer subtypes. Through the exploitation of these data, several models have been created to mimic the pathogenesis and to gain knowledge about the molecular mechanisms of the tumors. All the brain tumor models developed so far have shown some pitfalls in the correct modeling of the disease and the human translation of the findings (**Figure 2**). The first issue is related to the genetics, with all the mouse models and hiPSCs derived-brain organoid, relying only on a few of the genetic abnormalities found in patients with brain tumor. In this direction, it will be worth expanding the combination of genetic abnormalities inducing tumor in mice and organoids performing large genetic screens. Drosophila represents a valid complementary model to be used for performing a "low-cost" initial genetic screen for a new putative cancer driver. Secondly, the drug screen platforms used so far have mostly relied on 2D-cultured tumor cell lines. Therefore, the use of hiPSCs-derived brain organoid represents a unique platform for medium/high throughput screening of new molecules to hinder tumor progression. On the other hand, organoid cultures have some limitations. The lack of vascularization leads to reduced oxygenation and access to nutrients, with the consequent formation of an inner necrotic core in the tissue when cultures are kept for long-term studies. The absence of immune cells and microglia makes the studies of tumor-microenvironment preferable *in vivo*. Some limitations can be overcome at the current state-of-the-art by transplanting human organoids in the mouse brain (Mansour et al., 2018; Ballabio et al., 2020; Bhaduri et al., 2020). Furthermore, the ability to cultivate the original human primary tumor with PDO will be a breakthrough that will provide the possibility to personalize the treatments. Recently, patient-derived xenografts (PDXs) have been shown to be the most advanced model, recapitulating the human disease. These models might be used to model frequent as well as rare childhood brain tumor entities, including HGG, MB, anaplastic ependymoma, atypical teratoid rhabdoid tumor, and embryonal tumor (Brabetz et al., 2018; Smith et al., 2020). PDOX models will be valuable platforms for evaluating novel therapies and conducting pre-clinical trials to accelerate progress in the treatment of pediatric brain tumors. However, the usage of immunocompromised mice does not allow to investigate the interaction between tumor cells and immune system. Moreover, since PDO and PDX are derived from tumor biopsies, they should not be considered suitable for investigating the neoplastic transformation of brain cells. In this review, we depicted an overview of the *in vitro* and *in vivo* brain tumor models used in the past together with the most technologically advanced ones. Considering the entire pros and cons described in this review, the best model system must be chosen, depending on the specific biological question that needs to be addressed.

AUTHOR CONTRIBUTIONS

FA, GA, AS, and LT made substantial contributions to researching data for the article, to discussions of content, and to writing the manuscript. EM and LA reviewed and edited the manuscript before submission. All authors contributed to the article and approved the submitted version.

FUNDING

LT gratefully acknowledges financial support from the Armenise-Harvard Foundation, AIRC, CARITRO, Pezcoller Foundation and EMBO. FA has received funding from the European Union's Horizon 2020 Research and Innovation Program under the Marie Skłodowska Curie, with grant agreement No. 844677, and Fondazione Umberto Veronesi. GA was supported by a FIRC-AIRC fellowship for Italy. EM was supported by Italian Ministry of Health, Ricerca Finalizzata, No. GR-2018-12367328. AS and LA were supported by Fondazione Umberto Veronesi.

ACKNOWLEDGMENTS

We thank all the members of the Armenise-Harvard Laboratory of Brain Disorders and Cancer for helpful discussions.

REFERENCES

Abballe, L., and Miele, E. (2021). Epigenetic modulators for brain cancer stem cells: implications for anticancer treatment. *World J. Stem Cells* 13, 670–684. doi: 10.4252/wjsc.v13.i7.670

Aday, S., Cecchelli, R., Hallier-Vanuxeem, D., Dehouck, M. P., and Ferreira, L. (2016). Stem cell-based human blood–brain barrier models for drug discovery and delivery. *Trends Biotechnol.* 34, 382–393. doi: 10.1016/j.tibtech.2016.01.001

Ahir, B. K., Engelhard, H. H., and Lakka, S. S. (2020). Tumor development and angiogenesis in adult brain tumor: glioblastoma. *Mol. Neurobiol.* 57, 2461–2478. doi: 10.1007/s12035-020-01892-8

Aiello, G., Ballabio, C., Ruggeri, R., Fagnocchi, L., Anderle, M., Morassut, I., et al. (2019). Truncated BRPF1 cooperates with smoothened to promote adult Shh medulloblastoma. *Cell Rep.* 29, 4036.e10–4052.e10.

Akter, F., Simon, B., de Boer, N. L., Redjal, N., Wakimoto, H., and Shah, K. (2021). Pre-clinical tumor models of primary brain tumors: challenges and

opportunities. *Biochim. Biophys. Acta. Rev. Cancer* 1875:188458. doi: 10.1016/j.bbcan.2020.188458

Aldape, K., Brindle, K. M., Chesler, L., Chopra, R., Gajjar, A., Gilbert, M. R., et al. (2019). Challenges to curing primary brain tumours. *Nat. Rev. Clin. Oncol.* 16, 509–520. doi: 10.1038/s41571-019-0177-5

Ausman, J. I., Shapiro, W. R., and Rall, D. P. (1970). Studies on the chemotherapy of experimental brain tumors: development of an experimental model. *Cancer Res.* 30, 2394–2400.

Azzarelli, R., McNally, A., Dell'Amico, C., Onorati, M., Simons, B., and Philpott, A. (2022). ASCL1 phosphorylation and ID2 upregulation are roadblocks to glioblastoma stem cell differentiation. *Sci. Rep.* 12:2341. doi: 10.1038/s41598-022-06248-x

Azzarelli, R., Ori, M., Philpott, A., and Simons, B. D. (2021). Three-dimensional model of glioblastoma by co-culturing tumor stem cells with human brain organoids. *Biol. Open* 10:bio056416. doi: 10.1242/bio.056416

Ballabio, C., Anderle, M., Gianesello, M., Lago, C., Miele, E., Cardano, M., et al. (2020). Modeling medulloblastoma *in vivo* and with human cerebellar organoids. *Nat. Commun.* 11, 1–18. doi: 10.1038/s41467-019-13989-3

Ballabio, C., Gianesello, M., Lago, C., Okonechnikov, K., Anderle, M., Aiello, G., et al. (2021). Notch1 switches progenitor competence in inducing medulloblastoma. *Sci. Adv.* 7:eabd2781. doi: 10.1126/sciadv.abd2781

Bell, A. J., McBride, S. M. J., and Dockendorff, T. C. (2009). Flies as the ointment: drosophila modeling to enhance drug discovery. *Fly (Austin)* 3, 39–49. doi: 10.4161/fly.3.1.7774

Bhaduri, A., Andrews, M. G., Mancia Leon, W., Jung, D., Shin, D., Allen, D., et al. (2020). Cell stress in cortical organoids impairs molecular subtype specification. *Nature* 578, 142–148. doi: 10.1038/s41586-020-1962-0

Bian, S., Repic, M., Guo, Z., Kavirayani, A., Burkard, T., Bagley, J. A., et al. (2018). Genetically engineered cerebral organoids model brain tumor formation. *Nat. Methods* 15, 631–639. doi: 10.1038/s41592-018-0070-7

Boetto, J., Apra, C., Bielle, F., Peyre, M., and Kalamarides, M. (2018). Selective vulnerability of the primitive meningeal layer to prenatal Smo activation for skull base meningothelial meningioma formation. *Oncogene* 37, 4955–4963. doi: 10.1038/s41388-018-0328-7

Boetto, J., Peyre, M., and Kalamarides, M. (2021). Mouse models in meningioma research: a systematic review. *Cancers* 13:3712. doi: 10.3390/cancers13153712

Brabetz, S., Leary, S. E. S., Gröbner, S. N., Nakamoto, M. W., Şeker-Cin, H., Girard, E. J., et al. (2018). A biobank of patient-derived pediatric brain tumor models. *Nat. Med.* 24, 1752–1761. doi: 10.1038/s41591-018-0207-3

Brennan, C. W., Verhaak, R. G. W., McKenna, A., Campos, B., Noushmehr, H., Salama, S. R., et al. (2013). The somatic genomic landscape of glioblastoma. *Cell* 155, 462–477. doi: 10.1016/j.cell.2013.09.034

Bressan, R. B., Southgate, B., Ferguson, K. M., Blin, C., Grant, V., Alfazema, N., et al. (2021). Regional identity of human neural stem cells determines oncogenic responses to histone H3.3 mutants. *Cell Stem Cell* 28, 877.e9–893.e9. doi: 10.1016/j.stem.2021.01.016

Breznik, B., Motaln, H., Vittori, M., Rotter, A., and Turnšek, T. L. (2017). Mesenchymal stem cells differentially affect the invasion of distinct glioblastoma cell lines. *Oncotarget* 8, 25482–25499. doi: 10.18632/oncotarget.16041

Cargioli, T. G., Ugur, H. C., Ramakrishna, N., Chan, J., Black, P. M., and Carroll, R. S. (2007). Establishment of an *in vivo* meningioma model with human telomerase reverse transcriptase. *Neurosurgery* 60, 750–760. doi: 10.1227/01.NEU.0000255397.00410.8F

Casey, M. J., and Stewart, R. A. (2020). Pediatric cancer models in zebrafish. *Trends Cancer* 6, 407–418. doi: 10.1016/j.trecan.2020.02.006

Caussinus, E., and Gonzalez, C. (2005). Induction of tumor growth by altered stem-cell asymmetric division in Drosophila melanogaster. *Nat. Genet.* 37, 1125–1129. doi: 10.1038/ng1632

Chan, H. S. C., Ng, H. K., Chan, A. K. Y., Cheng, S. H., Chow, C., Wong, N., et al. (2021). Establishment and characterization of meningioma patient-derived organoid. *J. Clin. Neurosci.* 94, 192–199. doi: 10.1016/j.jocn.2021.10.035

Chen, X., Wanggou, S., Bodalia, A., Zhu, M., Dong, W., Fan, J. J., et al. (2018). A feedforward mechanism mediated by mechanosensitive ion channel PIEZO1 and tissue mechanics promotes glioma aggression. *Neuron* 100, 799.e7–815.e7. doi: 10.1016/j.neuron.2018.09.046

Cheng, P., Wang, J., Waghmare, I., Sartini, S., Coviello, V., Zhang, Z., et al. (2016). FOXD1-ALDH1A3 signaling is a determinant for the self-renewal and tumorigenicity of mesenchymal glioma stem cells. *Cancer Res.* 76, 7219–7230. doi: 10.1158/0008-5472.CAN-15-2860

Chi, K.-C., Tsai, W.-C., Wu, C.-L., Lin, T.-Y., and Hueng, D.-Y. (2018). An adult drosophila glioma model for studying pathometabolic pathways of gliomagenesis. *Mol. Neurobiol.* 56, 4589–4599. doi: 10.1007/s12035-018-1392-2

Chia, K., Keatinge, M., Mazzolini, J., and Sieger, D. (2019). Brain tumours repurpose endogenous neuron to microglia signalling mechanisms to promote their own proliferation. *Elife* 8:e46912. doi: 10.7554/eLife.46912

Chia, K., Mazzolini, J., Mione, M., and Sieger, D. (2018). Tumor initiating cells induce Cxcr4-mediated infiltration of pro-tumoral macrophages into the brain. *Elife* 7:e31918. doi: 10.7554/eLife.31918

Chizhikov, V. V., Lindgren, A. G., Mishima, Y., Roberts, R. W., Aldinger, K. A., Miesegaes, G. R., et al. (2010). Lmx1a regulates fates and location of cells originating from the cerebellar rhombic lip and telencephalic cortical hem. *Proc. Natl. Acad. Sci. U.S.A.* 107, 10725–10730. doi: 10.1073/pnas.0910786107

da Silva, B., Mathew, R. K., Polson, E. S., Williams, J., and Wurdak, H. (2018). Spontaneous glioblastoma spheroid infiltration of early-stage cerebral organoids models brain tumor invasion. *SLAS Discov.* 23, 862–868. doi: 10.1177/2472555218764623

Darmanis, S., Sloan, S. A., Croote, D., Mignardi, M., Chernikova, S., Samghababi, P., et al. (2017). Single-Cell RNA-Seq analysis of infiltrating neoplastic cells at the migrating front of human glioblastoma. *Cell Rep.* 21, 1399–1410. doi: 10.1016/j.celrep.2017.10.030

Day, C., Merlino, G., and Van Dyke, T. (2015). Preclinical mouse cancer models: a maze of opportunities and challenges. *Cell* 163, 39–53. doi: 10.1016/j.cell.2015.08.068

Dey, J., Ditzler, S., Knoblaugh, S. E., Hatton, B. A., Schelter, J. M., Cleary, M. A., et al. (2012). A distinct Smoothened mutation causes severe cerebellar developmental defects and medulloblastoma in a novel transgenic mouse model. *Mol. Cell. Biol.* 32, 4104–4115. doi: 10.1128/MCB.00862-12

Dhar, S., Zhao, D., Lin, T., Gu, B., Pal, K., Wu, S. J., et al. (2018). MLL4 Is Required to maintain broad H3K4me3 peaks and super-enhancers at tumor suppressor genes. *Mol. Cell* 70, 825.e6–841.e6. doi: 10.1016/j.molcel.2018.04.028

Eder, E., Roncaroli, F., Domart, M. C., Horswell, S., Andreiuolo, F., Flynn, H. R., et al. (2020). YAP1/TAZ drives ependymoma-like tumour formation in mice. *Nat. Commun.* 11:2380.

Eichmüller, O. L., Corsini, N. S., Vértesy, A., Morassut, I., Scholl, T., Gruber, V.-E., et al. (2022). Amplification of human interneuron progenitors promotes brain tumors and neurological defects. *Science* 375:eabf5546. doi: 10.1126/science.abf5546

Englund, C., Kowalczyk, T., Daza, R. A. M., Dagan, A., Lau, C., Rose, M. F., et al. (2006). Unipolar brush cells of the cerebellum are produced in the rhombic lip and migrate through developing white matter. *J. Neurosci.* 26, 9184–9195. doi: 10.1523/JNEUROSCI.1610-06.2006

Fareh, M., Turchi, L., Virolle, V., Debruyne, D., Almairac, F., de-la-Forest Divonne, S., et al. (2012). The miR 302-367 cluster drastically affects self-renewal and infiltration properties of glioma-initiating cells through CXCR4 repression and consequent disruption of the SHH-GLI-NANOG network. *Cell Death Differ.* 19, 232–244. doi: 10.1038/cdd.2011.89

Forget, A., Martignetti, L., Puget, S., Calzone, L., Brabetz, S., Picard, D., et al. (2018). Aberrant ERBB4-SRC signaling as a hallmark of Group 4 medulloblastoma revealed by integrative phosphoproteomic profiling. *Cancer Cell* 34, 379.e7–395.e7. doi: 10.1016/j.ccell.2018.08.002

Gangoso, E., Southgate, B., Bradley, L., Rus, S., Galvez-Cancino, F., McGivern, N., et al. (2021). Glioblastomas acquire myeloid-affiliated transcriptional programs *via* epigenetic immunoediting to elicit immune evasion. *Cell* 184, 2454.e26–2470.e26. doi: 10.1016/j.cell.2021.03.023

Gangwani, K., Snigdha, K., and Kango-Singh, M. (2020). Tep1 regulates Yki activity in neural stem cells in drosophila glioma model. *Front. Cell Dev. Biol.* 8:306. doi: 10.3389/fcell.2020.00306

Gao, Y., de Wit, M., Struys, E. A., van der Linde, H. C. Z., Salomons, G. S., Lamfers, M. L. M., et al. (2018). IDH1-mutated transgenic zebrafish lines: an in-vivo model for drug screening and functional analysis. *PLoS One* 13:e0199737. doi: 10.1371/journal.pone.0199737

Gibson, P., Tong, Y., Robinson, G., Thompson, M. C., Currle, D. S., Eden, C., et al. (2010). Subtypes of medulloblastoma have distinct developmental origins. *Nature* 468, 1095–1099. doi: 10.1038/nature09587

Golebiewska, A., Hau, A.-C., Oudin, A., Stieber, D., Yabo, Y. A., Baus, V., et al. (2020). Patient-derived organoids and orthotopic xenografts of primary and recurrent gliomas represent relevant patient avatars for precision oncology. *Acta Neuropathol.* 140, 919–949. doi: 10.1007/s00401-020-02226-7

Gómez-López, S., Lerner, R. G., and Petritsch, C. (2013). Asymmetric cell division of stem and progenitor cells during homeostasis and cancer. *Cell. Mol. Life Sci.* 71, 575–597. doi: 10.1007/s00018-013-1386-1

Goodrich, L. V., Milenkoviæ, L., Higgins, K. M., and Scott, M. P. (1997). Altered neural cell fates and medulloblastoma in mouse patched mutants. *Science* 277, 1109–1113. doi: 10.1126/science.277.5329.1109

Goranci-Buzhala, G., Mariappan, A., Gabriel, E., Ramani, A., Ricci-Vitiani, L., Buccarelli, M., et al. (2020). Rapid and efficient invasion assay of glioblastoma in human brain organoids. *Cell Rep.* 31:107738. doi: 10.1016/j.celrep.2020.107738

Gould, S. E., Junttila, M. R., and de Sauvage, F. J. (2015). Translational value of mouse models in oncology drug development. *Nat. Med.* 21, 431–439. doi: 10.1038/nm.3853

Grammel, D., Warmuth-Metz, M., von Bueren, A. O., Kool, M., Pietsch, T., and Kretzschmar, H. A. (2012). Sonic hedgehog-associated medulloblastoma arising from the cochlear nuclei of the brainstem. *Acta Neuropathol.* 123, 601–614. doi: 10.1007/s00401-012-0961-0

Gronych, J., Korshunov, A., Bageritz, J., Milde, T., Jugold, M., Hambardzumyan, D., et al. (2011). An activated mutant BRAF kinase domain is sufficient to induce pilocytic astrocytoma in mice. *J. Clin. Invest.* 121, 1344–1348. doi: 10.1172/JCI44656

Haag, D., Mack, N., Benites Goncalves da Silva, P., Statz, B., Clark, J., Tanabe, K., et al. (2021). H3.3-K27M drives neural stem cell-specific gliomagenesis in a human iPSC-derived model. *Cancer Cell* 39, 407.e13–422.e13. doi: 10.1016/j.ccell.2021.01.005

Hakes, A. E., and Brand, A. H. (2020). Tailless/TLX reverts intermediate neural progenitors to stem cells driving tumourigenesis *via* repression of asense/ASCL1. *Elife* 9:e53377. doi: 10.7554/eLife.53377

Hambardzumyan, D., Amankulor, N. M., Helmy, K. Y., Becher, O. J., and Holland, E. C. (2009). Modeling adult gliomas using RCAS/t-va technology. *Transl. Oncol.* 2, 89–95. doi: 10.1593/tlo.09100

Hede, S.-M., Hansson, I., Afink, G. B., Eriksson, A., Nazarenko, I., Andrae, J., et al. (2009). GFAP promoter driven transgenic expression of PDGFB in the mouse brain leads to glioblastoma in a Trp53 null background. *Glia* 57, 1143–1153. doi: 10.1002/glia.20837

Hicks, W., Bird, C. E., Traylor, J. I., Shi, D. D., Ahmadieh, T. Y. E., and Richardson, T. E. (2021). Contemporary mouse models in glioma research. *Cells* 10:712. doi: 10.3390/cells10030712

Hill, R. M., Kuijper, S., Lindsey, J. C., Petrie, K., Schwalbe, E. C., Barker, K., et al. (2015). Combined MYC and P53 defects emerge at medulloblastoma relapse and define rapidly progressive, therapeutically targetable disease. *Cancer Cell* 27, 72–84. doi: 10.1016/j.ccell.2014.11.002

Ho, V. K. Y., Reijneveld, J. C., Enting, R. H., Bienfait, H. P., Robe, P., Baumert, B. G., et al. (2014). Changing incidence and improved survival of gliomas. *Eur. J. Cancer* 50, 2309–2318. doi: 10.1016/j.ejca.2014.05.019

Hoffmann, N., Fernández, V., Cruz Pereira, R., Rancati, S., Pelizzoli, R., and De Pietri Tonelli, D. (2020). A Xenotransplant model of human brain tumors in wild-type mice. *iScience* 23:100813. doi: 10.1016/j.isci.2019.100813

Holland, E. C., Hively, W. P., DePinho, R. A., and Varmus, H. E. (1998). A constitutively active epidermal growth factor receptor cooperates with disruption of G1 cell-cycle arrest pathways to induce glioma-like lesions in mice. *Genes Dev.* 12:3675. doi: 10.1101/gad.12.23.3675

Hovestadt, V., Smith, K. S., Bihannic, L., Filbin, M. G., Shaw, M. K. L., Baumgartner, A., et al. (2019). Resolving medulloblastoma cellular architecture by single-cell genomics. *Nature* 572, 74–79. doi: 10.1038/s41586-019-1434-6

Huang, M., Tailor, J., Zhen, Q., Gillmor, A. H., Miller, M. L., Weishaupt, H., et al. (2019). Engineering genetic predisposition in human neuroepithelial stem cells recapitulates medulloblastoma tumorigenesis. *Cell Stem Cell.* 25, 433.e7–446.e7. doi: 10.1016/j.stem.2019.05.013

Huang, Y. C., Lin, S. J., Shih, H. Y., Chou, C. H., Chu, H. H., Chiu, C. C., et al. (2017). Epigenetic regulation of NOTCH1 and NOTCH3 by KMT2A inhibits glioma proliferation. *Oncotarget* 8, 63110–63120. doi: 10.18632/oncotarget.18668

Hubert, C. G., Rivera, M., Spangler, L. C., Wu, Q., Mack, S. C., Prager, B. C., et al. (2016). A three-dimensional organoid culture system derived from human glioblastomas recapitulates the hypoxic gradients and cancer stem cell heterogeneity of tumors found *in vivo*. *Cancer Res.* 76, 2465–2477. doi: 10.1158/0008-5472.CAN-15-2402

Jacob, F., Salinas, R. D., Zhang, D. Y., Nguyen, P. T. T., Schnoll, J. G., Wong, S. Z. H., et al. (2020). A patient-derived glioblastoma organoid model and biobank recapitulates inter- and intra-tumoral heterogeneity. *Cell* 180, 188.e22–204.e22. doi: 10.1016/j.cell.2019.11.036

Jacob, L., Sawma, P., Garnier, N., Meyer, L. A. T., Fritz, J., Hussenet, T., et al. (2016). Inhibition of PlexA1-mediated brain tumor growth and tumor-associated angiogenesis using a transmembrane domain targeting peptide. *Oncotarget* 7, 57851–57865. doi: 10.18632/oncotarget.11072

Jandial, R., Neman, J., Lim, P. P., Tamae, D., Kowolik, C. M., Wuenschell, G. E., et al. (2018). Inhibition of GLO1 in glioblastoma multiforme increases DNA-AGEs, stimulates RAGE expression, and inhibits brain tumor growth in orthotopic mouse models. *Int. J. Mol. Sci.* 19:406. doi: 10.3390/ijms19020406

Jones, D., Jäger, N., Kool, M., Zichner, T., Hutter, B., Sultan, M., et al. (2012). Dissecting the genomic complexity underlying medulloblastoma. *Nature* 488, 100–105. doi: 10.1038/nature11284

Joo, K. M., Kim, J., Jin, J., Kim, M., Seol, H. J., Muradov, J., et al. (2013). Patient-specific orthotopic glioblastoma xenograft models recapitulate the histopathology and biology of human glioblastomas in situ. *Cell Rep.* 3, 260–273. doi: 10.1016/j.celrep.2012.12.013

Ju, B., Chen, W., Orr, B. A., Spitsbergen, J. M., Jia, S., Eden, C. J., et al. (2015). Oncogenic KRAS promotes malignant brain tumors in zebrafish. *Mol. Cancer* 14:18. doi: 10.1186/s12943-015-0288-2

Ju, B., Chen, W., Spitsbergen, J. M., Lu, J., Vogel, P., Peters, J. L., et al. (2014). Activation of Sonic hedgehog signaling in neural progenitor cells promotes glioma development in the zebrafish optic pathway. *Oncogenesis* 3:e96. doi: 10.1038/oncsis.2014.10

Jung, I. H., Leem, G. L., Jung, D. E., Kim, M. H., Kim, E. Y., Kim, S. H., et al. (2013). Glioma is formed by active Akt1 alone and promoted by active Rac1 in transgenic zebrafish. *Neuro. Oncol.* 15, 290–304. doi: 10.1093/neuonc/nos387

Kalamarides, M., Niwa-Kawakita, M., Leblois, H., Abramowski, V., Perricaudet, M., Janin, A., et al. (2002). Nf2 gene inactivation in arachnoidal cells is rate-limiting for meningioma development in the mouse. *Genes Dev.* 16, 1060–1065. doi: 10.1101/gad.226302

Kalamarides, M., Stemmer-Rachamimov, A. O., Niwa-Kawakita, M., Chareyre, F., Taranchon, E., Han, Z.-Y., et al. (2011). Identification of a progenitor cell of origin capable of generating diverse meningioma histological subtypes. *Oncogene* 30, 2333–2344. doi: 10.1038/onc.2010.609

Kanton, S., Boyle, M. J., He, Z., Santel, M., Weigert, A., Sanchís-Calleja, F., et al. (2019). Organoid single-cell genomic atlas uncovers human-specific features of brain development. *Nature* 574, 418–422. doi: 10.1038/s41586-019-1654-9

Kawauchi, D., Robinson, G., Uziel, T., Gibson, P., Rehg, J., Gao, C., et al. (2012). A mouse model of the most aggressive subgroup of human medulloblastoma. *Cancer Cell* 21, 168–180. doi: 10.1016/j.ccr.2011.12.023

Kaye, A. H., Morstyn, G., Gardner, I., and Pyke, K. (1986). Development of a Xenograft glioma model in mouse brain. *Cancer Res.* 46, 1367–1373.

Kerstetter-Fogle, A. E., Harris, P. L. R., Brady-Kalnay, S. M., and Sloan, A. E. (2020). Generation of glioblastoma patient-derived intracranial xenografts for preclinical studies. *Int. J. Mol. Sci.* 21:5113. doi: 10.3390/ijms21145113

Kim, S. N., Jeibmann, A., Halama, K., Witte, H. T., Wälte, M., Matzat, T., et al. (2014). ECM stiffness regulates glial migration in Drosophila and mammalian glioma models. *Development* 141, 3233–3242. doi: 10.1242/dev.106039

Kirchberger, S., Sturtzel, C., Pascoal, S., and Distel, M. (2017). Quo natas, Danio?-Recent progress in modeling cancer in Zebrafish. *Front. Oncol.* 7:186. doi: 10.3389/fonc.2017.00186

Koschmann, C., Calinescu, A.-A., Nunez, F. J., Mackay, A., Fazal-Salom, J., Thomas, D., et al. (2016). ATRX loss promotes tumor growth and impairs non-homologous end joining DNA repair in Glioma. *Sci. Transl. Med.* 8:328ra28. doi: 10.1126/scitranslmed.aac8228

Krieger, T. G., Tirier, S. M., Park, J., Jechow, K., Eisemann, T., Peterziel, H., et al. (2020). Modeling glioblastoma invasion using human brain organoids and single-cell transcriptomics. *Neuro. Oncol.* 22, 1138–1149. doi: 10.1093/neuonc/noaa091

Kutscher, L., Okonechnikov, K., Batora, N. V., Clark, J., Silva, P. B. G., Vouri, M., et al. (2020). Functional loss of a noncanonical BCOR-PRC1.1 complex accelerates SHH-driven medulloblastoma formation. *Genes Dev.* 34, 1161–1176. doi: 10.1101/gad.337584.120

Kwon, C.-H., Zhao, D., Chen, J., Alcantara, S., Li, Y., Burns, D. K., et al. (2008). Pten haploinsufficiency accelerates formation of high-grade astrocytomas. *Cancer Res.* 68, 3286–3294. doi: 10.1158/0008-5472.CAN-07-6867

Lai, Y. J., Tsai, J. C., Tseng, Y. T., Wu, M. S., Liu, W. S., Lam, H. I., et al. (2017). Small G protein Rac GTPases regulate the maintenance of glioblastoma stem-like cells *in vitro* and *in vivo*. *Oncotarget* 8, 18031–18049. doi: 10.18632/oncotarget.14949

Lam, S. H., Chua, H. L., Gong, Z., Lam, T. J., and Sin, Y. M. (2004). Development and maturation of the immune system in zebrafish, Danio rerio: a gene expression profiling, in situ hybridization and immunological study. *Dev. Comp. Immunol.* 28, 9–28. doi: 10.1016/s0145-305x(03)00103-4

Lan, X., Jörg, D. J., Cavalli, F. M. G., Richards, L. M., Nguyen, L. V., Vanner, R. J., et al. (2017). Fate mapping of human glioblastoma reveals an invariant stem cell hierarchy. *Nature* 549, 227–232. doi: 10.1038/nature23666

Lee, Y., Kawagoe, R., Sasai, K., Li, Y., Russell, H. R., Curran, T., et al. (2007). Loss of suppressor-of-fused function promotes tumorigenesis. *Oncogene* 26, 6442–6447. doi: 10.1038/sj.onc.1210467

Li, Z., and Langhans, S. A. (2021). *In Vivo* and Ex Vivo pediatric brain tumor models: an overview. *Front. Oncol.* 11:620831. doi: 10.3389/fonc.2021.620831

Lin, C. Y., Erkek, S., Tong, Y., Yin, L., Federation, A. J., Zapatka, M., et al. (2016). Active medulloblastoma enhancers reveal subgroup-specific cellular origins. *Nature* 530, 57–62. doi: 10.1038/nature16546

Lindberg, N., Kastemar, M., Olofsson, T., Smits, A., and Uhrbom, L. (2009). Oligodendrocyte progenitor cells can act as cell of origin for experimental glioma. *Oncogene* 28, 2266–2275. doi: 10.1038/onc.2009.76

Linkous, A., Balamatsias, D., Snuderl, M., Edwards, L., Miyaguchi, K., Milner, T., et al. (2019). Modeling patient-derived glioblastoma with cerebral organoids. *Cell Rep.* 26, 3203.e5–3211.e5. doi: 10.1016/j.celrep.2019.02.063

Llaguno, S. A., Chen, J., Kwon, C. H., Jackson, E. L., Li, Y., Burns, D. K., et al. (2009). Malignant astrocytomas originate from neural stem/progenitor cells in a somatic tumor suppressor mouse model. *Cancer Cell* 15, 45–56. doi: 10.1016/j.ccr.2008.12.006

Llaguno, S. A., Sun, D., Pedraza, A. M., Vera, E., Wang, Z., Burns, D. K., et al. (2019). Cell-of-origin susceptibility to glioblastoma formation declines with neural lineage restriction. *Nat. Neurosci.* 22, 545–555. doi: 10.1038/s41593-018-0333-8

Llaguno, S. R. A., Wang, Z., Sun, D., Chen, J., Xu, J., Kim, E., et al. (2015). Adult lineage-restricted CNS progenitors specify distinct glioblastoma subtypes. *Cancer Cell* 28, 429–440. doi: 10.1016/j.ccell.2015.09.007

Louis, D. N., Perry, A., Reifenberger, G., von Deimling, A., Figarella-Branger, D., Cavenee, W. K., et al. (2016). The 2016 World Health Organization classification of tumors of the central nervous system: a summary. *Acta Neuropathol.* 131, 803–820. doi: 10.1007/s00401-016-1545-1

Louis, D. N., Perry, A., Wesseling, P., Brat, D. J., Cree, I. A., Figarella-Branger, D., et al. (2021). The 2021 WHO classification of tumors of the central nervous system: a summary. *Neuro. Oncol.* 23, 1231–1251.

Lyne, S. B., and Yamini, B. (2021). An alternative pipeline for glioblastoma therapeutics: a systematic review of drug repurposing in Glioblastoma. *Cancers (Basel)* 13:1953. doi: 10.3390/cancers13081953

Mansour, A. A., Gonçalves, J. T., Bloyd, C. W., Li, H., Fernandes, S., Quang, D., et al. (2018). An *in vivo* model of functional and vascularized human brain organoids. *Nat. Biotechnol.* 36, 432–441. doi: 10.1038/nbt.4127

Marumoto, T., Tashiro, A., Friedmann-Morvinski, D., Scadeng, M., Soda, Y., Gage, F. H., et al. (2009). Development of a novel mouse glioma model using lentiviral vectors. *Nat. Med.* 15, 110–116. doi: 10.1038/nm.1863

Matsui, T. K., Tsuru, Y., Hasegawa, K., and Kuwako, K. (2021). Vascularization of human brain organoids. *Stem Cells* 39, 1017–1024. doi: 10.1002/stem.3368

Mayrhofer, M., Gourain, V., Reischl, M., Affaticati, P., Jenett, A., Joly, J. S., et al. (2017). A novel brain tumour model in zebrafish reveals the role of YAP activation in MAPK- and PI3K-induced malignant growth. *Dis. Model. Mech.* 10, 15–28. doi: 10.1242/dmm.026500

McCutcheon, I. E., Friend, K. E., Gerdes, T. M., Zhang, B. M., Wildrick, D. M., and Fuller, G. N. (2000). Intracranial injection of human meningioma cells in athymic mice: an orthotopic model for meningioma growth. *J. Neurosurg.* 92, 306–314. doi: 10.3171/jns.2000.92.2.0306

Miele, E., Po, A., Begalli, F., Antonucci, L., Mastronuzzi, A., Marras, C. E., et al. (2017). β-arrestin1-mediated acetylation of Gli1 regulates Hedgehog/Gli signaling and modulates self-renewal of SHH medulloblastoma cancer stem cells. *BMC Cancer* 17:488. doi: 10.1186/s12885-017-3477-0

Minata, M., Audia, A., Shi, J., Lu, S., Bernstock, J., Pavlyukov, M. S., et al. (2019). Phenotypic plasticity of invasive edge glioma stem-like cells in response to ionizing radiation. *Cell Rep.* 26, 1893.e7–1905.e7. doi: 10.1016/j.celrep.2019.01.076

Miroshnikova, Y., Mouw, J. K., Barnes, J. M., Pickup, M. W., Lakins, J. N., Kim, Y., et al. (2016). Tissue mechanics promote IDH1-dependent HIF1α-tenascin C feedback to regulate glioblastoma aggression. *Nat. Cell Biol.* 18, 1336–1345. doi: 10.1038/ncb3429

Muguruma, K., Nishiyama, A., Kawakami, H., Hashimoto, K., and Sasai, Y. (2015). Self-organization of polarized cerebellar tissue in 3D culture of human pluripotent stem cells. *Cell Rep.* 10, 537–550. doi: 10.1016/j.celrep.2014.12.051

Narayanan, A., Gagliardi, F., Gallotti, A. L., Mazzoleni, S., Cominelli, M., Fagnocchi, L., et al. (2019). The proneural gene ASCL1 governs the transcriptional subgroup affiliation in glioblastoma stem cells by directly repressing the mesenchymal gene NDRG1. *Cell Death Differ.* 26, 1813–1831. doi: 10.1038/s41418-018-0248-7

Nayler, S., Agarwal, D., Curion, F., Bowden, R., and Becker, E. B. E. (2021). High-resolution transcriptional landscape of xeno-free human induced pluripotent stem cell-derived cerebellar organoids. *Sci. Rep.* 11:12959. doi: 10.1038/s41598-021-91846-4

Neftel, C., Laffy, J., Filbin, M. G., Hara, T., Shore, M. E., Rahme, G. J., et al. (2019). An integrative model of cellular states, plasticity, and genetics for glioblastoma. *Cell* 178, 835.e21–849.e21. doi: 10.1016/j.cell.2019.06.024

Northcott, P. A., Lee, C., Zichner, T., Stütz, A. M., Erkek, S., Kawauchi, D., et al. (2014). Enhancer hijacking activates GFI1 family oncogenes in medulloblastoma. *Nature* 511, 428–434. doi: 10.1038/nature13379

Northcott, P. A., Robinson, G. W., Kratz, C. P., Mabbott, D. J., Pomeroy, S. L., Clifford, S. C., et al. (2019). Medulloblastoma. *Nat. Rev. Dis. Prim.* 5:11.

Núñez, F. J., Mendez, F. M., Kadiyala, P., Alghamri, M. S., Savelieff, M. G., Garcia-Fabiani, M. B., et al. (2019). IDH1-R132H acts as a tumor suppressor in glioma *via* epigenetic up-regulation of the DNA damage response. *Sci. Transl. Med.* 11:eaaq1427. doi: 10.1126/scitranslmed.aaq1427

Ocasio, J., Babcock, B., Malawsky, D., Weir, S. J., Loo, L., Simon, J. M., et al. (2019). scRNA-seq in medulloblastoma shows cellular heterogeneity and lineage expansion support resistance to SHH inhibitor therapy. *Nat. Commun.* 10, 1–17. doi: 10.1038/s41467-019-13657-6

Ogawa, J., Pao, G. M., Shokhirev, M. N., and Verma, I. M. (2018). Glioblastoma model using human cerebral organoids. *Cell Rep.* 23, 1220–1229. doi: 10.1016/j.celrep.2018.03.105

Omuro, A., and DeAngelis, L. M. (2013). Glioblastoma and other malignant gliomas: a clinical review. *JAMA* 310, 1842–1850. doi: 10.1001/jama.2013.280319

Oppel, F., Tao, T., Shi, H., Ross, K. N., Zimmerman, M. W., He, S., et al. (2019). Loss of atrx cooperates with p53-deficiency to promote the development of sarcomas and other malignancies. *PLoS Genet.* 15:e1008039. doi: 10.1371/journal.pgen.1008039

Osswald, M., Jung, E., Sahm, F., Solecki, G., Venkataramani, V., Blaes, J., et al. (2015). Brain tumour cells interconnect to a functional and resistant network. *Nature* 528, 93–98. doi: 10.1038/nature16071

Ozawa, T., Arora, S., Szulzewsky, F., Juric-Sekhar, G., Miyajima, Y., Bolouri, H., et al. (2018). A de novo mouse model of C11orf95-RELA fusion-driven ependymoma identifies driver functions in addition to NF-κB. *Cell Rep.* 23, 3787–3797. doi: 10.1016/j.celrep.2018.04.099

Pajtler, K., Wei, Y., Okonechnikov, K., Silva, P. B. G., Vouri, M., Zhang, L., et al. (2019). YAP1 subgroup supratentorial ependymoma requires TEAD and nuclear factor I-mediated transcriptional programmes for tumorigenesis. *Nat. Commun.* 10:3914. doi: 10.1038/s41467-019-11884-5

Park, H.-J., Kim, J.-K., Jeon, H.-M., Oh, S.-Y., Kim, S.-H., Nam, D.-H., et al. (2010). The neural stem cell fate determinant TLX promotes tumorigenesis and genesis of cells resembling glioma stem cells. *Mol. Cells* 30, 403–408. doi: 10.1007/s10059-010-0122-z

Park, N., Guilhamon, P., Desai, K., McAdam, R. F., Langille, E., O'Connor, M., et al. (2017). ASCL1 reorganizes chromatin to direct neuronal fate and suppress tumorigenicity of glioblastoma stem cells. *Cell Stem Cell* 21, 209.e7–224.e7.

Patel, A. P., Tirosh, I., Trombetta, J. J., Shalek, A. K., Gillespie, S. M., Wakimoto, H., et al. (2014). Single-cell RNA-seq highlights intratumoral heterogeneity

in primary glioblastoma. *Science (80)* 344, 1396–1401. doi: 10.1126/science.1254257

Patmore, D., Jassim, A., Nathan, E., Gilbertson, R. J., Tahan, D., Hoffmann, N., et al. (2020). DDX3X suppresses the susceptibility of hindbrain lineages to medulloblastoma. *Dev. Cell* 54, 455.e5–470.e5. doi: 10.1016/j.devcel.2020.05.027

Pei, Y., Moore, C. E., Wang, J., Tewari, A. K., Eroshkin, A., Cho, Y. J., et al. (2012). An animal model of MYC-driven medulloblastoma. *Cancer Cell* 21, 155–167. doi: 10.1016/j.ccr.2011.12.021

Peyre, M., Salaud, C., Clermont-Taranchon, E., Niwa-Kawakita, M., Goutagny, S., Mawrin, C., et al. (2015). PDGF activation in PGDS-positive arachnoid cells induces meningioma formation in mice promoting tumor progression in combination with Nf2 and Cdkn2ab loss. *Oncotarget* 6, 32713–32722. doi: 10.18632/oncotarget.5296

Peyre, M., Stemmer-Rachamimov, A., Clermont-Taranchon, E., Quentin, S., El-Taraya, N., Walczak, C., et al. (2013). Meningioma progression in mice triggered by Nf2 and Cdkn2ab inactivation. *Oncogene* 32, 4264–4272. doi: 10.1038/onc.2012.436

Phillips, H. S., Kharbanda, S., Chen, R., Forrest, W. F., Soriano, R. H., Wu, T. D., et al. (2006). Molecular subclasses of high-grade glioma predict prognosis, delineate a pattern of disease progression, and resemble stages in neurogenesis. *Cancer Cell* 9, 157–173. doi: 10.1016/j.ccr.2006.02.019

Phoenix, T., Patmore, D. M., Boop, S., Boulos, N., Jacus, M. O., Patel, Y. T., et al. (2016). Medulloblastoma genotype dictates blood brain barrier phenotype. *Cancer Cell* 29, 508–522. doi: 10.1016/j.ccell.2016.03.002

Pine, A. R., Cirigliano, S. M., Nicholson, J. G., Hu, Y., Linkous, A., Miyaguchi, K., et al. (2020). Tumor microenvironment is critical for the maintenance of cellular states found in primary glioblastomas. *Cancer Discov.* 10, 964–979. doi: 10.1158/2159-8290.CD-20-0057

Po, A., Ferretti, E., Miele, E., Smaele, E., Paganelli, A., Canettieri, G., et al. (2010). Hedgehog controls neural stem cells through p53-independent regulation of Nanog. *EMBO J.* 29, 2646–2658. doi: 10.1038/emboj.2010.131

Pudelko, L., Edwards, S., Balan, M., Nyqvist, D., Al-Saadi, J., Dittmer, J., et al. (2018). An orthotopic glioblastoma animal model suitable for high-throughput screenings. *Neuro. Oncol.* 20, 1475–1484. doi: 10.1093/neuonc/noy071

Püttmann, S., Senner, V., Braune, S., Hillmann, B., Exeler, R., Rickert, C. H., et al. (2005). Establishment of a benign meningioma cell line by hTERT-mediated immortalization. *Lab. Invest.* 85, 1163–1171. doi: 10.1038/labinvest.3700307

Qian, X., Song, H., and Ming, G. L. (2019). Brain organoids: advances, applications and challenges. *Development* 146:dev166074. doi: 10.1242/dev.166074

Ragel, B. T., Elam, I. L., Gillespie, D. L., Flynn, J. R., Kelly, D. A., Mabey, D., et al. (2008). A novel model of intracranial meningioma in mice using luciferase-expressing meningioma cells. Laboratory investigation. *J. Neurosurg.* 108, 304–310. doi: 10.3171/JNS/2008/108/2/0304

Rampazzo, E., Persano, L., Pistollato, F., Moro, E., Frasson, C., Porazzi, P., et al. (2013). Wnt activation promotes neuronal differentiation of glioblastoma. *Cell Death Dis.* 4:e500. doi: 10.1038/cddis.2013.32

Read, R. D., Cavenee, W. K., Furnari, F. B., and Thomas, J. B. (2009). A drosophila model for EGFR-Ras and PI3K-dependent human glioma. *PLoS Genet.* 5:e1000374. doi: 10.1371/journal.pgen.1000374

Read, R., Fenton, T. R., Gomez, G. G., Wykosky, J., Vandenberg, S. R., Babic, I., et al. (2013). A kinome-wide RNAi screen in Drosophila Glia reveals that the RIO kinases mediate cell proliferation and survival through TORC2-Akt signaling in glioblastoma. *PLoS Genet.* 9:e1003253. doi: 10.1371/journal.pgen.1003253

Reilly, K. M. (2009). Brain tumor susceptibility: the role of genetic factors and uses of mouse models to unravel risk. *Brain Pathol.* 19, 121–131. doi: 10.1111/j.1750-3639.2008.00236.x

Reiter, L. T., Potocki, L., Chien, S., Gribskov, M., and Bier, E. (2001). A systematic analysis of human disease-associated gene sequences in drosophila melanogaster. *Genome Res.* 11, 1114–1125. doi: 10.1101/gr.169101

Rodrigues, J., Heinrich, M. A., Teixeira, L. M., and Prakash, J. (2021). 3D In Vitro Model (R)evolution: unveiling tumor-stroma interactions. *Trends Cancer* 7, 249–264. doi: 10.1016/j.trecan.2020.10.009

Royet, A., Broutier, L., Coissieux, M. M., Malleval, C., Gadot, N., Maillet, D., et al. (2017). Ephrin-B3 supports glioblastoma growth by inhibiting apoptosis induced by the dependence receptor EphA4. *Oncotarget* 8, 23750–23759. doi: 10.18632/oncotarget.16077

Sasaki, A., Ishiuchi, S., Kanda, T., Hasegawa, M., and Nakazato, Y. (2001). Analysis of interleukin-6 gene expression in primary human gliomas, glioblastoma xenografts, and glioblastoma cell lines. *Brain Tumor Pathol.* 18, 13–21. doi: 10.1007/BF02478920

Schüller, U., Heine, V. M., Mao, J., Kho, A. T., Dillon, A. K., Han, Y. G., et al. (2008). Acquisition of granule neuron precursor identity is a critical determinant of progenitor cell competence to form Shh-Induced medulloblastoma. *Cancer Cell* 14, 123–134. doi: 10.1016/j.ccr.2008.07.005

Seligman, A. M., Shear, M. J., and Alexander, L. (1939). Studies in Carcinogenesis: VIII. Experimental production of brain tumors in mice with methylcholanthrene. *Am. J. Cancer* 37, 364–395.

Shi, Y., Sun, L., Wang, M., Liu, J., Zhong, S., Li, R., et al. (2020). Vascularized human cortical organoids (vOrganoids) model cortical development *in vivo*. *PLoS Biol.* 18:e3000705. doi: 10.1371/journal.pbio.3000705

Shin, J., Padmanabhan, A., De Groh, E. D., Lee, J. S., Haidar, S., Dahlberg, S., et al. (2012). Zebrafish neurofibromatosis type 1 genes have redundant functions in tumorigenesis and embryonic development. *Dis. Model. Mech.* 5, 881–894. doi: 10.1242/dmm.009779

Shu, Q., Wong, K. K., Su, J. M., Adesina, A. M., Yu, L. T., Tsang, Y. T. M., et al. (2008). Direct orthotopic transplantation of fresh surgical specimen preserves CD133+ tumor cells in clinically relevant mouse models of medulloblastoma and glioma. *Stem Cells* 26, 1414–1424. doi: 10.1634/stemcells.2007-1009

Singh, S., Hawkins, C., Clarke, I. D., Squire, J. A., and Hide, J. B. T. (2004). Identification of human brain tumour initiating cells. *Nature* 432, 396–401. doi: 10.1038/nature03128

Smith, K. S., Xu, K., Mercer, K. S., Boop, F., Klimo, P., DeCupyere, M., et al. (2020). Patient-derived orthotopic xenografts of pediatric brain tumors: a St. Jude resource. *Acta Neuropathol.* 140, 209–225. doi: 10.1007/s00401-020-02171-5

Sumiyoshi, K., Koso, H., and Watanabe, S. (2018). Spontaneous development of intratumoral heterogeneity in a transposon-induced mouse model of glioma. *Cancer Sci.* 109, 1513–1523. doi: 10.1111/cas.13579

Susanto, E., Navarro, A. M., Zhou, L., Sundström, A., van Bree, N., Stantic, M., et al. (2020). Modeling SHH-driven medulloblastoma with patient iPS cell-derived neural stem cells. *Proc. Natl. Acad. Sci. U.S.A.* 117, 20127–20138. doi: 10.1073/pnas.1920521117

Swartling, F. J., Grimmer, M. R., Hackett, C. S., Northcott, P. A., Fan, Q. W., Goldenberg, D. D., et al. (2010). Pleiotropic role for MYCN in medulloblastoma. *Genes Dev.* 24, 1059–1072. doi: 10.1101/gad.1907510

Swartling, F. J., Savov, V., Persson, A. I., Chen, J., Hackett, C. S., Northcott, P. A., et al. (2012). Distinct neural stem cell populations give rise to disparate brain tumors in response to N-MYC. *Cancer Cell* 21, 601–613. doi: 10.1016/j.ccr.2012.04.012

Tang, M., Xie, Q., Gimple, R. C., Zhong, Z., Tam, T., Tian, J., et al. (2020). Three-dimensional bioprinted glioblastoma microenvironments model cellular dependencies and immune interactions. *Cell Res.* 30, 833–853. doi: 10.1038/s41422-020-0338-1

Taylor, M. D., Northcott, P. A., Korshunov, A., Remke, M., Cho, Y.-J., Clifford, S. C., et al. (2012). Molecular subgroups of medulloblastoma: the current consensus. *Acta Neuropathol.* 123:465. doi: 10.1007/s00401-011-0922-z

Thomas, R. S., Susil, B., and Kola, I. (1994). Activating point mutations of the neu oncogene in schwannomas induced by ethylnitrosourea exposure to day 15 and day 18 fetal rats. *Int. J. Oncol.* 5, 1219–1225. doi: 10.3892/ijo.5.6.1219

Thompson, E. M., Ashley, D., and Landi, D. (2020). Current medulloblastoma subgroup specific clinical trials. *Transl. Pediatr.* 9, 157–162. doi: 10.21037/tp.2020.03.03

Tiberi, L., Bonnefont, J., van den Ameele, J., Le Bon, S. D., Herpoel, A., and Bilheu, A. (2014). A BCL6/BCOR/SIRT1 complex triggers neurogenesis and suppresses medulloblastoma by repressing Sonic Hedgehog signaling. *Cancer Cell* 26, 797–812. doi: 10.1016/j.ccell.2014.10.021

Uhrbom, L., Kastemar, M., Johansson, F. K., Westermark, B., and Holland, E. C. (2005). Cell type-specific tumor suppression by Ink4a and Arf in Kras-induced mouse gliomagenesis. *Cancer Res.* 65, 2065–2069. doi: 10.1158/0008-5472.CAN-04-3588

Uziel, T., Zindy, F., Xie, S., Lee, Y., Forget, A., Magdaleno, S., et al. (2005). The tumor suppressors Ink4c and p53 collaborate independently with Patched to suppress medulloblastoma formation. *Genes Dev.* 19, 2656–2667. doi: 10.1101/gad.1368605

Vanner, R. J., Remke, M., Gallo, M., Selvadurai, H. J., Coutinho, F., Lee, L., et al. (2014). Quiescent Sox2+Cells drive hierarchical growth and relapse in sonic hedgehog subgroup medulloblastoma. *Cancer Cell* 26, 33–47. doi: 10.1016/j.ccr.2014.05.005

Vargas-Patron, L. A., Agudelo-Dueñãs, N., Madrid-Wolff, J., Venegas, J. A., González, J. M., Forero-Shelton, M., et al. (2019). Xenotransplantation of Human glioblastoma in Zebrafish larvae: *in vivo* imaging and proliferation assessment. *Biol. Open* 8:bio043257. doi: 10.1242/bio.043257

Velasco, S., Kedaigle, A. J., Simmons, S. K., Nash, A., Rocha, M., Quadrato, G., et al. (2019). Individual brain organoids reproducibly form cell diversity of the human cerebral cortex. *Nature* 570, 523–527. doi: 10.1038/s41586-019-1289-x

Verhaak, R. G. W., Hoadley, K. A., Purdom, E., Wang, V., Qi, Y., Wilkerson, M. D., et al. (2010). An integrated genomic analysis identifies clinically relevant subtypes of glioblastoma characterized by abnormalities in PDGFRA, IDH1, EGFR and NF1. *Cancer Cell* 17:98. doi: 10.1016/j.ccr.2009.12.020

Vittori, M., Breznik, B., Hrovat, K., Kenig, S., and Lah, T. T. (2017). RECQ1 helicase silencing decreases the tumour growth rate of U87 glioblastoma cell xenografts in Zebrafish embryos. *Genes (Basel)* 8:222. doi: 10.3390/genes8090222

Vo, B. H. T., Li, C., Morgan, M. A., Theurillat, I., Finkelstein, D., Wright, S., et al. (2017). Inactivation of Ezh2 Upregulates Gfi1 and drives aggressive myc-driven group 3 medulloblastoma. *Cell Rep.* 18, 2907–2917. doi: 10.1016/j.celrep.2017.02.073

Watanabe, M., Buth, J. E., Vishlaghi, N., de la Torre-Ubieta, L., Taxidis, J., Khakh, B. S., et al. (2017). Self-organized cerebral organoids with human-specific features predict effective drugs to combat Zika virus infection. *Cell Rep.* 21, 517–532. doi: 10.1016/j.celrep.2017.09.047

Wei, Q., Clarke, L., Scheidenhelm, D. K., Qian, B., Tong, A., Sabha, N., et al. (2006). High-grade glioma formation results from postnatal pten loss or mutant epidermal growth factor receptor expression in a transgenic mouse glioma model. *Cancer Res.* 66, 7429–7437. doi: 10.1158/0008-5472.CAN-06-0712

Wetmore, C., Eberhart, D. E., and Curran, T. (2001). Loss of p53 but not ARF accelerates medulloblastoma in mice heterozygous for patched. *Cancer Res.* 61, 513–516.

Willoughby, L. F., Schlosser, T., Manning, S. A., Parisot, J. P., Street, I. P., Richardson, H. E., et al. (2013). An *in vivo* large-scale chemical screening platform using Drosophila for anti-cancer drug discovery. *Dis. Model. Mech.* 6, 521–529. doi: 10.1242/dmm.009985

Xu, R., Boreland, A. J., Li, X., Erickson, C., Jin, M., Atkins, C., et al. (2021). Developing human pluripotent stem cell-based cerebral organoids with a controllable microglia ratio for modeling brain development and pathology. *Stem Cell Rep.* 16, 1923–1937. doi: 10.1016/j.stemcr.2021.06.011

Yamamoto, S., Jaiswal, M., Charng, W. L., Gambin, T., Karaca, E., Mirzaa, G., et al. (2014). A drosophila genetic resource of mutants to study mechanisms underlying human genetic diseases. *Cell* 159, 200–214. doi: 10.1016/j.cell.2014.09.002

Yamazaki, S., Ohka, F., Hirano, M., Shiraki, Y., Motomura, K., Tanahashi, K., et al. (2021). Newly established patient-derived organoid model of intracranial meningioma. *Neuro-Oncology* 23, 1936–1948. doi: 10.1093/neuonc/noab155

Yan, C., Brunson, D. C., Tang, Q., Do, D., Iftimia, N. A., Moore, J. C., et al. (2019). Visualizing engrafted human cancer and therapy responses in immunodeficient Zebrafish. *Cell* 177, 1903.e14–1914.e14. doi: 10.1016/j.cell.2019.04.004

Yang, X. J., Cui, W., Gu, A., Xu, C., Yu, S. C., Li, T. T., et al. (2013a). A novel zebrafish xenotransplantation model for study of glioma stem cell invasion. *PLoS One* 8:e61801. doi: 10.1371/journal.pone.0061801

Yang, X. J., Chen, G. L., Yu, S. C., Xu, C., Xin, Y. H., Li, T. T., et al. (2013b). TGF-β1 enhances tumor-induced angiogenesis *via* JNK pathway and macrophage infiltration in an improved zebrafish embryo/xenograft glioma model. *Int. Immunopharmacol.* 15, 191–198. doi: 10.1016/j.intimp.2012.12.002

Yang, Z. J., Ellis, T., Markant, S. L., Read, T. A., Kessler, J. D., Bourboulas, M., et al. (2008). Medulloblastoma can be initiated by deletion of patched in lineage-restricted progenitors or stem cells. *Cancer Cell* 14, 135–145. doi: 10.1016/j.ccr.2008.07.003

Yao, M., Ventura, P. B., Jiang, Y., Rodriguez, F. J., Wang, L., Perry, J. S. A., et al. (2020). Astrocytic trans-differentiation completes a multicellular paracrine feedback loop required for medulloblastoma tumor growth. *Cell* 180, 502.e19–520.e19. doi: 10.1016/j.cell.2019.12.024

Yi, H.-G., Jeong, Y. H., Kim, Y., Choi, Y.-J., Moon, H. E., Park, S. H., et al. (2019). A bioprinted human-glioblastoma-on-a-chip for the identification of patient-specific responses to chemoradiotherapy. *Nat. Biomed. Eng.* 3, 509–519. doi: 10.1038/s41551-019-0363-x

Yi, Y., Hsieh, I.-Y., Huang, X., Li, J., and Zhao, W. (2016). Glioblastoma stem-like cells: characteristics, microenvironment, and therapy. *Front. Pharmacol.* 7:477. doi: 10.3389/fphar.2016.00477

Youngblood, M. W., Duran, D., Montejo, J. D., Li, C., Omay, S. B., Özduman, K., et al. (2019). Correlations between genomic subgroup and clinical features in a cohort of more than 3000 meningiomas. *J. Neurosurg.* 133, 1345–1354. doi: 10.3171/2019.8.JNS191266

Zhang, P., Xia, Q., Liu, L., Li, S., and Dong, L. (2020). Current opinion on molecular characterization for GBM classification in guiding clinical diagnosis, prognosis, and therapy. *Front. Mol. Biosci.* 7:562798. doi: 10.3389/fmolb.2020.562798

Zhu, H., Acquaviva, J., Ramachandran, P., Boskovitz, A., Woolfenden, S., Pfannl, R., et al. (2009). Oncogenic EGFR signaling cooperates with loss of tumor suppressor gene functions in gliomagenesis. *Proc. Natl. Acad. Sci. U.S.A.* 106, 2712–2716. doi: 10.1073/pnas.0813314106

Zuckermann, M., Hovestadt, V., Knobbe-Thomsen, C. B., Zapatka, M., Northcott, P. A., Schramm, K., et al. (2015). Somatic CRISPR/Cas9-mediated tumour suppressor disruption enables versatile brain tumour modelling. *Nat. Commun.* 6:7391. doi: 10.1038/ncomms8391

Conflict of Interest: The authors declare that the research was conducted in the absence of any commercial or financial relationships that could be construed as a potential conflict of interest.

Advantages of publishing in Frontiers

OPEN ACCESS
Articles are free to read for greatest visibility and readership

FAST PUBLICATION
Around 90 days from submission to decision

HIGH QUALITY PEER-REVIEW
Rigorous, collaborative, and constructive peer-review

TRANSPARENT PEER-REVIEW
Editors and reviewers acknowledged by name on published articles

Frontiers
Avenue du Tribunal-Fédéral 34
1005 Lausanne | Switzerland

Visit us: www.frontiersin.org
Contact us: frontiersin.org/about/contact

REPRODUCIBILITY OF RESEARCH
Support open data and methods to enhance research reproducibility

DIGITAL PUBLISHING
Articles designed for optimal readership across devices

FOLLOW US
@frontiersin

IMPACT METRICS
Advanced article metrics track visibility across digital media

EXTENSIVE PROMOTION
Marketing and promotion of impactful research

LOOP RESEARCH NETWORK
Our network increases your article's readership